The First Annual Conference on Cold Fusion

Conference Proceedings

March 28-31, 1990
University Park Hotel
Salt Lake City, Utah

Sponsored by the

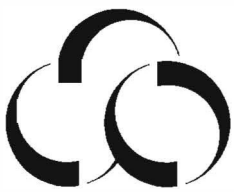

National Cold Fusion Institute

National Cold Fusion Institute

August 10, 1990

Dear Colleague:

I am pleased to be sending you these conference proceedings in connection with the First Annual Conference on Cold Fusion. As sponsors of the conference, we at NCFI and the University of Utah wish to thank you for your participation in the conference. We found that the exchange of ideas and information at the conference stimulated new experimental and theoretical research at our institute, and hope that many others were similarly prompted in their study of the interesting phenomena which were discussed during our meetings.

The papers which are presented in the enclosed proceedings will give interested readers an in-depth perspective on the material which was presented at the conference. Like the conference itself, we feel the proceedings will lead researchers to a greater depth of understanding in this emerging field of inquiry. We wish to extend our thanks to those who prepared the material presented in this volume, to those who attended the conference, and to those who will pursue research in these important phenomena.

With regards,
THE NATIONAL COLD FUSION INSTITUTE

Fritz G. Will

Dr. Fritz G. Will
Director

390 Wakara Way, Salt Lake City, Utah 84108/801-581-5571, Fax: 801-581-6674

The First Annual Conference on Cold Fusion

Conference Proceedings

March 28-31, 1990
University Park Hotel
Salt Lake City, Utah

Sponsored by the

National Cold Fusion Institute

OPENING ADDRESS

By

FRITZ G. WILL
Director
National Cold Fusion Institute

Welcome to the First Annual Cold Fusion Conference sponsored by the University of Utah National Cold Fusion Institute. My name is Fritz Will and, as director of the Institute, it is my pleasure to open this conference at which more than 200 attendees will have the opportunity to share the results in cold fusion research, as presented by 40 speakers from the United States, India, Italy and Taiwan.

The objectives of this conference are, as in any scientific meeting, to provide a forum for scientists to present the results of their research and to discuss the findings of others, thereby stimulating new ideas and advancing our understanding.

It has now been one year since Drs. Fleischmann and Pons announced that they had observed nuclear fusion at room temperature. They reported that they had observed unusually large amounts of excess heat and evidence for the occurrence of nuclear reactions when applying an electric current between a palladium cathode (negative pole) and a platinum anode immersed into an electrolyte solution of LiOD in heavy water (D_2O).

The announcement evoked euphoria in many, but skepticism in some. The possible technological implications were and are enormous. But, what was originally believed to be simple experiments that could be readily reproduced in other laboratories, turned out to be complex phenomena that defied confirmation in many laboratories and which cannot be explained on the basis of classical nuclear physics.

However, persistent and careful work by recognized experts in the fields of electrochemistry, nuclear measurements and materials science has now led to confirmation of the Fleischmann and Pons results in many laboratories in the United States, Japan, India, Italy, Russia and several other countries.

The papers to be presented during this conference will report on the generation of excess heat, determined in careful calorimetric measurements, observations of tritium levels far in excess of background, and the detection of strong neutron emissions. The multitude of results obtained by so many different groups can no longer be explained away as experimental artifacts. The reality of these effects is further underscored by the absence of such effects in carefully executed control experiments, employing hydrogen instead of deuterium or platinum instead of palladium. At this conference, another significant set of presentations will occur. Theoretical physicists will present novel theoretical models aimed at explaining why nuclear fusion can occur in solids, where classical nuclear physics (applicable to gases) fails to provide explanations.

While the key observations relating to cold fusion have been confirmed by many competent groups, it is also true that the phenomena cannot be reproduced on demand and that an understanding of the underlying mechanisms is not at hand. The phenomena involve surface chemistry and the behavior of a metal loaded with deuterium. Appreciating the complexities and well-known irreproducibilities involved in each of these cases individually, many scientists are not surprised that one year of research and development have not been sufficient to unravel the complexities of cold fusion, which combines both cases.

The history of science and technology has many examples where irreproducibility had been experienced for years. A prominent case is the metaloxide semiconductor. It took years of effort with multi-million dollar expenditures to achieve reproducible performance of such semiconducting devices. What ultimately led to reproducibility was the careful control of the level of impurities, most notably, sodium.

The basis of many critics for rejecting cold fusion out of hand has been that the experimental results violate the predictions of classical nuclear physics and, hence, must be erroneous. It is not the first time in science that a radically new finding has defied traditional thinking and existing theories. Nor is it the first time that a revolutionary discovery has been rejected by a large fraction of the scientific community. A prominent example is Galileo's declaration that the earth circles around the sun rather than vice versa. We recall that Galileo was ultimately forced to swear that his revolutionary new concept was false after all.

We know that we live in much more enlightened times today. We know that experimental results cannot be declared wrong by voting. We know that the reliable results obtained by a minority must not be regarded as wrong only because a majority of others has failed to confirm these results within one year.

Research into the intriguing phenomena of cold fusion must and will continue. It will continue because dedicated scientists will not rest before the phenomena of cold fusion are fully understood and because sponsors with vision will continue to support the progress of science. The scientific process of seeking understanding must not be interfered with. The freedom of science is just as basic as the freedom of speech.

March 29, 1990

PROGRAM

Wednesday, March 28, 1990

7:00 p.m. - 9:00 p.m. **REGISTRATION and RECEPTION**

Thursday, March 29, 1990

		PAGE
7:00-8:30 a.m.	**REGISTRATION**	
8:30	**OPENING COMMENTS** **F.G. Will**, Director **H. Rossi**, Conference Chair National Cold Fusion Institute (NCFI)	
	WELCOME **I. Cumming** Chair, Board of Trustees NCFI	
Session Chair:	**H. Rossi** University of Utah/NCFI	
8:45	**Calorimetry of the Palladium-Deuterium Systems** **S. Pons** and M. Fleischmann University of Utah/NCFI	1
9:30	**Calorimetry and Electrochemistry in the D/Pd System** **M.C.H. McKubre,** R.C. Rocha-Filho, S. Smedley, F. Tanzella, *J. Chao, *B. Chexal, *T. Passell, and *J. Santucci Stanford Research Institute *Electric Power Research Institute	20
10:00	**Anomalous Calorimetric Results During Long-Term Evolution of Deuterium on Palladium from Alkaline Deuteroxide Electrolyte** A.J. Appleby, Y.J. Kim, **O.J. Murphy,** and S. Srinivasan Texas A& M University	32
10:30	Break	
10:40	**Initial Calorimetry Experiments in the Physics Division at ORNL** ***(Paper not submitted)*** **D.P. Hutchinson**, C.A. Bennett, R.K. Richards, J. Bullock IV, and G.L. Powell Oak Ridge National Laboratory	
11:00	**Recent Measurements of Excess Energy Production in Electrochemical Cells Containing Heavy Water and Palladium** **M. Schreiber**, T.M. Gür, G. Lucier, J.A. Ferrante, J. Chao* and R.A. Huggins Stanford University *Electric Power Research Institute	44

PROGRAM

Thursday, March 29, 1990 (continued)

		PAGE
11:20	**Quartz Crystal Microbalance Study of Palladium/Hydrogen Interactions** **G.T. Cheek** and W.E. O'Grady Naval Research Laboratories	57
11:40	**Investigation of Nuclear Processes in Deuterated Metals** ***(Paper not submitted)*** **J. Santucci** Electric Power Research Institute	
12:00	Lunch Break	
Session Chair:	**J. O'M. Bockris** Texas A&M University	
1:30	**Overview of BARC Studies in Cold Fusion** **P.K. Iyengar** and M. Srinivasan Atomic Energy Commision, Bombay, India	62
2:15	**Experimental Considerations in Electrochemical Isoperibolic Calorimetry** **T.M. Gür,** M. Schreiber, G. Lucier, J.A. Ferrante, J. Chao* and R.A. Huggins Stanford University *Electric Power Research Institute	82
2:35	**Theoretical Ideas on Cold Fusion** **G. Preparata** University of Milan, Italy	91
3:20	**Status of Coherent Fusion Theory** **P.L. Hagelstein** Massachusetts Institute of Technology	99
3:40	**Quantum Mechanics of "Cold" and "Not-So-Cold" Fusion** S.R. Chubb and **T.A. Chubb** Naval Research Laboratories	119
4:00	Dinner Break	
4:15-6:00	Guided Tours of National Cold Fusion Institute (sign-up sheets at the conference registration desk) (walk east of hotel five minutes to 390 Wakara Way)	
Session Chair:	J. Brophy University of Utah	
7:30	**Nuclear Energy in an Atomic Lattice** **J. Schwinger**, Nobel Laureate UCLA	130
8:15	Adjourn	

PROGRAM

Friday, March 30, 1990		PAGE
Session Chair:	**R. Huggins** Stanford University	
8:15 a.m.	**Does Tritium Form at Electrodes by Nuclear Reactions?** **J. O'M. Bockris**, G.H. Lin, R.C. Kainthla, N.J.C. Packham, and O. Velev Texas A&M University	**137**
9:00	**A Study of Electrolytic Tritium Production** **E. Storms** and C. Talcott Los Alamos National Laboratory	**149**
9:45	**The Initiation of Excess Power and Possible Products of Nuclear Interactions During the Electrolysis of Heavy Water** **C.D. Scott**, J.E. Mrochek, T.C. Scott, G.E. Michaels E. Newman, and M. Petek, Oak Ridge National Laboratory	**164**
10:30	**Panel Discussion - Thermal Phenomena** **F.G. Will**, Moderator **J. O'M. Bockris** **M. Fleischmann** **R. Huggins** **M. McKubre** **S. Pons** **E. Yeager**	
11:30	Lunch Break	
Session Chair:	**H. Menlove** Texas A&M University	
1:30	**Cold Nuclear Fusion in Condensed Matter: Recent Results and Open Questions** ***(Paper not submitted)*** **S. Jones** Brigham Young University	
2:05	**Search for Nuclear Phenomena by the Interaction between Titanium and Deuterium** **F. Scaramuzzi,** F. D'Amato, A. DeNinno, P. Zeppa, C. Pontorieri, F. Lanza ENEA, Rome, Italy	**170**
2:15	**Statistical Analysis of Neutron Emission in Cold Fusion Experiments** **M. Srinivasan,** A. Shyam, S.B. Degwekar, and L.V. Kulkarni Bhabha Atomic Research Center, Bombay, India	**175**

PROGRAM

Friday, March 30, 1990 (continued) PAGE

3:00	**The Effect of Velocity Distribution and Electron Screening on Cold Fusion** R.A. Rice, G.S. Chulick, and **Y.E. Kim** Purdue University	**185**
	Surface Reaction Mechanism and Lepton Screening for Cold Fusion with Electrolysis **Y.E. Kim** Purdue University	**194**
3:30	Break	
3:40	**On Aspects of Nuclear Products** **G.H. Miley,** M.H. Ragheb and H. Hora University of Illinois	**202**
4:00	**Isotopic Mass Shifts in Cathodically-Driven Palladium via Neutron Transfer Suggested by a Transmission Resonance Model to Explicate Enhanced Fusion Phenomena (Hot and Cold) within a Deuterated Matrix** **R.T. Bush** California State Polytechnic University	**213**
4:20	**A Zero Gradient Calorimeter for the Measurement of Anomalous Heat from the Electrolysis of Deuterated Metals** **L.J. Droege** and T.F. Droege Black Hawk, CO and Batavia, IL	**229**
4:40	**Electric Field Distribution of the Palladium Crystal Lattice** **K.J. Bunch** and R.W. Grow University of Utah/NCFI	**243**
5:00	Session Adjourns	
6:00-7:30	Buffet Reception Remarks by the Governor of Utah **The Honorable Norman S. Bangerter** Hosted by Leucadia National Corporation Dessert provided by Mrs. Fields Cookies Home office located in Park City, Utah	

PROGRAM

Friday, March 30, 1990 (continued) PAGE

Session Chair: **S. Jones**
Brigham Young University

7:30 **High-Sensitivity Measurements of Neutron Emission from Ti Metal in Pressurized D_2 Gas** 250
H. Menlove
Los Alamos National Laboratory

8:15 **Technical Status of Cold Fusion Results** 252
D. Worledge
EPRI

8:35 Adjourn

Saturday, March 31, 1990

Session Chair: **M. Fleischmann**
University of Utah/NCFI

8:15 a.m. **Tritium Measurements and Deuterium Loading in D_2O Electrolysis with a Palladium Cathode** 261
R.R. Adzic, D. Gervasio, I. Bae, B. Cahan and E. Yeager
Case Western Reserve University

9:00 **Anomalies in the Surface Analysis of Deuterated Palladium** 272
D. Rolison, W.E. O'Grady, R.J. Doyle, Jr., and P.P. Trzaskoma
Naval Research Laboratories

9:45 **Anomalous Effects of Deuterated Metals**
(Scheduled but not presented)
T. Schneider
EPRI

10:30 **Panel Discussion - Nuclear Phenomena**
H. Rossi, Moderator
J. O'M. Bockris
S. Jones
T. Schneider
C.D. Scott
E. Storms
N. Hoffman

11:30 Lunch Break

PROGRAM

Saturday, March 31, 1990 (continued)		PAGE
Session Chair:	**E.B. Yeager** Case Western University	
1:20	**On Empirical System ID, Possible External Electromagnetic/Electronuclear Stimulation/Actuation and Automatic Feedback Control of Cold Fusion** **R.W. Bass** Thousand Oaks, CA	281
1:40	**An Investigation of Cold Fusion in This Titanium Films** ***(Paper not submitted)*** **G. Chambers,** G. Hubler, and K. Grabowski Naval Research Laboratory	
	Reformulation of the Cold Fusion Problem: Heterogeneous Nucleation - A Likely Cause of the Irreproducibility and Intermittency of Cold Fusion Observations **P.H. Handel** University of Missouri	288
	A New Theoretical Model (Nu-Q*) for Rationalizing Various Events of "Cold Fusion" in Deuterium Loaded Palladium Cathodes **G. Andermann** University of Hawaii	295
2:00	**Some Observations Related to the Presence of Hydrogen and Deuterium in Palladium** D.R. Coupland, M.L. Doyle, J.W. Jenkins, J.H.F. Notton, R.J. Potter, and **D.J. Thompson** Johnson-Matthey Technology Centre	299
2:20	**Three Dimensional Computer Simulation of an Isoperibolic Calorimeter for Cold Fusion Experiments** **J. Chao***, W. Layman*, C.M. Kang, T.M. Gür, M. Schreiber, R. Huggins, G. Lucier, and J. Ferrante Stanford University *Electric Power Research Institute	308
2:40	Break	
Session Chair:	**F.G. Will** NCFI	
2:45	**Metallurgical Aspects in Cold Fusion Experiments** **S. Guruswamy** and M.E. Wadsworth University of Utah/NCFI	314
3:05	**Electrochemical Calorimetric Studies of the Cold Fusion Effect** **M.H. Miles,** K.H. Park and D.E. Stilwell Naval Weapons Center	328

PROGRAM

Saturday, March 31, 1990 (continued)		PAGE
3:25	**Thoughts on Warm Fusion vs Cold Fusion** Y.-C. Cheng, W-Y.P. Hwang, and **S.N. Yang** National Taiwan University	**335**
3:45	**An Overview of Cold Fusion Phenomena** **M. Fleischmann** University of Utah/NCFI	**344**

PROCEEDINGS INDEX

PRESENTATION TITLE	PAGE
Calorimetry of the Palladium-Deuterium System **S. Pons** and M. Fleischmann University of Utah/NCFI	1
Calorimetry and Electrochemistry in the D/Pd System **M.C.H. McKubre,** R.C. Rocha-Filho, S. Smedley, F. Tanzella, *J. Chao, *B. Chexal, *T. Passell, and *J. Santucci Stanford Research Institute *Electric Power Research Institute	20
Anomalous Calorimetric Results During Long-Term Evolution of Deuterium on Palladium from Alkaline Deuteroxide Electrolyte A.J. Appleby, Y.J. Kim, **O.J. Murphy,** and S. Srinivasan Texas A& M University	32
Recent Measurements of Excess Energy Production in Electrochemical Cells Containing Heavy Water and Palladium **M. Schreiber**, T.M. Gür, G. Lucier, J.A. Ferrante, J. Chao* and R.A. Huggins Stanford University *Electric Power Research Institute	44
Quartz Crystal Microbalance Study of Palladium/Hydrogen Interactions **G.T. Cheek** and W.E. O'Grady Naval Research Laboratories	57
Overview of BARC Studies in Cold Fusion **P.K. Iyengar** and M. Srinivasan Atomic Energy Commision, Bombay, India	62
Experimental Considerations in Electrochemical Isoperibolic Calorimetry **T.M. Gür,** M. Schreiber, G. Lucier, J.A. Ferrante, J. Chao* and R.A. Huggins Stanford University *Electric Power Research Institute	82
Theoretical Ideas on Cold Fusion **G. Preparata** University of Milan, Italy	91
Status of Coherent Fusion Theory **P.L. Hagelstein** Massachusetts Institute of Technology	99
Quantum Mechanics of "Cold" and "Not-So-Cold" Fusion S.R. Chubb and **T.A. Chubb** Naval Research Laboratories	119
Nuclear Energy in an Atomic Lattice **J. Schwinger**, Nobel Laureate UCLA	130

PRESENTATION TITLE	PAGE
Does Tritium Form at Electrodes by Nuclear Reactions? **J. O'M. Bockris**, G.H. Lin, R.C. Kainthla, N.J.C. Packham, and O. Velev Texas A&M University	137
A Study of Electrolytic Tritium Production **E. Storms** and C. Talcott Los Alamos National Laboratory	149
The Initiation of Excess Power and Possible Products of Nuclear Interactions During the Electrolysis of Heavy Water **C.D. Scott**, J.E. Mrochek, T.C. Scott, G.E. Michaels, E. Newman, and M. Petek Oak Ridge National Laboratory	164
Search for Nuclear Phenomena by the Interaction between Titanium and Deuterium F. D'Amato, A. DeNinno, **F. Scaramuzzi,** P. Zeppa, C. Pontorieri, F. Lanza ENEA, Rome, Italy	170
Statistical Analysis of Neutron Emission in Cold Fusion Experiments **M. Srinivasan,** A. Shyam, S.B. Degwekar, and L.V. Kulkarni Bhabha Atomic Research Center, Bombay, India	175
The Effect of Velocity Distribution and Electron Screening on Cold Fusion R.A. Rice, G.S. Chulick, and **Y.E. Kim** Purdue University	185
Surface Reaction Mechanism and Lepton Screening for Cold Fusion with Electrolysis **Y.E. Kim** Purdue University	194
On Aspects of Nuclear Products **G.H. Miley,** M.H. Ragheb and H. Hora University of Illinois	202
Isotopic Mass Shifts in Cathodically-Driven Palladium via Neutron Transfer Suggested by a Transmission Resonance Model to Explicate Enhanced Fusion Phenomena (Hot and Cold) within a Deuterated Matrix **R.T. Bush** California State Polytechnic University	213
A Zero Gradient Calorimeter for the Measurement of Anomalous Heat from the Electrolysis of Deuterated Metals **L.J. Droege** and T.F. Droege Black Hawk, CO and Batavia, IL	229
Electric Field Distribution of the Palladium Crystal Lattice **K.J. Bunch** and R.W. Grow University of Utah/NCFI	243
High-Sensitivity Measurements of Neutron Emission from Ti Metal in Pressurized D_2 Gas **H. Menlove** Los Alamos National Laboratory	250

Technical Status of Cold Fusion Results **252**
David H. Worledge
Electric Power Research Institute

Tritium Measurements and Deuterium Loading In D_2O Electrolysis With A Palladium Cathode **261**
R. R. Adzic*, D. Gervasio, I. Bae, B. Cahan And E. Yeager
Case Western Reserve University

Anomalies in The Surface Analysis of Deuterated Palladium **272**
Debra R. Rolison, William E. O'Grady, Robert J. Doyle, Jr. and Patricia P. Trzaskoma
Naval Research Laboratory

Reformulation of The Cold Fusion Problem: Heterogeneous And Intermittency of Cold Fusion Observations Nucleation - A Likely Cause of The Irreproducibility **288**
Peter H. Handel
University of Missouri

A New Theoretical Model (N-Q*) For Rationalizing Various Events of 'Cold Fusion' In Deuterium Loaded Palladium Cathodes **295**
George Andermann
University of Hawaii At Manoa,

Some Observations Related to The Presence of Hydrogen And Deuterium In Palladium **299**
D R Coupland, M L Doyle, J W Jenkins, J H F Notton, R J Potter and D T Thompson.
Johnson Matthey Technology Centre

Three Dimensional Computer Simulation of An Isoperibolic Calorimeter For Cold Fusion Experiments **308**
J. Chao, Epri, W. Layman, Epri, C.M. Kang, AET T. Gur, M. Schreiber, R. Huggins, G. Lucier, J. Ferrante
Stanford University

Metallurgical Aspects in Cold Fusion Experiments **314**
Sivaraman Guruswamy And Milton E. Wadsworth
National Cold Fusion Institute, University of Utah

Electrochemical Calorimetric Studies of The Cold Fusion Effect **328**
M. H. Miles, K. H. Park, and D. E. Stilwell
Naval Weapons Center, China Lake, Ca 93555

Thoughts on Warm Fusion Versus Cold Fusion **335**
Yi-Chen Cheng, W-Y. P. Hwang, And Shin Nan Yang
National Taiwan University

An Overview of Cold Fusion Phenomena **344**
Martin Fleischmann
University of Southampton

AUTHOR INDEX

Adzic, R.R. - 261
Andermann, G. - 295
Appleby, A.J. - 32

Bae, I. - 261
Bass, R.W. - 281
Bennett, C.A. - *paper not submitted*
Bockris, J.O'M. - 137
Bullock IV, J. - *paper not submitted*
Bunch, K.J. - 243
Bush, R.T. - 213

Cahan, B. - 261
Chambers, G. - *paper not submitted*
Chao, J. - 20; 44; 82; 308
Cheek, G.T. - 57
Cheng, Y.-C. - 335
Chexal, B. - 20
Chubb, S.R. - 119
Chubb, T.A. - 119
Chulick, G.S. - 185
Coupland, D.R. - 299

D 'Amato, F. - 170
De Ninno, A. - 170
Degwekar, S.B. - 175
Doyle, M.L. - 299
Doyle, Jr., R.J. - 272
Droege, L.J. - 229
Droege, T.F. - 229

Ferrante, J. - 44; 82; 308
Fleischmann, M. - 1; 344

Gervasio, D. - 261
Grabowski, K. - *paper not submitted*
Grow, R.W. - 243
Gür, T.M. - 44; 82; 308
Guruswamy, S. - 314

Hagelstein, P.L. - 99
Handel, P.H. - 288
Hora, H. - 202
Hubler, G. - *paper not submitted*
Huggins, R. - 44; 82; 308
Hutchinson, D.P. - *paper not submitted*
Hwang, W.-Y. - 325

Iyengar, P.K. - 62

Jenkins, J.W. - 299
Jones, S. - *paper not submitted*

Kainthla, R.C. - 137
Kang, C.-M. - 308
Kim, Y.E. - 185; 194
Kim, Y.J. - 32
Kulkarni, L.V. - 175

Lanza, F. - 170
Layman, W. - 308
Lin, G.H. - 137
Lucier, G. - 44; 82; 308

McKubre, M.C.H. - 20
Menlove, H. - 250
Michaels, G.E. - 164
Miles, M.H. - 328
Miley, G.H. - 202
Mrochek, J.E. - 164
Murphy, O.J. - 32

Newman, E. - 164
Notton, J.H.F. - 299

Packham, N.J.C. - 137
Park, K.H. - 328
Passell, T. - 20
Petek, M. - 164
Pons, S. - 1
Pontorieri, C. - 170
Potter, R.J. - 299
Powell, G.L. - *paper not submitted*
Preparata, G. - 91

O'Grady, W.E. - 44; 272

Rice, R.A. - 185
Richards, R.K. - *paper not submitted*
Rocha-Filho, R.C. - 20
Ragheb, M.H. - 202
Rolison, D.R. - 272

Santucci, J. - 20
Scaramuzzi, F. - 170
Schneider, T. - *paper not submitted*
Schreiber, M. - 44; 82; 308
Schwinger, J. - 130
Scott, C.D. - 164
Scott, T.C. - 164
Shyam, A. - 175
Smedley, S. - 20
Srinivasan, M. - 32; 62; 175
Srinivasan, S. - 32
Stilwell, D.E. - 328
Storms, E. - 149

Talcott, C. - 149
Tanzella, F. - 20
Thompson, D.T. - 299
Trzaskoma, P.P. - 272

Velev, O. - 137

Wadsworth, M.E. - 314
Worledge, D.H. - 252

Yang, S.N. - 335
Yeager, E.B. - 261

Zeppa, P. - 170

WORD INDEX

Atom-Atom Collision - 335
Atomic Lattice - 130

Bloch State - 119
Bose-Einstein Statistics - 130
Boson - 119
Bulk Analysis - 299

Calibration - 82
Calorimeter - 229; 308
Calorimetry - 20; 82
Closed System - 164
Coherent Fusion - 91
Cold Deuterium Fusion - 194
Computer Simulation - 308
Control - 281
Coulomb Screening - 335

d-d Fusion - 335
de Broglie Waves - 215
D-Pd System - 44
Dendrites - 137
Deuteron Wave Functions - 130
Diagnostics - 202

Electrochemical - 82
Electrochemical Kinetics - 20
Electrolysis - 308
Electrolytic Cell - 149
Electron Screening Effect - 194
Energy Balance - 44
Enhanced Fusion - 213
Enhanced Tunneling - 91
Enthalpy - 328
Excess Heat - 164
Excess Heat Bursts - 314
Excess Power - 164

Films (Palladium) - 57

Gamma Rays - 164

Heavy Water - 328
Hydrogen Isotopes - 32

Internal Recombiner - 164
Ionic - 119
Isoperibolic - 82
Isoperibolic Calorimetry - 44

Lattice Potential - 243
Lithium - 299

Metallurgical Examination - 314
Metals - 243
Microcalorimetry - 32
Morphology of Deuterated Pd - 272
Muon Screening Effect - 194

Neutron Transfer - 213
Neutrons - 164
Nuclear Measurements - 314
Nuclear Products - 202
Nuclear Reactions - 202

Over Potential - 213

Palladium - 32; 149; 243; 328
Pd Isotopic Distribution - 272
Phonon Energies - 130
Plasmas - 91
Platinum - 328
Pressurized Cells - 20

Quantum Mechanics - 119
Quartz Crystal Microbalance - 57
Quasi-Equilibrium in Cluster Impact - 335

Reaction Mechanisms - 202
Resistance Ratio - 20
Resonant Transmission - 213

Stress - 57
Superradiance - 91
Surface Analysis - 32; 272; 299
Surface Enrichment - 272
Surface Material - 137
Surface Reaction Mechanism - 194
System Identification - 281

Temperature Programmed Absorption/Desorption (or TPA/TPD) - 299
Thomas-Fermi - 243
Tritium - 137; 149

CALORIMETRY OF THE PALLADIUM - DEUTERIUM SYSTEM

Stanley Pons*
Martin Fleischmann* **

*Department of Chemistry
University of Utah
Salt Lake City UT 84112

**Department of Chemistry
University of Southampton
Southampton, Hants. SO9 5NH
ENGLAND

Abstract

Our calorimetric measurements of the Pd/D system both in the period leading up to the preliminary publication[1] (for some corrections see[2]) and in the period leading up to the submission of the first full paper[3] showed that it is necessary to make measurements on a large number of electrodes for long times (the mean time chosen for a measurement cycle has been 3 months). It has therefore been necessary to adopt a low cost approach; our solution has been to use the single compartment Dewar cell type calorimeters illustrated in Fig.1 and we have maintained up to five of these cells in each of three specially constructed water baths (see Section 1 below). The same type of calorimeter has been used for blank measurements on the Pd-H, Pt-D, and Pt-H systems.

Section 1
Aspects of the Calorimeter and Electrochemical Experiment Design and Calorimetric Measurements

The general principles of the calorimeter design have been outlined elsewhere[3]. The choice of rod electrodes surrounded by a closely wound helical platinum anode allows the axially symmetric injection of heat and, moreover, the uniform charging of the Pd cathodes. Furthermore the choice of such a simple design of calorimeter coupled to the use of rod electrodes allows the iterative adjustment of the dimensions of the systems such that the excess enthalpy to be observed (if any) is large compared to the random errors (see Section 3). The use of a long, thin calorimeter increases the mixing in the calorimeter compared to other possible designs[3]; the minimum current used for most experiments with rod electrodes we have reported to date has been 200mA. Measurements of the mixing history using dye injection (tracer technique of chemical reaction engineering[4]) has shown that radial mixing is extremely rapid (time scale <3s). Axial mixing takes appreciably longer($\cong$ 20 s) but the axially uniform injection of heat ensures that this longer time scale is unimportant. As the thermal relaxation time is $\cong$ 1600 s (see Figs. 5A, 6A-C, 7) the cells behave as well stirred tanks. In agreement with this assessment, measurements of the temperature distribution within the cells (using ensembles of 5 thermistors which could be displaced radially and axially) showed that the temperature was uniform to within $\pm 0.01^{\circ}$ throughout the bulk of the cells; this variation rose to $\pm 0.02^{\circ}$ in contact with the Kel-F plugs at the bottom of the cells (all temperature measurements reported here have been made with specially calibrated thermistors (Thermometrics Ultrastable Thermoprobes, $\cong$ 10 kΩ, $\pm$0.02% stability per year)). Statements which have been made (e.g.[5]) about large temperature fluctuations in cells of this type are incorrect (for a further comment see [6])

All connections to the electrodes were covered in glass and special care has always been taken to ensure that the palladium cathodes and platinum anodes remained totally immersed throughout all of the measurement cycles. In consequence there was no recombination in the gas head spaces (assertions such as those in [7] are incorrect). Furthermore the volumes of gas evolved from the cells corresponded to that from Faraday's law to better than 99% for electrolysis times from approximately 5 diffusional relaxation times to times corresponding to the termination of the experiments ($\cong$ 7 to 200 diffusional relaxation times), and the

records of D_2O additions also matched that predicted for a 100% efficient process for experiments where the cell temperature was within 20° of the bath temperature (30°C). This somewhat surprising result, which has now also been noted in other work,[8,9] can be understood in terms of the inhibition of D_2 ionization at the anode by platinum oxide formation and by degassing of the electrolyte in the vicinity of the cathode by the rapidly evolving D_2 bubbles. This high current efficiency for gas formation greatly simplifies the analysis of the experimental data (see Section 2).

The cells were maintained in specially constructed thermostats (1/2" thick Plexiglas bath surrounded on 5 sides by 2" thick foam insulation bonded on both sides to aluminum foil, the whole structure being enclosed in a 1/16" thick sheet steel container); the water/air interface was allowed to evaporate freely. Stirring with oversized stirrer-temperature regulators ensured that the bath temperature could be controlled to ±0.01° of the set temperature (in the vicinity of 303.15K) throughout the whole space at depths greater than 0.5 cm below the water surface and to ± 0.003° at any given point. The water level in the thermostats was controlled using dosimeter pumps connected to a second thermostat.

All experiments were carried out galvanostatically (Hi-Tek DT2101 potentiostats connected as galvanostats as shown in Fig. 2A). The stability of the systems was monitored oscillographically; the ripple content was <0.04%. For work at current levels outside the operating range of the potentiostats, the circuit shown in Fig. 2B was used (which takes full advantage of the regulation achievable by the potentiostat used as a galvanostat). The systems could be calibrated at any given operating point by using metal film resistor chains in the cells (Digikey ±1% accuracy 5 x 20Ω). The procedure adopted was as follows: after the addition of D_2O (or of electrolyte following sampling for analysis for tritium or HDO) the system was allowed to equilibrate for at least 6 thermal relaxation times. A constant current was then applied to the resistor chain (again supplied by a potentiostat connected as a galvanostat) for 3 hours (i.e. > 6 thermal relaxation times) to give a temperature rise of ≅ 2° above the sloping base line; the current to the calibration system was then switched off and the relaxation of the system to the original base line was followed. Cell parameters and the bath temperature were monitored every 5 minutes using Keithley Model 199 DMM multiplexers to input data to Compaq 386 16MHz computers. The measuring circuits were maintained open except during the actual sampling periods (voltage measurements were allowed to stabilize for 2s before sampling and thermistor resistances 8s before sampling). Data were displayed in real time as well as being written to disks. Fig. 3 illustrates a typical experiment lay-out.

Experiments have been carried out on 0.1, 0.2, 0.4, and 0.8 cm diameter x 10 cm long Pd cathodes (special grade, Johnson Matthey) and on 0.1 x 10 cm Pt electrodes (Johnson Matthey). At the highest current densities used the electrode lengths were reduced to 1.25 cm and the spacings of the anode windings were also reduced. These shorter electrodes were placed at the bottom of the Dewar cells so as to ensure adequate mixing. Measurements reported here were made in D_2O (Cambridge Isotopes) of 99.9% isotopic purity; light water levels were monitored by NMR and never rose above 0.5%. Results reported here have been obtained in 0.1M LiOD prepared by adding Li metal (A.D. Mackay $^6Li/^7Li$ = 1/9) to D_2O, 0.1M LiOD + 0.1M Li_2SO_4 and 1M Li_2SO_4 were prepared by adding dried Li_2SO_4 (Aldrich 99.99% anhydrous, $^6Li/^7Li$ = 1/11) to 0.1M LiOD and D_2O respectively. A single batch of electrolyte was used for any given experimental series. Blank experiments were carried out using Pd cathodes in 0.1M LiOD in D_2O and Pt cathodes in both in 0.1M LiOD in D_2O and 0.1M LiOH in H_2O.

Section 2
The "Black Box" Representation of the Calorimeters

Data evaluation from the behavior of the Dewar-type electrochemical calorimeters requires the construction of adequately accurate "black-box" models such as that shown in Fig. 4A. In this particular case the models must account for the enthalpy and mass balances in the cell which can be combined through the current efficiency, γ, of the

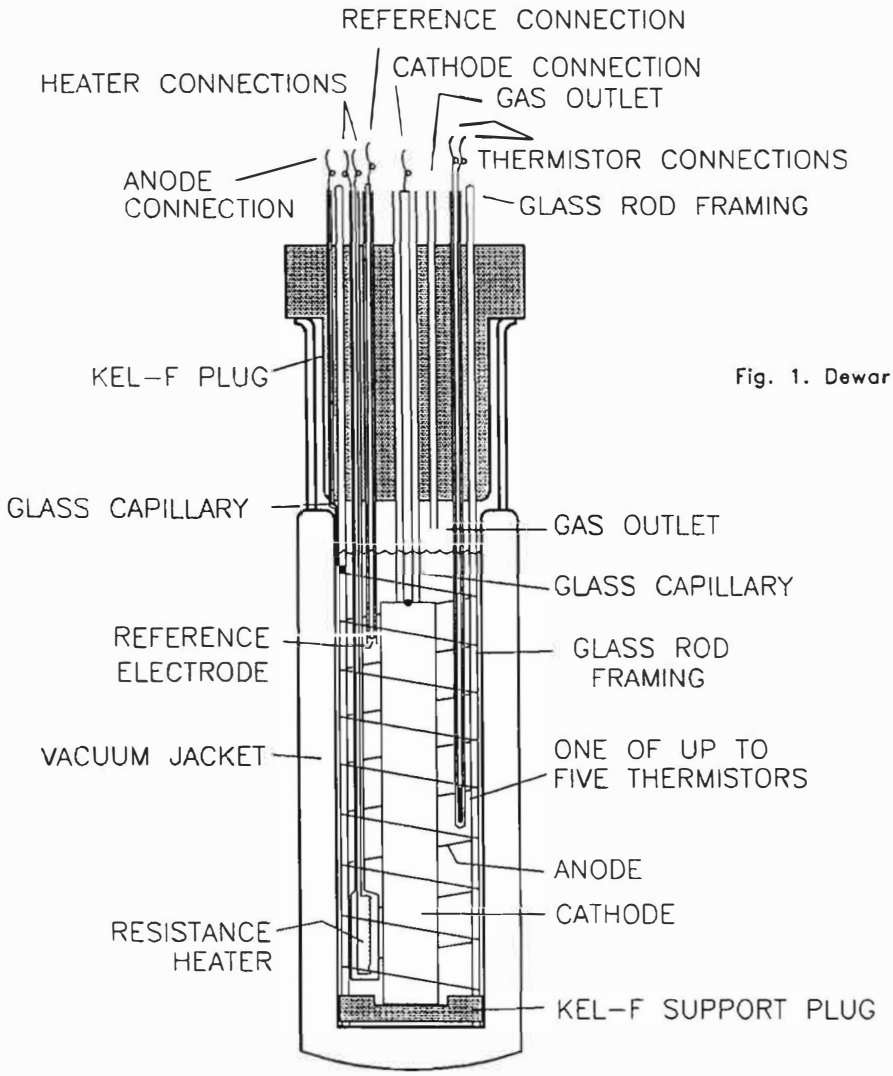

Fig. 1. Dewar calorimeter cell used in this work.

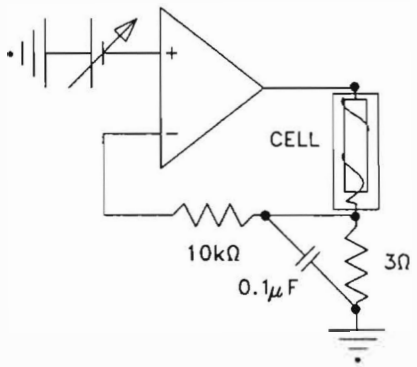

Fig. 2A. Schematic diagram of the feedback circuit used in this work for protection against galvanostat oscillations.

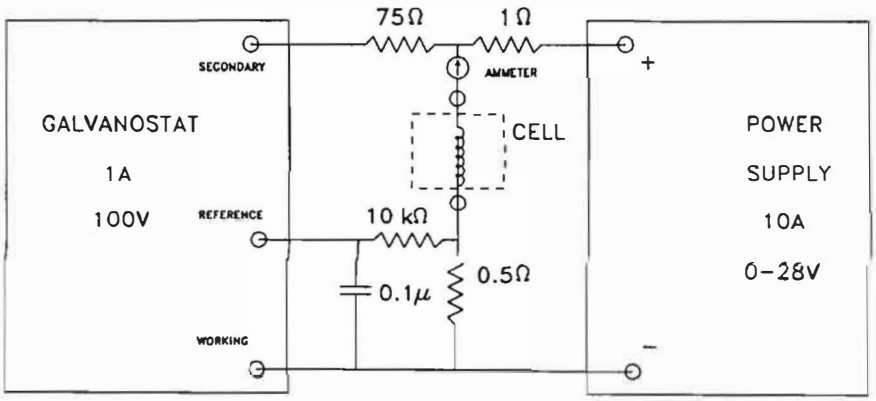

Fig. 2B. Schematic diagram of the circuit used in this work for high stabilization of a regulated power supply used as a high output current galvanostat.

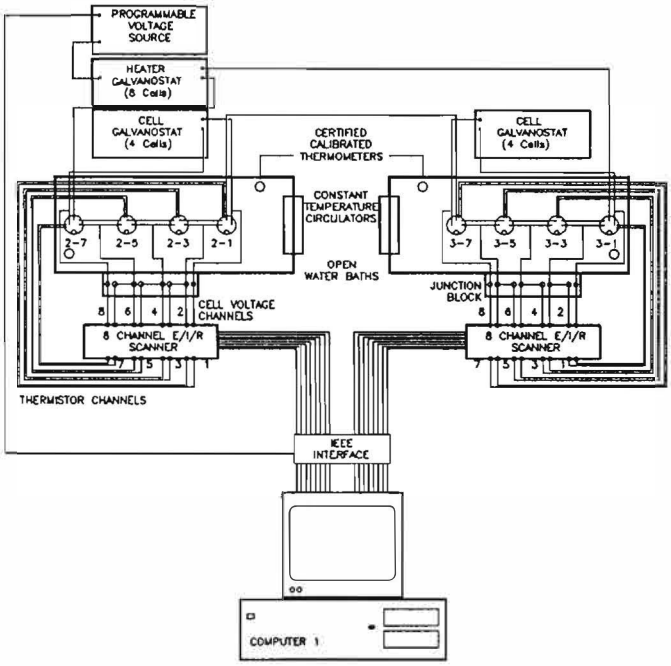

Fig. 3. Experimental layout for some of the calorimetric measurements reported in this paper.

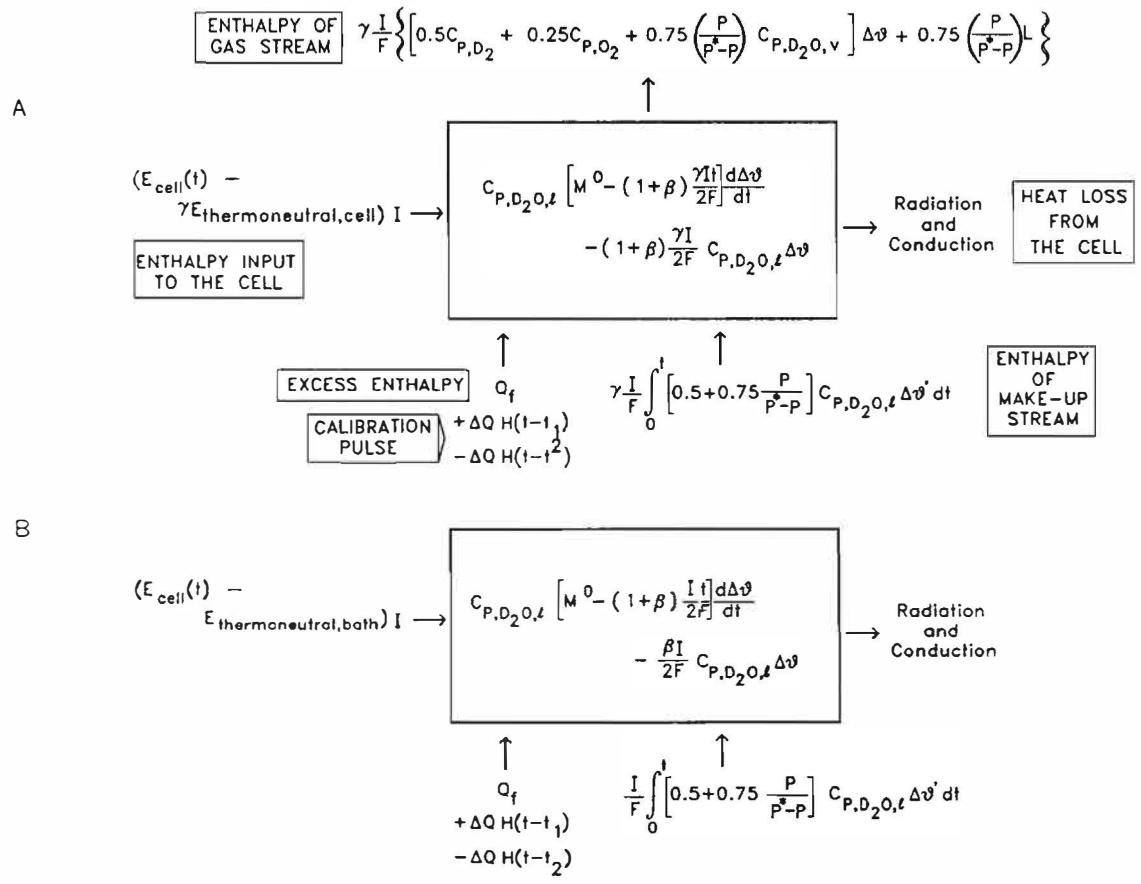

Fig. 4. The full (A) and the approximate (B) "black box" models of the calorimeter shown in Fig. 1.

electrolysis. The nature of the enthalpy flows into and out of the "black box" will be explained by the following comments:

a) the enthalpy flow into the cell due to the electrical input is $(E_{cell}(t) - \gamma E_{thermoneutral,cell})I$. The term $E_{thermoneutral,cell}$ is the cell voltage at which the electrolysis is thermoneutral; this differs from the reversible potential of the reaction $2D_2 + O_2 \rightleftarrows 2D_2O$ since the electrolysis takes place with an increase of entropy.

b) the current efficiency, γ, can be taken as unity (see Section 1).

c) in the analysis of the data we have neglected the enthalpy content of the gas stream due to the D_2O content, $0.75\left(\frac{P}{P^* - P}\right)C_{P,D_2O,v}\,\Delta\theta$, as well as that due to the evaporation of D_2O, $0.75\left(\frac{P}{P^* - P}\right)L$. Both these terms have been written assuming the gas stream is saturated with D_2O at the relevant cell temperature. The neglect of these terms causes an underestimate of the excess enthalpy. The terms are relatively small for values of $\Delta\theta < 20^o$ but the second, especially, becomes large and the dominant form of heat transfer from the cell as the temperature reaches the boiling point (See Section 4). Our calorimeters are unsuitable for measuring the heat outputs from the cells under these conditions.

There is a further term (not shown in Fig. 4A) which causes an additional underestimate of the excess enthalpy. This is due to the change in composition of the Pd-D electrode due to the increase of $\Delta\theta$ with time (see Fig.5). The dissolution of D in Pd is exothermic under the operating conditions so that a decrease of the D content with increasing $\Delta\theta$ will cause an absorption of heat in the cell. This effect is difficult to quantify since equilibrium cannot be maintained on the timescales of the measurement cycles. We have therefore neglected this term.

d) heat transfer from the calorimeter to the surroundings can be written in a variety of ways depending on its design and properties as well as the chosen level of approximation[3]. For the Dewar-type cells, Fig. 1, heat transfer for a hypothetical steady state generation of Q watts is controlled by a mixture of radiation and conduction

$$Q = k_R\left[\left(\theta_{bath} + \Delta\theta\right)^4 - \theta_{bath}^4\right] + k_C\Delta\theta \qquad (1)$$

Similarly for the steady state following the additional injection of ΔQ watts to calibrate the system we have

$$Q + \Delta Q = k_R\left[\left(\theta_{bath} + \Delta\theta + \Delta\Delta\theta\right)^4 - \theta_{bath}^4\right] + k_C\left[\Delta\theta + \Delta\Delta\theta\right] \qquad (2)$$

The separate determination of k_R and k_C leads to an increase in the random errors in the estimation of the heat flows from the cells. We have therefore adopted the strategy of neglecting the conductive term while making an appropriate increase in the radiative term

$$Q \cong k_R'\left[\left(\theta_{bath} + \Delta\theta\right)^4 - \theta_{bath}^4\right] \qquad (3)$$

and

$$Q \cong k_R'\left[\left(\theta_{bath} + \Delta\theta + \Delta\Delta\theta\right)^4 - \left(\theta_{bath} + \Delta\theta\right)^4\right] \qquad (4)$$

We have shown elsewhere[3] that this leads to a small systematic underestimate of the heat flow from the cell (and hence the excess enthalpy). However, as the correct value of the radiative term can be estimated from the Stefan-Boltzmann constant and the surface areas of the cells, a correction can readily applied (if this is desired) to give the heat output from the cells to within 1% of the enthalpy input or 1 milliwatt whichever is the greater. (for further comments on the application of equations (1) - (4) see Section 3. An important aspect of the approximations (3) and (4) is that any other term linear in $\Delta\theta$ can similarly be accounted for by making an appropriate increase or decrease in k_R (see Section 3).

A further factor which needs to be taken into account is that for a continuously reacting chemical system (open system) such as the electrochemical Dewar cells, the cell contents change with time. The extent of the radiant surface decreases with time while the length of any parallel conduction path increases with time. To a first approximation we

would therefore expect the heat transfer coefficients to decrease linearly with time and we write

$$Q \cong k_R'^0 \left[1 - \frac{(1+\lambda)\,\gamma I t}{2FM^0}\right] \cdot \left[\left(\theta_{bath} + \Delta\theta\right)^4 - \theta_{bath}^4\right] \qquad (5)$$

where the term λ allows for a more rapid decrease of the radiant surface area (and increase of the length of the conduction path) than would be predicted by electrolysis alone in view of the internal solid cell components. The superscript ^{0} here and elsewhere in this text denotes a value at a chosen time origin.

e) a general expression for the water equivalent is

$$M = M^0 - \frac{(1+\beta)\,\gamma I t}{2F} \qquad (6)$$

where, as for the heat transfer coefficient, the term β allows for a more rapid decrease of M with time than would be predicted by electrolysis alone. We expect $\beta < \lambda$.

f) the term $\frac{\gamma I}{F}\int_0^t \left[0.5 + 0.75\left(\frac{P}{P^* - P}\right)\right] \cdot C_{P,D_2O,\ell}\Delta\theta'\,dt$ is the enthalpy input to the cell due to the addition of D_2O to make up for the losses due to,electrolysis and evaporation. Here $\Delta\theta$ is the difference in temperature between the cell and make-up stream. In practice it has been found convenient to add D_2O at fixed intervals of time and, provided measurements are initiated at times longer than 6 thermal relaxation times following this addition, the effect of this term can be neglected in the further analysis.

We therefore obtain the differential equation governing the behavior of the calorimeter

$$C_{P,D_2O,\ell}\left[M^0 - \frac{(1+\beta)\,\gamma I t}{2F}\right]\frac{d\Delta\theta}{dt} - C_{P,D_2O,\ell}\frac{(1+\beta)\,\gamma I \Delta\theta}{2F} = -\left(E_{cell}(t) - \gamma E_{thermoneutral,cell}\right)I + Q_f(t) + \Delta QH(t-t_1) - \Delta QH(t-t_2)$$

$$- \frac{\gamma I}{F}\left\{\left[0.5C_{P,D_2} + 0.25C_{P,O_2} + 0.75\left(\frac{P}{P^* - P}\right)C_{P,D_2O,v}\right]\Delta\theta + 0.75\left(\frac{P}{P^* - P}\right)L\right\} - k_R'^0\left[1 - \frac{(1+\lambda)It}{2FM^0}\right] \cdot \left[\left(\theta_{bath} + \Delta\theta\right)^4 - \theta_{bath}^4\right] \qquad (7)$$

Equation (7) is difficult to apply because $E_{cell}(t)$ and $Q_f(t)$ are unknown functions of time. We note, however, that since we are only concerned with small changes of temperature at any given origin, θ^0, we can carry out a Taylor series expansion at this point and, retaining only the first derivatives we obtain

$$\left\{\frac{dE_{cell}}{d\theta} + \frac{d}{d\theta}\left[\frac{0.75I}{F}\left(\frac{P}{P^* - P}\right) \cdot \left(C_{P,D_2O,v}\,\Delta\theta + L\right)\right]\right\} I\Delta\theta' = -\frac{\psi I}{\theta^0}\Delta\theta' \qquad (8)$$

where $\Delta\theta' = \Delta\theta - \Delta\theta^0$ (see Glossary). We assume also that Q(t) is constant during any one measurement cycle and, taking note also of

$$\Delta H^{\circ}_{cell} = \Delta H^{\circ}_{bath} + \sum_i \nu_i C_{P,i}\,\Delta\theta \qquad (9)$$

as well as of b) and c) we can write (7) in the more tractable form

$$C_{P,D_2O,\ell}\left[M^0 - \frac{(1+\beta)It}{2F}\right]\frac{d\Delta\theta}{dt} - C_{P,D_2O,\ell}\frac{\beta I\Delta\theta}{2F} = -\left(E^0_{cell} - E_{thermoneutral,bath} + \frac{\psi\Delta\theta'}{\theta^0}\right)I + Q_f(t) + \Delta QH(t-t_1) - \Delta QH(t-t_2)$$

$$- k_R'^0\left[1- \frac{(1 + \lambda)It}{2FM^0}\right]\cdot$$

$$\left[\left(\theta_{bath} + \Delta\theta\right)^4 - \theta_{bath}^4\right] \qquad (10)$$

This equation describes the modified "black-box" shown in Fig. 4B.

Section 3
Data Evaluation and Error Analysis

As is well understood in the field of chemical kinetics, it is necessary to fit the integrated form of equation (10) to the experimental data in order to extract the parameters of the equations; application of such equations at a single point leads to erroneous results. It is naturally not possible to derive an analytical solution to (10) since this equation is non-linear and inhomogeneous. An approximate solution, however, can be obtained[3] using the linearized form of the heat transfer term $4k_R'^0\theta_{bath}^3\left[1 - \frac{(1 + \lambda)It}{2FM^0}\right]\Delta\theta$ and this solution shows that the heat transfer coefficient to be used in the evaluation of Q_f at a given point is $\left[4k_R'^0\theta_{bath}^3 - \frac{\psi I}{\theta^0}\right]\left[1 - \frac{(1 + \lambda)It}{2FM^0}\right]$ rather than the value $4k_R'^0\theta_{bath}^3\left[1- \frac{(1 + \lambda)It}{2FM^0}\right]$ which would be predicted from the thermal balance at a single point and it is the former rather than the latter value which has to be used in determining the thermal output of the cell in applying the linearized equations.[3]

These linearized equations can be shown to be in close accord with the experimental data for small values of $\Delta\theta$ but these equations will naturally not be applicable for large values of $\Delta\theta$ say, $>10^o$.[3] In order to obtain approximate values of Q, $k_R'^0\left[1 - \frac{(1 + \lambda)It}{2FM^0}\right]$, and Q_f we have therefore applied the calculation scheme illustrated in Fig. 5A and using equations (3) and (4). Fig. 5B illustrates a set of such calibration pulses determined during one measurement cycle and Fig. 5C illustrates the time dependence of the derived heat transfer coefficients. It can be seen that there is a systematic error due entirely to the uncertainty in the refilling of the Dewars at the beginning of any one measurement cycle. Superposition of the plots at the mid-point (27 hours after addition of the D_2O) shows that the standard deviation of the remaining 132 points in 33 experimental series is only 0.15%, a value which is roughly in line with the errors in measurement of the absolute temperatures in (3) and (4). These data show that it is essential to calibrate the cells for each desired measurement of the thermal output.

Nevertheless, such determinations are evidently approximate not only because of the underestimate of k_R' (see Section 2d) but also because of the assumption that Q is unchanged in applying the heater calibration pulse is strictly speaking not valid (see the decrease in E_{cell}) with t during the heater calibration period $t_1 < t < t_2$, Fig. 5A). Accurate values of Q can only be obtained by fitting the whole of the transient predicted from (10) (or any other chosen representation of the calorimeter)to the experimental data and making the estimate of Q and hence Q_f at the point designated ^{0} (where the term $\frac{\psi\Delta\theta'}{\theta^0}$ is zero) Such a fitting procedure must be carried out in an unbiased manner. We have used non-linear regression and, in this, have used the simplest forward integration method

$$\Delta\theta_{n+1} = \Delta\theta_n + \left(\frac{d\Delta\theta}{dt}\right)_n \Delta t \qquad (11)$$

and we have used the parameters Q, $k_R'^0$, Q_f and $(1 + \lambda)$ estimated according to Figs. 5A and 5B as starting values for the regression procedures. The parameter ψ has been estimated from the E_{cell} - t plot using linear regression. In this way the number of parameters to be fitted to (10) has been reduced from 5 to 4 thereby speeding the calculation. In view of the curvature of the parameter space hypersurfaces, it has also been found to be convenient to regard

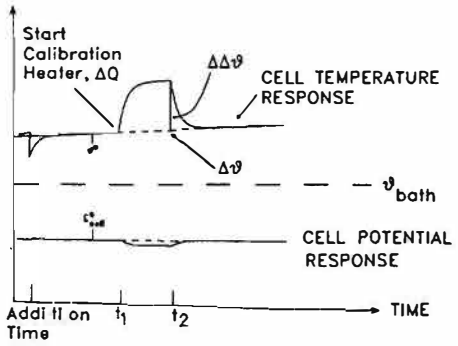

Fig. 5A. Schematic diagram for the experimental determination of approximate heat flow in the calorimeter. The response shows the application of the calibration pulse of strength ΔQ which leads to an eventual new sloping steady state temperature $\Delta\Delta\vartheta$ degrees above the linearly sloping baseline temperature. Calculation of the output heat flow at this level of approximation requires simply the measurement of the three temperatures indicated and the magnitude (ΔQ) of the calibration heater pulse. In applying equation (10) it is convenient to set the origin $t = 0$ at ~ 6 thermal relaxation times following the addition of D_2O to make up for losses due to electrolysis and evaporation. At this point $\vartheta = \vartheta^o$ $E_{cell} = E^o_{cell}$, $k'_R = k'^o_R$, and $M = M^o$.

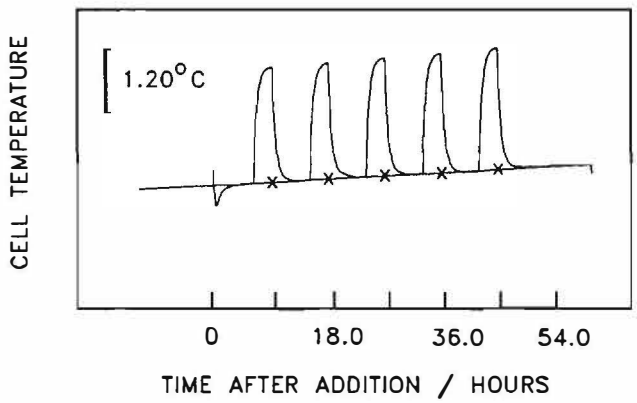

Fig. 5B. Typical set of heat flow calibration cycles made at 9, 18, 27, 36, and 45 hours after addition of D_2O. for a 0.1 x 10 cm Pd electrode in 0.1MLiOD. The current density was 64 mA cm^{-2}. x = calculated baseline.

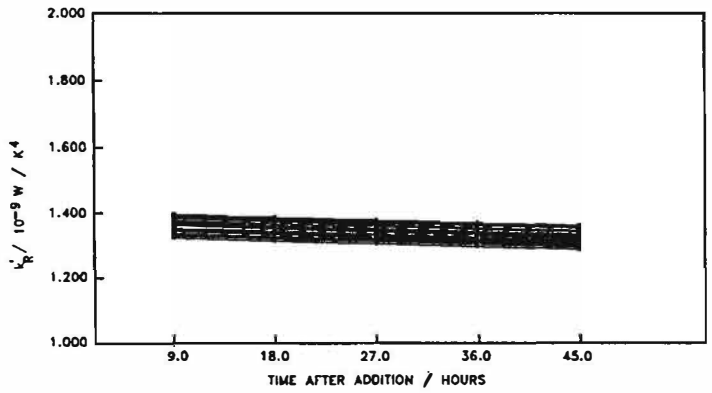

Fig. 5C. 165 derived heat transfer coefficients for 33 sets of calibration cycles for a typical cell, showing the effect of the systematic error discussed in the text.

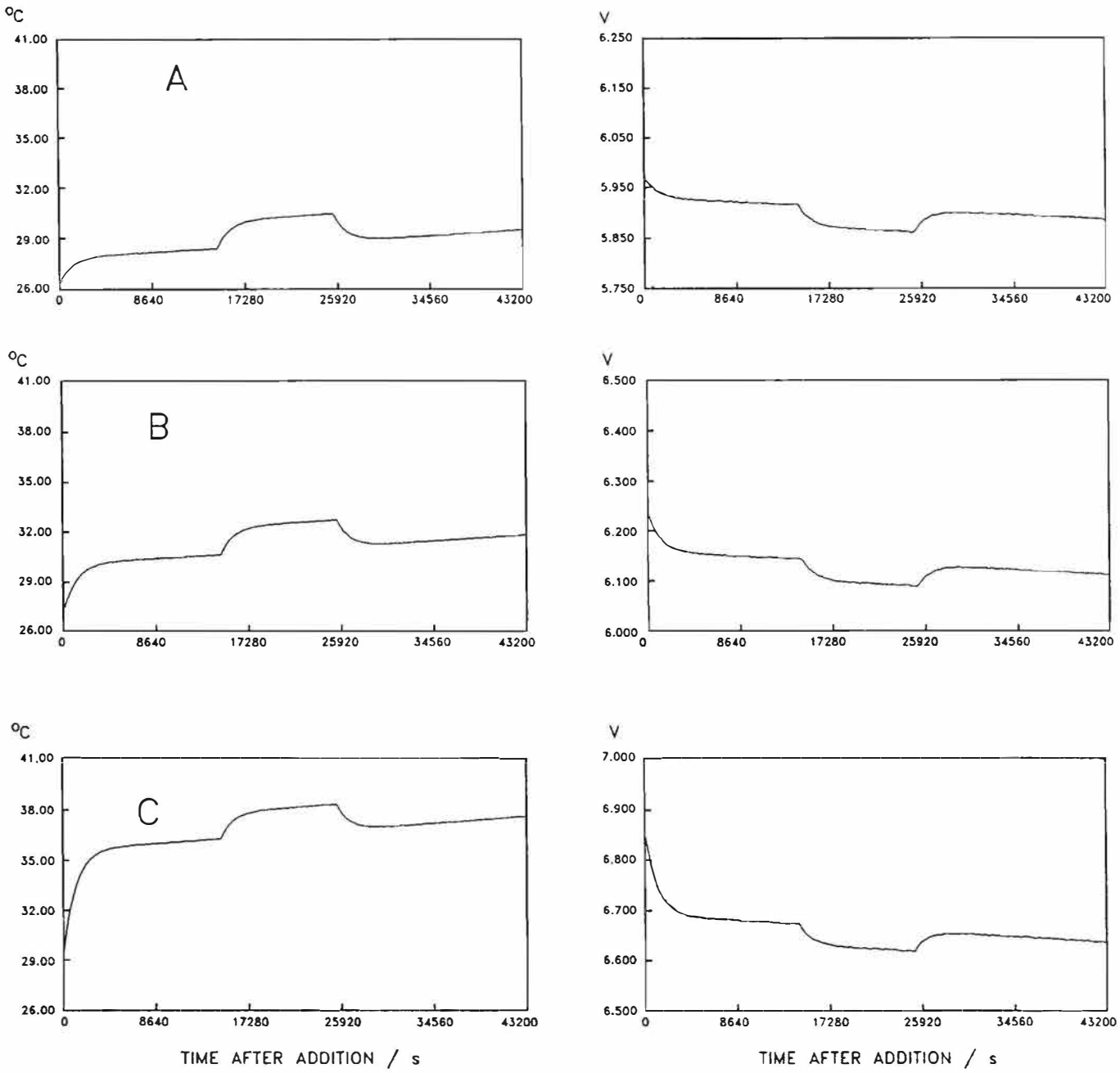

Fig. 6A. Temperature °C above bath vs. time (left plot) and cell potential (V) vs. time (lower right) data for a 0.4 x 10 cm Pd rod in 0.1M LiOD solution. The applied current was 800 mA, the bath temperature was 29.87°C, and the estimated Q_f was 0.158 W. The time of the measurement was approximately 0.45 x 10^6s after the beginning of the experiment.

Fig. 6B. Same as Fig. 6A except time of measurement approximately 0.89 x 10^6s. Estimated Q_f = 0.178 W.

Fig. 6C. Same as Fig. 6A except time of measurement approximately 1.32 x 10^6s. Estimated Q_f = 0.372 W.

$$\frac{\left(E^0_{cell} - E_{thermoneutral,bath} \right) I + Q_f}{C_{P,D_2O,\ell}\, M^0}$$

as one of the free parameters of the calculation.

We have used a Marquardt-type algorithm for the fitting procedure and it should be noted that the diagonal elements of the error matrix derived in this calculation (the inverse of the matrix used in the parameter estimation) directly give the standard deviation of the parameters. In this way we have shown that the parameter

$$\frac{\left(E^0_{cell} - E_{thermoneutral,bath} \right) I + Q_f}{C_{P,D_2O,\ell}\, M^0}$$

can be estimated to ±0.1% throughout the operating range. This is also the error of $\left(E^0_{cell} - E_{thermoneutral,bath}\right) I + Q_f$ since the independently derived value of M^0 has errors of ≅ ±0.01%. Even higher precisions could well be achieved by using a larger number of calibration pulses but we have not done this so far in our work as we have only estimated $\left(E^0_{cell} - E_{thermoneutral,bath}\right) I$ to ≅ 0.1% (the error of this quantity is controlled by σ_I). This error must be added to that of $\left(E^0_{cell} - E_{thermoneutral,bath}\right) I + Q_f$ to obtain the total error of the excess enthalpy listed in Tables 1 and 2.

Section 4
Results

An example of a set of temperature - time and the associated potential - time plots is illustrated for one experiment at three different times in Figs. 6A-C. Fig. 7 illustrates the degree of fit which can be obtained by using the non-linear regression procedure outlined in the previous section and Tables 1 and 2 illustrate the results of measurements of the excess enthalpy using both the approximate and exact methods of data analysis. We have also included some data[1,2] taken prior to our first publication which were obtained using only the approximate method of data analysis.

The marked excess enthalpy production on 0.1 and 0.2 and 0.4 cm diameter electrodes, (Table 1) must be viewed in terms of the slightly negative excess enthalpies for the blank experiments, Table 2.[1] This slightly negative value is due to the method of calculation which underestimates the heat output from the cell (see Section 2D). In many ways we regard the "zero" result on 0.8 cm diameter electrodes as the most significant blank as it shows that almost exact thermal balances can be obtained using our methodology for systems identical to those giving marked excess enthalpy. The differences between the 0.1, 0.2, 0.4 and the 0.8 cm electrodes also point to the importance of the metallurgical procedures in devising electrodes showing excess enthalpy generation.

Section 5
Discussion

It can be seen that many (perhaps all?) of the assertions e.g.[5,10-16] which have been made about our experiments are erroneous. We would stress here that it is perfectly possible to obtain accurate values of the heat output from the cells and, hence, the excess enthalpy provided due attention is paid to the design of the calorimeters and control of the environment and providing modern methods of data analysis are used. We would also stress the importance of deriving error estimates from a single experiment rather than from the variation of a parameter (here the excess enthalpy) from a set of experiments as the variability of the parameter may itself be a key feature of the phenomenon to be observed. In this context it is of interest that the variability of the results at low to intermediate current densities (which have been widely used in attempts to replicate our work) is large and far in excess of the errors of each individual experiment. This variability may point to the importance of the precise nature of the surface conditions and/or history of the

---

[1] Much of this data was available at the time of our first publication but the Editor of Nature refused to publish a letter to correct the many erroneous statements which had been made in the Editorials of the Journal.

Table 1. Excess enthalpy observed for 0.1, 0.2, and 0.4 cm diameter palladium rods as a function of current density and electrolyte composition.

Rod Dia.[a] /cm	Electrolyte[b]	Current Density /mA cm^{-2}	E_{cell} /V	Q_{input} /W	Q_{excess} /W	Approximate Specific Q_{excess} /W cm^{-3}	Specific Q_{excess} From Regression Analysis /W cm^{-3}	
0.1	$\mathcal{D}$	64	3.637	0.419	0.042	0.53	0.581	±0.003
0.1*	$\mathcal{S}$	64	2.811	0.032	0.001	0.140	0.1442	±0.0002
0.1	$\mathcal{D}$	128	4.000	0.984	0.160	2.04	2.043	±0.003
0.1*	$\mathcal{S}$	128	3.325	0.089	0.005	0.486	0.5131	±0.0006
0.1	$\mathcal{D}$	256	5.201	2.93	0.313	3.99	4.078	±0.007
0.1*	$\mathcal{D}$	512	9.08	1.51	0.17	17.3	18.19	±0.02
0.1	$\mathcal{D}$	512	6.085	7.27	1.05	13.4	13.77	±0.02
0.1*	$\mathcal{D}$	1024	11.640	4.04	1.03	105.	112.8	±0.1
0.2	$\mathcal{D}$	64	4.139	1.040	0.123	0.39	0.419	±0.003
0.2	$\mathcal{S}$	64	4.780	1.30	0.006	0.019	0.021	±0.001
0.2	$\mathcal{M}$	64	3.930	0.956	0.024	0.077	0.077	±0.001
0.2	$\mathcal{D}$	128	8.438	5.52	1.65	5.25	5.68	±0.01
0.2*	$\mathcal{S}$	128	4.044	0.250	0.028	0.713	0.714	±0.001
0.2*	$\mathcal{M}$	256	6.032	0.898	0.056	1.42	1.498	±0.002
0.2*	$\mathcal{D}$	512	8.25	2.68	0.66	16.8	17.02	±0.04
0.2*	$\mathcal{M}$	512	9.042	3.00	0.603	15.3	16.03	±0.01
0.2*	$\mathcal{S}$	1024	7.953	5.13	2.80	71.2	75.42	±0.08
0.4	$\mathcal{D}$	64	5.137	2.88	0.502	0.40	0.411	±0.001
0.4	$\mathcal{D}$	64	5.419	3.10	0.263	0.209	0.214	±0.003
0.4**	$\mathcal{D}$	64	4.745	2.24	0.117	0.106	0.145	±0.002
0.4*	$\mathcal{M}$	64	3.519	0.198	0.0005	0.002	0.0023	±0.0002
0.4	$\mathcal{D}$	128	6.852	8.50	1.05	0.84	0.842	±0.009
0.4*	$\mathcal{D}$	256	7.502	2.38	0.311	1.98	1.999	±0.003
0.4*	$\mathcal{D}$	512	8.66	5.70	2.18	13.9	14.41	±0.05
0.4*	$\mathcal{D}$	512	10.580	7.23	1.65	10.5	11.09	±0.02

(a) All rod lengths 10cm or *1.25cm or **8.75cm

(b) $\mathcal{D}$: 0.1M LiOD; $\mathcal{S}$: 0.50M Li_2SO_4; $\mathcal{M}$: 0.1M LiOD + 0.45M Li_2SO_4. All measurements were made in the same batch of D_2O of 99.9% isotopic purity. Measurements using electrolytes labelled $\mathcal{S}$ and $\mathcal{M}$ have been made since 23rd March, 1989.

Table 2. Results for blank experiments on platinum and palladium rods as a function of current density and electrolyte composition.

Rod Dia.[a] /cm	Electrolyte[c]	Current Density /mA cm^{-2}	E_{cell} /V	Q_{input} /W	Q_{excess} /W	Approximate Specific Q_{excess} /W cm^{-3}	Specific Q_{excess} From Regression Analysis /W cm^{-3}
Palladium Electrodes:							
0.1	*W*	32	3.605	0.212	-0.001	-0.009	-0.0097 ±0.0002
0.1	*W*	64	3.873	0.479	-0.001	-0.014	-0.0165 ±0.0005
0.1[d]	*W*	128	5.186	1.482	-0.001	-0.001	
0.1[d]	*W*	256	8.894	5.931	-0.001	-0.007	
0.1	*W*	512	11.29	15.70	-0.001	-0.008	-0.01 ±0.02
bd[b]	*D*	0.8	2.604	1.458	-0.001	-0.000	
0.8[d]	*D*	8	3.365	0.365	-0.001	-0.000	
0.8[d]	*D*	8	3.527	0.397	-0.003	-0.000	
Platinum Electrodes:							
0.1[d]	*D*	64	3.800	0.452	0.000	0.000	
0.1[d]	*D*	64	4.138	0.520	-0.001	-0.008	
0.1[d]	*D*	256	6.218	3.742	-0.001	-0.028	
0.1	*W*	64	4.602	0.624	-0.002	-0.023	-0.0232 ±0.0006
0.1	*W*	64	4.821	0.668	-0.003	-0.038	-0.0392 ±0.0006
0.1	*W*	512	12.02	16.86	-0.001	-0.007	-0.01 ±0.02

(a) All rod lengths 10cm.
(b) Palladium sheet electrode 8 x 8 x 0.2cm.
(c) *D*: 0.1M LiOD; *W*: 0.1M LiOH; All measurements in D_2O were made in the same batch as that used in the experiments in Table 1.
(d) Data available March 23, 1989. These data were evaluated by another method and not by those described in this paper.

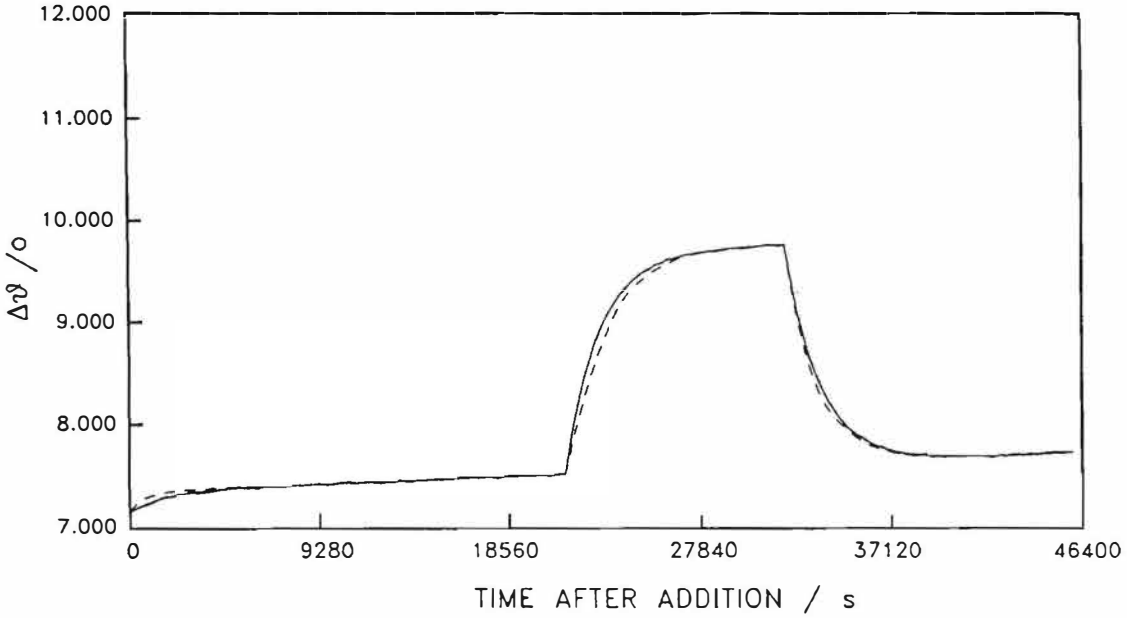

Fig. 7. Figure showing the degree of fit of the "black box" model in Fig. 4B to actual experimental data from an experiment using a 0.2 x 10cm Pd rod cathode in 0.1MLiOD. The dotted line in the figure represents the fit obtained using estimated values of the several cell parameters and was obtained by the forward integration technique described in the text to force the fit of the data to the model at the starting point (t = 0), the point of application of the calibration heater pulse, the point at the end of the calibration heater pulse, and the point at the end of the experiment. The solid line (which in this figure is coincident with the experimental data) is the fit obtained to the model by the Marquardt algorithm for the non-linear regression technique described in the text.

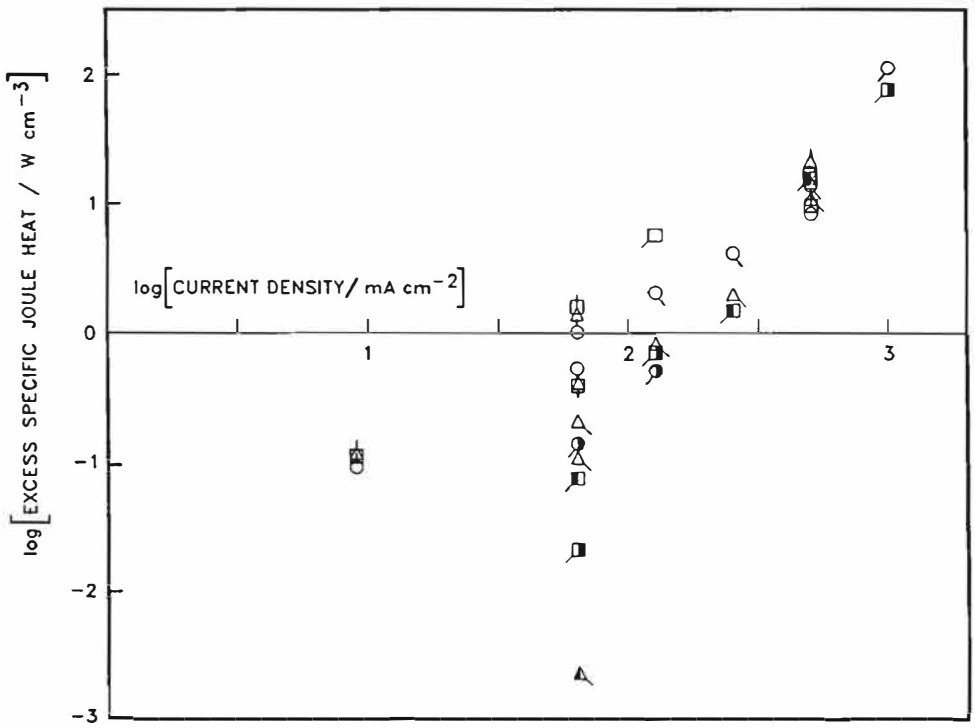

Fig. 8. Log-log plot (Excess enthalpy vs. current density) for a group of typical calorimetric experiments using Pd electrodes in D_2O electrolytes.

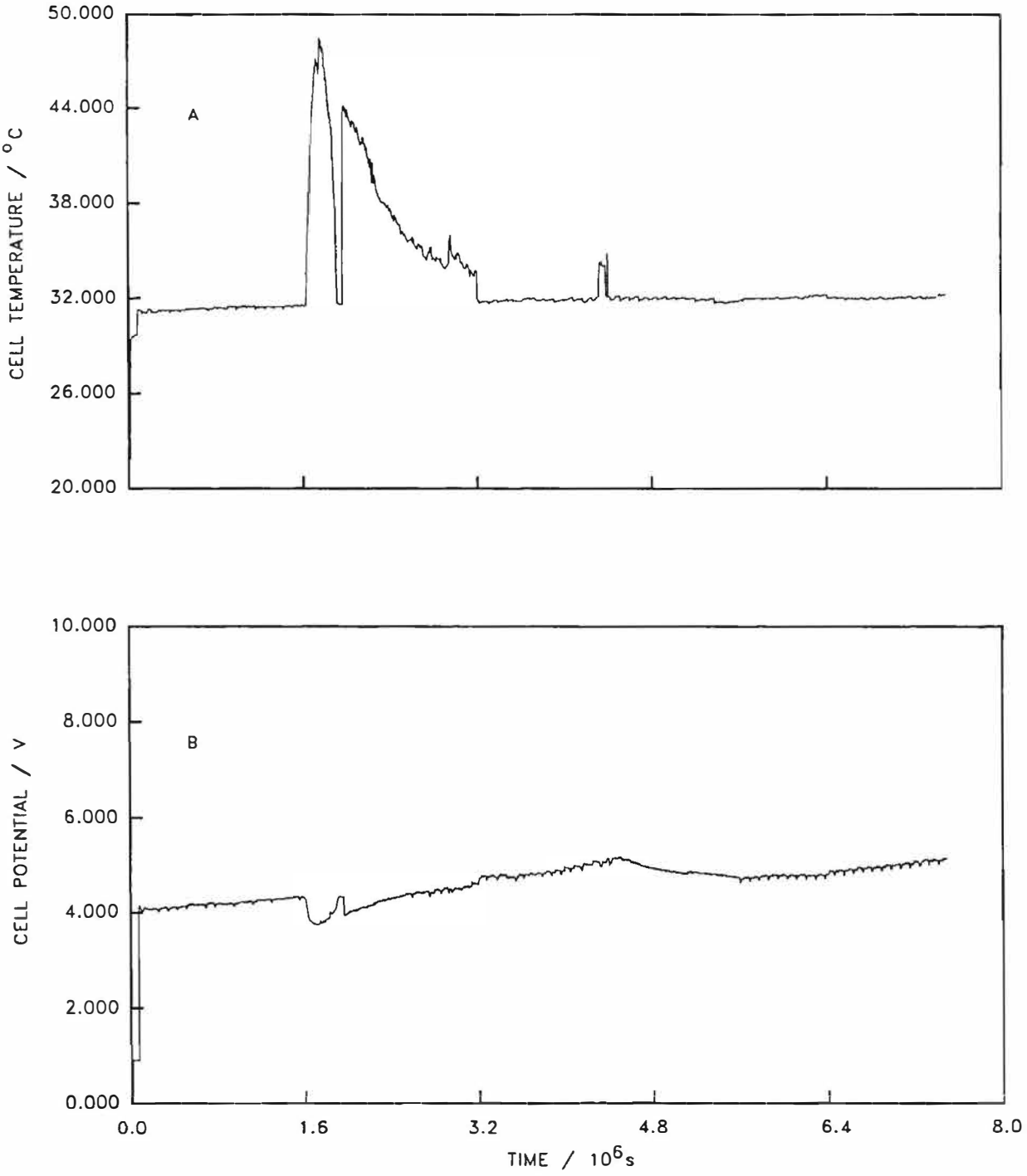

Fig. 9A. Demonstration of a "burst" of excess enthalpy for a long period of time. The upper plot is the cell temperature vs. time and the lower plot is the cell potential vs. time. The electrode was a 0.4 x 1.25 cm Pd rod in 0.1M LiOD solution. The current density was 64 mA cm^{-2}, and the bath temperature was held at 29.87°C.

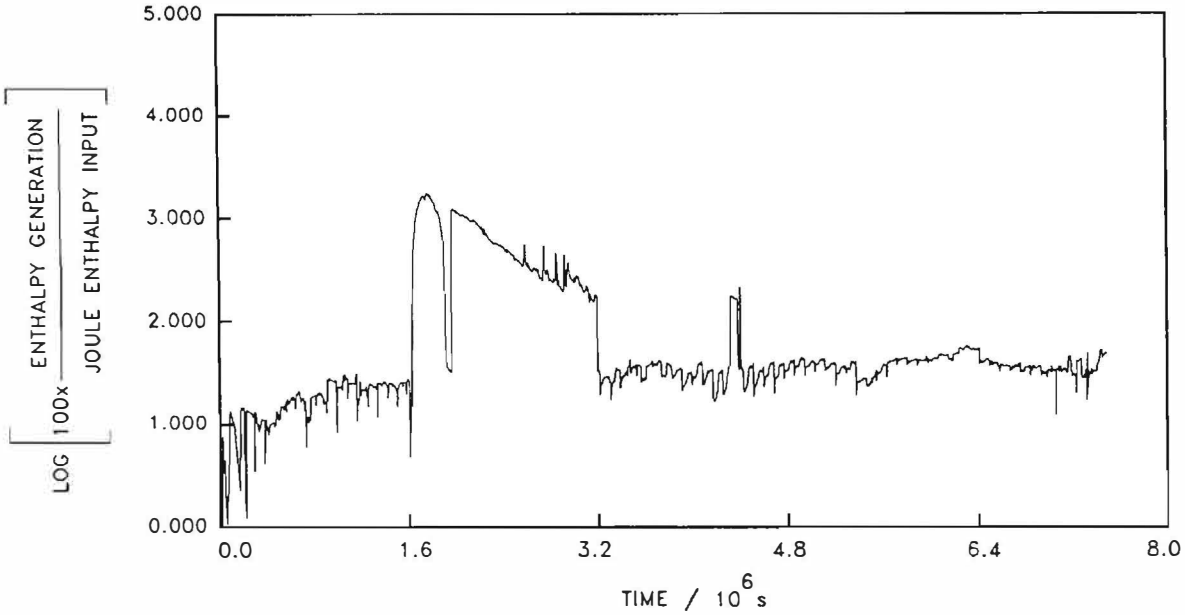

Fig. 9B. Figure showing the calculated rate of excess enthalpy generation as a function of time for Fig. 9A, and

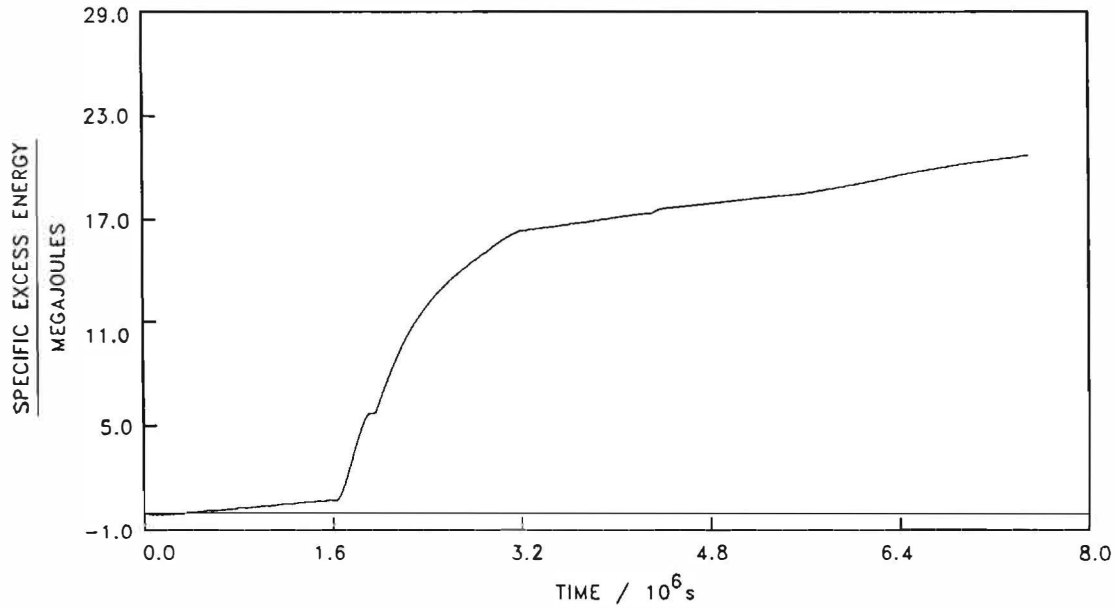

Fig. 9C. Figure showing the total specific excess energy output as a function of time for this cell.

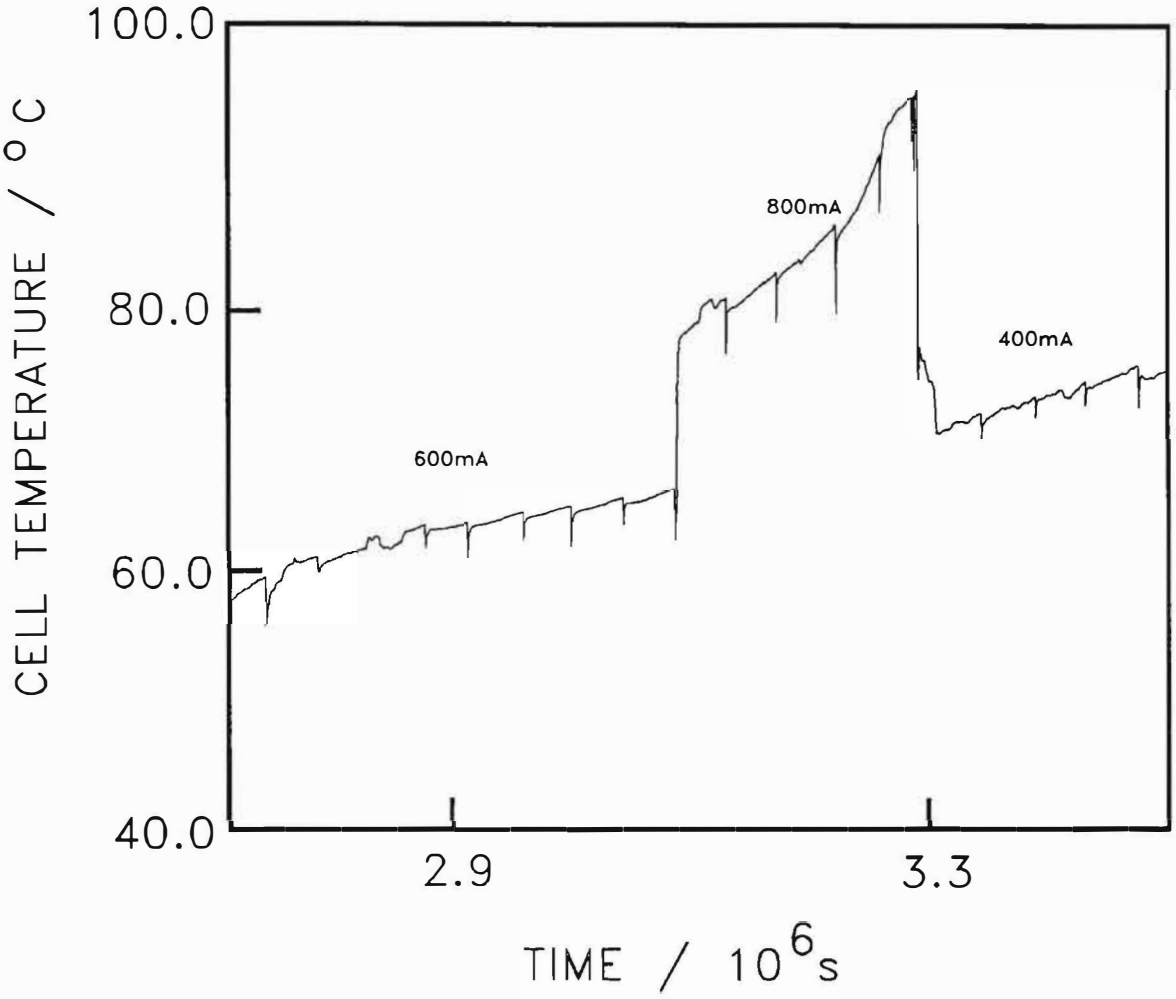

Fig. 10. A cell temperature vs. time plot for a 0.4 x 1.25 cm palladium rod electrode in 0.1M LIOD for a period during which the cell contents went to the boiling point.

electrodes in defining the phenomenon.

It can be seen that the excess enthalpies increase markedly with the current density so much so that the results have the appearance of a threshold phenomenon. However, experiments of very high precision at low current densities are required before this can be confirmed. On balance we still believe that the results confirm that excess heat generation is a bulk phenomenon, Fig. 8, although this cannot now be stated as firmly as it appeared from the results available in the spring of 1989. The levels of enthalpy generation during the duration of a typical experiment (3 months) are such (hundreds of Megajoules cm^{-3}) that they must be attributed to nuclear processes. In particular, it is inconceivable that chemical or non-nuclear physical energy could be stored in the system at these levels and then be released over prolonged periods of time[17]. The phenomenon of "bursts" in the enthalpy production which we first described[18] shortly after the publication of our preliminary paper[1] is also of interest in this context. Figs. 9A, B and C illustrate the $\Delta\theta$ - t , the specific excess enthalpy - t and the cumulative specific enthalpy - t data for the largest "burst" we have observed to date. The total specific excess over the period of the "burst" ($\cong$16 MJ cm^{-3} over 16 days) is again of such a magnitude that the heat release can only be attributed to nuclear processes. The heat output during this burst was 17 times (average value) and 40 times (peak value) of the enthalpy input. In some cells e.g. Fig. 10, the temperature rises rapidly to boiling. When this occurs, it is difficult to accurately measure the heat flows (see Section 2c above). The heat output, however, must be extremely high.

Our current work is concentrated on the design and implementation of factorial experiments in which we are seeking to define more closely the effects of the many variables which control the excess enthalpy. The instrumentation and procedures which we are using in the execution of these experiments are essentially the same as those described in this paper.

ACKNOWLEDGEMENTS

We thank the Office of Naval Research and the University of Utah for support of this work. All of the special grade electrodes used in this work were lent to us by Johnson-Matthey PLC, to whom we are indebted.

REFERENCES

[1] M. Fleischmann, S. Pons, and M. Hawkins, J. Electroanal Chem. 261 (1989) 301.

[2] M. Fleischmann, S. Pons, and M. Hawkins, J. Electroanal Chem. 263 (1989) 187.

[3] M. Fleischmann, S. Pons, M. Anderson, L. J. Li, and M. Hawkins, J. Electroanal. Chem., in the press.

[4] O. Levenspiel, "Chemical Reaction Engineering", J. Wiley & Sons, New York, 1972.

[5] N. Lewis, M. J. Heben, A. Kumar, S. R. Lunt, G. E. McManis, G. M. Miskelly, R. M. Penner, M. J. Sailor, P. G. Santangelo, G. A. Shreve, B. J. Tufts, M. G. Youngquist, C. A. Barnes, R. W. Kavanagh, S. E. Kellog, R. B. Vogelaar, T. R. Wang, R. Kondrat, and R. New, Nature340 (1989) 525, and 175th Meeting of the Electrochemical Society, Los Angeles, CA USA May, 1989.

[6] S. Pons and M. Fleischmann, J. Fusion Technology, in the press.

[7] G. Kreysa, G. Marx, and W. Plieth, J. Electroanal. Chem. 266 (1989) 437.

[8] V. J. Cunnane, R. A. Scannel, and D. J. Schiffrin, J. Electroanal. Chem. 269 (1989) 437. .

[9] L. L. Zahm, A. C. Klein, S. E. Binney, J. N. Reyes, Jr., J. F. Higgenbotham, A. H. Robinson, and M. Daniels, J. Electroanal. Chem., submitted.

[10] D. E. Williams, D. J. S. Findlay, D. H. Craston, M. R. Sené, M. Bailey, S. Croft, B. W. Hooten, C. P. Jones, A. R. J. Kucernak, J. A. Mason, and R. I. Taylor, Nature 342 (1989) 375.

[11] M. Chemla, J. Chevalet, R. Bury, and M. Perie, Cold Fusion Session, 40th Meeting of the International Society of Electrochemistry, Kyoto, Japan, 11-18 September 11-18, 1989.

[12] A. Bruggeman, M. Loos, C. Van der Poorten, R. Craps, R. Leysen, F. Poortmans, G. Verstappen, and M. Snykers, Studiecentrum voor Kernenergie Report, September 1989.

[13] V. Eberhard, G. Fieg, K. Flory, W. Heeringa, H. V. Karow, H. O. Klages, J. Lebkücher, M. Möschke, C. Politis, J. Römer, H. Schnider, G. Völker, H. Werle, H. Würtz, and B. Zeitnitz, Report INR-1653 of the Kernforschungszentrum Karlsruhe, West Germany (1989).

[14] R. D. Armstrong, Session on Cold Fusion, 40th Meeting of the International Society of Electrochemistry, Kyoto, Japan, 17-22 September, 1989.

[15] H. S. Bosch, G. A. Wurden, J. Gernhardt, F. Karger, and J. Perchermeier, Report IPP III / 149' of the Max-Planck Institut für Plasmaphysik, Garching bei München, West Germany.

[16] G. Kreysa International Society of Electrochemistry, Kyoto, Japan, 17-22 September, 1989 and Meeting of the Electrochemical Society, Los Angeles, CA, USA May (1989).

[17] R. C. Kainthla, M. Sklarczyk, L. Kaba, G. H. Lin, O. Velev, N. J. C. Packham, J. C. Wass and J. O'M. Bockris, Inst. J. Hydrogen Energy, 14 (1989) 771.

[18] M. Fleischmann and S. Pons, Meeting of the Electrochemical Society, Los Angeles, CA, USA May (1989).

GLOSSARY OF SYMBOLS USED

$C_{P,D_2O,\ell}$	Heat capacity of liquid D_2O, $JK^{-1}mol^{-1}$.
$C_{P.D_2O,v}$	Heat capacity of D_2O vapor, $JK^{-1}mol^{-1}$.
$C_{P,i}$	Heat capacity of O_2, D_2, or $(D_2O)_\ell$, $JK^{-1}mol^{-1}$.
E_{cell}	Measured cell potential, V.
$E_{cell,t=0}$	Measured cell potential time when the initial values of parameters are evaluated, V.
$E_{thermoneutral,bath}$	Potential equivalent of the enthalpy of reaction for the dissociation of heavy water at the bath temperature, V.
F	Faraday constant, 96484.56 $C\ mol^{-1}$
H	Heaviside unity function.
I	Cell current, A.
k_c	Heat transfer coefficient due to conduction, $W\ K^{-1}$.
k_R	Heat transfer coefficient due to radiation, $W\ K^{-4}$.
k_R^0	Heat transfer coefficient due to radiation at a chosen time origin, $W\ K^{-4}$.
k_R'	Effective heat transfer coefficient due to radiation, $W\ K^{-4}$.
$k_R'^0$	Effective heat transfer coefficient due to radiation at a chosen time origin, $W\ K^{-4}$.
ℓ	Symbol for liquid phase.
L	Enthalpy of evaporation, $J\ mol^{-1}$.
M	Heavy water equivalent of the calorimeter, mols.
M^0	Heavy water equivalent of the calorimeter at a chosen time origin.
n	Iteration number (data point number).
P	Partial pressure, Pa.
P*	Atmospheric pressure, Pa.

Q Rate of steady state heat generation at a given temperature, W.

Q_f Rate of generation of excess enthalpy, W.

t Time, s.

β Dimensionless term allowing for more rapid time dependent decrease of water equivalent of cell than that expected from electrolysis alone.

γ Current efficiency of electrolysis toward a given reaction.

$\Delta H^{\oslash}$ Standard free enthalpy change, J mol^{-1}.

ΔQ Rate of heat dissipation of calibration heater, W.

$\Delta\theta$ Difference in cell and bath temperature at a given rate of enthalpy release, K.

$\Delta\theta^0$ Difference in temperature between the cell and the bath at a chosen time origin, K.

$\Delta\theta'$ Difference in cell and make-up temperature, K.

$\Delta\theta'$ $\Delta\theta - \Delta\theta^0$, K.

$\Delta\theta_n$ Difference in cell and bath temperature at the n^{th} time interval, K.

$\Delta\theta_{n,calc}$ Calculated difference in cell and bath temperature at the n^{th} time interval, K.

$\Delta\theta_{n,exp}$ Difference in experimental cell and bath temperature at the n^{th} time interval, K.

$\Delta\Delta\theta$ Temperature rise in cell due to application of a calibration pulse of heat, K.

θ_{bath} Bath temperature, K.

λ Dimensionless parameter determining the more rapid decrease of the radiant surface area than would be predicted by electrolysis alone.

ν_i Stoichiometric coefficients.

σ_n Sample standard deviation of a given temperature measurement, K.

χ^2 Sum of inverse variance weighted deviations between experimental data and values predicted by the model using the non-linear regression fitting algorithm.

ψ Slope of the change of cell potential with temperature, V.

CALORIMETRY AND ELECTROCHEMISTRY IN THE D/Pd SYSTEM

Michael C.H. McKubre, Romeu C. Rocha-Filho*,
Stuart Smedley, Francis Tanzella
SRI International

Jason Chao, Bindi Chexal, Tom Passell, and Joseph Santucci
Electric Power Research Institute

* On leave from the Federal University of São Carlos, Brazil

ABSTRACT

Experiments have been performed to examine the anomalous effects associated with the D/Pd system, and to discover some of the experimental variables that might be important to the effects. Experiments were concerned with calorimetry of the D/Pd system, but also monitored those experimental variables that might be important in causing the effects: the D/Pd ratio and its rate of change, interfacial phenomena such as the reduction of D_2O, or reduction of contaminant species.

Two types of calorimeters were employed: a differential calorimeter and a flow calorimeter. In both of these instruments the electrochemical cell was pressurized with D_2 gas to 60 atm. The calorimeters were designed to facilitate on-line measurement of the resistance of the Pd cathode, and for high quality measurements of the interfacial impedance. In both calorimeters the electrochemical system has produced evidence of heat output appearing in bursts, apparently in excess of known input power sources. These bursts last for several hours or tens of hours, and produce energies up to several hundred thousand joules.

In electrodes that are heavily loaded with D, the electrical resistance of the Pd cathodes was observed to pass through a maximum with increasing time of cathodic charging, which is consistent with the known behavior of the H/Pd system. The electrochemical interfacial impedance of the cathode gives evidence of one, and at times two relaxation phenomena; it is also sensitive to accumulation of cathodically deposited impurities that may influence the rate and degree of D loading.

INTRODUCTION

Following the announcement last year by Fleischmann, Pons and Hawkins [1] of anomalous effects in the D/Pd system, we have performed a series of experiments designed to examine anomalous excess enthalpy associated with this system and to discover some of the experimental variables that might be important to the effects.

We have designed our experiments with two important principles in mind: the need in precise calorimetric measurements for a closed system, and for knowledge at all times of the composition of the reacting system. These principles were based on the understanding that calorimetry in an open system is subject to more error than in a closed one; this is especially important when seeking small excess enthalpies relative to the total power input into the system. The second principle is based on the belief that anomalous phenomena associated with the D/Pd system probably are related in some way to the D/Pd ratio, and that a high ratio, which is equivalent to a high D fugacity in the metal, is an important factor in determining the onset of the phenomena. In order to facilitate high loading we have operated our calorimetric electrochemical charging cells at an elevated pressure of D_2 gas, and at low temperatures. Deuterium solubility in Pd is a function of the applied emf, the D_2 gas pressure, and the temperature. The effect of temperature on solubility is very significant; the solubility at 5°C is 7 fold that at 50°C, so lowering the temperature (thereby increasing the deuterium solubility) is equivalent to increasing the gas pressure. A high pressure of D_2 has the important effect also of depolarizing the anode reaction hence reducing problems associated with O_2 production.

A further feature of all our experiments was to have comprehensive monitoring of all the experimental parameters, e.g. cell current and voltage, reference voltage, Pd cathode resistance, electrochemical impedance, gas pressure, and of all temperatures pertinent to the experiment.

RESISTANCE MEASUREMENTS

None of the "cold fusion" electrolysis experiments described to date contain any means of determining the D/Pd content *in situ*. Yet this ratio may be a crucial difference between those experiments that have produced a Fleischmann-Pons effect and those that have not. The resistance of Pd metal is a function of its hydrogen content [2] and is, in principle, the easiest way of determining the state of the Pd electrode as the experiment proceeds. Unfortunately, the relationship between the resistance and the D/Pd ratio is known only up to 0.65, but until further calibration experiments are performed, these data can be used at least as an indicator that the ratio is ≥ 0.65. Also, comparison can be made with the H/Pd system, which is calibrated in resistance change up to H/Pd = 1.1 [3].

Figure 1 shows the known data for the resistance ratio, R/R°, as a function of hydrogen loading from the data of Baranowski and Wisniewski [3] and deuterium loading from the data of Barton, Lewis and Woodward [4]. The solid line shows an extrapolation of the D/Pd resistance

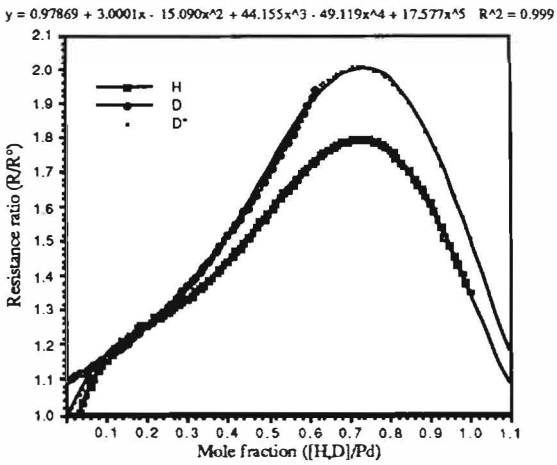

Figure 1. R/R° versus loading; data from references [4,H] and [5,D].

data, based on the assumption that the resistance behavior of the H and D systems are similar, and that resistance maxima occur at the same degree of loading. The inferences that we make about degrees of loading higher than 0.65 for D/Pd are based on this assumption, and are obtained by fitting the measured resistance ratio data to the fifth order polynomial given in Figure 1. It is clear that the assumption of similar resistance behavior for H and D in Pd, differing only in the magnitude of the effect, and the length of the extrapolation, results in significant quantitative uncertainty at high loading levels. We nevertheless expect the loading levels inferred from resistance measurement to be useful qualitatively.

Several factors may influence the measured resistance. Of these, temperature, the occurrence of cracking, and inhomogeneity of loading in the metal phase produce the most significant effects. As shown in Figure 2, the temperature coefficient of resistance for the H/Pd system varies over a considerable range from the pure metal to H/Pd $\simeq$ 0.7; however, we have no data on the behavior in this regard of D/Pd up to 0.7, or of any hydrogen isotope at higher loadings. Our own results suggest that the behavior shown in Figure 2 is closely obeyed in the deuterium system, but that the temperature coefficient remains more or less constant at $\sim 2 \times 10^{-3}$ K^{-1}, at higher loadings. This functional form is assumed in correcting our resistance data for temperature effects.

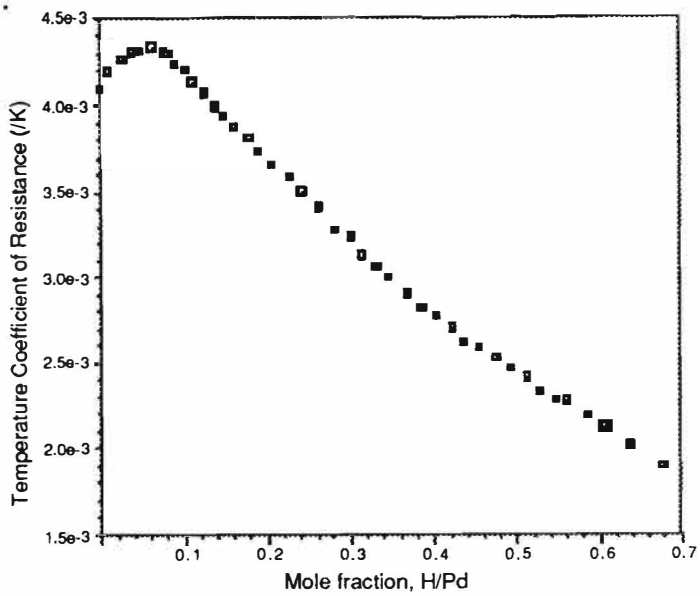

Figure 2. Temperature coefficient of resistance after reference [4].

When the profile of composition in the metal phase is significantly nonuniform, due to high absorptions or desorption fluxes, the average resistance may not reflect the average loading. This problem arises particular during anodic deloading, when the surface achieves the low resistance of the α-phase. At low absorption fluxes the concentration profiles are sufficiently flat that this seldom complicates the interpretation of resistance data.

Resistance inhomogeneities due to cracking or phase nucleation also may yield measured resistances that do not reflect the average composition of the D/Pd system. The extent of cracking can be minimized by loading the electrode unidirectionally, or by pre-loading at temperatures higher than ~350°C, to avoid the α to β phase transformation.

DIFFERENTIAL CALORIMETRY

Concept

Because of the applied current, electrochemical "cold fusion" cells produce Joule heat, and any extraneous heat producing reactions must be detected in addition to this heat. A convenient way of detecting chemical or nuclear reaction enthalpy is by comparing the temperature or heat flux from identical cells, where one cell is restricted to producing Joule heat only.

Heat is produced in an electrochemical cell with D_2O electrolyte and Pd cathode as a result of several phenomena: absorption of D in Pd, overvoltages on the

cathode and anode, and I^2R heating in the electrolyte. The first of these factors becomes less significant once the D/Pd ratio has reached a steady state. Ideally, the other two factors should be the same in the experimental cell and the reference cell, the latter being the cell where the heat production is limited to Joule heating only. Joule heating differences in the two cells were minimized by using electrode surfaces and cells of identical size and shape, as well as identical electrolytes. Any bulk phase reactions arising from the palladium were minimized in the reference cell by using a palladized Cu electrode. This approach to the construction of the reference cell is based upon the tenet that fusion reactions occur, if at all, in the bulk phase and not on the surface of the electrode. If surface reactions are heat producing, then they are likely to occur in the Cu/Pd cathode before comparable reactions occur in the bulk Pd rod, since the thin Pd layer on the Cu rod would become saturated with deuterium before the Pd rod.

An alternative approach is to use H_2O in the reference cell. However, because H_2O electrolytes have different overpotentials and different electrical and thermal conductivities than their D_2O equivalents, the Joule heating will be different. In addition, the heat of adsorption of D in Pd is significantly different from that of H in Pd. For these reasons, light water provides a poor blank for the experiments described below.

The electrolysis of water in our cells was minimized by keeping the applied cell voltage below that required for oxygen evolution. From the known thermodynamic and kinetic values, we calculated the minimum cell voltage required for the evolution of oxygen from light water, as 1.27 V, and even at 1.8 V the electrolysis current would not be above 1 mA.

Experimental Approach

Figure 3 illustrates a cell design that incorporates the features referred to above, which, except for the Pd electrode, represents identically both the experimental and reference cells.

The body of the cell was constructed from copper, which was chosen for its high thermal conductivity and low solubility and diffusivity of hydrogen isotopes, and its ability to accommodate a pressure of at least 50 atm. All interior surfaces were platinum coated on nickel. Both these metals are resistant to corrosion in LiOD under the conditions applicable to this experiment. Temperature was measured with a four terminal resistance temperature device (RTD) embedded in each cathode.

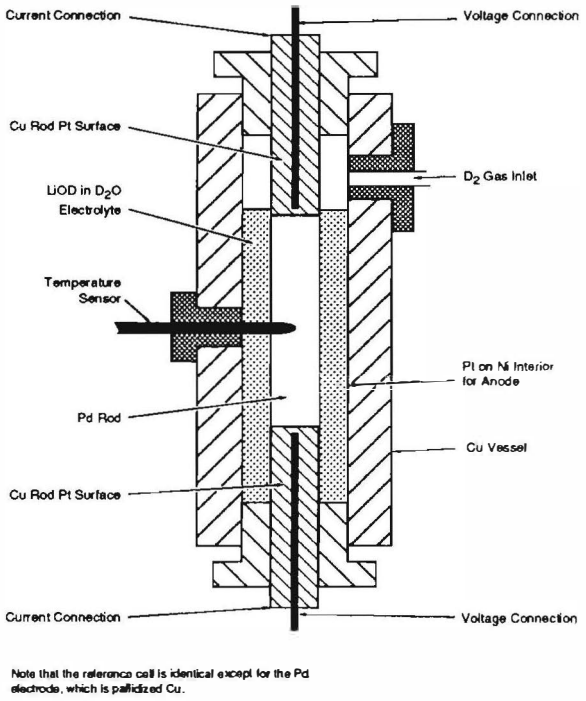

Figure 3. Cell for differential calorimeter

For the experimental cell, the cathode was made from twice vacuum melted Pd, which was machined, then annealed in a vacuum at 800°C for three hours, then backfilled at temperature with D_2. Palladized copper was used for the reference cell cathode. The electrolyte was prepared by the addition of 99.9% Li metal (Ventron Alfa Products) to 99.9% D_2O (Aldrich Chemicals).

The cells were placed, as shown in Figure 4, in an insulated bath cooled to ~ 7°C. Pressure was applied to the cells from a D_2 gas cylinder. Each cell could be pressurized independently or removed from the gas system; a relief valve was also included to prevent overpressurization of the system in the event of a large exothermic reaction.

An Apple Macintosh microcomputer with a Keithley data acquisition system was used to monitor every minute the temperature of the Pd and Cu cathodes, the bath temperature, both cell voltages and the current. The interfacial impedances were measured every ten minutes during the latter part of the experiment.

The cells were filled with electrolyte, and the cathodes charged galvanostatically in series at 10 mA cm^{-2} for five days. On the establishment of steady-state temperatures and voltages, the Pd electrode resistance was measured, and the current increased by an amount just sufficient to keep the applied cell voltage below 1.5 V, to prevent oxygen evolution. The above sequence was repeated periodically.

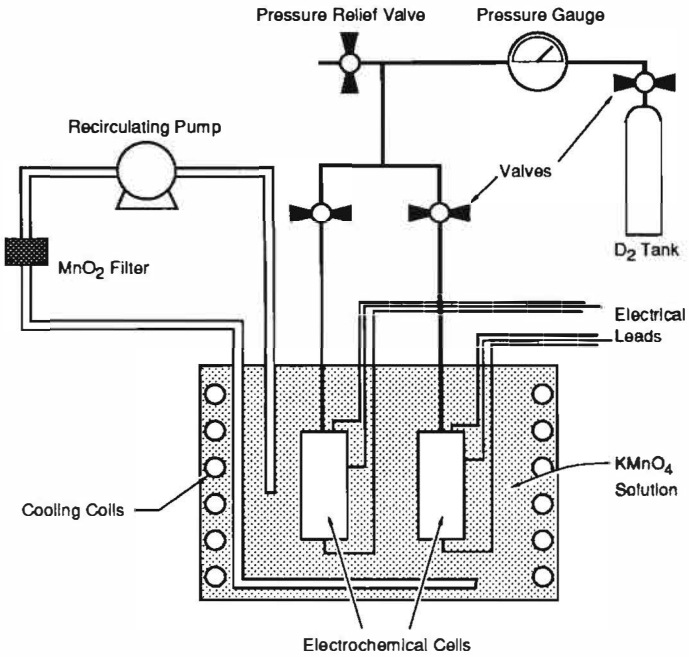

Figure 4. Schematic diagram of differential calorimeter

At intervals during the charging process, the resistance of the bulk palladium electrode was measured using a four terminal ac measurement of the longitudinal impedance to determine the deuterium loading level. Measurements also were made of the two-terminal cell impedance, to determine what fraction of the dc cell voltage was associated with IR drop in the electrolyte and what was due to the deuterium redox overpotential.

Calorimetry

If I is the current and V the cell voltage then, in the steady state, the input power is the sum of the product IV and any extraneous sources of heat, Q_u. If the calorimeter heat capacity and cooling constant are C_p and K respectively, then, for an elapsed time t

$$IV + Q_u/t = (C_p + K)\,\Delta T \qquad [1]$$

where

$$\Delta T = T_{cell} - T_{bath}$$

this relationship can be further expressed as:

$$IV = C_p'\Delta T - Q_u/t \qquad [2]$$

The calorimeter was calibrated by varying the input electrochemical power to the two cells in series. With $Q_u = O$ we expect a linear relationship between the input Joule power to each cell, IV, and the observed temperature difference between cell and bath;

$$IV = a\Delta T + b \qquad [3]$$

The cells were calibrated according to equation [3], using both stepped and ramped currents, to establish a steady state slope and intercept: a and b for the working cell and a' and b' for the reference cell. We do not make any attempt to calculate or calibrate the temporal response of these cells to a change in input Joule heat or thermal conditions. Instead, in the differential mode, we assume that the only differences between the response of the working and reference cells are those due to the difference in the steady-state calibration coefficients (a and a', b and b'), and the possible existence of extraneous heat, Q_u, in the working cell. That is,

Working cell: $a\,\Delta T + b = IV + Q_u$

Reference cell: $a'\,\Delta T' + b' = IV'$

$$Q_u = a\,\Delta T + b - (a'\,\Delta T' + b')\,V/V' \qquad [4]$$

Equation [4] reflects the extraneous heat if all influences on the two cells are the same except for the quantified and calibrated differences between the primed and unprimed variables. This procedure yields a positive excess if the extraneous heat occurs in the working (solid Pd) cell, a "negative excess" if this heat occurs in the reference (Pd coating) cell, and zero if there are no extraneous, uncorrelated influences.

Results

Table 1 displays a chronology of observations. Except for the times noted in Table 1, the differential calorimeter operated with Q_u close to zero, with a statistical fluctuation of $\pm$ 200 mW. We observed anomalous enthalpic effects from the experimental cell, and possibly also from the reference cell. The enthalpic events referred to occurred when the output power, observed as heat, was in excess of the input power.

The events described as δV, refer to occasions when the cell voltage underwent spontaneous changes at constant current, temperature and pressure. These events occurred without accompanying bursts of power in excess of that provided by the input electrical power, and were observed for the experimental cell only.

Table 1

Chronology of Anomalous Events in the Differential Calorimeter

#	DATE	TIME	TYPE	H/kJ
1	5/15	2300	$\partial H\ XS_{Cu}$	<3
2	5/17	1800	$\partial H\ XS_{Cu}$	~10
3	5/18	0530	∂V_{Pd}	0
4	5/18	2100	$\partial H\ XS_{Pd}$	5
5	5/19	0800	$\partial H\ XS_{Pd}$	32
6	5/20	0100	∂V_{Pd}	0
7	5/21	2200	∂V_{Pd}	0
8	5/22	1900	∂V_{Pd}	0
9	5/24	1800	$\partial H\ XS_{Pd}$	<3
10	5/26	1700	∂V_{Pd}	0
11	5/31	1300	$\partial H\ XS_{Pd}$	26
12	6/01	0700(2)	$\partial H\ XS_{Pd}$	6

where H=enthalpy, V=voltage, XS=excess.

Figures 5 and 6 show data for Q_u calculated using equation [4]. Also displayed is the excess energy for the two periods of essentially twelve hours, although the features in Figure 6 presumably are continuations of the event in Figure 5. The event in Figure 5 appears to have been initiated by a transient decrease in the cell temperature, both of which occurred in the interval between 16 and 17 hours in that figure. During this time a slow increasing current ramp was begun, although this was initiated some 20 minutes after the leading edge of the apparent positive power excess.

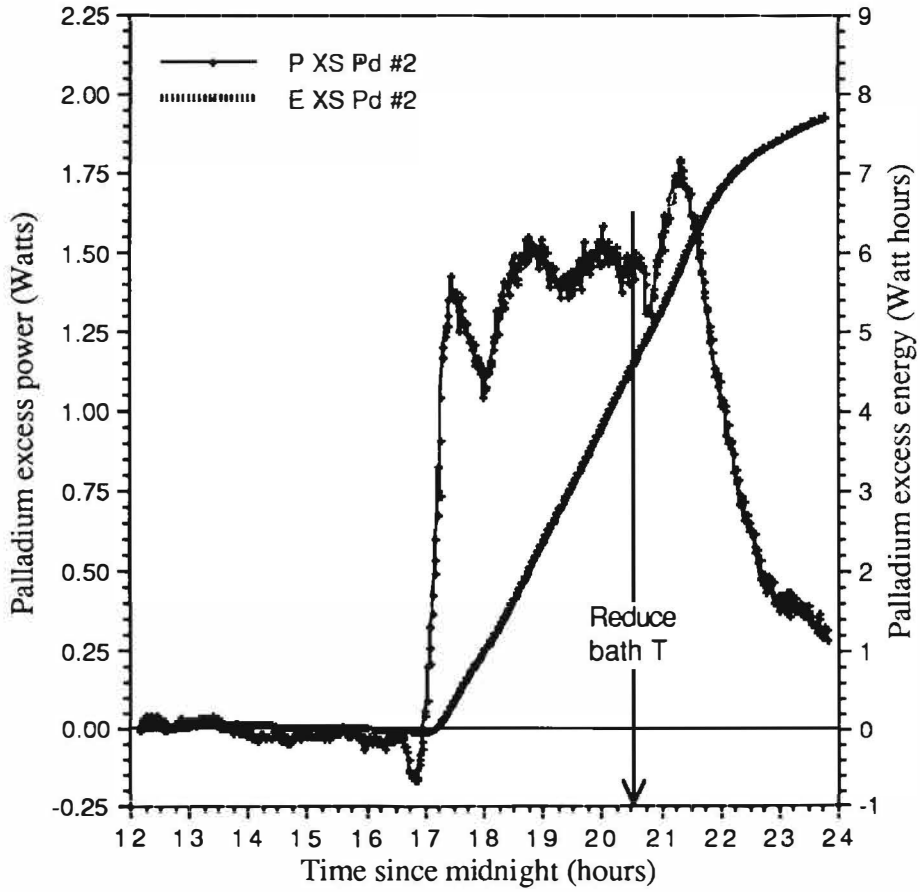

Figure 5. Differential calorimeter excess power and energy: May 31, 1989.

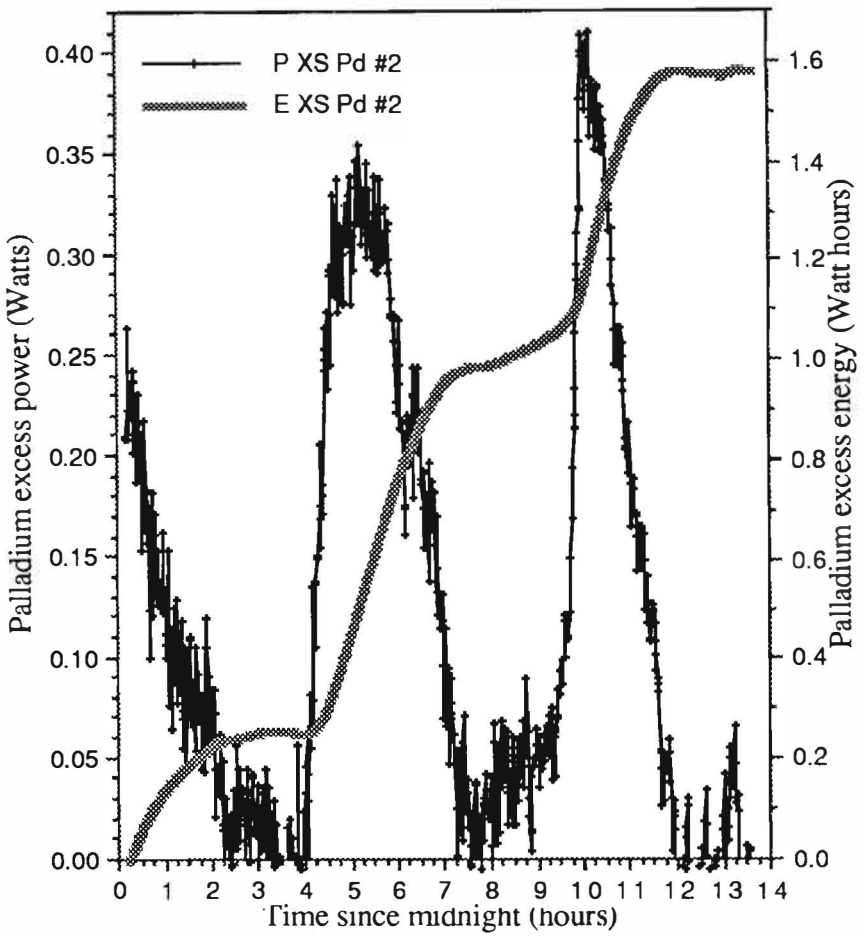

Figure 6. Differential calorimeter excess power and energy; June 1, 1989.

FLOW CALORIMETRY

Concept

A second series of experiments was performed in a flow calorimeter operated isothermally. Figure 7 depicts the calorimeter schematically. In the experiment described here only one calorimeter cell was used. During operation the electrochemical cell was contained inside the calorimeter Dewar flask, and the heat transfer fluid (silicone oil) was pumped through it. Temperature control was maintained by mounting the calorimeter in a well regulated bath (± 0.01°C) and by equilibrating the temperature of the oil with that of the bath before it was pumped into the Dewar flask. The flow rate was maintained constant to within ± 1% by means of an FMI metering pump; this was monitored continuously with a rotameter-type flow meter, and periodically by weighing timed samples removed from the flow. Two RTD temperature sensors were placed in the inlet to, and outlet from the calorimeter; turbulence promoters were employed to ensure that the fluid was well mixed before it passed over the outlet sensors.

The electrochemical cell was a nickel pressure vessel whose interior and all other fittings were coated with Pt. Provision was made for four-terminal resistance measurements, and a reference electrode. A helical electrical heater was mounted in grooves on the outside of the pressure vessel.

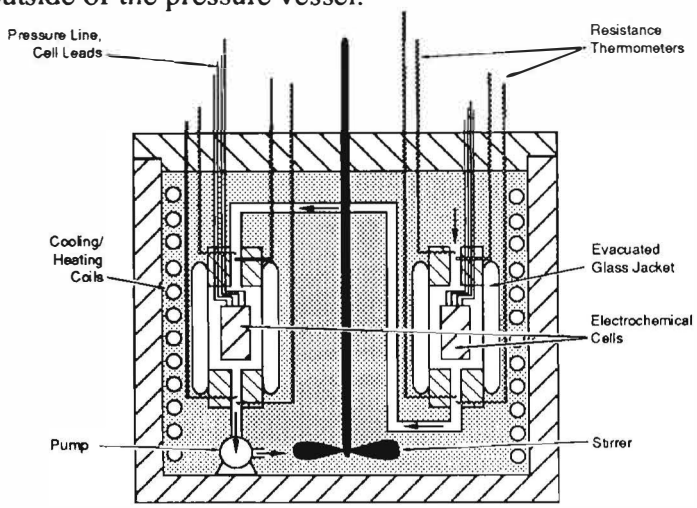

Figure 7. Schematic diagram of differential calorimeter.

Calorimetry

To assist in rapid transfer of heat to the heat transfer fluid a "finned jacket" was placed around the outside of the vessel. In operation, the total input power to the calorimeter was maintained at a preset constant value by using the data acquisition computer to calculate the input electrochemical power and adjust the heater power. In this way, at constant mass flow of calorimetric fluid, the presence of excess power could be inferred from an increase in the temperature difference measured between the inflow and outflow. In the absence of excess power any second order effects of heat loss should remain constant since the temperature profile inside the Dewar flask is essentially constant.

The calorimeter was calibrated by several methods: by adjusting the heater power, and the electrochemical power in a stepwise manner allowing the system to come to a steady state, and by dynamic methods where a sinusoidal or sawtooth waveform was applied to the heater.

The thermal output of the calorimeter is observed to have the following dependence on input power:

$$P_{heater} + P_{electrochem} = (\mathbf{C_p\ dm/dt + k'})\ \Delta T \quad [5]$$

where C_p is the heat capacity of the calorimetric fluid, **dm/dt** the rate of mass flow through the calorimeter, and **k'** is a small loss term due primarily to heat loss through the electrical and pressure interconnects that penetrate the top of the calorimeter vessel.

The values of the constants $\mathbf{C_p}$ and **k'** were determined by a series of calibrations, varying the input heater power at constant flow rate, and the flow rate at constant input power. The value of $\mathbf{C_p}$ obtained was in precise accord with that obtained by independent heat capacity measurements, and with the value supplied by the manufacturer. At the flow rates normally employed in the calorimeter (2-3 g/s), **k'** represents less than 5% loss due to conduction.

Experimental

LiOD of 0.1 M concentration was prepared by reacting pure Li metal with D_2O under nitrogen in a glove box.

The Pd electrode was prepared by etching in aqua regia, annealing the sample in a vacuum for 4 hours at 800°C, and then cooling under D_2. Upon cooling to room temperature the electrode was placed in the electrochemical cell.

Parameters monitored were the cell current and voltage, reference voltage, Pd resistance, two inlet and two outlet temperatures, two cell temperatures, cell pressure, and calorimetric fluid flow rate. Electrochemical impedance measurements were made at regular intervals to monitor the kinetic processes at the Pd/LiOD interface.

The cell was operated with 60 atm of D_2 pressure, and with varying cathodic current densities up to 600 mA cm^{-2}. Experiments were performed at 25 and 4°C.

Table 2 displays a chronology of excess heat observations, where ΔT increased spontaneously in the apparent absence of any spurious effects. Figure 8 shows the raw data for event #2, calculated from the difference between the calorimeter output power from equation [5], and the known input power $P_{electrochem} + P_{heater}$. This figure provides a good indication of the level of baseline variation of the "excess" power; for some period prior to and subsequent to the positive excursion shown in Figure 8, the "excess" power registers zero with a random variation of roughly 0.2 W. The structured variation of the "excess" power apart from the burst is due to the enthalpy of partial recombination of D_2 and O_2. At high current densities, the anodic reaction is not completely depolarized by the D_2 pressure, and electrolysis occurs. The products of this reaction (and all the associated enthalpic effects) are contained within the calorimeter. Recombination occurs on the inner exposed surfaces of the Pt coated pressure vessel, and its progress can be monitored by the pressure. We observe oscillations in the pressure of period approximately 30 minutes, consistent with small positive and negative fluctuations of the "excess" heat. No significant change was observed in the cell pressure associated with the heat burst in Figure 8, and the recombination fluctuations occurred throughout this positive heat excursion.

Also shown in Figure 8 is the electrochemical input power. At this time the heater was employed for power calibration only at the times marked "P". The average of the positive excursion is approximately 1.25 W; nearly 33% of the total input power to calorimeter at that time. The excess energy was calculated from the area of the envelope of the event in Figure 8 to be 49 kJ, excluding the effects of heater calibration pulse which are incompletely removed from the steady state calculation. At no times were negative excursions observed in the data record of similar form or comparable magnitude. The energy total of the four events of apparent excess heat in this experiment was 298 kJ, this is 7.45 MJ/mol for an electrode which comprised 0.04 mol of Pd.

Table 2

Cell P2 Excess Enthalpy

#	DATE	TIME	DURATION/h	H/kJ
	10/11	21:40	Cell Start Up	
1	11/1	22:00	13	49
2	11/3	10:00	11	49
3	11/5	23:00	24	154
4	12/10	12:00	46	46
			TOTAL	298

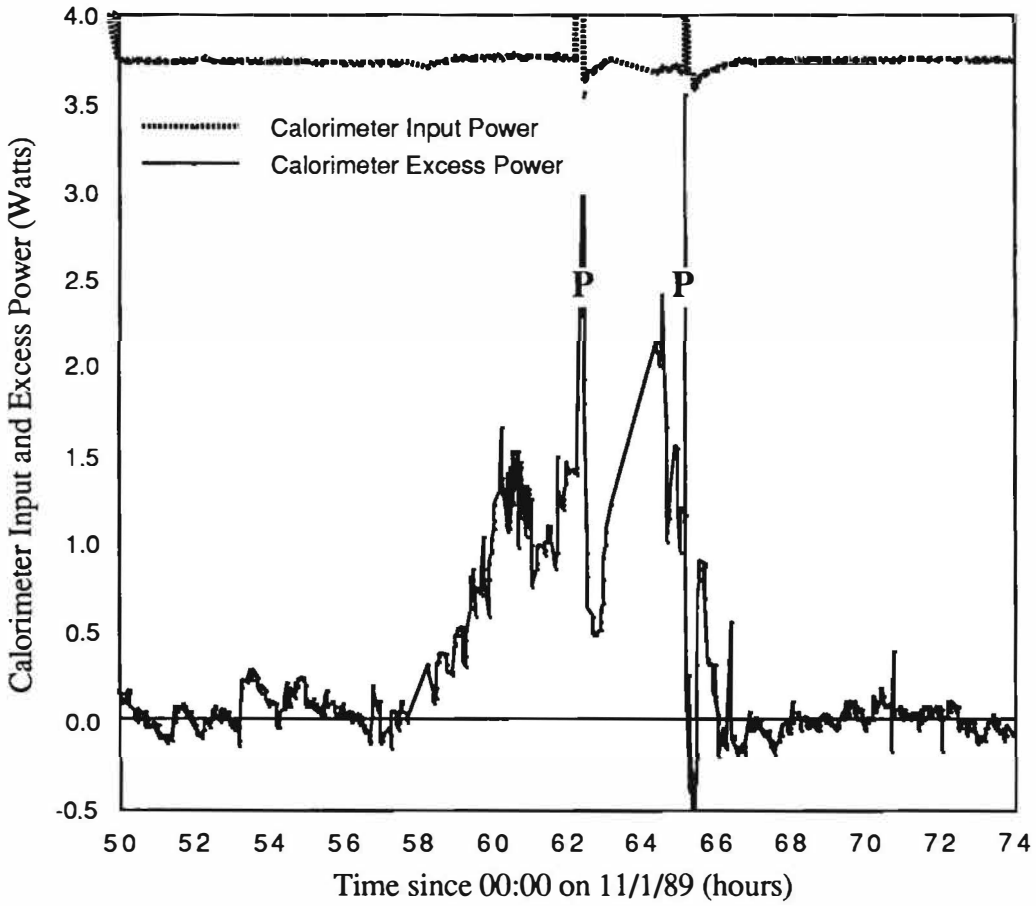

Figure 8. Isothermal flow calorimeter excess heat event #2.

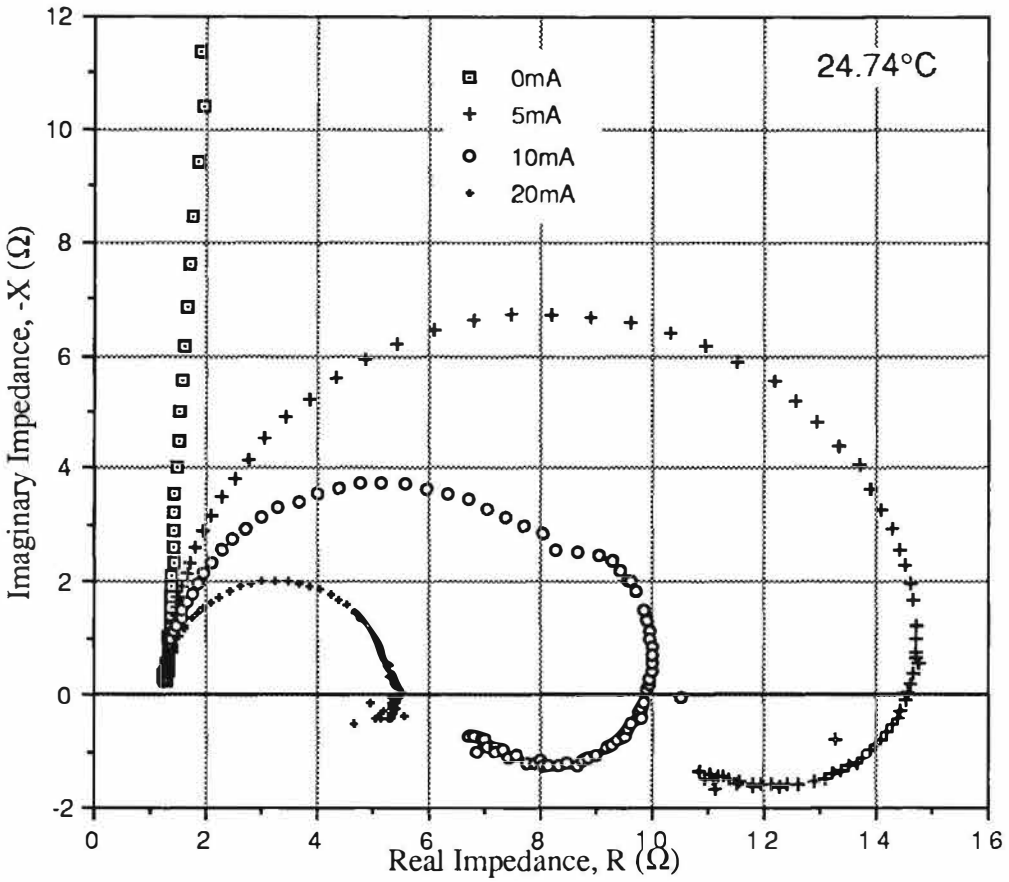

Figure 9. Pressurized Cell P2; complex plane Impedance plot as a function of applied cathodic bias.

Impedance Measurement

At low loading levels the electrochemical impedance of the Pd/LiOD interface exhibits a single semicircle in the complex plane suggesting that the response is due to the double layer capacitance and charge transfer resistance. At high rates of loading (high surface loading) or high equilibrium loading levels (high bulk loading) the interfacial impedance response exhibits a more complex behavior.

Figure 9 shows the impedance response of the electrode in the pressurized isothermal flow calorimeter, at 25°C, as a function of applied cathodic current (for an electrode with area ≈ 4 cm^2). Based on the measured resistance ratio and the extrapolation of known data suggested by Figure 1, the electrode in this experiment had a bulk D/Pd loading of approximately 1.

Post Test Analysis

One week after the electrode was removed from the pressurized isothermal flow calorimeter it was placed between two layers of Polaroid ASA 3000 film for 12 days. Details of the resulting films are shown in Figure 10. Clear evidence of some type of ionizing radiation is observed. The points of light with diffuse halo exposure suggest that some of the radiation may be coming from point sources within the metal, being scattered by the lattice structure.

The surface and near surface of the sample were subjected to surface analysis by laser ionization (SALI) and compared to an identically treated blank electrode. No changes in isotopic composition were observed, and no unexpected elements were observed that might be consistent with fission products.

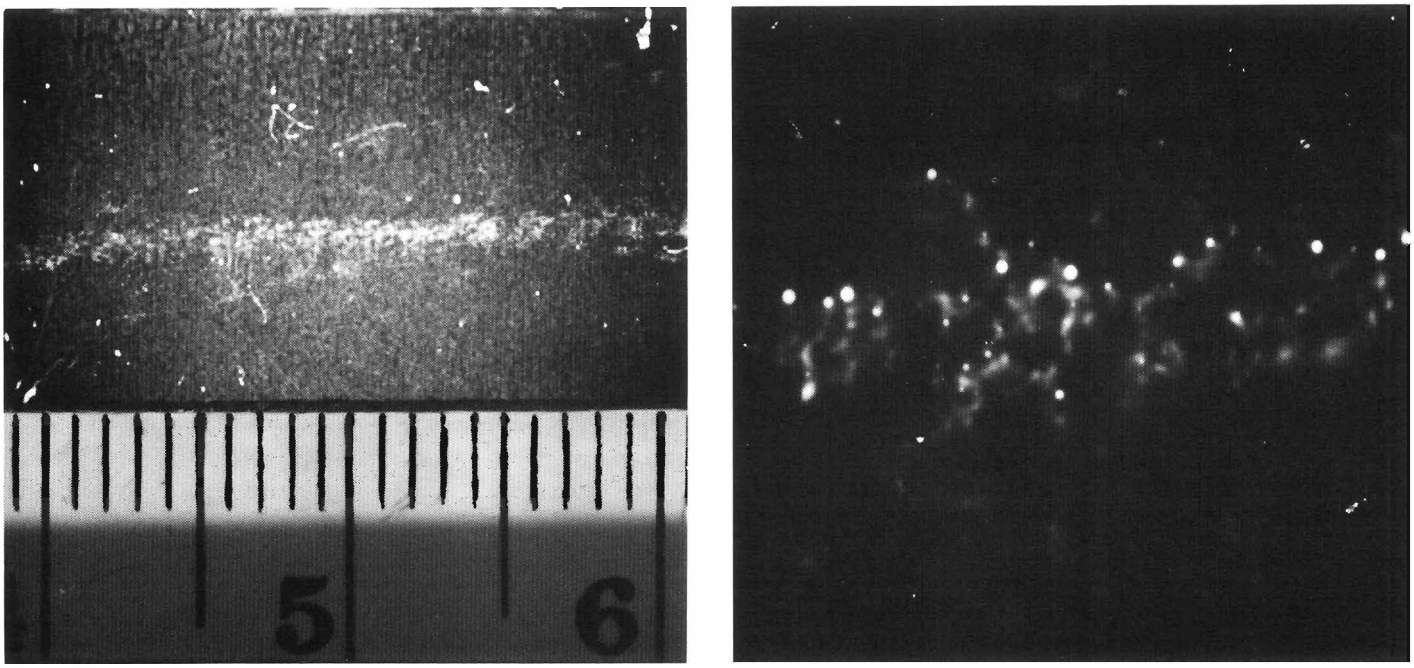

Figure 10. Autoradiograph of flow calorimeter, pressurized cell P2 electrode, after 12 day exposure; shown at 4x and 50x magnification (markings in centimeters).

Approximately 10% of the total mass of the electrode, comprising one sample from the surface and one from the bulk, were analyzed by Rockwell International for ^3He and ^4He by mass spectrometry of a molten sample. This technique is capable of detecting 10^{11} atoms; no He was observed at that detection level.

Mass spectrometry was used to analyze the residual D_2 gas in the pressure vessel for ^3H, ^3He and ^4He. At a detection level of 1 ppm, none of these isotopes were found.

The electrolyte was sampled for tritium before emplacement in the cell and after removal; no increase in tritium was observed above the background level.

DISCUSSION

Experiments were performed in two electrochemical cells comprising a Pt anode, LiOD electrolyte, Pd cathode and D_2 gas. Both experiments appear to give bursts of heat output in excess of the known sources of Joule input heat. In one experiment differential calorimetry was employed; in a subsequent experiment a more sophisticated isothermal flow calorimeter was used. The results nevertheless were qualitatively similar - considerable periods in which the calorimeters were poised in thermal balance, with occasional positive excursions of output power, lasting hours or tens of hours, and in magnitude several tens of kilojoules.

It is difficult to discuss the initiation of these events given the apparent stoichastic nature of the excess heat bursts. Nevertheless, we have observed no heat excess from electrodes that were loaded to D/Pd $\lesssim$ 1 (based on an extrapolation of known resistance ratio data). It may be that such loading is necessary. However, it is clearly <u>not</u> sufficient to produce the anomalous heat effects. In both cases the Pd had achieved its minimum resistance (from which we infer maximum loading) condition, several weeks prior to the observation of anomalous heat.

The interfacial impedance data may give a clue to other conditions that are necessary for anomalous heat effects to be observed. The impedance feature evidenced at low frequencies and appearing in the fourth quadrant of Figure 9 is not present at all times, even for a highly loaded electrode. In a subsequent paper we will demonstrate that the impedance spectra can be accounted for quantitatively by the double layer capacitance in combination with the charge transfer resistance for D adsorption coupled with recombination and absorption at a fractional monolayer coverage of D. The fourth quadrant feature derives from the coupling of the potential dependent adsorption coverage, and the concentration dependent absorption flux. In qualitative terms, this "inductive" feature appears only when there is a significant absorption flux; it can be used as an

indicator that the electrode surface is in a state such that the electrode is capable of further absorbing D.

Extended cathodization provides an opportunity for electro-reducible minority components to deposit on the cathode surface. While we did not observe macroscopic fouling of the electrodes in this study, one might expect that the presence of a film of cathodically deposited contaminant species on the surface would block D absorption. In our experience, however, the presence of certain deliberately added impurities appears to create the inductive term and facilitate loading, whereas anodic stripping of the Pd appears to eliminate the fourth quadrant term. is therefore likely that the inductive effect is a feature of a specifically modified Pd surface, of unknown origin, but which may be beneficial to loading.

The presence or absence of the inductive term, the existence of which effectively reduces the dc interfacial resistance, can be used also to account for the anomalous changes observed in the cathodic overvoltage of highly loaded electrodes. For both calorimeter cells we have observed cases where the voltage measured between the surface of the cathode and an adjacent Pt pseudo-reference electrode have spontaneously, and over a period of several hours, increased at constant current, decreased at constant current, and, in one case, the overvoltage was observed to decrease with increasing current.

It is possible that both high loading and high interfacial flux are necessary for the anomalous effects to be manifest. In our experience, certain conditions facilitate high loading: high temperature gas loading prior to cathodization, electrode activation in strong acid, low temperature electrochemistry, high current densities, and high pressures of D_2. In a number of instances the occurrence of "excess heat bursts" appears to correlate with a change in condition that might well stimulate high D fluxes at the interface of a highly loaded electrode: transient or stepped increases or decreases in the cathodic current and decreases in the temperature. The event shown in Figure 5 occurred 20-30 minutes after a transient decrease in the cell temperature. A decrease in the temperature might be expected to result in an increased absorption flux since the solubility and thus the equilibrium loading level of D in Pd is increased. Additionally, lower temperature is likely to result in an increased electrochemical impedance for the recombination step which, at constant current, may result in a higher adsorption coverage, a larger dynamic overvoltage and facilitate the adsorbed to absorbed reaction step.

The last excess heat event observed in the isothermal flow calorimeter (event #4 in Table 2) was associated with a decrease in cell current, and persisted for some hours following the reversal of cell potential for anodic deloading. If a flux of D is necessary, then it may be that the direction is not important. If both high flux and high loadings are necessary, then it is difficult to maintain high loading at a high steady-state outward D flux, while it is difficult to achieve a high steady-state inward flux at a high loading level. It might be possible to resolve this apparent impass by periodically reversing the direction of the flux.

In both experiments the excess energy in any burst represents at most 1% of the total energy input to the calorimeter before the excess heat event. The precision with which we establish our calorimetric baseline is not sufficient to eliminate the possibility that energy is being stored in the system during the long periods of time that calorimeters are in apparent thermal balance, and released in bursts. While the thermodynamic properties of the D/Pd system are not known for mole fractions of D near 1, we consider it nevertheless unlikely that the excess energies represented by the events chronicled in Tables 1 and 2 can be accounted for by chemical processes. In particular it is unlikely that spontaneous transformation is occurring to a more stable (and hitherto unobserved) phase. If this were so, we would expect to see some evidence in the mechanical character and some evidence in the resistance. No such evidence is observed.

We do not claim to have examined all possible sources of systematic error in our calorimetry. However, highly instrumented and monitored experiments, using calorimeters of considerably different design and principle have resulted in qualitatively and quantitatively similar results of apparent excess heat bursts outside the standard deviation of the random errors by factors up to 50.

It has been suggested [1] that excess heat is produced in the D/Pd system by nuclear processes. The evidence that we have from the isothermal flow calorimeter cell that produced 300 kJ of excess heat is that sources of ionizing radiation are contained within the Pd cathode, that are not present in a blank electrode prepared identically from the same stock. Experience from autoradiographs of other electrodes heavily electrolyzed in LiOD and LiOH suggests strongly that the exposure evidenced in Figure 10 is not due to contact printing or to chemical exposure by reducing species such as lithium or hydrogen. Autoradiography while sensitive is not specific, and we were unable to identify the species that produced the film exposure, or any other species that might be a product of nuclear reaction. We were unable to identify any isotopic changes or the presence of ^3He or ^4He in the metal, the presence of ^3H in the electrolyte or the presence of ^3H, ^3He or ^4He in the gas. Within the respective detection limits of the various techniques employed, it is not clear that we would expect to see the 3×10^{15} atoms of product that would be associated with 300 kJ of heat from a nuclear process.

ACKNOWLEDGEMENT

We gratefully acknowledge the financial support and considerable technical assistance of the Electric Power Research Institute.

REFERENCES

1. M. Fleischmann, S. Pons and M. Hawkins, "Electrochemically Induced Nuclear Fusion of Deuterium", J. Electroanal. Chem., 261 (1989), p. 301 and errata, 203 (1989), p. 87.

2. D. D. Macdonald, M.C.H. McKubre, A. C. Scott and P. R. Wentrcek, "Continuous In-Situ Method for the Measurement of Dissolved Hydrogen in High-Temperature Aqueous Systems", I&EC Fundamentals, 20, p. 290, (1981).

3. B. Baranowski and R. Wisniewski, Phys. Stat. Sol., 35 (1969), p. 539.

4. J. C. Barton, F. A. Lewis, and I. Woodward, Trans. Faraday Soc., 59 (1963), p. 1201.

A more readable copy of this paper is here: http://lenr-canr.org/acrobat/ApplebyAJanomalousc.pdf

ANOMALOUS CALORIMETRIC RESULTS DURING LONG-TERM EVOLUTION OF DEUTERIUM ON PALLADIUM FROM ALKALINE DEUTEROXIDE ELECTROLYTE

A. John Appleby, Young J. Kim,
Oliver J. Murphy, and Supramaniam Srinivasan

Center for Electrochemical Systems and Hydrogen Research
Texas Engineering Experiment Station
Texas A&M University
College Station, Texas 77843, USA

ABSTRACT

Convincing evidence of anomalous thermal fluxes from palladium cathodes in LiOD solutions is provided. When combined with other evidence for tritium formation, these argue for the existence of solid state nuclear processes in this system. Compared with previous work, effects are only seen at a relatively low level, and they appear to decrease with decreasing electrode surface/volume ratio. They are also observed in a sealed cell with internal gas recombination, which requires no thermodynamic corrections. The effect of lithium ion is seen to be specific, and the effect seems to involve only the palladium surface layers.

INTRODUCTION

In a recent publication, Fleischmann, Pons and Hawkins[1] have alluded to anomalous enthalpy production when deuterium is evolved on palladium from solutions of lithium deuteroxide in deuterium oxide after polarization over long periods of time. These experiments were conducted using a classical calorimetric technique, in which temperature changes were measured using Beckmann thermometers. The authors concluded that nuclear reactions of unknown type involving deuterons dissolved in palladium beyond the composition corresponding to that of the end of the (α+β) phase were taking place, since no significant neutrons or γ-radiation much above background were observed. The total excess thermal energy (4MJ), observed over a period of 120 hours, was much greater than the heat output from any possible chemical process. Such results have not been reported for cathodes that do not significantly absorb deuterium (e.g., platinum), or during hydrogen evolution on palladium from light water. In this paper, we report the results of work on anomalous heat production from palladium cathodes during deuterium evolution from lithium deuteroxide solutions in deuterium oxide. We also present results of control experiments with platinum cathodes evolving deuterium under identical conditions, and with palladium electrodes evolving hydrogen from lithium hydroxide-light water solutions.

EXPERIMENTAL

The investigations were conducted using an automatic precision microcalorimeter (Tronac Model 350, Orem, UT). This is a differential heat conduction instrument with a noise level of less than 0.3 μW and a precision better than 1 μW. The temperature fluctuations of the water bath in the microcalorimeter are controlled to $\pm$0.0002°C. The instrument operates by electrically comparing the voltage signal ΔV across a thermoelectric junction assembly mounted around the working chamber with a similar signal from a reference chamber in the

instrument, which avoids fluctuations in the baseline or in the instrument constant. The voltage determined is proportional to the temperature difference across the ends of the thermoelectric pile, and thus to the heat flux. The instrument includes a built-in calibration resistor (about 1000 Ω), with a maximum heat output of 25 mW. Since this level was much below the heat outputs measured, we constructed an extended calibration curve using a standard resistor of smaller value inside the electrochemical cell with and without electrolyte (Fig. 1). It includes any effects of temperature change inside the cell, and is linear over a wide heat flux range. The voltage signal ΔV is monitored using a high-impedance digital voltmeter and the instrument also provided a continuous chart-paper printout of these data, which is available for inspection. The heat flux from the calorimeter is given by $\Delta V.C$, where C is the slope from Figs. 1a and 1b, the calibration plots for the two chambers of the calorimeter. Since the bath temperature of the calorimeter can be adjusted in the range 2°-30° C, it was possible to verify the temperature-independence of the the calibration. The value of C was 184.0 with a standard deviation of ±1.23.

Heat generation rates were measured in a closed stainless steel cell, which was used because of its high thermal conductivity. The cell fitted snugly in the working chamber of the microcalorimeter (1cm x 5cm x 5cm) which was located in a large aluminum block in contact with a water bath maintained at 25°C. The latter temperature could be varied by means of a freon bath. Preliminary results established negligible corrections for the heat generated by oxidation of the stainless steel cell in the electrolyte.

Electrochemical cells were assembled with palladium wire cathodes (1 cm long, 0.05 cm diameter) surrounded by spirally wound platinum wire anodes (99.9995% pure, Alfa Products). All cathodes were cut from the same batch of palladium wire (99.997% pure, Alfa Products). Platinum wire leads (0.05 cm diameter) were spot welded to one end of the palladium cathodes and isolated from the solution by means of Teflon. In control cells, a similar electrode configuration was used with a platinum wire substituted for the palladium. All electrode specimens were cleaned using acetone followed by thorough rinsing with ultrapure water. The electrolytes initially used were 0.1 M lithium deuteroxide in 99.8% pure deuterium oxide (Aldrich Chemical Company), and 0.1 M lithium hydroxide in ultrapure light water. Both solutions were prepared by dissolving natural lithium metal ("nLi" 99.9% pure containing 93 wt % ^{7}Li, Aldrich Chemical Company) in light and heavy water. The cells with the palladium cathodes were examined in the heavy and light water electrolytes, and those with platinum cathodes in the deuterium oxide electrolyte only. In later experiments, 0.1 M NaOD, 1.0 M ^{n}LiOD, 0.1 M ^{7}LiOD and 0.17 M ^{6}LiOD electrolytes were used. They were prepared by dissolving "nuclear" grade sodium metal sealed under argon (Alfa Products), ^{7}Li (99.9% chemical purity, 99.8% isotopic purity, Eagle-Picher Industries) and ^{6}Li (99.97 % chemical purity, 98.67% isotopic purity, Oak Ridge National Laboratory). The ^{7}Li isotope was supplier-sealed under argon, whereas the ^{6}Li was under oil, and was Soxhlet-extracted with hexane before use.

The electrical circuits were carefully checked for leakage currents to ground via the metal cell and it was verified that the working and counter electrodes connected to a constant-current power supply were indeed floating. Any AC component from the power line was verified to be less than 20 mV in 5 V. The cell voltage (V) was continuously monitored using a high-impedance digital voltmeter.

After allowing the stainless steel cell and its contents to thermally equilibrate in the microcalorimeter, palladium working electrodes were polarized cathodically in 0.1 M ^{n}LiOD at 0.06 A/cm^2 for 40 hours to allow saturation of the palladium with deuterium (or hydrogen) beyond the end of the $(\alpha+\beta)$ phase composition. In preliminary work, this was immediately followed by the application of current densities of 0.6 A/cm^2, 1.0 A/cm^2, and 0.3 A/cm^2 for various times (see for example Fig. 2). In this example, the cell currents were 97.2 mA, 161 mA and 49.2 mA, respectively. The voltages were about 4.5V, 5.6V and 3.4V. Some voltage variation, discussed below, was seen as a function of time. While the cells were being polarized, the rates of heat generation were monitored. The heat input could be determined from instantaneous readings of the cell voltage, which could be read to within three (but not four) significant figures. The voltage at constant current showed a random noise in the range ±2 to ± 10 mV due to variations in effective cell resistance resulting from gas evolution. The cell current, which showed small variations with time, could be determined to a precision of 0.1%. The calorimeter output was a low noise signal typically in the range 1500 to 2500 μV, which was read by a digital voltmeter to a precision of ±10 μV.

Solvent was periodically added every 48 h to the cell to maintain constant volume due to loss of solution by electrolysis and any entrainment by evolved gas. The measured amount of solvent was 1.7 ml at a current density of 0.6 A/cm^2. This

quantity corresponds to the theoretical amount for 100% dissociation of the electrolyte to hydrogen or deuterium and oxygen at a total cell current close to 0.1 A. In no case was the electrolyte level allowed to fall so that platinum or palladium wires were exposed above the electrolyte. After each addition, the cell and its contents were allowed to reequilibrate before further recordings were made.

RESULTS

Plots of the cell potential and of the excess rate of heat generation, recorded as a function of time for a palladium wire cathode in 0.1 M ^{n}LiOD, are presented in Figure 2. The rate of excess enthalpy generation, ΔQ, is given by:

$$\Delta Q = Q - \{E - (\Delta H/F)\} I \qquad (1)$$

where Q is the total rate of enthalpy generation, E is the cell potential, ΔH is the heat of formation of gaseous D_2 or H_2 and O_2 from liquid D_2O or H_2O, as appropriate, F is the numerical value of the Faraday in joules, and I is the current passing through the cell. The value of $\Delta H/F$ is 1.527 V for D_2O (rounded to 1.53 V) and 1.48 V for H_2O. The excess enthalpy flux for D_2O was therefore:

$$\Delta Q = \Delta V.C - (E - 1.53)I \qquad (2)$$

The correction for evaporation of solvent and the smaller effect of heat loss in the escaping gas was determined to be small (certainly less than -2 mW at a cell temperature maintained close to 25°C by the heat conduction calorimeter), compared with the order of magnitude of the heat flux changes sought. Consideration of the precision of reading ΔV, E and I, along with the standard deviation of C, suggests the error in determining ΔQ using Equation 2 is ±3 mW. However, to verify that Equ. 2 can be used to accurately calculate the irreversible heat flux, it is necessary to show that recombination of the gases is small. Although it is possible to estimate the extent of recombination from the measured amount of solvent periodically added to the cell, for a more precise determination gas volumes from the operating cell were measured using a gas burette during electrolysis, both on the bench and in the calorimeter. Results obtained were always slightly less than, but within about 1% of, the theoretical value, indicating a small amount of recombination, presumably by diffusion of oxygen through the electrolyte to the cathode. If the fraction of gases recombining during the experiment is x, the heat flux input to the calorimeter will be (E - [1.53][1-x])I. If x is indeed 0.01, then the error in ΔQ will be positive and equal to about +1.5 mW. Thus, a small amount of recombination will tend to compensate the heat loss resulting from evaporation and other heat losses. Since these corrections are within the overall estimated error bars, the latter are shown as ± 3 mW on the plots of the experimental results. Breaks are shown in the plots corresponding to the re-equilibration times for the calorimeter after the cells were opened for verification or electrolyte addition. These corresponded to intervals of 1-2 hours.

The result in Fig. 2 shows an excess rate of heat generation (i.e. over and above the rate of heat generation due to irreversible losses in the electrochemical cell) several hours after the current density was increased to 0.6 A/cm^2 from 0.06 A/cm^2, the current density for charging of palladium with deuterium. It is interesting to note that at current densities of 0.6 and 1.0 A/cm^2, the excess rate of heat generation was 38 mW, whereas at 0.3 A/cm^2 it decreased to 29 mW. As a percentage of the irreversible heat flux input to the calorimeter, the excess heat was 6.1%, 13.2%, and 31.5% at 1.0, 0.6, and 0.3 A/cm^2 respectively. The fact that the rate of excess heat evolution increases as heat input (i.e., the reaction rate) to the calorimeter decreases is a strong argument against a spurious chemical explanation of this effect, particularly anomalous (and unobserved) recombination of deuterium and oxygen. The highest heat generation rate observed (at 0.6A/cm^2) corresponded to 19.3 W/cm^3 of Pd, which is comparable to that reported by Fleischmann, Pons and Hawkins (26 W/cm^3).

A similar experiment to that shown in Figure 2 was carried out using a platinum cathode in 0.1 M ^{n}LiOD for a period of 80 hours. Since platinum does not form a hydrogen or deuterium bulk alloy, a current density of 0.6 A/cm^2 was applied from the beginning of the experiment. From the data in Figure 3, it is clear that there was no excess heat generation in this case. In a third experiment, electrolysis of H_2O from 0.1 M ^{n}LiOH using a palladium cathode, and the same current density sequence as in Fig. 2, did not reveal any excess heat generation, as shown in Figure 4. These results again demonstrate that recombination of evolved oxygen and deuterium gases within the electrochemical cell should not be a chemical source of the excess rate of heat generation observed for deuterium evolution on a palladium cathode from the ^{n}LiOD electrolyte. The experiments in Figures 3 and 4 have been repeated three times with palladium cathodes in ^{n}LiOH electrolyte, and three times with platinum cathodes in ^{n}LiOD electrolyte, each giving identical results to the examples shown.

The sequence of current densities shown in Fig. 2 for palladium cathodes in ^{n}LiOD electrolyte was repeated for several different specimens of different dimensions, origins, and pretreatments. In all cases, some excess heat generation was observed, the quantity varying according to the nature of the specimen. All results are shown in Table 1. Following Fleischmann and Pons, anomalous heat flux results are expressed in W/cm^3. The highest value obtained (about 25 W/cm^3) was for an annealed wire, 0.05 cm diameter, from the same lot as that used for Fig. 2. These results are shown in Fig. 5. Relatively lower values (6-12 W/cm^3) were obtained on a spherical electrode, 0.2 cm diameter, prepared by melting another sample of the same wire. A further result was obtained on a 0.1 cm diameter wire of "investment" quality. Before stepping up the current density to 0.6 A/cm^2, charging was this time conducted at 0.06 A/cm^2 for two weeks. Results for this wire, expressed in terms of raw data (i.e., ΔV.C and [E - 1.53]I), are shown in Fig. 6. It can be seen that from the start of deuterium evolution at 0.6 A/cm^2, this electrode produced an excess heat flux at a low level. However, after about 12 hours, about 30-60 mW excess heat flux was produced, corresponding to 4-7 W/cm^3. In the case of the specimens shown in both Fig. 5 and Fig. 6, the anomalous heat production was associated with a falling cell potential as a function of time, although this was not consistently true of the other specimens studied. In contrast to the results shown in Figs. 2 and 5, some decay of anomalous heat occurs after 25 h in this case.

Results for two experiments for 0.5 mm diameter annealed Pd wires in 0.1 M ^{n}LiOD and ^{n}LiOH are shown in a more detailed form as a function of time in Table 2. In ^{n}LiOH solution, the cell voltage starts at 4.325 V and shows a slight initial rise as electrolysis proceeds, which we suggest may be due to the effect of impurities. This is followed by a fall as electrolysis proceeds and as the solution becomes more concentrated, hence more conductive. On adding 1.7 ml of solvent, the voltage increases to a value 200 mV greater than that initially observed, which again falls smoothly by 200 mV as the solvent is consumed. In all cases, the heat output from the calorimeter is slightly less than the heat input corrected assuming 100% Faradaic efficiency for electrolysis. In contrast, the cell voltage in ^{n}LiOD solution starts at a considerably higher voltage, reflecting its lower conductivity than that of ^{n}LiOH. This voltage initially falls as the solution concentrates over the first 24 h, then it shows a rise as the production of anomalous heat becomes more evident.

More results are shown in Fig. 7 for a 0.05 cm diameter "as-received" palladium wire initiated in ^{n}LiOD solution. An excess rate of heat generation can be seen starting about 3.5 h after the current density was increased to 0.6 A/cm^2 from 0.06 A/cm^2. After a rise time of a further 14 h, excess enthalpy generation had reached a maximum value of 36 mW, equivalent to 18.3 W/cm^3, compared with 19.3 W/cm^3 observed in Figure 2 for a specimen cut from the same wire sample. However, a rise time of 50 h was required to show the maximum effect in this case. After allowing the excess enthalpy generation to stabilize for 10 h, 0.1 M NaOD electrolyte was substituted, giving a rapid decay of the effect, most having disappeared after 4 h. The cell potential was about 340 mV lower in the NaOD solution, whose specific conductivity is higher than that of 0.1 M ^{n}LiOD. After 24 h, the excess heat flux had fallen to 4 mW and the electrolyte was again changed to 0.1 M ^{n}LiOD. The excess heat flux then rapidly redeveloped, reaching a maximum similar to that observed earlier within 12 h. After a further 12 h, the electrolyte was changed for 1.0 M ^{n}LiOD. In this case build-up of the excess heat after recovery from switching off the current was slow, perhaps due to impurity accumulation by plating-out on the electrode surface from the more concentrated solution, in which the cell voltage was about 3.5 V, compared with about 5.2 V in 0.1 M ^{n}LiOD. The final rate of excess heat production was similar to that in the latter.

After 23 h the current was switched off and heat generation was allowed to decay. Fig. 8 shows the cell voltage and absolute heat decay rates on switch-off. The former is very rapid: After a change of scale, an open-circuit voltage of about 1 V is observed, corresponding to that for the oxidized platinum anode against the deuterium-charged palladium cathode. Within about 1 hour, the open circuit voltage decayed to about 350 mV, followed by a slow decay as deuterium was lost from the palladium and the platinum surface became reduced. The rate of heat decay is the same as that for a heated electrical resistance within the cell, hence it can also be described as instantaneous, corresponding in practice to the time constant of the microcalorimeter.

A similar set of results is shown in Fig. 9 for an annealed wire. In obtaining these, 0.1 M ^{7}LiOD electrolyte, rather than 0.1 M ^{n}LiOD, was substituted for 0.1 M NaOD. Results are broadly similar to those shown in Fig. 7, however, while the time interval from changing the current density tenfold to the appearance of excess enthalpy production on the palladium cathode was rapid (about 1 h), the rise time was slower (about 20

hours instead of 14 hours). It was also much slower than for the annealed wire studied in the same electrolyte in Fig. 5, where initiation of the phenomenon from switching the current density from 0.06 A/cm^2 to 0.6 A/cm^2 took only 2.2 h, reaching close to the maximum value after a further 3.5 h. The maximum excess enthalpy production was this time 34 mW, or 94% of that in Fig. 7. In the previous work reported, a similarly treated annealed wire produced 49 mW (25 W/cm^3). These differences may be due to the presence of trace impurities, since the palladium cathode surface blackens and roughens with use. Surface examination by the SEM shows mossy surface growths, and SIMS and Auger data (to be reported separately) show the presence of transition metals other than Pd, as well as a relatively large amount of Li, at the surface.

Fig. 10 shows similar data to those on Fig. 9, this time on an annealed wire immersed from the beginning in 0.17 M ^{6}LiOD electrolyte. Initiation time from the application of 0.6 A/cm^2 was almost instantaneous, and the slope of the rise was about the same as for ^{n}LiOD in Fig. 8. The final result obtained in this series of experiments is given in Fig. 11, which shows results for an untreated palladium electrode 2 mm in thickness cut from a 4 mm diameter rod (Johnson-Matthey) cut from the same rod stock used by the authors of Ref. 1. The disk-shaped electrode was immersed in 0.1 M ^{n}LiOD in a sealed cell containing a platinum black fuel cell electrode for gas recombination. In this case, no thermodynamic corrections at all are required in evaluating the results, which are shown in tabular form in Table 3. After precharging in 0.1 M ^{n}LiOD at 0.06 A/cm^2 for two weeks, the maximum excess enthalpy production was similar to that in other cells, about 30 mW, however it represented only about 3% of the maximum heat flux input of 900 mW. Because of limitations in the power supply used, the maximum current density was limited to 400 mA/cm^2. The most interesting effect noted is the abrupt fall in excess enthalpy production on reducing the current density from an initial value of 350 mA/cm^2 to 200 mA/cm^2, which is followed by a slow rise over 20 h. A further change to 400 mA/cm^2 results in a short horizontal characteristic, followed by a further slow rise. This may be interpreted as suggesting that 200 mA/cm^2 is perhaps close to a threshold current density for the anomalous heat phenomenon to occur, at least under the conditions used by us.

DISCUSSION

The detailed results reported above show that excess enthalpy production during electrolysis of D_2O solutions on Pd is a real effect, at least in certain electrolytes, and we thus confirm at least some aspects of the rather limited details given in the paper by Fleischmann, Pons and Hawkins[1]. By expressing their results in terms of the excess heat flux per unit volume of the electrode, these authors presumably assumed that they were observing a bulk phenomenon. However, their data scarcely suggest this, since in their reported work[1] at 0.008 A/cm^2, a change of electrode volume by a factor of 16 increased the excess heat flux by only 28%. The corresponding increase at 0.064 A/cm^2 was 38%, and at 0.512 A/cm^2, 257%. For a wire of diameter similar to that in Fig. 6, Fleischmann and Pons obtained 8.33 W/cm^3 excess enthalpy production at 0.512 A/cm^2. Hence, the high values for the 0.05 cm diameter wires used in this work, particularly the annealed specimen, may be atypical.

The results shown in Figs. 7, 9 and 10 show that excess enthalpy production required the presence of lithium in the electrolyte, indifferently ^{6}Li or ^{7}Li isotopes. Replacement of lithium-containing alkaline electrolyte by sodium causes a rapid fall in excess enthalpy production. The rate of this fall suggests that it is due to lithium leaching from the surface. This strongly suggests that a superficial chemical process underlies the effect, although it does not necessarily mean that the excess heat is of chemical origin. Furthermore, the results on the platinum cathodes, compared with those obtained with palladium, indicate that the effect is not exclusively at the metal surface, but appears to be only associated with dissolved (i.e., alloyed) deuterium (and not protonic hydrogen) present in the surface layers of palladium. When the current to the cell was switched off, rapid decay of the excess heat occurred, since ΔV decayed as a function of time in the same way as heat produced by an electric heater inside the cell. If we can discount continuously-occurring chemical explanations such as gas recombination for this phenomenon, other chemical events also seem unlikely. For example, 15 W/cm^3 for 80 h represents over 40,000 kJ/mole or 0.45 keV/Pd atom, which is far greater than either the bond strength of palladium (about 0.67 eV/Pd atom) or the latent heat of sublimation of the metal (4 eV/Pd atom). Even if all of the electrolyte had been involved in some chemical or physical change, this must involve about 17 kJ/mole, which should have been detected.

In the present work, the specific effect of lithium has been shown. This should be contrasted

with the recent results of Iyengar[2], which show anomalous heat, with tritium formation, in 5M NaOD at current densities in the 0.2 -0.3 A/cm^2 range at Pd-Ag alloy electrodes. While lithium metal (with a deposition potential from pH 13 LiOH solution of -2.310 V vs H_2 under the same conditions) is unlikely to plate out on the palladium cathode, LiD (deposition potential of LiH is -806 mV on the same scale) may well do so. We therefore suggest that the deposition of a lithium deuteride layer from a concentrated, i.e., almost D_2O-free electrolyte, at the cathode surface under high current density conditions for deuterium evolution may be responsible. Such a coating, once formed, may easily lose lithium ions into the palladium lattice, to form a superficial lithium alloy. Similarly, D^- could lose its two electrons and also pass into the metal. Sodium deuteride, whose deposition potential is close to that of LiD, would also be expected to form on the electrode surface from NaOD solutions, but it may be less likely to alloy with the palladium lattice. With Pd-Ag electrodes and a 5M NaOD solution[2], the situation is evidently different. When electrodes exposed to LiOD solution are exposed to NaOD under the conditions used in this work, the superficial compounds formed may leach out, and anomalous enthalpy production stops. The NaOD data reported here are highly reproducible, and have been repeated a total of five times to date on different palladium cathode samples.

Whether nuclear events are responsible for anomalous heat production depends on the detection of nuclear products. In parallel work at this University, Wolf et al.[3] have examined neutron fluxes from cells containing the same 0.1 cm palladium wires reported in Figure 6, again operating in the 0.6 A/cm^2 range. Results have been inconsistent, neutrons occasionally being observed at a level of about five times background, i.e., many orders of magnitude less than that corresponding to the level of the excess heat flux observed, assuming the usual approximately equal branching ratios for $^2D + {}^2D \rightarrow {}^3He + {}^1n$ or $^3T + {}^1p$. Iyengar[2] has suggested a branching ratio of 10^8. Our collaborators at this University (Bockris et al.[4]) have observed high levels of tritium in the electrolyte (> 10^6 disintegrations/ml/min, compared with background values (200 disintegrations/ml/min) at the start of experiments. Their work showed that more tritium was formed in the gas phase than was present in the electrolyte. However, results have been sporadic, suggesting that tritium is formed within the electrode, at least initially. If the tritium formed corresponds to the anomalous heat, about 10^{16} atoms, (or 0.01% of the total palladium atoms present), should be formed over 80 h. High tritium levels in the electrolyte are only observed after charging for long times (2-6 weeks) at 0.06 A/cm^2. We have observed no significant amounts of tritium in the electrolyte during the course of the relatively short-term experiments reported above.

Samples of 0.05 cm and 0.1 cm diameter palladium wires in "as-received" form and after serving as cathodes in the above experiments were analyzed at Atomics International Division of Rocketdyne Corporation, Canoga Park, CA, and at Lawrence Livermore National Laboratory. Neither ^3He nor ^4He were observed above background (10^{12} and 2.5 x 10^{11} atoms per ml respectively). However, if no significant neutrons are observed, ^3He as a primary reaction product would not be expected. It is usually considered that ^4He is an improbable fusion product in a plasma phase, but perhaps it is not in a lattice, as noted in a recent paper by Walling and Simons[5]. If the process involves a skin effect, ^4He would probably escape in the solution. We should note that lack of ^3He in the bulk of the palladium indicates that no known deuterium fusion process involving the classical branching ratio between the $^3He + {}^1n$ and $^3T + {}^1p$ channels is occurring in the bulk at a enthalpy production level greater than a fraction of 1 μW. Similarly, the quantitative upper limit for tritium production in the bulk palladium in an electrode that was assayed 5 days after a series of experiments was about 1.5 x 10^{15} atoms/ml, about 3000 times less than the amount expected from the enthalpy evolved. However, this electrode had degassed, and tritium and deuterium would have been lost both from the surface layers and the bulk. Further work is clearly needed to clarify the origin of the observed heat flux.

The ensemble of results, however, show that chemical enthalpy resulting from spurious gas-phase processes is a highly improbable explanation of the heat flux effects seen with LiOD isotopic species present. The results also persuasively show that the phenomena do not appear to be true bulk effects, but that they occur within the surface skin. The time-integrated results are much too large[1] to be explained by continuous chemical processes taking place in a thin superficial skin of palladium. It is also improbable that they can be cyclic chemical processes, for example lithium deposition taking place in surface cracks, followed by its dissolution to produce hydrogen, as one reviewer of this paper suggested. This would be akin to an a.c. impedence effect, and as such it should be detectable at the levels observed. The anomalous heat effects are however chemically initiated by Li ions, and they may well not be identical to those

noted by Fleischmann, Pons and Hawkins[1]. Indeed, with larger electrodes, the excess enthalpy production observed here is relatively low grade compared with that reported by the latter authors. Our results on 0.1 cm diameter wires were about the same as those reported in Ref. 1, but as stated above, those with 0.05 cm diameter wires were significantly higher. We presently have no explanation of either this, or as to why the excess heat went through a maximum in the experiment shown in Fig. 2, or for the fall shown at 24 h in Fig. 6.

If the excess enthalpy production is due to nuclear fusion, lithium ions are most unlikely to be involved due to their s-electron screen and the apparent lack of an isotope effect. Further evidence is required to say whether they are due to some unusual form of $^2D + {}^2D$ fusion associated with the presence of the palladium lattice[5]. Finally, the fact that surface phenomena initiate the anomalous enthalpy production effects may explain the lack of success of many laboratories in reproducing the Fleischmann-Pons results, since such reactions are known to be very sensitive to surface pretreatment and to the effect of impurities that might be present.

REFERENCES

1. M. Fleischmann, S. Pons, and M. Hawkins *J. Electroanal. Chem.* 261, 301 (1989).
2. P.K. Iyengar, Proc. Fifth Intl. Conf. on Emerging Nuclear Energy Systems (ICENES V), Karlsruhe, FRG, July 3-6, 1989.
3. K.L. Wolf, N.J.C. Packham, D.R. Lawson, J. Shoemaker, F. Cheng and J.C. Wass, *J. Fusion Tech.*, (to be published).
4. N.J.C. Packham, K.L. Wolf, J.C. Wass, R.C. Kainthla and J. O'M. Bockris, *J. Electroanal. Chem.* 270, 451 (1989).
5. C. Walling and J. Simons, *J. Phys. Chem.* 93, 4593 (1989).

Exp. #	Electrode Material		Electrolyte	Current Density	Rate of Excess Heat Generation
	Cathode	Anode		mA/cm^2	W/cm^3 of Pd
1	as-received Pd 0.5mm dia. 10mm long	Pt	0.1M LiOD	300	16.3
				600	19.3
				1000	18.5
2	as-received Pd 1.0mm dia. 10mm long	Pt	0.1M LiOD	600	4-7
3	annealed Pd 0.5mm dia. 10mm long	Pt	0.1M LiOD	600	22-25
4	arc-melted Pd 2.0mm dia. sphere	Pt	0.1M LiOD	600	6-12

Table 1: Excess Enthalpy Production from Various Pd Specimens in 0.1 M LiOD at 0.6 A/cm^2.

TABLE 2

Date	Time	Cell Current (mA)	Cell Voltage (V)	Power In (mW)	Power Out (mW)	Excess Heat (mW)
5/11	10:30	98.18	5.26	359.33	385.00	25.67
5/11	12:50	98.02	5.13	351.89	381.20	29.31
5/11	16:15	97.79	5.06	344.22	381.50	37.28
5/12	08:45	97.81	4.91	329.62	367.50	37.88
5/12	12:10	97.80	4.92	330.566	371.00	40.44
5/12	16:00	97.91	4.97	335.83	375.00	39.17
5/12	17:00	98.20	5.04	343.37	382.37	38.96
5/12	21:45	97.80	4.90	328.61	371.46	42.85
5/13	11:00	97.53	4.75	313.07	358.77	45.70
Calorimeter opened at 11:00 on 5/13 to measure electrolyte volume--1.7 ml/2 days consumed. 1.7 mls of D_2O was added.						
5/14	09:00	97.03	4.70	306.61	341.25	34.64
5/15	08:00	97.03	4.75	311.46	350.05	38.59

Date	Time	Cell Current (mA)	Cell Voltage (V)	Power In (mW)	Power Out (mW)	Excess Heat (mW)
5/27	11:30	96.40	4.325	274.46	271.80	-2.66
5/27	13:00	96.35	4.335	275.08	271.80	-3.28
5/27	18:00	96.40	4.330	274.74	271.80	-2.94
5/28	10:00	96.55	4.295	271.79	271.80	0.01
5/28	11:30	96.60	4.295	271.93	271.80	-0.13
5/28	20:00	96.61	4.280	270.51	268.18	-2.33
5/29	08:10	96.60	4.232	265.84	264.55	-1.29
Calorimeter opened at 08:15 on 5/29 to measure electrolyte volume--1.7 ml/2 days consumed. 1.7 mls of H_2O was added.						
5/29	12:00	96.58	4.532	294.47	293.54	-0.93
5/29	15:00	96.56	4.525	293.83	291.73	-2.10
5/29	17:00	96.45	4.520	293.20	291.73	-1.47
5/29	22:00	96.60	4.500	291.73	289.92	-1.81
5/30	08:10	96.61	4.450	286.90	286.30	-0.60
5/30	11:00	96.58	4.430	284.91	284.48	-0.43
5/30	15:30	96.55	4.410	282.89	282.67	-0.22
5/31	08:00	96.60	4.330	275.31	273.62	-1.69
5/31	15:30	96.58	4.320	274.29	273.62	-0.67

Table 2: Enthalpy data for Pd in 0.1 M LiOD and 0.1 M LiOH electrolytes. The cathodes consisted of a palladium wire (0.5 mm diameter, 1 cm in length, 0.159 cm^2, 1.96 x 10^{-3} cm^3, 99.997% pure) supplied by Johnson-Matthey. The electrodes were annealed at 950°C for 0.5 hr at 10^{-6} torr and afterwards allowed to cool in the furnace under vacuum. The electrodes were previously charged at 60 mA cm^{-2} for two days. The "closed" electrochemical cells initially contained 7.8 ml of electrolyte. The anodes were a spiral of platinum wire.

Date	Time	Cell Current (mA)	Cell Voltage (V)	Power In (mW)	Power Out (mW)	Excess Heat (mW)
7/4	08:00	100.75	4.440	447.33	465.85	18.52
7/4	10:30	175.60	6.175	1,084.33	1,122.18	37.85
7/4	12:50	175.25	6.090	1,067.27	1,110.70	43.43
7/4	15:10	175.25	6.030	1,059.77	1,095.70	36.00
7/4	16:25	175.70	6.010	1,055.96	1,089.14	33.18
7/4	22:55	175.70	6.050	1,062.99	1,099.50	36.51

Table 3: Excess enthalpy production in a sealed cell. The cathode consisted of a palladium disc (4 mm diameter, 2 mm thick, 0.501 cm^2, 2.51 x 10^{-2} cm^3, 99.997% pure) supplied by Johnson-Matthey. The electrode was previously charged at 60 mA cm^{-2} for two weeks. The sealed electrochemical cell initially contained 7.8 ml of 0.1 M D_2O. The anode was a spiral of platinum wire and the O_2-D_2 recombination catalyst was a segment of a fuel cell electrode.

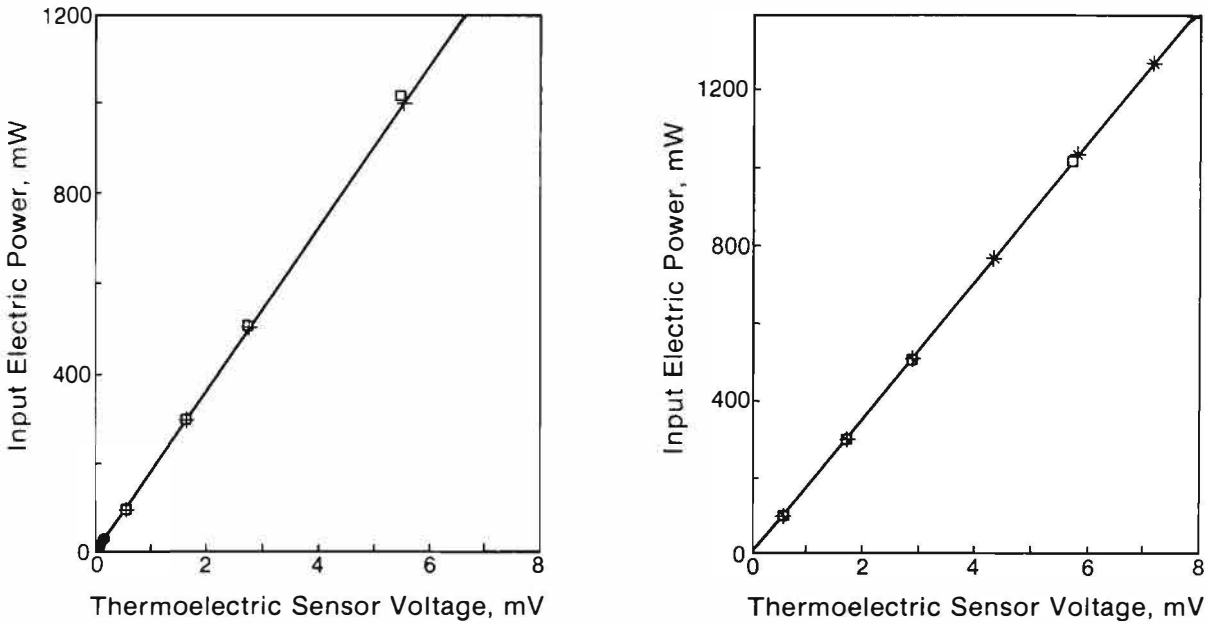

Figure 1: Calibration curve for microcalorimeter. ● : With built-in resistor (limited to 25 mW); + : With resistor in cell without electrolyte; □ : With resistor in cell containing electrolyte.

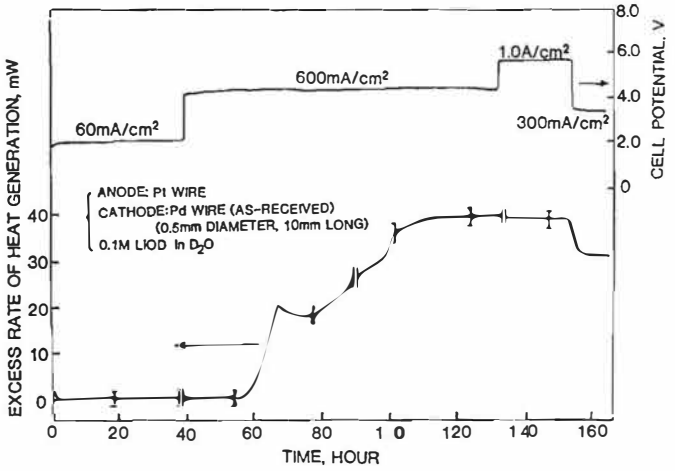

Figure 2: Cell potential and excess rate of heat generation on a 0.05 cm diameter as-received palladium cathode at various current densities as a function of time in 0.1M LiOD in D_2O.

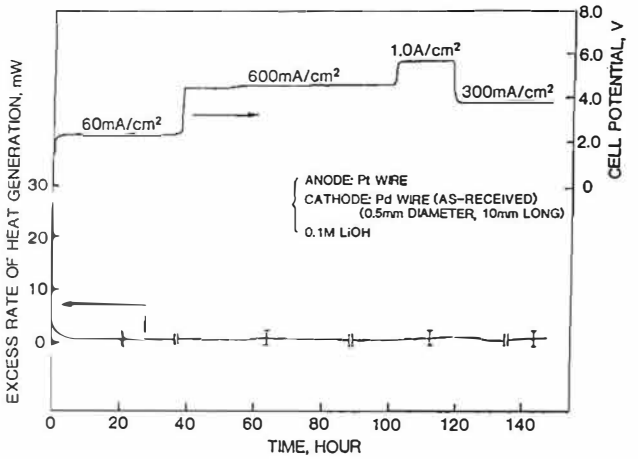

Figure 4: Cell potential and excess rate of heat generation on a 0.05 cm diameter as-received palladium cathode at various current densities as a function of time in 0.1M LiOH.

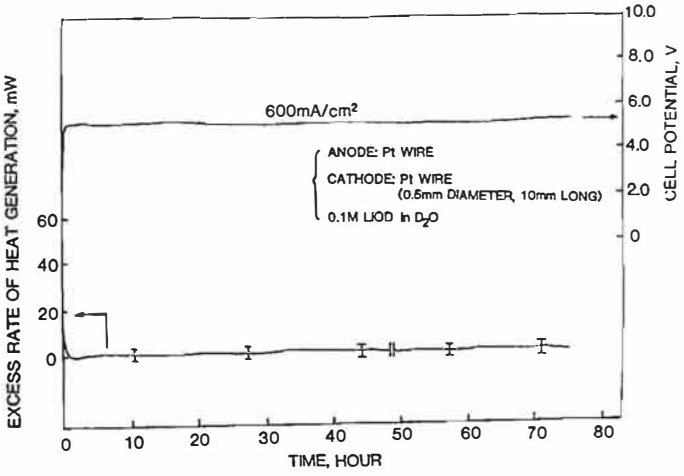

Figure 3: Cell potential and excess rate of heat generation on a 0.05 cm diameter as-received platinum cathode at 0.6 A/cm^2 as a function of time in 0.1M LiOD in D_2O.

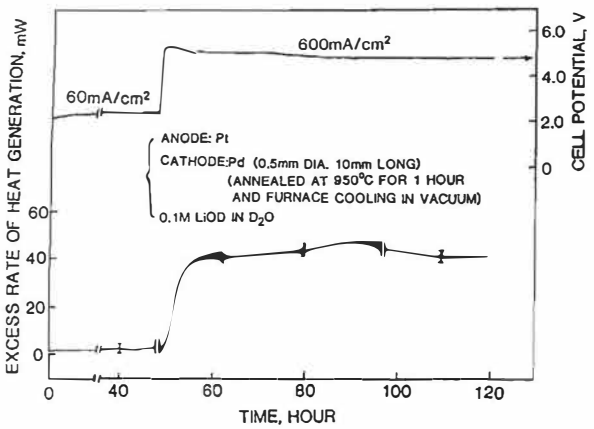

Figure 5: Cell potential and excess rate of heat generation on a 0.05 cm diameter annealed palladium cathode at various current densities as a function of time in 0.1M LiOD in D_2O.

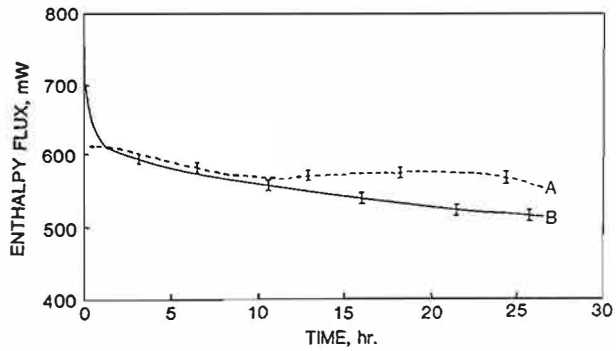

Figure 6: Heat flux: B - entering calorimeter and A - leaving calorimeter, for deuterium evolution at 0.6 A/cm^2 in 0.1M LiOD in D_2O on a 0.10 cm diameter as-received palladium cathode after charging for two weeks at 0.06 A/cm^2 as a function of time.

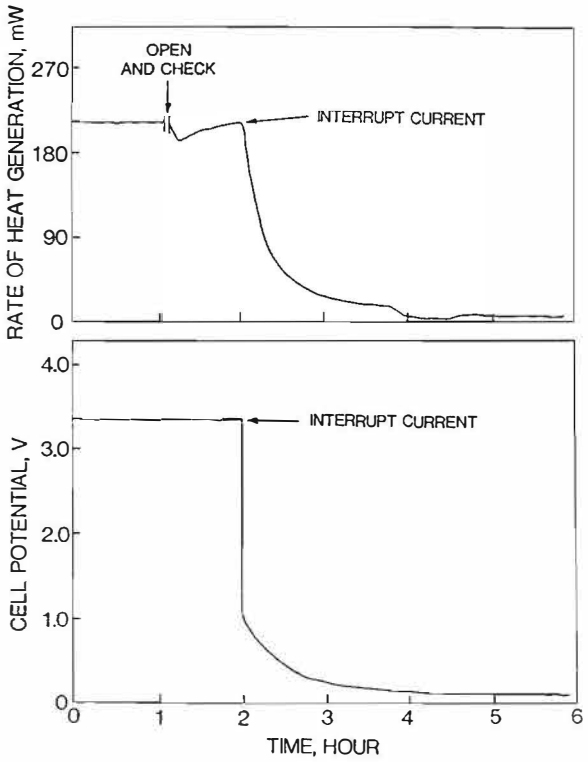

Figure 8: Chart recorder tracings showing the rapid decay of enthalpy generation rate on interruption of the electrolysis current. The decay of the open-circuit potential of the cell is apparent.

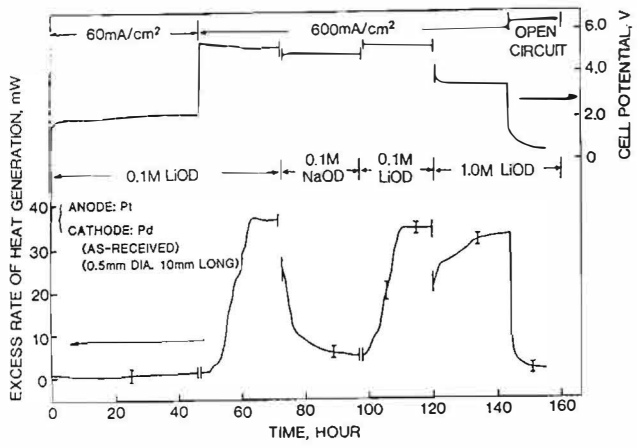

Figure 7: Excess enthalpy generation rates during electrolysis of D_2O on a Pd cathode in alkaline solutions showing the specific effect of lithium cation.

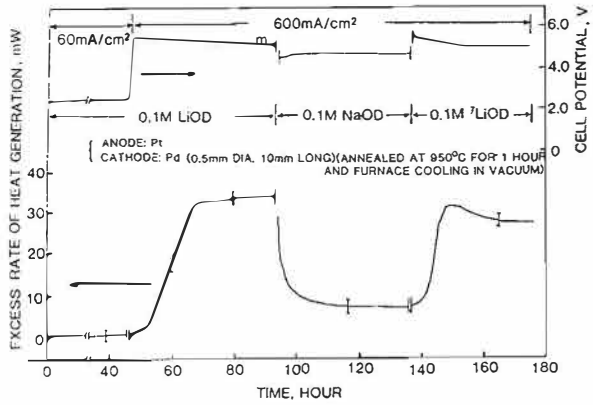

Figure 9: Excess enthalpy generation rates during electrolysis of D_2O on a Pd cathode in alkaline solutions showing 0.1 M electrolyte changes in the sequence $^{n}LiOD \rightarrow NaOD \rightarrow {}^{7}LiOD$.

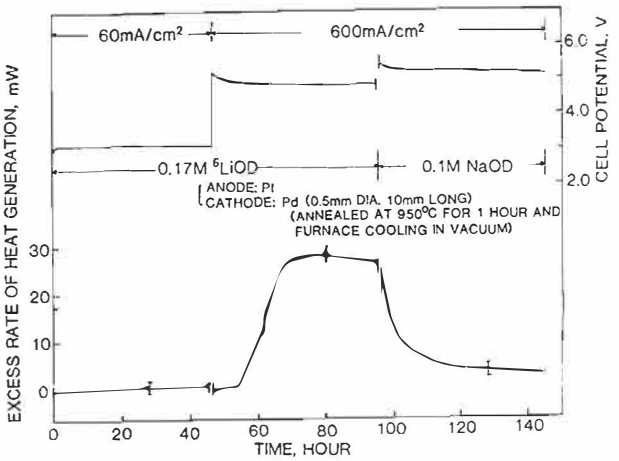

Figure 10: Excess enthalpy generation rates during electrolysis of D_2O on a Pd cathode in 0.17 M ^{6}LiOD as a function of time, showing the decay of excess heat flux to negligible values when the electrolyte was changed to 0.1 M NaOD.

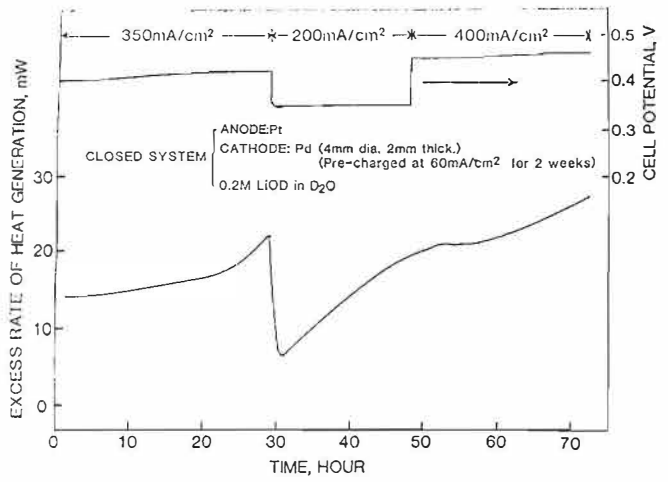

Figure 11: Excess enthalpy generation rates on a palladium disc electrode on electrolyzing a 0.1 M LiOD solution in a sealed cell.

RECENT MEASUREMENTS OF EXCESS ENERGY PRODUCTION IN ELECTROCHEMICAL CELLS CONTAINING HEAVY WATER AND PALLADIUM

Martha Schreiber, Turgut M. Gür, George Lucier, Joseph A. Ferrante, Jason Chao* and Robert A. Huggins

Department of Materials Science and Engineering
Stanford University, Stanford, CA 94305

** Electric Power Research Institute*
Palo Alto, CA 94303

ABSTRACT

This paper reports calorimetric experiments related to the energy breakeven issue during heavy water electrolysis using a Pd cathode in thermodynamically closed cells. A comparison with light water electrolysis under the same conditions is also given. Excess power has been observed in a number of cases in which the overall energy balance becomes positive after a short period, leading to the generation of significant amounts of excess energy. In one case, excess power was maintained over a period of ten days, and produced over 23 MJ of excess energy per mole of palladium.

INTRODUCTION

Since the announcement of Martin Fleischmann and Stanley Pons, and the publication of their related preliminary note [1], which reported the production of excess heat during the insertion of deuterium into palladium electrochemically, a number of laboratories have also claimed to have measured substantial rates of excess heat generation.

Nevertheless, there has been the persistent question whether the excess heat generation that has been observed might be related to some type of (perhaps chemical) energy storage mechanism, such that the magnitude of energy that had been produced in this way would be limited to an amount that had been somehow previously invested in the system.

In order to address this question one has to investigate whether one could operate a cell long enough in the excess power mode to achieve a significant positive energy balance. Our definition of the energy balance in this context is the difference between the energy produced by the system during a certain period of time and the total energy consumed for its operation during that period.

Our prior work was focussed upon the direct comparison of the thermal behaviour of the hydrogen - palladium and deuterium - palladium systems. In four pairs of electrochemical experiments we observed excess power generation in the deuterium - palladium cells but not in the hydrogen - palladium cells [2-4]. Our early experiments were performed in thermodynamically open type cells, where the gases produced by the electrolysis reaction escaped from the system and the electrolyte had to be replenished constantly.

Our more recent work has concentrated on the energy breakeven issue, and all the experiments described in this paper were performed in thermodynamically closed cells, where the gases from the electrolysis process were recombined by a catalyst within the cell. This eliminates the question of a possible uncontrolled contribution to the heat production due to partial recombination in open cells. It also avoids any complications related to the enthalpy carried out of the system by evolved gases. Thus this approach is conceptually less complex, and completely eliminates several of the issues and potential problems that have been raised by some of the critics of previous calorimetric measurements.

As mentioned later, we have also designed a new type of isoperibolic calorimeter that neatly eliminates earlier questions or hypotheses related to that mode of calorimetry. These include the possibility that temperature measurements might not be indicative of the actual experimental steady state power balance because of temperature non-uniformity due to insufficient stirring, differences in the locations of the heat sources and the temperature measurement device, or that calibration was performed under non-representative conditions. A detailed discussion of this new design is presented in another paper [5], and thus will not be included here.

THE ENERGY BALANCE

As stated above, the energy balance can be written as

$$\text{Net Energy} = \text{Energy Produced} - \text{Energy Consumed} \quad (1)$$

The experiments reported here were conducted using isoperibolic calorimetry. This is a two - compartment steady state power balance method in which heat is generated within one compartment, and is conducted through an intermediate thermally - conducting wall into the other compartment, which is maintained at a fixed lower temperature. Under steady state conditions, a temperature distribution is established in which the temperature difference across the thermally - conducting wall between the two compartments transports heat at a rate that just balances the power generated within the first compartment. Thus, measurement of the difference in the temperature of the two compartments ($T_1 - T_2$) provides information about the thermal power generated in the first compartment, P_{therm}, that is passed out as heat flux through the thermally - conducting wall into the second compartment. This can be expressed as

$$\text{Thermal power produced} = P_{therm} = K\ (T_1 - T_2) \quad (2)$$

where K is the calorimeter calibration constant.

The energy produced within an isoperibolic calorimeter system is the time integral of the thermal power, which is evaluated by measurement of the time dependence of the temperature difference between the two compartments, ($T_1 - T_2$).

In an electrochemical cell undergoing electrolysis with an applied voltage E_{appl} producing a current I_{appl} the power consumed is simply the product $E_{appl}\ I_{appl}$. In a thermodynamically open system under steady state conditions one divides the applied power into two terms, one a chemical term related to the thermodynamic properties of the electrolysis reaction, and the other a Joule heating term related to the passage of current across the several impedances in the system. This can be expressed as

$$P_{consumed} = E_{appl}\ I_{appl} = I_{appl}\ E^o + I_{appl}^2 *(Z_c + Z_a + Z_e) \quad (3)$$

The value of E^o is related to the standard Gibbs free energy change per mole ΔG^o of the electrolytic reaction, by

$$E^o = \Delta G^o / 2\ F \quad (4)$$

where F is the Faraday constant. Z_c, Z_a, and Z_e are the impedances at the cathode/electrolyte interface, the anode/electrolyte interface, and in the bulk of the electrolyte, respectively.

On the other hand, in a thermodynamically closed system in which the products of the electrolysis reaction are catalytically recombined within the cell, there is no net power invested in the chemical process, and the chemical term $I_{appl}\ E^o$ is eliminated.

The energy consumed under these steady state conditions is thus simply the time integral of the product $E_{appl}\ I_{appl}$, or of $I_{appl}^2\ (Z_c + Z_a + Z_e)$.

However, in order to determine a proper total energy balance for the whole experiment, we also have to consider several other factors. As a result of the application of the electrical power to the system and the establishment of a new temperature distribution, an investment of sensible energy proportional to the heat capacity of the electrochemical cell and calorimeter is required. Therefore an additional term must be added to the total amount of energy consumed related to the heating of the electrochemical cell and calorimeter up to the temperature of operation. Likewise, any other process that causes a positive change in the cell and calorimeter temperature will consume sensible energy.

There also are additional processes whereby thermal energy is produced when electrolysis takes place upon a palladium cathode. These include the heat of solution when hydrogen or deuterium is inserted into the palladium, and if the concentration is sufficiently high, the enthalpy change related to the α - β phase transformation.

The magnitudes of these effects are relatively small, for example, 9.55 kcal/mole for the α - β transformation in the H-Pd case, and 8.55 kcal/mole in the D-Pd case [6], and they only contribute to the observed behavior when these particular processes are under way. As the diffusion of the guest species into the interior is relatively slow in the time span of a particular measurement, and the rate of this insertion reaction decreases with time (being approximately proportional to $t^{-1/2}$) this contribution to the power production becomes less and less important the longer the cell has been in operation.

If, in addition to these processes, there is some other phenomenon within the system (presumably within the cathode or upon its surface) that produces excess heat, it will provide an extra contribution to the thermal power, and thus to the production term in the energy balance.

$$\text{Net Energy} = \int_{t_1}^{t_2} (K\,(T_1 - T_2)\,dt - \int_{t_1}^{t_2} (I_{appl}\,E_{appl})\,dt \quad (5)$$

EXPERIMENTAL ASPECTS

The electrochemical cell used in these experiments had a Pd cathode and either a Pt or Pd anode. The electrolyte was 0.1 molar LiOD or LiOH, and a dispersed platinum recombination catalyst was present to recombine the produced gases (Figure 1).

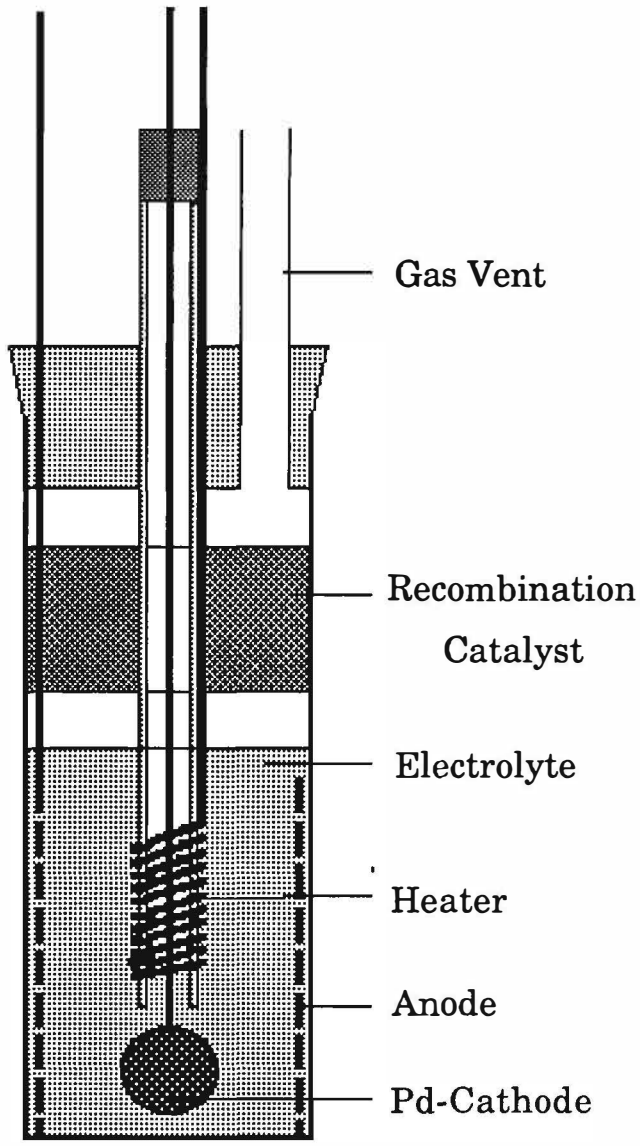

Figure 1. Electrochemical cell.

This cell was mounted inside the concentric cylinder isoperibolic calorimeter described elsewhere [5] that was equipped with three redundant sets of differential thermocouple pairs for the measurement of $(T_1 - T_2)$. The calorimeter was imbedded in a large water bath in order to dissipate the power generated.

The palladium was obtained by arc melting pieces cut from a palladium crucible that contained an appreciable amount of hydrogen, and other possible impurities. In order to get rid of such contaminants, the samples were re-melted at least 10 times, using an arc-melting apparatus with a water cooled tungsten electrode and a water cooled copper hearth, which acted as the other electrode. The environment was argon, and the procedure consisted of first melting some titanium sponge in order to getter species from the argon, such as oxygen, just prior to melting the palladium. After melting the palladium, the argon atmosphere was replaced, and the procedure repeated again. It was quite obvious from the change in the color of the arc during repeated melting that the impurity content of the palladium was gradually being changed. This process was repeated until re-melting caused no further visible change in the arc color.

The resulting palladium, in the form of a distorted sphere, was then mechanically converted into coin - shaped disks 2 - 3 mm thick and roughly 1 cm in diameter, with weights in the range of 2 to 3 grams each. Fine palladium wire was employed to hold the sample and act as the current collector.

The anodes were made either from approximately 2 meters of fine platinum wire or from a spiral length of thin Pd ribbon of equivalant surface area, and were coiled just inside the cell periphery.

Heavy water is a getter for light water, and therefore precautions were taken to prevent contact between the electrolyte and (moist) air or water, both during assembly and operation of the cells. The cell components were stored, as well as assembled and loaded into the cells, inside a dry nitrogen - filled glove box. All cells were connected to a one-way gas bubbler system containing silicone oil to allow the escape of unrecombined oxygen during the charging period without back flow of atmospheric gas.

Questions have been raised about possible errors in calorimetric measurements upon electrochemical cells in which electrolysis is taking place. The key issues have involved the calibration process whereby the value of K is determined, and the comparability of the measurements of T_1 and T_2 during the calibration and during the actual experiments.

Of special concern have been questions such as the influence of the physical locations at which heat is produced and at which the temperatures are measured in the two cases, and the magnitude of the stirring of the electrolyte fluid, which should have some influence upon thermal homogeniety.

In order to avoid these potential problems a new type of isoperibolic calorimeter was designed in which, under steady state conditions, essentially all the heat generated within the electrochemical cell passes to the external environment radially through a pair of concentric heavy aluminum cylinders that are separated by a well - defined thermal conduction layer. As a result, it is not necessary to measure the temperature either inside the electrochemical cell itself, or in a surrounding water bath. Instead, temperature measurements are made inside the two aluminum cylinders. Detailed information about the performance of this new calorimeter design, as well as documentation of the calibration procedure, are the subject of a separate paper [5].

The electrochemical cell, with an outer diameter of about 1.16 inches and a length of 4 inches, was placed into the calorimeter as shown in Figure 2. The inner (T_1) aluminum cylinder is 4 inches long, and the outer (T_2) cylinder is 7 inches long. The inner diameter of the T_1 cylinder is about 1.16 inches, and its outer diameter 2.0 inches. The inner diameter of the T_2 cylinder is 2.25 inches, and its outer diameter is 3.0 inches. Thus the gap across which the heat conduction takes place, and the temperature difference measured, is 0.125 inches.

The general calibration procedure involved the introduction of several levels of electrical power and the measurement of the temperature difference between the two aluminum cylinders (T_1-T_2) in each case. Two different methods were employed in the experiments reported here. One involved the introduction of Joule heat by use of a resistive heater immersed within the cell electrolyte. The second made use of an internal electrolysis method and a three - electrode cell configuration.

The latter method was used in order to simulate the electrolysis process, with its attendent gas evolution and recombination during calibration. A special cell was designed that allowed electrolysis of the heavy water electrolyte at an additional cathode made of Pt wire and of equal surface area to the Pd cathode. This three electrode arrangement is shown in Figure 1. Our results confirmed those of Appleby et al. [7], based on microcalorimeter measurements, that heavy water electrolysis using a Pt cathode does not produce excess power. Therefore, conducting electrolysis with such an electrode within the cell itself serves as a blank and can be used for calibration of the calorimetric system.

This three electrode arrangement has a further advantage. The Pt cathode serves as a collector for impurities in the heavy water electrolyte, and may be especially useful if the calibration procedure is done before starting electrolysis on the Pd cathode.

Observation of the time behavior of the gas evolution through the bubbler system provided confirmation that there was no insertion of deuterium into the Pt, as would be indicated by the evolution of uncombined oxygen. When current was passed through the Pd cathode gas was evolved, and observations showed that the rate decreased with time as the Pd cathode became saturated with deuterium.

Electrolysis was performed under controlled voltage, and all electrical and thermal measurements were monitored using a Macintosh data aquisition system controlled by Lab View software.

In total, eleven samples of palladium were prepared and measured in the way described above, but the results from only three will be reported here. One, designated as P2, was operated in an H_2O, rather than D_2O, electrolyte, and produced no excess energy. A second, P9, was operated in a D_2O electrolyte for 10 days, and produced a large amount of excess energy under quasi - steady state conditions. The third, P11, was prepared in a different way, and demonstrates a substantial "heat burst". The sample history and specific data relating to these are shown in Tables 1-3.

EXPERIMENTAL RESULTS

The time dependence of the energy balance of the cell that contained sample P2 and had a light water electrolyte is shown in Figure 3. It is seen that, after the initial transient period the energy input and output remained essentially balanced over a period of 106 hours.

Sample P9, which was run in the D_2O electrolyte, showed very different behavior, with the production of a large amount of excess energy over a period of 10 days.

Figure 4 shows both the power and energy balances during the early part of the electrolysis. It is seen that there is an initial energy investment or deficit of roughly 500 kJ/mole of Pd during the first hour of operation. This resulted mostly from the energy consumption necessary to heat the cell and calorimeter mass to the equilibrium operating temperature. There are also two other contributions at the start. One is due to the insertion of deuterium into the palladium cathode, which is exothermic, and the other is an endothermic effect due to the loss of

enthalpy in the cell due to the evolution of unrecombined oxygen. This unbalanced oxygen, which amounted to about 100 ml at a D/Pd ratio of 0.6 for this 3.055 gm sample, escaped from the system through the bubbler.

After this initial energy investment, the cell began producing excess power at a low, but gradually increasing rate, and reached energy breakeven after about 13 hours. Thereafter, the energy balance became increasingly positive.

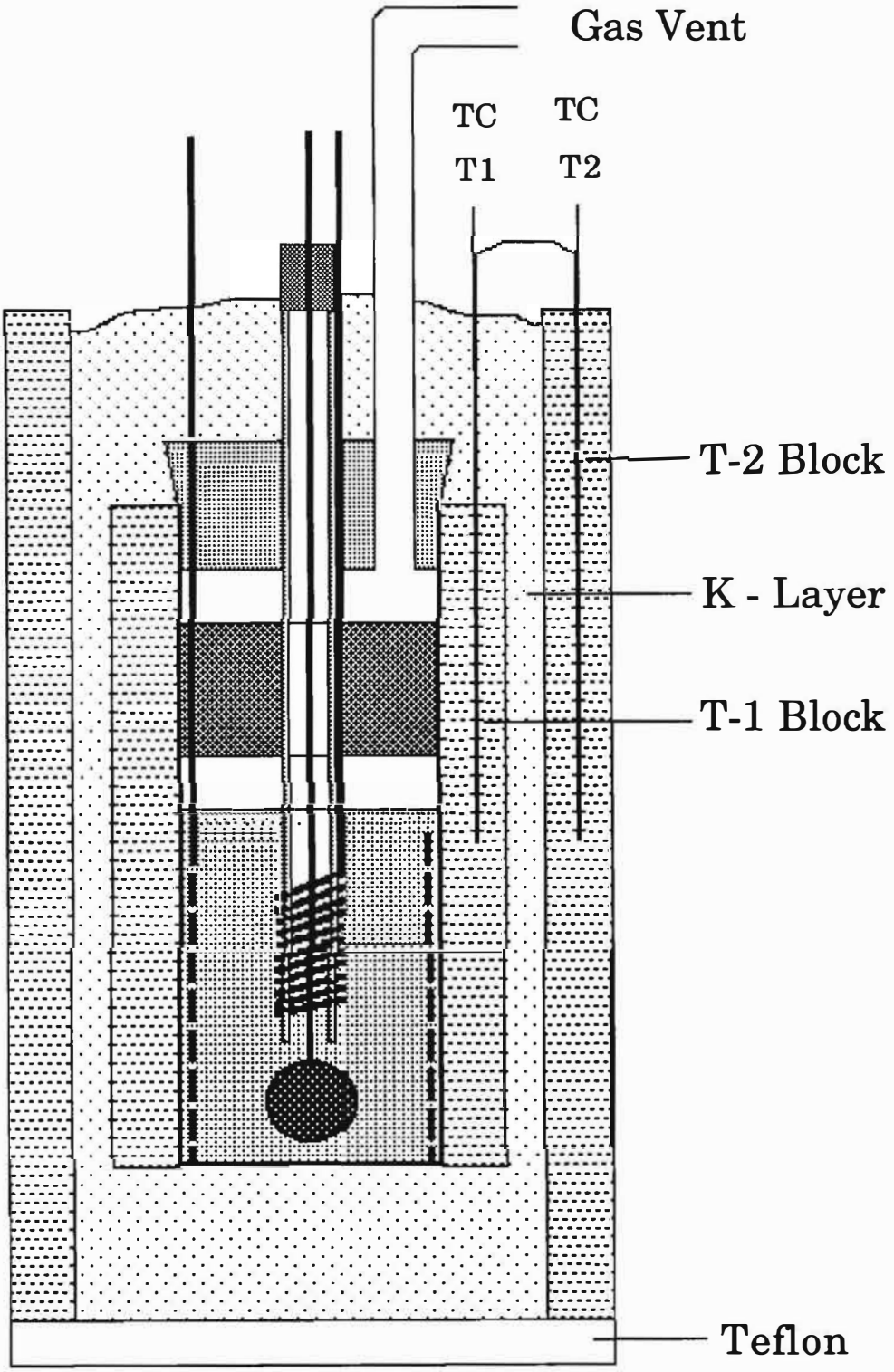

Figure 2. Electrochemical cell mounted in the concentric cylinder calorimeter.

As shown in Figure 5, this cell produced a total of 22.5 MJ/mole of Pd excess energy in a quasi - steady state reaction over the following 10 days. If one compares this total excess energy output to the initial investment of about 0.5 MJ/mole, we see that it indicates a factor of 45 over energy breakeven.

The other sample, P11, was treated in about 1 atm. D_2 gas at 400 °C for several hours and cooled in this D_2 atmosphere to room temperature. It was then inserted into a heavy water electrochemical cell with a Pd anode and a Pt cathode heater and put into the calorimeter. The calibration was done using the Pt

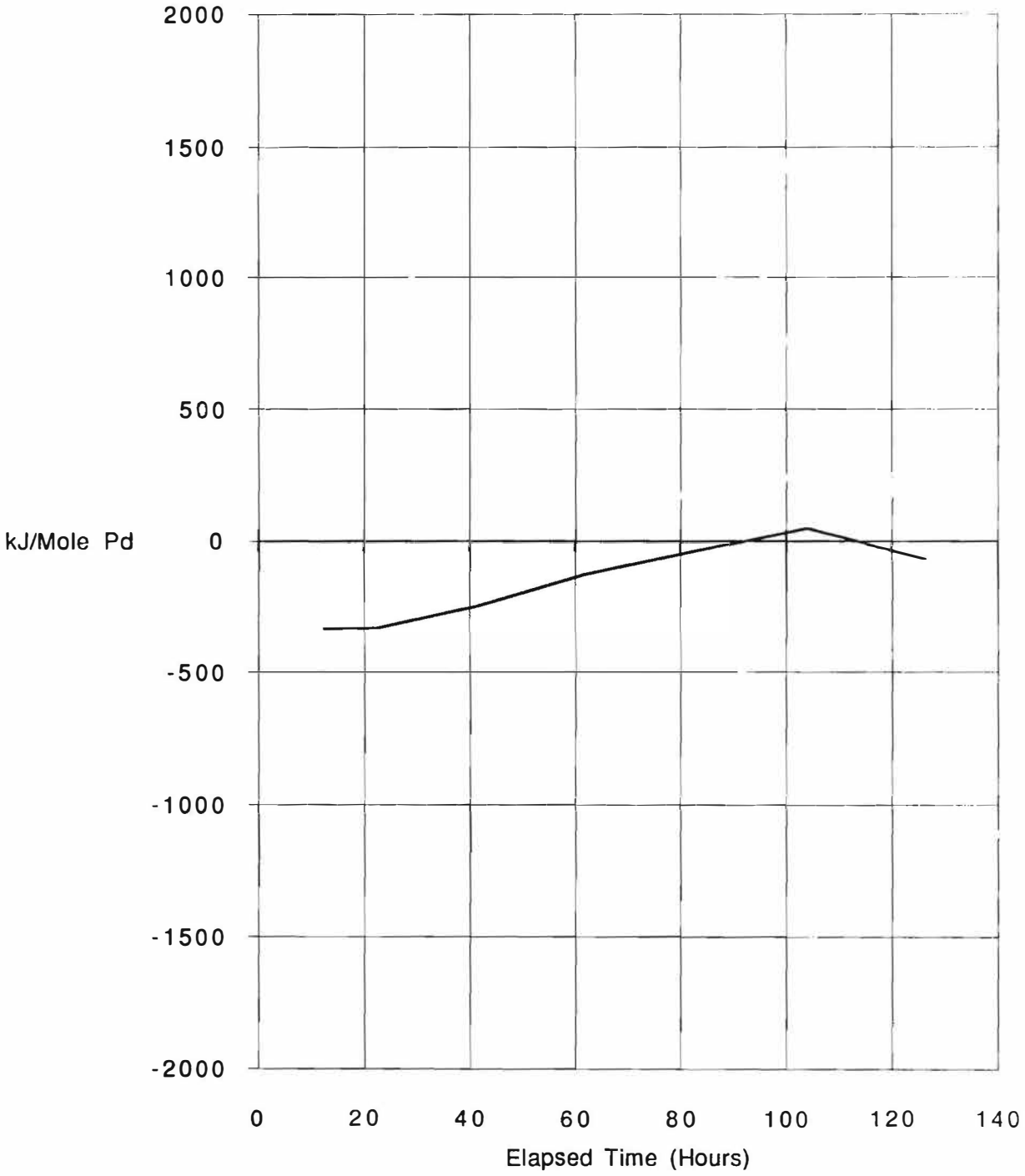

Figure 3. Time dependence of the net energy in a light water cell.

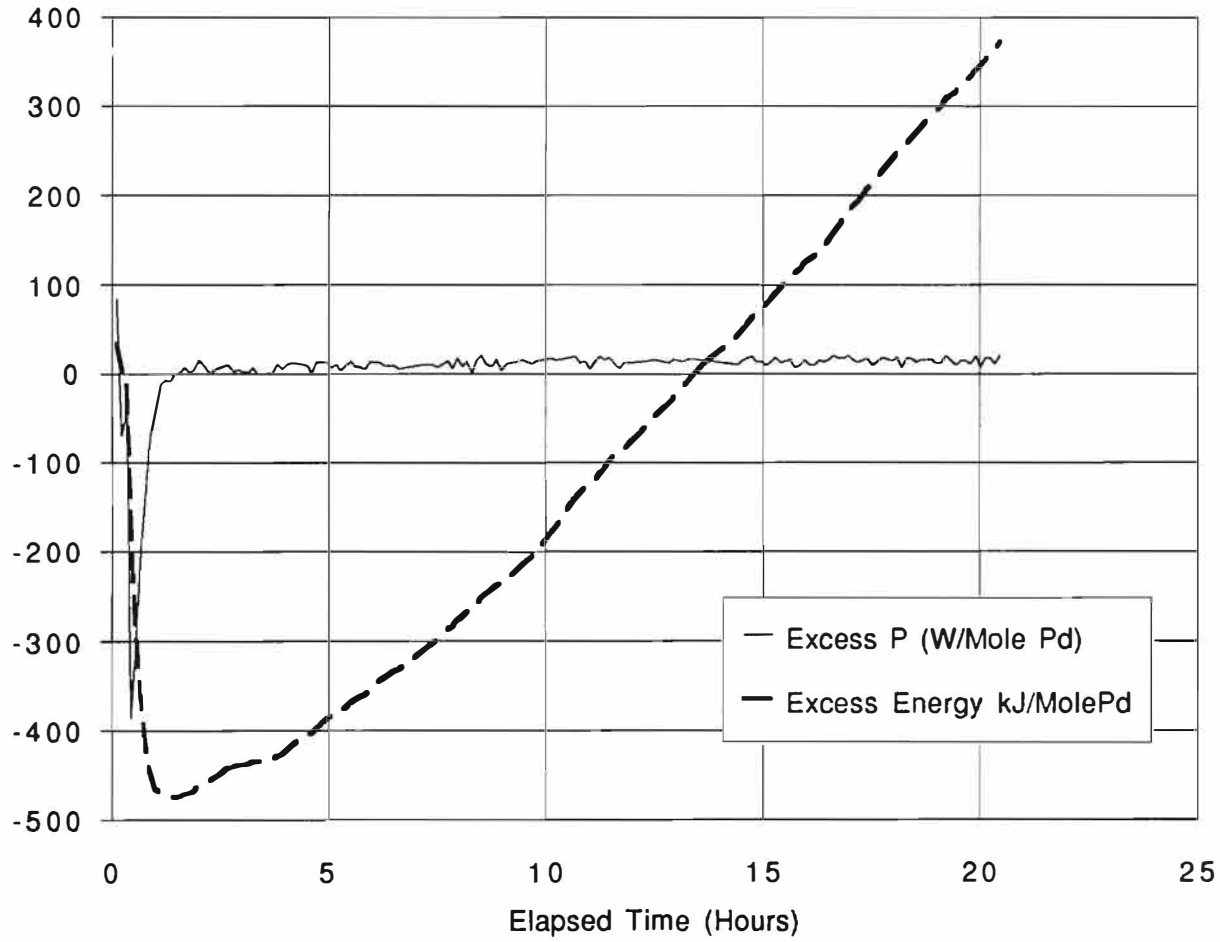

Figure 4. Time dependence of the excess power and net energy for sample P 9 during the early stages of electrolysis.

wire cathode, and was performed during electrolysis on the Pd cathode, so the sample did not sit in the electrolyte without a negative potential applied for any appreciable time.

The energy balance profile of sample P11 is shown in Figure 6. The initial energy investment is similar to that of sample P9, but the level of excess power production was much lower. It took about 17 hours to reach energy breakeven. Somewhat later, after about 18.5 hours of operation, there was a sudden increase in excess power, giving rise to a sharp increase in the slope of the energy balance profile, as shown in Figure 6. This "thermal excursion" is shown in more detail in Figure 7, in which the excess power, as indicated by two sets of differential thermocouples (whose data were so close that they are shown on top of each other), and the applied power are plotted versus the elapsed time.

Also shown is the apparent percent excess power during this period. However, one should not literally believe the time dependence of the excess power shown in this figure as a true measure of what was occurring, because of the thermal mass of the cell and calorimeter system, and the associated sensible heat absorption and time delay.

The magnitudes of these observations are substantial. The cell temperature went through an excursion over a period of about an hour, with a maximum temperature rise of about 7 °C. The apparent excess power rose to over 50 % of the input power. The energy released during this "heat burst" amounted to about 290 kJ/mole or 32 kJ/cm^3 Pd. During the first 9 days of operation P11 produced a total of about 7 MJ/mole Pd excess energy.

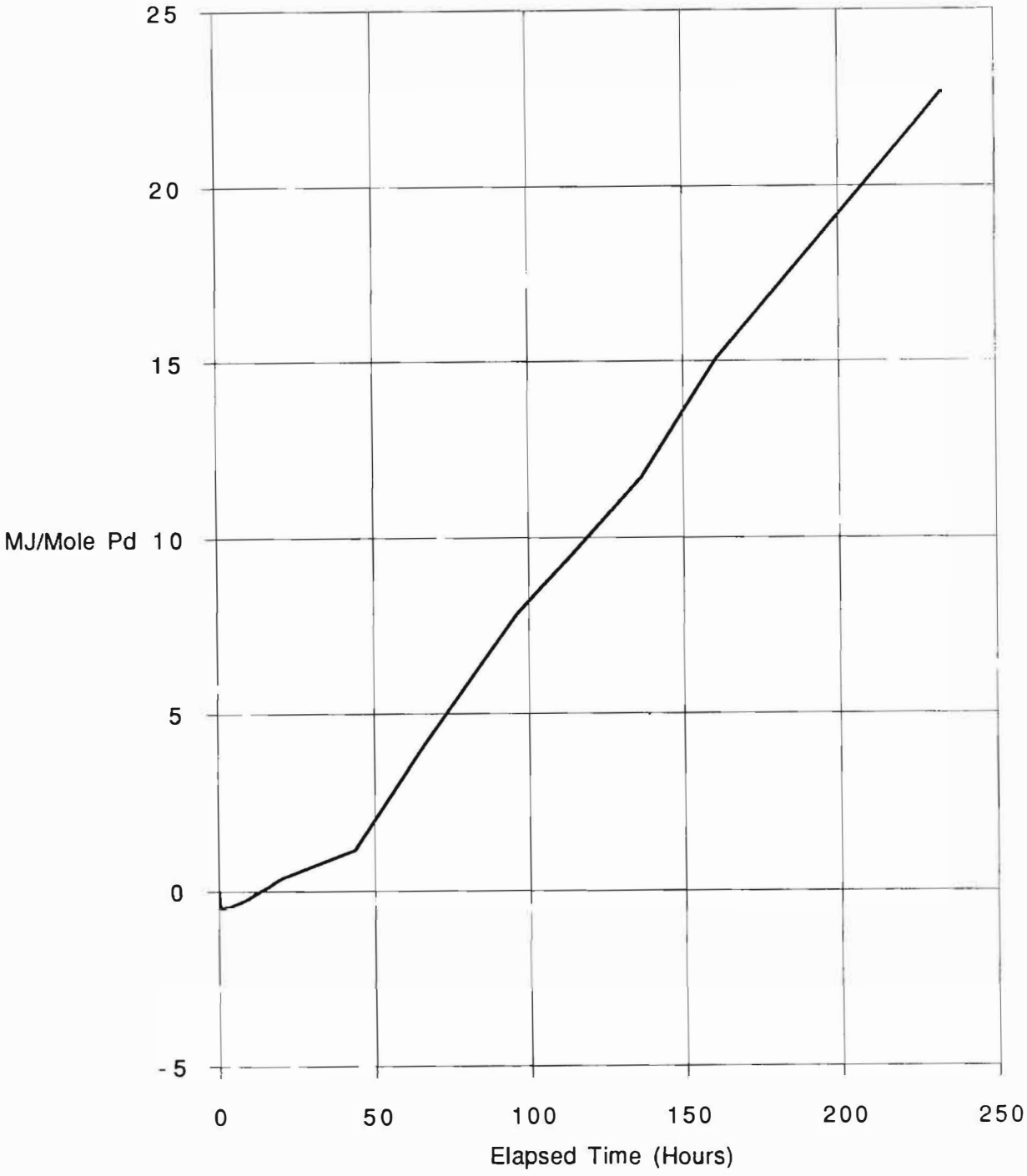

Figure 5. Time dependence of the net energy for sample P 9.

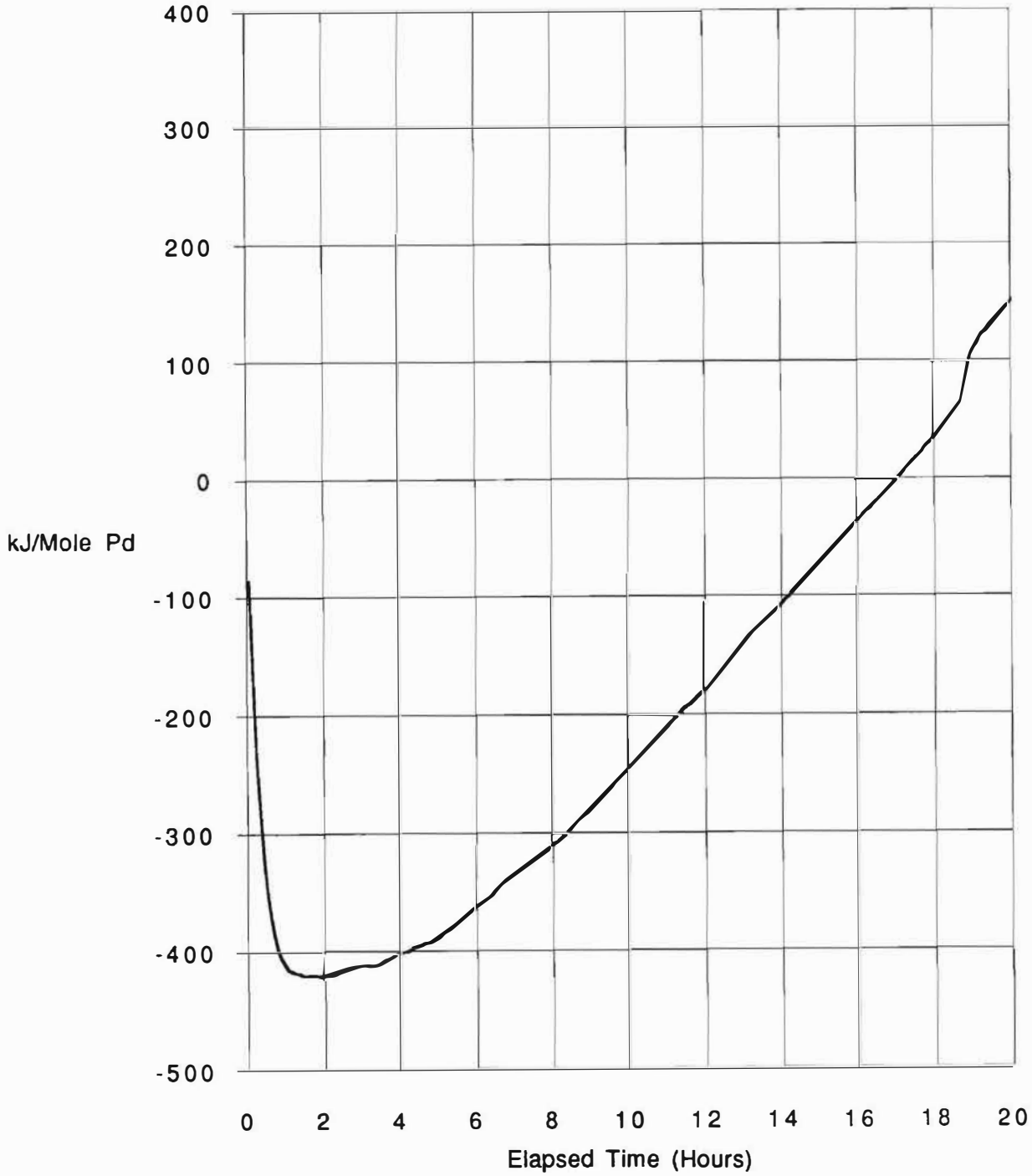

Figure 6. Time dependence of the net energy for sample P 11 during the early stages of electrolysis.

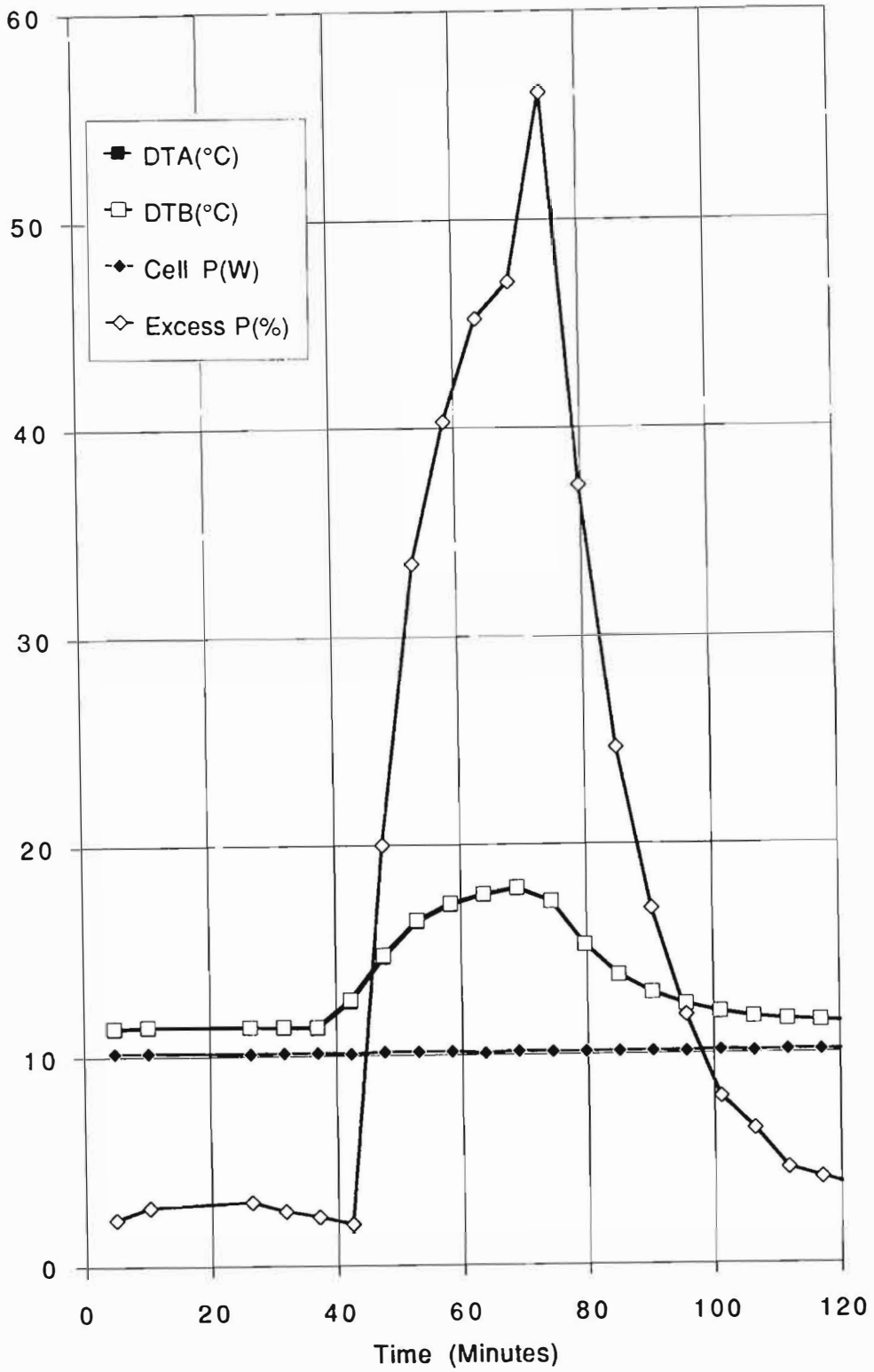

Figure 7. Time dependence of the temperature, applied cell power, and apparent excess power during a thermal excursion in sample P 11.

Table 1

Palladium Sample	P 2
Source	Engelhard*
Processing	Arc Melted in Argon 5-10 Times
Shaping	Deformed by Hammer Blows into "Fat Dime"
Weight	2.39 g
Pretreatment	-
Electrolyte	0.1 molar LiOH (Li2O in H2O)
Anode	Pt - Wire
Anode/Cathode Surface Area	7
Heater for Calibration	Resistive J-Tube Heater
Calibration	Before and During Electrolysis
Operation Mode	Constant Voltage
Cell Current	
Cell Power	2W
Excess Power	-
Excess Energy	-
Duration of Experiment	106 Hours or 4.4 Days

* Crucible used for Hydrogen Permeation Measurements in LiCl-KCl-LiH Molten Salt

Table 2

Palladium Sample	P 9
Source	Engelhard 3.125 mm Wire
Processing	Arc Melted in Argon 5-10 Times
Shaping	Deformed by Hammer Blows into "Fat Dime"
Weight	3.055 g
Pretreatment	Precharged with D electrochemically
Electrolyte	0.1 molar LiOD (Li2O in D2O)
Anode	Pd - Ribbon
Anode/Cathode Surface Area	10
Heater for Calibration	Pt-Wire Electrode (0.01", 24cm)
Calibration	Before and During Electrolysis
Operation Mode	Constant Voltage 14-23 V
Cell Current	1-1.3 A
Cell Power	14,20,23,25,30 W
Excess Power	6 - 7 %
Excess Energy	22,500 kJ/Mole Pd 2,537 kJ/cm3 Pd
Duration of Experiment	240 Hours or 10 Days

Table 3

Palladium Sample	P 11
Source	Engelhard 3.125 mm Wire
Processing	Arc Melted in Argon 5-10 Times
Shaping	Deformed by Hammer Blows into "Fat Dime"
Weight	3.29 g
Pretreatment	Precharged in D2 gas
Electrolyte	0.1 molar LiOD (Li2O in D2O)
Anode	Pd - Ribbon
Anode/Cathode Surface Area	14
Heater for Calibration	Pt-Wire Electrode (0.01",24 cm)
Calibration	During Electrolysis
Operation Mode	Constant Power: 2, 10, 20 Watts
Cell Voltage	10 - 30 V
Excess Power	1-3%, 56% burst (30 min)
Excess Energy	7,200 kJ/Mole Pd
	812 kJ/cm3 Pd
Duration of Experiment	210 Hours or 8.75 Days

SUMMARY AND DISCUSSION

A direct comparison has been made, using careful calorimetric techniques, of the behavior of the light water (H_20) - palladium system and the heavy water (D_2O) - palladium system under conditions in which electrolysis was taking place at high rates and the gases produced were internally recombined within the cell.

Experimental results demonstrate that it is possible to obtain substantial amounts of excess energy production as well as excess power generation in such thermodynamically "closed" electrochemical cells when deuterium is inserted into palladium. Similar experiments with light water and hydrogen insertion do not produce either excess energy or excess power. These conclusions are similar to those reached earlier [2-4] with similar, but thermodynamically "open" cells.

Of equal, or perhaps greater importance, these experiments have also demonstrated that it is possible to generate large amounts of excess energy, far above breakeven, in the deuterium - palladium case.

Our calorimetric measurements give no information about the mechanism causing the generation of this excess power.

One of the major problems in this "cold fusion" area at the present time is the apparent lack of evidence for some product that could verify that there is a process taking place that causes the production of the experimentally observed large values of excess power and energy, and give some guidance concerning its nature. Efforts have been undertaken in many laboratories to look for either radiation products or chemical products.

Because of the limitations of analytical methods, the observation of chemical products is especially difficult. Let us consider two possible examples to illustrate this. For example, if the important reaction were either of the following:

$$D + {}^{6}Li = {}^{7}Li + H \qquad + 5.0\ MeV \qquad (6)$$

$$D + {}^{6}Li = 2\ {}^{4}He \qquad + 22.4\ MeV \qquad (7)$$

one might look for decreases in the amount of ^6Li or enhancements in the amounts of ^7Li or ^4He.

If we recall that 1 MeV is 1.603×10^{-13} Joules, we can calculate the number of events that would have been necessary to produce the 22.5 MJ per mole of excess energy observed from sample P9. In the case of reaction (6) this would require about 2.8×10^{19}

events per mole of Pd, whereas if reaction (7) were relevant, it would require about 6.27×10^{18} events per mole of Pd. If we convert these numbers to events per cm^3 of Pd, we have 3.167×10^{18} events per cm^3 for reaction (6), and 7.066×10^{17} events per cm^3 for reaction (7).

The natural abundance of ^6Li in Li is about 7.5 %, and measurements of the ratio of ^6Li to ^7Li generally have an accuracy of 5 to 10 %, or 0.75 % of the total lithium present. Thus if a sample of palladium had a total lithium concentration of 1 %, or 6.79×10^{20} Li atoms per cm^3, the ^6Li analysis would have an accuracy of about 5.1×10^{18} ^6Li atoms per cm^3.

Compare this with the estimated ^6Li atom concentration in sample P9 if reaction (6) were occurring, of 3.167×10^{18} ^6Li atoms per cm^3. If reaction (7) were occurring, the resulting ^6Li concentration would be 7.066×10^{17} ^6Li atoms per cm^3.

Thus we see that if ^6Li were a major reactant, the detection of a change in its concentration would be quite difficult.

Measurements were undertaken to evaluate the content of ^4He in sample P9, and concentrations well below the values discussed here were found. Therefore, we tentatively conclude that reaction (7) did not play a substantial role in the heat generation process taking place in that case.

ACKNOWLEDGEMENT

The assistance of Dr. Prodyot Roy of the General Electric Co. in acquiring the palladium used in some of our early experiments, and of Dr. Howard Rogers of Hughes Aircraft Co., who provided the recombination catalyst, is gratefully acknowledged. This work was partially supported by the Electric Power Research Institute.

REFERENCES

1. M. Fleischmann and S. Pons, Jour. Electroanal. Chem. 261, 301 (1989).

2. Andreas Belzner, Ulrike Bischler, Steven Crouch-Baker , Turgut M. Gür, George Lucier, Martha Schreiber, and Robert A. Huggins, to be published in the Journal of Fusion Energy

3. Andreas Belzner, Ulrike Bischler, Steven Crouch-Baker , Turgut M. Gür, George Lucier, Martha Schreiber, and Robert A. Huggins, to be published in Solid State Ionics

4. Steven Crouch-Baker , Joseph A. Ferrante, Turgut M. Gür, George Lucier, Martha Schreiber and Robert A. Huggins, to be published in the Proceedings of the NSF-EPRI Workshop on "Anomalous Effects in Deuterated Metals" that was held October 16-18, 1989.

5. Turgut M. Gür, Martha Schreiber, George Lucier, Joseph A. Ferrante, Jason Chao, and Robert A. Huggins, this volume

6. A. Maeland and T.B. Flanagan, Jour. Phys. Chem. 68, 1419 (1964)

7. S. Srinivasan and A. J. Appleby, to be published in the Proceedings of the NSF-EPRI Workshop on "Anomalous Effects in Deuterated Metals" that was held October 16-18, 1989.

QUARTZ CRYSTAL MICROBALANCE STUDY OF PALLADIUM/HYDROGEN INTERACTIONS

Graham T. Cheek* and William E. O'Grady

Code 6170, Chemistry Division
Naval Research Laboratory
4555 Overlook Avenue SW
Washington, DC 20375-5000

*on sabbatical leave from the
United States Naval Academy
Chemistry Department

ABSTRACT

Thin palladium films deposited on quartz have been loaded with hydrogen (deuterium) by electrochemical reduction of 0.1 M LiOH (LiOD) in H_2O (D_2O). Coulometric measurements during both the hydrogen deposition and subsequent removal steps have shown that H:Pd ratios of 0.7 are reached under these conditions, in accord with accepted values for bulk samples. The frequency decrease observed at AT-cut crystals during hydrogen (deuterium) loading is larger than that expected for the mass of hydrogen deposited into the film. Considering that palladium undergoes a substantial increase in volume upon hydrogen uptake, the role of the resulting film stress in influencing the observed frequency must be addressed. It has been found that such film stresses at an AT-cut crystal produce frequency decreases and that these effects can be accounted for using techniques which are well established in the frequency control field. Measurements at BT-cut crystals, the stress/frequency response of which is opposite to that of AT-cut crystals, have confirmed that stress plays a major role in the present work and have allowed the determination of a quantitative value for this stress. Investigations of mixtures of H_2O and D_2O have also been carried out and shed some light on the effect of small amounts of H_2O in determining the H/D content in the palladium.

INTRODUCTION

It has become apparent that the extent of deuterium loading in palladium is important in producing excess heat and other phenomena as discovered by Fleischmann, Pons, and Hawkins [1]. Another interesting effect which is dependent upon loading is superconductivity in palladium/hydrogen systems [2]. With these considerations in mind, we decided to investigate the uptake of hydrogen into palladium by using the electrochemical quartz crystal microbalance. This device has been used in a number of studies to more clearly define mass changes accompanying various electrochemical processes [3,4]. In the present case, we were particularly interested in determining relative extents of H and D loading from mixtures of H_2O and D_2O.

EXPERIMENTAL

Palladium film electrodes were vapor-deposited onto quartz crystals (Valpey-Fisher) as 8.0 mm diameter discs, with thicknesses ranging from 400 nm to 500 nm.

A 5 nm underlayer of chromium was deposited directly onto the quartz to promote good adhesion of the palladium. Both AT-cut and BT-cut 5.00 MHz crystals were used in this work. These quartz discs were clamped between two O-rings into an electrochemical cell (Figure 1). This cell features a Luggin probe for the reference electrode. Electrochemical experiments were carried out in H_2O (0.1 M LiOH) and D_2O (0.1 M LiOD) solutions. Instrumentation consisted of a Wenking Model PCA 72M potentiostat and a PARC Model 175 Universal Programmer for producing voltammograms, and a Philips Model 6674 Universal Frequency Counter for frequency measurements. Keithley 197 multimeters were used for current/potential measurements. A Lotus Measure data acquisition package was used in the IEEE488 mode for obtaining and processing information from these instruments.

RESULTS AND DISCUSSION

Initial studies were directed toward an understanding of the processes occurring upon loading of palladium with hydrogen. This loading was carried out by electrochemical reduction of H_2O at the palladium cathode under potentiostatic conditions. The potential was scanned toward more negative potentials until the current density reached approximately 0.3 mA/cm^2, at which point the potential was held constant. As the loading process began, a decrease in frequency was observed. The current density typically reached a value of 50 $\mu A/cm^2$ at the end of the loading process, which was apparent when the frequency no longer decreased. A subsequent positive-going sweep resulted in the anodic removal of the hydrogen, with a corresponding frequency increase to the initial value. This behavior is illustrated in Figure 2. In this figure, a frequency decrease of 370 Hz was found; however, scaling the results to a film thickness of 400 nm gives a value of 351 Hz. From the Sauerbrey equation [5], one can obtain the sensitivity of the microbalance as 9 ng/Hz. Assuming that the entire frequency shift is due to hydrogen uptake, this approach leads to a H:Pd ratio of approximately 1.4, whereas coulometric measurements on the anodic hydrogen removal indicate a ratio of only 0.7. This latter result is in accord with values obtained at bulk palladium samples [6]. It is evident that an effect other than simple mass loading is at work in the hydrogen uptake process. Considering that palladium undergoes an 11% volume expansion upon loading with hydrogen [7], it is expected that the film, and therefore the underlying crystal, would be subjected to considerable strain as loading occurs. From other work in thin films, this strain involves compressive forces in the film itself, giving rise to tension in the quartz crystal and a resulting frequency decrease for an AT-cut crystal [8]. Using the coulometry data to obtain the mass of deposited hydrogen, the frequency shift due to mass loading can be calculated using the Sauerbrey equation and gives a value of −185 Hz. The remaining 166 Hz decrease is due, then, to the strain effect.

A very important aspect of this work involves the use of BT-cut crystals in assessing the role of film stresses during the loading process. It is known that tension in a BT-cut crystal produces a frequency increase as hydrogen is introduced into the palladium film [8], so that measurements carried out at such crystals can be used to confirm that film stress is an important factor in this process. From the results given above, it is apparent that the mass loading and film stress effects are approximately of the same magnitude, so that one would expect a virtual cancellation in the corresponding frequency shifts at a BT-cut crystal. This is indeed found to be the case, and an overall frequency decrease of 20 Hz is measured for H uptake (400 nm film). The mass loading effect can again be calculated for this case, although the mass sensitivity for the 5.00 MHz BT-cut crystal is lower than that of the 5.00 MHz AT-cut crystal by a factor of 0.654 due to the different shear moduli for the AT and BT cuts [4,9]. The various frequency shifts for H loading into palladium on both AT and BT crystals are summarized in Figure 3.

The amount of stress in the film can be calculated according to a method, developed in the frequency control field, known as the "double resonator" technique [10,11]. This technique involves measurements at both AT and BT-cut crystals, and the interested reader is referred to the original work [10,11] and more recent investigations by the present authors [4] for details of the calculations. Using this approach, an integrated stress value of -3.9×10^5 dyne/cm has been found for H loading into palladium.

Analogous measurements for deuterium loading into palladium have been carried out and are summarized in Figure 4. As with the H system, it is apparent that stress is also very important in determining the frequency response in the D system. The greater mass of deuterium is responsible for the greater decreases in frequency observed for the D case. The integrated stress value for D loading into palladium was calculated to be -2.6×10^5 dyne/cm. It is interesting that this finding is in accord with the fact that the Pd-D force constant for interstitial binding is less than that for the Pd-H force constant [12].

As seen from the frequency shifts reported above, the cases of H and D loading are very readily distinguishable from one another, so that in a "competitive" situation of a solution containing both H_2O and D_2O one can easily determine the relative amounts of H and D loading into palladium. In this manner, it is possible to find the extent to which the presence of H_2O as an impurity in D_2O affects the loading of D. Such an experiment has been carried out at an AT-cut crystal in a solution initially containing D_2O/0.10 M LiOD. As expected, the frequency decrease observed upon D loading is 442 Hz (400 nm film). As H_2O is added, the frequency decrease becomes progressively lower, reaching the value seen for pure H_2O (-351 Hz) at 10 volume percent H_2O. This result indicates that a

significant separation factor is involved, favoring H reduction, as has been observed by other methods [13]. Even at low (1 %) levels of H_2O, the effect is noticeable (approximately 10% of the ultimate effect) by the present technique, indicating the importance of maintaining the purity of D_2O solutions in "cold fusion" investigations.

CONCLUSIONS

By carrying out measurements at both AT- and BT-cut crystals, the roles of mass loading and film stress have been defined for H and D loading into palladium films. A method has been developed for determining the effect of H_2O impurities on deuterium loading by cathodic reduction of D_2O solutions.

ACKNOWLEDGEMENT

We acknowledge the funding of this work through the Office of Naval Research.

REFERENCES

1. M. Fleischmann, S. Pons, and M. Hawkins, J. Electroanal. Chem., 261 (1989) 301; erratum 263 (1989) 187.

2. T. Skoskiewicz, Phys. Status Solidi A 11 (1972) K123.

3. M.R. Deakin and O. Melroy, J. Electroanal. Chem., 239 (1988) 321.

4. G.T. Cheek and W.E. O'Grady, J. Electroanal. Chem., 277 (1990) 341.

5. O. Melroy, K. Kanazawa, J.G. Gordon II and D. Buttry, Langmuir, 2 (1986) 697.

6. M. Hansen, Constitution of Binary Alloys, McGraw-Hill, New York, 1958, pp. 790-793.

7. T.B. Flanagan and W.A. Oates in R. Bau, ed., Transition Metal Hydrides (ACS Advances in Chemistry Series 167), ACS, Washington, DC, 1978, Ch. 20.

8. E.P. EerNisse, Proc. 29th Annual Symposium on Frequency Control, Atlantic City, NJ, 1975, Electronics Industries Association, Washington, DC, 1975, p. 1.

9. K.K. Kanazawa and J.G. Gordon II, Anal. Chem., 57 (1985) 1770.

10. E.P. EerNisse, J. Appl. Phys., 43 (1972) 1330.

11. E.P. EerNisse, J. Appl. Phys., 44 (1973) 4482.

12. A. Rahman, K. Skold, C. Pelizzari and S.K. Sinha, Phys. Rev. B, 14 (1976) 3630.

13. M. Fleischmann and B. Dandapani, J. Electroanal. Chem., 39 (1972) 39.

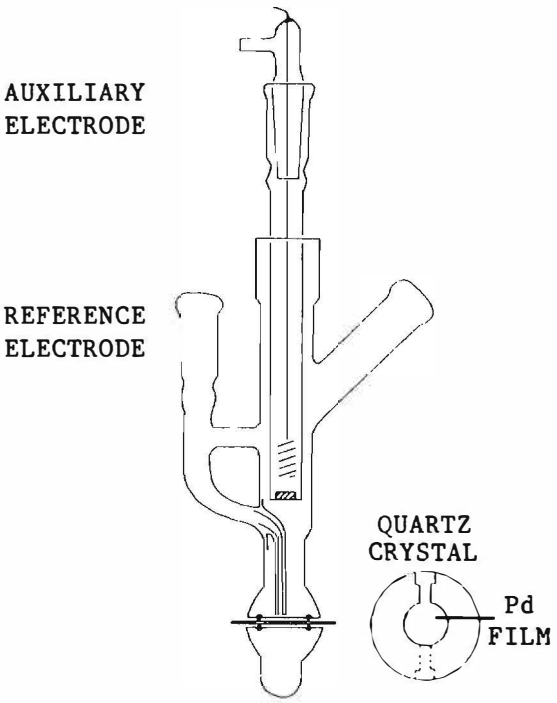

Figure 1. Electrochemical cell used in this work.

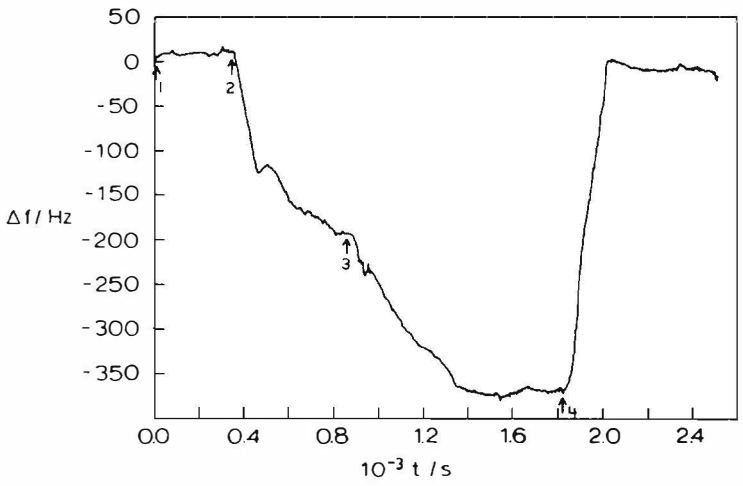

Figure 2. Frequency shift (Hz) vs time (s) for a 367 nm Pd film on an AT-cut crystal (0.10 M $LiOH/H_2O$ solution). The applied potential is indicated by the numbered arrows: (1) 0.00 V; E scanned and held successively at (2) -1.14 V (3) -1.27 V (4) 0.00 V.

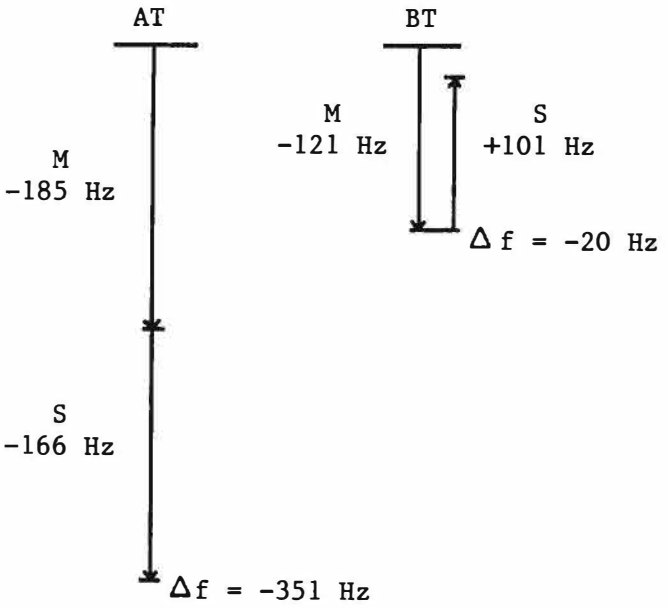

Figure 3. Frequency shifts at 5.00 MHz quartz crystals in 0.10 M $LiOH/H_2O$ solution. Shifts due to stress (S) and mass (M) are indicated on the figure.

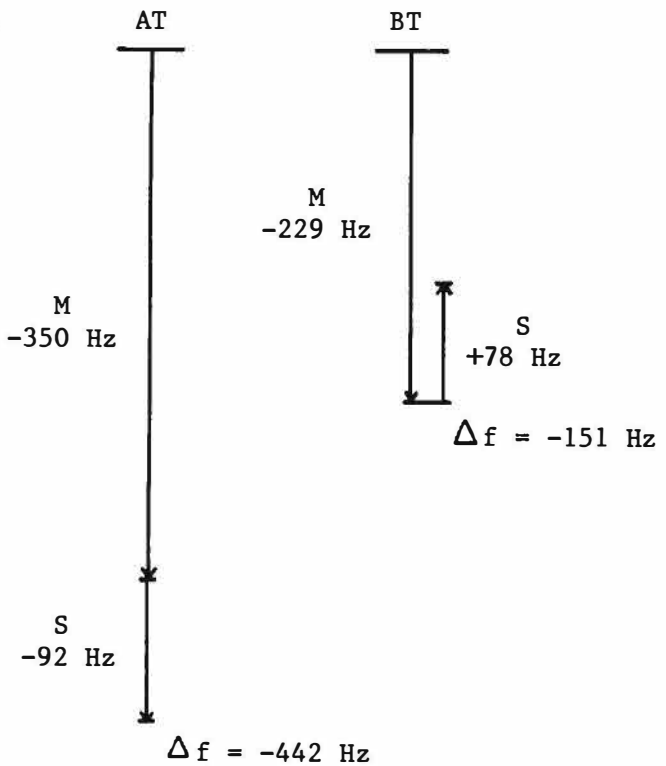

Figure 4. Frequency shifts at 5.00 MHz quartz crystals in 0.10 M $LiOD/D_2O$ solution. Shifts due to stress (S) and mass (M) are indicated on the figure.

OVERVIEW OF BARC STUDIES IN COLD FUSION

P.K. Iyengar
Atomic Energy Commission
CSM Marg, Bombay 400 039, India
and
M. Srinivasan
Neutron Physics Division
Bhabha Atomic Research Centre
Trombay, Bombay 400 085, India

ABSTRACT

A wide variety of experiments have been carried out by twelve independent teams employing both electrolytic and gas phase loading of deuterium in Pd and Ti metals to investigate the phenomenon of cold fusion first reported by Fleischmann and Pons in March 1989. The experiments were primarily devoted to the study of the emission of nuclear particles such as neutrons and tritium, with a view to verify the "nuclear origin" of cold fusion. In 22 different electrolytic experiments whose cathode surface areas ranged from 0.1 to 300 cm^2, large bursts of neutrons and/or tritium were measured. Some of these gave clear evidence that these two nuclear particles were being generated simultaneously. The neutron–to–tritium yield ratios in majority of these experiments was in the range of 10^{-6} to 10^{-9}. The specific neutron and tritium yields expressed per cm^2 of cathode surface area also fitted into a systematic pattern. A unique feature of the BARC electrolysis results is that the first bursts of neutrons and tritium occurred (in 8 out of 11 cells) on the very first day of commencement of electrolysis, when hardly a few amp–hrs of charge had been passed.

In gas phase studies copious neutron emission was observed in a Frascati type absorption/desorption mode experiment with Ti shavings. Presence of tritium in D_2 gas loaded Pd and Ti samples was established through the technique of autoradiography as well as Ti K X–ray counting. In the case of Ti, it was noted that RF heating of samples, in leau of resistance furnace heating, somehow promotes tritium formation. Most recently it was found that $\approx 10^{16}$ atoms of tritium had been "produced" on the top end surface of the central Ti electrode of a deuterium filled Plasma Focus device after it was subjected to $\approx$ 80 charge/discharges shots. All in all the BARC studies have unambiguously confirmed the anomalous production of neutrons and tritium in deuterium loaded Pd and Ti lattices.

1. INTRODUCTION

The announcement in March 1989 by Fleischmann and Pons /1/ of the occurrence of (d–d) fusion reactions (or possibly some other unknown nuclear processes) in Pd metal cathodes electrolytically loaded with deuterium , followed by reports of the observation of "2.45 Mev fusion neutrons" independently by Jones et al during the electrolysis of D_2O, resulted in a frenzy of activity the world over to reproduce these measurements. At Trombay several groups having expertise in various areas such as hydriding of metals, electrochemistry, isotope exchange processes in the upgrading of heavy water, fusion plasma experiments and neutron and tritium measurements devised and set up a variety of electrolytic cells during the early days of April 1989. In a centre such as BARC which has nurtured the development of the heavy water moderated line of reactors in India for over three decades, equipment and expertise for the measurement of neutrons and tritium was readily available. In the initial experiments the emphasis was naturally on the detection of nuclear particles rather than "excess heat" which required intricate calorimetry. The first positive evidence for the emission of neutrons and tritium was obtained on 21st April 1989 and since then several different cells have confirmed these results.

Meanwhile reports from Frascati of the detection of neutrons from pressurized D_2 gas loaded Ti shavings /2/ opened up a second channel of cold fusion investigations. Neutrons / or tritium have since been measured in a variety of D_2 gas loaded Ti and Pd targets at Trombay. A brief summary of the early BARC work /3/ was presented at Karlsruhe in July 1989. Report BARC–1500 issued in December 1989 is a compendium of twenty papers, documenting in an informal style the status of ongoing work, and

covers "BARC Studies in Cold Fusion" over the period April to September 1989 /4/. The experimental papers of this compilation are also being published in Fusion Technology /5/. The present paper is an overview of all the experimental work done at Trombay during the first year of the 'cold fusion era' including new results obtained since the publication of BARC–1500 and summarizes the efforts of about a dozen independent groups comprising over 60 scientists and engineers drawn from different divisions of BARC.

PART A: ELECTROLYTIC STUDIES

2. EXPERIMENTS WITH HIGH CURRENT NaOD ELECTROLYZERS (HWD/N$_t$PD/DD)

2.1 NEUTRON MONITORING

Three different neutron detectors were available for monitoring the neutron yield in these experiments. The first was a bank of three BF_3 counters (each of 25 mm dia x 450 mm length) sensitive mainly to slow neutrons, embedded in a paraffin moderator block. The second was a similar bank of three paraffin encased thermal neutron detectors except that they were of the He^3 type. The third neutron detector was an 80 mm dia x 80 mm high proton recoil type plastic scintillator (NE 102A) sensitive both to fast neutrons as well as high energy gammas. During the electrolysis experiments usually one of the thermal neutron banks and the fast neutron detector were mounted close to the cell while the other thermal neutron bank was located about 1.5 m away to serve as background monitor. The neutron detection efficiency was determined with the help of a calibrated Pu–Be neutron source placed at the cell location and was typically in the region of 0.05% to ~1.5%. In later experiments a personal computer became available to display on line the count rate variations.

2.2 MILTON ROY COMMERCIAL ELECTROLYZER/5/

A diffusion type water electrolyzer using Pd–Ag alloy tubes as cathodes designed to generate ultra pure (oxygen free) hydrogen gas had been procured from the Milton Roy company of Ireland, sometime in 1988 for the purpose of generating D_2 gas for use in Plasma Focus experiments. Thus it so happened that when news of the cold fusion phenomenon reached Trombay in March 1989, this cold fusion cell was all set to be switched on with D_2O as electrolyte. 5M NaOD in D_2O was selected as the electrolyte based on the recommendation of the suppliers of the Milton Roy cell. A schematic view of this cell is shown in Fig.1. The outer nickel body along with a central Ni pipe serve as coaxial anodes. The cathode comprises of 16 numbers of specially activated Pd–Ag alloy membrane tubes having a total surface area of 300 cm^2.. These tubes are sealed at the top and open at the bottom into a plenum through which the D_2 (or H_2) gas is drawn.

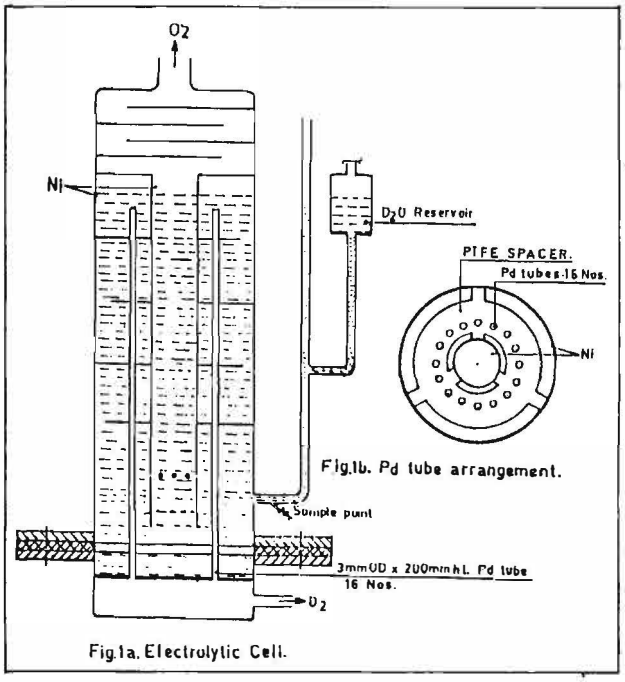

Fig.1 Schematic View of Milton–Roy Commercial Electrolyzer

D_2O of >99.75% isotopic purity, containing ~0.075 nCi/ml (or ≃2.8 Bq/ml) of tritium and moisture free Na were employed for preparing the NaOD electrolyte. The electrolyzer can be operated upto a current level of 100 amps corresponding to a current density of ~330 mA/cm^2, although for continuous operations only 60 amps is recommended in order to avoid overheating.

Run No.1 (21st April 1989)

The cell was initially operated for about 48 hours with 20% NaOH in ordinary water. It was later flushed with D_2O and filled with 20% NaOD solution in D_2O prior to commencement of electrolysis on 21st April 1989. Following brief operation at 30 amps, the current was slowly raised to 60 amps. After about 3 hours at this current level both the neutron detectors viewing the cell started showing counts well above background values. At this time the current was raised further and this resulted in a number of distinct neutron peaks appearing in both neutron detector channels (See Fig.2). The experiment was

terminated when the cell current increased on its own to over 120 amps at the time of the last peak, resulting in the power supply getting damaged. The total number of neutrons generated during the four hour duration of this run is estimated to have been ~4 x 10^7.

the large burst of 21st April.

Electrolysis commenced on 12th June at a current level of ~60 amps. The BF_3 neutron detector bank monitored the cell while the He^3

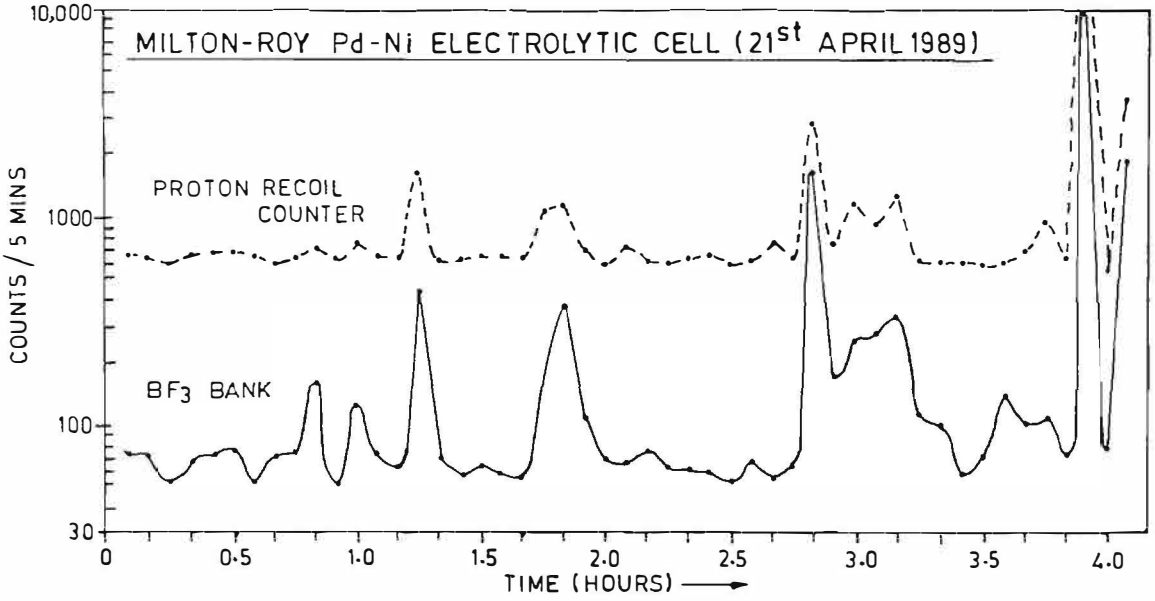

Fig.2 Neutron Counts Variation During Run No. 1 of Milton Roy Cell (21st April 1989)

A sample of the electrolyte drawn after the run, indicated a tritium content of ~1.5μCi/ml (55.5 KBq/ml), an increase by a factor of ~20,000 in comparison to the tritium content of the initial stock heavy water. Taking into account the total volume of the electrolyte (250 ml) as well as the amount of make up D_2O added, it is estimated that an excess of ~8 x 10^{15} atoms of tritium were generated in this run. The corresponding neutron–to–tritium yield ratio works out to be 0.5 x 10^{-8}. This was the first indication to us that the neutron–to–tritium yield ratio in cold fusion experiments is anomalously low.

Run No.2 (12th to 16th June 1989)

A second series of electrolysis runs was carried out with this cell in June 1989 after it was drained and thoroughly flushed with D_2O several times. Prior to this a drain tap with a valve had been welded to the bottom of the cell to enable periodic withdrawal of electrolyte samples. Fresh electrolyte solution prepared with stock D_2O was charged and left in the cell over a weekend. A sample of this electrolyte taken on the following Monday morning gave a high tritium level of ~0.32 nCi/ml (11.8Bq/ml), presumably due to leach out of tritium left over in the cathodes from bank served as background monitor. Except for a few small neutron bursts which were observed within about half an hour of commencement of electrolysis, no neutrons were recorded for the next couple of days, although electrolysis continued until 17.45 hrs of Wednesday 14th June, when the cell was put off. A couple of hours later there was another small neutron burst lasting ~15 minutes. (These small bursts are shown plotted in Fig.1 of the companion paper from BARC /6/.) But on the evening of Friday 16th June, there was a large neutron burst (>10^6 neutrons) lasting for a couple of hours. (see Fig. 3)

The week long experiment was terminated at this point but the electrolyte was left in the cell and the D_2 gas plenum closed leaving the gas at an excess pressure of ~ 1kg/cm^2 above atmospheric pressure. Samples of electrolyte were drawn every day during the week of the experiment and sent for tritium analysis. The sample drawn on 23rd June indicated a high tritium level of 121 nCi/ml (4.5KBq/ml). After a lapse of about a month the tritium level in the electrolyte was found to have further increased to a value of ~460 nCi/ml (17KBq/ml), a four fold increase since the termination of the experiment. Fig.3 shows the variation of tritium concentration

during the entire course of Run No.2. It may be noted that after the large neutron burst the tritium level has shown a thousand fold jump suggesting that tritium is produced at the same time as the neutrons.

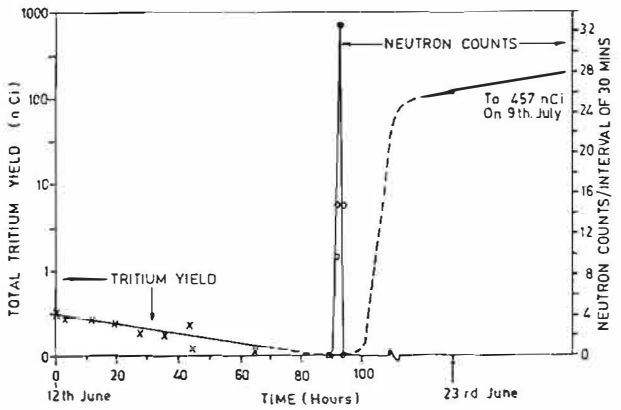

Fig.3 Neutron and Tritium Output During Run No.2 of Milton–Roy Cell

The integrated neutron yield during this experiment was ~0.9 x 10^7 neutrons while the total number of tritium atoms generated was 1.9 x 10^{15}. The corresponding neutron–to–tritium yield ratio is 0.5 x 10^{-8}. This is in remarkably good agreement with the results of the earlier Milton Roy run, although the absolute neutron and tritium yields are lower by a factor of ~5. Thus the Pd–Ag cathode appears to have partly lost its capability to support "cold fusion reactions" after the first run..

2.3 FIVE MODULE CELL WITH DISC ELECTRODES/5/

This modular five unit cell represents our early attempts at obtaining experience with an electrolyzer design which can be scaled up to higher capacities if required. Five cathode discs each of 78 cm^2 area and 1 cm^3 volume are fabricated out of Johnson & Matthey palladium(75%)–silver(25%)–alloy sheets (0.12 mm thickness); the anode plates are made of porous nickel. The individual modules of the cell are clamped together and connected in series. Fig.4 gives a schematic sectional view of the cell. The cell is capable of operating at currents of upto 80 A corresponding to current densities of ~1A/cm^2. Operating electrolyte temperatures close to 100 C are possible as the unit can withstand internal pressures of a few atmospheres.

Two neutron detectors, namely a BF_3 bank and a fast neutron recoil detector, were mounted close to the cell to monitor the neutron output. The system was filled with freshly prepared 20% NaOD in D_2O on 5th May 1989 and electrolysis commenced at a current of 60 to 65 amps (applied voltage was 12.5 V). When the cell had operated for about four hours a big burst of neutrons overlapping two consecutive counting intervals was recorded in both channels. Knowing the neutron detection efficiencies it is estimated that ~5 x 10^6 neutrons were generated during that burst. It was found that the tritium level had jumped by a factor of ~3500 from an initial value of 0.055 nCi/ml (2Bq/ml) to a final post burst value of 190.3 nCi/ml (7KBq/ml). Considering that the total inventory of electrolyte in the system was ~1 liter, this corresponds to an overall excess tritium production of ~190 μCi or 4 x 10^{15} atoms. It must however be emphasized that this does not include the tritium carried away by the electrolytic gas stream which was allowed to escape. Thus an upper bound to the neutron–to–tritium yield ratio in this experime is 1.2 x 10^{-9}.

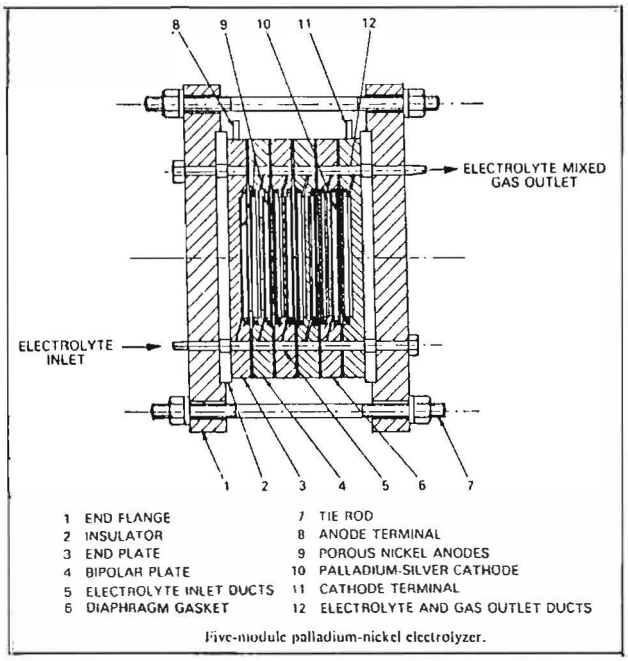

Fig.4 Schematic Sectional View of Five Module Cell With Disc Electrodes

2.4 EXPERIENCE WITH A Ti–SS CELL/5/

A Ti–SS cell was quickly fabricated in April 89 using readily available components in order to obtain some experience with use of Ti as cathode material. A 22 mm dia x 150 mm long rod (surface area = 104 cm^2) of Ti with a flange at the bottom served as cathode. An SS pipe of 40 mm ID served as anode leaving an annular inter

electrode gap of ~9 mm. PTFE gaskets at the bottom ensured coaxial alignment, as well as leak tightness. A vent at the top permitted free escape of electrolytic gases. A second cell of identical design was also fabricated for use as a control cell with H_2O.

5M NaOD in D_2O was used as electrolyte. The current density was ~400 mA/cm^2. The main problem with this cell was the continuous deposition of a dull black coating of iron on the cathode which impaired operation. The electrolytic solution also developed a pale greenish yellow colour. The electrode surface had therefore to be cleaned frequently and fresh electrolyte charged, interrupting electrolysis. On the whole it was a messy operation.

The neutron yield during this experiment was monitored by the bank of 3 He^3 counters embedded in paraffin. The count rate was initially about 240 counts/10s, comparable to the count rates observed during an initial H_2O electrolysis run. After about 3 hours of D_2O electrolysis the count rate increased slowly to ~ 590 counts/10s. Since no big neutron bursts as in the Pd cathode cells were observed it was suspected that this gradual increase in counts could have been due to amplifier drifts, etc. On switching off the cell current it was noted that the count rate came down to ~385 counts/10s, but it did not quite reach the earlier background levels. When the cell was switched on again however the count rate attained levels of about ~590 counts/s once again. Thereafter operation of the cell was terminated and it was confirmed that the count rate decreased to the original background levels when the cell was removed from the vicinity of the neutron detector.. Throughout this experiment the counts of the plastic scintillator channel monitoring the background did not show any significant variation. In all ~ 3 x 10^7 neutrons were generated during this experiment.

A sample of the electrolyte sent for analysis at the end of the experiment indicated tritium activity of ~48 nCi/ml (1.78KBq/ml), a three order of magnitude increase over the initial stock solution value of ~0.05 nCi/ml (1.9 Bq/ml). The net excess tritium produced after correcting for tritium input through make up D_2O addition etc, works out to ~7 μCi or ~1.4 x 10^{14} atoms of T. Admittedly this was not a very clean experiment, but even so one can obtain a very rough value for the neutron–to–tritium yield ratio as ~2 x 10^{-7} for this experiment.

2.5 Pd–Ti PARALLEL PLATE CELL

A simple parallel plate cell with teflon button spacers was fabricated with Pd (0.5 mm thick) and Ti (1 mm thick) plates (40 x 50 mm^2) as electrodes. The inter–electrode gap was ~2 mm. A thin platinum strip was spot welded at the top of the Pd to serve as current feed through. The parallel plate assembly was suspended inside a 300 ml glass bulb having a wide mouth at the top. A vent hole in the stopper permitted escape of electrolytic gases. An advantage of this cell was that either Pd or Ti could be selected as cathode, the other serving as anode.

Electrolysis was commenced on 15th March 1990 with Pd as cathode and 5M NaOD in D_2O as electrolyte. Current density was adjusted to be ~200 mA/cm^2. Three neutron detectors were available for monitoring neutron output, two for viewing the cell and the third for serving as background monitor. Two consecutive neutron bursts occurred about 4 hours after commencement of electrolysis. The background counts was absolutely flat during this run (see Fig.5). It was noted that the Pd cathode had buckled outwards and had become extremely hardened. The buckling can be explained on the basis of differential loading of D_2 across the thickness of the metal.

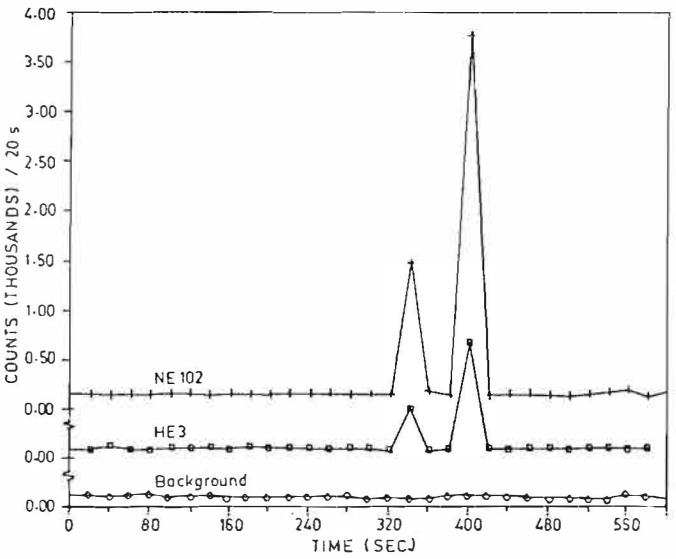

Fig.5 Neutron Burst of Pd–Ti Parellel Plate Cell (15th March 1990)

The Pd cathode was immediately taken for X–ray counting to a low energy NaI detector assembly. Later it was kept overnight in contact with a medical X–ray film for autoradiography. (These techniques are discussed in detail in Ref/5/). However these did not give any evidence

of presence of radioactivity. Samples of the electrolyte taken immediately after the experiment also did not show any significant increase in tritium activity which is indeed very puzzling to the authors. It is possible that the tritium generated had fully escaped along with the electrolytic gases.

3. Pd CATHODE CELLS WITH LiOD ELECTROLYTE

3.1 HOLLOW Pd CYLINDER EXPERIMENT (AnCD)/5/

In this quartz cell the cathode was a hollow Pd cylinder of 1.7 g mass, having a wet surface area of 5.9 cm^2; the anode was a Pt guaze; the electrolyte was 0.1 M LiOD in D_2O (99.87% isotopic purity). To begin with a current of 1 A was used for the electrolysis. After about 30 hours when the temperature attained 60 C, current pulsing between 1 and 2 A at 1 second intervals was adopted. In the absence of a direct neutron detector, this group looked for neutron emission through the 1186 Kev window of the gadolonium capture gamma ray peak. The detector was a 3 x 3 NaI crystal mounted behind a gadolonium compound coated converter plate. After a charge of 17.5 amp–hrs had been passed, the first neutron emission was detected on 21st April 1989. As seen in Fig. 6, in all three distinct neutron bursts of 14

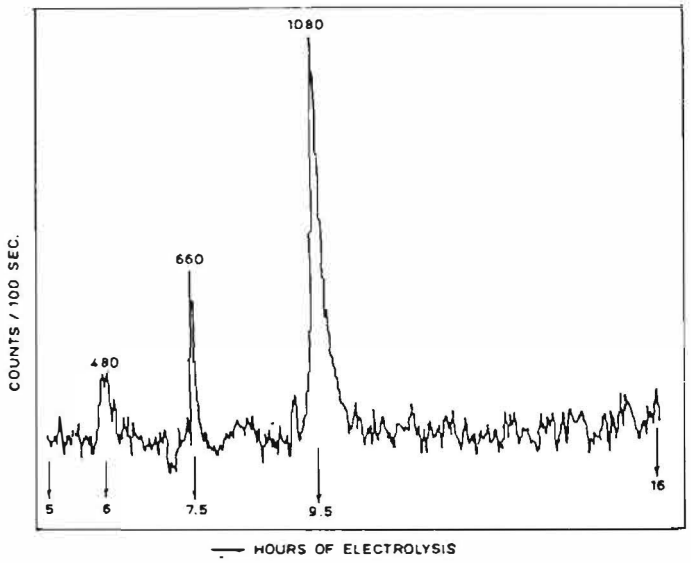

Fig.6 Neutron Yield PDC–I Cell:
1186 Kev Capture gamma Counts

to 20 minutes duration each were produced amounting to an integrated yield of 3 x 10^6 neutrons. Subsequent analysis of a sample of the electrolyte indicated that a total of 3.85 μCi or 7.3 x 10^{13} atoms of tritium had been generated in this experiment. This corresponds to a neutron–to–tritium yield ratio of 4 x 10^{-8}.

3.2 Pd CUBE EXPERIMENT (ROMG)/5/

In this experiment the cathode was a 1 cm^3 of Pd and anode a Pt wire gauze formed into a cylinder surrounding the cube. The electrolyte was 0.1 M LiOD in D_2O. The electrolytic gases were recombined using a Pd catalyst; excess D_2 was converted into D_2O using hot copper oxide. Although the main objective of these experiments was measurement of excess heat, in this paper only the neutron and tritium results are reported.

The neutron yield was monitored by means of a paraffin encased BF_3 counter mounted immediately underneath the table where the cell was located. A second BF_3 detector placed about a metre away monitored background neutrons. The cell electrolyte as well as the D_2O collected in the various cold traps in the system were periodically sampled for tritium measurements. Electrolysis was carried out at a current of ~0.6 amps. After about 24 hrs when ~14.7 amp–hrs of charge had been passed, bursts of neutrons began to be observed. In all 17 neutron bursts lasting from 2 mins to 55 mins each were recorded. The neutron yield in the bursts varied from 5 x 10^3 (2 min burst) to 5 x 10^5 (8 min burst). Altogether a total of 1.4 x 10^6 neutrons was estimated to have been generated. Thereafter there were no more neutron bursts although the electrolysis continued for a further period of seven weeks (a total of 1365 amp–hrs).

A detailed accounting of tritium distributed in various constituents such as electrolyte, vapour condensate recovered from recombined gases, gases extracted from Pd electrode etc was carried out by this group. It was concluded that in all about 35 nCi or 6.7 x 10^{11} atoms of excess tritium was produced in this experiment. This corresponds to a gross neutron–to–tritium yield ratio of 1.7 x 10^{-6}.

3.3 CYLINDRICAL Pd PELLET EXPERIMENT (ROMG)/7/

Here the cathode was a cylindrical Pd pellet 11 mm dia x 11.2 mm height and anode a Pt gauze as before. The concentration of the LiOD electrolyte (120 ml) was increased progressively from 0.1M to ~3M and accordingly the applied voltage decreased, with the current being maintained constant at ~4A. The neutron detection set up was the same as in the previous ROMG experiment. On 13th Feb 1990 when ~3400 amp–hrs had been passed, there was a sharp

burst of 3 x 10^6 neutrons lasting approximately for about 100 s (see Fig.7).

A sample of the electrolyte which was taken the day after this burst, showed a clear eight fold increase in tritium level (64.5 Bq/ml vs preburst value of 7.9 Bq/ml). The tritium level thereafter continuously decreased as shown in Fig.7. But a significant observation was that the rate of decrease was not commensurate with dilution effects caused by make up D_2O addition. The dotted lines commencing from each experimental point in the figure indicates how one would have expected the tritium level to fall if only dilution was playing a role. This implies that additional tritium is continuously entering the electrolyte for many days after the sharp neutron burst. If this is attributed to diffusion of tritium from the inner regions of the pellet, it would support the theory that tritium (and neutron) generation is not restricted to the surface of the cathode alone.

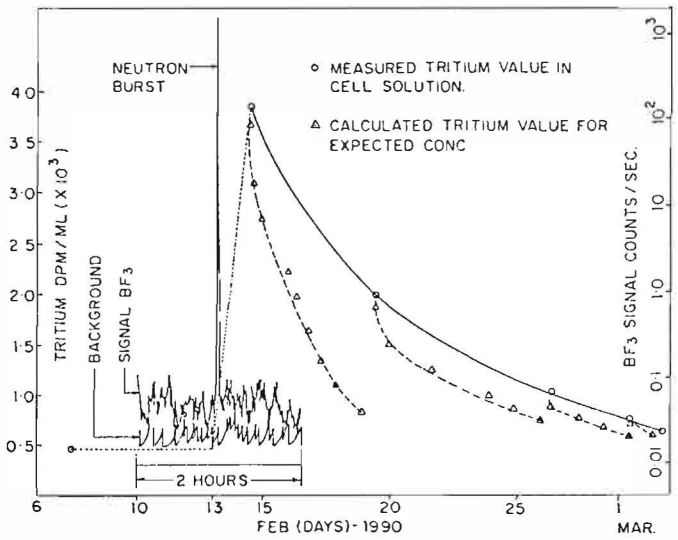

Fig.7. Neutron and Tritium Output of RCS–11 Experiment

After the experiment was terminated following several weeks of electrolysis, the Pd electrode which was found to have developed many cracks on the surface, was degassed at 900 C, and from the volume of D_2 liberated the D/Pd ratio at saturation was deduced to be ~0.85.

3.4 Pd RING AND Pd COIL CELLS WITH NAFION MEMBRANE (ApCD)

In both these experiments the cathodes were thoroughly degassed and vacuum annealed (<10^{-3} mm Hg, 1070 K, ~10 hours) prior to electrolysis. The anode was a cylindrical Pt mesh covering the cathode on all sides. In the first experiment the Pd ring cathode (2.5 cm dia, 1 cm height and 0.1 cm thickness) was charged from both the sides /5/. In the second experiment a thin Pd rod (1 mm dia x 14 cm length) formed into a coil was employed as cathode /8/. In both these experiments the anodes were loosely sandwiched between pairs of Nafion membranes so as to prevent the oxygen evolved at the anode to diffuse back to the cathode surface. The electrolyte (0.1M LiOD in D_2O of 99.86% isotopic purity) was circulated through the quartz electrolytic cell to reduce the dissolved oxygen level further. A saturated calomel electrode dipping in the electrolyte was used to monitor the cathode potential. The cell was operated at a relatively low current density of ~60 mA/cm^2.

Neutron detection was carried out by means of a well type counter containing 24 He^3 detectors embedded in an annular block of paraffin. The test cell was located at the centre of this well, giving a neutron detection efficiency of 8.6%. Data acquisition was carried out with the help of a personal computer having multi–scaling mode facility. The counting time per channel was set as 40s. It was ensured that the overall neutron detection system was immune to extraneous influences which could give false counts. The background reference counts was observed to be steady at ~1.6 cps for about 10 days before start of experiments.

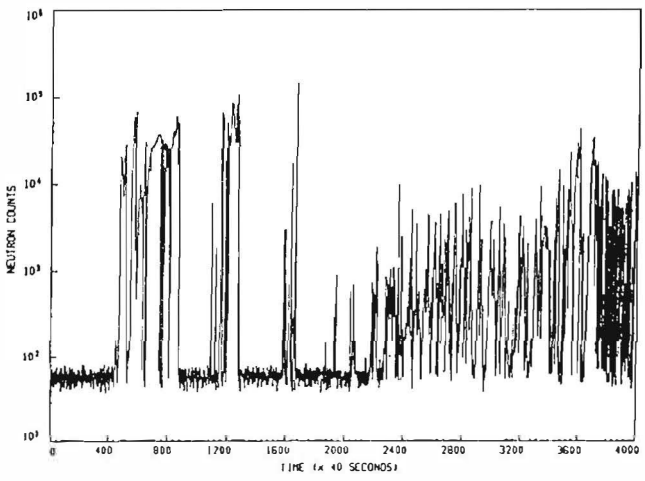

Fig.8 Neutron Bursts of Pd Ring Cathode Experiment of ApCD

The ring cathode electrolysis experiment was run for 32 days commencing from 6th of July 1989. Between the 14th and 17th days from start of electrolysis copious emission of neutrons in the form of bursts was recorded. Otherwise the count

rate remained close to background levels for the rest of the period. Fig. 8 depicts the neutron counts variation over the entire 44 hour (4000 x 40s) duration, while Fig 9 gives an expanded view of a part of the same data. The log scale of the counts axis should be noted, indicating that the bursts were indeed intense, the peak neutron emission rate being ~1000 times background levels. The total neutron emission over the 40 hour neutron active phase was 1.8×10^8 neutrons. It is interesting to note however that even during an intense phase of neutron production the count rate suddenly dropped to near background levels and remained so for several seconds before abruptly climbing back to levels over a 100 times the background value.

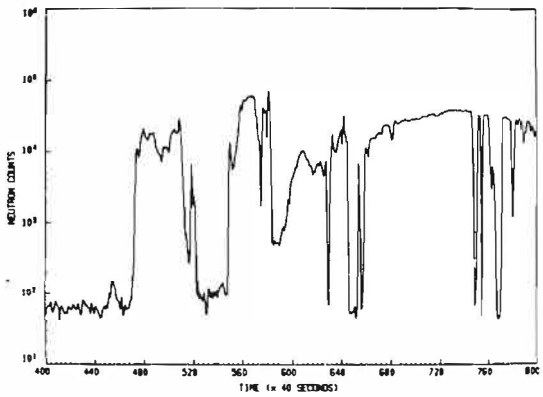

Fig.9 Expanded View of Portion of Fig.8

The electrolyte was sampled once in 6 days during the experiment and analyzed for tritium content using standard liquid scintillation techniques. After the neutron active phase, the tritium level of the electrolyte showed an increase from 0.4 to 1.3 Bq/ml. The cell electrolyte volume being 250 ml, this corresponds to an excess tritium generation of 1.8×10^{11} atoms. This does not include the tritium carried away by the gas stream. Degassing of the Pd cathode at 680 K and reformation of water over hot CuO turnings yielded an additional 3×10^9 tritium atoms only. Thus an upper limit to the overall neutron–to–tritium yield ratio in this experiment works out to $\sim 10^{-3}$.

The electrolysis experiment with the Pd coil cathode was carried out for 24 days. The electrolyte was 0.05M Li_2SO_4. Neutron emission started within 4 hours of commencement of electrolysis and lasted for a total period of 15 hrs spread over the first five days of the electrolysis. The integrated neutron yield was 5.8×10^6 while the tritium yield at the end of the experiment amounted to 1.8×10^{10} atoms. The neutron–to–tritium yield ratio in this experiment works out to be 3.2×10^{-4}.

It is significant that the neutron to tritium yield ratios of 10^{-3} to 10^{-4} observed in both these experiments are several orders of magnitude larger than the values of 10^{-6} to 10^{-8} obtained in all the previous cells. One possible explanation could be that the employment of Nafion membrane in conjunction with the very low levels of dissolved oxygen in these cells might have been responsible for preventing recombination of T back into DTO and instead have allowed most of the T to escape along with the gas stream. As noted earlier the tritium carried away by the gas stream was not measured in this experiment also.

4. SUMMARY OF ELECTROLYSIS EXPERIMENTS WITH NEUTRON AND TRITIUM GENERATION

Table I presents a summary of the successful electrolysis experiments conducted so far at Trombay wherein significant amounts of both neutron and tritium production has been observed. Also included (last column of Table I) for comparison and completeness are the results of an experiment /9/ conducted at the Indira Gandhi Centre for Atomic Research (IGCAR) in Kalpakkam, Tamil Nadu, a sister Institution of BARC. The main conclusions to emerge out of these results are discussed later.

5. OTHER TRITIUM PRODUCING CELLS / EXPERIMENTS

Besides the above electrolysis experiments wherein both tritium and neutron production has been observed, there have been an additional 11 cells / experiments wherein clear evidence for excess tritium generation has been obtained. Majority of these experiments were carried out in the various divisions belonging to the "Chemical Group " of BARC. Table II summarises these results. In most of these experiments neutron yield, if any, was not monitored due to non–availability of detectors with the groups concerned. In the few cases where neutron detectors were present the increase in count rates if any was not significant enough within the statistics of the background count rate variations. Some of the cells of Table II were of closed type wherein the electrolytic gases were recombined by means of a suitable catalyst.

The MR(Jr) cell was a smaller version of the Milton Roy cell with 6 Pd–Ag alloy tubes. This cell has earlier been used for routine H_2 generation for several years at the Chemistry

TABLE I: SUMMARY OF ELECTROLYSIS EXPERIMENTS WITH NEUTRON AND TRITIUM GENERATION

Sr. No.	#1	#2	#3	#4	#5	#6	#7	#8	#9	#10	#11
Division	DD/ HWD NtPD	NtPD/ HWD	NtPD/ HWD	DD/ HWD NtPD	HWD/ NtPD	AnCD	ROMG	ROMG	ApCD	ApCD	IGCAR
Cell (Name)	Ti–SS	MR–1	MR–2	5 Module	Par. Plate	PDC–I	RCS–11	RCS–19	Nafion–1	Nafion–2	RCP–II
Date	1989 21 May	1989 21 April	1989 12–16 Jun	1989 5 May	1990 15 March	1989 21 April	1989 June–Aug.	1990 Jan.–Apr.	1989 July	1990 Feb.	1989 Dec.
Cathode:											
Material	Ti	Pd–Ag	Pd–Ag	Pd–Ag	Pd	Pd	Pd	Pd	Pd	Pd	Pd
Geometry	Rod	Tubes	Tubes	Discs (5)	Plate	Hollow Cyl.	Cube	Pellet	Ring	Coil	Button
Dimensions (in mm)	22 ϕ x 150 long	← 3 o.d. x → 200 ht		115 ϕ x 0.1 thk	40 x 50 x 1 thk	–	1 cm^3	11 ϕ x 11.2 ht.	25ϕ x 10 ht x 1 thk.	1 ϕ x 140 long	–
Area (Cm^2)	104	300	300	78	20	5.9	6	5.7	18	4.4	8
Anode	S.S. Pipe	Ni–Pipes	Ni–Pipes	Porous–Ni	Ti Plate	Pt Mesh	Pt Mesh	Pt Mesh	Pt Mesh	Pt Mesh	Pt Mesh
Electrolyte	NaOD (5M)	NaOD (5M)	NaOD (5M)	NaOD (5M)	NaOD (5M)	LiOD (0.1 M)	LiOD (0.1 M)	LiOD (0.1 M)	LiOD (0.1 M)	Li_2SO_4 (.05 M)	LiOD (0.1 M)
Volume (ml)	135	250	250	1000	300	45	150	120	250	140	–
Current Density (mA/ cm^2)	$\leq$400	~300	~300	~800	~200	$\leq$340	~100	~700	~60	~50	<100
Switching On:											
Charge ($\frac{A-hrs}{cm^2}$)	1.2	0.6	–	3.2	0.8	3.0	2.5	650	34	0.15	36.7
Time (hrs)	3	5	0.5	4	4	9	24	930	330	3	300
Active Life	Few hrs	~3.5 hrs	~2 hrs	$\leq$3 mins	<1 min	~5 hrs	~5 d	~100 sec	~40 hrs.	~5 d	8 hrs
Neutron Yield:											
No. of Bursts	Continuum	9	1	1	1	3	17	1	Many	Many	2
Total	$3x10^7$	$4x10^7$	$.9x10^7$	$5x10^6$	$1x10^6$	$3x10^6$	$1.4x10^6$	$3x10^6$	$1.8x10^8$	$5.8x10^6$	$2.4x10^6$
n/ cm^2	$2.9x10^5$	$1.7x10^5$	$1.3x10^4$	$1.3x10^4$	$5x10^4$	$5x10^5$	$2.3x10^5$	$5.2x10^5$	10^7	$1.3x10^6$	$3x10^5$
Tritium Yield:											
Total (Bq)	$2.6x10^5$	$1.5x10^7$	$3.8x10^6$	$7x10^6$	–	$1.42x10^5$	$1.3x10^3$	$7.7x10^3$	325	32.5	$6.3x10^3$
Total (Atom)	$1.4x10^{14}$	$8x10^{15}$	$1.9x10^{15}$	$4x10^{15}$	–	$7.2x10^{13}$	$6.7x10^{11}$	$4x10^{12}$	$1.8x10^{11}$	$1.8x10^{10}$	$3.5x10^{12}$
t/ cm^2	$1.3x10^{12}$	$2.7x10^{13}$	$6x10^{12}$	10^{13}	–	$1.2x10^{13}$	$1.1x10^{11}$	$5.2x10^{13}$	$1x10^{10}$	$4x10^9$	$4.4x10^{11}$
(n/t) Ratio	$2x10^{-7}$	$0.5x10^{-8}$	$0.5x10^{-8}$	$1.2x10^{-9}$	–	$4x10^{-8}$	$1.7x10^{-6}$	10^{-6}	10^{-3}	$3.2x10^{-4}$	$7x10^{-7}$

TABLE II: SUMMARY OF OTHER TRITIUM PRODUCING ELECTROLYTIC EXPERIMENTS

Sr. No.	#1	#2	#3	#4	#5	#6	#7	#8	#9	#10	#11
Division	Heavy Water Divn.		ROMG	Analytical Chemistry Division					Chemistry Division		
Cell (Name)	MR (Jr)–I	MR (Jr)–II	RCS–18	PDX–0	PDC–II	PDC–III	PDC–IV	PDR–I	CD–4	CD–6	CD–5
Date	1989 21 Sept.	1990 5 March	1989 24 Oct.	1989 24 April	1989 10 July	1989 6 Sept.	1989 29 Sept.	1989 9 Nov.	1989 21 July	1989 22 Dec.	1989 24 Oct.
Cathode:											
Material	–Pd–Ag Alloy–		Cold Rolled Pd	Pd	Pd			Pd	Pd ingot	Pd	Pd wire
Geometry	Tubes		Hollow Cyl.	Ring	Hollow Cylinder			Rod	Cylinder	Pellet	Grid
Dimensions (in mm)	3 ϕ x 150 ht		–	2 thk.	–	–	–	4 ϕ x 19 long	8 ϕ x 16 long	4 ϕ x 4 ht.	0.5 ϕ x 800 long
Area (Cm^2)	113		19	14.5	6.37			2.75	0.57	0.126	4
Anode	Ni Pipe		Pt gauze	Pt Discs	Pt Mesh	Pt Mesh	Pt Mesh	Pt Mesh	Pt Coil	Pt Wire	Pt Wire
Electrolyte	NaOD (5M)		LiOD (0.1 M)	LiOD (0.14 M)	LiOD (0.1 M)	LiOD (0.1 M)	LiOD (0.14 M)	LiOD (0.1 M)	LiOD (0.1 M)	LiOD (0.1 M)	KOD (Cone) (Paste)
Volume (ml)	150		150	65	60	100	80	80	28	3	1.5
Open/ Closed	Open		Open	Closed	Open	Open	Closed	Closed	Open	Semiopen	Closed
Current (A)	40		~ 2	$\leq$ 2	1~2 Pulsed	1~3 Pulsed	1~2 Pulsed	0.2~2.2 RF Superposed	100 mA	$\leq$ 35 mA	30 mA
Current Density (mA/cm^2)	350		~105	~160	<350	$\leq$470	<350	<800	~100	~278	7.5
Duration of Electrolysis	12 hrs	30 hrs	13 d	7.4 d	366.2 hrs	183.3 hrs	5.8 d	40 d	190 d	17 d	80 d
Tritium Measurements:											
Initial Concn. (Bq)	1.44	3.33	3.6	2.7	2.81	2.77	2.70	2.68	4.6	2.0	2.5
Maximum Concn. (Bq/ml)	225.7	18.5	–	0.93×10^{4}	5.88×10^{4}	4.6	–	–	72.1	65.0	22.9
Output to Input Ratio	156.7	5.6	3.36	3425	20,925	1.66	2.5	1.91	15.7	32.5	9.16
Net Excess:											
(Bq)	3.3×10^{4}	2.28×10^{3}	2.71×10^{3}	6.02×10^{5}	2.08×10^{6}	2.96×10^{3}	6.29×10^{2}	1.1×10^{3}			
(Atoms)	1.76×10^{18}	1.2×10^{12}	1.44×10^{12}	3.2×10^{14}	1.1×10^{15}	1.56×10^{12}	3.96×10^{11}	5.83×10^{11}	10^{12}	10^{11}	2×10^{10}
t/ cm^2	1.6×10^{11}	1.1×10^{10}	0.8×10^{11}	2.2×10^{13}	1.7×10^{14}	2.4×10^{11}	6.2×10^{10}	2.12×10^{11}	1.8×10^{12}	0.8×10^{12}	0.5×10^{10}

Division. Cell #11 was a very novel cell wherein the electrolyte was KOD in the form of a paste applied on a multiwire grid electrode system made of alternate wires (0.5 mm dia) of Pd and Pt. Although this gave excess tritium of only 2 X 10^{10} atoms (lowest in the Table) it must be noted that the total inventroy of electrolyte in this microcell was hardly 1.5 ml. In Cell #8 (PDR–I) an RF voltage was superposed on the applied DC voltage with a view to ascertain whether this would help improve the tritium production. As seen from the results there is no evidence of any improvement.

The Cells # 5, 6, & 7 used the same hollow Pd cylinder cathode deployed in Cell # 6 of Table I (Expt. PDC–I). As in the case of PDC–I current pulsing was resorted to in these three PDC series of experiments also. On completion of PDC–I the hollow Pd cathode was degassed at 300 C in a vacuum furnace for over 2 hrs. Subsequent electrolysis in 0.1 M LiOD (Expt. PDC–II) terminated in an explosion after a charge of 423 amp–hrs had been passed. Careful measurements of the tritium content indicated that over 2 MBq (1.1 x 10 ^{15} atoms) of excess tritium had been generated during this experiment. (see Table II). This corresponds to an increase in tritium inventory by a factor of more than 20,000 relative to the total tritium input to this experiment.

This same cathode generated tritium two more times after degassing and reuse. (PDC–III & IV). But as seen from Table II in each subsequent run the quantum of tritium generated decreased further. For example in PDC–III while excess tritium recovered was 2.96 KBq, in PDC–IV the excess tritium was only 629 Bq even after 123 amp–hrs of charging. Prior to commencement of PDC–IV the electrode had been heated to 850 C for 4 hrs in vacuum, cooled and again heated to 800 C in D_2 gas atmosphere at 1 cm pressure for 3 hrs followed by degassing again under vacuum for 3 hrs. This very elaborate pretreatment would have cleansed the Pd of any remnant tritium within its interior, confirming that the fresh amount 629 Bq obtained in PDC–IV must have been generated during this run of electrolysis only. But the more important implication of this result is that even vacuum heating–annealing does not appear to have restored the ability of the Pd cathode to support nuclear reactions.

6. REAL TIME NEUTRON DIFFRACTION STUDY OF DEUTERON LOADING IN A Pd CATHODE /11/

Cell #9 (CD–4 of Chemistry Division) was primarily designed for conducting an online neutron diffraction study of the phase changes occurring during the deuteration of a Pd rod. It comprised of a covered pyrex glass beaker with an 8 mm dia x 16 mm long Pd cathode of which 11 mm protruded underneath the cell and was set up in front of one of the neutron beams at the Dhruva research reactor at Trombay. The portion of the Pd rod exposed to atmosphere was given thin protective coating of tin to minimise escape of deuterium. A platinum cell above the cathode served as anode and the electrolyte was 0.1M Li_2O in D_2O. A 0.18 mm thick Nafion membrane between the electrodes helped prevent direct recombination of deuterium and oxygen. Electrolysis was carried out at a steady current of 100 mA extending over a period of more than 8 weeks. Powder diffraction patterns were recorded periodically with the help of a 1 metre wide position sensitive neutron detector mounted so as to provide a 30^0 angular span. With this arrangement the real time development of the (111),(200) and (311) reflections could be studied.

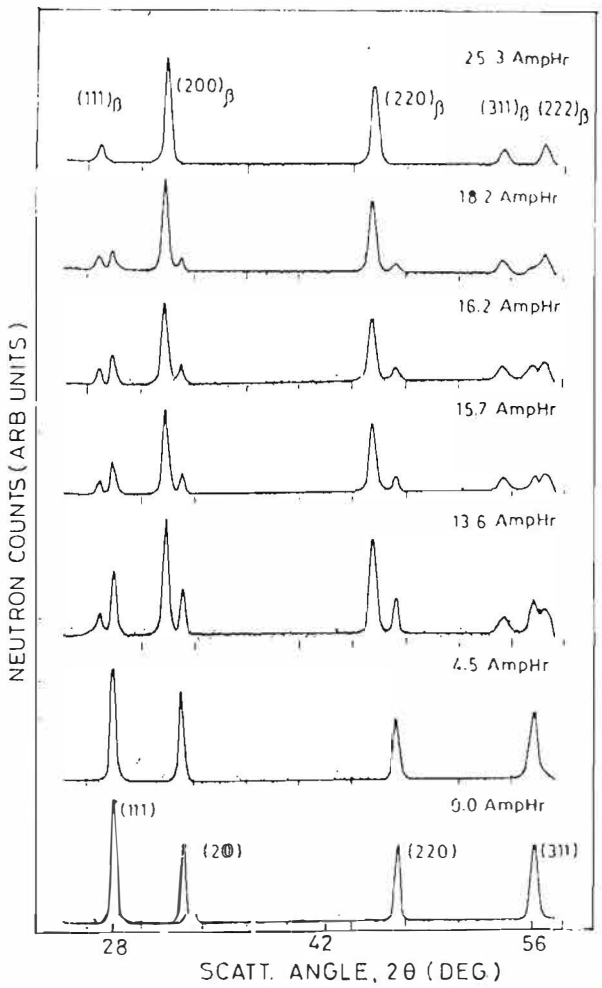

Fig.10 Neutron Diffraction Patterns at Different Deuterium Loadings of Palladium Rod

Fig.10 displays the recorded diffraction patterns at various loading stages measured in terms of amp–hrs of electrolysis. It took an hour's reactor time for each spectrum. The Pd electrode was initially in pure fcc(metallic) form with the lattice constant of 3.89 A^0 characterized by the four peaks corresponding to α phase seen in the bottom most pattern of Fig.10. New peaks indicative of the precipitation of the β phase of the Pd–D system (lattice constant of 4.02 A^0) showed up at around 10 amp–hrs of electrolysis. As electrolysis proceeded the intensity of the β phase peaks built up at the cost of α phase peaks. It was found that within about 25 amp–hrs the upper part of the Pd electrode projecting underneath the cell was completely converted to β phase wherein the lower part required nearly 60 amp–hrs for this. From the ratio of the structure factors of the odd to even reflections (S(111)/S(200)) the stochiometry in the β phase could be deduced. It was summarised from the study that the stochiometry at saturation was $PdD_{0.55}$. The main conclusion of this experiment relevant to cold fusion is that no new phases develop in Pd even after 100 amp–hrs of electrolysis.

PART B: D_2 GAS LOADING EXPERIMENTS

7.1 SEARCH FOR TRITIUM IN GAS LOADED Pd SAMPLES/5/

In these experiments D_2 gas was loaded into Pd samples after thoroughly degassing them and a search was made for the possible production of tritium in the samples. The tritium produced if any along with that in the initially loaded deuterium was extracted through isotopic exchange with distilled light water wherein the Pd sample itself served as a catalyst. From the activity measured in the water the amount of tritium "produced" in the Pd was computed.

D_2 gas was generated by reducing D_2O with Na in vacuum and stored under pressure in an SS dewar with liquid nitrogen cooling, in the presence of activated charcoal. The stock D_2O used had a tritium content of 0.075 nCi/ml (2.8 Bq/ml), corresponding to a (T/D) isotopic ratio of 3 x 10^{-14}. Pd samples either in the form of Pd black powder or Johnson & Matthey Pd–Ag foils were taken in an SS reaction vessel connected to a vacuum system (10^{-5} mm) through a buffer tank of 1 litre volume equipped with a pressure gauge. After degassing and cooling under vacuum, D_2 gas at 1 atm pressure was let into the buffer tank and the system sealed off for equilibration with the Pd contained in the reaction vessel for several hours or days at times. From the pressure drop observed the quantity of gas absorbed in the Pd could be deduced. The deuterated Pd samples were later immersed inside a measured quantity of distilled water for a few hours and the concentration of tritium in the water measured through standard liquid scintillation counting systems. The tritium content in the Pd was deduced therefrom knowing the gram moles of D_2 absorbed in Pd as well as the relevant equilibration constant (K).

TABLE III
TRITIUM PRODUCTION IN D_2 GAS LOADED Pd SAMPLES

Experiment No	#1	#2	#3	#4	#5
Nature of sample	Pd black powder	Pd–Ag foil	Pd–Ag foil	Pd–Ag foil	Pd–Ag foil
Mass (g)	20	0.96	10.9	10.6	0.43
Date of loading	20 June 89	24 Aug 89	19 Sept 89	7 Mar 90	19 Sept 89
Volume of D_2 absorbed (ml)	1325	34.5	518.4	222	20.2
(D/Pd) ratio	63	46	45	20	45
Equilibration time (hrs)	16	16	240	40	240
Water used for extraction (ml)	50	6	50	50	5
Tritium activity of water (bq/ml)	8.1	5.9	8.5	12.5	32.6
T/D ratio in Pd	3.2×10^{-11}	1.1×10^{-11}	$.87\times10^{-11}$	3.4×10^{-11}	8.3×10^{-11}
Absolute tritium activity (bq)	410.7	37.0	429.2	717.8	159.1
Total tritium atoms in Pd	2.31×10^{11}	2.02×10^{10}	2.4×10^{11}	4.1×10^{11}	8.96×10^{10}
Tritium atoms per g of Pd	1.2×10^{10}	2.1×10^{10}	2.2×10^{10}	3.6×10^{10}	20.8×10^{10}

Table III summarizes the results. The tritium activity measured in the distilled water was a small fraction of a nCi/ml (5 to 30 Bq/ml). The total quantity of tritium estimated to have been generated in the Pd foils is in the region of 10^{10} to 10^{11} atoms. It is observed that the (D/Pd) ratios attained following D_2 absorption are approximately similar in all the cases (0.20 to 0.63). The amount of tritium produced per gram of Pd sample varies widely, from ~1.2 to 20.8 x 10^{10} atoms/g. As may be expected the higher value is consistent with the longer duration of equilibration time (240 hours) between D and Pd, but the large Pd foil (column #3) which was also equilibrated for 240 hours has given only 2.2×10^{10} atoms of t/g of Pd. In all cases the finally attained (T/D) ratios which are in the range of .3 x 10^{-11} to 8.3 x 10^{-11} are two to three orders of magnitude higher than that of the initial gas value namely ~ 3 x 10^{-14}. Thus fresh tritium amounting to about 10^{10} or 10^{11} atoms appears to have been created in the Pd, presumably due to "cold fusion" reactions. It is not clear whether the tritium was produced during the absorption process or during the subsequent "curing" or equilibration phase.

The presence of tritium in the Pd–Ag foils has also been independently confirmed through autoradiography. Fig 11 shows the radiograph of a triangular Pd–Ag foil.The image displays some non–uniformity in fogging. It was however observed that the intensity of fogging of these Pd–Ag foils rapidly decreased when attempts were made to reproduce the radiographs on subsequent days, indicating that the tritium retention capability of Pd–Ag is not as good as that of titanium.

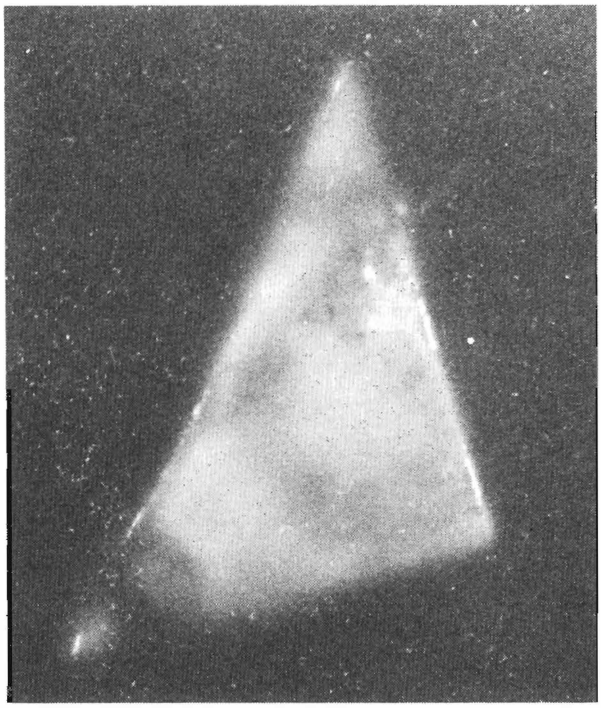

Fig.11 Autoradiograph of Deuterated Triangular Pd–Ag Foil

7.2 FRASCATI TYPE EXPERIMENTS WITH Ti SHAVINGS (CD)/5/

A readily available set up employed earlier for high pressure hydriding studies was used for these experiments/12/. Ti metal pieces cut from a sheet were surface cleaned and subjected to activation treatment prior to loading in the high pressure cell. D_2 gas pressure or temperature was cycled between high and low values using liquid nitrogen. The well type neutron counter employing 24 He^3 detectors embedded in paraffin, along with the associated data acquisition system described in Sec 3.4 was used for the neutron yield measurements. The counting efficiency was determined to be 10%.

In these experiments first conducted in June 1989, Ti pieces were to begin with equilibrated with D_2 gas at 10 atm and 77 K for ~20 minutes. The temperature was then allowed to increase slowly to ambient level, with simultaneous evacuation resulting in desorption of D_2 gas from the Ti shavings. This resulted in large neutron bursts lasting between half an hour to ~2 hours each as shown in Figs. 12a to 12d. Prior to the experiments of Figs 12c & 12d, the D_2 gas pressure and temperature were simultaneously cycled. While the first three measurements were carried out with the same charge of Ti, the last one was done with a fresh charge which could be the reason for the slightly different characteristics of Fig. 12d. The integrated neutron yield in these experiments varied in the range of 10^5 to 10^7 neutrons.

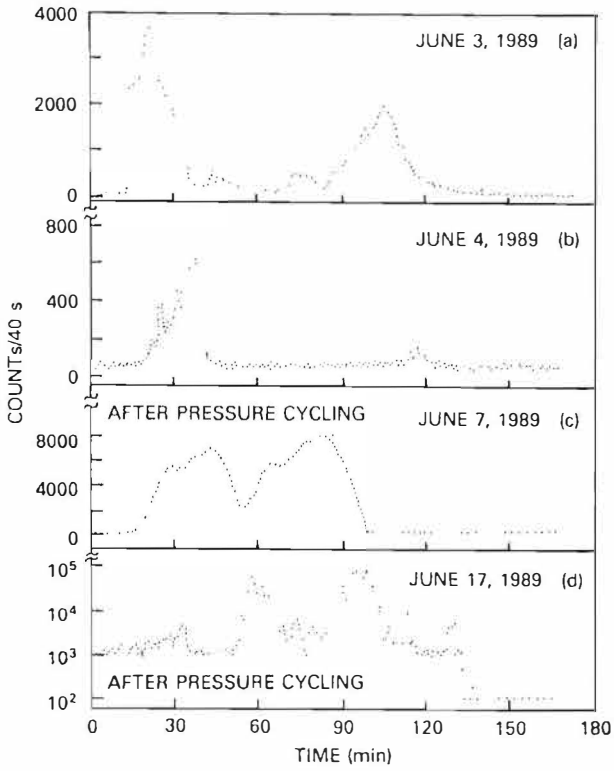

Fig.12 Neutron Counts Variation During Frascati Type Experiment with Ti Shavings

The authors of these measurements have reportedly been unsuccessful in their attempts to measure neutrons again in repeated attempts to reproduce the earlier results /13/. However they have detected the presence of tritium in some of the newly loaded Ti shavings through the technique of autoradiography. For this they employed a high speed polaroid camera. A 25 μm thick aluminium foil placed between the shavings and the photo sensitive film ensured that false images are not produced due to mechanical scratching of the film by the sharp edges of the shavings. The aluminium foil converts the tritium betas into soft X–rays which emerge from the foil

giving rise to image formation.(see Sec. 8.3).

7.3 EVIDENCE FOR TRITIUM IN Ti TARGETS SUBJECTED TO RF HEATING IN D_2 ATMOSPHERE (TPPED/NtPD) /5/

In these experiments machined and chemically cleaned targets of Ti were individually heated to temperatures of upto 900 C in a glass chamber using a surrounding induction heating coil (1 to 2 MHz frequency, 3 to 6 KW power). The glass chamber was connected to a vacuum system as well as H_2 and D_2 gas bottles. Degassing was initially carried out at 900 C for several hours until a vacuum of 10^{-5} mm was maintained steadily. The targets were later heated to 600 C in H_2 atmosphere at a few mm of pressure. The induction heater was then switched off and the target allowed to cool absorbing H_2 in the process. Atleast three cycles of H_2 absorption /desorption was given "to create active sites for D_2 absorption". Three such heating/cooling cycles were then carried out with D_2 gas. Pressure drop recorded by an oil manometer indicated the quantity of gas absorbed during each cooling cycle. It was observed that the quantity of gas absorbed increased each time saturating in the 3rd or 4th cycle.

The targets typically absorbed $<10^{19}$ molecules of D_2. Since the mass of Ti was a few hundred milligrams, this corresponds to a gross (D/Ti) ratio of hardly 0.001. However we have reason to believe that most of the absorption would be confined to the surface region. This is because when a metallic object is heated by induction heating the current distribution falls off exponentially with increasing depth. The skin depth δ characterizing this phenomenon is given by $\delta^2 = (s/f\pi\mu)$ where s and μ are the resistivity and permeability respectively of the workload and f is the frequency of the applied electromagnetic field. For a frequency of 1 to 2 MHz, δ for Ti is 0.1 mm. Consequently we believe that the (D/Ti) ratio in the near surface region would be much higher than the gross value of 0.001 noted earlier.

After loading, all the targets were subjected to various tests such as autoradiography, K X–ray counting etc in search of tritium. Although several dozen targets were successfully loaded with D_2 gas, only a few of them gave positive evidence for the presence of tritium. Interestingly the samples which soaked up large amounts of D_2 gas did not give any positive results. The best results were obtained from a disc shaped button (10 mm dia x 2 mm thick) and a couple of conical pieces meant for use as electrodes. Table IV summarizes the results. Figs. 13 and 14 are the autoradiographs of a deuterated disc and cone respectively. The radiographs of the Ti disc shows about 50 to 60 spots randomly distributed within the boundary. The occurrence of spots all along the rim of the machined disc is very intriguing. It is estimated

TABLE IV

TRITIUM CONTENT IN D_2 GAS LOADED Ti TARGETS

Date of loading	14 June 89	9 June 89	21 Mar 90
Shape of sample	Disc	Cone	Cone
Sample mass (g)	.98	.206	.2
D_2 absorbed (mg)	.42	.07	.29
T activity from X–ray counts(bq)	290	1300	5.5×10^{6}
Date of counting	16 June 89	16 June 89	28 Mar 90
Tritium atoms	1.5×10^{11}	6.5×10^{11}	3.0×10^{11}
T/D ratio	1.2×10^{-9}	3.2×10^{-8}	7.1×10^{-5}

that each spot corresponds roughly to 10^9 to 10^{10} atoms of tritium. The total number of tritium atoms in the whole target works out to be $\sim10^{11}$. This is to be compared with the 10^{19} to 10^{20} atoms of D absorbed in all by the Ti, pointing to a gross (T/D) ratio of $>10^{-9}$.

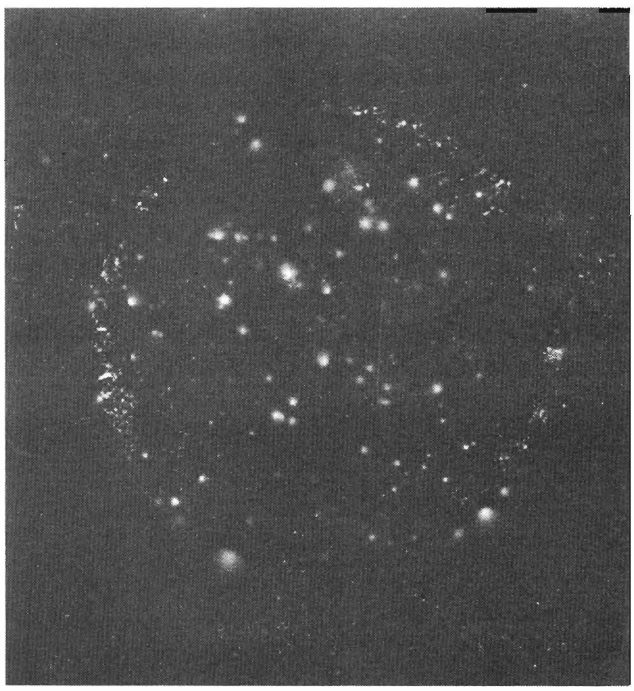

Fig.13 Autoradiograph of Deuterated Ti Disc

Interestingly one of these disc targets which was kept in front of a paraffin encased BF_3 neutron detector and monitored over a week end,

suddenly emitted a large burst of neutrons on its own lasting over a time span of 85 mins. (See Fig.2 of companion BARC paper /6/)
The most intriguing feature of this experiment is that ever since the RF heating system became defective in September 89, these results could not be reproduced even once using a resistance furnace

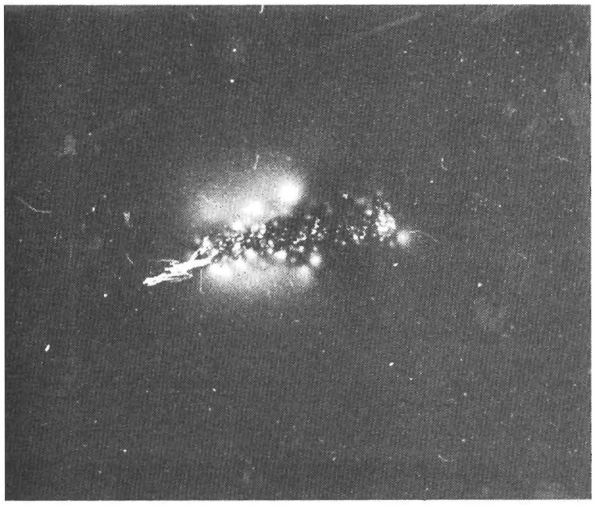

Fig.14 Autoradiograph of Deuterated Ti Cone

even though the power was higher and much greater quantities of D_2 gas could be absorbed. It was only in March 90 when a 1MHz furnace became available that a conical target once again indicated the presence of μCi amounts of tritium (See Table IV). The authors are therefore obliged to conclude that oscillatory electric and magnetic fields somehow play a crucial role in stimulating anomalous nuclear reactions on the surface of these machined Ti targets. In this context the recent Coherent Theory of Cold Fusion proposed by Hagelstein /14/ appears to give some theoretical insight as to possible mechanisms which could explain these observations.

7.4 ANOMALOUS TRITIUM PRODUCTION IN TITANIUM ELECTRODE OF A PLASMA FOCUS DEVICE (NtPD)/15/

A Plasma Focus (PF) device forms a high density (10^{25} ions/m^3), high temperature (10^7 K) plasma which produces an intense burst of neutrons when operated with deuterium gas/16/. This device has a vacuum chamber consisting of coaxial cylindrical electrodes connected through a Corning glass insulator at the bottom end and left open at the top. Fig.15 shows a schematic diagram of a plasma focus device of the type used in the present experiments. When this coaxial gun is connected to a high voltage (15 to 50 KV) capacitor bank with the help of a spark gap switch, a surface discharge is initiated at the insulator end. This then develops into a radial current sheath which is accelerated by J x B forces down the length of the electrode system, sweeping the gas ahead of it. On reaching the open end, the current sheath turns around on itself forming a quasi–cylindrical implosion resulting in a dense hot "plasma focus" a few cm long and few mm in diameter just above the tip of the central anode.

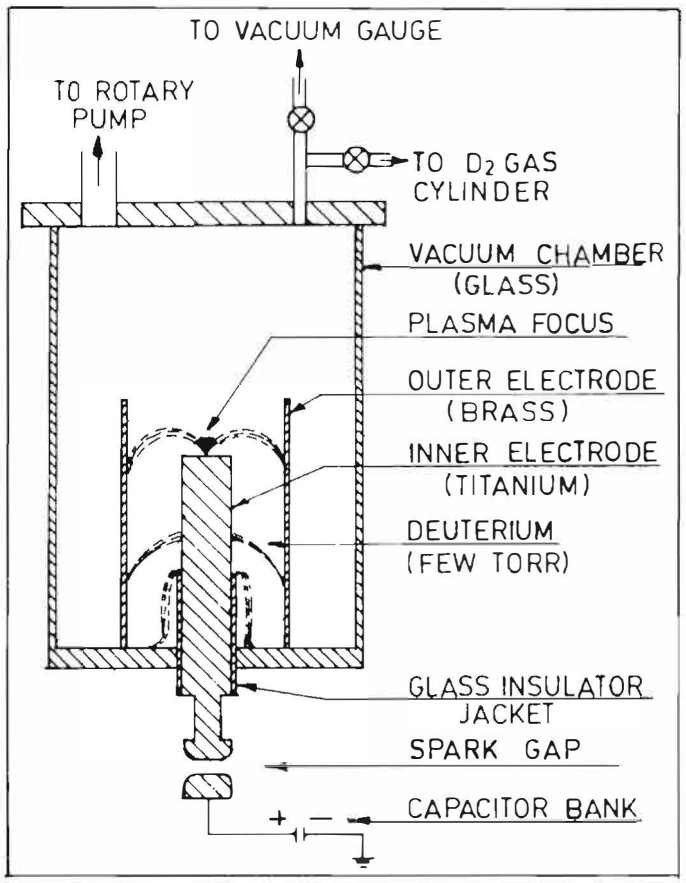

Fig.15 Schematic Diagram of a Plasma Focus Device With Central Ti Electrode

During January 90 an experimental program was underway to study the influence of anode material on the characteristics of the plasma created and consequently on the neutron production mechanisms of a PF device. Brass, aluminium, stainless steel and titanium were investigated for neutron yield systematics under various deuterium filling pressures (1–10 mbar).

During the experiments with a Ti anode, about 80 charge/discharge shots were carried out. After each shot the chamber was flushed and filled with fresh D_2 gas. Some of these shots were performed with the central electrode operated

with negative polarity. This mode of operation would direct the deuteron beams of a few hundred KeV energy which are known to be generated in PF devices, towards the central electrode. The neutron yield in every shot was recorded with the help of a bank of calibrated activation type silver cathode Geiger Muller counters located close to the device. Typically with ~3 KJ of stored energy, 10^7 neutrons were produced in each normal shot i.e. when the central electrode is used as anode. In the polarity reversed mode of operation also neutrons were produced but the magnitude of the neutron burst was an order of magnitude smaller.

In view of the special role of Ti in D_2 gas loaded cold fusion experiments, the Ti electrode was tested for induced radioactivity using autoradiography immediately after the experiment on two consecutive nights (4^{th} and 5^{th} Jan.90). No image was found at that time. But five weeks later (on 9^{th} Feb 90) using a new NaI detector set up it was discovered that a surprisingly high activity of ~392 μCi (~ 10^{16} atoms of tritium) had built up on the surface of the Ti electrode which had been exposed to the plasma focus shots. To confirm this, the rod was subjected to overnight autoradiography once again. As seen in Fig. 16 a very beautiful and impressive image was obtained.

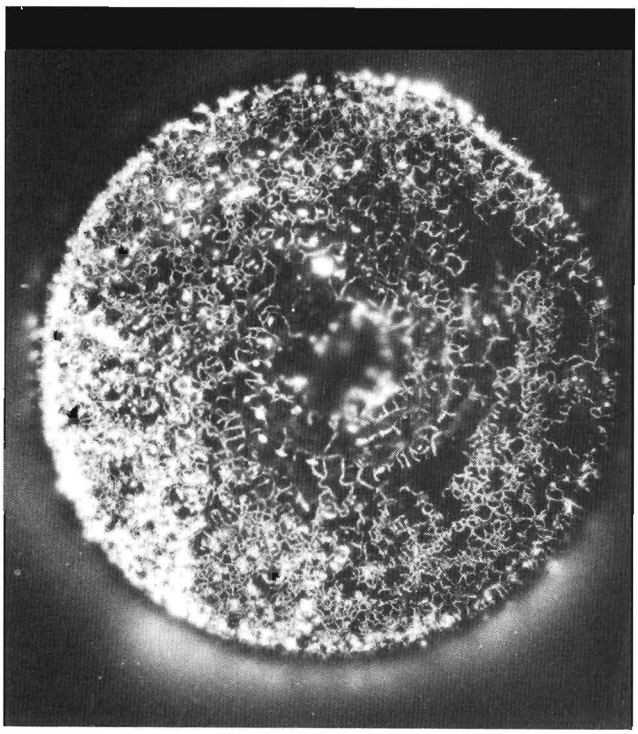

Fig.16 Autoradiograph of Central Ti Electrode of PF Device (5 Weeks After Charging)

This image has since been reproduced several times through repeated autoradiographic exposures. There has been no change in the resolution or clarity of the images even after a gap of a few months. The very sharp worm like lines are believed to be due to β^s from tritium bearing grain boundary regions near the surface, while the intense diffuse spots are due to soft X–rays (Ti K X–rays) emanating from deeper layers of the titanium electrode. As in the case of the RF heated Ti disc autoradiographs (Fig 13) the presence of spots all along the periphery of the rod is noteworthy. In order to rule out the possibility of image formation due to tritium contamination in the D_2 gas, the other electrodes (Al, SS and brass) were also tested for radioactivity. But none of them showed any activity confirming that the phenomenon is unique to Ti.

During all the 80 PF shots it is estimated that atmost 10^9 (d–d) neutrons could have been generated due to hot fusion reactions. Since in conventional (d–d) reactions (both beam target and hot fusion) the neutron–to–tritium branching ratio is ~ 1, it follows that not more than 10^9 tritium atoms could therefore have been produced during the shots. It is totally unrealistic to expect or postulate that all this tritium would have succeeded in getting absorbed on the Ti anode surface. Even if that were true, it still can not explain the 10^{16} atoms of tritium measured on the tip of the Ti anode. But the even more intriguing question is why was it not seen in the radiographs taken on the same night of the experiment as well as on the following night? Although the presence of large amounts of tritium was first detected only five weeks later, it is possible that it might have been produced any time in the intervening period.

The authors suggest that the intense electric and magnetic fields involved in the operation of a PF must have had some role to play in causing "cold fusion" reactions on the tip of the anode. Repeat experiments using planchets of Ti mounted at the top of a brass anode have however not shown any activity so far. A fresh stock of pure D_2 gas as well as a new Ti electrode are awaited for repeating the experiments under identical conditions prevalent in the earlier successful experiment.

7.5 OBSERVATION OF HIGH TRITIUM LEVELS IN AGED DEUTERATED Ti TARGETS/5/

The Division of Radiological Protection of BARC had procured a number of deuterated titanium targets on copper backing during 1972 to 1981 for dosimetry studies with accelerator based neutron sources. Twelve such targets were available, nine procured from M/S Amersham

International of U.K. and the remaining three from the Isotope Division of BARC. In view of the various studies involving deuterated titanium targets described in the earlier sections, it was conjectured that cold fusion reactions might have occurred in these "aged" targets over the past 9 to 18 years and if so, it was argued, they should contain considerable amounts of tritium. In order to check this hypothesis these aged targets were subjected to various studies for establishing the magnitude of tritium in them. Five different techniques namely autoradiography, Ti K X–ray counting with NaI and high purity germanium detectors, β counting with proportional counters and current measurements with an ionization chamber were used. The details of the targets, measurements and results are described in Ref /5/. It was found that the absolute tritium content in the targets varied between 0.3 and 150 MBq. Inquiries with the suppliers of these targets indicate that while inadvertent contamination during manufacture to the extent of a few hundred Bq is in principle a likely possibility, contamination levels in the MBq region is difficult to explain. The tritium levels in these aged TiDx targets expressed in terms of the (T/D) isotopic ratios was seen to vary in the range of 0.07 to 3.5 x 10^{-4}. For comparison the tritium activity of the D_2O moderator of a CANDU type power reactor is atmost 30 Ci/l even at saturation, corresponding to a (T/D) ratio of 10^{-5}. In contrast the (T/D) ratio of fresh D_2O from a factory is typically in the region of 10^{-14} to 10^{-13} only. Hence the authors are inclined to speculate that a plausible explanation for the unexpectedly high tritium levels in aged deuterated Ti targets could be the occurrence of cold fusion reactions..

8. MEASUREMENT OF TRITIUM LEVELS IN AQUEOUS AND METALLIC SAMPLES

As a consequence of the many years of operational experience with heavy water moderated research and power reactors in India, considerable expertise has been built–up in the area of tritium measurements, particularly in moderator and coolant circuits as well as in environmental samples. The status of development of the field of "Tritium Measurement and Applications" was reviewed recently at a Symposium /17/ held in Bombay to mark the golden jubilee of the discovery of tritium in 1939.

8.1 Analysis of Acqueous Samples

The tritium levels in the electrolytes and other aqueous samples was measured by expert groups at the Isotope and Health Physics Divisions of BARC. Commercial liquid scintillation counting systems such as Packard Instruments Model 4530 or LKB Systems Model 1215 (RACKBETA–II) which provide automatic quench correction facilities were employed. ^{40}K free vials were used. Commercially available scintillation cocktail, INSTAGEL, was found most suitable as it gave minimum chemiluminiscence. Double distilled water was used for diluting samples to reduce PH level as well as quenching impurities. In some electrolyte samples chemiluminiscence effects entirely masked the true tritium signal. Fig.17 shows the chemiluminiscence decay curve of one such "difficult" sample which did not cool down even after several hours of dark adaptation and decay time.

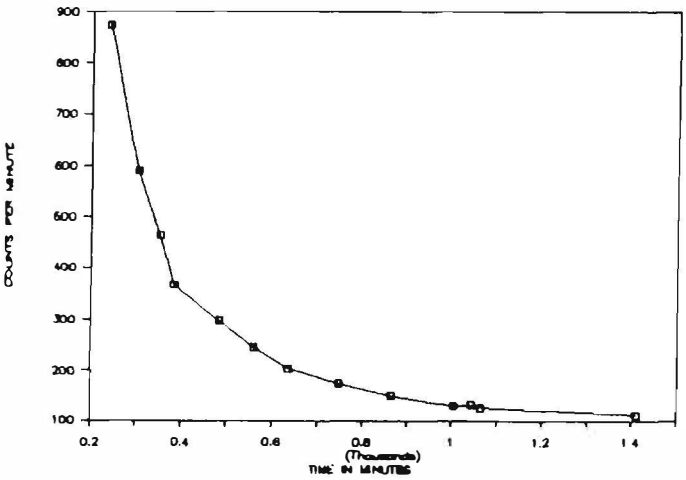

Fig.17 Chemiluminscence Decay Curve of a Severe Electrolyte Sample

Chemical and photon quenching effects were encountered in other samples resulting in compression of the tritium spectrum. In order to confirm that the spectral output of the electrolytic samples falls well within the tritium spectral region, an experimental sample which did not show any chemiluminiscence or quenching effects was spiked with a tritium standard and the pulse height spectrum was checked and compared with that of the test sample. In the case of LiOD based electrolytes a systematic study has been carried out to study the influence of alkalinity on the measurements.

The Pollution Monitoring Section of BARC has recently developed a flow detector for on line measurement of tritium levels in gas and liquid phases /17/. The flow cell has a volume of 15ml and is packed with 5 μm thick plastic scintillating fibres. A pair of photomultiplier tubes viewing from the sides and operating in coincidence measure the scintillation rates, due to tritium.

8.2 β–particle and K X–ray Counting of Deuterated Ti and Pd Targets

The presence of tritium in the near surface region of deuterated Ti and Pd targets has been established through the technique of β particle and Ti K X–ray counting. The βs were counted using either a proportional gas counter or a plastic scintillator. In some of the strong sources pico amp levels of ionization current could be measured using an ionization chamber. The range of the tritium β^s (energy < 18.6 keV) in metallic samples is < 1mg/cm^2. Some of the β^s excite the characteristic K X–rays of Ti (~4.5 kev) whose mean free path for absorption in Ti is however 10mg/cm^2. Thus these X–rays are able to escape from deeper layers of the Ti than the β^s. Using a high resolution germanium detector or a 1mm thick NaI detector these soft X–rays can be conveniently counted.

8.3 Autoradiography

As mentioned already the technique of auto radiography has been employed very effectively at BARC to study the spatial distribution of near surface tritium produced in deuterated Ti and Pd targets. In order to obtain good resolution the samples were kept in contact with medical X–ray film and exposed overnight. The fogging of the film is due to the combined effect of tritium β^s and the K X–rays excited in the host metal lattice. Sometimes a stack of two films was mounted close to the sample and it was observed that the second film also gives a similar but fainter image ruling out the suspicion that image formation could be due to mechanical (scratching of films) or chemical reduction effects.

9. CONCLUSIONS

Experiments carried out by a number of totally independent groups employing diverse experimental set ups have unambiguously confirmed the production of neutrons and tritium both in electrolytically loaded and gas loaded Pd/Ti lattices.

Tables I & II present in a nut shell the main results of the BARC electrolysis experiments. It may be noted that in all 22 cells/experiments have yielded excess tritium varying over a wide margin of 10^{10} to 10^{16} atoms. Roughly half of these may be described as having been "doubly successful" since in these both neutrons and tritium were measured. The main conclusions to emerge from the electrolysis experiments may be summarized as under:

(a) The most important observation is the surprisingly low neutron–to–tritium yield ratio, first reported by us at the Karlsruhe meeting in July 1989 /3/. 8 out of the 11 doubly successful cells of Table I have given values in the region of 10^{-6} to 10^{-9} for this ratio, while two experiments have given a comparatively larger value of 10^{-3} to 10^{-4}. These ratios may be considered as overestimates since in most of the experiments the tritium escaping with the electrolytic gases has not been accounted for.

(b) The Trombay electrolytic experiments have also convincingly demonstrated that both neutrons and tritium are generated concomitantly. This is evident from the sharp increase in the tritium concentration of the electrolyte immediately after a large neutron burst in several of the experiments.

(c) Another significant observation pertains to the specific charge passed per unit of cathode surface area, namely amp–hrs/cm^2 at the time of the first neutron burst. This quantity which may be called the "switching on charge" is seen to be in the range of 0.6 to 3.2 amp–hrs/cm^2 in 8 out of the 11 experiments of Table I. In the remaining three cells (all of which have used LiOD as electrolyte) the switching on charge is an order of magnitude or more higher.

(d) It is significant that in all the five experiments which used 5 M NaOD as electrolyte the switching on charge was $\leq$ 3 amp–hrs/cm^2. In the isolated instance where Li_2SO_4 was used the switching on charge was the lowest namely 0.15 amp–hr/cm^2 among all the experiments reported in Table I.

(e) In 8 out of the 11 cases of Table I the first neutron burst has occurred on the very first day of electrolysis, in fact within 9 hrs of commencement of electrolysis (except for experiment #7 where it occurred after ~24 hrs). This seems to be a unique feature of the Trombay results.

(f) It is also worth noting that one amp–hr or 3600 coulombs corresponds roughly to the charge carried by the deuterons required to load a few grams of Pd (associated with each cm^2 of cathode surface) to a (D/Pd) ratio of ~0.6. In practice since only a fraction (10 ~ 30%) of the deuterons bombarding the cathode actually get absorbed in it, the experimentally observed switching on charge of $\leq$ 3 amp–hr/cm^2) is consistent with the common sense expectation that a (D/Pd) ratio of atleast 0.6 should be achieved before nuclear processes involving

deuterons can be expected to take place.

(g) Except for the Ti–SS cell (Cell#1 of Table I) in all the other ten cells neutrons are produced in one or more large bursts of magnitude several times the background values. But in all cases after a limited period of nuclear activity the cells becomes inactive, no matter for how long the electrolysis is continued.

(h) Inspite of the wide disparity in cell designs, it is observed that the specific neutron yield i.e the integrated neutron yield per unit area of cathode surface, lies in the range of 10^4 to 10^5 n/cm^2 except for the two experiments where a Nafion membrane was present between the cathode and anode (Cells # 9 & 10). The specific neutron yield in these two cases is 1 or 2 orders of magnitude higher.

(i) The specific tritium yield (see Tables I & II) has shown a greater overall variation ranging from 4 x 10^9 to 1.7 x 10^{14} t/cm^2. In 10 of of 22 cells it is in the range of 10^{12} to 10^{14} t/cm^2 while most of the other cells have given values in the region of 10^{10} to 10^{12} t/cm^2.

(j) The BARC teams generally operated only one cell at a time. The overall "success rate" defined as the percentage of cells which produced tritium or neutrons in relation to the total number of cells operated is estimated to be more than 70%. The groups who used NaOD as electrolyte had perhaps an even higher success rate.

(k) The BARC experiments possibly include the largest sized electrolytic cold fusion cells (measured in terms of either cathode surface area (300 cm^2) or total current (100 amps)) to have been employed so far.

(l) Unfortunately it has not been possible to conclusively establish whether the neutron and tritium producing reactions occur only on the surface of the electrode or over the whole volume of the cathode. But the delayed appearance of additonal tritium in the electrolyte, at times even when the cell was off, indicates that tritium slowly leaches out from the inner regions of the electrode, giving some credence to the volume effect theory.

The gas phase experiments of BARC have spanned a variety of novel approaches and diagnostic techniques. The observation that RF heating of titanium targets in D_2 atmosphere promotes tritium production is interesting. The large amount of tritium (10^{16} atoms) found on the top end surface of the central titanium electrode of a plasma focus device, particularly the very impressive high resolution autoradiogrpah, is puzzling indeed. Finally the unexpectedly large levels of tritium in decades old deuterated titanium targets adds to the pool of puzzling results.

On the whole however, the results obtained by a number of independent experimental groups at BARC during the first year of the 'cold fusion era' has provided ample evidence of the occurrence of anamolous nuclear processes in Pd and Ti lattices loaded with deuterium.

ACKNOWLEDGEMENTS

We are very grateful to all the authors of the individual BARC cold fusion papers for readily supplying experimental details and results for the preparation of this overview paper. We wish to thank Drs R.M. Iyer and T.S. Murthy for many fruitful discussions. The considerable help rendered by A. Shyam, T.C. Kaushik, R.K. Rout, V. Chitra, S. Ranganekar and D.V. Periera in the time consuming task of editing and formatting of this manuscript is warmly acknowledged.

REFERENCES

1. M. Fleischmann et al, J. Electranal. Chem. Vol.261, pp301–308 (1989)

2. A. De Ninno et al, Europhys. Lett. Vol.9, p221 (1989)

3. P.K. Iyengar, "Cold Fusion Results in BARC Experiments", Proc. Fifth Int. Conf. on Emerging Nuclear Energy Systems, Karlsruhe (FRG) World Scientific, Singapore, p291 (1989)

4.P.K. Iyengar & M. Srinivasan (Eds), BARC Studies in Cold Fusion (April–September 1989) Report BARC–1500, (1989)

5. P.K. Iyengar et al, Bhabha Atomic Research Centre Studies in Cold Fusion, Technical Note, Fusion Technol.August (1990).

6. M. Srinivasan et al, Statistical Analysis of Neutron Emission in Cold Fusion Experiments, Proc. First Annual Conf. on Cold Fusion, Salt Lake City, Utah March 28th–31st (1990).

7. H. Bose et al, Cold Fusion Cell Experiments with Cylindrical Palladium Cathode at Sub–Ambient Temperatures. Unpublished Note, March (1990).

8. G. Venkateswaran, Personal Communication, 11th March (1990).

9. C.K. Mathews, Personal Communication 2nd March (1990).

10. N.J.C. Packham et al, J. Electroanal. Chem. Vol.270 pp451–458 (1989).

11. R. Mukopadhyay et al, Accepted for publication in Solid State Comm. (1990).

12. P. Raj et al, J. Less–Common Metals, Vol 130 p 139 (1987).

13. P. Raj, Personal Communication 11th March (1990).

14. P.L. Hagelstein,"Status Report on Coherent Fusion Theory", Proc. First Annual Conf. on Cold Fusion" Salt Lake City, Utah,March 28th–31st (1990).

15. R.K. Rout et al, Unpublished Note, (1990).

16. Symposium on "Tritium Measurements and Applications Feb 22–23, 1990, BARC, Bombay., Bulletin of the Indian Association for Radiation Protection Vol 13,No.1, (1990).

17. A.N. Singh et al, An Instrument for On–line Monitoring of Tritium–in–Air in Heavy Water Reactors, Nucl.Instru. & Meth, Vol 258 p 250, (1987).

EXPERIMENTAL CONSIDERATIONS IN ELECTROCHEMICAL ISOPERIBOLIC CALORIMETRY

Turgut M. Gür, Martha Schreiber, George Lucier, Joseph A. Ferrante, Jason Chao* and Robert A. Huggins

Department of Materials Science and Engineering
Stanford University
Stanford, CA 94305-2205

** Electric Power Research Institute*
Palo Alto, CA 94303

ABSTRACT

A novel concentric cylinder isoperibolic calorimeter was designed and fully characterized. Several different methods of introducing calibration power to the calorimeter were studied and the calibration constant was found to be independent of the method. Calibration constants could be determined with a precision to $\pm$ 0.5 %. Furthermore, they were independent of the input power level up to 22 W and with a cell temperature up to 60 °C over appreciable periods of time. This new design possesses many advantages that makes it suitable for careful studies of the thermal behavior of electrochemical systems, such as the electrochemical insertion of deuterium into Pd cathodes.

INTRODUCTION

Calorimetric techniques have widely been used to study thermochemical properties of both static and reacting systems with great success. A great deal of attention has been drawn to this experimental method recently as a result of the announcement by Fleischmann and Pons last year [1] that they had observed the generation of large amounts of excess heat when deuterium is electrochemically inserted into palladium. This paper describes the design and performance characteristics of a new type of isoperibolic calorimeter that has been employed for heat flux measurements during the electrolysis of both light and heavy water upon palladium cathodes.

The word "isoperibol" denotes uniform surroundings. So, isoperibolic calorimetry refers to methods in which thermal energy is transferred from a heat source to a surrounding heat sink that is maintained at a constant temperature. It is generally operated in a steady state power balance mode. When applied to electrolysis systems, heat is typically generated within the electrochemical cell and transferred through a intermediate thermally-conducting layer to a surrounding water bath held at constant temperature. Under steady state conditions, a temperature distribution is established in which the temperature difference across the thermally - conducting layer transports heat at a rate that just balances the power generated within the electrochemical cell. Thus, in principle, measurement of the temperature difference between the cell and the surrounding bath provides information about the thermal power generated in the electrochemical cell, P_{therm}. This can be simply expressed as

$$P_{therm} = K\ (T_1 - T_2) \qquad (1)$$

where K is the calorimeter calibration constant, and T_1 and T_2 are the temperatures of the cell and bath.

As will be shown below, if the electrical power applied to the cell causes a chemical or electrochemical reaction to occur that involves a change in the enthalpy of the system, the thermal power generated P_{therm} is not equal to the applied electrical power P_{appl} . This is described as a thermodynamically "open system", and is the case if the gaseous products of the electrolysis reaction are allowed to escape. As a result, the temperature difference between the cell and the surrounding bath is less than it would be if the applied electrical power produced only Joule heating.

On the other hand, if a thermodynamically "closed cell" design employing an in-cell recombination catalyst is used, so that no enthalpy is transported out of the system, P_{therm} and P_{appl} will be equal if

there is no other heat generation or absorption process present. This is thus a conceptually simpler situation, and any measured difference between the input and output powers must have some other origin. One possibility is that it might be due to some additional power generation process taking place inside the electrochemical cell, as proposed by Fleischmann and Pons [1].

CALORIMETER DESIGN

A new type of isoperibolic calorimeter has been designed in which various issues such as the influence of the physical locations at which heat is produced and at which the temperatures are measured during both calibration and operation, and the magnitude of the stirring of the electrolyte fluid are not relevant.

The new design consists of two concentric heavy aluminum cylinders that are separated by a well - defined thermally conducting layer. The electrochemical cell fits snugly inside the axial hole of the inner cylinder. Under steady state conditions, essentially all the heat generated within the electrochemical cell passes to the external environment radially through the surrounding cylinders.

Instead of relying upon measurement of the temperature within the electrochemical cell itself, as well as of the assumed homogeneous environment, this design involves the measurement of the temperatures of the two aluminum cylinders. Because of their dimensions and excellent thermal conductivity, the aluminum cylinders provide temperature uniformity. Thus possible sources of error related to issues such as the amount of stirring and the locations of the heat sources and temperature measurement within the electrochemical cell are avoided.

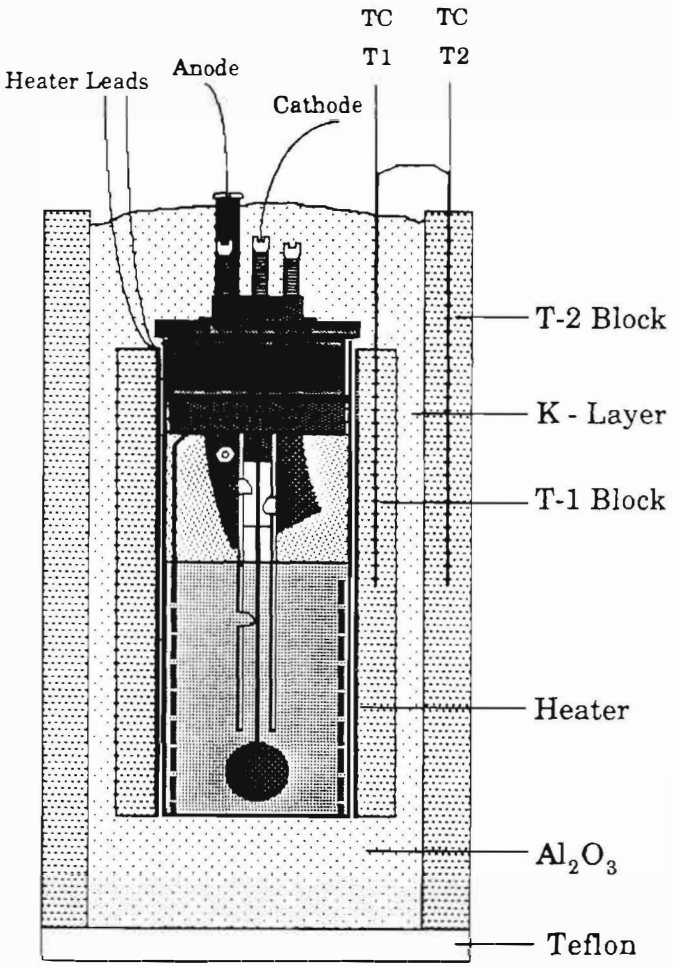

Figure 1. Schematic design of the concentric cylinder isoperibolic calorimeter with the external thin sheet Joule heater wrapped around the electrochemical cell and inserted inside the inner aluminum cylinder.

The design of this new isoperibolic calorimeter is shown schematically in Figure 1. The inner (T_1) aluminum cylinder has an outer diameter of 2 inches and an inner diameter of 1.17 inches. It is 4 inches long, and weighs about 365 g. The outer (T_2) aluminum cylinder is 7 inches long and weighs 958 g. Its inner diameter is 2.25 inches, and its outer diameter, 3.0 inches. Thus the gap across which the heat conduction takes place, and the temperature difference is measured, is 0.125 inches. The container for the electrochemical cell that fits snugly inside the (T_1) cylinder is a quartz tube 1.14 inches (29 mm) in outside diameter and 4 inches long.

The inner (T_1) cylinder housing the electrochemical cell is mounted on Teflon supports and placed concentrically inside the outer (T_2) cylinder in such a way that 1.5 inches of vertical space is left above and below the inner cylinder. This vertical space above and below as well as the 0.125 inch wide radial gap between the two cylinders is packed with Al_2O_3 powder. This thick layer of Al_2O_3 powder insulation above and below the cell and inner cylinder forces the heat to be transfered in the radial direction across the gap between the two cylinders. The effective thermal conductivity of this Al_2O_3 powder, which has a particle size range of 50-200 mm, was experimentally determined to be about 1.6×10^{-3} W/cm.^{o}C.

Three small thermocouple holes 1/16 inches in diameter were drilled vertically down to half-height of each aluminum cylinder. The holes are located at midpoints of the wall thickness of the cylinders and

are spaced 120° circumferentially from each other. Copper-constantan (Type T) thermocouples were firmly fixed into these holes so as to make good physical contact with the aluminum. A few drops of silicone oil were put at the bottom of these holes to enhance the thermal contact between the thermocouples and the aluminum cylinders. The thermocouples are used in a differential mode such that each calorimeter contains four pairs of thermocouples. In each case, the outer members are copper, so as to avoid any thermoelectric effects when they are joined to the measuring circuitry. Two pairs are connected between the inner (T_1) and outer (T_2) aluminum cylinders to sense the temperature difference between the cylinders. The other two pairs of thermocouples are connected between each aluminum cylinder and the surrounding constant temperature water bath. Thus all possible adverse thermoelectric contributions from dissimilar contacts are eliminated. The linear response of these T-type thermocouples is 39 mV/°C. A 6 1/2 digit Keithley Model 193A microvoltmeter is used for reading the thermocouple output and it thus provides a resolution of about 0.025 °C.

Eight such calorimeters have been built and tested. Their 1/e time constants were determined from their transient response to step changes in the level of the input power, and were found to range between 13 and 15 minutes.

ELECTROCHEMICAL CELL DESIGN

The electrochemical cells used in this work are thermodynamically "closed" cells, i.e., they contain an internal recombination catalyst made of finely divided Pt supported on Teflon with a nickel backing to recombine the D_2 and O_2 formed by the electrolysis and return it by gravity back into the electrolyte. In contrast, the gaseous products of electrolysis are vented off to the outside in "open" cells.

The cells were connected externally to silicone oil bubblers by plastic tubing. This served two purposes. One is to prevent atmospheric moisture to diffuse back into the electrolyte of the electrochemical cells, which contain about 20 ml of 0.1 M LiOD in D_2O. This is an important consideration since D_2O attracts light water strongly, and hydrogen is selectively absorbed into the Pd cathode.The other reason for the bubbler is to allow the escape of gas in the amount of uncombined oxygen. Observation of the time behavior of the bubble evolution provided information about this process, and showed that it ceased as the Pd cathode became saturated with deuterium.

The Pd cathodes were prepared by repeated arc melting in a gettered argon atmosphere, followed by mechanical deformation to produce a "fat dime" shape. Earlier, thin Pt and Au wires were used to make electrical connections to the Pd cathodes. However, due to surface contamination problems, the cathode current collector was changed to fine Pd wire, which was shielded by a thin Teflon tube to prevent appreciable electrolysis taking place on it, rather than on the Pd cathode.

Three different cell designs have been studied. In the first design, a static immersion heater shielded in J - shaped quartz tubing was used to provide the Joule heating for calibration. The cell was sealed with a rubber stopper, which housed the feed-throughs for cathode and anode lead connections, the immersion Joule heater, and the gas vent to the silicone bubbler. The anode was about 200 cm of 0.010 inch thick Pt wire spirally wound inside the cell. The anode to cathode surface area ratios were between 10 and 15 to assure that most of the applied voltage drop was at the Pd cathode.

Although this general design provided reproducible calibration and stable electrochemical performance, the problems associated with the cramped space inside the cell as well as in the rubber stopper and the occasional and unpredictable breakage of the quartz shielding around the Joule heater led to a modified design.

Energy dispersive spectroscopy studies of the surface of the Pd cathodes indicated the presence of substantial amounts of Pt coverage, which can block deuterium insertion. Therefore, the fine wire Pt anodes were replaced by large surface area thin Pd ribbon anodes, produced by rolling 1/8 inch O.D. Pd wire. This modification has the advantage of continuously depositing fresh Pd upon the cathode surface, which could cover up any potentially blocking metallic or other impurities that might be deposited during the electrolysis process.

The second design used a modified three-electrode configuration, in which heat generated by electrolysis upon an auxiliary Pt wire cathode centered within the cell was utilized for calibration purposes. Passing current between this Pt cathode (instead of the Pd cathode) and the Pd anode caused only the generation of Joule heat, so that measurement of the electrical input to this configuration provided a simple calibration method, with gas generation, bubble - driven stirring, and recombination similar to that which takes place during electrolysis with the Pd cathode. Of course, one had to be sure to open the Pt cathode circuit during operation of the Pd cathode to insure that there was no electrical cross talk between

the two cathodes. Again, rubber stoppers were used to support the electrical feed-throughs and the gas vent to the bubbler.

The third design used a simple Pd cathode and Pd ribbon anode arrangement inside the cell. Joule heater power for calibration was provided by a thin film sheet heater which was snugly fitted between the outside of the quartz cell and the inside of the inner aluminum cylinder of the calorimeter. Rubber stoppers were abandoned because of concern about their possible contamination of the electrolyte, and were replaced by cell caps machined out of Delrin.

EXPERIMENTAL PROCEDURES

Calorimeter Calibration Principles

The basic equation for an isoperibolic calorimeter was given earlier as equation (1), which relates the thermal power output to the measured temperature change through the calibration constant, K.In the current design, the value of K is determined by the construction of the concentric cylinder calorimeter, and is independent of the particular experiment being performed within it.

The most common way of supplying the power for calibration is by the use of an internal Joule heater. Several levels of electrical power are applied, and the corresponding increases in the steady state temperature evaluated. A plot of (T_1-T_2) versus applied electrical power gives a linear relation, whose slope is the reciprocal of the calibration constant K.

However, it is often desirable to perform a calibration of the calorimeter while electrolysis is also taking place. In that case, the total applied thermal power introduced is the sum of that which is provided by the Joule heater and that contributed as a result of the electrolytic process. In addition, we must consider the possibility that there may also be another phenomenon present that introduces additional thermal power, P_{int}.

In the absence of any other energy generating or consuming effects, so that P_{int} is zero, electrolysis conducted in a "closed" cell in which the gaseous products of the electrolysis are internally recombined, produces exactly the same results as a simple Joule heater [2-4].

This is not true in the case of an "open" cell, however, as enthalpy is carried out of the system by the escape of evolved gases. Therefore the contribution to (T_1-T_2) due to the electrical power applied to the electrolysis process will be lower than if the same amount of power were applied to a simple Joule heater, and the apparent value of K would be greater than the proper one.

There is an additional effect that must be considered in order to obtain a proper calibration of a calorimeter by adding Joule heat in the presence of electrolysis. This is because changes in applied Joule heater power cause changes in the temperature of the electrolyte. This causes changes in electrolyte resistance, and can thus influence the amount of thermal power introduced in connection with the electrolysis reaction.

As an example, if additional heater power ΔP_{htr} is applied, the electrolyte temperature will increase. Because of this increased temperature, the overall cell resistance decreases.

If the electrolysis is being conducted under constant voltage conditions, the electrolysis current will increase. This increases the electrolysis thermal power input by an amount ΔP_{el}. On the other hand, if the electrolysis is conducted under constant current conditions, the voltage and the thermal power introduced by the applied electrolysis power will both decrease.

Thus we see that the total change in thermal power introduced into the calorimeter is the sum of two factors, that simply due to the added calibration heater power ΔP_{htr}, and that due to a change in the electrolysis power ΔP_{el} due to the concommitant decreased electrolyte resistance.

Therefore, we can not merely compare the observed value of (T_1-T_2) to the sum of the electrical power applied to the heater and that applied to the electrolysis reaction. We must separate these two effects. The total power, P_{tot} , put into the cell during calibration while electrolysis is also taking place is

$$P_{tot} = P_{htr} + P_{el} + P_{int} \qquad (2)$$

Additional Joule heater power increases the temperature difference (T_1-T_2) by ΔT_{htr} such that the total temperature rise, ΔT_{tot} , is given by

$$\Delta T_{tot} = \Delta T_{htr} + \Delta T_{el} + \Delta T_{int} \qquad (3)$$

where ΔT_{el} is the change in (T_1-T_2) due to the change in the electrolysis power, and ΔT_{int} is the change in (T_1-T_2) due to any related change in the additional internal heat generation process, if one is present.

We can also write

$$\Delta T_{tot} = \Delta P_{htr}/K + \Delta P_{el}/K_{el} + \Delta P_{int}/K_{int} \quad (4)$$

if the values of K, K_{el} and K_{int} are not the same. In that case, we note that (4) is not the same as

$$\Delta T_{tot} = (\Delta P_{htr} + \Delta P_{el} + \Delta P_{int})/K \quad (5)$$

which would be the case if all the K values were the same.

The apparent value of K that would result from this experiment is given by

$$K_{apparent} = (\Delta P_{htr}+\Delta P_{el}+\Delta P_{int})/(\Delta T_{htr}+\Delta T_{el}+\Delta T_{int}) \quad (6)$$

which can be quite different from the real value characteristic of the calorimeter, K.

This problem can be solved by assuming that ΔP_{el} and ΔP_{int} are coupled, and can be represented by a single value of K_{el}, which can be found from the values of (T_1-T_2) and P_{el} in the absence of any heater power. If the magnitude of K_{el} varies with electrolysis power level, it can be determined over any desired power range by performing an additional experiment, in which the value of this composite K_{el} is determined by observing the change in temperature difference $(\Delta T_{el} + \Delta T_{int})$ that results from a change in the electrical power input ΔP_{el} applied to the electrolysis process. For that case,

$$K_{el} = \Delta P_{el} / (\Delta T_{el} + \Delta T_{int}) \quad (7)$$

Thus if we have the value of K_{el} we can find the proper value of K for the calorimeter from

$$K = \Delta P_{htr} / (\Delta T_{tot} - (\Delta T_{el} + \Delta T_{int})) = \Delta P_{htr} / (\Delta T_{tot} - (\Delta P_{el} / K_{el})) \quad (8)$$

An alternative strategy is to operate the cell in a different mode, maintaining the electrolysis power constant, with the computer, rather than keeping the electrolysis voltage constant. If we did this, the electrolysis power would not go up when the heater power is introduced, and the observed temperature rise would be due to the effect of the heater power alone. This would allow direct evaluation of K without the need for a separate experiment to evaluate K_{el} and to separate out the two factors.

However, if the electrolyte temperature increases, and thus its resistance decreases, as the result of the addition of heater power, the relationship between electrolysis voltage and current will change, even under constant electrolysis power.

Calibration Procedure

Experiments were performed to determine the values of K for the calorimeters using three different methods of introducing power, an immersion Joule heater within the electrochemical cell, internal electrolysis, and a Joule heater placed between the external wall of the electrochemical cell and the inside surface of the inner cylinder of the calorimeter. Each of these methods can be readily incorporated into the electrochemical cell design, as discussed earlier. The calibration procedure simply involved the introduction of several levels of Joule heating power, in both increasing and decreasing steps, and the measurement of the temperature difference between the two aluminum cylinders in each case. Calibrations were carried out both with and without concurrent "closed cell" electrolysis, and with the electrolysis conducted in either the constant power mode or the constant voltage mode. In the latter case, the corrections discussed above were applied.

Measurement and Data Acquisition System

The power for both the electrolysis and the Joule heater were supplied by Lambda LLS series power supplies. In the case of constant electrolysis power, the power supplies for the electrolysis process were computer controlled. A Macintosh IIx computer was used for this purpose as well as for calorimeter data acquisition, using a Keithley 193A microvoltmeter and a Keithley 706 scanner. For each calorimeter, a total of ten experimental parameters were monitored. They included four differential and two absolute thermocouple values, as well as two voltage and two current (read as voltage across precision resistors) values. They were measured sequentially, and each point was averaged over ten readings and stored every 5 to 15 seconds. The hardware allowed five calorimeters to be monitored and controlled simultaneously. Both the cell operation and the data acquisition were controlled using the LabView software from National Instruments Co.

CALIBRATION RESULTS

As mentioned earlier, the temperature distribution within the calorimeter is measured by the use of six copper-constantan (Type T) thermocouples located at different positions in the calorimeter. They were configured in a differential mode such that only the copper ends of each pair were connected to the microvoltmeter, eliminating spurious thermoelectric effects. Figure 2 shows the exceptional agreement between three temperature difference measurements, made at the six points in the calorimeter by the four

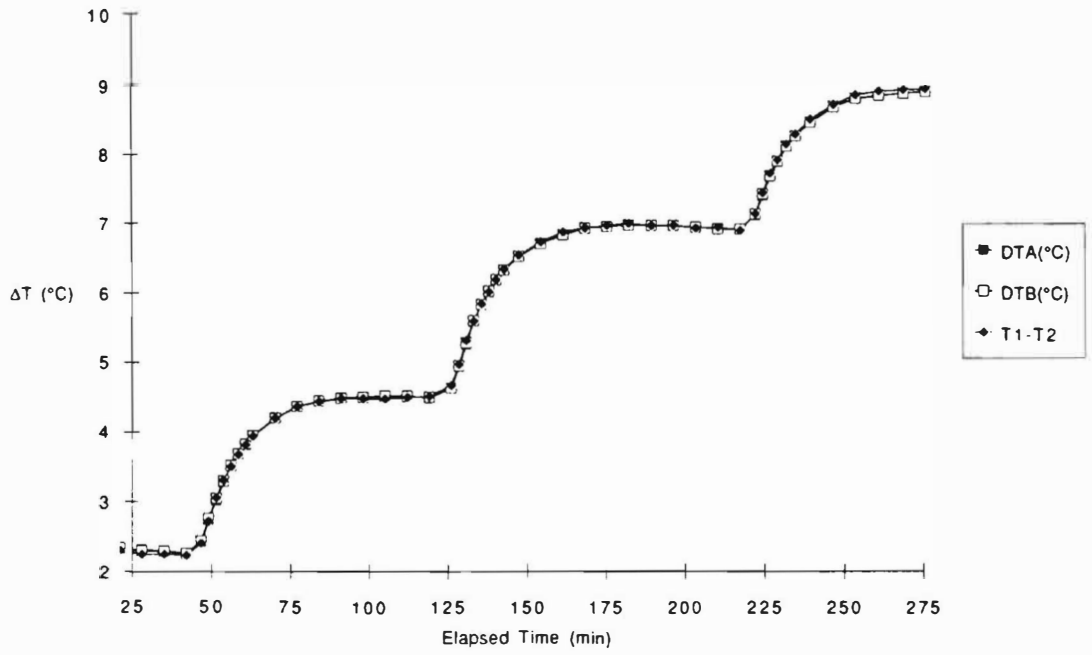

Figure 2. The variation of temperature with time during a calibration experiment at three levels of power input using an immersion Joule heater. All three differential temperatures measured at different locations lie exactly on top of each other indicating a uniform temperature distribution within the inner aluminum cylinder in the calorimeter.

pairs of differential thermocouples, and clearly demonstrates the uniformity of the temperature distribution within the calorimeter. This is an important advantage. It eliminates any ambiguity about the locations of the sources of heat and the temperature probes within the electrochemical cell. Hence the extent of stirring to distribute the heat within the electrochemical cell becomes irrelevant.

These data also illustrate the typical time - dependent variation of the temperature during a calibration carried out by the use of an immersion Joule heater.

A typical time variation of the two electrical power inputs during a calibration experiment is shown in Figure 3(a). The Joule heat for calibration was supplied by a thin sheet heater external to the electrochemical cell, and the electrolysis was operated in the constant power mode in this case. Note that all are very flat and steady with time. High total power levels, sometimes in excess of 20 watts, as was the case here, have been commonly used in both our calibration and electrochemical insertion experiments.

The time variation of the calibration constant extracted from these data using equation (8) is shown in Figure 3(b). The spikes on the graph are due to the transient behavior of the calorimeter when the input power level is varied abruptly. The steady state behavior, however, clearly shows that the calibration constant values are very consistent, lying in a band less than 0.5 % wide, and independent of the input power level as well as time.

The effect of different modes of Joule heating during calibration experiments was also studied. It was found that the value of the calibration constant was independent of the manner in which power was supplied to the calorimeter. This is illustrated in Figure 4, which compares the results of experiments using the external thin sheet Joule heater with those using the electrolytic heater, both with and without simultaneous electrolysis taking place. Over a wide range of power levels the calibration constant was independent of the type of calibration heat source, and in this case was equal to 0.83 W/°C with a precision to $\pm$0.5 %.

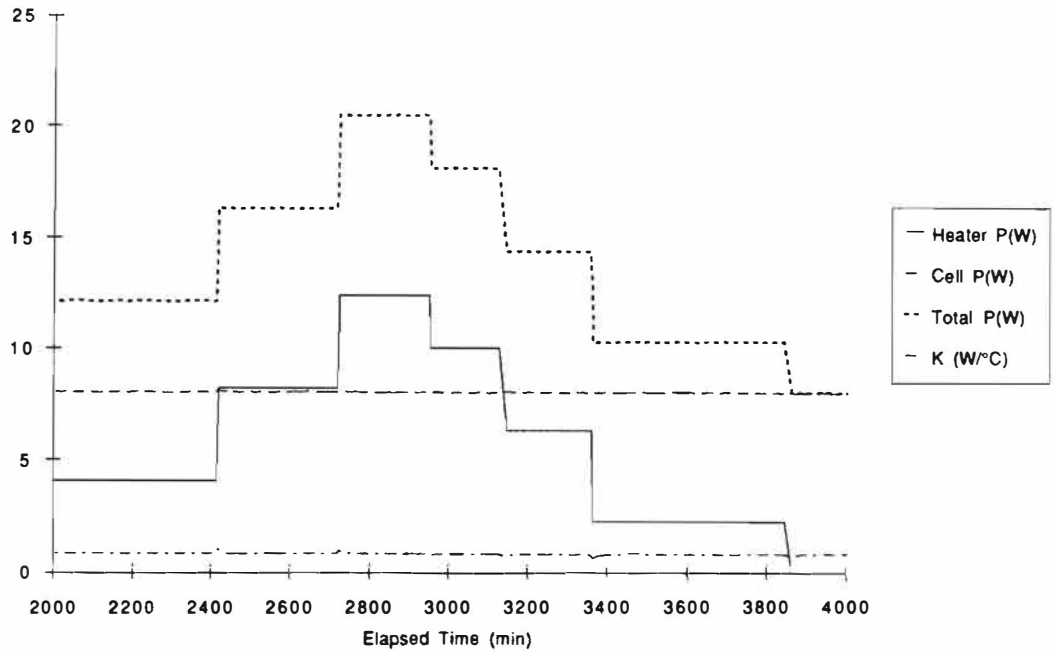

(a)

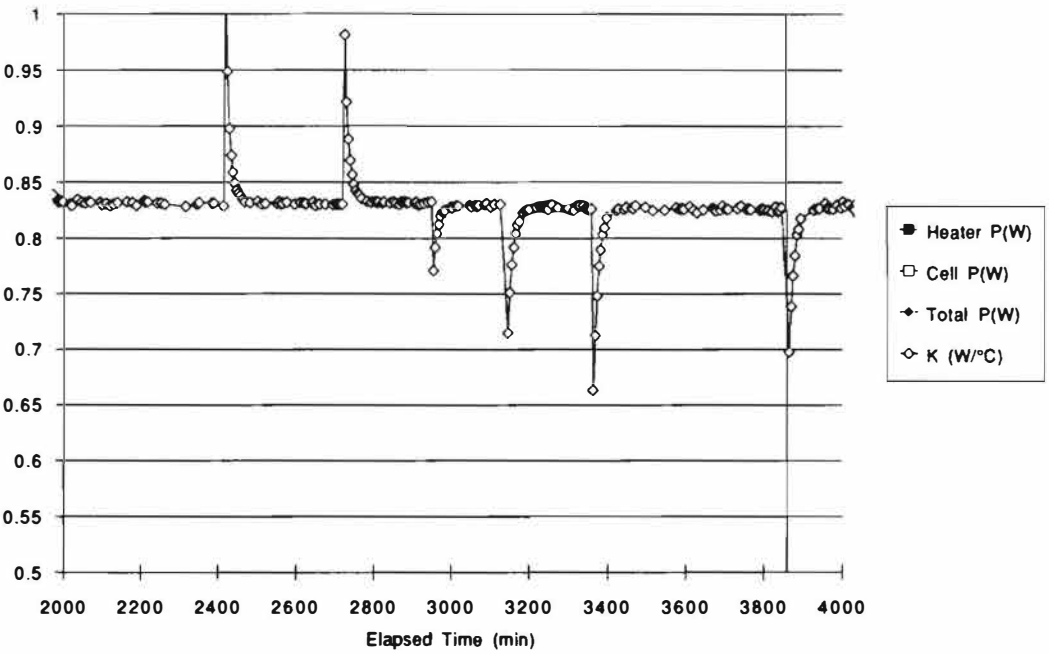

(b)

Figure 3. (a) The variation of Joule heater, electrolysis and total input power as a function of time during a calibration experiment using an external thin sheet Joule heater. The electrolysis was operated in the constant power mode. (b) The corresponding values of the calibration constant, K, as a function of time and the input power level. It is clear that K is practically independent of the input power level as well as time.

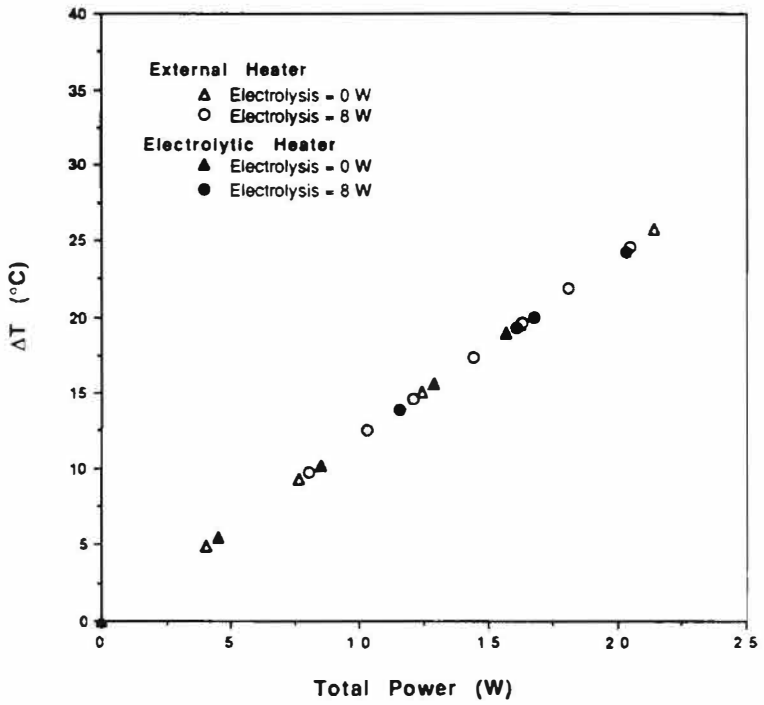

Figure 4. Calibration plot to compare two different ways of introducing calibration heat using external thin sheet and electrolytic Joule heaters both with and without electrolysis taking place.

The variation of the calibration constant with the cell temperature is also of interest. The data shown in Figure 5 indicate that K is practically constant over a wide range of temperature.

DISCUSSION AND CONCLUSIONS

It has been shown that the novel concentric cylinder isoperibolic calorimeter design has consistent and attractive features, providing reliable information with a high degree of precision. The general design feature whereby heat is uniformly distributed throughout heavy aluminum cylinders, where the temperature measurements are made, eliminates the uncertainities associated with the exact nature and location of the heat source and the temperature probe. It also renders the issue of the adequacy of stirring irrelevant, and thus makes these calorimeters attractive for the study of the thermal characteristics of the electrochemical insertion of deuterium into Pd, as well as other electrochemical studies.

The major construction materials are aluminum and alumina, both of which allow operation at quite high temperatures, perhaps up to 600 °C. Materials used for the construction of the electrochemical cell will be the major factor limiting the maximum temperature of operation.

Calibration has been conducted using three different modes of introducing calibration heat. The calibration constant was found to be independent of whether the power was supplied by an immersed Joule heater, internal electrolysis, or an external thin film Joule heater. This provides flexibility in experiments using this design.

Experiments on the time dependence of the response to step changes in the input power level have demonstrated 1/e times of about 15 minutes. This enables one to observe relatively rapid changes in the thermal behavior of electrochemical systems.

The calibration constants have been found to be independent of both time, input power level, and cell temperature over quite a wide ranges, with uncertainities less than $\pm$ 0.5 %.

This high level of precision makes it possible to accurately study questions such as the thermal behavior of Pd during the electrochemical insertion of deuterium.

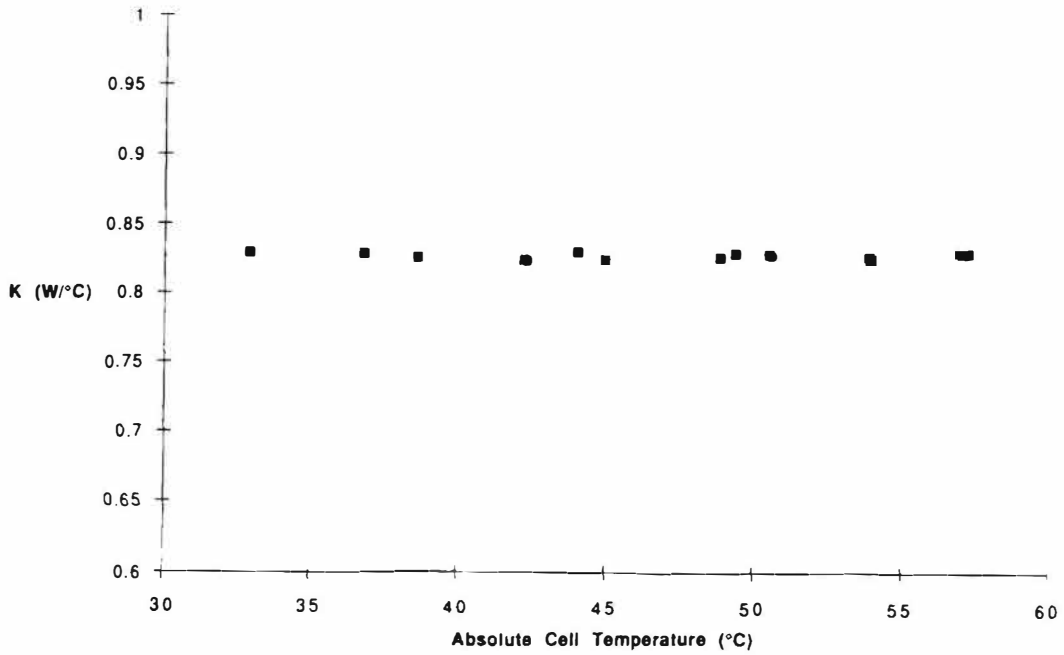

Figure 5. Temperature dependence of the calibration constant over a wide range of cell temperatures.

ACKNOWLEDGEMENTS

The authors were indebted to Roger Hart of Hart Scientific for valuable discussions and suggestions. This work was partially supported by the Electric Power Research Institute.

REFERENCES

1. M. Fleischmann and S. Pons, Jour. Electroanal. Chem. 261, 301 (1989)

2. Andreas Belzner, Ulrike Bischler, Steven Crouch-Baker, Turgut M. Gür, George Lucier, Martha Schreiber, and Robert A. Huggins, to be published in the Journal of Fusion Energy

3. Andreas Belzner, Ulrike Bischler, Steven Crouch-Baker, Turgut M. Gür, George Lucier, Martha Schreiber, and Robert A. Huggins, to be published in Solid State Ionics

4. Steven Crouch-Baker, Joseph A. Ferrante, Turgut M. Gür, George Lucier, Martha Schreiber and Robert A. Huggins, to be published in the Proceedings of the NSF-EPRI Workshop on "Anomalous Effects in Deuterated Metals" that was held October 16-18, 1989.

THEORETICAL IDEAS ON COLD FUSION

Giuliano Preparata
Dipartimento di Fisica, Università di Milano
and
INFN Sezione di Milano, Via Celoria 16, Milano, Italy

ABSTRACT: The rapidly expanding experimental body of information on the phenomena attributed to cold nuclear fusion poses several fundamental challenges to the generally accepted physical picture of both condensed matter and nuclear physics. In this presentation I will show how a recently proposed approach to the coherent electrodynamic processes in condensed matter, in terms of the so called "superradiant" behavior, can be used to provide for explicit coherent mechanisms for: (a) greatly enhancing the tunneling probability in the DD fusion process; (b) ultrarapid electron cooling of the excited compound nucleus, thus strongly suppressing the usual n-^{3}He and p-T channels of DD fusion in vacuum.

INTRODUCTION

In the year that has elapsed since the Fleischmann-Pons announcement of anomalous heat production in the electrolysis of heavy water with a Pd cathode, the experimental activity in the field of "cold" nuclear fusion has been steadily going on, so that today we can identify roughly 5 distinct lines, or broad categories of experimental results, with which present day theoretical efforts must confront themselves; namely

(1) The Fleischmann-Pons (FP) line[1], where an excess heat of the order of a few tens of $\frac{W}{cm^3}$ (corresponding to $\sim 10^{12}$ fusion $sec^{-1}cm^{-3}$) is produced over periods of time of a few days. The observed excess heat is at least 9 orders of magnitude larger than the rate of production of both neutrons and tritium;

(2) The Jones (J) line [2], where the electrolysis of heavy water is performed with both Pd and Ti cathodes, but with a very different choice for the electrolytes (in FP case LiOD 0.1 molar). The 2.45 MeV neutrons of DD fusion have been observed significantly above background, with rates typically 9-10 orders of magnitude smaller than those implied by FP excess heat. We may attribute to this line, due to the similarity in the fusion rates, also absorption experiments of gaseous D_2, such as Scaramuzzi's[3];

(3) The Texas A& M (TAM) line [4], where the excess heat production in similar electrolysis setups has been observed, accompanied by the occasional large release of tritium (with rate only a few orders of magnitude smaller than the FP rate) and of a much smaller numbers of neutrons (compatible with Jones' rate $\sim 10^2 \div 10^3$ fusions $sec^{-1}cm^{-3}$)

(4) The Brookhaven (B) line [5], where Titanium deuteride is bombarded with very small clusters of heavy water (of the typical size of a few hundred molecules) with average D energy of the order of few hundred eV. DD fusion is detected in the p-T channel with a cross section about 10^{10} times bigger than expected;

(5) The Caltech-Harwell-Yale (CHY) line[6], where FP types of experiment were conducted with sophisticated equipment to detect nuclear fusion products. No significant effects of any type have been observed.

Three of the four positive lines have received rather significant confirmation; here is a very incomplete and rather arbitrary selection:

(FP) The Minnesota group [7] experiment

(J) The Gran Sasso [8] and Los Alamos [9] experiments;

(TAM) The Oak Ridge [10] and Rome [11] experiments;

The most remarkable aspect, however, of the four positive lines is their general lack of reproducibility that, in a sense, makes them not totally incompatible with the CHY line.

Thus if we accept that, as J. Schwinger puts it, nuclear energy appears in an atomic lattice, we must face the hard and heavy task to understand theoretically how MeV physics (nuclear energy) can arise from eV physics (the energy that is at play in an atomic lattice). In other words we must address two basic problems:

i) how does the Coulomb barrier, that inhibits DD fusion in the D_2 molecule, get suppressed in a metal (Pd, Ti) matrix so as to enhance the tunneling probability by more than 50 orders of magnitude ($\sim 10^{-40}$ to account for J-line rates);

ii) how can DD fusion take place in a Pd lattice differently than in vacuum, and with a gain in rate of an extra ten orders of magnitude (to explain the FP rate).

Needless to say, the answer to both questions appears desperate within the generally accepted physical picture of condensed matter, where the elementary matter systems (nuclei, electrons, atoms) are held together by electrostatic and magnetostatic short-range forces. Indeed, as for i) the diffuse conduction electrons' cloud cannot substantially lower the DD Coulomb barrier, nor can the electrons' enhanced effective mass, that sometimes characterizes their propagation through the lattice, be invoked at the small distances ($\leq$ .5Å)

where tunneling takes place. As for ii) it appears sheer science fiction that for the times ($\sim 10^{-21}$ sec) and the distances ($\sim 10^{-12}$ cm) involved in DD fusion the lattice may be any different from the perturbative QED vacuum.

In this presentation I shall illustrate how a recent approach to the coherent interaction between the matter constituents and the electromagnetic radiation field [12] in condensed matter ("Superradiance") can provide natural mechanisms to give a solution to both problems i) and ii). Much of the material that I shall present has already appeared in print [13,14].

THE "PLASMAS" OF COLD FUSION

Let me first briefly illustrate the ideas and the main results of the application of "Superradiance" to plasmas [12].

A plasma is, as usual, a system of N charged particles, of charge Q and mass M, in a volume V oscillating around their equilibrium positions, immersed in a fluid of opposite charge that insures overall neutrality. Such a system is characterized, as well known, by a plasma frequency (I shall use throughout the natural units $\hbar = c = 1$)

$$\omega_p = \frac{Q}{(M)^{1/2}}(\frac{N}{V})^{1/2}, \qquad (1)$$

the frequency of small amplitude oscillations of the charged particles around their equilibrium positions. The "Superradiant" program describes a plasma by a quantum wave field $\Psi(\vec{x}, \vec{\xi}, t)$, $\vec{x}$ denoting the equilibrium position and $\vec{\xi}$ the small deviation therefrom (obviously the particle position is $\vec{X} = \vec{x} + \vec{\xi}$). For large N it is possible to show that:

(a) the wave field can be written as

$$\Psi(\vec{x}, \vec{\xi}, t) = \Psi_0(\vec{x}, \vec{\xi}, t) + \eta(\vec{x}, \vec{\xi}, t), \qquad (2)$$

where $\Psi_0(\vec{x}, \vec{\xi}, t)$ is a complex c-number wave function such that

$$|\Psi_0(\vec{x}, \vec{\xi}, t)|^2 \sim O(\frac{N}{V}), \qquad (3)$$

while $\eta(\vec{x}, \vec{\xi}, t)$, the field of quantum fluctuations, is in general $O[\frac{|\Psi_0(\vec{x}, \vec{\xi}, t)|}{\sqrt{N}}]$;

(b) the wave function $\Psi_0(\vec{x}, \vec{\xi}, t)$ is $\vec{x}$ independent within space domains of at least the size of the e.m. field wave length λ_p associated with the plasma frequency ω_p,

$$\lambda_p = \frac{2\pi}{\omega_p}, \qquad (4)$$

such space regions shall be called "coherence domains";

(c) at temperature T=0, within a coherence domain all charges oscillate in phase performing oscillations of well defined amplitude, depending on the anharmonicities of the real system. These coherent charge oscillations are also in phase with a peculiar coherent mode of the e.m. field, of wave length λ_p and frequency $\omega < \omega_p$, that remains trapped in matter;

(d) the coherent e.m. field interacts also with the quantum fluctuations $\eta(\vec{x}, \vec{\xi}, t)$, creating energy gaps in their spectrum. When T increases the quantum fluctuations get excited with a Boltzmann spectrum up to the point when the condensed phase described by $\Psi_0(\vec{x}, \vec{\xi}, t)$ is totally depleted, thus leading to a phase transition.

In the following these results shall be applied to the three plasmas of a Pd deuteride:

(α) the electron plasma of the 10 peripheral d electrons, with plasma frequency

$$\omega_{ep} \simeq 30\ eV, \qquad (5)$$

implying that the minimum size of coherence domains is

$$\lambda_{ep} = \frac{2\pi}{\omega_{ep}} \simeq 400\mathring{A}; \qquad (6)$$

(β) the Pd nuclei plasma(*) whose plasma frequency is

$$\omega_{Np} \simeq .85\ eV, \qquad (7)$$

with coherence length

$$\lambda_{Np} = 1.5\mu; \qquad (8)$$

(γ) the D plasma with

$$\omega_{Dp} = x^{1/2}.13\ eV, \qquad (9)$$

and

$$\lambda_{Dp} \simeq 10\ x^{-1/2}\mu; \qquad (10)$$

where x denotes the ratio D/Pd.

Before proceeding I should sound the warning that in real life $T \neq 0$, and the different systems may considerably deviate from the behavior of an ideal plasma. However I shall assume that these factors do not qualitatively change the picture.

(*)Actually in the analysis of this paper, this plasma does not play any important role.

THE COHERENT ELECTRON PLASMA AND THE ENHANCED TUNNELING

Let's consider a plane of the Pd lattice (see Fig.1). Suppose that the d electrons oscillate coherently in one of the direction connecting nearest Pd neighbors (say ξ);

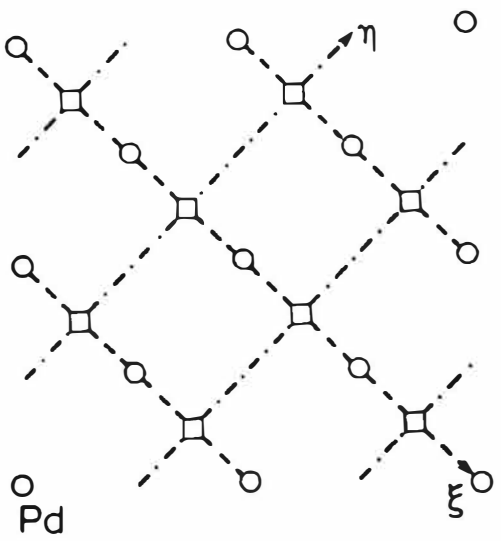

Fig.1 A plane of the Pd-lattice. The sites denoted by a circle are occupied by the Pd-nuclei, while those denoted by a square are occupied by D-nuclei. ξ and η are the two orthogonal directions linking nearest Pd neighbors. The dashed lines shall be called ξ-lines, the dash-dotted η-lines.

then from Thomas-Fermi theory we have approximately the situation depicted in fig.2. We can imagine in fact the d-electrons concentrated in a spherical shell at about 1.5 a_o (a_o = .57 Åis the Bohr radius) from the Pd nucleus, performing coherent oscillations of amplitude approximatively a_o in the ξ-direction. It is clear that in the hatched region of fig.2 a static negative charge distribution will be seen by any D nucleus moving along the orthogonal direction η . A simple application of the Gauss theorem to the disc-like region around the positions denoted by squares in fig.1, of height (in the ξ direction) a_o and radius R, together with symmetry considerations [the electric field in the ξ-direction vanishes for symmetry reasons on the circles at $\xi = \pm a_o/2$ (fig.2)], yields (e is the electron charge; $\alpha = \frac{e^2}{4\pi} \simeq \frac{1}{137}$)

$$e\,V(R) \simeq Z_d \frac{\alpha}{a_o} \frac{R^2}{R_o^2} \qquad (11)$$

where $R_o \simeq \sqrt{2} a_o$ (the maximum radius of the disc within which the stationary electron plasma is contained) and $Z_d \simeq \frac{10}{3}$ is the charge contained in the disc. Thus along any η-line we have the potential profile reported in fig.3(a).

Suppose a D_2 molecule of the approximate size of $\simeq 2a_0$ enters the lattice, the electrostatic forces will be strong enough to tear it apart and send the deuterons into contiguous minima, thus modifying the potential profile as depicted in figure 3(b). The modification of the nearest wells (by about 10 eV at the bottom) is then, presumably, strong enough that molecular D_2 cannot be dissociated there. This would explain easily and naturally why the β-phase of D_2 absorbed in Pd, in a wide span of p and T, is at $x \simeq 2/3$. This physical situation does not apply to the D nucleus (which is presumably the form in which deuterium enters the lattice in appropriate electrolytical conditions), and its wandering around will bring it to fill one of the vacant deep holes. In the process it may be trapped in one of the shallow holes(fig.3(b)), but it will have no chance to tunnel toward the D nucleus sitting close, for there are around empty deep holes that are better accessible. The situation will clearly change when all the deep holes are filled, i.e. when

$$x \simeq 1, \qquad (12)$$

for then the D nucleus trapped inside the lattice will evolve to a stationary state, and its tunneling amplitude can be computed by the well known semiclassical formula:

$$D_T^{1/2} \sim exp - (2\mu)^{1/2} \int_{r_n}^{r_0} dr \sqrt{V(r) - E}, \qquad (13)$$

where $\mu = \frac{m_p}{2}$, $E \simeq 0$,

$$V(r) \simeq \frac{\alpha}{r} - V_0 \qquad (V_0 \simeq 100\ eV), \qquad (14)$$

the classical turning point r_o is given by

$$r_0 = \frac{\alpha}{V_0} \simeq 1.4 \cdot 10^{-9} cm,$$

and r_n is the distance between the two protons ($\sim 10^{-12}$) where Yukawa attraction overtakes Coulomb repulsion. A simple calculation yields:

$$D_T^{1/2} \simeq exp\{-(2\mu\alpha r_0)^{1/2}[\frac{\pi}{2} - 2(\frac{r_n}{r_0})^{1/2}]\} =$$

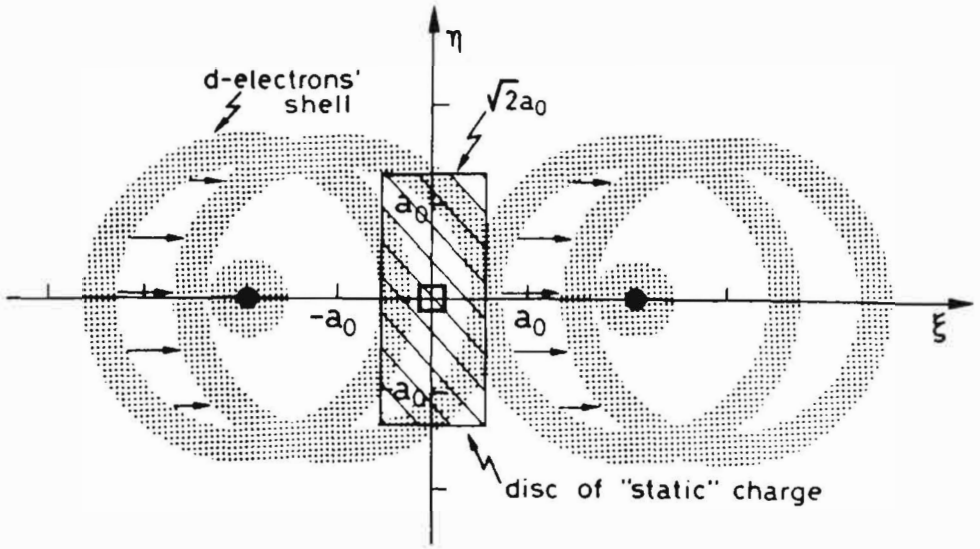

Fig.2 The d-electrons' plasma oscillations between nearest Pd-neighbors. a_o is the Bohr radius (.57Å)

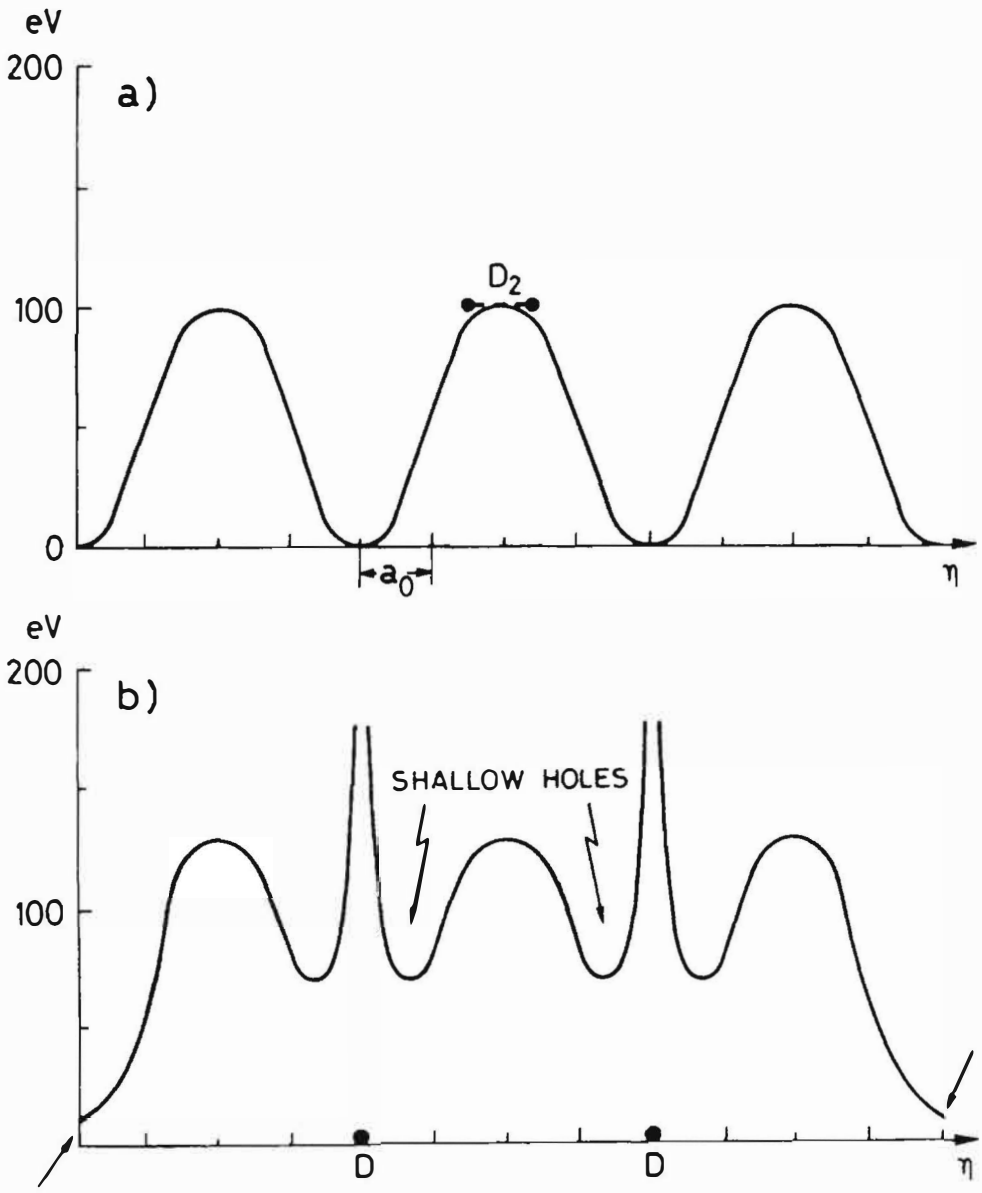

Fig.3
(a) The potential profile along η that a D_2 molecule sees in an empty Pd-lattice.
(b) Same, when two contiguous square-sites are occupied by a D-nuclei. The arrows indicate the modification of the deep holes close to the D's.

$$= 10^{-21.5} \cdot 10^{3(r_n)^{1/2}} \sim \quad (r_n \text{ in fermis})$$

$$\sim 10^{-20} \quad \text{for } r_n \simeq 20F, \qquad (15)$$

thus realising an enhancement of some 30 orders of magnitude over the tunneling amplitude for molecular deuterium. For titanium deuteride similar mechanisms can be envisaged, but an explicit analysis has still to be performed.

COHERENT vs. INCOHERENT FUSION

If the coherent electron plasma oscillations, just described, were the whole story, that part (10^{-40}) of all the D nuclei in excess of $x_0 N (x_0 \simeq 1)$ that tunnels beyond r_n would undergo usual (in vacuo) DD fusion with an incoherent fusion rate ($\Gamma \sim 10^{21} sec^{-1}$)

$$R_{inc} = D_T(x - x_0) N \Gamma \simeq$$

$$\simeq 5 \cdot 10^3 (x - x_0) sec^{-1} cm^{-3} \qquad (16)$$

some ten orders of magnitude smaller than the rate of excess heat production. This, however, may explain the results belonging to the J-line. Furthermore, the incoherent fusion will yield the same fusion products as hot fusion, namely p-T and n-^{3}He in an approximately fifty-fifty proportion.

Where then can one find the factor of about ten billion that we need to account for the observed excess heat? Let's suppose that x_0 has been reached and therefore no "deep hole" is accessible to the extra $(x - x_0)$N deuterons that are jammed into the lattice. Then the plasma of deuterons in the deep holes within a coherence domain (10μ across) will be in a collective state and will be "seen" by the incoming excess deuteron as **a single quantum mechanical system**, described by **a single quantum mechanical wave function.** This simply means that the DD fusion amplitude will be constructed coherently by summing over all N_{cd} (N_{cd} is the number of D's in a coherence domain) "classical paths of fusion". However in order for coherence to hold up we must require that very little or no energy be transferred to the D plasma. As a consequence we must have somebody else in the metal to carry away the several MeV involved in a fusion process.

We shall now see how the electron plasma can do this job most efficiently. By applying perturbation theory, we need compute the diagram in fig.4, according to which the fusion amplitude at the time T, for an energy release E to the plasma, is given by

$$A_n(E,T) = -i \int_0^T dt \langle e'_p n | \vec{d} \cdot \vec{E}(t) | e_p \rangle, \qquad (17)$$

where $\vec{d}$ is the electric dipole operator for the electron plasma [12],

$$\vec{d} = e(\frac{1}{2m_e \omega_{ep}})^{1/2}(\vec{a}^\dagger + \vec{a}),$$

and the electric field $\vec{E}(t)$ is given by the matrix element

$$\langle final\ state, -E | \vec{E}(t) | DD_p \rangle =$$

$$= \frac{ie^{-iEt}}{E} - \langle final\ state, -E | \vec{J}_{em}(0) | DD_p \rangle, \qquad (18)$$

where use has been made of the Maxwell equations and the fact that, due to the condensation of the plasma of deuterons D_p, no substantial $\vec{x}$-dependence can arise in the problem. Thus in order for the matrix element (18) to be non zero beyond r_n we must have nuclear configurations that allow for the large e.m. current needed in the cooling process.

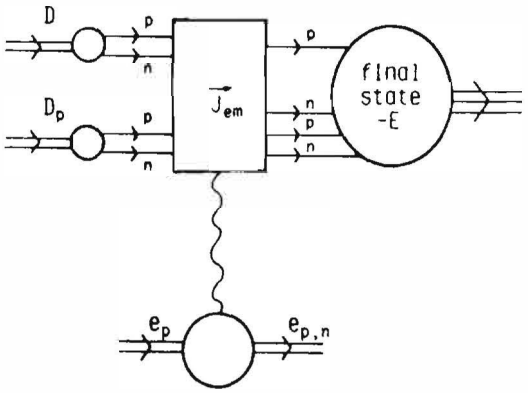

Fig.4 The perturbative amplitude for the electromagnetic cooling of the initial DD_p-state by the electron plasma.

A look at fig.5 immediately shows that the most favorable configuration for the long range Yukawa interaction (that requires a neutron and a proton to "face" each other) in order to give rise to large e.m. currents (through the rapid motion of the peripheral proton) must evolve into a p-T^* configuration.

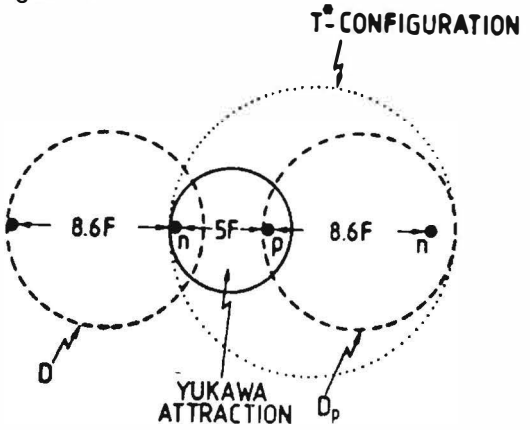

Fig.5 The preferred configuration for DD_p-tunneling (p n facing each other) evolves toward a p-T^* state in order to maximize the e.m. current, necessary to the couple the electron plasma.

The n-$^3He^*$ configuration being clearly suppressed for in this case it is the neutron that is rapidly moving. Thus we can write

$$\vec{E}(t) \sim \frac{e^{-iEt}}{E} e\vec{v}_p(E) D_T^{1/2} \left(\frac{N}{V}\right) =$$

$$= ie^{-iEt}\vec{E}_0 D_T^{1/2}, \qquad (19)$$

where $|\vec{v}_p| \simeq .1$ for $E \simeq 5MeV$. The probability for an energy release E after the time T can be easily calculated from (17). We obtain:

$$P(E,T) = \sum_n |A_n(E,T)|^2 =$$

$$= \frac{4e^2}{E^2}|\vec{E}_0|^2 \frac{D_T N_e^2}{2m_e\omega_{ep}} \sin^2\left(\frac{ET}{2}\right), \qquad (20)$$

where N_e is the number of "condensed" electrons contained in a coherence domain of the D plasma (with volume $V_{cd} \simeq \lambda_p^3$):

$$N_e \simeq 10\frac{N}{V}V_{cd} \cdot f \simeq 6 \cdot 10^{14} f, \qquad (21)$$

$f \leq 1$ being the fraction of the correlated component of the electron plasma. In order to determine the "coherent" fusion rate we must evaluate the energy E that the electron plasma can absorb in a cycle $ET = \pi$. From the classical equation ($\vec{v}_e$ is the velocity of the electron plasma)

$$\frac{dE}{dt} = e\vec{E}_0 \cdot \vec{v}_e N_e \sin(Et), \qquad (22)$$

and Eq.(19) one obtains

$$E^3 = 2e^2(\vec{v}_p \cdot \vec{v}_e)\frac{N}{V}N_e, \qquad (23)$$

and putting numbers in one gets

$$E \simeq 3.6\, f^{1/3} MeV. \qquad (24)$$

The time in which this energy is released is given by

$$T = \frac{\pi}{E} \simeq f^{-1/3}\ .5 \cdot 10^{-21} sec, \qquad (25)$$

very short indeed! We can now estimate the coherent fusion rate

$$R_{coh} = (x - x_0)N\Gamma_{coh} \simeq$$

$$\simeq f(x - x_0)3.5 \cdot 10^{13} sec^{-1} cm^{-3}, \qquad (26)$$

$$\Gamma_{coh} = \frac{P(E,T)}{T} = f\ .7 \cdot 10^{-9} sec^{-1}, \qquad (27)$$

some ten orders of magnitude larger than R_{inc}. For $x - x_0 \simeq .1$ and $f \simeq 1$, we obtain a power output

$$W \simeq 20\, Watt/cm^3. \qquad (28)$$

In spite of the definite crudeness of the calculation reported here, we seem to obtain rather naturally numbers in the right ball park.

HAS A COHERENT PICTURE EMERGED?

I shall address this question by assuming that superradiant behavior sets in in all plasmas of the metal-deuteride under consideration. Then for the various lines, sketched in the Introduction, the following is a possible scenario arising from the previous discussion:

(a) The CHY line, that reports consistently negative results can be explained by the failure of the groups involved to reach the obligatory threshold value $x_0 \simeq 1$ (*).

(*) From a discussion with Dr. F.G.Will, this possibility seems strongly suggested by his survey of all negative and positive results so far reported.

The threshold condition may also be a convincing explanation for the universally observed erratic reproducibility of the cold fusion phenomena.

(b) The B line: if the kind of potential wells ($\sim 100\ eV$) that surround D in the Pd lattice also hold in the Ti lattice (we have not been able to work it out yet, however) then the enhancement by 10 orders of magnitude of the DD fusion cross-section, observed in [4], can be easily explained.

(c) The J line: the conditions prevailing in this line of experiment are most likely non-stationary, so that the incoherent fusion processes with rate (16) is the only possible. This agrees with observation.

(d) The FP line: the substantial excess heat of the order of a few tens of $Watts/cm^3$ observed by Fleischmann and Pons is just in agreement with (28). The lack of observation of both neutrons and tritium can be understood if we make the hypothesis that they have reached almost ideal conditions ($f \simeq 1$). In this case, after the coherent interaction with the electron plasma has cooled the DD system, according to (24) by about $3.6\ MeV$, the successive cooling steps will occur with rates

$$\Gamma \simeq \frac{1}{T} = \frac{E}{\pi} \simeq 1.2\ MeV,$$

[see Eq. (25)], competing in principle with the rate of a p-T^* configuration to turn into a p T state with a Q value of about $400\ KeV$. It is reasonable that in this condition the latter rate will be much smaller than 1 MeV (or $1.5 \cdot 10^{21} sec^{-1}$).

(e) The TAM line: abundant production of tritium in a late stage of excess heat yield may be attributed to some ageing effect of the electron plasma, which substantially lowers f by the presumable creation of vortices in the cooling processes. If this is the case, for, say, $f \simeq 10^{-2}$ according to (24) the cooling steps carry away about $800\ KeV$ each, and their rate is [see Eq.(25)] about $0.5 \cdot 10^{21} sec^{-1}$ (or $250\ KeV$). This means that after about 5 steps the system p-T^*, having consumed all its Q($\sim 4MeV$), will be close to a p-T configuration where both nuclei are at rest, thus decoupling from the electrons' plasma. Coulomb repulsion will then succeed in producing, some of the times, a (almost) zero-energy p-T final state at a rate between two and three orders of magnitude smaller than the FP-rate, as observed. Obviously much more theoretical work is needed to turn this plausible arguments into a quantitative description. We hope to get back to this important problem soon.

Finally, about the question of the main fusion product in the FP and TAM lines the inevitable conclusion is that ^4He is produced. It is very unlikely, however, that in the condition prevailing in a "successful" electrolysis atomic He, which most probably gets formed, lingers on in the Pd lattice, being expelled by the flux of incoming D nuclei that strenuously compete to occupy the shallow holes available to them.

Acknowledgements

Let me thank most deeply Dr. Frits G. Will, Director of the Cold Fusion Institute, for his kind invitation to present my and my colleagues' (Tullio Bressani and Emilio Del Giudice) thoughts on the fascinating subject of cold fusion. I should likewise thank Profs. M. Fleischmann and S. Pons for illuminating discussions. I have also greatly benefitted from conversation with, among many others, J. Appleby, S. Jones, N. Packham, J. Rafelsky, F. Will and K. Wolf.

REFERENCES

[1] M. Fleischmann, M. Hawkin and S. Pons, J. Electroanal. Chem. 261,301 (1989).

[2] S.E. Jones, E.P. Palmer, J.B. Csirr, D.L. Decker, G.L. Jensen, J.M. Thorne, S.F. Taylor and J. Rafelsky, Nature 338,737 (1989).

[3] A. De Ninno et al., Nuovo Cim. 101A, 841 (1989).

[4] R.C. Kainthlia, O. Velev, L. Kaba, G.H. Sin, W.J.C. Packham, M. Szklarczyk, J. Wass and J.O'M. Bockris, Electrochimica Acta 34, 1315 (1989);
K.L. Wolf et al., Proc. DOE Workshop, Santa Fe, NM, May 1989.

[5] R.J. Beuhler, G. Friedlander and L. Friedman, Phys. Rev. Lett. 63, 1292 (1989).

[6] M. Gai et al., Nature 340, 29 (1989);
N.S. Lewis et al., Nature 340, 525 (1989);
D.E. Williams et al., Nature 342, 375 (1989).

[7] R.A. Oriani et al., Calorimetric measurements of excess power output during the cathodic charging of Deuterium into Palladium. Univ. of Minnesota preprint (1989).

[8] A. Bertin et al., Nuovo Cim. 101A, 997 (1989).

[9] H.O. Menlove, E. Garcia and S.E. Jones, Update on the measurement of neutron emission from Ti sample in pressurized D_2 gas, Los Alamos LA-UR 89-3633 preprint (1989).

[10] C.D. Scott et al., A preliminary investigation of Cold Fusion by Electrolysis of Heavy Water-ORNL/TM-11322(1989).

[11] D. Gozzi et al., Nuovo Cim. 103A, 143(1990).

[12] G. Preparata, Quantum field theory of super-

radiance, in Problems of Fundamental Modern Physics, R. Cherubini, P. Dal Pias and B. Minetti Eds. World Scientific (1990).

[13] T. Bressani, E. Del Giudice and G. Preparata, Nuovo Cim. 101A, 845 (1989).

[14] T. Bressani, E. Del Giudice and G. Preparata, A possible coherent dynamics underlying "Cold" Nuclear fusion, in "Understanding Cold Fusion Phenomena", R.A. Ricci, E. Sindoni and F. De Marco, Ed. SIF Bologna (1989).

STATUS OF COHERENT FUSION THEORY

Peter L. Hagelstein

Massachusetts Institute of Technology
Research Laboratory of Electronics
Cambridge, Massachusetts 02139

ABSTRACT

Nuclear reactions which may exhibit coherent effects have been studied as a candidate explanation for cold fusion effects.

An analysis of a general class of two-step coherent reactions involving charged nucleons has been performed, and very small reaction rates are found. This result is due to the small tunneling factors associated with coulomb repulsion.

We are investigating two-step coherent reactions which begin through weak interaction mediated electron capture, which in hydrogen isotopes would produce off-shell (virtual) neutrons. No coulomb repulsion occurs for virtual neutrons. Virtual neutron capture by deuterons would yield tritium, and virtual neutron capture by protons would yield deuterons; the latter process is favored by a factor of 10^4 in the square of the matrix element on a per nucleon basis, and corresponds to a heat-producing reaction. The nuclear reaction energy would be coupled into the electrolysis process, with the final reaction products stationary.

We have found that the weak interaction process can in principle be superradiant in the Dicke sense. If so, then considerable acceleration of this type of coherent reaction may occur.

I. INTRODUCTION

Much controversy has surrounded the area of cold fusion research since its inception last March following the initial papers of Fleischmann and Pons at Utah[1,2] and Jones et al. at BYU[3]. During the months that followed numerous experiments were performed, most of which did not reproduce any of the various "miracles" that have become associated with cold fusion.[4–22] Especially disconcerting was the apparent inability of the principle advocates of cold fusion to reproduce their own results.

Based on these points, and based also on the complete lack of any supporting theory or basic mechanism, the scientific community views cold fusion research of any sort with extreme skepticism. The ERAB review board[23] politely summarized this position with the comment: "Based on these many negative results and the marginal statistical significance of reported positive results, the Panel concludes that the present evidence for the discovery of a new nuclear process termed cold fusion is not persuasive." *Nature* has gone further and has published a number of obituaries for cold fusion.[24–26]

The arguments that have been given for the fundamental unsoundness of cold fusion research in general are numerous. Among them is the basic physics problem associated with overcoming the coulomb barrier at room temperature, and accounting for heat with no apparent nuclear byproducts. Additionally, the positive cold fusion results appear to be in direct contradiction to very basic precepts of nuclear physics, and it seems that an extremely fundamental and totally unexpected change in our understanding of physics would be required even to begin accounting for the various "miracles" that have been claimed. Finally, it has been remarked in private countless times that the single strongest argument against cold fusion is that the experimental effects simply vanish whenever a competent physicist performs the relevant measurements with adequate instrumentation, and that anyone claiming to observe a positive result is self-deluding.

D. Morrison is studying the progress of cold fusion as an example of pathological science.[27]

In spite of the views of the majority of physicists, positive experimental results in support of anomalous effects persist (as described in a recent review by Bockris[28]). Evidence for very substantial excess heat generation in closed system calorimetry experiments has been obtained at

Stanford.[29] The isoperibolic calorimeter is simple and well-calibrated; the error bars are at the 1 % level, and the signals exceed 20 %. This evidence is compelling. Observations of heat have been reported by numerous other laboratories.[30–37]

Perhaps the strongest evidence for substantial tritium production comes from Texas A&M.[38] Additionally, tritium production has been reported numerous times.[39–44] Neutron emission in electrolysis cells has been reported by BYU,[3] and has been claimed at other laboratories.[33,45,46] Neutron emission in gas cells has been reported by Frascati[47] (who have recently seen more neutrons[48]), LANL,[40,49] and elsewhere.[50] Fast protons have been reported in Ref. 51.

Heat bursts have been reported by many workers. Pons and Fleischmann reported early on in their work that a cubic centimeter cube exploded. Bockris mentions exploding rods in his review. Extreme heat production was reported by Gozzi et al.,[52,53] in a non-reproduced experiment.

There are proponents of cold fusion and there are skeptics. The skeptics have demonstrated that no cold fusion effects occur. The proponents have answered most if not all of the skeptics criticisms with respect to experimental methodology, and have demonstrated that the effect is real. Unfortunately the skeptics and proponents rarely meet and discuss physics, and this is very unfortunate for all involved.

We have adopted the position of devil's advocate (relatively). We have looked at the problem from the point of view that the effect may both be real and be all that was originally claimed for it, and from there inquired how it could possibly come about, without breaking basic physical laws in the process. The current experimental evidence from the proponents largely supports such a view, even at this late date after the obituaries have appeared in print.

We have speculated given the assumptions that the heat is real and of nuclear origin. It seems to follow that if the heat is real and accurately measured, that it must be nuclear since the total energy production that is reported would correspond to more than 10 eV per atom of electrode. Additionally, if the tritium production is real, it most certainly involves nuclear processes since tritium cannot be made chemically. Finally, if the neutrons are real, then they too would provide evidence for the occurrence of a nuclear process.

But what nuclear process? Certainly conventional binary nuclear reactions cannot do it, for two compelling reasons: (1) there is no way known to overcome the coulomb barrier at room temperature to the degree required under electrolysis conditions, and (2) there is no experimental support for any known conventional reaction that can produce either heat or tritium as it is reportedly produced.

Furthermore, if the tritium is real at the levels reported, and if it is actually produced with a low accompanying secondary 14 MeV neutron emission rate that is smaller by many orders of magnitude as is reported, then it implies a very severe constraint on the final state tritium kinetic energy that may occur. This constraint is described in this paper, and more or less implies that no conventional binary fusion reaction is likely to be responsible, since the tritium which is produced is essentially sitting still by nuclear standards.

Another constraint must be obeyed by any nuclear reaction that is proposed to account for the "miracles." Not only do the reactions have to be consistent with the observed stability of heavy water and deuterium gas not involved in cold fusion experiments, but they must be consistent with stellar evolution models. The existence of a binary fusion reaction that occurs at room temperature would in all probability be impossible to reconcile with stellar models at higher temperatures.

Our general approach has been to explore what we have termed coherent nuclear reactions. These are proposed reactions that would proceed collectively due to some unique feature of the reaction, and occur only rarely as incoherent or binary reactions. Such reactions certainly can be postulated and are certainly physical, but most occur with an utterly negligible reaction rate. To our knowledge there is no previous work or speculation on such reactions; aside from the recent cold fusion results there would be no motivation aside from curiosity to explore collective nuclear reactions.

Our initial efforts involved the consideration the implications of coherent *dd* reactions between coupled nuclear/lattice states that were degenerate. The idea is interesting, but finding microscopic mechanisms that support such a picture has been difficult. We analyzed a rather general class of coherent fusion reactions between charged hydrogen isotopes, and we were able to show that

all such reactions in general occur with reaction rates that are quite small. The basic problem is that the matrix elements between initial and final states are too small due to exponentially small tunneling factors to support reaction rates in the range of those reported.

One solution to this very general problem is to consider coherent reactions wherein the fusion occurs between a neutral nucleon (neutron) and a charged nucleon. The weak interaction can provide a mechanism to reduce the charge of a hydrogen isotope, and the resulting problem becomes one of studying virtual neutron states, since the process is by necessity off-shell. A weakness of the approach is that one very difficult problem is replaced by another very difficult problem: that off-shell neutrons almost never stray far from their point of origin.

A second perceived weakness of the approach is that a reaction that begins with a weak interaction matrix element is probably going to be vanishingly small. We have found, or so we believe, an interesting situation in which a coherence effect has the potential to enhance neutrino emission (and therefore the effective strength of the weak interaction) by a large factor. This effect can be described briefly as Dicke superradiance of neutrinos. If it occurs, a condition that must be obeyed is that the final nucleon states be stationary. This condition is consistent with the constraint imposed by the low neutron emission observations during heat generation and tritium production. In order for this to occur, the nuclear energy must be transferred elsewhere in a nondisruptive manner, a process which has no precedent in nuclear physics.

This is our general approach, and the specific scenario that we envision is one in which deuterons generate virtual neutrons through electron capture and coherent neutrino emission, and heat and tritium generation occurs through virtual neutron pickup by protons and deuterons. The nuclear energy is transferred to the macroscopic level coherently through M1 interaction of the nuclear dipoles with the current in the presence of a high order nonlinearity. Protons are substantially more reactive than deuterons in virtual neutron pickup as is discussed later in this work (section VI).

The fuel for heat production in this scenario are protons, deuterons and electrons; the palladium is in a sense a catalyst by virtue of its electrochemical and magnetic properties. The byproducts of the reaction are deuterons and soft neutrinos (which are probably unobservable), and the deuterons are born stationary. This scenario is qualitatively consistent with many of the reported observations. The process would not occur in stars due to the coherency and current requirements. It remains to be seen whether the scenario can become a predictive theory.

The remainder of this report is divided up as follows: In section II we consider the implications of the low values of observed neutron emission. We review the basic reactions that we have considered during this work in Section III. The relative strengths of M1 matrix elements for slow neutron pickup by protons and deuterons is considered in Section IV. We show that neutrino emission can occur coherently in section V; and we discuss the coupling of energy from the microscopic to the macroscopic in section VI. We provide further discussion in Section VII. Proposals for experiments that would help elucidate reaction mechanisms within the framework of our scenario are given in Section VIII.

We will not discuss other theoretical approaches in this paper. A very critical article[26] by Lindley summarizes the most popular models and their drawbacks.

II. LIMITS ON THE KINETIC ENERGY OF FINAL PRODUCTS

Consensus is appearing among some cold fusion experimentalists regarding upper bounds on neutron production when either heat or tritium is observed. It is found at numerous laboratories that the neutron production rate occurs at a rate which is less than 10^{-8} of the rate at which tritium production occurs. A stronger bound occurs in the case of heat production, under the assumption that heat producing reactions evolve MeV-level energy per reaction.

Such upper bounds imply a maximum kinetic energy possible for final state reaction products. In conventional exothermic fusion reactions, the nuclear energy released appears as kinetic energy of the products or as gamma radiation. There are no reports of the observation of gamma emission from any cold fusion experiments, and the bounds on neutron emission can be used to limit directly the final reaction product kinetic energy.

If tritium is created initially at high (MeV) kinetic energy, then the probability that a DT reaction which produces a 14 MeV neutron occurs can be computed from the yield formula to be in the vicinity of $10^{-5} - 10^{-4}$ per triton. In order to obtain a neutron to triton ratio which is as low as 10^{-8}, the emitted triton energy must be quite low. We have estimated the neutron yield for fast tritons in a deuterated palladium lattice from

$$Y(E) = \int_0^\infty N_D \sigma_{DT}(\epsilon) \left[\frac{d\Delta E}{dx}\right]^{-1} d\epsilon \quad (II.1)$$

following Batra et al[54] and Armstrong et al[55], where N_D is the deuterium number density, and σ_{DT} is the fusion cross section. We have adopted the range data of Janni[56] for palladium. The result is shown in Figure 1. A neutron yield of 10^{-8} would correspond to an upper limit on tritium kinetic energy of about 25 keV.

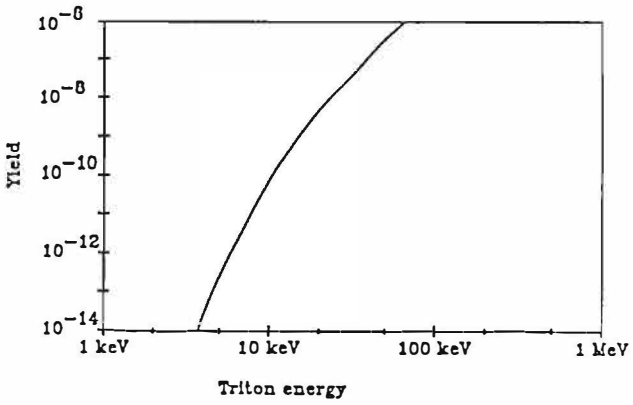

Figure 1: Yield of 14 MeV DT neutrons through fusion of fast tritons in deuterated palladium as a function of triton energy.

A point of interest here is that the neutrons which have been reported to date are not consistent with 14 MeV emission, but rather the observed neutrons are thought to be 2 MeV neutrons (consistent with dd fusion neutrons). If so, then the relevant constraint on 14 MeV neutron yield emission is more severe, and bounds the maximum triton kinetic energy to even smaller values. Kevin Wolf at Texas A&M estimates that this bound can currently be taken to be 15 keV.[57]

The relative lack of neutron emission can be used to rule out essentially all known nuclear fusion reactions which evolve tritium, even if some mechanism were found to overcome the coulomb barrier. Furthermore, any proposed theoretical explanations for Pons-Fleischmann effects (heat and tritium) should be consistent with these observations.

We have considered the possibility that heat production occurs through virtual neutron capture by protons. The end product of such a capture process would be a deuteron, and the above arguments can be repeated to obtain an upper limit on the deuteron kinetic energy. The yield formula

$$Y(E) = \int_0^\infty N_D \sigma_{DD}(\epsilon) \left[\frac{d\Delta E}{dx}\right]^{-1} d\epsilon \quad (II.2)$$

was evaluated using the dd cross section of Brown and Jarmie[58], and the result is shown in Figure 2. One is tempted to apply this yield formula to the original Pons-Fleischmann data, and take the upper bound on neutron yield from Ref. 4. This gives an upper bound on neutron yield on the order of 10^{-11}. By itself, this would give an upper bound of less than 20 keV for a deuteron kinetic energy, under the two assumptions that the Pons-Fleischmann heat is real and that deuteron production is responsible.

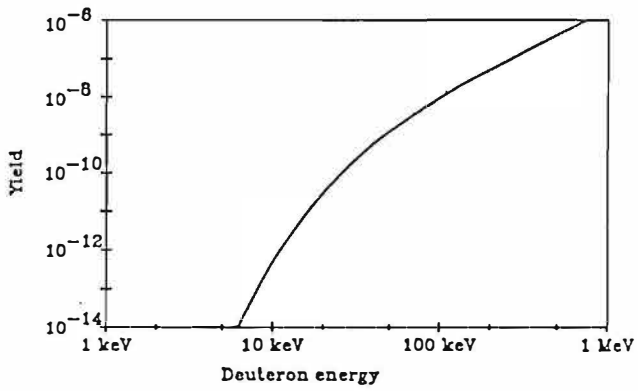

Figure 2: Yield of 2.4 MeV DD neutrons through fusion of fast deuterons in deuterated palladium as a function of triton energy.

III. SUMMARY OF REACTIONS EXAMINED

In the course of our efforts, we have focussed on the general notion that collective effects may be involved.[59] This notion will be illustrated in the examples under discussion. We have looked

for effects which involve primarily deuterium and protons.

A. $d + d \longleftrightarrow {}^4He$

The initial report of Pons and Fleischmann proposed that *dd* fusion was responsible for the effects, and we considered initially what would be required for this to occur. One idea was that a lattice under stress might show multiphonon response in the MeV range due to fractures, and that in some way the electromagnetic interaction could get the energy out coherently at an enhanced rate.

The principal drawback to this approach is the exponentially damped electric quadrupole moment between initial and final states due to the Coulomb barrier between nucleons.

B. Fusion/Beta Two step reactions: $p + d \longleftrightarrow ({}^3He)_V \rightarrow t + e^+ + \nu_e$

Two step reactions in which fusion is followed by an incoherent decay process have the possibility of behaving coherently if the exchanged photon is soft. We were able to formulate a many-body theory for this class of reaction based on the analogy with laser physics models. We found that the model was mathematically tractable but that all effects due to this type of reaction were quite small due to the small electromagnetic moment between initial and final fusing states. In essence, if there were some way to enhance the tunneling, then coherent two-step reactions of this type might occur. The detailed analysis of such processes is documented in our ASME paper.

C. Beta/Fusion Two-step Reactions: $d + e + 2p \longrightarrow (\nu_e + 2n + 2p)_V \longleftrightarrow \nu_e + 2d + 2.05\ MeV$

The exponential inhibition of fusion reactions due to the coulomb barrier is responsible for the general view among physicists that no cold fusion effects are possible in spite of supporting experimental results. If weak interaction electron capture by a deuteron occurs first, then the fusion reaction is between a neutral and charged nucleus, with no accompanying coulomb barrier. The price to be paid for this is twofold: the weak interaction is not so large of an effect, and the intermediate states with neutrons present is virtual. The detailed analysis of this reaction as an incoherent process is straightforward, and one finds that the range of the virtual neutrons is measured in tens of fermis.

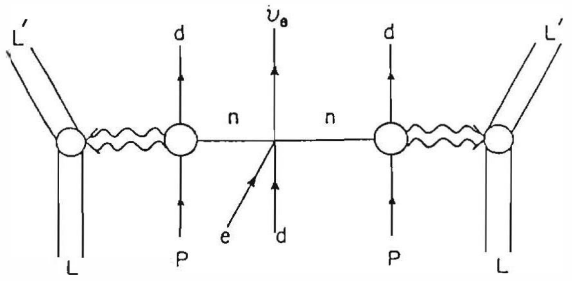

Figure 3: Feynman-like diagram for the proposed heat-producing two-step *depp* reaction.

We have been exploring a coherent version of this reaction as a many-particle process. The most interesting result which we have found is the possibility that the neutrino emission has the potential to be superradiant in the Dicke sense. In order to reach maximum superradiance, the fusion states would have to retain phase coherence, which is consistent with the requirement that the final states be stationary.

IV. MAGNETIC DIPOLE STRENGTHS

One approach towards developing an explanation for tritium production is to adopt a scenario in which tritium is formed through the capture of a neutron by deuterium. One proposed version of this reaction is

$$d + e + p + d \longrightarrow (2n + \nu_e + p + d)_V \longrightarrow \nu_e + d + t$$

We are interested in the strength of this reaction in comparison with the strength of the *depp* reaction mentioned above. An examination of the known slow neutron capture cross sections leads to the conclusion that virtual neutron capture by protons is favored over capture by deuterons by a moderately large factor. We conjecture that the magnetic dipole matrix element for neutron capture by protons is larger than for any other system by a large factor as well, and we have concluded this based on an examination of a relatively small number of capture cross sections.

Our approach will be very simple; we shall view the capture process as a radiative decay from an extended bound state. For example, in the presence of a magnetic field, neutrons of the appropriate spin polarization will see an attractive potential which is very weak. For low enough neutron

energy, bound states will exist (although they will be unstable to collisions by thermal nucleons). Such states will decay radiatively according to

$$\gamma_R = \frac{4}{3}\frac{\omega^3}{\hbar c^3}\frac{1}{(2J_u+1)}\left|\langle \Gamma_u J_u \left|\left| \mu \right|\right| \Gamma_l J_l \rangle\right|^2 \quad (IV.1)$$

where $|\Gamma_u J_u\rangle$ denotes the upper state in which the neutron is relatively delocalized, and $|\Gamma_l J_l\rangle$ denotes the lower state in which neutron capture has occurred. By necessity for these arguments, these states are many-particle states.

The radiative decay rate is related to the capture cross section through

$$\gamma_R = N\sigma_c(v)v \quad (IV.2)$$

where N is the number density of target nucleons, and $\sigma_c(v)$ is the capture cross section into the ground state. For M1 capture of neutrons by protons and deuterons, the capture cross sections vary as $1/v$ at low energy.

It follows that the reduced matrix element can be related to the capture cross section through

$$\frac{1}{N}\frac{1}{(2J_u+1)}\left|\langle \Gamma_u J_u \left|\left| \mu \right|\right| \Gamma_l J_l \rangle\right|^2 = \frac{3}{4}\frac{\hbar c^3}{\omega^3}\sigma_c(v)v \quad (IV.3)$$

We may define a single particle reduced matrix element in terms of the left hand side

$$\frac{|\langle u \,||\, \mu \,||\, l\rangle|^2}{(j_u+1)} = \frac{1}{N}\frac{1}{(2J_u+1)}|\langle \Gamma_u J_u \,||\, \mu \,||\, \Gamma_l J_l\rangle|^2 \quad (IV.4)$$

which can be used to obtain a ratio of the reduced matrix elements for neutron capture by protons and deuterons.

$$\frac{(2j_{np}+1)^{-1}\,|\,(np \,||\, \mu \,||\, d)\,|^2}{(2j_{nd}+1)^{-1}\,|\,(nd \,||\, \mu \,||\, t)\,|^2} = \left(\frac{\omega_t}{\omega_d}\right)^3 \frac{(\sigma_c v)_d}{(\sigma_c v)_t} \quad (IV.5)$$

Experimental measurements on slow neutron capture by protons have yielded a value of the capture cross sections for room temperature neutrons (2200 m/sec) which we may use

$$(\sigma_c v)_d = (3.342\times 10^{-25} cm^2)(2.200\times 10^5 \frac{cm}{sec})$$
$$= 7.35\times 10^{-20} cm^3/sec \quad (IV.6)$$

from Cox et al[60] (for a theoretical examination of this, see Mathiot[61]). For neutron capture by deuterons, and similar estimate gives

$$(\sigma_c v)_t = (5.7\times 10^{-28} cm^2)(2.200\times 10^5 \frac{cm}{sec})$$
$$= 1.25\times 10^{-22} cm^2/sec \quad (IV.7)$$

where we have used the somewhat dated value from Kaplan et al[62], which is in rough agreement with the CRC value of $5.1\times 10^{-28} cm^2$.

The ratio of (IV.5) actually requires channel specific cross sections to be valid. Neutron pickup by a proton requires a singlet initial state, and so we may require this unique channel in our ratio. Neutron capture by a deuteron involves two channels, and we do not have data for the two channels individually. In order to get a general estimate, we shall take the deuteron capture quantities to imply an averaged sum, and we then obtain for the ratio of (IV.5)

$$\frac{(2j_{np}+1)^{-1}\,|\,(np \,||\, \mu \,||\, d)\,|^2}{(2j_{nd}+1)^{-1}\,|\,(nd \,||\, \mu \,||\, t)\,|^2} = \left[\frac{6.25 MeV}{2.22 MeV}\right]^3 \left[\frac{7.35\times 10^{-20}}{1.25\times 10^{-22}}\right] = 1.3\times 10^4 \quad (IV.8)$$

This ratio is relatively independent of photon energy, and would be valid in the limit that the emitted photons are soft. The key result here is that protons would be substantially more reactive in terms of accepting a virtual neutron in a coherent fusion model than deuterons. It is this point which has focused our attention on the importance of protons in our coherent fusion work.

The two step beta/fusion reaction under discussion is essentially a generalized neutron transfer reaction, which is proposed to deposit S-wave neutrons in the ground state of an isotope through an M1 transition. Reactions in which a neutron is transferred into an s-orbital of an acceptor isotope are of most interest. Candidate 1s orbital isotopes are presented in Table I. It is observed that out of the three possible candidates, two are implicated in the present scenario. We have not yet obtained an estimate of the gamma channel of the low energy neutron-^{3}He reaction, so we are not in a position to predict how strongly ^{3}He would react relative to protons or deuterons.

Isotope	Abundance	$(J_i)^{\pi_i}$	$(J_f)^{\pi_f}$	τ_f	Q(MeV)
^{1}H	99.985 %	$(\frac{1}{2})^+$	$(1)^+$	∞	2.32
^{2}H	0.015 %	$(1)^+$	$(\frac{1}{2})^+$	12.26 y	6.16
^{3}He	0.00014 %	$(\frac{1}{2})^-$	$(0)^+$	∞	20.58

Table I: Parameters for slow neutron pickup mediated by M1 electromagnetic transitions to nuclear 1s orbitals.

Candidate 2s orbital isotopes are given in Table II. Of interest in the list is silicon, which was used in Claytor's tritium experiments and which is the subject of a number of undocumented reports concerning Wada's neutron experiments. Also of interest is ^{31}P, which would be activated to ^{32}P upon capture of a neutron; the product is radioactive with a half-life of 14 days (the decay mode is β^- with a 1.7 MeV energy), which would make a useful marker for autoradiography experiments. If we assume that the branching ratio is 0.7 % from Lycklama and Kennet,[63] and adopt the CRC value of 0.233 b for the total thermal neutron cross section, then we obtain a partial cross section of 1.6 mb. The ratio of equation (IV.8) evaluates to about 9.4×10^3 for ^{31}P, which is similar to that for deuterium. Hence, if the scenario is right, then we might hope to activate phosphorous as a second order effect (on par with tritium production) if P is present in quantity.

Isotope	Abundance	$(J_i)^{\pi_i}$	$(J_f)^{\pi_f}$	τ_f	Q(MeV)
^{26}Mg	11.01%	$(0)^+$	$(\frac{1}{2})^+$	9.45m	6.44
^{28}Si	92.23	$(0)^+$	$(\frac{1}{2})^+$	∞	8.47
^{30}Si	4.67	$(\frac{1}{2})^+$	$(0)^+$	∞	10.61
^{31}P	100.	$(\frac{1}{2})^+$	$(1)^1$	14.28d	7.94

Table II: Parameters for slow neutron pickup mediated by M1 electromagnetic transitions to nuclear 2s orbitals.

The branching ratios for slow neutron capture in ^{29}Si have been given by Beard and Thomas.[65] The partial cross sections for capture of thermal neutrons to the ground state of ^{30}Si can be estimated to be 0.26 mb.

Although we have assembled a table of candidate transitions for slow neutron capture into 3s neutron orbitals,[66] the resulting table is moderately long due to the mixing of the 3s orbital with other neutron shells. The list includes isotopes between Cd and Ba. Of most interest may be the cadmium and tin isotopes, which include a small number which are unstable following neutron activation (for example, ^{112}Sn lead to ^{113}Sn with a half-life of 115 days).

We note that tritium cannot be an acceptor in this scenario.

The spin flip transitions under discussion here can proceed in principle coherently, in which case there can arise an N^2 factor associated with the coherence. It is this effect which is proposed to account for the observation that deuterons are favored over protons as sources of virtual neutrons. We expect that such processes would be enhanced by net nuclear spin polarization locally, which would follow from electronic spin polarization.[67–69] Unfortunately the case is not strong for this since the magnetic susceptibility is known to be very low in PdD_x at high loading.[70–71] A reduction in hopping at high loading would improve coherence and may provide a rationalization of the observed loading requirements.

V. COLLECTIVE EFFECTS IN NEUTRINO EMISSION

In this section we shall explore a semi-classical model of neutrino emission. This analysis is motivated by analogous models for photon emission in quantum electronics. Starting from QED, an evolution equation for the expectation value of the electric and magnetic fields can be developed readily. The equations obeyed by the averages are Maxwell's equations, and the source terms are found explicitly in terms of averages of the quantum equivalents of the classical sources.[72–75]

Neutrino emission can in principle be viewed analogously. The expectation value of the neutrino field obeys the Weyl equation with a source term, and this model is in essence a semiclassical model for neutrino emission in the quantum electronics sense. This semi-classical model can be used to explore conditions under which neutrino

emission occurs as a collective process. The motivation for this analysis is that the phenomenon of Dicke superradiance is accounted for within the framework of the semiclassical model for electromagnetics, and it follows that neutrino emission may show an equivalent effect.

It is known that neutrinos can participate in coherent phenomenon. Based on the analogy with photons, Weber suggested that neutrinos would scatter coherently proportional to N^2 the number of scatters in a crystal.[76-77] A detector based on this principle has been constructed and there is evidence for the detection of neutrinos.[78] The extension to coherent emission of neutrinos is straightforward conceptually.

Our starting point is the Dirac equation for the classical neutrino field, which is the expectation value of the field-theoretic neutrino field operator. This equation is

$$\left[i\hbar\frac{\partial}{\partial t} - \alpha\cdot c\mathbf{p}\right]\psi_\nu = \frac{1}{\sqrt{2}}s_\nu \qquad (V.1)$$

where s_ν is the semiclassical neutrino source function, analogous to electromagnetic polarization. The semiclassical source function s_ν is

$$s_\nu(\mathbf{r},t) = \langle gC_V\sum_i \tau_i^{(-)}\delta^3(\mathbf{r}-\mathbf{r}_i)(1+\gamma_5)\gamma_4\hat{\psi}_e\rangle + \langle gC_A\sum_i \sigma_i\tau_i^{(-)}\delta^3(\mathbf{r}-\mathbf{r}_i)(1+\gamma_5)\sigma\gamma_4\hat{\psi}_e\rangle \qquad (V.2)$$

where the expectation value is over a macroscopic lattice.

If we adopt a Furry picture for the electron field operator, where the potential is taken to be due to many nucleii in a lattice, then the individual electron orbitals which are converted are Bloch waves. If we define the expectation value to be between a state with an electron present in a Bloch state Γ_j and a state with no electron present, then we may write

$$s_j(\mathbf{r},t) = gC_V\langle\sum_i \tau_i^{(-)}\delta^3(\mathbf{r}-\mathbf{r}_i)\rangle(1+\gamma_5)\gamma_4\psi_j(\mathbf{r},t) + gC_A\langle\sum_i \tau_i^{(-)}\sigma_i\delta^3(\mathbf{r}-\mathbf{r}_i)\rangle\cdot(1+\gamma_5)\sigma\gamma_4\psi_j(\mathbf{r},t) \qquad (V.3)$$

The electron orbitals which have strong overlap with the deuterons will be well described in a nonrelativistic approximation. In this case we may take the 4-vector $\psi_j(\mathbf{r},t)$ and break it down into two components

$$\psi_j(\mathbf{r},t) \approx \begin{bmatrix} \phi_j(\mathbf{r},t) \\ \frac{\sigma\cdot c\mathbf{p}}{2mc^2}\phi_j(\mathbf{r},t)\end{bmatrix} \qquad (V.4)$$

It follows that

$$(1+\gamma_5)\gamma_4\phi_j(\mathbf{r},t) \approx \begin{bmatrix} (I+\frac{\sigma\cdot c\mathbf{p}}{2mc^2})\phi_j(\mathbf{r},t) \\ -(I+\frac{\sigma\cdot c\mathbf{p}}{2mc^2})\phi_j(\mathbf{r},t)\end{bmatrix} \qquad (V.5)$$

and

$$(1+\gamma_5)\sigma\gamma_4\phi_j(\mathbf{r},t) \approx \begin{bmatrix} \sigma(I+\frac{\sigma\cdot c\mathbf{p}}{2mc^2})\phi_j(\mathbf{r},t) \\ -\sigma(I+\frac{\sigma\cdot c\mathbf{p}}{2\ \ \sigma\hbar^2})\phi_j(\mathbf{r},t)\end{bmatrix} \qquad (V.6)$$

The form of these formulas shows explicitly the choice of helicity of the neutrino source. A unitary transformation can be used to simplify the computation

$$\begin{bmatrix}\phi_\nu\\ \chi_\nu\end{bmatrix}' = \frac{1}{\sqrt{2}}\begin{bmatrix}1 & -1\\ 1 & 1\end{bmatrix}\begin{bmatrix}\phi_\nu\\ \chi_\nu\end{bmatrix} \qquad (V.7)$$

We find that

$$i\hbar\frac{\partial}{\partial t}\begin{bmatrix}\phi_\nu\\ \chi_\nu\end{bmatrix} = \begin{bmatrix}0 & \sigma\cdot c\mathbf{p}\\ \sigma\cdot c\mathbf{p} & 0\end{bmatrix}\begin{bmatrix}\phi_\nu\\ \chi_\nu\end{bmatrix} + \frac{1}{\sqrt{2}}\begin{bmatrix}s_\phi\\ s_\chi\end{bmatrix} \qquad (V.8)$$

transforms into

$$i\hbar\frac{\partial}{\partial t}\begin{bmatrix}\phi_\nu\\ \chi_\nu\end{bmatrix}' = \begin{bmatrix}-\sigma\cdot c\mathbf{p} & 0\\ 0 & \sigma\cdot c\mathbf{p}\end{bmatrix}\begin{bmatrix}\phi_\nu\\ \chi_\nu\end{bmatrix}' + \begin{bmatrix}s_\phi\\ 0\end{bmatrix} \qquad (V.9)$$

using $s_\chi = -s_\phi$. We may therefore simplify our analysis, and use the Weyl equation with a source

$$\left[i\hbar\frac{\partial}{\partial t} + \sigma\cdot c\mathbf{p}\right]\phi'_\nu = s'_\nu \qquad (V.10)$$

where $s'_\nu = s_\phi$.

We shall henceforth omit the primes and work with unprimed variables. The source term will in general have a distribution of frequencies. If we assume that the frequencies are discrete, then

$$s_j(\mathbf{r},t) = \sum_l s_{jl}(\mathbf{r}) e^{i\omega_l t} \qquad (V.11)$$

and (V.10) becomes

$$[\hbar\omega_l + \sigma\cdot c\mathbf{p}]\,\phi_{jl}(\mathbf{r}) = s_{jl}(\mathbf{r}) \qquad (V.12)$$

for a component of ϕ_j at ω_l. If we operate on both sides of V.12 with $[\hbar\omega_l - \sigma\cdot c\mathbf{p}]$, we obtain

$$[\hbar\omega_l - \sigma\cdot c\mathbf{p}]\,[\hbar\omega_l + \sigma\cdot c\mathbf{p}]\,\phi_{jl}(\mathbf{r}) = [\hbar\omega_l - \sigma\cdot c\mathbf{p}]s_{jl}(\mathbf{r}) \qquad (V.13)$$

which can be recast as

$$\left[\nabla^2 + \left(\frac{\omega_l}{c}\right)^2\right]\phi_{jl}(\mathbf{r}) = \frac{1}{\hbar^2c^2}\,[\hbar\omega_l - \sigma\cdot c\mathbf{p}]\,s_{jl}(\mathbf{r}) \qquad (V.14)$$

It follows that

$$\phi_{jl}(\mathbf{r}) = -\frac{1}{4\pi}\int d^3\mathbf{r}'\frac{e^{i\omega_l|\mathbf{r}-\mathbf{r}'|/c}}{|\,\mathbf{r}-\mathbf{r}'\,|}\frac{1}{\hbar^2c^2}\,[\hbar\omega_l - \sigma\cdot c\mathbf{p}]\,s_{jl}(\mathbf{r}') \qquad (V.15)$$

In the far-field we may approximate (V.15) by

$$\phi_{jl}(\mathbf{r}) \longrightarrow -\frac{\omega_l}{4\pi\hbar c^2}\frac{e^{i\omega_l|\mathbf{r}|/c}}{|\,\mathbf{r}\,|}\int d^3\mathbf{r}'e^{-i\kappa_l\cdot\mathbf{r}'}\,[I + i\frac{\sigma\cdot\nabla'}{|\,\kappa_l\,|}]s_{jl}(\mathbf{r}') \qquad (V.16)$$

where

$$\kappa_l = \frac{\omega_l}{c}\frac{\mathbf{r}}{|\,\mathbf{r}\,|} \qquad (V.17)$$

and where the radiator is assumed centered at $\mathbf{r} = 0$.

The total emission rate of neutrinos is

$$\Gamma_\nu = \sum_j\sum_l c\int d\Omega\;|\,\phi_{jl}(\mathbf{r})\,|^2|\,\mathbf{r}\,|^2 \qquad (V.18)$$

which is expanded out to be

$$\Gamma_\nu = \sum_j\sum_l \frac{\omega_l^2}{16\pi^2\hbar^2c^3}\int d\Omega\Big|\int d^3\mathbf{r}'e^{-i\kappa_l\cdot\mathbf{r}'}\left[I + \frac{\sigma\cdot\nabla'}{|\,\kappa_l\,|}\right]s_{jl}(\mathbf{r}')\Big|^2 \qquad (V.19)$$

We shall define the function

$$\zeta_{jl} = \int d^3\mathbf{r}'e^{-i\kappa_l\cdot\mathbf{r}'}\left[I + i\frac{\sigma\cdot\nabla'}{|\,\kappa_l\,|}\right]s_{jl}(\mathbf{r}') \qquad (V.20)$$

and split it into Fermi and Gamow-Teller terms

$$\zeta_{jl} = \zeta_{jl}^V + \zeta_{jl}^A \qquad (V.21)$$

Explicitly, we have

$$\zeta_{jl}^V = \int d^3\mathbf{r}'e^{-i\kappa_l\cdot\mathbf{r}'}\left[I + i\frac{\sigma\cdot\nabla'}{|\,\kappa_l\,|}\right] gC_V\langle\sum_i\tau_i^{(-)}d^3(\mathbf{r}'-\mathbf{r}_i)\rangle_{jl}\left[I + \frac{\sigma\cdot c\mathbf{p}}{2mc^2}\right]\phi_j(\mathbf{r}') \qquad (V.22)$$

and

$$\zeta_j^A = \int d^3\mathbf{r}'e^{i\kappa_l\cdot\mathbf{r}'}\left[I + i\frac{\sigma\cdot\nabla'}{|\,\kappa_l\,|}\right] gC_A\langle\sum_i\tau_i^{(-)}\sigma_i\delta^3(\mathbf{r}'-\mathbf{r}_i)\rangle_{jl}\sigma(I + \frac{\sigma\cdot c\mathbf{p}}{2mc^2})\phi_j(\mathbf{r}') \qquad (V.23)$$

The electron orbitals are Bloch orbitals, and are composed of the product of an oscilltory and periodic term.

$$\phi_j(\mathbf{r}) = e^{i\mathbf{k}_j\cdot\mathbf{r}}u_j(\mathbf{r}) \qquad (V.24)$$

We are in a position to integrate (V.22) and (V.23) with respect to $\mathbf{r}'$. We note that

$$\int d^3\mathbf{r}'e^{-i\kappa_l\cdot\mathbf{r}'}\left[I + i\frac{\sigma\cdot\nabla'}{|\,\kappa_l\,|}\right]f(\mathbf{r}') = \int d^3\mathbf{r}'\left[[I - i\frac{\sigma\cdot\nabla'}{|\,\kappa_l\,|}]e^{i\kappa_l\cdot\mathbf{r}'}\right]f(\mathbf{r}') \qquad (V.25)$$

from which it follows that

$$\zeta_{jl}^V = gC_V\langle\sum_i\tau_i^{(-)}e^{i(\mathbf{k}_j-\kappa_l)\cdot\mathbf{r}_i}\rangle_{jl}[I + \sigma\cdot\hat{\kappa}_l]u_j(0) \qquad (V.26)$$

where $u_j(0)$ is the value of the periodic part of the Bloch wave at the deuteron nucleus. In this formula we have dropped the electron spin-orbit term. Similarly we have

$$\zeta_{jl}^{A} = gC_A\langle\sum_i \tau_i^{(-)}\sigma_i e^{i(\mathbf{k}_j-\kappa_l)\cdot\mathbf{r}_i}\rangle_{jl}[I+\sigma\cdot\hat{\kappa}_l]\sigma u_j(0) \quad (V.27)$$

We define the generalized Fermi and Gamov-Teller expectation values

$$M_{jl}^{F}(\mathbf{k}_j-\kappa_l) = \langle\sum_i \tau_i^{(-)} e^{i(\mathbf{k}_j-\kappa_l)\cdot\mathbf{r}_i}\rangle \quad (V.28)$$

and

$$M_{jl}^{GT}(\mathbf{k}_j-\kappa_l) = \langle\sum_i \tau_i^{(-)}\sigma_i e^{i(\mathbf{k}_j-\kappa_l)\cdot\mathbf{r}_i}\rangle \quad (V.29)$$

which allows us to write

$$\zeta_{jl}^{V} = gC_V M_{jl}^{F}(\mathbf{k}_j-\kappa_l)[I+\sigma\cdot\hat{\kappa}_l]u_j(0) \quad (V.30)$$

and

$$\zeta_{jl}^{A} = gC_A \mathbf{M}_{jl}^{GT}(\mathbf{k}_j-\kappa_l)\cdot[I+\sigma\cdot\hat{\kappa}_l]\sigma u_j(0) \quad (V.31)$$

At this point we are in a position to explore coherent neutrino emission. If the electron momentum and the neutrino momentum coincide, then the Fermi average becomes

$$M_{jl}^{F}(0) = \langle\sum_i \tau_i^{(-)}\rangle$$

$$= 2\langle T^{(-)}\rangle \quad (V.32)$$

where $T^{(-)}$ is the many-particle isospin operator. The emission of neutrinos with momentum equal to the converted electron momentum can be coherent. We may show this explicitly by considering the Fermi emission rate

$$\Gamma_j^{VV}\mid_{(\mathbf{k}_j-\mathbf{K}_l=0)} = \frac{\omega_l^2}{4\pi^2\hbar^2c^3}g^2$$

$$C_V^2 \mid (I+\sigma\cdot\mathbf{K}_l)u_j(0)\mid^2 \mid \langle T^{(-)}\rangle\mid^2 \quad (V.33)$$

If the many-particle nuclear states are Dicke states, then

$$\mid\langle T^{(-)}\rangle\mid^2 \propto [T(T+1)-M_T(M_T+1)] \quad (V.34)$$

If $\mid M_T \mid$ is much less than $\mid T \mid$, then the neutrino emission will be coherent and proportional to the square of the number of emitters. The physical content of this result is that in the Dicke limit all of the nucleons participate on an equal basis in the neutrino emission process, in phase with one another throughout the lattice. The resulting emission rate can be much larger than N times the single particle incoherent neutrino emission rate.

In order for this process to occur, phase coherence must be maintained between the initial and final states, which implies that the final states must be stationary. This requirement seems to be consistent with the experimental observations of low neutron yield. In order for this to occur the nuclear energy must be transferred elsewhere coherently, and we discuss this problem in the following sections.

VI. COUPLING OF ENERGY FROM THE MICROSCOPIC TO THE MACROSCOPIC

In order to achieve superradiance in the neutrino emission in the coherent scenario, the neutrino energy must be very low (on the order of 1 eV or less), and the final state nucleons must be stationary. The overall reactions of interest are exothermic by multiple MeV, hence the nuclear energy must be deposited elsewhere in a nondisruptive manner in order for coherence to be maintained. Coupling nuclear energy from the microscopic to the macroscopic coherently is unprecedented, and we require a fundamentally new mechanism to do this.

In our earlier efforts, we have proposed coupling of the nuclear energy into phonons in the palladium lattice. The phenomenon of deexcitation of electronic transitions into phonons is known in molecules and solids,[79–83] and the fundamental quantum mechanics seems to be qualitatively similar between these well-known systems and our earlier coherent fusion model. However, in essentially all systems in which a relatively high quantum energy transition is coupled with phonons,

the non-radiative processes proceed through at most a relatively small number of phonons at a time. The rate of phonon emission decreases exponentially with increasing number of phonons generated, which is characteristic of a high order emission process.[80] As a result, unless some new and compelling physical mechanism is found, it seems improbable that nuclear energy can be coupled directly to lattice phonons in bunches of 10^7 or more at a nonvanishing rate.

The arguments above apply to radiation of large numbers of quanta in a system which is fundamentally linear or near linear. Phonons within a macroscopic lattice or large molecule are well-described by linear or weakly nonlinear models, which is ultimately why the emission rate is exponentially damped for large numbers of emitted phonons. Radiation of photons into a vacuum is exponentially weak for large number of photons for the same reason. As a result, if we hope to make any progress at all, we must search for a mechanism which is fundamentally nonlinear to very high order in order to avoid exponential extinction of emission rate at high quantum energy.

There are examples of systems which appear to behave in this fashion. One such mechanism is the electrochemical process, as can easily be seen. Consider an electrochemical cell which is driven by a low frequency LC-circuit (an example which we shall focus on in this section), and assume that when in operation gas molecules are generated from chemical species within the electrolyte. The generation of each gas molecule requires a relatively high chemical energy quanta, which must be supplied by relatively low energy electrical quanta from the LC circuit. In order for this to occur, a mechanism must exist which is capable of exchanging a very large number (10^6 to 10^{12}) of electrical quanta for a single chemical quanta. Such a mechanism would have to be nonlinear to extreme order, and in what follows in this section we explore the possible application of this type of nonlinearity to the coherent fusion problem.

We begin by considering the quantization of a simple LC circuit. The Hamiltonian is derived from the classical electric and magnetic field energies

$$H = \frac{1}{2}Cv^2 + \frac{1}{2}Li^2 \qquad (VI.1)$$

which leads to the Schrödinger equation for the probability amplitude

$$i\hbar\frac{\partial}{\partial t}\psi(v,t) = -\frac{\hbar^2}{2LC^2}\frac{\partial^2}{\partial v^2}\psi(v,t) + \frac{1}{2}Cv^2\psi(v,t) \qquad (VI.2)$$

where we have used the current operator

$$i_{op} = -i\frac{\hbar}{LC}\frac{\partial}{\partial v} \qquad (VI.3)$$

The quantization of the LC circuit is of course well known,[84,85] and is usually written in terms of creation and destruction operators as we shall shortly do also. In this form, it is emphasized that the current operator is to within a constant simply a derivative of the voltage. This will be of use later.

In terms of raising and lowering operators, the current and voltage operators are

$$\hat{v} = \sqrt{\frac{\hbar\omega}{2c}}(a^\dagger + a) \qquad (VI.4)$$

$$\hat{i} = -\sqrt{\frac{\hbar\omega}{2L}}\frac{(a^\dagger - a)}{i} \qquad (VI.5)$$

The Hamiltonian for this system is

$$\hat{H}_{LC} = \hbar\omega a^\dagger a \qquad (VI.6)$$

where $\omega = 1/\sqrt{LC}$, and where we have suppressed the zero-point contribution which is not important for our discussion. The eigenfunction solutions for this problem are completely standard, and the energy levels are quantized with a constant spacing of $\hbar\omega$. That the inductance or capacitance might be somewhat nonlinear in the corresponding physical system has no impact on the present arguments. The presence of resistive losses can be included directly using standard techniques of coupling to a heat bath,[84–86] however, such processes play no role in the nuclear coupling process of interest here. We may add such resistive terms to our Hamiltonian at our pleasure; they will show up additively at the end of the computation – hence there is no reason to carry them along here.

We may consider the coupling of the LC circuit to a two-level nuclear system, which is in essence a toy model for virtual neutron capture in our scenario. A full model including superradiant neutrino emission cannot be described as a two-level system, however, if we focus on a two-level system

we will have a better chance of elucidating the basic mechanism. A more complete model will have to follow in a future work. The Hamiltonian for the coupled system is

$$\hat{H} = \hat{H}_{LC} + \hat{H}_N + \hat{H}_I \qquad (VI.7)$$

where

$$\hat{H}_N = \frac{\hbar\omega_N}{2}\sum_j (b_j^\dagger b_j - b_j b_j^\dagger) = \frac{1}{2}\hbar\omega_N \hat{\Sigma}_z \quad (VI.8)$$

$$\hat{H}_I = \frac{\partial^2 H}{\partial a \partial b}\frac{(a^\dagger - a)}{i}\sum_j (b_j^\dagger + b_j)$$

$$= \frac{\partial^2 H}{\partial a \partial b}\frac{(a^\dagger - a)}{i}\hat{\Sigma}_x \qquad (VI.9)$$

The Σ_x and Σ_z operators are many-particle "spin" operators, which are used commonly in this type of model. The b and $b^\dagger$ operators are fermionic creation and annihilation operators. The interaction term is appropriate for $-\mu\cdot\mathbf{B}$ coupling where the magnetic field is uniform throughout and where the magnetic field is in the near-field (which couples the nuclear energy directly to current increments). The microscopic coupling links a single energetic spin flip with the creation or destruction of a single current quantum.

This model is simple and can be diagonalized approximately through a unitary transformation:

$$\Psi' = e^{i\hat{R}}\Psi \qquad (VI.10)$$

$$\hat{H}' = e^{i\hat{R}}\hat{H}e^{-i\hat{R}} \qquad (VI.11)$$

The rotation operator which accomplishes this is

$$\hat{R} = \frac{1}{2}\tan^{-1}\left[\frac{2}{\hbar\omega_N}\frac{\partial^2 H}{\partial a \partial b}\frac{(a^\dagger - a)}{i}\right]\hat{\Sigma}_y \quad (VI.12)$$

The resulting Hamiltonian is

$$\hat{H}' = \hat{H}_{LC} + \hat{H}'_N + \hat{H}'_I \qquad (VI.13)$$

where

$$\hat{H}'_N = \frac{1}{2}\hbar\hat{\omega}'_n\hat{\Sigma}_z \qquad (VI.14)$$

$$\begin{aligned}\hat{H}_I &= e^{i\hat{R}}\hat{H}_{LC}e^{-i\hat{R}} - \hat{H}_{LC} \\ &\approx i\left[\hat{R}, \hat{H}_{LC}\right]\end{aligned} \qquad (VI.15)$$

The diagonalization of this Hamiltonian is similar to rotations discussed elsewhere.[87–89]

The coupling term in the rotated picture is very small, and we have achieved a relatively accurate diagonalization through this transformation. One result of this diagonalization is that it becomes apparent that the interaction term, which is of low order, does not help the transfer of net nuclear excitation to a linear circuit. The nuclear quanta can only be transferred in units of 10^n quanta at a time in order to conserve energy, and such processes are exponentially inhibited as remarked upon above. There is some small degree of mixing between the nuclear levels and the oscillator levels which will be of use shortly.

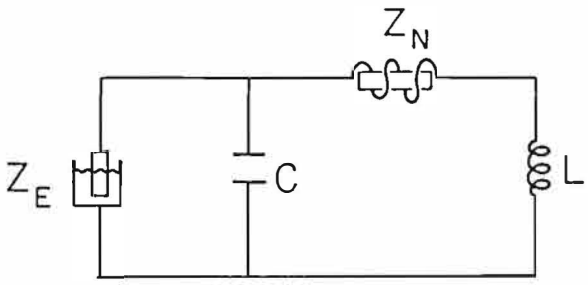

Figure 4: LC circuit couple to a nuclear spin system at high energy and a nonlinear element.

The coupling of the LC circuit to the electrolysis process is to be considered next, and for this we adopt a model Hamiltonian of the form

$$\hat{H} = \hat{H}_{LC} + \hat{H}_N + \hat{H}_I + \hat{H}_E + \hat{H}_C \qquad (VI.16)$$

where we include the "bath" for the chemical system through

$$\hat{H}_E = \sum_j \frac{1}{2}\hbar\omega_j(c_j^\dagger c_j - c_j c_j^\dagger) \qquad (VI.17)$$

where c and $c^\dagger$ are fermionic creation and destruction operators relevant to chemical species. The coupling with the chemical bath is accounted for through $\hat{H}_C$, which we conjecture has the form

$$\hat{H}_C = \sum_j \Theta(\hat{v} - v_j)\Delta H_j \qquad (VI.18)$$

The important feature of the coupling Hamiltonian is that is must have an explicit nonlinearity of high order in order for the electrolysis process to be able to convert low energy electrical quanta

to chemical quanta. The use of a step function to describe this coupling is conjecture (we expect it to be sharp, be we do not know whether it is sharp to the degree to which we will shortly require). The summation over j in this equation is a summation over available quantum mechanical microscopic channels. A summation over channels weighted by a thermal occupation average of this Hamiltonian would give a nonlinear current-voltage characteristic which is more gentle and locally linear.

If we apply a unitary transformation to diagonalize the coupling between the nucleii and the current to first order in the presence of the electrochemical terms, we obtain a new and very interesting term due to the resulting commutation. If we rotate:

$$\hat{H}' = e^{i\hat{R}}\hat{H}e^{-i\hat{R}} \qquad (VI.19)$$

using the transformation described above, then we obtain

$$\hat{H}' = \hat{H}'_{LC} + \hat{H}'_N + \hat{H}'_I + \hat{H}'_E + \hat{H}'_C \qquad (VI.20)$$

where

$$\begin{aligned} \hat{H}'_C &= e^{i\hat{R}}\hat{H}_C e^{-i\hat{R}} \\ &\approx \hat{H}_C + i\left[\hat{R}, \hat{H}_C\right] \\ &= \hat{H}_C + \sum_j A_j \left[\hat{i}, \Theta(\hat{v} - v_j)\right] \hat{\Sigma}_y \\ &= \hat{H}_C + \sum_j A_j \delta(\hat{v} - v_j)\hat{\Sigma}_y \end{aligned} \qquad (VI.21)$$

In the dressed state picture, a new term appears which couples nuclear energy into the LC circuit, assisted by the electrochemical process. This term is extremely nonlinear, and is approximated by a delta-function in voltage in this simple model. Depending on how strong the nonlinearity is, it has the potential to exchange a nuclear quantum into a very large number of LC circuit quanta in a nondisruptive manner required for the coherence in neutrino emission.

The scenario described in this paper rests on the conjecture that the electrochemical process is nonlinear to a somewhat higher degree than is required in order for electrochemisty to occur. Some consideration of the microscopic physics suggests that this conjecture is not entirely unreasonable. The voltage operator is approximately proportional to the number operator of electrons within an electrode, and the nonlinearity comes about because the electrode orbitals are filling (or emptying) as the voltage increases. Each newly entering electron sits on the shoulders of previous electrons in energy; at some point a newly entering electron will fill an orbital through which electrochemical current flow is energetically allowed. This microscopic picture leads to a coupling Hamiltonian of the general form given above, except that the step function will be replaced by something softer depending on the details of the tunneling between metal orbitals and surface orbitals.

We note that the nonlinearity, if it worked as conjectured here, might provide under certain conditions, a source of $1/f$ electrical noise.

The extension to the full model would require analysis of superradiance in a multi-level system, and some work has been done on this type of system.[90–92]

VII. DISCUSSION

The binary fusion of two charged nucleons at room temperature as an explanation for cold fusion effects seems to us to be hopeless due to the presence of the coulomb barrier, in spite of the proposals which have been suggested for ways to circumvent coulomb repulsion. Even if a way were found, there remains the problem of developing a reaction which produces cold reaction products. The *dd* binary fusion reaction which has been discussed so much in the last year simply does not begin to fit the reaction profile of the observations.

The fusion of a virtual neutron with a charged nucleon can provide a way to circumvent the coulomb barrier, and our current effort is based on the exploration of this possibility. In place of the problem of coulomb repulsion, an issue of nearly equal severity arises, specifically one of transport. The range of virtual neutrons is quite small (fermi scale) unless the energy deficit can be somehow reduced. Additionally, the weak interaction is a numerically small effect; it is difficult to understand how any reaction, whether coherent or not, could have a substantial reaction rate if the weak interaction is a part of it.

We have proposed that the neutrino emission can be superradiant if the neutrino momentum is

equal to the Bloch wave momentum of the electron and if the reaction final products are stationary. This provides a possible mechanism to boost the weak interaction by a considerable factor.

The neutron transport problem may in principle be solved if the coupling of the nuclear energy to the current occurs collectively, which preferentially favors long wavelength virtual neutron states. In conventional incoherent nuclear reactions where off-shell neutrons occur, the time-duration of the excursion of the neutrons can be obtained from the uncertainty principle if the energy deficit is known. In a coherent reaction, which is ultimately a resonance process, the transition width can be very small (less than 1 eV) even though the energy deficit is large. This translates directly into a potentially large spatial excursion for the off-shell neutrons.

There is considerable interest in defining what factors are required to produce cold fusion effects, under the assumption that they are real. This has been of concern, especially to the experimentalists, and there have been some attempts at assembling a list of requirements. No such list has been produced by theorists at this point, and that fact is a consequence that no theory currently exists. Our work is speculative, and although we have not produced a theory as recognized by physicists, we have developed a scenario which may lead to a predictive theory. It is of some interest to address the problem of what requirements would follow under the assumption that the scenario is at least partially correct.

With the above proviso in mind, we offer a list of factors which would be required in our scenario for heat production:

1. A source of virtual neutrons: specifically deuterium or tritium are possible sources. Within the scenario, deuterons would be favored by an N^2 coherent factor over protons.

2. A regular potential which supports electron Bloch waves to enable coherent neutrino emission. This is probably not a requirement that the lattice be perfect, but clearly water will have less order of this sort than a palladium rod.

3. An exothermic sink for virtual neutrons: protons are proposed to be the recipients of virtual neutrons in current heat-producing experiments. As discussed earlier, protons are favored over deuterons in this respect due to the larger M1 matrix element.

4. A magnetic field which is due to a current which sees a highly nonlinear impedance. Although the magnetic field must be present where virtual neutrons are converted, the nonlinearity may be separate. This mode of coupling is specific to M1 interactions.

5. Net (local) nuclear spin polarization.

For tritium production, the requirements would be very similar as the above list applicable to M1 neutron pickup, except that protons would no longer be required. It is likely that they will be helpful, in that the conversion of two virtual neutrons (from electron capture on deuterium) may be enhanced if one is captured onto a proton.

The outstanding issues in the field are: (1) the unequivocable proof that there is indeed a new effect, (2) reproducibility, and (3) mechanism. Engineering and applications must ultimately wait for some very basic level of demonstrable physical understanding. It seems unlikely that the theoretical situation will improve much without more experimental input.

If neutrino emission can occur superradiantly, and if the nonlinearity in current-voltage characteristic actually can take up the nuclear energy, then it may be possible that the various "miracles" can be explained rationally. Future theoretical efforts towards the development of our scenario must involve further quantification of the scenario.

Consideration of these issues has its motivation in the controversial cold fusion experiments. If the experiments are right, then there ought to be some sensible explanation. It is important to establish firmly whether there are indeed cold fusion effects, and if so, a second generation of experiments focusing on mechanism need to be started. We have developed what amounts to a wish list for experiments which would help clarify whether our scenario is indeed a correct approach. This list is given in the following section.

Theory and experiment need to go hand in hand. If proton depletion in heat experiments can be demonstrated quantitatively, then this would be regarded as strong motivation for pursuing our scenario. But it remains to be settled as to

whether there is an effect at all, and this must still be regarded as a top priority.

VIII. PROPOSALS FOR EXPERIMENTS

At this point, it is still not accepted that cold fusion effects are real rather than experimental artifacts. If we take the position that the heat and tritium are real effects that can be reproduced by one or more groups, then the question arises as to what new or related experiments can be done which might help clarify mechanisms.

A. Reproducibility

Ever since the initial announcement of the effect, the issue of apparent nonreproducibility has plagued the field. It almost seems as if some researchers have the "magic touch," while most do not, and this has been used as a primary argument that the effect is not real. Currently, numerous researchers are apparently able to obtain one or more of the miracles with much improved probability of success for a given experiment.

Probably the highest priority project which is faced by workers in the field is to define one or more experiments which produce either heat, tritium, neutrons or isotope shifts at some probability level. This accomplishment would go far to make the effect accessible to the scientific community in general. From the large variety of positive experimental results which are being reported now, I think that the definition of an "industry standard" set of cells could be done.

B. Proton Loss

Within the framework of the coherent fusion scenario discussed in this work, protons play a key role in constituting the primary fuel for heat production. A demonstration of this would represent a fundamental step in the elucidation of a mechanism for the Pons-Fleischmann effect. A null result in this area would serve to eliminate the proposed scenario. The key experiment which we recommend is a proton loss experiment, in which the proton concentration is monitored (which presents severe experimental difficulties) over the course of an extended experiment in which multiple megajoules of heat is produced.

C. Proton Concentration

Pons-Fleischmann cells are often run at low levels of light water (on the order of 1%). The initial pre-march work of Pons and Fleischmann suggested that there is an optimum mix of proton and deuterons which gave the best results. The question of interest is: what is the sensitivity of the effect to relative proton concentration within the palladium? Associated with this is whether a rod loaded with less than 0.01% protons can show heat. Within the scenario, such a rod should not exhibit heat, although it could in principle evolve tritium.

C. Tritium loss

Tritium production has been reported in a number of laboratories. A small number of reports of tritium loss exists. The question which arises, is simply whether there is such an effect and whether it is reproducible. An experiment could be done in which a heat producing closed cell is injected with a known amount of tritium, after which tritium content is monitored. Noise levels in the $\frac{\mu\text{Curie}}{ml}$ range have been reported, and an added signal of 100 times this level would be of interest. Within the present scenario, tritium may serve as the source for virtual neutrons, although the primary *teppp* reaction is not allowed energetically.

D. Production of slow neutrinos

Electron capture through the weak interaction involves the emission of a neutrino. If the neutrinos were energetic (which is not consistent with the present scenario), then they could be observed by conventional solar neutrino detectors.[93,94] A point source of $10^{13} - 10^{14}$ neutrinos in the MeV range would be detected by the Kamiokande detector, for example.

If the neutrinos are low energy neutrinos (< 1 eV) as might be produced superradiantly, then they would be detectable only through use of a Weber neutrino detector specifically designed and optimized for a large flux of soft neutrinos.

E. Activation of Phosphorous

Natural phosphorous occurs as ^{31}P. Neutron activation to the ground state of ^{32}P involves an M1 virtual neutron pickup reaction analogous to proton and deuteron reactions discussed above. The activated phosphorous isotope is unstable with a 14 day half-life, and produces a 1.7 MeV electron. If this process can be demonstrated, it would be important mechanistically in that it would be much more difficult to imagine how ^{32}P could be produced through the types of mecha-

nisms which have been discussed elsewhere. A clean demonstration of a new neutron activation reaction would be of great value.

F. Separation of Reactants and Nonlinearity

The mechanism proposed to convert the nuclear energy works through a near field magnetic field generated by a current which sees a high order nonlinearity. This nonlinearity need not necessarily be in the same location as the reactants, and an extremely interesting experiment would be to demonstrate this effect. If the current running through the palladium electrolysis cell were run through another element exhibiting a high order nonlinearity (for example, another electrolysis cell, a battery, a diode or other systems), then it is possible that anomolous energy deposition into the series nonlinear element might occur. A demonstration of this effect would strongly support the present scenario. More interesting still would be the replacement of the original palladium cell with a crystal containing deuterium and hydrogen as constituents (partially deuterated LiH, etc.).

G. Net Nucleon Spin Polarization

Spin-spin coupling between electrons and nuclear spins can be a relatively rapid process. Protons and deuterons undergoing electrolysis in palladium or titanium will see some degree of net nuclear spin alignment. Any coherent mechanism for fusion effects of the class which we have been considering may be sensitive to the state of net nuclear spin polarization. Questions which are of interest involve the relation of nuclear spin polarization to the Pons-Fleischmann effect.

1. Is net nuclear spin polarization present in a heat producing cell? What is the direction, spatial dependence, and strength of proton and deuteron polarization.

2. Can a Pons-Fleischmann cell produce heat if the nuclear spins are randomized?

3. What does the NMR spectrum of a working Pons-Fleischmann cell look like?

IX. SUMMARY AND CONCLUSIONS

We have proposed a new coherent fusion scenario involving exotic two-step beta/fusion reactions to account for the still highly controversial Pons-Fleischmann effect. The previous discussions of *dd* reactions as candidates for explaining the observations suffered from the fact that the reported observations simply do not fit the *dd* reaction profile, and that reactions at room temperature involving fusion of charged nucleii have exceedingly small reaction rates.

The present scenario offers a number of advantages relative to the claimed observations, including

1. Heat production without fast reaction products, neutrons or gammas.

2. Tritium production as a second order process, unaccompanied to first order by secondary neutron production.

3. No explicit exponential damping factors occur at room temperature.

4. The scenario is consistent with the known stability of heavy water and can be consistent with stellar evolution models.

5. The time-dependence of a superradiant system is qualitatively consistent with the dynamics of the observations of the heat and tritium observations.

6. The dependence of the strength of the effect on current density is in qualitative agreement (maximum di/dv is favored, rather than maximum i).

7. The scenario is consistent with contamination-dependent production of low levels of residual radioactivity.

Real neutron production can occur as an incoherent process parasitic with the coherent processes described in the paper. It is at best a third order process in comparison to heat and tritium production in the model.

The principle weakness of the scenario at this point is the lack of quantitative predictions. This weakness is not inherent in the model; the effects discussed here are amenable to precise quantification. Further effort is required to obtain predictions.

Acknowledgements

The author would like to thank his friends for their encouragement and technical support. This work was supported under DOE contract DEFG02/89CR14012.

REFERENCES

1. M. Fleischmann, S. Pons and M. Hawkins, *J. Electroan. Chem.* **261** 301 (1989), **263** 187 (1989).

2. M. Fleischmann, S. Pons and R. J. Hoffman, *Nature* **339** 667 (1989).

3. S. E. Jones, E. P. Palmer, J. B. Czirr, D. L. Decker, G. L. Jensen, J. M. Thorne, S. F. Taylor and J. Rafelski, *Nature* **338** 737 (1989).

4. R. D. Petrasso, X. Chen, K. W. Wenzel, R. R. Parker, C. K. Li, C. Fiore, *Nature* **339** 183 (1989); *Nature* **339** 667 (1989).

5. J. F. Ziegler, T. H. Zabel, J. J. Cuomo, V. A. Brusic, G. S. Cargill, E. J. O'Sullivan and A. D. Marwick, *Phys. Rev. Lett.* **62** 2929 (1989).

6. M. Gai, S. L. Rugari, R. H. France, B. J. Lund, Z. Zhao, A. J. Davenport, H. S. Isaacs and K. G. Lynn, *Nature* **340** 29 (1989).

7. N. S. Lewis, C. A. Barnes, M. J. Heben, A. Kumar, S. R. Lunt, G. E. McManis, G. M. Miskelly, R. M. Penner, M. J. Sailor, P. G. Santangelo, G. A. Shreve, B. J. Tufts, M. G. Youngquist, R. W. Kavanagh, S. E. Kellogg, R. B. Vogelaar, T. R. Wang, R. Kondrat and R. New, *Nature* **340** 525 (1989).

8. D. Albagli, R. Ballinger, V. Cammarata, X. Chen, R. M. Crooks, C. Fiore, M. J. P. Gaudreau, I. Hwang, C. K. Li, P. Linsay, S. Luckhardt, R. R. Parker, R. D. Petrasso, M. O. Schloh, K. W. Wentzel, M. S. Wrighton, submitted to *J. of Fusion Energy* (1989).

9. H. Hsuan, D. M. Manos, S. Cohen, S. Cowley, R. Motley, A. L. Roquemore, T. Saito, J. Timberlake, W. Ayers, T. Bennet, M. Bitter, F. E. Cecil, J. Cuthbertson, J. Dong, H. F. Dylla, J. Evans, H. Furth, L. Grisham, H. Hendel, K. Hill, R. Kulsrud, D. Meade, S. S. Medley, D. Mueller, E. Nieshmidt, R. Shoemaker and J. Thomas, "Lack of neutron and gamma radiation from PPPL's cold fusion experiments," presented at the Workshop on Cold Fusion Phenomena at Santa Fe, May 1989.

10. M. H. Salamon, M. E. Wrenn, H. E. Bergeson, K. C. Crawford, W. H. Delaney, C. L. Henerson, Y. Q. Li, J. A. Rusho, G. M. Sandquist, and S. M. Seltzer, *Nature* **344** 390 (1990).

11. G. Schrieder, H. Wipf and A. Richter, *Z. Phys. B: Condensed Matter* **76** 141 (1989).

12. E. Kashy, W. Bauer, Y. Chen, A. Galonsky, J. Gaudiello, M. Maier, D. J. Morrissey, R. A. Pelak, M. B. Tsang and J. Yurkon, *Phys. Rev C* **40** R1 (1989).

13. S. H. Faller, R. W. Holloway and S. C. Lee, *J. Radioanal. Nucl. Chem. Letters* **137** 9 (1989).

14. J. J. G. Durocher, D. M. Gallop, C. B. Kwok, M. S. Mathur, J. K. Mayer, J. S. C. McKee, A. Mirzai, G. R. Smith, Y. H. Yeo, K. S. Sharma and G. Williams, *Can. J. Phys.* **67** 624 (1989).

15. R. Behrisch, W. Moller, J. Roth, B. M. U. Scherzer, *Nuclear Fusion* **29** 1187 (1989).

16. A. Baurichter, W. Eyrich, M. Frank, H. Gohr, W. Kreische, H. Ortner, B. Roseler, C. A. Schiller, G. Weeske and W. Witthun, *Z. Phys. B: Condensed Matter* **76** 1 (1989).

17. D. Alber, O. Boebel, C. Schwartz, H. Duwe, D. Hilsher, H. Homeyer, U. Jahnke and B. Spellmeyer, *Z. Phys A: Atomic Nuclei* **333** 319 (1989).

18. D. Abriola, E. Achterberg, M. Davidson, M. Debray, M. C. Etchegoyen, N. Fazzini, J. Fernandez Niello, A. M. J. Ferrero, A. Filevich, M. C. Galia, R. Garavaglia, G. Garcia Bermudez, R. T. Gettar, S. Gil, H. Grahmann, H. Huck, A. Jeck, A. J. Kreiner, A. O. Macchiavelli, J. F. Magallanes, E. Maqueda, G. Marti, A. J. Pacheco, M. L. Perez, C. Pomar, M. Rameriz and M. Scasserra, *J. Electroanal. Chem* **265** 355 (1989).

19. R. D. Armstrong, E. A. Charles, I. Fells, L. Molyneux and M. Todd, *J. Electroanal. Chem* **272** 293 (1989).

20. J. Balej and J. Divisek, *J. Electroanal. Chem.* **278** 85 (1989).

21. J. Divisek, L Furst, and J. Balej, *J. Electroanal. Chem.* **278** 99 (1989).

22. M. Chemla, J. Chevalet, R. Bury and M. Perie, *J. Electroanal. Chem.* **277** 93 (1990).

23. "Cold Fusion Research," a report of the Energy Research Advisory Board to the U. S. Department of Energy, November 1989.

24. *Nature* **343** 6 (1990).

25. "Farewell (not fond) to cold fusion," *Nature* **344** 365 (1990).

26. D. Lindley, *Nature* **344** 375 (1990).

27. D. R. O. Morrison, "The Rise and Decline of Cold Fusion," to appear in *Physics World* (1990).

28. J. O'M. Bockris, G. H. Lin and N. J. C. Packham, "A Review of the Investigations of the Fleischmann-Pons Phenomena," (unpublished) Dept. of Chemistry, Texas A&M University, March, 1990.

29. R. Huggins et al., presented at the Technology and Society Division of the *ASME Winter Meeting* in San Francisco, December 12, 1989. Huggins described recent experiments that employ closed cell calorimetry, and reported the production of 1.15 MJ in 260 hours in one experiment. He mentioned that in another cell he was able to sustain 8.5 Watts for 275 hours. Extensions of this work were presented at the First Anuual Cold Fusion Conference, Utah, 1990.

30. A. J. Appleby, S. Srinivasan, Y. J. Kim, O. J. Murphy and C. R. Martin, "Evidence for excess heat generation rates during electrolysis of D_2O in LiOD using a palladium cathode - a microcalorimetric study," presented at the Workshop on Cold Fusion Phenomena at Santa Fe, May 1989.

31. O. J. Murphy, A. J. Appleby and S. Srinivasan, presented at the First Annual Conference on Cold Fusion, Utah, (1990).

32. R. C. Kainthla, O. Velev, N. J. C. Packham, L. Kaba and J. O'M. Bockris, *Electrochim. Acta* **34** 1315 (1989).

33. C. D. Scott, J. E. Mrochek, E. Newman, T. C. Scott, G. E. Michaels and M. Petek, "A preliminary investigation of cold fusion by electrolysis of heavy water," ORNL report TM-11322, Nov. 1989. G. Michaels et al, presented at the Technology and Society Division of the *ASME Winter Meeting* in San Francisco, December 12, 1989. Presented at the First Annual Conference on Cold Fusion, 1990.

34. D. Hutchinson, C. A. Bennett, R. K. Richards, J. Bullock and G. L. Powell, Oak Ridge National Lab Report ORNL/TM-11356 (1989).

35. M. C. H. McKubre, R. C. Rocha-Filho, S. Smedley, F. Tanzella, B. Chexal, T. Passell and J. Santucci, "Calorimetric and Electrochemical Studies of the Deuterium-Palladium System," First Annual Cold Fusion Conference, Utah (1990).

36. L. L. Zahm, A. C. Klein, S. E. Binney, J. N. Reyes, J. F. Higginbotham, A. H. Robinson and M. Daniels, Oregon State University Report OSU-NE-8914 Dec. 1989.

37. S. Pons and M. Fleischmann, to appear *J. Fusion Tech.*.

38. K. L. Wolf, N. Packham, J. Shoemaker, F. Chung and D. Lawson, "Neutron emission and the tritium content associated with deuterium loaded palladium and tritium metals," presented at the Workshop on Cold Fusion Phenomena at Santa Fe, May 1989.

39. N. J. C. Packham, K. L. Wolf, J. C. Wass, R. C. Kainthla and J. O'M. Bockris, *J. Electroanal. Chem.* **270** 451 (1989). Also K. Wolf, private communication (1990).

40. T. N. Claytor, P. A. Seeger, R. K. Rohwer, D. G. Tuggle and W. R. Doty, "Tritium and neutron measurements of a solid state cell," LANL report LA-UR-89-39-46, October 1989. There is a LANL memorandum of Jan. 23, 1989 from T. N. Claytor, D. G. Tuggle, P. Seeger, H. O. Menlove, R. K. Rohwer and W. Doty which contains an update of this work. Claytor reported the production of tritium in gas cell experiments. A number of his cells produced tritium between 8 and 245 μCuries.

41. E. Storms and C. Talcott, "Electrolytic Tritium Production," LANL report LAUR: 89-4138. This work was presented at the First Annual Cold Fusion Conference, Utah, 1990.

42. "BARC Studies in cold fusion," edited by P. K. Iyengar and M. Srinivasan, Bhaba Atomic Research Centre, Trombay, Bombay, India, December (1989). This work was presented at the First Annual Cold Fusion Conference, Utah, 1990.

43. C. Sanchez, J. Sevilla, B. Escarpizo, F. Fernandez and J. Canizares, "Cold Fusion during Electrolysis of Heavy Water with Ti and Pt Electrodes," Societa Italiana di Fisica Conference Proceedings Vol. 24 - Understanding Cold Fusion Phenomena- Edited by R. A. Ricci, E. Sindoni, and F. DeMarco, (1989).

44. J. Chene and A. M. Brass, *J. Electroanal. Chem.* **280** 199 (1990).

45. A. Bertin, M. Bruschi, M. Capponi, S. De-Castro, U. Marconi, C. Moroni, M. Piccunini, N. Semprini-Cesari, A. Trombini, A. Vitale, A. Zoccoli, J. B. Czirr, G. L. Jensen, S. E. Jones and E. P. Palmer, "Experimental evidence for cold fusion in a measurement in the Gran Sasso Massif," *Il Nuovo Cimento* **101** 997 (1989).

46. P. Perfetti, F. Cilloco, R. Felici, M. Capozi and A. Ippoliti, *Il Nuovo Cimento* **11D** 921 (1989).

47. A. De Ninno, A. Frattolillo, G. Lollobattista, L. Martinis, M. Martone, L. Mori, S. Podda, and F. Scaramuzzi, *Europhysics Letters* **9** 221 (1989).

48. F. Scaramuzzi, presented at the First Annual Cold Fusion Conference, Utah, 1990.

49. H. O. Menlove, M. M. Fowler, E. Garcia, A. Mayer, M. C. Miller, M. C. Miller, R. R. Ryan and S. E. Jones, "The measurement of neutron emission from Ti plus D_2 gas," presented at the Workshop on Cold Fusion Phenomena at Santa Fe, May 1989. This work was presented at the First Annual Cold Fusion Conference, Utah, 1990.

50. N. Wada and K. Nishizawa, *Jap. J. Appl. Phys.* **28** L2017 (1989).

51. R. Taniguchi, T. Yamamoto and S. Irie, *Jap. J. Appl. Phys.* **28** L2021 (1989).

52. D. Gozzi, P. L. Cignini, L. Petrucci, M. Tomellinin, G. De Maria, S. Frullani, F. Garibaldi, F. Ghio, M. Jodice and E. Tabet, "Nuclear and thermal effects during electrolytic reduction of deuterium at a palladium cathode," presented at the Workshop on Cold Fusion Phenomena at Santa Fe, May 1989.

53. D. Gozzi, P. L. Cignini, L. Petrucci, M. Tomellini and G. De Maria, *Il Nuovo Cimento* **103A** 143 (1990).

54. G. J. Batra, D. K. Bewley and M. A. Chaudhri, *Nucl Inst Meth* **100** 135 (1972).

55. D. D. Armstrong, C. R. Emigh, K. L. Meier, E. A. Meyer, and J. D. Schneider, *Nucl Inst Meth* **145** 127 (1977).

56. J. F. Janni, *Atomic Data Nucl Data Tables* **27** 341 (1982).

57. K. Wolf, private communication. This conclusion was discussed by Wolf at the NSF/EPRI meeting October 16-18, 1989.

58. R. E. Brown and N. Jarmie, submitted to *Phys Rev C* (1989). LANL Preprint LA-UR-89-953 (1989).

59. P. L. Hagelstein, "Coherent Fusion Theory," Presented at the ASME Winter Meeting, San Francisco, Dec. 1989, paper TS-4.

60. A. E. Cox, J. A. R. Wynchank and C. H. Collix, *Nucl. Phys.* **74** 497 (1965).

61. J. F. Mathiot, *Nucl. Phys.* **A412** 201 (1984).

62. L. Kaplan, G. R. Ringo and K. E. Wilzbach, *Phys. Rev.* **87** 785 (1952).

63. H. Lycklama and T. J. Kennett, *Can. J. Phys.* **45** 3039 (1967).

64. K. Kaminishi, *Jap. J. Appl. Phys.* **19** 1399 (1980).

65. G. B. Beard and G. E. Thomas, *Nucl. Phys.* bf A157, 520 (1970).

66. P. L. Hagelstein, "Status of Coherent Fusion Theory," DOE annual report, Jan. 1990.

67. J. Korringa, *Physica* **XVI** 601 (1950).

68. B. Hohler and H. Kronmuller, *Phil. Mag. A* **45** 607 (1982).

69. W. Gotz and W. Ketterle, *Z. Phys. B - Condensed Matter* **54** 49 (1983).

70. T. R. P. Gibbs, *Prog. Inorg. Chem.* **3** 315 (1962).

71. R. E. Norberg, *Phys. Rev.* **86** 745 (1952).

72. R. H. Dicke, *Phys. Rev.* **93** 99 (1954).

73. N. E. Rehler and J. H. Eberly, *Phys. Rev. A* **3** 1735 (1971).

74. J. H. Eberly, *Am. J. Phys.* **40** 1374 (1972).

75. R. Bonifacio and G. Preparata, *Lettre al Nuovo Cimento* **1** 887 (1969).

76. J. Weber, *Foundations of Physics* **14** 1185 (1984).

77. J. Weber, *Phys. Rev. C* **31** 1468 (1985).

78. J. Weber, *Phys. Rev. D* **38** 32 (1988).

79. M. Bixon and J. Jortner, *J. Chem. Phys.* **48** 715 (1968).

80. R. Englman and J. Jortner, *Mol. Phys.* **18** 145 (1970).

81. A. Nitzan and J. Jortner, *J. Chem. Phys.* **56** 3360 (1972).

82. A. Nitzan and J. Jortner, *Mol. Phys.* **25** 713 (1973).

83. R. Englman, *Non-radiative decay of ions and molecules in solids*, North-Holland, NY (1979).

84. J. Weber, *Phys. Rev.* **90** 977 (1953).

85. J. Weber, *Phys. Rev.* **94** 211 (1954).

86. R. Silbey and R. A. Harris, *J. Chem. Phys.* **80** 2615 (1984).

87. M. Wagner, *Z. Phys.* **256** 291 (1972).

88. E. Sigmund and M. Wagner, *Z. Phys.* **268** 245 (1974).

89. V. Denner and M. Wagner, *Z. Phys. B - Condensed Matter* **58** 255 (1985).

90. D. F. Walls and R. Barakat, *Phys. Rev. A* **1** 446 (1970).

91. M. Takatsuji, *Phys. Rev. A* **4** 808 (1971).

92. Z. C. Wang and H. Haken, *Z. Phys. B - Condensed Matter* **55** 361 (1984).

93. J. N. Bahcall, *Rev. Mod. Phys.* **50** 881 (1978).

94. K. S. Hirata, T. Kajita, M. Koshiba, M. Nakahata, Y. Oyama, N. Sato, A. Suzuki, M. Takita, Y. Totsuka, T. Kifune, T. Suda, K. Takahashi, T. Tanimori, K. Miyano, M. Yamada, E. W. Beier, L. R. Feldscher, W. Frati, S. B. Kim, A. K. Mann, F. M. Newcomer, R. Van Berg, W. Zhang, and B. G. Cortez, *Phys. Rev. D* **38** 448 (1988).

Quantum Mechanics of "Cold" and "Not-so-cold" Fusion

Scott R. Chubb
9822 Pebble Weigh Ct.
Burke, Va. 22015

and

Talbot A. Chubb
5023 N 38th Street
Arlington, Va. 22207

Abstract

Cooperative ionic fluctuations, which become energetically favorable during the overcharging of a sufficiently ordered, stoichiometric Pd-D lattice, provide a means for an entirely new form of nuclear interaction, "cold" or "solid state" fusion. As a consequence, 1) nucleons separated by macroscopic distances *in a classical sense* may interact in a nuclear fashion *quantum mechanically*, and 2) nuclear fusion may occur in which unfamiliar products are released. The evolution of such an ionic fluctuation, which we have named a Bose Bloch Condensate (BBC), becomes favorable as the concentrations of D and Pd become comparable because of large energy costs from lattice strain at individual lattice sites that result from coulombic repulsion associated with the occupation of a site by more than one D. These strain energy costs are removed through the evolution of long-ranged, periodic, ionic fluctuations in which equal (though small) amounts of excess charge are distributed uniformly to unit cells throughout the crystal. We provide the underlying quantum mechanical theory that governs both the evolution of these fluctuations and the associated selection rules of the resulting nuclear interactions. We also use a critical element of this theory (associated with the electrostatically induced changes in volume that accompany the binding of D^+ ions to an external environment) to explain how it is possible to initiate the kinds of low temperature fusion reactions that apparently have been seen in the recent Cluster Impact Fusion experiments performed by Beuhler, Friedlander, and Friedman.

Introduction

It has not been generally recognized that at the current time there is an evolving taxonomy of fusion processes. The first and best known form is "hot fusion", which is initiated from free space collisions of deuterons at high temperature. The two remaining forms were discovered during the last year. In both forms, fusion seems to be initiated at considerably lower temperature. These recently discovered processes are "cold fusion" as observed by Fleischmann and Pons[1], and "not-so-cold" fusion as observed in ion cluster impact experiments by Beuhler, Friedlander and Friedman[2]. In cold fusion, heat is produced without proton or neutron generation, whereas in not-so-cold fusion there is a release of neutrons and protons, as in conventional hot plasma fusion, but the process occurs at deuteron bombardment energies well below those known to be effective in D-D fusion-inducing collisions.

Both cold and not-so-cold fusion are manifestations of the quantum wave character of particles at low energy. The behavior of a particle as it undergoes collisions at low energies is determined both by the intrinsic properties of the particle and by the environment in which the particle resides. In the language of physics and chemistry, the wave function of a particle is determined by the interaction possibilities and by the boundary conditions applied. In a semantic extrapolation, one could say that the structure of a particle is affected by the boundary conditions it sees. Disregarding the semantics, quantum mechanics provides procedures for calculating particle behavior; namely, one calculates the wave function in accordance with the boundary conditions and pertinent interactions, and one calculates reaction rates using overlap integrals in accord with the Fermi Golden Rule or its equivalent.

Once it is recognized that the boundary conditions associated with bound deuterons may profoundly affect the quantum mechanical dynamics of colliding deuterons, it is possible to understand 1) how it is possible (contrary to conventional expectation) to initiate fusion in low temperature environments, and 2) that there is a relationship between the two lower temperature forms of fusion. Because Cluster Impact Fusion is highly reproducible while cold fusion is difficult to reproduce, the fact

that such a relationship can be explained quantum mechanically is significant.

The key difference between free space, unbound deuterons and deuterons that are bound to an attractive potential is that unbound deuterons may occupy any region of space with an appreciable probability, while the probability of finding a bound deuteron in a region of space beyond the classical turning point of its motion is exponentially small. Thus, when the active reactants in a fusion process obey the boundary conditions associated with bound deuterons, the potential for overlap during collisional processes becomes very different. As a consequence, if the active reactants are bound, many of our preconceived notions about fusion (which are based on the boundary conditions associated with unbound deuterons) do not apply.

Cold fusion is more complicated than ion cluster impact fusion, but both fusion processes depend on the existence of deuteron wave functions broadened to ~ 0.2 A by zero point motion. This wave function broadening is a consequence of electrostatic interaction between bound D^+ ions and the electrostatic potential provided by the other atoms and electrons of the larger structure that bind the D^+ ions to a particular region of space.

Quantum Mechanics of "Not-so-cold" Fusion

Let us first consider the cluster ion impact experiments. In the cluster impact studies D_2O ion clusters are accelerated onto a Ti target containing deuterium. The cluster ions are mass filtered so as to remove any light ion clusters or "naked" D^+ ions present in the beam prior to acceleration. (Here, a "naked" D^+ ion refers to a singly charged ion which is not bound to a cluster.) Control studies have shown that no high energy light ions contaminate the filtered heavy ion beam. The studies are carried out at ion impact velocities that correspond to D^+ kinetic energies relative to the target frame of ~100 eV. Fusion reactions are observed[2] at a rate that exceeds conventional expectation (based on the free space picture associated with the Gamow theory of a point particle electrostatic barrier) by more than a factor of 10^{10} . Fusion is not observed when the target contains H instead of D. Beuhler et al measured the fusion rate for impacting clusters over a wide range of cluster sizes having a fixed 300-KeV total energy. They found beginning at low mass that the fusion rate increases with cluster mass, going through a maximum near $D^+(D_2O)_{200}$. For this case the kinetic energy of the impacting D^+ ions in the target frame is 150 eV, far below the value at which a D^+ beam impact fusion would be expected based on Gamow theory.

It is clear from calculations given below that Gamow theory does not apply when the zero point motion broadening of the wave function is included in the target D that results from binding of the target D to the Ti host. To our knowledge, it is an open question what the actual value is of the fusion rate of a beam of D^+ incident on a TiD_2 target at these energies. Presumably, this rate is considerably smaller than when the incident D resides either within a cluster or bound to a single O atom or to an OD because when the D is bound to any of these polyatomic entities, its wave function is also broadened as a consequence of the binding that results from its interaction with its environment. Even for the case in which the incident D are "naked" (i.e., not bound to a cluster as they are in these Cluster Impact Fusion Experiments), for a wide range of energies Gamow theory simply does not apply when the target D is bound (as shown below), and the exponentially small value (associated with conventional wisdom) for the fusion rate at the energies associated with the average D energy (~100's of eV) in these collisions does not apply.

Because the effect of wave function broadening in the target D dramatically expands the "effective", electrostatic volume of each D by many orders of magnitude relative to its "point-like", free space size, even a crude calculation can be used to demonstrate how this wave function broadening effect may significantly alter the electrostatic barrier that inhibits fusion. Specifically, we may approximate the broadening effect by using for the target D wave function Φ^{target} the ground state wave function for a harmonic well, whose curvature is defined by the characteristic zero point motion R_{zp} (as determined by neutron scattering experiments) of D in TiD_2.

$$\Phi^{target}(R) = (2/(R_{zp}^2\pi))^{3/4} \exp(-R^2/R_{zp}^2) \qquad (1)$$

For the incident D wave function Φ^{inc} we may use a minimal uncertainty wave packet of characteristic size λ_{inc}, defined by the approximate variance of the deuteron wave function during the collision.

$$\Phi^{inc}(R) = (2/(\lambda_{inc}^2 \pi))^{3/4} \exp(-R^2/\lambda_{inc}^2) \qquad (2)$$

Depending upon the circumstances associated with the collisional process, λ_{inc} may take on a wide range of values. Since 80 percent of the momentum in each D_2O molecule is given to the oxygen atom, and the oxygen atom possesses 90 percent in each OD molecule, it is clear that as the cluster breaks up during the impact with the solid, transfer of energy and momentum from the O to the solid provides the dominant mechanism for slowing down the incident particles. In addition, as these momentum transfers occur, it is to be expected that significant interaction through changes in the vibrational modes of the D through bonding with the O will occur. Thus, we expect that the wave function broadening associated with O-D bonding and with changes in this bonding associated with interaction of the O with the solid will provide the dominant effects associated with the characteristic dimension λ_{inc}. The associated zero point motion is again on the order of 10^{-9} cm provided that the D remains bound to the O. If it becomes unbound, its characteristic dimension can vary considerably, with a lower bound corresponding to the situation in which the incident D has energy of ~100's eV. This case leads to the value $\lambda_{inc} \sim 10^{-10}$ cm.

Not surprisingly, when a realistic value of R_{zp} (~2 x 10^{-9} cm) is assumed, each deuteron is only "weakly" bound to a particular zero point volume of the lattice (it has a zero point energy of 10's of meV). The result of a first Born calculation of the shift $\Delta E^{(1)}$ in eigenvalue of each target deuteron that results through Coulombic interaction then is a "large", repulsive perturbation relative to both this electrostatic binding energy and to the binding energy of the deuteron to the entire crystal (given by ~ the heat of desorption ~ several eV). Thus, not only will the incident projectile unbind the target from its zero point volume, it will unbind the target completely from the lattice. Specifically,

$$\Delta E^{(1)} = e^2 \iint d^3R\, d^3R' \frac{\Phi^{target}(R)^2\, \Phi^{inv}(R')^2}{|R - R'|}$$

$$= e^2 (2/(\pi(R_{zp}^2 + \lambda_{inc}^2)))^{1/2}$$

$$\sim 30 \text{ eV} \qquad (3)$$

Then, the collision induces an electrostatic repulsive shift in the eigenvalue that is several hundred times larger than the zero point energy of the target, and about ten times larger than its total binding energy to the lattice. However, this shift in eigenvalue is 5 orders of magnitude less in absolute value than the accompanying attractive shift in eigenvalue that results from the strong interaction. The shift is also five orders of magnitude less than the comparable electrostatic shift that results when "point-sized" particles of nuclear dimension collide in this fashion. As a consequence, prior to and in the presence of the perturbation, the characteristic electrostatic and nuclear energies remain very different when the target D is initially bound, while this is not the case when the target and incident D are both unbound. Because these energy scales are so different, it becomes possible to write the "complete" wave function $\Phi = \Phi(r_n, r_p)$ (r_n and r_p respectively are the coordinates of the proton and neutron) for the target and incident D approximately in a Born-Oppenheimer separable form in which variations in the center of mass coordinate, $r_{cm} = (r_n + r_p)/2$, (which are associated with electrostatic interaction, as in the R and R' dependencies of Eqs. 1-3), are independent from the short-ranged variations in neutron-proton separation $r_{n-p} = r_n - r_p$ that are associated with the strong interaction.

$$\Phi = \Phi^{elect}(r_{cm})\, \Phi^{nuc}(r_{n-p})$$

Here, $\Phi^{elect}(r_{cm})$ is a slowly varying function, whose value is appreciable on the length scale of the electrostatic interaction, while $\Phi^{nuc}(r_{n-p})$ has appreciable value only on the length scale of the strong interaction. When this separability condition is imposed, it then follows that the first Born shifts in eigenvalue are extremely negative, indicating that fusion *may* occur. However, because the electrostatic perturbation is large on the scale of the initial energy (10's of meV) of the target D, the perturbation expansion must be viewed

as asymptotic at best, and coupling to higher order perturbations may alter the eigenvalue shift in a manner that would invalidate this conclusion.

On the other hand, it is also true that during the collision process, coupling to electrons (and other atoms through the electron coupling), could broaden the wave function further. Because there are wide possibilities associated with this effect, it is probable that perturbation theory may be applied. Then, it follows that fusion becomes permissible. In this manner, we see that as a consequence of broadening induced by the target, it becomes possible for a very different scenario to unfold in which fusion *may* occur. The additional broadening that results as a consequence of binding between the incident D with other atoms before and during the collision process probably plays a role in the resulting enhancement in fusion rate. Through even these crude arguments, we see that 1) cluster impact fusion follows as a consequence of wave functioning broadening due to binding effects associated with interaction between both the target and incident deuterons with their respective external environments, and 2) the effect should be sensitive to variations in cluster size. Thus the observation of cluster impact fusion and our explanation of the phenomenon provide a convincing demonstration of how the effect of wave function broadening may significantly alter the coulomb barrier to fusion.

Since the boundary conditions associated with cluster impact fusion and with colliding particles in free space are very different, it would be surprising if the Gamow theory (associated with free space collisions) has bearing on this new form of fusion. In fact, a crude application of the theory can be used to demonstrate that even for the case of a "naked" unbound deuteron incident on a target D, binding of the target to the Ti host may so significantly alter the resulting Coulomb barrier that in the majority of cases (i.e., when the incident D has an energy greater than ~70 eV), the underlying principle associated with the barrier concept (i.e., that "tunnelling" is required) breaks down. Specifically, when the incident D is sufficiently energetic so that the overlap of its wave function with the target wave function of Eq. 1 is sufficiently small, it follows that the repulsive Coulombic barrier V^{Coul} associated with the tunnelling problem may be evaluated in the limit in which the response of the target density to the presence of the incident deuteron is neglected. In this limit, the tunnelling probability T is given by

$$T = \exp(-2\lambda) \qquad , (4)$$

where

$$\lambda = \int_0^{r_{tp}} dR \left(\left(V^{Coul}(R) - E\right) 2M_D \right)^{1/2} / \hbar \qquad , (5)$$

r_{tp} is the classical turning point (defined by $V^{Coul}(r_{tp}) = E$), E is the incident energy, $\hbar = h/(2\pi)$, where h is Planck's constant, and M_D is the mass of a deuteron. Also, because the response of the target to the incident D is neglected, $V^{Coul}(R)$ is the Coulombic potential that the incident D "experiences" due to the presence of the target D.

$$V^{Coul}(R) = e^2 \int d^3R' \Phi_{target}(R')^2 / |R - R'| \qquad (6)$$

Using Eq. 1, it follows that

$$V^{Coul}(R) = e^2 \left(2/(R_{zp}^2 \pi) \right)^{3/2} \frac{1}{2\pi^2} \times \int d^3Q \int d^3R' \left\{ \exp(i(Q \cdot (R-R')) \times \exp(-2R'^2/R_{zp}^2) / Q^2 \right\}$$

$$< (8/\pi)^{1/2} e^2 / R_{zp}$$

$$\sim 70 \text{ eV} \qquad .(7)$$

This last inequality means that there is no classical turning point whatsoever associated with Eq. 5 when the incident energy is greater than 70 eV. Thus, for E>70 eV, the fundamental idea associated with a tunnelling requirement (as in Eq. 4) breaks down since the forbidden region in which exponential decay of the wave function occurs is never involved in the collision process.

Quantum Mechanics of "Cold" Fusion

Zero point motion plays an important role in cold fusion, but its role is different than in cluster impact fusion. It causes a reduction in the electrostatic interaction energy associated with the transient multiple occupation of a lattice site. Multiple occupations arise quantum mechanically from self-interaction of identical bosons in a periodic lattice. A key aspect of this self-interaction is the approximate notion of periodicity. When periodicity prevails for a sufficiently long period of time, for each Bravais vector of the lattice R_n, the single particle wave functions ψ associated with the stable particles (with respect to the electrostatic interaction) obey Bloch's theorem,

$$\psi_{\mathbf{k}}(r+R_n) = \exp(i\mathbf{k}\cdot R_n)\psi_{\mathbf{k}}(r) \quad . \quad (8)$$

Because the long-lived states obey Eq. 8, it follows that at an isolated location, the density is constructed from a superposition of states, formed from the eigenstates that obey Eq. 8. In this context, at any moment in time, at an individual lattice site the density must be viewed as a transitory entity, which oscillates in time. Of greater significance, when the many-body wave function is constructed from wave functions that obey Eq. 8, it follows that at any moment in time, there exists the possibility at a given site of fluctuations involving one, two,...N_B bosons (N_B is the number of bosons in the entire crystal), where the lifetime of this kind of fluctuation is determined by the interaction time associated with self-interaction.

The main effect of wave function broadening is a lengthening of the electrostatic lifetime (due to self-interaction) of the resulting multiple occupation virtual states. Because there exist a large set of self-interaction processes (each of which may be constructed self-consistently), in which Born-Oppenheimer separability applies as a consequence of large disparities in the energy, length and time scales between the perturbations associated with electrostatic and nuclear self-interaction, it follows that once states become occupied in which the scales of these interactions are sufficiently different, analogous to the evolution of the separability condition that arises in cluster impact fusion through wave function broadening, Born-Oppenheimer separability applies both prior to and in the presence of a well-prescribed perturbation.

The major distinction in the case of cold fusion is that the perturbation is always derived from self-interaction between bosons in which Born-Oppenheimer separability applies and is maintained. (When only those perturbations which preserve the separability between nuclear and electrostatic wave functions are included, the theory becomes self-consistent.) A necessary and sufficient condition which unambiguously preserves the condition of separability is that the wave function field associated with the single particle electrostatic interaction (from which the stable entities are constructed) must evolve in a manner that is independent of the more rapidly varying wave function fields associated with the nuclear interaction. This condition, once the fields are quantized, can only be maintained when the stable entity from which the field theory is formulated involves tightly bound proton-neutron pairs, which on the scale of electrostatic interaction behave as bosons. This result leads to the selection rule of cold fusion: *when the initial state is composed of tightly bound proton-neutron pairs, the final state is composed of tightly bound proton-neutron pairs.*

The distinction between the electrostatic and nuclear self-interactions is somewhat arbitrary. As long as there exists a well-defined set of perturbations, all of which are of sufficiently short length and time scale, and a second set of perturbations which are considerably longer in length and time scale, Born-Oppenheimer separability can be maintained. In fact, because, to an excellent approximation, the strong interaction remains invariant with respect to rigid displacements of the reactants and products, the strong interaction associated with a given multi-particle fluctuation is cyclic in the center of mass coordinate of the fluctuation. In practice, by expanding any of the relevant many-body interactions about the center of mass coordinate of all of the entities involved, it always becomes possible as a consequence to separate the self-interaction into two pieces, one of which is "slowly varying" and depends on the center of mass of the fluctuation, while the second is considerably more rapidly varying and does not depend on the center of mass. As the number of particles involved in the fluctuation increases, this kind of

separability procedure becomes artificial in the sense that there is no clear-cut difference in length scale. Provided, however, we restrict consideration to sufficiently simple forms of fluctuation, the ratio of the electrostatic lifetime (where this lifetime is associated with the slowly varying perturbation) to nuclear fluctuation time (associated with the rapidly varying portion of the perturbation) becomes sufficiently small that the wave function of the multi-particle fluctuation can always be written as a product of functions, in which one function is slowly varying and depends only on the center of mass coordinate of the fluctuation, while the remaining functions do not depend on the center of mass. This prescription provides a means of generalizing the Born-Oppenheimer separability of the many-particle fluctuation in a manner in which the kinds of perturbation theory arguments associated with cluster impact fusion can be applied to cold fusion.

Let us now consider the band theory of cold fusion[3-6]. The theory applies the quantum mechanics associated with the energy band theory of solids to D^+ ions in a periodic solid and examines the self-interactions implicit in the many body bosonic wave function that describes band state D^+ ions. The theory is a composite theory in the sense that it depends on a number of possibly controversial steps. These steps are:

* The occupation of band states by a macroscopic number of indistinguishable D^+ ions,

* the use of quantum mechanics and many-body theory to account for the associated quantum field behavior of the D^+ that occupy these band states,

* the effect of the environment on the structure of particles at low energy that are initially bound to a lattice, and the incorporation of this effect in the initial state band picture from which fusion commences,

* the relevance in this quantum field problem (as it relates to the nuclear fusion problem) of transient, cospatial multiple occupations of lattice sites by band-state D^+ ions (which are present in the initial state as a consequence of Bloch symmetry),

* the relevance to the fusion problem of a category of self-induced potentials associated with the short-range behavior of the field theory, each of which preserves Born-Oppenheimer separability, and the neglect of all other perturbations,

* the subsequent transfer of momentum to the environment from a model final state in which both the electrostatic and nuclear wave functions are of comparable dimension but are uncorrelated with respect to each other.

Each of these steps is in accordance with the laws of physics. It is not necessarily clear that the realization of the limit in which our theory would apply has been observed. However, even rudimentary calculations indicate important predictions of the theory seem to apply. These include the following: 1) it is necessary to achieve an over-potential condition prior to obtaining the anomalous heating effects in the electrolysis experiments, 2) in the case of Pd, the anomalous heating will occur very near the concentration $x=1$ in PdD_x, 3) there is a selection rule that is required by Born-Oppenheimer separability (as discussed above) and the nature of the interaction that mandates that in the primary cold fusion reactions, when the initial state involves only deuterons, the final state can only be formed from particles that consist of proton-neutron pairs. Thus, the theory predicts heat release without production of primary neutrons or protons. The possibility of the release of 23.8 MeV alpha particles is indicated, but a prediction of the number of alphas per joule of energy release requires a better understanding of the final step. Although there undoubtedly are refinements in the details of the theory that will be needed to understand all aspects of cold fusion, even in its initial (somewhat crude) form, the theory seems to provide a framework for an understanding of the cold fusion phenomenon.

Let us now summarize the band state D^+ cold fusion model. We can then discuss the individual statements making up the summary.

"Cold" Fusion in PdD_x at $X=1+\epsilon$

Injection of deuterium into metals containing a maximum loading of chemically

bonded D creates a population of band state deuterium ions. The band state deuterium forms a cooperative, collective matter phase called a Bose Bloch condensate (BBC), which infuses a host crystal, and in which the mean concentration of D^+ per unit cell is << 1. The properties of the BBC are those implicit in its many body wave function and the Fermi Golden Rule.

The BBC confers onto each unit cell of a crystal a low duty cycle transient occupation by single and multiple-occupation BBC deuterons. The wave function of these transient occupations reflects the zero point motion of interstitial deuterium. The multiple occupations are subject to reversible coalescence self-interactions in which there is a rapid fluctuation between chemical and nuclear density configurations. The nuclear density configuration of the 4-fold occupation state can decay into two 23.8 McV alpha particles. Less certain, the double occupation state in Pd can result in successive scatterings of chemically bonded interstitial D, resulting in lattice heating without alpha particle decay.

Though the name Bose Bloch Condensate places special emphasis on the bosonic character of the D^+ ion, the Bose behavior of this particular "condensate" is only significant on the length and time scales associated with electrostatic interaction. The use of terminology that involves "Bose" and "condensate" in this context should not be confused with the more commonly used term "Bose Condensate". A Bose Bloch Condensate only resembles a "Bose Condensate" at low temperatures and only then on length scales that are much larger than nuclear dimension. At elevated temperatures, the bosonic nature of the BBC is important primarily because its presence means that the dynamics of each of the thermally accessible BBC states may be described in terms of a single, exchange-symmetrized many body wave function. The condensate aspect of the state refers to the fact that collectively the identity of each D^+ ion has been lost with respect to the others. The Bose Bloch Condensate is present at all temperatures in which each deuteron in a periodic host may be viewed as an independent particle that has become indistinguishable from a macroscopic number of other deuterons.

Our statement that the formation of band state D^+ becomes favorable in β PdD_x at $x\sim1$ is based on the following reasoning. The chemical potential for the reaction $D^+ + PdD_x \rightarrow PdD_{x+\varepsilon}$ has been described by Wicke and Brodowsky[7] as the sum of four terms, involving a single statistical term and three energy terms. These authors provide a figure which illustrates how the behavior of these four factors contribute to the chemical potential as x varies between 0 and 1. The statistical term shows the effect of the availability of unoccupied unit cells. It is negative at low x and positive as $x\rightarrow 1$. The energy terms include a zero point motion term, which is endothermic and independent of x, an electrostatic interaction term, which is exothermic at low x and becomes endothermic as $x\rightarrow 1$, and a lattice strain energy term, which is endothermic at low x and exothermic as $x\rightarrow 1$. The electrostatic term includes the summed effect on the system energy of: (1) adding a D^+ charge to the center of an octahedron whose vertices are Pd atoms, (2) adding an electron to the pool of Pd conduction electrons, and (3) rearrangement of electron charges associated with the conduction electrons so as to provide neutralization of the added D^+ ion. The term is exothermic at low x, where vacancies exist in the Pd 4-d electron band, and becomes increasingly endothermic when these vacancies become filled and the electrons are forced to occupy higher energy 5-s band states. The term we are most interested in, however, is the lattice strain term. This term is positive at low x since the addition of isolated D^+ ions to the lattice forces expansion of isolated unit cells in a lattice whose lowest energy condition occurs with unit cells of smaller size. The term becomes negative as $x\rightarrow 1$ because most unit cells are then occupied and only isolated cells are unoccupied. The lattice strain caused by the isolated unoccupied cells is relieved as D^+ is added, resulting in energy release.

One now asks the question: what happens when highly non-equilibrium electrochemistry forces D^+ ions into a stoichiometric PdD crystal. If additional D is to be added in the form of a normal chemical occupation of a unit cell, isolated unit cells must become doubly occupied, and the lattice strain energy term jumps from strongly exothermic to strongly endothermic. However, if the added D^+ ion can enter a band state and be shared by all the unit cells of the crystal, it will contribute only a fractional charge (ε <<1) to each unit cell of the lattice and all unit cells will be affected equally. As

a result the endothermic lattice strain energy cost is avoided. For this reason the band state D^+ is favored for the non-stoichiometric component of $PdD_{1+\varepsilon}$. Because this process involves an "overcharging" of the electrode by effectively adding a small amount of D^+, accompanying this condition will be a polarization of the charge in opposition to the normal charge flow prior to the overcharging. This polarization is the origin of the over-potential condition that is seen during the observation of anomalous heating.

Consider now the statement that band state D^+, which we call Bose Bloch Condensate D^+, or BBC D^+ is a cooperative, collective matter phase whose properties are determined by its many body wave function. It is standard solid state physics practice to describe band state electrons in terms of a set of collective states characterized by many body wave functions. The wave functions are fabricated from sums of products of single particle wave functions, with the sums made up of permutations of an initial set of wave function products, and with signs applied to the products to reflect the antisymmetry of the fermion wave function of the electron under particle exchange. The same procedure is applicable to band state deuterons, except that all component wave functions are positive, reflecting the symmetric wave function of D^+, which is a boson. This procedure reflects the existence of collective states formed from indistinguishable particles and is simply the application of the exchange principle to multiparticle states. For both band state electrons and band state deuterons the electrostatic potential controlling the collective state is periodic and imposes Bloch symmetry on the single particle wave functions, and thus also on the many body wave function describing the collective state. The Bose character of the D^+ band system impacts the behavior of the collective state mainly by its removal of the Pauli exclusion principle. As a result the collective states have high degeneracy and can support cooperative behavior. In the limit of low temperature, only a single state of the band system is occupied, and a fully cooperative condensate, exhibiting ionic superconductivity, is to be expected.

The statement that the BBC confers onto each unit cell of a crystal a low duty cycle transient occupation by single and multiple-occupation BBC deuterons is a reflection of the quantum field character of the many body cooperative state, and the fundamental wave-particle duality of quantum mechanics. The time-independent description of the BBC is in terms of Bloch functions (defined by Eq. 8), which are wavelike and have equal amplitude distributions over each of the unit cells of the crystal. The Bloch functions are the eigenstates of the BBC and their density integrals show an equal and fractional charge contribution to each unit cell. However, the many body wave function can just as well be expressed in terms of Wannier functions, which describe the BBC in terms of transient, low duty cycle, single particle occupations of each unit cell of the crystal. When the many body Bloch wave functions are expanded in terms of Wannier functions, the new expression has terms corresponding to both transient single particle occupations, and transient multiple particle occupations of each unit cell. The transient multiple particle occupation terms in the many body wave function are the source of the nuclear self-interactions predicted by our theory.

The mathematics associated with these transient multiple particle occupations can be understood by writing the many-body wave function first in terms of Bloch states $\psi_{\mathbf{k}}(\mathbf{r})$ and then rewriting each Bloch state in terms of Wannier states $\Phi_s(\mathbf{r_m})$. Specifically if we use the symbol (ε_p,r) to denote the set of all of the many-body spatial coordinates $\{r\}$ and occupied energy bands $\{\varepsilon_p\}$, the many-body wave function $\Psi(\varepsilon_p,r)$ is given by

$$\Psi(\varepsilon_p,r) = (1/N_B!)^{1/2} \sum_{\{\mathbf{r}_m\}} \left\{ \prod_{m=1}^{N_B} \psi_{\mathbf{km}}(\mathbf{r}_m) \right\} \qquad ,(9)$$

where N_B is the number of BBC bosons in the crystal, and the sum over $\{\mathbf{r_m}\}$ includes interchange of each coordinate $\mathbf{r_m}$ with the remaining N_B-1 coordinates, ensuring that Ψ is suitably Bose symmetric. Then, we may rewrite each Bloch state $\psi_{\mathbf{km}}(\mathbf{r_m})$ in terms of Wannier states $\Phi_s(\mathbf{r_m})$.

$$\psi_{\mathbf{km}}(\mathbf{r_m}) = (1/N_L)^{1/2} \sum_{s=1}^{N_L} \Phi_s(\mathbf{r_m}) \exp(i\mathbf{k}_m \cdot \mathbf{R}_s) \qquad ,(10)$$

where N_L is number of unit cells in crystal. Substituting Eq. 10 into Eq. 9, we find

$$\Psi(\varepsilon_p,r) = (1 N_B!)^{1/2} \times \sum_{\{r_m\}} (1/N_L)^{N_B/2} \{ \prod_{m=1}^{N_B} \sum_{s=1}^{N_L} \Phi_s(\mathbf{r}_m) \exp(i\mathbf{k}_p\cdot\mathbf{R}_s) \} . \quad (11)$$

In Eqs. 10 and 11, $\Phi_s(\mathbf{r}_m)$ is a Wannier function for boson **m** occupying unit cell **s**. In the harmonic approximation, it is appropriate to construct each Wannier function, at time t=0, using the ground state wave functions of a harmonic well whose curvature is defined by the classical turning point **a** of the motion.

$$\Phi_s(\mathbf{r}) = (2/\pi a^2)^{3/4} \exp(-(r_s-\mathbf{r})^2/a^2) \quad (12)$$

Most of the terms in the bracketed product of sums of terms in Eq. (11) contain products in which the unit cell designator **s** is not repeated, since $N_L >> N_B$. A small fraction of the terms contain products in which the unit cell designator **s** is repeated twice. These terms describe double occupation of unit cell **s**. These terms contain factors $\Phi_s(\mathbf{r}_m)\Phi_s(\mathbf{r}_n)$, each of which is a product of cospatial wave functions centered on the center of unit cell s. Similarly, there are terms in which **s** is repeated three, four,....N_B times, corresponding to occupations of the unit cell **s** by three, four,...N_B deuterons. In each of these multi-particle occupations, each Wannier function has the same spatial distribution about the center of its unit cell, reflecting the zero point motion of a D^+ ion in the 3-dimensional potential well provided by the lattice. The collection of terms containing products corresponding to more than one deuteron occupying unit cell **s** are the only terms which contribute to nuclear self-interactions in unit cell **s**. They form the active portion of the input function to the Fermi Golden Rule expression as applied to unit cell **s**.

Both single and multiple occupation Wannier function products are transient due to the electrostatic self-interaction energy associated with unit cell occupation. The lifetime of each of the transient states is set by the Planck uncertainty principle $\Delta E \cdot \Delta t \sim h$. The uncertainty principle permits a short duration violation of the conservation of energy. The electrostatic self-interaction energies are calculable from the spatial distribution of the Wannier states, and are about 80 eV and 400 eV for the double and quadruple occupation states. The corresponding lifetimes are 5×10^{-17} and 1×10^{-17} s.

The statement that the wave functions reflect the zero point motion of D^+ ions in the lattice was discussed in conjunction with the ion cluster fusion observation.

The statement that multiple occupations of unit cells are subject to coalescence self-interactions between chemical and nuclear density configurations follows from: (1) the Fermi Golden Rule, (2) the cospatial form of the wave function products that are part of the initial state in the Fermi Golden Rule, (3) the existence of a nuclear interaction potential between paired neutron-proton elements in a nuclear density final state, and (4) our use of interaction potentials that are constructed from self-interaction in the limit in which electrostatic self-interaction and nuclear self-interaction occur on sufficiently different length and time scales that Born-Oppenheimer separability can be applied in the construction of the interaction potential and in the initial state. Because the quadruple and double occupancy electrostatic self-interaction energies (80 and 400 eV) are considerably smaller than the associated nuclear self-interaction energies (~10's of MeV), Born-Oppenheimer separability does apply to the initial state wave function, and in the construction of the interaction potential. (In the construction of the interaction potential associated with the quadruple particle case, it is necessary to perform an expansion about the center of mass of the four particle fluctuation in order to regroup terms in a suitable manner in which the rapidly and slowly varying contributions to the self-interaction become identifiable.)

The simplest mode of energy release through nuclear interaction that is consistent with momentum conservation and the selection rule in which the fusion products only involve configurations constructed from proton-neutron pairs when the initial state consists of deuterons is the coalescence reaction initiated from the quadruple occupation a site. In the limit in

which Born-Oppenheimer separability can be applied both to the reactants and the interaction potential, such a quadruple occupation provides an initial step in the decay of a virtual $^8Be^*$ nucleus to two alpha particles. We use the Fermi Golden Rule expression,

$$N = 2\pi/\hbar \; \Sigma \langle i|V|f\rangle \langle f|V|i\rangle \; \delta(E_i - E_f)$$

to calculate the associated reaction rate; N is the number of reactions per second within the crystal. This expression has been evaluated for a square well nuclear potential and a Gaussian input wave packet.

The possible modes of energy release through nuclear interaction that are consistent with momentum conservation and the selection rule in which the fusion products only involve configurations constructed from proton-neutron pairs when the initial state consists of deuterons are:

1) fusion via a nuclear configuration resembling $^8Be^*$, in which two 23.8 MeV alpha particles are released,

$$4D^+ \rightleftarrows {}^8Be^* \rightarrow 2 \text{ alpha} + 47.6 \text{ MeV}, \quad (13)$$

and

2) deexcitation of virtual $^4He^*$ states (associated with double deuteron [i.e., di-deuteron] occupation) through scattering between BBC di-deuterons with chemically bonded D. Schematically, the formation of such $^4He^*$ virtual states occurs through reversible coalescence reactions, of the form

$$2D+ \rightleftarrows {}^4He^* \quad .(14a)$$

The subsequent deexcitation of these virtual states through scattering processes involving the chemically bonded D may occur through a series of scattering events:

$$^4He^* + D_{lattice} \rightarrow {}^4He^{**} + D_{lattice,scat} \quad (14b)$$

$$^4He^{**} + D_{lattice} \rightarrow {}^4He^{***} + D_{lattice,scat} \quad (14c)$$

---------- --------

$$^4He^{**\cdots *} + D_{lattice} \rightarrow {}^4He + D_{lattice,scat} \quad (14d)$$

Here, each additional asterisk (in $^4He^{**\cdots *}$) is used to denote deexcitation of the nucleus. The chemically bonded (i.e., non-BBC) D are denoted by $D_{lattice,scat}$. (The chemically bonded deuterium refer to the D that are to be associated with the stoichiometric compound PdD.) Once reaction 14b takes place, the reverse reaction is blocked (even when the He state is virtual) through energy conservation. If one calculates the rate of Eq. 13 using the known size of the zero point motion of D^+ in PdD_x and assumes that the decay of the coalesced state into 2 alphas is prompt, then a BBC D^+ concentration of 3×10^{-7} BBC D^+ per unit cell is sufficient to produce the volumetric energy release of 10 W/cm^3 observed by Fleischmann and Pons[1].

However, it is not clear that alpha emission is the primary mode of energy release. It is probable that both the alpha particle emission mode (Eq. 13) , and the possible nuclear scattering mode involving virtual coalescence reactions from the double occupation state (Eq. 14a) could both be at work in the heating process . Scattering from the primary lattice constituent Pd also seems possible in imperfect crystals where wave function overlap occurs at lattice imperfections and at the crystal boundary. The nuclear scattering mode could liberate heat without release of any high energy particles. It is possible that the Li plays a role (as discussed in ref. 3) in a nuclear fashion, but it is probable that the most important impact of Li on the process is of an electronic nature, due to the Li-induced changes in surface chemistry. In regions where Bloch symmetry breaks down or is reduced, such as at interfaces, surfaces, or in other regions where periodicity is lost, it is to be expected that secondary reactions, initiated from the high energy D states (formed from Eqs. 14b-14d) will occur.

Finally let us consider experimental evidence for the validity of our theory. At last year's Utah meeting Chambers et al.[8] described a study in which a 130 A film of Pd sandwiched between two stainless steel diffusion barriers was loaded with deuterium by ion impact. The film was observed by a silicon particle detector. In two runs totaling a few hours a total of 8 abnormally high amplitude pulses were recorded. The 8 pulses could have been due to pick-up of unknown origin, as suggested by the authors, but if the pulses were due to high energy particles, the recorded energy losses averaged about 21

MeV. Our theory predicts emission of 23.8 MeV alpha particles. These authors also found a large number of low energy pulses due to response to a glowing ion-source filament. The lack of pulses outside the 21 MeV region supports the validity of the alpha particle interpretation.

1 M. Fleischmann and S. Pons , J. Electroanal. Chem. **261**, 301 (1989).

2 R.J. Beuhler, G. Friedlander, and L. Friedman, "Cluster-Impact Fusion", *Phys Rev Lett.* **63**, 1292 (1989).

3 S. R. Chubb and T. A. Chubb, "Distributed Bosonic States and Condensed Matter Fusion", NRL Memorandum Report 6600 (Documents, code 2627, Naval Research Laboratory, Washington, DC 20375-5000), (1990). Also submitted to NATURE, 1989.

4 T. A. Chubb and S. R. Chubb, "Nuclear Fusion in a Solid via a Bose Bloch Condensate", NRL Memorandum Report 6617, (Documents, code 2627, Naval Research Laboratory, Washington, DC ,20375-5000), (1990). Also submitted to *Phys. Rev. Lett.*, 1989

5 T. A. Chubb and S. R. Chubb, "Bloch-symmetric Fusion in PdD_x", *Fusion Technology,* in press , to appear May, 1990.

6 S. R. Chubb and T. A. Chubb, "Fusion Within a Solid via Solid State Effects: the Grand Identity Crisis", *Proceedings of the NSF/EPRI Workshop on Anomalous Effects in Deuterated Metals,* in press (1989).

7 E. Wicke and H. Brodowsky in *Hydrogen in Metals II,* edited by G. Alefield and J. Volkl (Springer , Berlin, 1978), p. 73.

8 G. P. Chambers, J. E. Eridon, K, S. Grabowski, B. D. Sartwell, and D. B. Chrisey, Journal of Fusion Energy: *Proceedings of the Utah Conference on Cold Fusion (May 23-25, 1989),* in press.

A more readable copy of this paper is here: http://lenr-canr.org/acrobat/SchwingerJnuclearene.pdf

NUCLEAR ENERGY IN AN ATOMIC LATTICE

Julian Schwinger

Department of Physics, University of California
Los Angeles, CA 90024

ABSTRACT

The distinct nature of the cold fusion regime is emphasized: electromagnetic selection rules suppress radiation, permitting excess energy transference to the lattice; the coherent nature of the wave-function is at variance with the standard separation between barrier penetration and nuclear reactivity. The discussion is restricted to tritium production, based on the dd reaction that populates the first excited state of ^{4}He, which decays into t+p, whereas the formation of ^{3}He+n is energetically forbidden. Production rates compatible with the broad range of experimental results are realized within a narrow parametric interval. The great sensitivity to the physical circumstances is reminiscent of the reproducibility problems that have plagued this field.

I believe it was Nils Bohr who defined an expert in some subject as one who has already made all possible mistakes. I stand before you as one who, in the field of cold fusion, is rapidly attaining expert status.

It began the night of March 23, 1989, when I caught the tail end of the MacNeil/Lehrer news report, which was somewhat amplified the next day by the New York Times article. As an old nuclear physicist I was, of course, quite excited by the remark – and here, for precision, I quote from the paper of Pons and Fleischmann as submitted a few days earlier – that "the bulk of the energy release is due to a hitherto unknown nuclear process or processes (presumably . . . due to clusters of deuterons)."

Surely, if something new is taking place, it ought to be associated with what – from a nuclear point of view – is new in the electrochemical arrangement. And that is the atomic lattice environment within which the putative nuclear reactions occur. Apart from a brief period of apostasy, when I echoed the conventional wisdom that atomic and nuclear energy scales are much too disparate, I have retained my belief in the importance of the lattice, as witnessed by the title of this talk.

But there must be more to the story. The early experimental situation suggested the hypothesis that two different nuclear reactions are at work. One is the apparently familiar DD reaction that, for example, produces tritium and hydrogen. The other stems from the inevitable contamination of D_2O by H_2O. An HD reaction produces ^{3}He – no tritium, no neutrons. Of course, a well trained hot fusioneer will instantly object that there must also be a 5.5 Mev γ-ray. He will not fail to point out that no such radiation has been observed. Indeed.

But consider the circumstance of cold fusion. At very low energies of relative motion, the proton and deuteron of the HD reaction are in an s-state, one of zero orbital angular momentum, and therefore of positive orbital parity. The intrinsic parities of proton, deuteron, and ^{3}He are also positive. Then, the usually dominant electric dipole radiation – which requires a parity change – is forbidden. To be sure,

as in the capture of a slow neutron by a proton, magnetic dipole radiation can occur, but at a significantly slowed rate. It is not unreasonable, then, that a good fraction, or, indeed, all of the available energy will be transferred to the phonon excitations of the heavily deuterided lattice. No 5.5 Mev γ-rays.

Incidentally, I did not advance the HD hypothesis as something to be proved theoretically – that is not the nature of a hypothesis – but as the basis for obvious critical experiments in which the H_2O/D_2O ratio is altered in small steps and heat production is monitored. To my knowledge, no systematic tests along these lines have yet been completed.

From what has been said, it is clear that cold fusion and hot fusion are quite different physical domains. The following qualitative remarks present that fact in an extreme form.

To my knowledge, all treatments of nuclear fusion between positively charged particles represent the reaction rate as the product of two factors. The first factor is a barrier penetration probability. It refers entirely to the electric forces of repulsion. The second factor is an intrinsic nuclear reaction rate. It refers entirely to the nuclear forces.

This representation of the overall probability, per unit time, as the product of two independent factors, may be true enough under the circumstances of hot fusion. But in very low energy cold fusion one deals essentially with a single state, or wave function, all parts of which are coherent. It is not possible to totally isolate the effect of the electric forces from that of the nuclear forces. The correct treatment of cold fusion will be free of the collision-dominated mentality of the hot fusioneers.

This audience needs no reminder of the extreme reactions that cold fusion has engendered. Happily, the psychological situation has been stabilized by a Christmas present from Los Alamos, re-enforcing an earlier announcement by Oak Ridge, as supported by findings at Texas A & M. It is no longer possible to lightly dismiss the reality of cold fusion.

Within the general context of "Nuclear Energy in an Atomic Lattice", my focus here is on the nuclear energy generation revealed by tritium production, as it occurs within the heavily deuterided palladium lattice. It is accepted that the DD reaction is the relevant mechanism. Two deuterons in close proximity can be thought of as an excited state of ^{4}He. It is advisable, then, to review what is known about such states.

Under cold fusion circumstances, the two deuterons have zero relative angular momentum, implying even parity, and a total spin angular moment of 0 or 2, as restricted by Bose-Einstein statistics. The energy of this state – twice the deuteron energy of binding – is -4.4_5 Mev.

The ground state of ^{4}He is a 0^+ state with a binding energy of 28.3 Mev. The first excited state, which is also 0^+, has a binding energy of 8.2 Mev. It is unstable, with a width ~ 0.3 Mev, decaying into a triton (^{3}H) and a proton (^{1}H), which continuum has its threshold at -8.5 Mev, 0.3 Mev below the 0^+ excited state. In contrast, the threshold for ^{3}He and a neutron is at -7.7 Mev, 0.5 Mev above the first

excited state. Thus the formation of the first excited state produces a source of tritium, but not of neutrons.

Now, the two-deuteron state, with energy -4.4 Mev, lies 3.8 Mev above the first excited state of ^{4}He. How can this excess energy, of roughly 4 Mev, be carried away? Certainly not by electric dipole emission of a photon; that is forbidden by the lack of parity reversal. And there is no counterpart to the weak magnetic dipole radiation in the HD reaction, because angular momentum 2 and angular momentum 0 do not yield a vector. There are more exotic possibilities: two photon emission, the creation of an electron-positron pair. But, the essential point, as in the HD reaction, is the likelihood that the excess energy will be transferred to the lattice.

A good deal is known about the lattice structures of pure palladium and deteurided palladium, except for the situation relevant to cold fusion, that of heavy deuteron loading. At least, I am unaware of any x-ray (or possibly neutron?) studies that would help clarify matters. There is, however, a theoretical conjecture [1] that new D_2 sites come into being, with an equilibrium separation of 0.94 Å. Inasmuch as this is significantly greater than the equilibrium separation in D_2 gas, 0.74 Å, the authors concluded that fusion in the lattice is highly improbable. To the contrary, I propose to accept their hypothesis as a basis for attempting to validate the cold fusion concept.

I have given only two public lectures on cold fusion. The first one, in October, was delivered at Albuquerque; the second one, two months ago, at Dijon, whence comes the mustard and the cassis. Although not hostile, both audiences were certainly skeptical, thus requiring detailed mathematical proof for all assertions. In this, more receptive atmosphere, perhaps precise details are less important than a qualitative survey, although if one is to come to grips with quantum mechanical subtleties, the natural language of atom physics can hardly be absent.

I begin with two important atomic parameters — those of length and of frequency. Consider a deuteron, of mass M, in the ground state of some localized site, about which it has the oscillation angular frequency ω. Let the mean square displacement from the equilibrium position, along one direction, be called Λ^2. By equating the relevant average potential energy, $\frac{1}{2} M\omega^2 \Lambda^2$ to half the corresponding zero-point energy, $\frac{1}{2}(\frac{1}{2}\hbar\omega)$, one learns that $\Lambda^2 = \hbar/(2M\omega)$.

The X-ray measurements on hydrided palladium, converted to the deuteron mass, indicate the Λ value: $\Lambda \simeq 10^{-9}$ cm = 0.1 Å. I shall accept this, as well, for the hypothetical D_2 sites. Given Λ, one infers that $\hbar\omega = (\hbar/\Lambda)^2/2M \simeq 0.1$ ev, which sets the scale of individual phonon energies. A convenient way to express the corresponding angular frequency scale is $2\pi\omega \simeq 10^{15}$ s^{-1}.

In the early days of radar, prior to, and at the start of the second World War, although the British had begun with radio waves that were called high frequency, HF, the need for better resolution led them to VHF, very high frequency, which inexorably brought about VHFI, very high frequency indeed. I mention this ancient history because, in our study of cold fusion, CF, it is useful, and implies no serious loss of

relevance, to consider VCFI, very cold fusion indeed. That is, we examine the lattice state at absolute zero. Then there are no phonon excitations – it is the phonon vacuum state – at least initially.

The latter phrase is the recognition that the phonon vacuum state is unstable. Through nuclear fusion, the deuteron constituents of the lattice are transformed, in pairs, at a certain rate, into tritium, hydrogen, and phonon energy. The anticipated number of phonons, per reaction, is measured by the ratio 3.8 Mev/0.1 eV ~ 4×10^7.

Recall that the simple independent phonon description of lattice excitations is based on the approximation of linear restoring forces or quadratic potential energies. The Hamiltonian for that phonon system will be called H_L.

Now consider a particular D_2 pair in the heavily loaded lattice. When the two deuterons are so close that fusion can occur, one is far outside the phonon domain of linear restoring forces. An additional potential energy – call it $V(\vec{R})$, with $\vec{R}$ the spatial displacement between the deuterons – comes into play. The Hamiltonian of this system is $H = H_L + V(\vec{R})$. Contact is made between $V(\vec{R})$ and the phonon description by introducing $\vec{R}_0$, the equilibrium separation of the deuterons, and writing $\vec{R} = \vec{R}_0 + \vec{r}$. Of course, an expansion in powers of $\vec{r}$, for $V(\vec{R}) = V(\vec{R}_0 + \vec{r})$, begins with cubic terms; any lesser power is already incorporated in H_L.

Time dependent perturbation theory gives the rate of transition out of the phonon vacuum state, which is the reciprocal of the mean lifetime T, as the vacuum expectation value

$$\frac{1}{T} = \frac{2\pi}{\hbar} {}_o\!<\! V\ \delta(H-E)\ V \!>_o \quad ,$$

where ${}_o\!<\!\ ,\ \!>_o$ symbolize the phonon vacuum state. Although, for simplicity, V is written, the symbol stands for the part of V that generates one or more phonons. As already noted, it must, in fact, be a rather large number of phonons. Also, whereas one would ordinarily assign zero energy to the lattice excitations, in the phonon vacuum state, E = -4.4 Mev appears here as the nuclear measure of energy appropriate to the two deuterons.

The next steps require some mathematical details. First, one introduces the Fourier integral representation for the delta function that enforces energy conservation:

$$\frac{1}{T} = \frac{1}{\hbar}\int_{-\infty}^{\infty} d\left(\frac{\tau}{\hbar}\right) {}_o\!<\! V\ e^{-\frac{i}{\hbar}(H-E)\tau}\ V \!>_o \ .$$

Then one adopts a Fourier integral representation for $V(\vec{R}) = V(\vec{R}_0 + \vec{r})$:

$$V = \int \frac{(d\vec{p})}{(2\pi\hbar)^3} V(\vec{p})\ e^{\frac{i}{\hbar}\vec{p}\cdot(\vec{R}_0+\vec{r})}$$

$$\equiv \int dV(\vec{p})\ e^{\frac{i}{\hbar}\vec{p}\cdot\vec{R}_0}\ e^{\frac{i}{\hbar}\vec{p}\cdot\vec{r}} \quad ,$$

along with the complex conjugate version, which is used for the left-hand V-factor:

$$\frac{1}{T} = \frac{1}{\hbar}\int_{-\infty}^{\infty} d\left(\frac{\tau}{\hbar}\right) dV(\vec{p})^*\ dV(\vec{p}')\ e^{-\frac{i}{\hbar}(\vec{p}-\vec{p}')\cdot R_0}$$

$$\times\ {}_o\!<\! e^{-\frac{i}{\hbar}\vec{p}\cdot\vec{r}}\ e^{-\frac{i}{\hbar}(H-E)\tau}\ e^{\frac{i}{\hbar}\vec{p}'\cdot\vec{r}} \!>_o \ .$$

The exponential factor $e^{\frac{i}{\hbar}\vec{p}'\cdot\vec{r}}$ acts on the phonon vacuum state to produce states

with every possible number of phonons. The simplification adopted here ignores all details about the phonons except their number. The related neglect of the vector character of $\vec{p}'$ will be corrected shortly. Then, the probability amplitude for creating n phonons is

$$ {}_n\langle e^{\frac{i}{\hbar}\vec{p}'\cdot\vec{r}} \rangle_o = \frac{1}{[n!]^{1/2}} \left[\frac{2^{1/2}\, p'\Lambda}{\hbar}\right]^n e^{-(p'\Lambda/\hbar)^2}, $$

which satisfies the physical requirement of unit total probability,

$$ \sum_{n=0}^{\infty} \left| {}_n\langle e^{\frac{i}{\hbar}\vec{p}'\cdot\vec{r}} \rangle_o \right|^2 = \sum_{n=0}^{\infty} \frac{[2(p'\Lambda/\hbar)^2]^n}{n!} e^{-2(p'\Lambda/\hbar)^2} = 1 . $$

Also correctly incorporated is the fact that, as a description of the relative motion of the two deuterons, the appropriate mass is the reduced mass $\frac{1}{2}$ M.

One function of the Hamiltonian H is to record the total energy of the n phonons, $n\hbar\omega$. Then the phonon part of the vacuum expectation value,

$$ {}_o\langle e^{-\frac{i}{\hbar}\vec{p}'\cdot\vec{r}}\, e^{-\frac{i}{\hbar}(H-E)\tau}\, e^{\frac{i}{\hbar}\vec{p}'\cdot\vec{r}} \rangle_o , $$

is

$$ \sum_{n=0}^{\infty} e^{-(p\Lambda/\hbar)^2} \frac{1}{[n!]^{1/2}} \left[\frac{2^{1/2}p\Lambda}{\hbar}\right]^n e^{-\frac{i}{\hbar}n\hbar\omega\tau} \times \left[\frac{2^{1/2}p'\Lambda}{\hbar}\right]^n \frac{1}{[n!]^{1/2}} e^{-(p'\Lambda/\hbar)^2} $$

$$ \longrightarrow e^{-(p\Lambda/\hbar)^2}\, e^{2\vec{p}\cdot\vec{p}'(\Lambda/\hbar)^2 e^{-i\omega\tau}}\, e^{-(p'\Lambda/\hbar)^2} $$

$$ = e^{-(\vec{p}-\vec{p}')^2(\Lambda/\hbar)^2}\, e^{2\vec{p}\cdot\vec{p}'(\Lambda/\hbar)^2(e^{-i\omega\tau}-1)} $$

where the correct vectorial relation between p and p' appears. In particular, it satisfies the requirement that only $\vec{p}-\vec{p}'$ occurs for $\tau = 0$.

The other function of the Hamiltonian H is to describe the formation of the 0^+ excited bound state of ^{4}He:

$$ e^{-\frac{i}{\hbar}(H-E)\tau} \longrightarrow {}_b\rangle\, e^{\frac{i}{\hbar}E_N\tau}\, \langle b $$

$$ E_N = 8.2-4.4 = 3.8 \text{ Mev} $$

where $\rangle_b$, $_b\langle$ symbolize the excited bound state. E_N, the nuclear energy released, sets the scale for τ, $\tau \sim \hbar/E_N \sim 10^{-22}$ s. As a result, $\omega\tau \sim 10^{14}\times 10^{-22} \sim 10^{-8}$, and $e^{-i\omega\tau} - 1 \cong -i\omega\tau$.

The special treatment of the two deuterons requires a corresponding splitting off, from the phonon vacuum state, of the description given the relative motion of the two deuterons, each in the ground state about its equilibrium position. That is the meaning of the subscript E, for Einstein, in the following summary:

$$ {}_o\langle e^{-\frac{i}{\hbar}\vec{p}'\cdot\vec{r}}\, e^{-\frac{i}{\hbar}(H-E)\tau}\, e^{\frac{i}{\hbar}\vec{p}'\cdot\vec{r}} \rangle_o $$

$$ \longrightarrow e^{-(\vec{p}-\vec{p}')^2\left(\frac{\Lambda}{\hbar}\right)^2} e^{-\frac{i}{\hbar}\left[\frac{\vec{p}\cdot\vec{p}'}{M} - E_N\right]\tau} \left| {}_b\langle \rangle_E \right|^2 . $$

The first, Gaussian, factor limits the magnitude of $\vec{p}-\vec{p}'$ to momenta $\sim \hbar/\Lambda$, which, Λ being $\sim 10^{-9}$ cm, is small on the nuclear scale. Now a crucial step is taken by recalling the additional factor $e^{-\frac{i}{\hbar}(\vec{p}-\vec{p}')\cdot R_0}$, and by writing

$$e^{-(\vec{p}-\vec{p}')^2(\Lambda/\hbar)^2}\; e^{-\frac{i}{\hbar}(\vec{p}-\vec{p}')\cdot R_0}$$

$$= e^{-\left[(\vec{p}-\vec{p}')\frac{\Lambda}{\hbar}+\frac{i}{2}\frac{\vec{R}_0}{\Lambda}\right]^2}\; e^{-1/4\,(R_0/\Lambda)^2} \quad .$$

The complex substitution

$$\vec{p} \to \vec{p} - \frac{i}{4}\frac{\hbar}{\Lambda}\frac{\vec{R}_0}{\Lambda} \quad , \qquad \vec{p}' \to \vec{p}' + \frac{i}{4}\frac{\hbar}{\Lambda}\frac{\vec{R}_0}{\Lambda} \quad ,$$

which has little effect elsewhere, converts this into

$$e^{-(\vec{p}-\vec{p}')^2(\Lambda/\hbar)^2}\; e^{-1/4\,(R_0/\Lambda)^2} \quad .$$

That Gaussian factor can be approximated by a delta function:

$$e^{-(\vec{p}-\vec{p}')^2(\Lambda/\hbar)^2} \to \pi^{3/2}\left(\frac{\hbar}{\Lambda}\right)^3 \delta(\vec{p}-\vec{p}') \quad ,$$

which permits a further reduction to a statement about magnitudes,

$$e^{-(\vec{p}-\vec{p}')^2(\Lambda/\hbar)^2} \to \frac{\pi^{1/2}}{2}\left(\frac{\hbar}{\Lambda}\right)^3 \frac{1}{Mp}\,\delta\left(\frac{p^2}{M}-\frac{p'^2}{M}\right).$$

But, prior to the last step, one would have carried out the τ-integration that exhibits energy conservation. With the distinction between $\vec{p}$ and $\vec{p}'$ removed, this integral appears as, for example,

$$\int_{-\infty}^{\infty} d\left(\frac{\tau}{\hbar}\right)\; e^{-\frac{i}{\hbar}\left[\frac{p'^2}{M}-E_N\right]\tau} = 2\pi\delta\left[\frac{p'^2}{M}-E_N\right].$$

Then one can return to the Gaussian function and give it the equivalent form

$$e^{-(\vec{p}-\vec{p}')^2(\Lambda/\hbar)^2} \to \frac{\pi^{1/2}}{2}\left(\frac{\hbar}{\Lambda}\right)^3 \frac{1}{Mp}\,\delta\left(\frac{p^2}{M}-E_N\right)$$

$$= \hbar\omega\left(\frac{2\pi\hbar\omega}{E_N}\right)^{1/2}\delta\left(\frac{p^2}{M}-E_N\right) \quad . \qquad \left[\frac{(\hbar/\Lambda)^2}{2M}=\hbar\omega\right]$$

Here is where we are now:

$$\frac{1}{T} = \frac{1}{\hbar}\int dV(\vec{p})^*\; dV(\vec{p}')\; 2\pi\;\hbar\omega\left(\frac{2\pi\hbar\omega}{E_N}\right)^{1/2}$$

$$\times\;\delta\left(\frac{p^2}{M}-E_N\right)\;\delta\left(\frac{p'^2}{M}-E_N\right)$$

$$\times\; e^{-1/4\,(R_0/\Lambda)^2}\;\left|\;{}_b\!<\;>_E\;\right|^2 \quad .$$

Attention is directed to the squared presence of the factor

$$v = \int dV(\vec{p})\;\delta\left(\frac{p^2}{M}-E_N\right)$$

$$\equiv \int \frac{(d\vec{p})}{(2\pi\hbar)^3}\,V(\vec{p})\;\delta\left(\frac{p^2}{M}-E_N\right) \quad ,$$

which is dimensionless and predominantly nuclear in content. That gives us

$$\frac{1}{T} = 2\pi\omega\left(\frac{2\pi\hbar\omega}{E_N}\right)^{1/2} v^2\; e^{-1/4\,(R_0/\Lambda)^2}\;\left|\;{}_b\!<\;>_E\;\right|^2.$$

It would be pointless to ask a precise number for v from this crude nuclear model. But, as a pure number that involves only nuclear magnitudes, the natural provisional value is $v \sim 1$. The dimensional factor that appears is

$$2\pi\omega\left(\frac{2\pi\hbar\omega}{E_N}\right)^{1/2} \sim 10^{15}\left(\frac{10^{15}}{10^{22}}\right)^{1/2} \sim 10^{12}\ s^{-1} \quad .$$

So, the inverse mean lifetime, measured in inverse seconds, is

$$\frac{1}{T} \sim 10^{12}\; e^{-1/4\,(R_0/\Lambda)^2}\;\left|\;{}_b\!<\;>_E\;\right|^2 \quad .$$

The wavefunction for the relative motion of the two deuterons, in their respective ground states, is

$$\psi_E(\vec{R}) = \text{const.}\;\exp\left[-\frac{1}{2}\,\frac{1/2\;M\omega}{\hbar}\,(\vec{R}-\vec{R}_0)^2\right]$$

$$= \frac{1}{(4\pi)^{3/4}}\,\frac{1}{\Lambda^{3/2}}\,\exp\left[-\frac{1}{2}\,\frac{1}{4\Lambda^2}\,(\vec{R}-\vec{R}_0)^2\right].$$

What counts in

$$ {}_b\langle\ \rangle_E = \int (d\vec{R})\ \psi_b^*(\vec{R})\ \psi_E(\vec{R}) $$

is the behavior at short distances, $R \ll \Lambda$:

$$ \psi_E(R \ll \Lambda) \cong \psi_E(0) = \frac{1}{(4\pi)^{3/4}} \frac{1}{\Lambda^{3/2}} e^{-1/8 (R_0/\Lambda)^2} . $$

As for the wavefunction of the bound state, in this oversimplified model, one can say that it has a linear dimension $\ell \sim 10^{-13}$ cm, and a corresponding amplitude $|\psi_b| \sim \ell^{-3/2}$. That gives the estimate

$$ \left| \int (d\vec{R})\ \psi_b^*\ \psi_E \right| \sim \ell^3\ \ell^{-3/2} \frac{1}{\Lambda^{3/2}} e^{-1/8 (R_0/\Lambda)^2} $$

$$ = (\ell/\Lambda)^{3/2}\ e^{-1/8 (R_0/\Lambda)^2} , $$

from which one gets

$$ e^{-1/4 (R_0/\Lambda)^2} \left| {}_b\langle\ \rangle_E \right|^2 \sim (\ell/\Lambda)^3\ e^{-1/2 (R_0/\Lambda)^2} , $$

where $(\ell/\Lambda)^3 \sim (10^{-13}/10^{-9})^3 \sim 10^{-12}$. The final outcome is

$$ \frac{1}{T} \sim e^{-1/2 (R_0/\Lambda)^2} . $$

With the two parameters chosen as $R_0 = 0.94$ Å and $\Lambda = 0.10$ Å, one gets

$$ \frac{1}{T} \sim e^{-44} \sim 10^{-19}\ s^{-1} , $$

per D_2 pair. If, for example, there are 10^{22} pairs, the rate of tritium production is 10^3/s. Changing Λ to 0.125 Å, a 25% increase, yields

$$ \frac{1}{T} \sim e^{-28} \sim 10^{-12}\ s^{-1} , $$

which, for 10^{22} pairs, is a production rate of 10^{10}/s. To my knowledge, these two examples more than span the observed range of tritium production.

But what is particularly striking is that a change in a parameter by 25% alters the production rate by a factor of ten million, a degree of sensitivity that verges on chaos. Inasmuch as the single parameter R_0/Λ combines, albeit crudely, the effects of all the forces at work within the lattice, the difficulties encountered in reproducing the cold fusion phenomena become more understandable.

REFERENCE

[1] Z. Sum and D. Tomanek, Phys. Rev. Lett. 63 p. 59:1989.

A more readable copy of this paper is here: http://lenr-canr.org/acrobat/BockrisJdoestritiu.pdf

DOES TRITIUM FORM AT ELECTRODES BY NUCLEAR REACTIONS ?

J. O'M. Bockris, G.H. Lin, R.C. Kainthla,
N.J.C. Packham and O. Velev

Surface Electrochemistry Laboratory
Texas A&M University
College Station, TX 77843

ABSTRACT

This paper reports tritium formed in $LiOD-D_2O$ solutions in which Pd cathodes are used to evolve D_2. Electrolysis was carried out for up to 4½ months. Excess heat has been observed from 5 electrodes out of 28, tritium in 15 out of 53 but 9 out of 13 if the electrodes are limited to 1 mm diameter. Steady state tritium concentrations were 10^4-10^7 disintegrations min^{-1} ml^{-1}. A weak correlation may exist between heat observed and tritium produced. The rate of production of tritium was c. 10^{10} atoms cm^{-2} sec^{-1}. The branching ratio of tritum to neutrons was ~ 10^8.

A theoretical dendrite enhanced fusion model is suggested. Growing gas layer breakdown occurs at sufficiently high surface potential dendrite tips and correspondingly fusion reactions occur. The model gives quantitative consistence with experiment, especially the sporadic nature and the observed branching ratio.

INTRODUCTION

Since Fleischmann, Pons and Hawkins [1] and Jones [2] reported the cold fusion phenomena, which is difficult to explain by conventional nuclear physics, several attempts to interpret the excess heat as well as radiative particle emission have been made. Such explanations fall into two large categories: chemical reaction and nuclear fusion. The heat released by a chemical reaction corresponds to the range of a few electron volts (eV) per atom in contrast to the energy liberated in a nuclear reaction - on the order of millions of electron volts (MeV) per nucleus. In an earlier paper [3], we summarized the eight possible chemical contributions to the excess heat seen in reference 1, and arrived at the conclusion that any chemical explanation would be improbable. No one chemical explanation will suffice to explain the magnitude of the excess heat observed, and the large amount of tritium produced in the solution and gas phases [4,5] cannot be explained by any kind of chemical reaction. The second category of explanation is a nuclear one. Different models [6-9] to explain the cold fusion experiments have been suggested since they cannot be simply interpreted by todays nuclear physics. In a review paper [10], different fusion experiments and theoretical explanations have been summerized.

There are two main characteristics of the cold fusion experiments. One is the large tritium to neutron ratio, on the order of 10^8, and the other is the sporadicity and irreproducibility of the phenomena. A suitable cold fusion theory or model must explain both of the these two features.

A large amount of tritium has been observed both in the solution and gas phases in this laboratory, which can not simply explained by isotopic enrichment. The maximum tritium concentration in the solution due to isotopic separation at infinitely long times, is about 2 times the tritium concentration in the original solution [5], which is very small compared to the experimental results.

EXPERIMENTAL

(a) Sources of Electrode Materials

The 1mm and 3mm Pd cathodes used in the present study were cut from 99.9% pure rods made by Hoover and Strong, Richmond, VA and purchased from the Texas Coin Exchange, College Station, while the 6mm diameter electrodes were cut from the 99.9% pure rod purchased from Sure Pure Chemicals, NY. The 4mm cathodes were cut from high purity "fusion" Pd on loan from Johnson Matthey. The lengths of the electrodes were cut about 4cm, 3cm, 2.5cm and 2.5cm, respectively.

Pt electrodes were of 99.9% purity, from Alfa Products, Danvers, MA, titanium (99.99%), from Johnson Matthey, Seabrook, NH, and Ni gauze (99.9%), from the

Belleville Metals Company, Belleville, NJ.

99.9% pure D^2_O was obtained from Aldrich Chemical Co.

(b) Pre-treatment

After cutting to appropriate sizes, the electrodes were pre-treated. This involved either; no pre-treatment, acid etching, annealing, electrochemical, hammering, electrodeposition of Pd, electroless deposition of Pd.

(c) Charging

After pre-treatment, a Ni wire was spot welded to the electrode, and put into small electrolytic cells with appropriate electrolyte and counter electrodes (Table 1).

The cells were then put on a charging current of ~64 mAcm~2 while the cell voltage was ~3.0-4.0 V. The cells were refilled with D_2O for a few weeks to a few months. Sometimes, th Ni anode was repaired or replaced along with the solution and the glass tube.

(d) Heat Measurements

After charging, for times varying from 1025 weeks, the electrodes were transferred to a calorimeter for the measurement of heat.

The calorimeter used in the study was of the heat transfer type, and has been described elsewhere [11].

(e) Tritium Measurements

Tritium analysis was performed on the alkaline electrolyte by in-situ Liquid Scintillation Counting (LSC). Multiple blank samples of H_2O, D_2O, and 0.1 M LiOD werre included for analysis. A test for chemiluminescence was made using samples ranging from 1M to 1M LiOD, including samples that had been neutralized by potassium hydrogen phthalate. Results are shown in Fig.1. One minute and ten minute analyses (some samples were run overnight) were performed. A detailed analysis of the energy spectra from the Cyclotron Institute counters yielded the correct β energy end point for tritium (18keV) c.f. Figs. 2a and 2b.

The results are shown in Table 2. The tritium content of the liquids resulting from the electrolyses, including a tritium (HTO) standard and blanks of LiOD and D_2O, was examined by Los Alamos National Laboratory, Argonne National Laboratory, Battelle Pacific Northwest Laboratory and the General Motors Research Laboratory. These results are shown in Table 3.

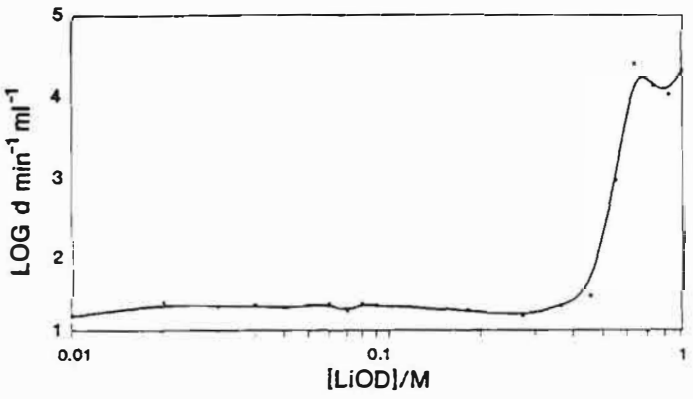

Fig. 1. The effect of electrolyte concentration on chemiluminescence of the scintillation cocktail [4].

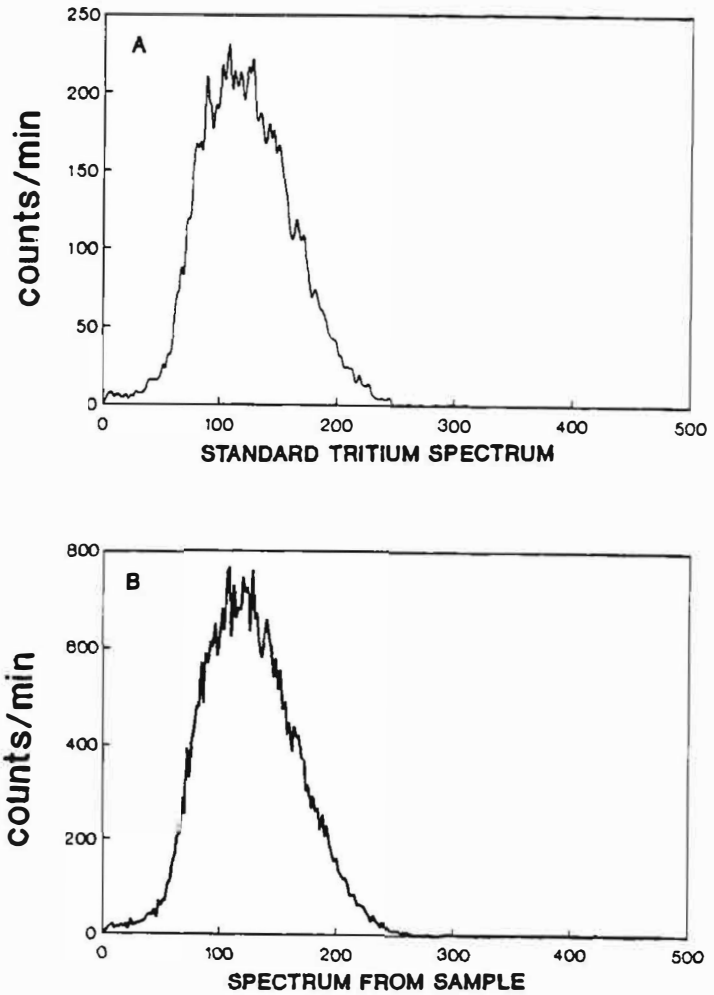

Fig. 2. (a) The spectrum of a tritiated water sample.

TABLE 1
SPORADIC OBSERVATIONS OF TRITIUM AND HEAT DURING D_2 EVOLUTION FROM D_2O ON PD

CELL	ELECTRODE PRETREATMENT	SOLUTION	TRITIUM	EXCESS HEAT
A1 (1mm)	No treatment	0.1M LiOD	Yes	NM
A2 (1mm)	No treatment	0.1M LiOD + 0.1mM NaCN	Yes	NM
A3 (1mm)	Annealed, 800°C, 6 hrs	0.1M LiOD	Yes	NM
A4 (1mm)	Annealed, 800°C, 6 hrs	0.1M LiOD + 0.1mM NaCN	Yes	NM
A5 (1mm)	Acid Etch	0.1M LiOD	Yes	NM
A6 (1mm)	Acid Etch	0.1M LiOD + 0.1mM NaCN	Yes	NM
A7 (1mm)	Electrochemical	0.1M LiOD	Yes	NM
A8 (1mm)	Electrochemical	0.1M LiOD + 0.1mM NaCN	Yes	NM
A9 (1mm)	No treatment, charged in U tube	0.1M LiOD	No	Yes
M1 (1mm)	No treatment	0.1M LiOD	Yes	NM
M2 (1mm)	Acid Etch	0.1M LiOD	No	NM
B1 (3mm)	No treatment	0.1M LiOD	No	No
B2 (3mm)	No treatment	0.1M LiOD + 0.1mM NaCN	No	No
B3 (3mm)	Annealed, 800°C, 6 hrs	0.1M LiOD	Yes	No
B4 (3mm)	Annealed, 800°C, 6 hrs	0.1M LiOD + 0.1mM NaCN	No	No
B5 (3mm)	Acid etch	0.1M LiOD	No	No
B6 (3mm)	Acid etch	0.1M LiOD + 0.001M NaCN	No	No
B7 (3mm)	Electrochemical	0.1M LiOD	No	No
B8 (3mm)	Electrochemical	0.1M LiOD + 0.001M NaCN	No	Yes
B9 (3mm)	No treatment, charged in U tube	0.1M LiOD	No	Yes
C8 (6mm)	Electrochemical	0.1M LiOD + 0.001M NaCN	No	No
CELL 1 (6mm)	No treatment	0.1M LiOD	No	No
CELL 4 (3mm)	Annealed, 1200°C, 12 hrs	0.1M LiOD	Yes	Yes
JM1 (4mm)	No treatment	0.1M LiOD	No	No
JM2 (4mm)	Annealed, 800°C, 24 hrs	0.1M LiOD	No	No
CELL 4A (3mm)	No treatment	0.1M LiOD	No	No
H1 (3mm)	Hammered; Electrochemical	0.1M LiOD	No	No
AH1 (3mm)	Annealed, 800°C, 8 hrs Hammered, Electrochemical	0.1M LiOD	No	No
Cell 1A (6mm)	Annealed, 800°C, 8 hrs	0.1M LiOD	No	No
CEll 1B (3mm)	Electrodeposited Pd on Pd	0.1M LiOD	No	No
B5A (3mm)	Annealed, 800°C, 24 hrs	0.1M LiOD	No	No

NM = No attempt made to measure.

TABLE 2
CELL IDENTIFICATION, ELECTRODE TREATMENT, SOLUTION TYPE AND TRITIUM ACTIVITY
OF ELECTROLYTE SAMPLES PERFORMED ON 1219 LSC

CELL	ELECTRODE PRETREATMENT	SOLUTION	CORRECTED ^3H ACTIVITY ($dpmml^{-1}$)
A1	No treatment	0.1M LiOD	3.8×10^4
A2	No treatment	0.1M LiOD + 0.1mM NaCN	
	After 16 days at 50 $mAcm^{-2}$ then for 8 hours at 500 $mAcm^{-2}$ (5/1/89)		168
	50 $mAcm^{-2}$ for 4 days (5/5/89)		134
	50 $mAcm^{-2}$ for 3 hours, 110 $mAcm^{-2}$ for 2 hours, 200 $mAcm^{-2}$ for 20 minutes (5/6/89)		1.1×10^4
	50 $mAcm^{-2}$ (5/7/89)		1.4×10^4
	(5/7/89 - 5/13/89)		1.1×10^4
	(5/13/89 - 6/6/89)		7.5×10^3
A3	Anneal	0.1M LiOD	4.9×10^6
A4	Anneal	0.1M LiOD + 0.1mM NaCN	1.2×10^5
A5	Acid Etch	0.1M LiOD	3.7×10^6
A6	Acid Etch	0.1M LiOD + 0.1mM NaCN	3.3×10^4
A7	Electrochemical	0.1M LiOD	
	Before high current density		102
	After 2 hours at 500 $mAcm^{-2}$		5223
	After 6 hours at 500 $mAcm^{-2}$		5.0×10^5
	After 12 hours at 500 $mAcm^{-2}$		7.6×10^5
A8	Electrochemical	0.1M LiOD + 0.1mM NaCN	
	After 16 days charging and 8 hours high current density (5/1/89)		192
	Electrolyte levels after 6 weeks at 50 $mAcm^{-2}$		5.0×10^5
	Recombined gas levels after 2 weeks of external recombination at 50 $mAcm^{-2}$		5.0×10^7
B3 (3mm)	Anneal	0.1M LiOD	6.3×10^4
B5 (3mm)	Acid Etch	0.1M LiOD	48
CELL 1 (6mm)	No treatment	0.1M LiOD	117
CELL 4		SEE FIG. 5	
M1	No Treatment	0.1M LiOD	3000

TABLE 3
CONFIRMATORY RESULTS FROM OUTSIDE SOURCES ON VARIOUS SAMPLES
CORRECTED ^3H ACTIVITY IN $dpmml^{-1}$

SAMPLE	CELL 1	CELL 2	HTO STANDARD	0.1M LiOD	D_2O
INSTITUTION					
Texas A&M	2.13×10^6	1157	7.23×10^5	93	47
Battelle	1.96×10^6	1170	8.08×10^5	127	140
Argonne	1.96×10^6	1020	7.59×10^5	90	114
Los Alamos	1.97×10^6	800-1300	6.50×10^5	113	161
General Motors	1.80×10^6	1000	----------NOT ANALYZED--------		

(f) Contamination

The possibility that large amounts of tritium were present in either the D_2O or the Li used to make the LiOD, is ruled out by the Results of Tables 4a and 4b. Each batch of D_2O that was used for refilling the cells was analyzed for tritium content, both on the 1219 instrument (Table 4a), and the 1410 (Table 4b, shown as a mean of 10 results). Many experiments were run in which no significant increase of tritium was observed, including identical cells to the ones which did produce tritium, except for the electrolyte, which was 0.1M LiOH in H_2O (Tables 4b and 5). Possible contamination from the nickel anode was examined by neutralization and then counting, with negative results.

Virgin palladium and nickel of the same batch used for all 1mm Pd cells were sent for analysis to LANL with no tritium being detected.

If it is supposed that the Pd had, earlier in its history, suffered prolonged exposure as a cathode in D_2O, T would have diffused into the electrode. Simple calculation shows [12] that it would take $<10^2$ hours to diffuse out again for a Pd rod kept in air.

Finally, some of the electrodes which gave tritium had been heavily annealed just prior to emmersion in the D_2O-LiOD. Thus, contamination would seem unlikely.

EXPERIMENTAL RESULTS

1) Reproducibility and Repeatability

The special difficulty of the present work is poor repeatability. Table 1 summarizes some of the results of heat and tritium measurements on all the electrodes studied so far in this laboratory. Excess heat has been observed in only 5 out of the 28 electrodes, tritium in 15 out of 53. The observation of tritium with 1mm diameter wires has been more successful with 9 out of 13 1mm electrodes yielding tritium. None of the seven 6mm electrodes have shown any excess heat or tritium for observation periods of up to 6 months. Both heat and tritium has been observed together only for one electrode. However, in some half of the present work, heat and tritium were not regularly recorded together. Further, heat and tritium come in bursts. T may have been produced during some heat bursts (as DT) and sparged out before measurement was be made. The duration of the experimental work covered in this paper is about 25 weeks.

2) Rise Times during Switch-on

In one of the cells (cell A7 c.f. Table 2) the build up of tritium as a function of time was followed at high current density. The results shown in Fig. 3 indicate either the time for reaching equilibrium of DT in solution to DT in the gas over the solution; or represent the time in which a burst occured, the product being largely DTO.

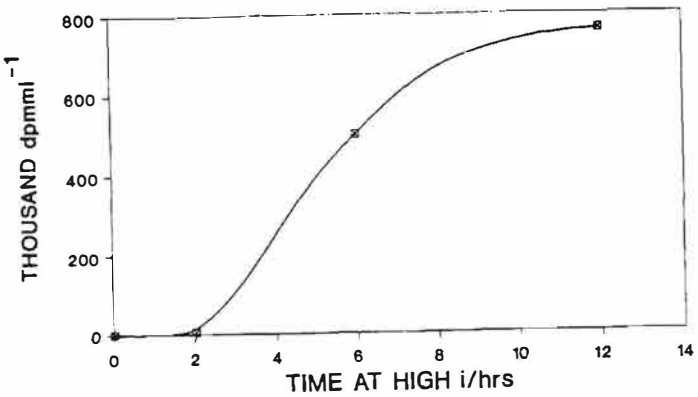

Fig. 3. The production of tritium in the electrolyte of cell A7 as a function of time [4].

3) Fall Time during Switch-off.

Another cell (cell A2 in Table 2) was tested for tritium over an extended period of time. It was run at a low current density for 16 days, followed by a 10 hour period at high current density, after which, tritium was not produced. The cell was then transferred to the Cyclotron Institute where it remained at low current density for another week, with no tritium production. On May 6, the current was increased to 110 mAcm^{-2} for two hours, increased again to 300 mAcm^{-2} for 20 minutes, decreased to 90 mAcm^{-2} for seven days then returned to 50 mAcm^{-2} until June 22. The tritium content of the solution was monitored during this time and the results are shown in Fig. 4, which indicates the production period was about 2 days, and the decay period about 3 days.

4) The Steady State Tritium Values

The steady state concentrations in T producing cells varied between 10^4 and 5 x 10^6 dpm ml^{-1}. These are shown in Table 2. The tritium production rate is 2 x 10^8 - 2 x 10^9 atoms sec^{-1} for the first and second bursts in the experiment, respectively. The maximum rate we observed is about 10^{10} atom sec^{-1}.

TABLE 4a

BLANK EXPERIMENTS DURING TRITIUM ANALYSIS
PERFORMED ON THE 1219 COUNTER

SAMPLE	$cpmml^{-1}$	BACKGROUND CORRECTED ACTIVITY ($dpmml^{-1}$)
D_2O Analysis #1	65	48
D_2O Analysis #2	70	63
D_2O Analysis #3	67	54
D_2O Analysis #4	60	33
D_2O Analysis #5	50	3
D_2O Analysis #6	71	66
D_2O Analysis #7	75	78
D_2O Analysis #8	62	39
0.1M LiOD Analysis #1	75	78
0.1M LiOD Analysis #2	70	63
0.1M LiOD Analysis #3	74	75
0.1M LiOD Analysis #4	65	48
0.1M LiOD Analysis #5	60	33
0.1M LiOD Analysis #6	66	51
0.1M LiOD Analysis #7	76	81
0.1M LiOD Analysis #8	70	63
Neutralized 0.1M LiOD	73	72
Neutralized 0.1M LiOD + 0.1mM NaCN	76	81
Dissolved nickel in acid Analysis #1	78	87
Dissolved nickel in acid Analysis #2	80	93
Dissolved nickel in acid Analysis #3	76	81
Scintillation cocktail	49	--

TABLE 4b
MEAN OF 10 BLANK EXPERIMENTS DURING TRITIUM ANALYSIS
PERFORMED ON THE 1410 COUNTER

SAMPLE	$cpmml^{-1}$	BACKGROUND CORRECTED ACTIVITY ($dpmml^{-1}$)
BIOSAFE II COCKTAIL	170±13	---
H_2O Analysis	161±16	0
D_2O Analysis	210±16	100
0.1M LiOD Analysis	220±20	125
0.1M LiOH Analysis	157±12	0
Dissolved Nickel in Nitric Acid	140±20	0
Tygon Tubing in NaOH	105±20	0
Rubber Stoppers in NaOH	150±20	0
Recombination Catalyst in NaOH	140±15	0
Dissolved Shavings from Cutters	160±11	0
Dissolved Shavings from Vacuum Chamber	164±17	0
Dissolved Shavings from Spotwelder	155±10	0

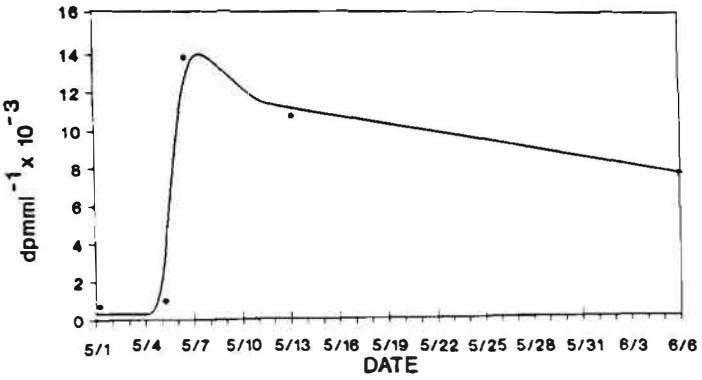

Fig. 4. The production of tritium in the electrolyte of cell A2 as a function of time (ordinate gives date) [4].

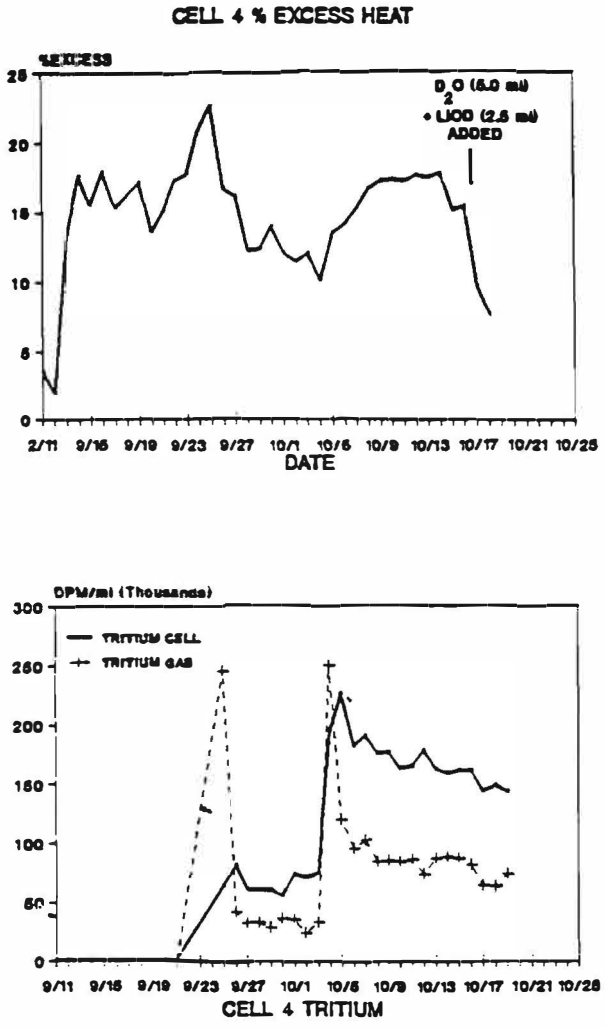

Fig. 5. The heat measurements and tritium activity levels from cell 4 showing a possible correlation between the two.

5) Pre-treatment and Degree of Tritium Production

Details on the pretreatment of the electrodes that produced tritium are given in Table 1.

The cell 4 electrode, the only electrode which has shown excess heat twice and two tritium bursts, was vacuum annealed at 10^{-6} torr at 1200-1300°C for 12 hrs. The excess heat was observed for the first time after about 3.5 months, while the combined tritium and excess heat were observed after about 4.5 months of electrolysis.

Correlation of Tritium Production to Heat

Some relation between heat and tritium production is indicated qualitatetively by the shape of the relation shown in Fig. 5.

Branching Ratio

The tritium production rate is about 10^9 atoms sec^{-1} cm^{-2} from our experiments. Neutron bursts have been observed by Wolf et al. [13], at the level of 1 to 2 sec^{-1} cm^{-2}. Thus, the branching ratio is on the order of 10^9. However, other results [14,15], show that the neutron production rate may be about 10^2 sec^{-1} cm^{-2}. Thus, on his basis, the branching ratio would be ~ 10^7.

FUSION MODELS

In Fig. 6, the take-off time for the growth of promontories occurs at times between 2 and 100 days for assumed impurity concentrations in the range 10^{-7} - 10^{-5} M. It is the time at which rapid increase of dendritic growth begins which fixes the time at which the production of tritium commences. The "Impurity" is likely to be the anode material but a surprising number of metals on the cathode have been observed on electron after prolonged electrolysis [16]. These are the most likely places where high electric fields or high stress fields may develop which make fusion more probable.

Such a hypothesis is consistent with the sporadicity of the effects, and the variety of the nature of the cathode deposits. Large electrodes would tend not to produce tritium. Their surface area getters the solution of impurities before the transition time for rapid dendrite growth has been reached.

The electric field in the double layer at an electrode is usually taken as having an order of magnitude of 10^8 V cm^{-1}.

TABLE 5
DETAILS OF CELLS THAT PRODUCED NO TRITIUM
WITH 1410 LSC (CORRECTED ACTIVITY)

EXPERIMENT	$dpmml^{-1}$
3mm x 3cm Ti Cathode in 0.1M LiOD with internal gas recombination	275
3mm x 3cm Pd Cathode in 0.1M LiOD with internal gas recombination	235
3mm x 3cm Ti Cathode in 0.1M LiOD with internal gas recombination	285
0.5mm x 1cm Pd Cathode in 0.1M LiOD with internal gas recombination	55
4mm x 2mm Pd disc Cathode in 0.1M LiOD with internal gas recombination	365
0.5mm x 1cm Pd Cathode in 0.1M LiOD with external gas recombination (recombined gases measured)	315
1mm x 4cm Pd Cathode in 0.1M LiOD with external gas recombination (recombined gases measured 7/18/89)	75
1mm x 4cm Pd Cathode in 0.1M LiOD with external gas recombination (recombined gases measured 7/21/89)	33
1mm x 4cm Pd Cathode in 0.1M LiOH (H_2O) No gas recombination	0
1mm x 4cm Pd Cathode in 0.1M LiOH (H_2O) No gas recombination	18

TABLE 6. THE RELATIONSHIP BETWEEN REQUIRED ENERGY AND THE FUSION RATE, f

E (eV)	G	$f(i=1A/cm^2)$	$f\Gamma\ (i=1A/cm^2)$
1000	2.63×10^{-14}	1.64×10^{5}	1.64×10^{2}
1500	8.18×10^{-12}	5.11×10^{7}	5.11×10^{4}
2000	2.50×10^{-10}	1.56×10^{9}	1.56×10^{6}
2500	2.59×10^{-9}	1.61×10^{10}	1.61×10^{7}
3000	1.44×10^{-8}	9.00×10^{10}	9.00×10^{7}
3500	5.52×10^{-8}	3.45×10^{11}	3.45×10^{8}
4000	1.62×10^{-7}	1.01×10^{12}	1.01×10^{9}

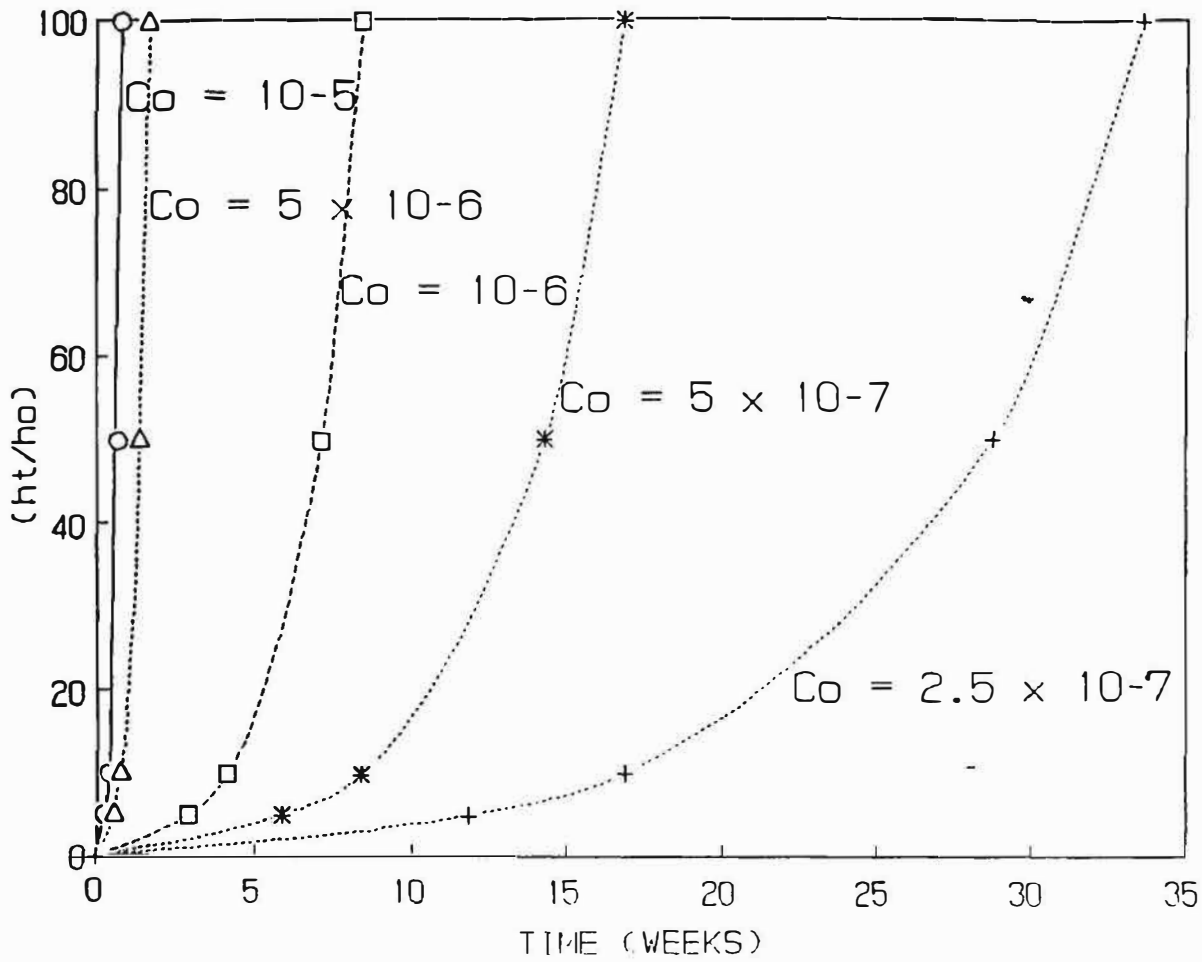

Fig. 6. The growth of promontories on the surface of electrodes as a function of time and impurity concentration.

However, recently Kolb and Franke [17] have concluded that it can be $\sim 10^9$ V cm^{-1} in certain areas. The enhancement is due to surface states on the electrode which concentrate the field lines near these states.

The tips of dendrites are the points at which local dielectric breakdown is likely. It seems reasonable to accept values for the local double-layer field of $> 10^9$ volts cm^{-1}. There is no simple method of calculating the enhancement in field due to the dendrite tip. It will therefore be assumed (somewhat conservatively) that this serves to double the large values of the field deduced by Kolb and Franke [17].

The breakdown of the water dielectric is likely to begin at sharp points (i.e. the dendrite tips) on the electrode surface, and thereafter a D_2 gas layer will be formed at the surface [18] (Fig. 7). When the gas layer grows, a transient large electric voltage drop may be developed onthe dendrite tips. Electron emission will ccur from dendrite tips into the gas, and in the gas layer the breakdown reaction:

$$D_2 + e_o \rightarrow D^+ + D + 2e \qquad (1)$$

seems feasable. Indeed, dark blue sparks have been seen in certain electrolyzing cells.

The D^+ produced will be pulled by the field lines through the gas to the cathode surface on the nearest available surface, the dendrite tip. Such a surface will be likely to retain adsorbed D with which the D^+ would be expected to collide.

The D^+ path length may be of the order of the thickness of the gas layer, c. 100 Å. Hence, the transient voltage drop would be about 2000 ev.

Suppose i is the current density in amps

cm^{-2}, then $N_A i/F$ is the number of D-D collisions on the electrode surface[1] in atoms cm^{-2} sec^{-1}, where F is the charge on one gram ion, in coulombs.

Let it be supposed that a fraction, Γ of the surface is occupied with sharpened tip material. Then, let the probability of tunnelling at such places be P_T, equivalent to:

$$P_T = \exp\{-\pi e_o^2 M^{1/2} / \hbar E^{1/2}\} \quad (2)$$

Therefore, the rate of T formation in atoms sec^{-1} cm^{-2} is given by:

$$\Gamma\ i/F\ P_T \quad (3)$$

In Table 6, this function is tabulated for i = 1 amp cm^{-2} and $\Gamma = 10^{-3}$. It is seen that the calculated fusion rate is about 2 x 10^6 compared with the experimental rate of 10^8 to 10^{10} atoms cm^{-2} sec^{-1}.

Quantitative agreement with the model can be obtained by doubling the field to allow for its concentration at a sharp point. The assumption that Γ might be ~ 10^{-3} is based on the appearance of the electron microscope pictures of Pd electrodes after prolonged electrolysis. It is possible that $\Gamma < 10^{-3}$, reducing the degree of agreement.

On the other hand, quantitative treatments of two factors neglected in this first approach would tend to increase the rate.

(i) The double layer involves electron overlap [19]. The electron cloud existing at the tip of the dendrite acts as a screen and reduces repulsion. Correspondingly, the adsorbed deuteron is shielded by the loss of cationic character. Recently, Kim [20] has shown that electron screening may grately reduce the needed collision energy. Hence, it would be possible to dispense with the reliance on the specially high electric fields arising from the work of Kolb and Franke and use those normally seen by electrochemists, i.e. 10^8 volts cm^{-1}.

(ii) Worledge et al. [9] have suggested that the effective mass of the deuteron is less than the rest mass in a force-free field. On this basis, the needed E in Gamow expression declines in proportion to the reduction of M_D. At M_D = 0.01, 4 x 10^7 volts cm^{-1} would give agreement with experiment and this is generally available in the electrical double layer at electrodes without the enhancement arising from low radius dendritic tips.

In the plasma nuclear fusion, two deuterons collide with a random orientation, the two product channels, helium and neutrons or tritium and hydrogen, have almost the same probobility. However, at the electrode, the deuteron, during its acceleration across the thin gas layer, will be subject to a vectorial force which will cause it to orient preferentially. One of the two branches will then be favored.

The deuteron is known to be a loosely bound entity, the wave function of which may effectively extend to 20 fermi. When a deuteron is incident on the surface, it feels a strong negative electric field (~ 2 x 10^9 V cm^{-1}) because of the pure negative excess surface electric charge. The electric field leads to an effective polarization of the deuteron or a p-wave component term in the deuteron's internal wavefunction. However, when this deuteron is close to the classical turning point, it will experience a strong positive electric field (> 10^{12} V cm^{-1}). This field forces the incident deuteron to reverse its orientation in a specific manner. The deuteron would gain the energy in such a fast reversal of the electric field. Then, the angular momentum of the incident deuteron may be excited from the J=0 state to J=2 or even partly to J=4 states. This fast (~ 10^{-17} sec) reversal of orientation may cause an induced porolization and loosen the structure of the deuteron nucleus, which may create a condition favor to Philips-Oppenheimer type stripping reaction - the tunneling neutron transfer reaction D + D → T + P [21]. The reasons for this kind of stripping reaction are (1) the orientation may help the neutron transfer process; (2) the proton transfer reaction has to penetrate an extra Coulomb barrier compared to the neutron transfer process.

The smaller electrodes (1 mm diameter) are much more likely to give tritium than those which are larger, e.g., 4-6 mm diameter. The reason may come from the dendrite growth [5]. For successful

[1]The collisions arise in the Volmer-Heyrovsky mechanism due to D_2O discharging a proton onto an adsorbed D to give D_2.

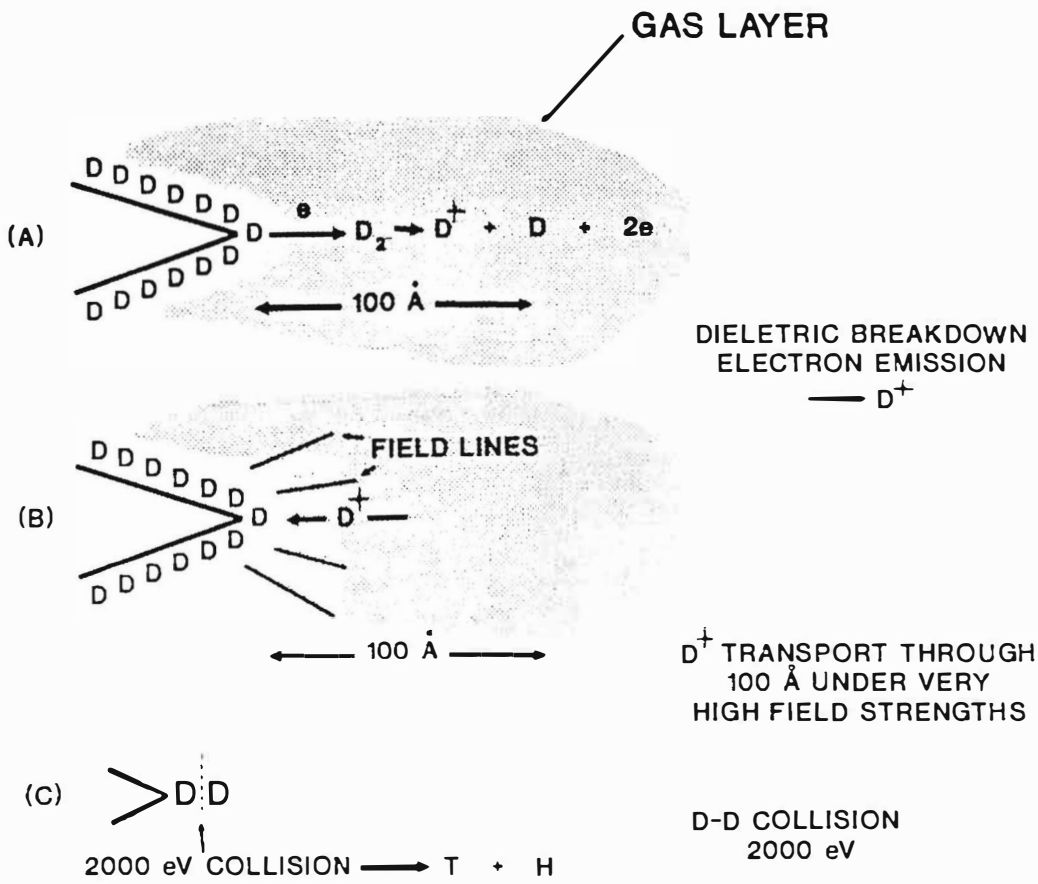

Fig. 7. Dielectric breakdown on a gas covered dendrite tip.

tritium formation,

$$V_{sol}\, V_{met}\, C_o/\delta A > 1 \qquad (4)$$

Hence, the larger A, the greater must be the concentration of depositing ions to attain the condition indicated. Large electrodes will thus be less likely to show the phenomena.

Thus, with V_{sol} ~ 100 ccs, V_{met} = 8.8 ccs/mol, $C_o = 10^{-1}$ moles L^{-1}, $\delta = 10^{-3}$, 5 x 10^{-3} M is sufficient impurity concentration. With r = 0.3 mm, the required impurity concentration is 6 times larger and unreasonably large impurity concentrations for switch on times ~ 100 days are necessary.

Finally, the factors, which would likely increase Fleischmann-Pons effects, are

(1) Pd or alkaline solutions may not be necessary. The metal has to exhibit a Volmer-Heyrovsky path with coupled electrochemical desorption in rate control, because this mechnism of deuterium evolution gives surfaces completely covered with D at high current densities.

(2) Surfaces should be spiky. The tip radii should be minimal [22]. The promontories must grow for a time long enough to penetrate the diffusion layer of the flat electrode.

(3) Surface states should be promoted.

(4) Any method which causes the field in the double layer to fluctuate (e.g. heterodyne beats of superimposed a.c.) would be advantageous.

(5) The working region for D_2 evolution should be as far as possible negative to the electrode p.z.c. of the dendrite forming material.

The most needed information concerns the influence of Li, gas phase tritium production and He. X-ray and γ emission during the rare bursts should be sought.

CONCLUSIONS

(1) The Fleischmann-Pons effects (Heat and Tritium) have been observed in around one quarter of the electrodes used in the cathodic evolution of deuterium after very long times. The success rate improves greatly, ~ up to 70% for T, ~ if the electrode diameter is ~ 1 mm or less.

(2) Tritium reaches 10^4-10^7 disintegration min^{-1} ml^{-1} in the solution. Bursts of T last for c. 5-50 hours.

(3) The tritium increases to steady state concentration in solution over ~ 12 hours.

(4) There is a weak suggestion for some correlation between heat and tritium.

(5) The frequency with which the phenomena are observed falls as the electrode size increases. No effects have been observed when the electrode diameter exceeded 4 mm.

(6) The repeated formation of tritium from deuterium establishes the nuclear nature of the sporadic effects occurring. No non-nuclear explanation for the heat has yet been found [3].

(7) It is difficult to justify a fugacity of D in Pd of > 10^6 ats. Fusion within Pd is therefore unlikely.

(8) D^+ ions are made from D_2O in the double layer during dielectric breakdown which begins near tips of promontories of foreign material growing on the electrode surface. Reasonable numerical agreement with experiment arises if the effective mass of the proton is as small as 0.01 or the electric field at the dendrite tip is ~ 2×10^9 volts cm^{-1}, or some combination of reduced effective mass and enhanced field.

(9) The model explains the long delay times, the sporadicity and the size effects. It may explain the high branching ratio.

ACKNOWLEDGEMENT

We are grateful for financial support from the Electric Power Research Institute (EPRI), the Welch Foundation, and Texas A&M University.

REFERENCES

1. M. Fleischmann, S. Pons and M. Hawkins, J. Electroanal. Chem., 261, 301 (1989); err 263, 187 (1989).
2. S.E. Jones et al., Nature, 338, 737 (1989).
3. R.C. Kainthla, M. Szklarczyk, L. Kaba, G.H. Lin, O. Velev, N.J.C. Packham, J.C. Wass and J.O'M. Bockris, Int. J. Hydrogen Energy 14, 771 (1989).
4. N.J.C. Packham, K.L. Wolf, J.C. Wass, R.C. Kainthla and J.O'M. Bockris, J. Electroanal. Chem., 270, 451 (1989).
5. G.H. Lin, R.C. Kainthla, N.J.C. Packham, O. Velev, and J.O'M. Bockris, Int. J. Hydrogen Energy (in press).
6. F.J. Mayer, Proceedings of the Workshop on Cold Fusion Phenomena, Santa Fe, NM., May 1989.
7. M. Gajda, D. Harley, J. Rafelski and M. Sawicki, Proceedings of the Workshop on Cold Fusion Phenomena, Santa Fe, NM., May 1989.
8. K. Nagamine et al., Proceedings of the DOE Workshop on Cold Fusion Phenomena, Santa Fe, (1989)
9. M. Rabinowitz and D.H. Worledge, Private Communication to G.H. Lin, September, 1989.
10. J.O'M. Bockris, G.H. Lin, and N.J.C. Packham, Fusion Technology (to be published).
11. O. Velev and R.C. Kainthla, submitted to Fusion Technology, March (1990).
12. J.O'M. Bockris, M.A. Genshaw and M. Fullenweider, Electrochimica Acta, 15 (1970) 47.
13. K.L. Wolf, N.J.C. Packham, D. Lawson, J. Shoemaker, F. Cheng and J.C. Wass., Proceedings of the Workshop on Cold Fusion Phenomena, Santa Fe, NM., May 1989.
14. P.K. Iyengar, Fifth International Conference on Emerging Nuclear Energy Systems (ICENES V), Karlsruhe, West Germany, July, 1989.
15. T. Mizuno, Private Communication to J.O'M. Bockris, October 1989.
16. W.A. Adams, E.E. Criddle, G. Jerkiewicz, B. E. Conway, V.S. Donepudi and J. Hebert, Proceedings of the Electrochemical Society Meeting, Hollywood, Florida, October 1989.
17. D.M. Kolb and C. Franke, Submitted to J. Appl. Phys. (1989).
18. M. Szklarczyk, R.C. Kainthla and J.O'M. Bockris, J. Electrochem. Soc., 136 (9), (1989) 2512.
19. W. Schmickler and E. Henderson, J. Phys. Chem., 85, (1986) 1.
20. Y.E. Kim, Proceedings of the First Annual Conference on Cold Fusion, Salt Lake City, UT, March 1990.
21. J.R. Oppenheimer and M. Philips, Phys. Rev., 48, (1935) 520.
22. J.L. Barton and J.O'M. Bockris, Proc. Roy. Soc., A268, (1962) 485.

A STUDY OF ELECTROLYTIC TRITIUM PRODUCTION

Edmund Storms and Carol Talcott
Nuclear Materials Technology, and Material Science and Technology Divisions
Los Alamos National Laboratory, MS C348, Los Alamos, New Mexico 87545

ABSTRACT

Tritium production is being investigated using cathodes made from palladium and its alloys (with Li, C, S, B, and Be) to which are applied various surface treatments. Three anode materials (Pt, Ni and stainless steel), and various impurities in the electrolyte have also been used. Tritium has been produced in about 10% of the cells studied, but there is, as yet, no pattern of behavior that would make the effect predictable.

INTRODUCTION

Since the first studies by Pons and Fleischmann[1], evidence for excess tritium production in electrolytic cells continues to be reported[2; 3; 4; 5; 6; 7; 8; 9]. In a few cases, relatively large increases in tritium content ($x10^{4-5}$)[2; 4] have been observed in electrolytic cells while smaller but significant increases (x1.5-80)[3; 5; 6; 7; 8] have been seen by many others. Electrode materials from many sources have been used as well as cells of various designs including sealed cells with gas recombiners and a high pressure cell[6]. Tritium also has been made (x1300) using D_2 gas in a solid electrolytic cell[10]. Although we can now reasonably assume that the effect is real, no patterns have emerged from these efforts to suggest ways to make the phenomenon reproducible. Apparently, a special environment must first be created on or near the electrode surface before the rather novel nuclear reactions can start. Because this special environment is, as yet, seldom achieved, an exhaustive study of the nuclear products using the necessarily expensive equipment is not cost effective and often frustrating. This study was undertaken to learn how the initiating conditions could be produced in order to improve the reproducibility of the nuclear reactions before attempts are made to study them in detail. Tritium production was used as an indication that a nuclear reaction had occurred.

Over 150 cells were examined involving over 5000 tritium measurements. Only about 10% of the cells produced tritium. Although the success rate is still rather low, a number of conditions can be ruled out as not being important.

EXPERIMENTAL

The cell design shown in Fig. 1 was used for most of this work. The cell consists of a 120 ml, wide mouth glass jar with a bakelite lid. Most cells had a paper lid liner. Gases generated by electrolysis flow through a stainless hypodermic needle sealed in the lid with epoxy and are routed to an IV drip system where the recombination catalyst is located. About 1 ml of

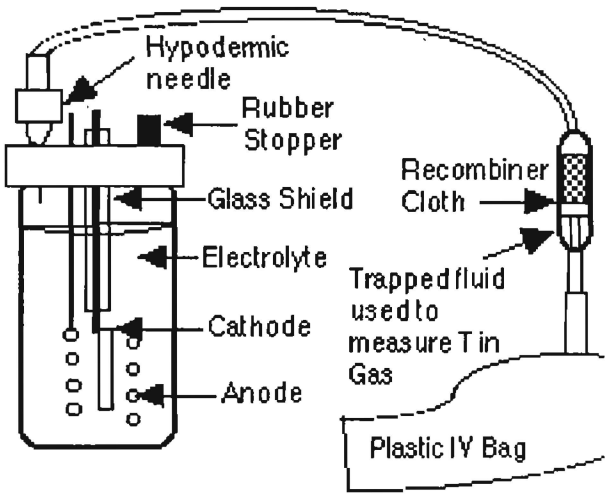

FIGURE 1. Cell with gas collection system

recombined liquid collects in this region before the excess enters a plastic IV bag. A rubber stopper seals a small hole in the lid and allows the electrolyte to be sampled using a 1.00±0.01 ml disposable, automatic pipette. Thus, the cell was completely sealed except for a small time during sampling. Tritium in the cell was determined daily, and a 1 ml sample of recombinate was taken approximately every other day if the electrolysis rate permitted. These samples as well as tritium-free water were each mixed with 10 ml of Opti-Fluor[11] and counted using a Packard Tri-Carb Liquid Scintillation Spectrometer. Measured quantities of D_2O[12] and electrolyte[13] were returned to the cell to replace that lost by electrolysis and sampling, respectively.

Palladium alloys were made by arc-melting Pd powder[14] with the other element in an Ar atmosphere to make the alloys listed in Table I. The X/Pd ratios are indicated for each alloying component.

TABLE I
Pd Alloys Studied as Cathodes

Pd-Li (0.011, 0.012, 0.013, 0.023, 0.051, 0.22)
Pd-C (0.005, 0.012, 0.026, 0.034)
Pd-Li-C (Li 0.038, C 0.019), (Li 0.039, C 0.040) (Li 0.012, C 0.012)
Pd-Be (0.01, 0.04)
Pd-S (0.0043)
Pd-B (0.028)

Most of these cathodes were studied using Pt gauze anodes although nickel wire was used in a few cases. The cathodes were either coin shaped, made by rolling an arc-melted button or were strips cut from a coin using a low speed diamond saw. Several of the Pd-Li alloys were swaged into 1-to 2-mm-diameter rods. In most cases, the surface was cleaned with concentrated HNO_3, water, and acetone.

TABLE II
Surface Treatment

Washed with	Heated in
HNO_3,	Paraffin + H_2S,
HCl,	Paraffin followed by H_2S, or
H_2O_2, or	H_2S alone
Acetone	

Unalloyed Pd was studied sometimes as strips cut from a 0.050" thick sheet, coins, and as wires. These cathodes were given various surface treatments as summarized in Table II. Only one treatment was applied to each strip. The paraffin + H_2S treatment was applied by heating the strip in vapor produced by heating paraffin and sulfur together.

Various materials were added to the electrolyte in order to plate a component onto the cathode surface. Some were present as unintentional impurities. The known impurities are listed in Table III. Not listed are the impurities in the D_2O and the components electrolyzed from the anode, both of which are largely unknown at the present time. The neutrons were obtained from a ^{252}Cf source (≈7200n/min) located near the cells.

Several of the electrodes were examined using an electron microscope and

TABLE III
Materials Present in Electrolyte

Added	Unintentional
Thiourea	Bakelite from lid
Wheat flour	Stainless from hypodermic needle
Fe metal	Glass components
Ag metal	
Hg metal	
Li_2S	
As_2O_3	
Ag_2S	
^{238}U metal	
Neutrons	

an ion probe to determine the surface composition.

RESULTS

The results from the various surface treatments and alloys will be discussed individually starting with the Pd-Li alloys.

Alloys

Pd-Li: The repeated ability of R. Huggins at Stanford University[15] to produce heat using impure Pd containing at least lithium and the observed migration of Li from the electrolyte into the cathode suggests that the presence of Li might be a precondition to a nuclear reaction. Cells were studied using the conditions listed in Table VII located at the end of the paper. No excess tritium was detected in any of the cells. All of the alloys except 22 % Li were ductile and easily rolled into a coin shape and swaged into rods.

Two alloys, Li/Pd = 0.011 (3mm Ø) and Li/Pd=0.034 (2mm Ø) were examined as rods for heat production, by T. Guilinger (Sandia National Laboratory) and by S. Gottesfeld (Los Alamos National Laboratory), respectively. No excess heat was observed in either case.

The presence of lithium was found to increase the ease of deuterium uptake and to increase the limiting D/Pd ratio over that observed using cathodes made with ordinary grade, arc-melted powder. However, there is no difference in properties when a comparison is made to ultrapure, arc-melted powder. Apparently the presence of lithium offsets the effect of impurities that are present in ordinary grade palladium.

Pd-C: Carbon, when present in Pd, resides mainly in the grain boundaries as graphite because of its very low solubility. This impurity would be expected to inhibit the diffusion of D through the grain boundaries thereby reducing the uptake rate, increasing the D concentration gradient near the surface, and reducing the limiting, average composition during the early history. When carbon was arc-melted with Pd powder, the resulting coins showed these effects. None of the cells listed in Table VII produced excess tritium.

Pd-C-Li: When Li was added to an alloy containing carbon, the effects produced by carbon were reduced. Thus, the addition of Li to ordinary grade Pd is thought to improve the D uptake rate because it tends to offset the effect of the usual carbon impurity. These alloys, as listed Table VII, did not produce excess tritium.

Pd-Be: Because beryllium has a relatively weak, neutron rich nucleus, a suggestion was made by Edward Teller that its presence might augment the neutron source provided by the deuterium atom. The two listed compositions were sufficiently ductile to be rolled into a coin shape and cut into strips using a diamond saw. These were used as cathodes in cells described in Table VII. No excess tritium was detected.

Pd-S: Although tritium was produced in some cells when a sulfide treatment was applied to the cathode surface, this Pd-S alloy produced no tritium. However, the sulfur does, in both forms, accelerate recombination of the evolving D_2 with oxygen in the air causing intense self-heating.

Pd-B: Two cathodes containing boron were studied as listed in Table VII. One which was run with As_2O_3 in the electrolyte produced a small amount of tritium. The other cathode did not produce tritium.

Surface Treatment

Heated in H_2S: A number of pure palladi-

um samples were heated in H_2S from a gas cylinder. This treatment causes an insulating sulfide layer to form on Pd. Unless the electrode is run as an anode for awhile, the Pd will not take up deuterium. Samples treated only with H_2S, without paraffin, have not produced excess tritium.

Heated in Paraffin Vapor: Several pure palladium samples, both strips as well as wire, were heated in paraffin or paraffin + H_2S from a cylinder. As can be seen in Table VII, several of these cells produced excess tritium. In this series, the electrolyte dissolved some of the bakelite lid because the lid liner had been removed. Surface examination showed the presence of large amounts of Ca which is a major component of bakelite. This Ca, as well as a lesser amount of Zn, formed a complex surface layer on the electrode. Residual paraffin was also observed as clumps. Electrolytic action was uneven where the paraffin was present.

Control Cells

The amount of tritium produced in most of the cells described in this study is so small that the possibility of contamination must be considered. This is especially important because the work is being done in an area where tritium might be present in the air. Two methods were used to determine the contamination level produced by the environment and by the cell construction materials. In addition, a cell was contaminated on purpose so that the time behavior of such contamination could be studied.

Seven inactive cells listed in Table VII were run during this study using materials from the same lot as were used in the cells that produced tritium (active cells). In addition, many cells of conventional, potentially active design did not produce tritium even though they were being studied at the same time, using the same materials and design as the active cells.

Open jars containing 60 ml of initially tritium-free water were situated in the room so that any tritium in the environment would be detected by observing an increase in their tritium content.

Finally, a little tritiated water was added to an inactive cell in order to see how this known contamination would behave compared to the time history of active cells.

The results from inactive cells are described first.

TABLE IV
Control Cells

	Cathode	Anode	Electrolyte	# Cells
A.	Pd	Ni	H_2O	3
	Pt	Pt	D_2O, Aldrich	1
	Ni	Ni	D_2O, MSD	1
	Ti	Pt	H_2O	1
B.	5 open water jars			
C.	1 cell to which tritium water was added			

(A) Inactive Cells: Three cells (#117, #123 and #132) contained water electrolyte (0.2M LiOH), and construction materials from the lots used in several active cells (#73, #98). Tritium measurements for these cells and for tritium-free water were taken over a 35 day period (23 data points in each set). The average excess tritium in the D_2O cells is 4 count/min-ml greater than tritium-free water (instrument background). Although there may be a slight pickup of tritium from the environment, the amount is well within the uncertainty of ±5 count/min-ml (±14 d/min-ml) found in the tritium measurement for the cells containing D_2O electrolyte. None

of the other control cells shows evidence for contamination beyond this level.

(B) Open Jars: One ml samples were taken from each open jar every working day. During times that a small amount of tritiated-water vapor was present in the air, the tritium content of the jar increased. When the air became tritium-free, the tritium content of the jars decreased. This reduction occurred because ≈4 ml/day evaporated in addition to the loss of 1 ml owing to sampling. This loss was replaced by tritium-free water. The rate of change, corrected for dilution, gives a measure of the tritium content of the air. The quantities present in the room are too small to have biological importance and are too small to affect sealed cells as used in this study. This conclusion will be seen more clearly in the following discussion about individual cells.

(C) Addition of tritiated water: A small amount of tritium water was added to an inactive cell (#82) so that the count rate was increased to a value similar to that found in some active cells. Corrections were made for enrichment during electrolysis and dilution by replacement fluid. The result is shown in Fig. 2 as the fraction excess tritium over that at the beginning of electrolysis. No tritium was produced during the 123 days preceding the addition of tritium water. After the addition, the quantity remained constant, consistent with normal enrichment and dilution. This steady value is in sharp contrast to the behavior of tritium loss from active cells as seen below. After this cell was terminated, the electrolyte was replaced by tritium-free water containing 0.2N LiOH and the current was reversed so that the cathode would lose any absorbed tritium to the water. After electrolyzing in this mode for 24 hrs, no increase in tritium content was seen. Therefore, the tritium which had been added to the electrolyte had not absorbed into the Pd cathode to any significant extent.

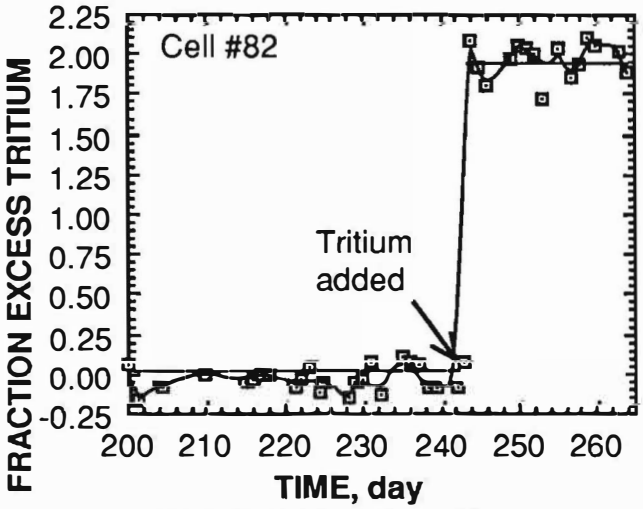

FIGURE 2. Effect of adding tritium water

Statistical Analysis of Data

A series of closed (recombinate run back into the cell) and, unfortunately, inactive cells allowed the total random error in the tritium measurements to be determined. These cells were unsealed such that there was a small hole to allow excess gas to escape after passing by the recombinate cloth. No enrichment or pickup of tritium was observed. Thus, the recombiner worked properly and no tritium entered from the environment in spite of the hole. The standard deviation based on 446 measurements using 13 cells over a 40 day period is listed in Table V as (A).

A similar analysis of a sealed cell was made, but where the recombinate was collected separately. The value is based on 80 data points, after correction for enrichment, and is listed as (B). When an enrichment correction was not made, the standard deviation, designated (C) was larger because of the slow increase in count rate over the life of the cell. This study shows that the total random error in the tritium measurement is ±14 decom-

TABLE V
Summary of Count Rate and Standard Deviation for Various Inactive Cells

	Data Set	Average d/min-ml	SD	#Values
A	Closed Cells	138	±14	446
B	Open Cell, corrected	120	±14	80
C	Open Cell, uncorrected	140	±31	96

position/min-ml (±5.3 count/min-ml) with an occasional outlier near ±25 d/min-ml. Because of such outliers, unusually high or low values are ignored if they are isolated from the trend of the data. In other words, only patterns supported by many points are used as evidence for tritium production. In addition, data are considered significant only if greater than 5 sigma from the behavior produced by enrichment and dilution.

Distribution Ratio

During electrolysis, the tritium concentration in the gas is generally less than that in the liquid. This difference causes enrichment of tritium in the liquid. In order to calculate the amount of tritium that is lost to the gas phase, thereby allowing tritium enrichment to be calculated, the distribution ratio (tritium in the gas/tritium in the liquid) must be determined. This quantity was measured directly for a number of active and inactive cells as listed in Table VI. In addition, this quantity was calculated by an indirect approach using the rate at which tritium was enriched in an inactive cell #70 (slope in Table VI). Values as high as 1.1 have been observed in the past (averaged over the life of the cell) although recent cells (>#91) have a mean of 0.55±0.02 based on 13 cells.

Behavior of Active Cells

A total of 13 cells have shown some evidence for tritium production as of 3/8/90, as listed in Table VII. However, only the more recent observations have been made with sufficient detail to eliminate any doubt about the source of tritium. The time history of various cells is summarized in Fig. 3. The square points indicate the time at which the cell was started, and the corresponding + indicates when the cell was stopped. A few of these point-pairs are connected in the figure to show how the connection should be made. Tritium was produced in some cells during the interval between each set of vertical lines. A

TABLE VI
Measured Distribution Ratio and Standard Deviation

Cell #	Gas/Liquid	SD	#Values
70 (ratio)	0.91	0.16	15
70 (slope)	0.84		
74	1.12	0.17	13
73*	0.83	0.12	9
82(before)	0.69	0.09	4
82(after)	0.44	0.06	3
85	0.53	0.05	10
86	0.52	0.08	8
87	0.76	0.15	21
91	0.53	0.04	7
98*	0.53	0.04	8
110	0.58	0.02	5
118	0.58	0.05	10
119	0.59	0.09	10
120	0.54	0.06	11
121	0.55	0.04	13
124	0.57	0.07	11
127	0.53	0.08	11
128	0.57	0.05	9
129	0.55	0.08	9
130	0.53	0.06	9
131	0.52	0.06	10

Values before and after addition of tritium to cell #82 are shown,
* Active cells

box is drawn around the cells that were active during this time. The number of active cells and the total running at the time are also indicated. For example, between 100 and 125 days after 6/1/89, seven cells out of a total of 34 produced tritium. These active cells continued to run after day 125 without producing tritium until they were turned off on day 180. Eleven cells were started during the time when tritium was being produced in these seven cells but none became active. Presence of low level tritium in the room air, as detected by the open water jars, is shown by the boxes at the bottom of the figure. Some tritium could have been in the air before day 125 but no open jars were present to detect its presence. Although some tritium was present in the air when excess tritium appeared in some cells, other cells showed no tritium production. In addition, all of the active cells eventually stopped production even though a small amount of tritium continued to be present in the air.

Two active (#73 and #98) and two inactive (#70 and #99) cells are compared in Fig. 4 where the fraction excess is plotted as a function of time from the start of electrolysis. The fraction excess is calculated as described previously[9]. In brief, the amount of tritium lost to the gas phase is calculated from the electrolysis rate and the measured distribution ratio. The small amount of tritium in D_2O that is added to the cell each day to replace fluid loss is also taken into account. The expected inventory of tritium in the cell is calculated and compared to the actual amount. The fraction excess is the difference between these values divided by the initial amount. For example, a calculated excess fraction of 1.0 means that the tritium content has doubled over that in the cell when electrolysis started, taking into account tri-

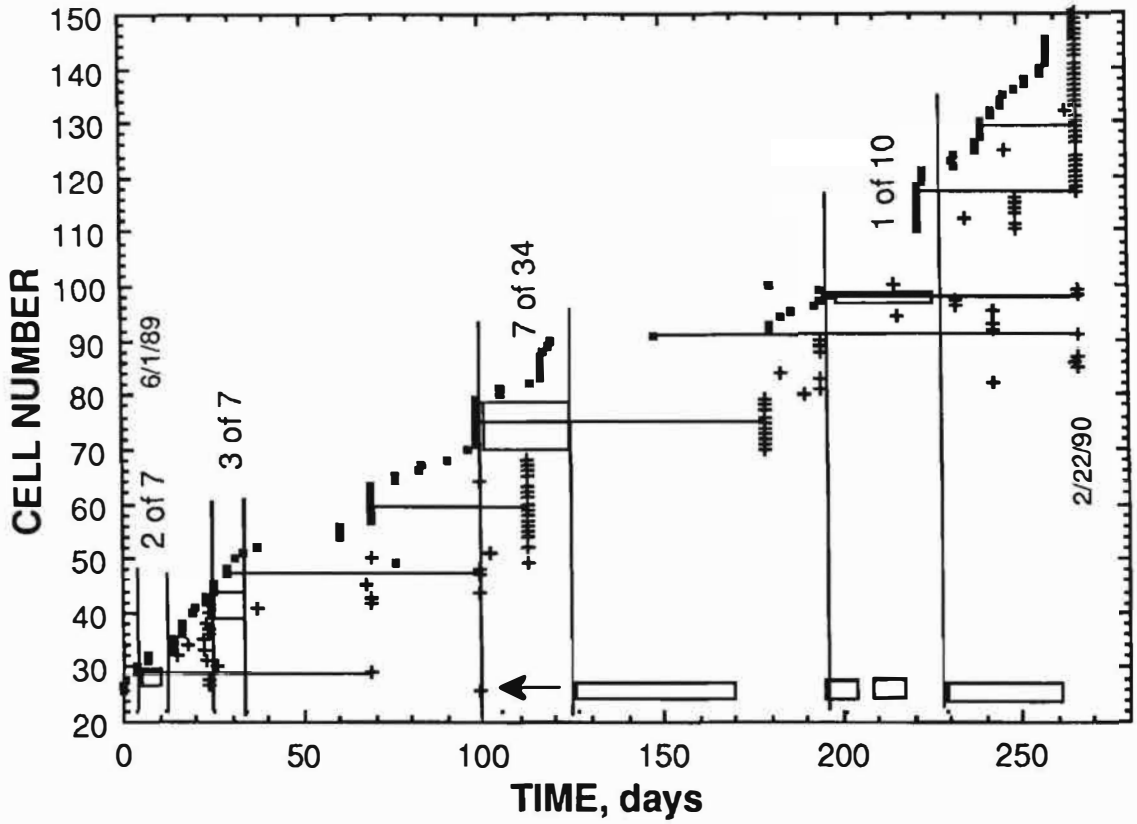

FIGURE 3. Time history of cells

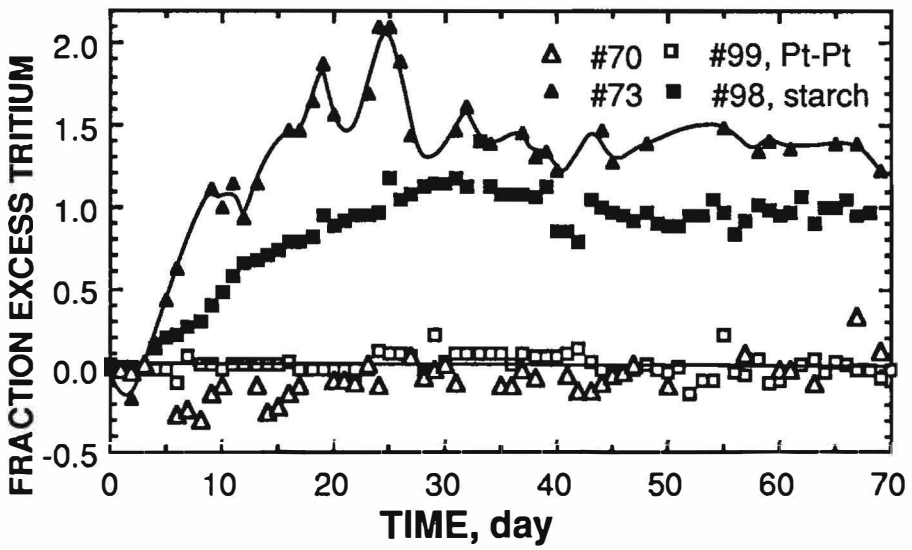

FIGURE 4. Fraction excess tritium calculated for cells #70, #73, #98 and #99.

tium from all known sources. Because the calculated excess does not take into account the small amount of tritium that is in the electrode, the plotted values are lower limits.

The amount of fluid added to the cells on a daily basis was recorded and compared to the amount lost, calculated using the cell current. Except when a cell occasionally started to leak fluid, the amount added agreed with the amount calculated. Of the two active cells compared in Fig. 4, only cell #98 started to leak after 40 hr. Because this leak occurred after tritium production had stopped, it could not have been the cause of excess tritium.

Cells #70 and #73 were electrolyzed at the same time and at the same current. The cathode in cell #73 had been heated in paraffin vapor before being electrolyzed. Other factors in the cell design are listed in Table VII. This cell produced tritium over a 25 day period with evidence for two bursts. After the last burst, the tritium content decreased to a constant value over a 10 day period. This decrease is thought to be caused by the removal of tritium that is present as DT gas dissolved in the liquid. The tritium that remained was present as DTO. This initial decrease is in contrast to the stable tritium content that results when tritiated water is placed in a cell as seen in Fig. 2.

Cells #98 and #99 were electrolyzed at the same time but not at the same current. The cathode in cell #98 was not pretreated although 3.4 mg of wheat flour was placed in the electrolyte. Such large molecules are thought to inhibit the growth of surface dendrites. Indeed, the tritium production rate was decreased, production lasted for a longer time, and there were no bursts. However, attempts to duplicate this effect using other cells containing various amounts of wheat flour have failed.

CONCLUSION

We have produced tritium in electrolytic cells containing a Pd cathode, a Ni or Pt anode, and an electrolyte containing 0.1M or 0.2M LiOD. However, we can not yet suggest a design that will have a high probability of success.

A high, bulk deuterium content in Pd does not appear to be essential because tritium has been produced by electrodes having an average D/Pd ratio between 0.55 and 0.80. However, local concentrations might be higher.

Most active cells, but not all, have produced tritium using MSD[12] heavy water in contrast to that obtained from Aldrich[16]. In addition, the Aldrich water has a larger variation of tritium con-

tent between bottles than does the MSD. This suggests that other, important impurities might have a similar variation.

The presence of Li, Be, C, or S alloyed with Pd does not increase the probability of tritium production at the concentrations studied in this work. A surface layer of only palladium sulfide does not help either. A small concentration of ^{238}U, Hg, Fe, thiourea, Li_2S, or Ag_2S in the electrolyte does not increase the rate of success. However, sulfur in the lattice or on the surface increases the rate at which evolved D_2 reacts with O_2 in the air.

The effect of (1) paraffin alone or paraffin plus sulfide on the surface, (2) wheat flour or As_2O_3 in the electrolyte, or (3) a Pd-B alloy is uncertain, although the chance of tritium production seems to be improved by these conditions.

Distribution ratios for tritium (gas/liquid) have been measured with values between 1.1 and 0.52, the most probable value being 0.55.

ACKNOWLEDGEMENTS

The authors wish to thank M.A. David (MST-3) for help in making many of the tritium measurements and R. Sherman (MST-3) for early discussions. We are grateful for financial support provided by the Department of Energy, Division of Basic Energy Sciences and continued support given by MST and NMT Divisions, and the weapons program.

References

[1] M. Fleischmann and S. Pons, "Electrochemically Induced Nuclear Fusion of Deuterium", J. Electroanal. Chem. **261** (1989) 301 and errata **263** (1989) 187.

[2] N. J. C. Packham, K. L. Wolf, J. C. Wass, R. C. Kainthla and J. O'M. Bockris, "Production of Tritium from D_2O Electrolysis at a Palladium Cathode", J. Electroanal. Chem. **270** (1989) 451.

[3] C. Sanchez, J. Sevilla, B. Escarpiz, F. J. Fernandez and J. Canizares, Solid State. Comm. **71**, #12, (1989) 1039.

[4] P. K. Iyengar, "Cold Fusion Results in BARC Experiments", Proc. of Fifth International Conference on Emerging Nuclear Energy Systems, Karlsruhe, Federal Republic of Germany, July 3-6, 1989. See also BARC-1500 Dec. 1989, Government of India, Atomic Energy Commission and this Proceeding.

[5] C. D. Scott, J. E. Mrochek, E. Newman, T. C. Scott, G. E. Michaels and M. Petek, "A Preliminary Investigation of Cold Fusion by Electrolsis of Heavy Water", Oak Ridge National Laboratory, ORNL/TM-11322 (1989).

[6] C. H. McKubre, S. I. Smedley, F. L. Tanzella and R. D. Weaver, "Calorimetric and Kinetic Observation of D_2-Pressurized LiOD/D_2O/Pd Cells", Presented at Electrochemical Soc. Meeting, Hollywood, Florida, Oct. 19-20, 1989.

[7] R. Alqasmi and H. -J. Scaller, "Neutrons and Tritium from Cold Fusion in Pd-D", Presented at Electrochemical Soc. Meeting, Hollywood, Florida, Oct. 19-20, 1989.

[8] R. Adzic, D. Gervasio, I. Bae, B. Cahn and E. Yeager, "Investigation of Phenomena Related to D_2O Electrolysis at a Palladium Cathode", Presented at Electrochemical Soc. Meeting, Hollywood, Florida, Oct. 19-20, 1989.

[9] E. Storms and C. Talcott, "Electrolytic Tritium Production", accepted by Fusion Technology (1990).

[10] T.N. Claytor, P.A. Seeger, R.K. Rohwer, D.G. Tuggle, W.R. Doty, "Tritium and Neutron Measurement of a Solid State Cell", NSF/EPRI Workshop on Anomalous Effects in Deuterated Materials, Washingon, DC. Oct 16-18 (1989).

[11] Opti-Fluor was obtained from Packard Instrument Company, 2200 Warrenville Rd, Downers Grove, IL 60515. This fluid shows no chemiluminescence after 20 min when mixed 10 to 1with 0.2 N LiOD.

[12] Obtained from MSD Isotopes, Montreal, Canada (>99.9 % D).

[13] Made by mixing Li metal with the D_2O to give a 0.1M or 0.2 M solution.

[14] Obtained from Johnson-Matthey Company as 100 % Pd, batch #V7114307 and #V8368501.

[15] A. Belzer, U. Bischler, S. Crouch-Baker, T. M. Gur, M. Schrieber, and R. Huggins "Two Fast Mixed Conductor Systems-Deuterium and Hydrogen in Palladium", Cold Fusion Workshop, Santa Fe, NM May 22-25 (1989).

[16] Obtained from Aldrich Chemical Company, (99.9 % D).

TABLE VII
Description of Cell Treatment

#	Form	wt. (g)	area (cm2)	Alloy	Cleaning	Pre-Treatment	Electrolyte	Kind	Anode	Container	lead covering	Max. D/Pd	Date Started	T
	A			B	C	D	E	F	G	H	I	J	K	L
Pd+Li Alloys														
33	coin	4.87	4.7	Li/Pd(1)=0.051	std	none	0.5N,thio	MSD	Pt	plastic(2)	none	0.77	6/15	n
34	coin	4.96	4.2	Li/Pd(1)=0.023	std	none	0.5N,thio	MSD	Pt	plastic(2)	none	0.83	6/15	n
35	coin	4.99	4.7	Li/Pd(1)=0.012	std	none	0.5N,thio	MSD	Pt	plastic(2)	none	0.77	6/15	n
49	wire	0.74	1.5	Li/Pd(2)=0.0343	HNO3	none	0.2N	MSD	Pt, small	plastic(3)	glass		8/15	n
55	coin	3.67	4.2	Li/Pd(4)=0.025	std	none	0.2N	MSD,pe	Pt	plastic(4)	glass	0.73	7/31	n
69	coin*	10.26	7.9	Li/Pd(1)=0.013	std	none	0.2N	MSD	Pt	quartz	glass		9/5	n
88	button	4.05	2.0	Li/Pd(1)=0.22	none	none	0.1N	MSD,Ald.	Pt	glass(5)	glass		9/25	n
111	strip	1.26	2.3	Li/Pd=0.012	HCl	pol.,annealed	0.1N	Aldrich	Ni(2)	glass(5)	glass	0.79	1/9	n
113	strip	0.82	1.7	Li/Pd=0.012	HCl	polished	0.1N	Aldrich	Ni(2)	glass(5)	glass	0.76	1/9	n
Pd + C Alloys														
2	coin	6.00		C/Pd(1)=0.0344	std	none	0.2N	MSD	Pt	plastic(3)	torr seal		7/2	n
52	coin	5.46	5.4	C/Pd(1)=0.026	Na2S	oxidized	0.2N	MSD	Pt	plastic(3)	1.yes, 2.no	0.88	7/8	n
56	coin	3.52	3.7	C/Pd(1)=0.0191	Li2S	oxidized	0.2N	MSD	Pt	plastic(4)	glass	0.66	7/31	n
65	coin	4.10	4.0	C/Pd=0.005	std	none	0.2N	MSD	Pt	plastic(4)	glass	0.77	8/15	n
110	strip	0.92	1.8	C/Pd=0.012	HCl	polished	0.1N	Aldrich	Ni(2)	glass(5)	glass	0.73	1/9	n
116	strip	0.83	1.8	C/Pd=0.012	HCl	pol.,annealed	0.1N	Aldrich	Ni(2)	glass(5)	glass	0.75	1/9	n
Pd + Li + C Alloys														
89	coin	4.90	3.0	Li/Pd(5)=0.038 C/Pd=0.019	H2O2	none	0.1N	MSD,Ald.	Pt	glass(5)	glass	0.70	9/27	n
90	coin	4.65	3.0	Li/Pd(5)=0.039 C/Pd=0.040	none	none	0.002N	MSD,Ald.	Pt	glass(5)	glass	0.53	9/28	n
114	strip	0.97	2.0	Li,C/Pd=0.012	HCl	polished	0.1N	Aldrich	Ni(2)	glass(5)	glass	0.76	1/9	n
115	strip	0.80	1.7	C,Li/Pd=0.012	HCl	pol.,annealed	0.1N	Aldrich	Ni(2)	glass(5)	glass	0.71	1/9	n
Pd-B Alloy														
43	coin	4.69		Pd(1)+B	std	none	0.2N,As2O3	MSD	Pt	plastic(3)	torr seal		6/24	y
118	strip	1.41	2.7	B/Pd=0.028	HCl	none	0.1N	Aldrich	Ni(3)	glass(5)	glass		1/9	n
Pd + S Alloy														
42	coin	4.47		S/Pd(1)=0.0043	std	none	0.2N	MSD,pe	Pt	plastic(3)	torr seal		6/24	n

TABLE VII (Continued)
Description of Cell Treatment

#	Form	wt. (g)	area (cm2)	Alloy	Cleaning	Pre-Treatment	Electrolyte	Kind	Anode	Container	lead covering	Max. D/Pd	Date Started	T
Pd + Be Alloys														
92	strip	1.63	3.0	Be/Pd(2)=0.01	none	none	0.1N	Aldrich	Ni(1)	glass(5)	glass	0.75	11/28	n
93	strip	1.66	2.9	Be/Pd(2)=0.04	none	none	0.1N	Aldrich	Ni(1)	glass(5)	glass	0.71	11/28	n
PURE Pd														
68	coin	2.09	2.6	ultra pure	std	none	0.2N	MSD	Pt	plastic(4)	glass	0.79	8/30	n
32	coin	5.10		Pd(1)	std	none	0.2N,thio	MSD	Pt	plastic(2)	torr seal		6/8	n
137	coin	6.21		Pd(3), W sw	sanded,HNO3	vac	0.1N	Aldrich	Pt, Ni(4)	plastic(2a)	glass		2/8	
138	coin	7.48		Pd(3), W sw	sanded,HNO3	anneal	0.1N	Aldrich	Pt, Ni(4)	plastic(2a)	glass		2/8	
54	coin	4.08	4.3	Pd(4)	std	none	0.2N	MSD,pe	Pt	plastic(4)	glass	0.77	7/31	n
50	coin	5.26		Pd(2)(am)	std	none	0.2N	MSD	Pt	plastic(3)	torr seal		7/2	n
51	coin	5.89	5.3	Pd(2)(am)	std	anneal	0.2N	MSD	Pt	plastic(3)	torr seal	0.80	7/4	n
58	sheet	1.79	2.5	Pd(2)	HNO3	none	0.2N,thio	MSD	Pt	plastic(4)	glass	0.83	8/9	n
59	sheet	2.44	3.5	Pd(2)	HNO3	none	0.2N,thio	MSD	Ni gauze	plastic(4)	glass	0.71	8/9	n
66	strip	1.71	1.5	Pd(2)	HNO3	none	0.2N	MSD	Ni(1)	plastic(4)	glass		8/22	n
104	strip	0.59		Pd(2)	HNO3	anneal	0.1N	Aldrich	Pt	glass(5a)	none		12/12	n
106	strip	1.11		Pd(2)	HNO3	none	0.1N	Aldrich	Pt	glass(5a)	none		12/12	n
107	strip	1.16		Pd(2)	HNO3	none	0.1N	Aldrich	Pt	glass(5a)	none		12/12	n
108	strip	0.93		Pd(2)	HNO3	none	0.1N	Aldrich	Pt	glass(5a)	none		12/12	n
109	strip	0.77		Pd(2)	HNO3	none	0.1N	Aldrich	Pt	glass(5a)	none		12/12	n
121	strip	0.68	1.5	Pd(2),sw Ni(4)	HCl	none	0.1N	Aldrich	Ni(2)	glass(5)	glass		1/10	n
127	strip	0.82	1.6	Pd(2),sw Ni(4)	HNO3	reverse	0.1N LiOD	Aldrich	Ni(4)	glass(5b)	glass		1/26	n
139	strip	1.06	2.0	Pd(2),sw Ni(4)	none	none	0.1N	Aldrich	Pt, Ni(4)	paraffin	glass		2/12	
140	strip	1.02	2.0	Pd(2),sw Ni(4)	HNO3	none	0.1N	Aldrich	Pt, Ni(4)	paraffin	glass		2/12	
41	wire	1.90	7.6	Pd, Marshall	HNO3	none	0.2N,thio	MSD	Pt	plastic(3)	torr seal	0.86	6/21	y
82	wire	1.66		Pd,Marshall	std	none	0.05N	MSD,Ald.	Ni(1)	glass(5)	glass		9/25	n
70	wire		2.0	Pd, Martin	HNO3	none	0.1N	MSD	Ni(1)	glass(5)	glass		9/5	n
79	wire	0.37	2.0	Pd,Martin	HNO3	none	0.2N,Ag	MSD	Ni(1),Ag	glass(5)	glass	0.94	9/7	y
80	bar	8.45	9.4	Pd investment	none	none	0.2N	MSD	Pt	glass(5)	glass		9/14	n
81	bar	7.44	8.4	Pd investment	none	none	0.2N	MSD	Pt	glass(5)	glass	0.74	9/14	n
Paraffin														
73	strip	0.68	1.0	Pd(2)	C	paraffin	0.2N	MSD	Ni(1)	glass(5)	glass	0.81	9/7	y
74	strip	0.69	1.5	Pd(2)	C	paraffin	0.2N	MSD	Ni(1)+S	glass(5)	glass	0.78	9/7	n
83	strip			Pd(2)	HNO3	paraffin	0.2N	MSD	Ni(1)	glass(5)	glass		9/25	n
84	strip	0.54	1.6	Pd(2)	HNO3	paraffin	0.1N	MSD	Ni(1)	glass(5)	glass	0.76	9/25	n

TABLE VII (Continued)
Description of Cell Treatment

#	Form	wt. (g)	area (cm2)	Alloy	Cleaning	Pre-Treatment	Electrolyte	Kind	Anode	Container	lead covering	Max. D/Pd	Date Started	T
Paraffin (Continue)														
85	strip	0.64		Pd(2)	HNO3	paraffin	0.1N	MSD,Ald.	Ni(1)	glass(5)	glass		9/25	n
86	strip	0.42		Pd(2)	HNO3	paraffin	0.1N	MSD,Ald.	Pt	glass(5)	glass		9/25	n
87	strip	0.47		Pd(2)	HNO3	paraffin	0.1N	MSD,Ald.	Pt	glass(5)	glass		9/25	n
91	sheet			Pd(2)	HNO3	paraffin	0.2N	MSD,Ald.	Ni(1)	glass(5)	glass		10/27	n
100	strip	1.13		Pd(2)	HNO3	paraffin	0.1N	Aldrich	Ni(1)	glass(5a)	none		11/28	n
101	strip	0.97		Pd(2)	HNO3	paraffin	0.1N	Aldrich	Ni(1)	glass(5a)	none		11/29	n
102	strip	0.69		Pd(2)	HNO3	paraffin	0.1N	Aldrich	Ni(1)	glass(5a)	none		11/28	n
105	strip	0.87		Pd(2)	HNO3	paraffin	0.1N	Aldrich	Pt	glass(5a)	none		12/12	n
Paraffin+H2S														
40	coin	6.97		Pd(1)	S	H2S+C	0.2N	MSD	Pt	plastic(3)	no	0.84	6/20	n
44	coin	4.93	4.6	Pd(1)	S	H2S+C	0.2N	MSD	Pt	plastic(3)	torr seal	0.75	6/26	n
45	coin	5.53		Pd(2)	S	H2S+C	0.2N	MSD	Pt	plastic(3)	torr seal	0.67	6/26	n
46	coin	5.15		Pd(1)	S	H2S+C	0.2N	MSD	Pt	plastic(3)	torr seal		6/27	n
71	strip	0.73	2.5	Pd(2)	C-S	paraffin, H2S	0.2N	MSD	Pt small	glass(5)	glass	0.55	9/7	y
72	strip	0.73	2.1	Pd(2)	C-S	paraffin, H2S	0.2N	MSD	Pt small	glass(5)	glass	0.81	9/7	y
75	strip	0.50	1.4	Pd(2)	C-S	paraffin, H2S	0.2N	MSD	Pt small	glass(5)	glass	0.71	9/7	y
77	strip	0.72	1.4	Pd(2)	C-S	paraffin, H2S	0.2N	MSD	Pt small	glass(5)	glass	0.69	9/7	y
H2S														
62	sheet	2.61	3.5	Pd(2)	S	H2S	0.2N	MSD	Pt	plastic(4)	glass	0.56	8/9	n
63	sheet	2.56	3.5	Pd(2)	S	H2S	0.2N	MSD,pe	Pt	plastic(4)	glass	0.67	8/9	n
64	sheet	2.27	3.4	Pd(2)	S	H2S	0.2N	MSD	Pt	plastic(4)	glass	0.69	8/15	n
Wheat Flour														
98	strip	0.79	1.8	Pd(2), sw stainless	HNO3	none	0.1N, 3.5mg	Aldrich	Ni(2)	glass(5)	glass	0.93	12/15	y
120	strip	0.86	1.7	Pd(2), sw Ni(4)	HCl	none	0.1N, 15mg	Aldrich	Ni(2)	glass(5)	glass		1/10	n
122	strip	0.68	1.6	Pd(2), sw Ni(4)	HNO3	none	0.1N, 5.4 mg	Aldrich	Ni(1)	glass(5)	glass		1/19	n
124	strip	0.96	1.8	Pd(2), sw Ni(4)	HNO3	none	0.1N, 4.0 mg	Aldrich	Ni(3)	glass(5)	glass		1/19	n
125	strip	0.75	1.6	Pd(2), sw Ni(4)	HNO3	reverse	0.1N, 5.2mg	Aldrich	Ni(3)	glass(5)	glass		1/25	n
126	strip	0.83	1.7	Pd(2), sw Ni(4)	HNO3	reverse	0.1N, 4.7mg	Aldrich	Ni(3)	glass(5)	glass		1/25	n
128	strip	0.79	1.6	Pd(2), sw Ni(4)	HNO3	reverse	0.1N,15mg	Aldrich	Ni(4)	glass(5b)	glass		1/26	n
129	strip	0.61	1.4	Pd(2), sw Ni(4)	HNO3	reverse	0.1N, 7.2mg	Aldrich	Ni(4)	glass(5b)	glass		1/26	n
130	strip	0.92	1.8	Pd(2), sw Ni(4)	HNO3	reverse	0.1N, 4.2mg	Aldrich	Ni(4)	glass(5b)	glass		1/26	n

TABLE VII (Continued)
Description of Cell Treatment

#	Form	wt. (g)	area (cm2)	Alloy	Cleaning	Pre-Treatment	Electrolyte	Kind	Anode	Container	lead covering	Max. D/Pd	Date Started	T
Thiourea														
26	coin	3.63	3.7	Li/Pd(1)=0.047	std	none	0.2N	MSD	Pt	plastic(2)	torr seal	0.82	6/1	n
28	coin	4.88	3.0	Rh/Pd=0.1	std	none	0.2N	MSD	Pt	plastic(2)	torr seal		6/2	n
29	coin	3.63	3.7	Pd(1)	S	H2S+C	0.2N	MSD	Pt	plastic(2)	torr seal	0.72	6/5	y
31	coin	4.93	4.7	Pd(1)+Rh+Li	std	none	0.2N	MSD	Pt	plastic(2)	torr seal	0.88	6/8	n
32	coin	5.10		Pd(1)	std	none	0.2N	MSD	Pt	plastic(2)	torr seal		6/8	n
33	coin	4.87	4.7	Li/Pd(1)=0.051	std	none	0.5N	MSD	Pt	plastic(2)	no	0.77	6/15	n
34	coin	4.96	4.2	Li/Pd(1)=0.023	std	none	0.5N	MSD	Pt	plastic(2)	no	0.83	6/15	n
35	coin	4.99	4.7	Li/Pd(1)=0.012	std	none	0.5N	MSD	Pt	plastic(2)	no	0.77	6/15	n
36	coin	5.86		Rh/Pd=0.1	std	none	0.5N	MSD	Pt	plastic(2)	no	0.86	6/17	n
37	coin	5.35	4.8	Rh/Pd=0.1	std	none	0.3N	MSD	Pt	plastic(2)	no	0.90	6/17	n
38	coin	5.13	4.7	Rh/Pd=0.1	std	none	0.2N	MSD	Pt	plastic(2)	no	0.85	6/17	n
41	wire	1.90	7.6	Pd, Marshall	HNO3	none	0.2N	MSD	Pt	plastic(3)	torr seal	0.86	6/21	y
58	sheet	1.79	2.5	Pd(2)	HNO3	none	0.2N	MSD	Pt	plastic(4)	glass	0.83	8/9	n
59	sheet	2.44	3.5	Pd(2)	HNO3	none	0.2N	MSD	Ni gauze	plastic(4)	glass	0.71	8/9	n
Uranium														
57	strip	0.46	1.1	Pd(2)	HNO3	none	0.2N	MSD	Pt, small	plastic(4)	glass		8/9	n
Iron														
61	sheet	2.08	2.9	Pd(2)	HNO3	none	0.2N	MSD	Pt	plastic(4)	glass	0.80	8/9	n
Sliver														
79	wire	0.37	2.0	Pd,Martin	HNO3	none	0.2N	MSD	Ni(1),Ag	glass(5)	glass	0.94	9/7	y
Mercury														
95	strip	1.19	2.3	Pd(3)	HNO3	none	0.1N	Aldrich	Ni(1)	glass(5)	glass	0.88	12/4	n
LI2S														
60	sheet	1.98	2.8	Pd(2)	HNO3	none	Li2S+alcohol	MSD	Ni gauze	plastic(4)	glass	0.71	8/9	n
As2O3														
43	coin	4.69		Pd(1)+B	std	none	0.2N,As2O3	MSD	Pt	plastic(3)	torr seal		6/24	y
131	strip	1.05	2.0	Pd(2), sw Ni(4)	HNO3	reverse	0.127g As2O3	Aldrich	Ni(4)	glass(5b)	glass		1/29	n
Ag2S														
135	strip	0.86		Pd(2), sw Ni(4)	HNO3	none	0.1N	Aldrich	Pt, Ni(4)	glass(5)	glass		2/2	n

TABLE VII (Continued)
Description of Cell Treatment

#	Form	wt. (g)	area (cm2)	Alloy	Cleaning	Pre-Treatment	Electrolyte	Kind	Anode	Container	lead covering	Max. D/Pd	Date Started	T
CONTROL CELLS														
Water electrolyte														
117	strip	0.98		Pd(2)	HCl	none	0.2NLiOH	H2O	Ni(3)	glass(5)	glass		1/9	n
123	strip	0.85	1.7	Pd(2), sw Ni(4)	HNO3	none	0.2N LiOH	H2O	Ni(1)	glass(5)	glass		1/18	n
132	strip	0.90	1.8	Pd(2), sw Ni(4)	HNO3	reverse	0.1N LiOH	H2O	Ni(4)	glass(5b)	glass		1/29	n
144	strip	0.44	4.2	Ti(1), sw Ni(4)	HNO3	none	0.1N LiOH	H2O	Pt, Ni(4)	glass(5)	glass		2/14	n
Pt Cathode														
99	wire			Pt	HNO3	none	0.1N	Aldrich	Pt	glass(5)	glass		12/12	n
Ni Cathode														
27	coin	6.97	6.4	Ni	std	none	0.2N	MSD	Pt	plastic(2)	torr seal	0.09	6/1	n
TRITIUM PRODUCING CELLS														
29	coin	3.63	3.7	Pd(1)	S	H2S+C	0.2N,thio	MSD	Pt	plastic(2)	torr seal	0.72	6/5	y
30	coin	5.40		Pd(1)	S	H2S+C	0.2N	MSD	Pt	plastic(2)	torr seal		6/5	y
41	wire	1.90	7.6	Pd, Marsh. 0.032"	HNO3	none	0.2N,thio	MSD	Pt	plastic(3)	torr seal	0.86	6/21	y
43	coin	4.69		Pd(1)+B	std	none	0.2N,As2O3	MSD	Pt	plastic(3)	torr seal		6/24	y
71	strip	0.73	2.5	Pd(2)	C-S	paraffin, H2S	0.2N	MSD	Pt small	glass(5)	glass	0.55	9/7	y
72	strip	0.73	2.1	Pd(2)	C-S	paraffin, H2S	0.2N	MSD	Pt small	glass(5)	glass	0.81	9/7	y
73	strip	0.68	1.0	Pd(2)	C	paraffin	0.2N	MSD	Ni(1)	glass(5)	glass	0.81	9/7	y
75	strip	0.50	1.4	Pd(2)	C-S	paraffin, H2S	0.2N	MSD	Pt small	glass(5)	glass	0.71	9/7	y
77	strip	0.72	1.4	Pd(2)	C-S	paraffin, H2S	0.2N	MSD	Pt small	glass(5)	glass	0.69	9/7	y
78	strip	0.66	1.4	Pd(2)	none	none	0.2N	MSD	Ni(1)+S	glass(5)	glass	0.79	9/7	y
79	wire	0.37	2.0	Pd,Martin	HNO3	none	0.2N,Ag	MSD	Ni(1),Ag	glass(5)	glass	0.94	9/7	y
98	strip	0.79	1.8	Pd(2)	HNO3	none	0.1N,3.5mg WF	Aldrich	Ni(2)	glass(5)	glass	0.93	12/15	y

A coin= arc melted and rolled into coin shape
sheet= 0.05" thick sheet cut into square shape
strip= strip cut from sheet or button to give a parallelepiped
wire= a cylinder having a diameter from 0.03" to 0.04"
button= used as arc-melted
am= used after arc-melting
sw Ni= spot welded to nickel lead
Marshall or Martin=source of wire

B Alloys made by arc melting Pd with the other component
Pd(1)= Johnson Matthey powder, Batch V7114307
Pd(2)= Englehart sheet
Pd(3)= Johnson Matthey powder, Batch V8368501
Pd(4)= Englehart Powder, Batch A4934
Pd(5)= Englehart Powder, Batch F01567
sw = spot welded using tungsten electrodes, otherwise copper electrodes were used.

TABLE VII (Continued)

C Various surfaces applied as described under "D"
std.= sanded with 200 grit paper and washed with nitric acid
none=not cleaned

D H2S+C= heated in H2S mixed with paraffin vapor
paraffin, H2S= heated in paraffin vapor first than in H2S
H2S+H2O= heated in H2S that was bubbled through H2O
H2S= heated in pure H2S to form Pd sulfide on surface
oxidized= heated in air to produce microfractures on surface
annealed = heated in vacuum

E thio= thiourea added to electrolyte
pe= current was passed through electrolyte using a Pt dummy electrode before Pd was used
All cells after #70 contained stainless hypodermic needles
Hg= mercury metal in electrolyte
U=uranium metal in electrolyte
WF= Whole wheat flour added

F MSD = D2O from MSD Isotopes, 99.9 at. %
Aldrich = D2O from Aldrich Cemical Co., 99.9 at %
pe= preelectrolyzed using a Pt cathode and anode

G Pt=platinum gauze in a large "C" shape around cathode
Ni wire= nickel wire was made into a spiral (0.3" ID) around the anode
Ni+S wire= Ni wire heated in H2S
Pt small= Pt gauze made into 0.3" in diameter tube that surrounded the cathode
Ni gauze= gauze obtained from Texas A and M
Ni(1)= 0.04" wire from Driver-Harris Company
Ni(2)= 0.04" welding wire
Ni(3)= 0.06"
Ni(4)= 0.04" protonic JM batch W12918

H Glass= flint glass
Plastic= polyethylene
Cell Design #1 = 120ml glass jar
Cell Design #2 = 120ml glass jar with 40 ml plastic insert
Cell Design #3 = 100ml plastic jar
Cell Design #4 = 100ml plastic jar with glass tube covering cathode lead. Recombined liquid returned to cell.
Cell Design #5 = 120ml glass jar with recombined gas collected separately.
Cell Design #5a = 10ml glass test-tube with recombined gas collected separately.
Cell Design #5b = 120ml glass jar with recombined gas collected separately in hot water bath.
Cell Design #2a = 120ml glass jar with 40 ml plastic insert-recombinate collected separately

I torr seal= Pt wire from Pd electrode was covered with Torr Seal to prevent Cu and Pb pickup
glass=lead covered with glass tube
no=bare lead

J Maximum determined from weight gain

K Month and day cell started

L y = excess tritium measured
n = no excess tritium measured
? = no tritium measurement made

A more readable copy of this paper is here: http://lenr-canr.org/acrobat/ScottCDtheinitiat.pdf

THE INITIATION OF EXCESS POWER AND POSSIBLE PRODUCTS OF NUCLEAR INTERACTIONS DURING THE ELECTROLYSIS OF HEAVY WATER

Charles D. Scott, John E. Mrochek, Timothy C. Scott,
Gordon E. Michaels, Eugene Newman, and Milica Petek

Chemical Technology Division
Oak Ridge National Laboratory
Oak Ridge, Tennessee 37831-6226

ABSTRACT

The electrolysis of heavy water is being investigated with an insulated flow calorimetric system. In each of a series of tests, the electrolyte was 0.1 to 1.0 N LiOD in D_2O and cylindrical palladium cathodes surrounded by wire-wound platinum anodes were used at cathode current densities of 100 to 800 mA/cm^2. The most recent test was made with a "closed system" without off-gas in which the electrolysis gases were internally recombined. Fast neutrons and gamma rays were measured continuously during each test. It was shown that certain system perturbations could initiate and extend the generation of excess power. In one test, an apparent increase in the neutron count rate was also coincident with system perturbations.

INTRODUCTION

The generation of excess energy and possible products of nuclear interactions, as proposed by Fleishmann and Pons [1] and Jones et al., [2] has been the rationale for the continued experimental investigation of the electrolysis of heavy water with a LiOD electrolyte solution and palladium cathodes. Our experimental approach has been to utilize an electrolysis system with positive heat removal by circulating cooling water and the continuous monitoring of fast neutrons and gamma rays. The most recent test also incorporates an internal recombination of the gases generated by electrolysis so that the system is totally closed without off-gas. The goal of this research is to carry out careful experiments with a complete energy balance while simultaneously measuring the products of possible nuclear interactions. Excess power and apparent increases in the neutron and gamma-ray count rates have been observed.

MATERIALS AND METHODS

Experimental System

A complete description of the experimental system has been reported previously [3,4]. To summarize, the approach is to use an insulated electrolysis cell, typically 4-cm-diam, made from Pyrex glass that is enclosed in a water cooling jacket. The electrolyte volume is 100 to 125 mL contained in 10- to 12-cm of height with an internal gas space of 4 to 9 cm enclosed with a Teflon top flange. Most of the tests have been made in an "open system" mode with the electrolysis gases exiting, but one extended run (1900 h) was made with an internal catalytic recombiner that resulted in a "closed system" without off-gas.

The total system also included constant-current DC power supplies for the cell current; an internal calibration heater; the catalytic recombiner; a heating/cooling system coupled to a cooling water pump; a syringe attached to a plastic tube for sampling or replenishment of the electrolyte; thermocouples for measuring inlet and outlet cooling water temperatures and the electrolyte temperature; NE-213 and NaI scintillation systems for measuring fast neutrons and gamma rays; and a strip-chart recorder and microcomputers for data acquisition and processing (Fig. 1).

Materials

The heavy water was deuterium oxide obtained from Aldrich Chemical Company, Inc., and designated as 99.9% atom % D with a tritium content of 2000 Bq/L. The electrolyte was prepared by dissolving reagent-grade, natural lithium in the D_2O at a concentration of 0.1 to 1 N.

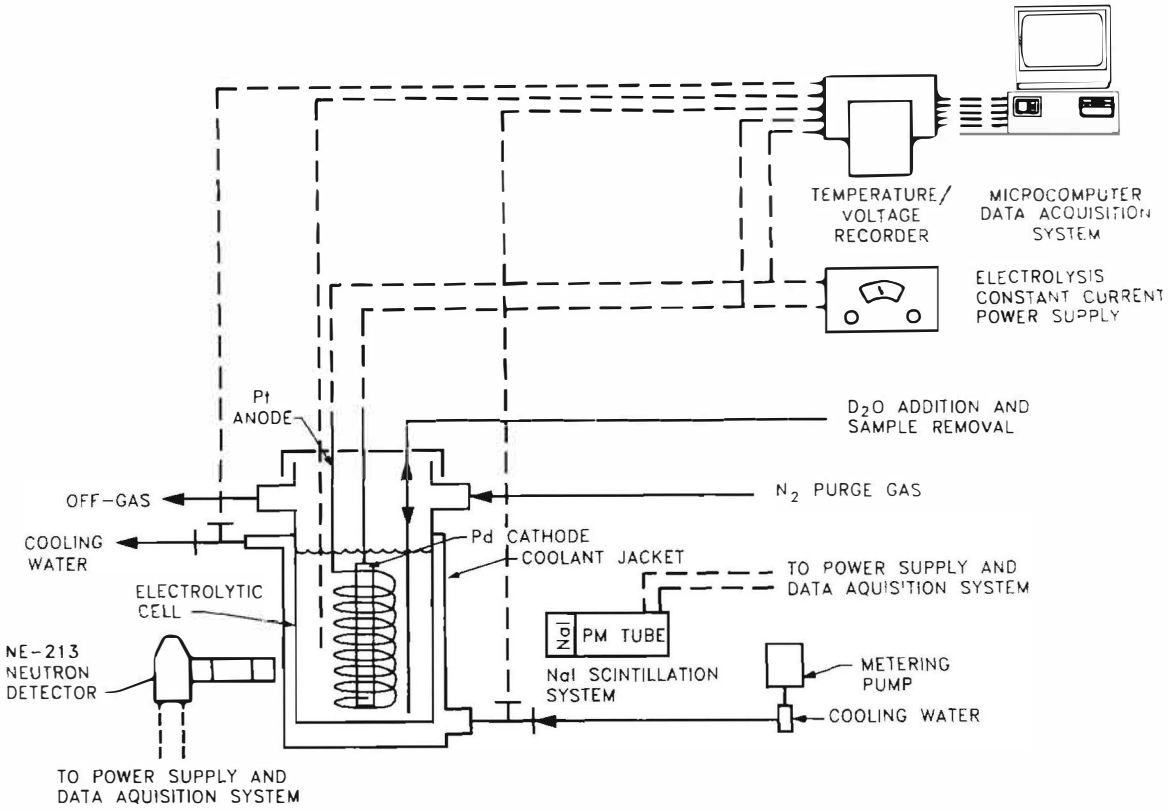

Fig. 1. Electrochemical system for the study of electrolysis of heavy water.

All of the cathodes were cylindrical rods of 99.9% palladium, obtained from Materials Research Corporation, that were cast in argon and swaged to the desired diameter (0.28 or 0.58 cm diam x 8.5 cm). A platinum connecting wire was then attached, and the rods were annealed at 900°C for 2 to 4 h in vacuum. All of the anodes and the recombiner were coils of wire fabricated from 99.9% platinum wire in the size range of 24 to 32 gauge (Englehard Corporation) [3,4].

Energy Balance

The energy balance for each test was determined by assuming that (1) the electric current was 100% efficient for electrolysis, (2) there was no accumulation of D_2, (3) the electrolysis gases were not recombined except in the closed-system test, and (4) there was no heat loss to the ambient. For the open and closed systems, the rate of energy input is [volts x amps]. The rate of energy removal in the open system was a combination of forced cooling [cooling water temperature increase x flow rate], electrolysis [negative heat of formation of the electrolysis products], and the increase of latent heat of the off-gases. For the closed system, the rate of energy removal was simply that of forced cooling.

RESULTS AND DISCUSSION

Several long-term (hundreds of hours) electrolysis tests have been made. Periods of excess power were observed in almost all cases; in a few tests, apparent increases in the neutron and gamma-ray count rates were also evident.

Excess Power

Apparent excess power has been observed in both open and closed electrolysis systems. There were periods of several hours when apparently spontaneous (no obvious initiation) excess power was measured at levels as high as 50% excess (Fig. 2). It was also shown that excess power could be initiated and extended for many hours by varying system parameters such as cathode current density, electrolyte concentration,

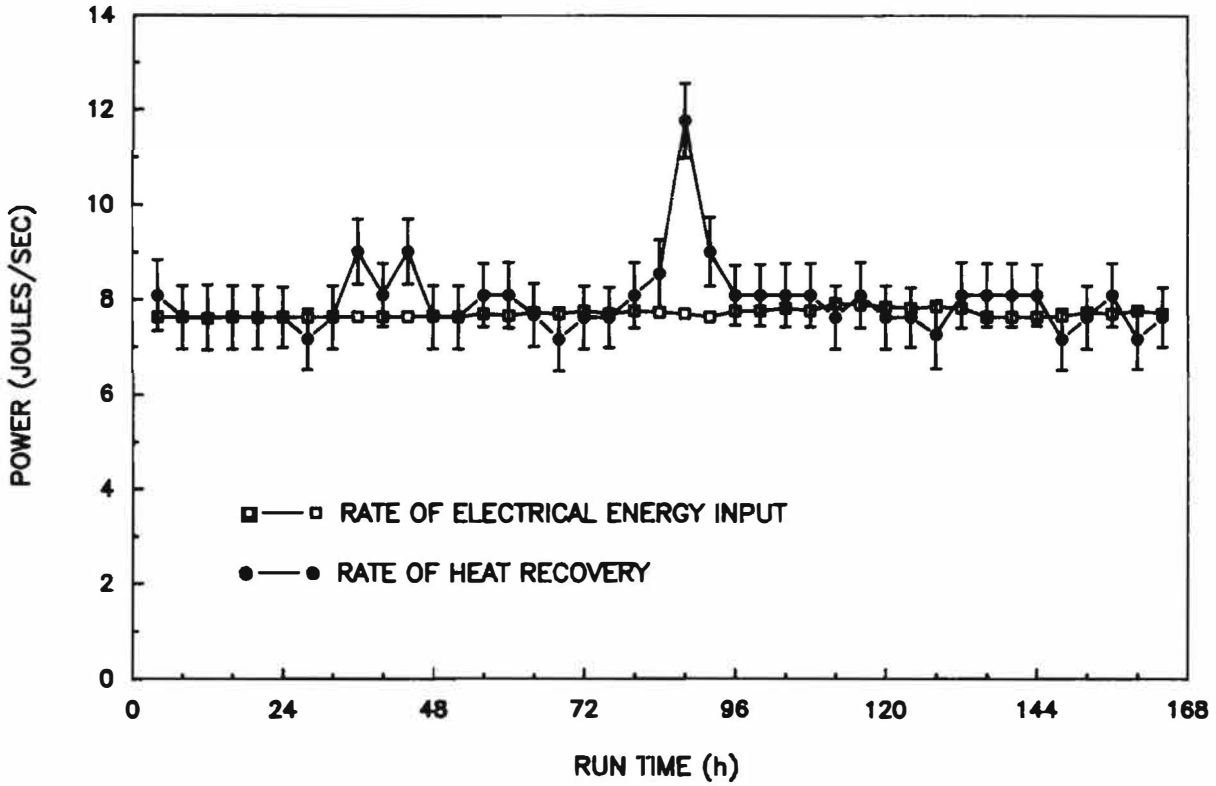

Fig. 2. Power balance for an open-system test in which a 0.56-cm-diam x 8.5-cm palladium cathode was used in 0.2 N LiOD at a cathode current density of 100 mA/cm^2. The error bar represents calculated uncertainty in the experimental value.

and electrolyte temperature (Fig. 3). The latter parameter seemed to be the most effective means for producing system perturbations that initiated excess power. This approach was of particular utility in the closed system where excess power was initiated and extended for hundreds of hours by reducing the electrolyte temperature (Fig. 4).

Increased Neutrons and Gamma Rays

In various tests, the neutron count rate spontaneously exceeded the background by over three standard deviations on several occasions. Typical of these was an open-system test where, during the first few hours, the neutron count rate exceeded the background by about three and one-half standard deviations (Fig. 5).

Perhaps the most interesting neutron result was obtained in a closed system where an apparent coincidence of increased neutron count rate was observed during the period of induced excess power (Fig. 6).

CONCLUSIONS

On several occasions, excess power was observed during the electrolysis of heavy water in the presence of a palladium cathode. In some cases, the excess power was apparently spontaneous; however, it could also be induced for many hours by system perturbations caused by varying certain operating parameters. Apparent increases in the neutron count rate were also observed in several instances, including one period that was coincident with induced excess power.

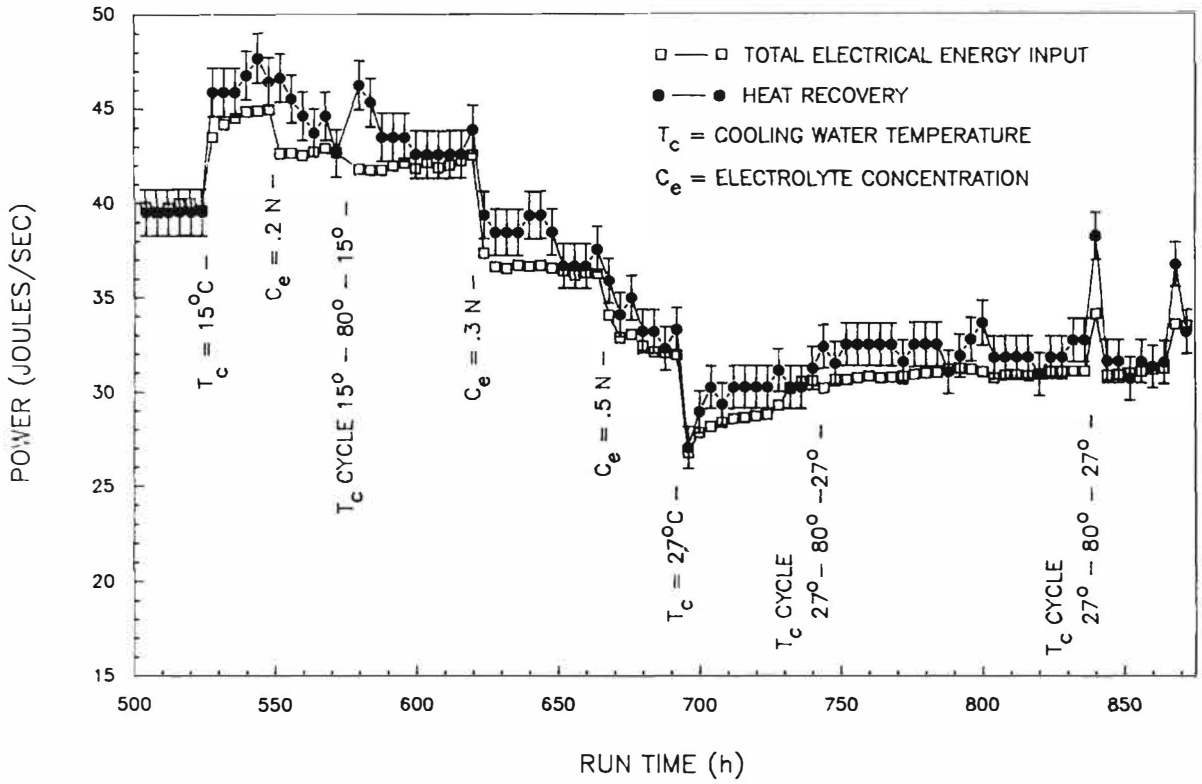

Fig. 3. Power balance for an open-system test in which a 0.28-cm-diam x 8.5-cm palladium cathode was used at a cathode current density of 600 mA/cm^2. Excess power was initiated and extended by varying certain system parameters.

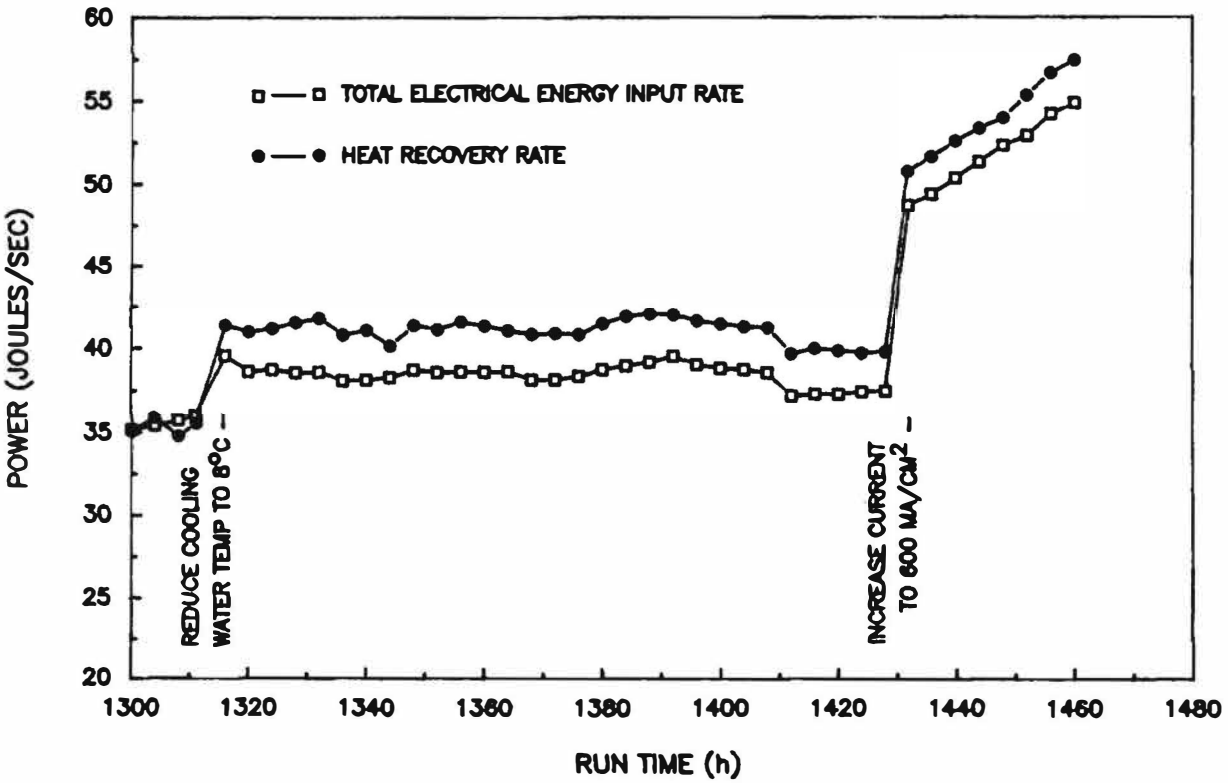

Fig. 4. Power balance of a closed-system test in which a 0.28-cm-diam x 8.5-cm palladium cathode was used in 0.1 N LiOD at a cathode current density varying from 500 to 600 mA/cm^2. The experimental uncertainty is approximately 0.4 joules/sec.

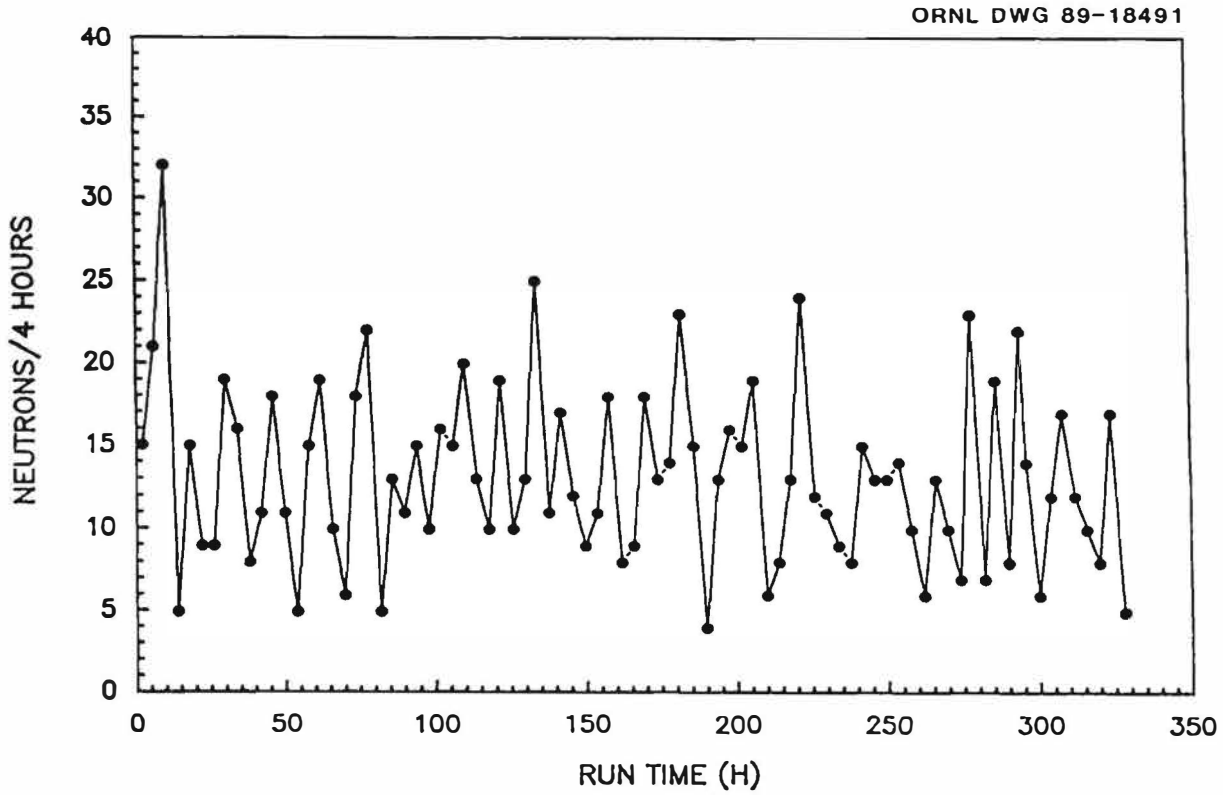

Fig. 5. Neutron count rate for an open-system test in which a 0.28-cm-diam x 8.5-cm palladium cathode was used in 0.2 N LiOD at a cathode current density of 100 mA/cm^2.

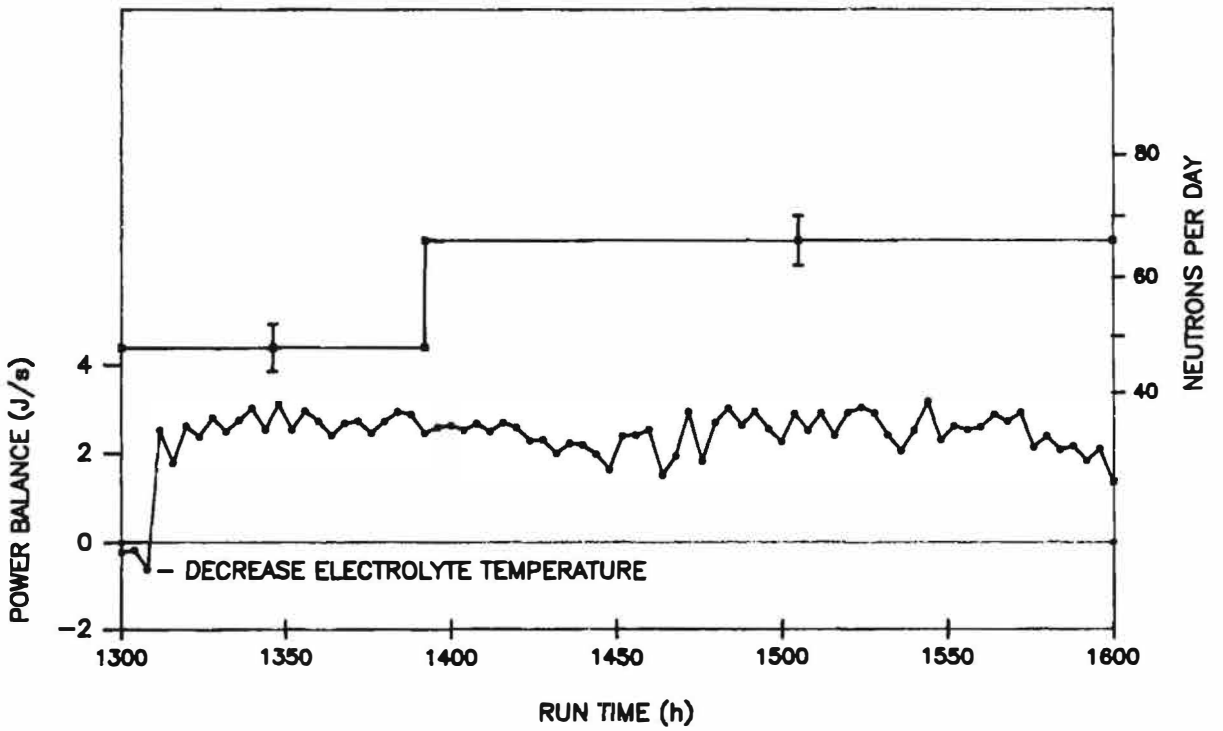

Fig. 6. Apparent coincidence of an increased neutron count rate during the period of induced excess power in a closed-system test in which a 0.28-cm-diam x 8.5-cm palladium cathode was used in 0.1 N LiOD at a cathode current density varying between 500 and 600 mA/cm^2. The error bars represent the 95% confidence level for neutron counts during the indicated period of time.

REFERENCES

[1] M. Fleishmann and S. Pons, "Electrochemically Induced Nuclear Fusion of Deuterium," J. Electroanal. Chem. 261, 301:1989.

[2] S. E. Jones, E. P. Palmer, J. B. Czirr, D. L. Decker, G. L. Jensen, J. M. Thorne, S. F. Taylor, and J. Rafelski, "Observation of Cold Nuclear Fusion in Condensed Matter," Nature, 338, 737:1989.

[3] C. D. Scott, J. E. Mrochek, E. Newman, T. C. Scott, G. E. Michaels, and M. Petek, "A Preliminary Investigation of Cold Fusion by Electrolysis of Heavy Water," Martin Marietta Energy Systems, Inc., Report ORNL/TM-11322: 1989.

[4] C. D. Scott, J. E. Mrochek, T. C. Scott, G. E. Michaels, E. Newman, and M. Petek, "Measurement of Excess Heat and Apparent Coincident Increases in the Neutron and Gamma-Ray Count Rates During the Electrolysis of Heavy Water," submitted to Fusion Technology:1990.

SEARCH FOR NUCLEAR PHENOMENA BY THE INTERACTION BETWEEN TITANIUM AND DEUTERIUM

F. D'Amato, A. De Ninno, F. Scaramuzzi

ENEA, Dip. TIB, Divisione Fisica Applicata, C. R. E. Frascati,
C.P. 65 - 00044 Frascati, Rome, Italy

P. Zeppa
ENEA, Dip. COMB, C.R.E. Casaccia
Via Anguillara, 301 - 00060 S. Maria di Galeria, Rome, Italy

C. Pontorieri - ENEA Student

F. Lanza
JRC EURATOM Ispra, I-21020 Ispra, Italy

ABSTRACT

Following the preliminary results obtained in the Spring of 1989 [see ref.3], a second generation of experiments aimed to the detection of nuclear particles from a titanium-deuterium system has been designed. Here very preliminary results from the new (even though not yet complete) experimental setup are presented: neutron burst emission from the system and tritium production in the samples.

INTRODUCTION

In March 1989 the evidence of "cold fusion" phenomena was claimed by two experimental groups in Utah; in both instances an electrolytic cell was used with heavy water. Fleischmann and Pons [1] attributed the excess heat produced during the elctrolysis to nuclear fusion reactions. Jones et al. [2] measured the emission of neutrons of the correct energy (2.45 MeV) during the electrolysis. Our group in Frascati made the assumption that, if a nuclear phenomenon was present in the quoted results, it could be attributed to the interaction between deuterium and some metals - in particular, palladium and titanium - with the electrolysis playing the role of an intermediary. A simple experiment was devised, with the purpose of avoiding the complications of electrolysis; it consisted in putting in contact gaseous deuterium with titanium (in shavings), and then changing the thermodynamical parameters of the system (temperature, pressure, stoichiometric ratio, etcetera) and looking for neutron emission. Positive results were obtained and published in reference 3: we refer to the latter for more details. Here we need to remember only two main features, that have influenced the design of a second generation experiment, which is the object of this communication.

- The neutron emission appeared to be structured in "bursts", i.e., many neutrons were emitted in a short time, of the order of 100 μs.
- Lack of reproducibility characterized our tests (and all the positive tests performed throughout the world): we had a total of 4 positive runs out of about 12 (each lasting roughly a week).

Since then we have been moving in three directions:

- improving the neutron detector,
- searching for tritium in our samples,
- trying to study the thermodynamics of the system.

Here the preliminary results of our second generation experiments are reported.

NEUTRON DETECTION

In detecting neutrons produced in nuclear reactions, like those apparently present in these experiments, four features are important:

- identification of neutrons,
- localization of the source,
- time structure of the bursts,
- energy of the neutrons.

As a first approximation, we decided to solve the first three problems, aiming in the

search for better reproducibility of the experiments, and postponing the measure of the neutrons' energy to a third generation experiment. We follow the solution chosen by the Los Alamos group [4], using a system of many ^{3}He detectors, arranged in a cylindrical geometry and embedded in polyethylene: this ensures high sensitivity. The presence of an outer ring of detectors gives information about the region where the neutrons come from. The use of a veto counter system, consisting in a set of ^{3}He tubes without moderator and connected to the same electric feed, allow us to exclude noise effects, and contributes to a good identification of neutrons. The burst structure is examined by opening a time window - usually 128 μs - every time a neutron is counted and seeing whether other neutrons are present in the window. A comparison with a similar window opened 2 ms later allows us to correct for the case of multiple events present in the background. In this way a multiplicity index n is measured, which is related to the number of neutrons R in the shift register by the expression

$$n = R(R-1)/2$$

If the efficiency of the detector is e, the number of neutrons emitted is, with good approximation,

$$N = e\sqrt{2n}$$

A detector with these characteristics is under construction and will be ready by the end of Spring 1990.

While waiting for the new detector we had the chance to use since last October a standard neutron detector (normally used to detect the amount of plutonium in a sample) with 15 operating ^{3}He tubes and an overall efficiency of about 15% (measured with a ^{252}Cf source). We were not yet able to use an outer ring and a veto counter. We could look at the burst structure of the emission, but with quite a high background. This meant that "meaningful" bursts needed to have multiplicities greater than 35. With this apparatus we performed a series of 19 runs, for a total of about 2100 hours between October 1989 and February 1990. Figure 1 shows the outcome of these runs. In 1a the kinds of sample are listed with the corresponding measurement time; in 1b for every kind of sample the number of runs and the number of bursts is reported. We could measure a total of 19 bursts, ranging from 40 to 320 in multiplicity, 17 of which were obtained in experiments on samples constituted by titanium (or titanium alloy) in the presence of deuterium. No bursts were observed in "blank" samples, i.e.: only the counter, titanium with hydrogen, titanium under vacuum. In one run with deuterium at 50 bar in the experimental cell, but without titanium, 2 bursts (of the minimum multiplicity) were seen. Figure 2 shows the distribution of the bursts with respect to multiplicity. During the tests the samples were subjected to temperature and pressure changes. The stoichiometric ratio in these experiments ranged in a very wide interval of values, from 10 at.% to 190 at.%. The positive data are too few at present to attempt any correlation with these parameters. The only conclusion that we can get is of statistical order: we see bursts when in the system there is deuterium, we do not see bursts when in the system there is no deuterium. The next step will be, with the new detector, to decrease substantially the background, in order to be able to consider multiplicity factors down to less then 10. This has already been done by the Los Alamos group [4], showing that the number of bursts strongly increases at low multiplicities. This seems a reasonable route to pursue in order to aim at reproducibility.

SEARCH FOR TRITIUM

If tritium is produced within the deuterated titanium sample because of a nuclear reaction, it is most probable that it is absorbed in the metal, with few chances of escaping. Thus, it is possible to search for tritium in samples even days or months after the experiment has been performed.

The technique used has been set up by one of us (FL) and is described in detail in reference 5. Here a short description of the method is presented. The metal sample is slowly heated up to 1000 °C in a slow flow of helium gas (roughly 1 cm^3 NTP/s). The outgoing gas passes through a catalyzer (CuO heated to a temperature of 400 °C), where the hydrogen and its isotopes are changed in water, and then through two scrubbers in series, where the water is condensed and collected: each scrubber is a glass tube containing distilled water, kept at a temperature of 4 °C (in order to have a low vapor pressure). Water from each scrubber is then mixed with a scintillator cocktail, and its disintegration rate is measured. The second scrubber normally does not show tritium: this is a check that all tritium and deuterium have been condensed in the first scrubber. Two independent measurements from the same sample are performed, using for each test 5 to 10 grams of metal. The amount of deuterium extracted is obtained by weighing the sample before and after heating it.

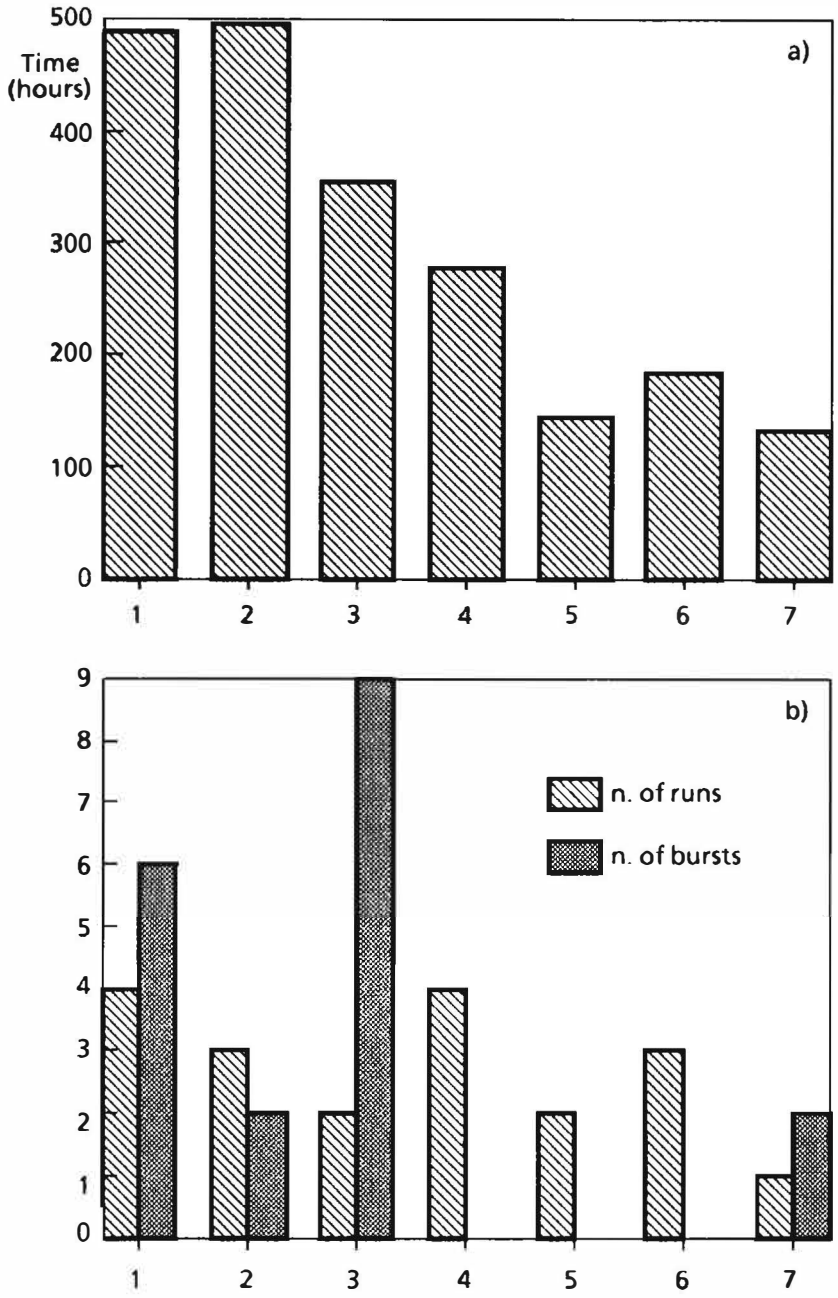

Figure 1. Emission of neutron bursts. (a) The number of hours of neutron detection for every kind of samples. N.1: titanium shavings with deuterium. N.2: titanium alloy 6-6-2 (6% Va, 6% Al, 2% Sn) with deuterium. N.3: titanium sheet (1 mm thick) with deuterium. N.4: blank with the detector containing a piece of metal of the same mass of the experimental cell, in order to keep the number of neutrons produced by cosmic rays constant. N.5: blank with the cell containing titanium and hydrogen. N.6: blank with titanium under vacuum in the cell. N.7: the cell, without titanium, with 50 bars of deuterium inside. (b) For each kind of sample the corresponding number of runs (each lasting roughly one week) is shown on the left, and the number of bursts on the right.

Previous to all measurements, the amount of tritium contained in the original deuterium must be determined. This is obtained with a similar procedure, in which the first step is substituted by flowing gas from the deuterium bottle, mixed with an appropriate amount of helium, which acts as the carrier. We found that the tritium content in commercial deuterium bottles can be quite different. The first bottle we used contained up to 360 Bq/g (becquerel per gram of deuterium), quite a high value. A second bottle contained only 9 Bq/g and with this one we

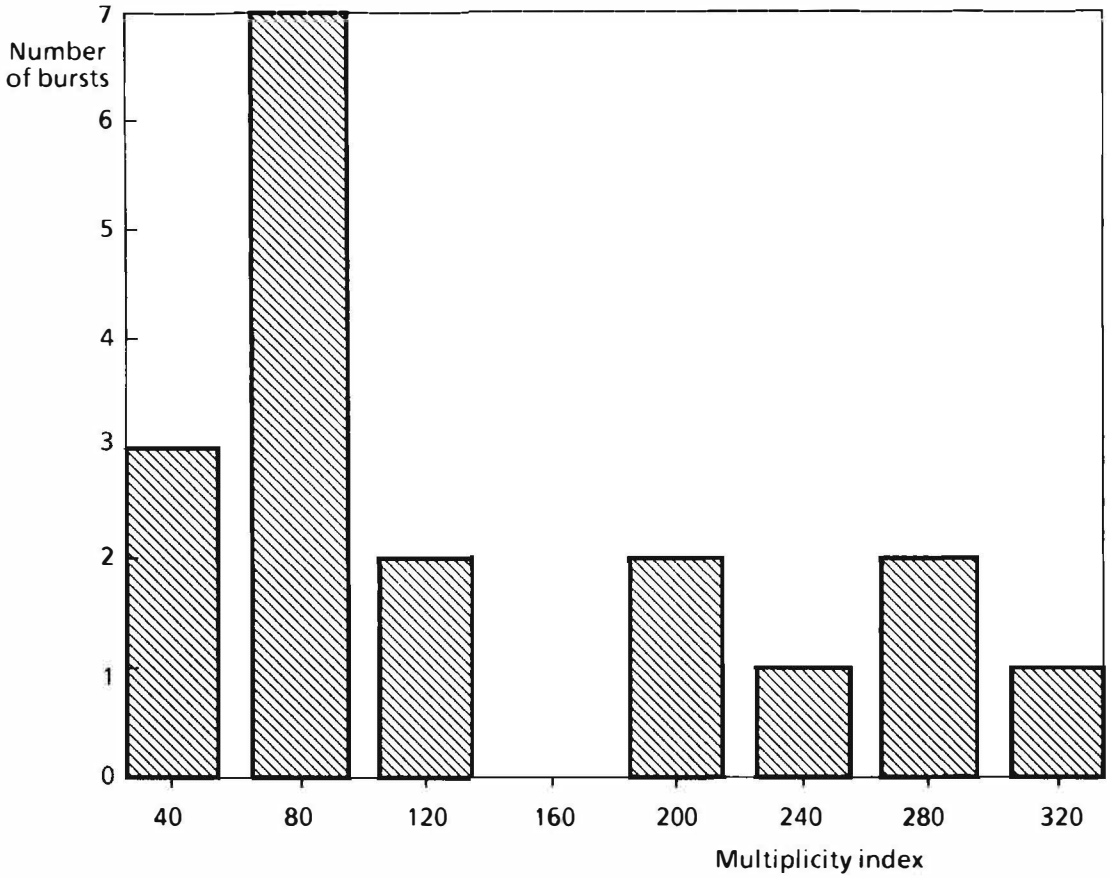

Figure 2. The distribution of the bursts as a function of multiplicity. Multiplicities lower than 35 have not been considered as "meaningful" bursts. The two bursts found in sample 7 of Figure 1 have multiplicity 40.

performed a few preliminary experiments. In order to have enough deuterium to minimize errors, in these experiments we strongly deuterated the titanium samples, with stoichiometric ratios higher than 140 at.%.

Table 1 shows the results obtained in the first 5 tests. The data reported have already been corrected for the tritium content in the original deuterium, by subtracting 9 Bq/g from the readings of the scintillator. Even in these experiments it is almost impossible to look for correlations between the results and the other parameters, such as the thermal cycles of the sample, the kind of material (shavings or powder), the stoichiometric ratio, etcetera. In all cases but one (n.1) we were not looking for neutrons during the experiment. We did not measure any neutron emission in experiment n.1. The only conclusions that we can draw at this point is that it seems that it is possible to form tritium during the interaction of deuterium gas with titanium, in amounts well above the standard deviation.

Table 1. The amount of tritium found in titanium samples that have been subjected to experiments of interaction with deuterium gas. The values reported under "T-production", expressed in becquerel per gram of deuterium, have been already corrected, by subtracting 9 Bq/g, for the tritium content in the original deuterium. All samples were Ti shavings, with the exception of sample 1, consisting of Ti powder. Samples 2 and 3 had no low temperature thermal cycle (see Reference 3). In all samples the stoichiometric ratio was more than 140 at.% of deuterium. 1 Bq/g corresponds to about 5×10^{8} atoms of tritium.

Sample N.	T-Production Bq/g	Standard Dev. Bq/g
1	13.68	1.26
2	26.91	0.89
3	4.60	0.92
4	7.29	0.93
5	3.11	0.85

THERMODYNAMICS

We are convinced that the main problem to face is the correlation between the nuclear phenomena described above and the thermodynamical features of the metal-deuterium system. By this we mean all the microscopic transformations that the interaction between deuterium and the metal lattice can produce. This kind of research has proved up to now quite difficult, because of the lack of reproducibility of the experiments. This justifies our present effort aimed at increasing reproducibility. If and when this target will be reached, we think that it is very important to look for correlations between nuclear phenomena and these parameters, i.e.: temperature; pressure; deuterium concentration; temperature, pressure and concentration gradients; changing rate of these parameters; phase transformations; purity and thermal history of the material; and considering materials other than titanium.

At present we are building a new cell in which we will be able to change the temperature of the sample in a programmed way, while looking for neutron emission. This cell should be operating with the new neutron detector next Summer.

ACKNOWLEDGEMENTS

The authors are very grateful to Messrs. G. Lollobattista, L. Martinis, L. Mori and C. Ronsecco for very valuable technical help.

REFERENCES

[1] M. Fleischmann, S. Pons., J. Electroanal. Chem., 261, 301 (1989).

[2] S.E. Jones, E.P. Palmer, J.B. Czirr, D.L. Decker, J.L. Jensen, J.M. Thorne, S.F. Taylor, J. Rafelski, Nature, 338, 737 (1989).

[3] A. De Ninno, A. Frattolillo, G. Lollobattista, L. Martinis, M. Martone, L. Mori, S. Podda, F. Scaramuzzi, Europhysics Letters, 9, 221 (1989).

[4] H.O. Menlove, M.M. Fowler, E. Garcia, A. Mayer, M.C. Miller, R.R. Ryan, S.E. Jones, submitted for publication and this conference.

[5] F. Lanza, C. Ronsecco, Technical note I.90.08, Joint Research Center - Ispra site - Italy.

STATISTICAL ANALYSIS OF NEUTRON EMISSION IN COLD FUSION EXPERIMENTS

M. Srinivasan, A. Shyam, S.B. Degwekar[1] and L.V.Kulkarni

Neutron Physics Division
[1]Reactor Physics Section
Bhabha Atomic Research Centre
Trombay, Bombay 400 085 India

ABSTRACT

The paper discusses two techniques for studying the multiplicity spectrum of neutron emission in cold fusion experiments. In the first method the multiplicity distribution of counts in 20 ms time intervals is analysed to give information about the statistics of neutron emission in cold fusion. The results of six such experiments indicate that about 10 to 25% of the neutrons produced in cold fusion are emitted in the form of bunches 400 to 600 neutrons each. The other method discussed is an adaptation of the Artificial Dead Time method developed originally for reactor noise analysis as well as for the passive neutron assay of plutonium. An expression for the fractional loss of counts in the presence of dead time is derived. It is shown that a neutron detection efficiency of ~ 1% is adequate to estimate the average multiplicity as well as the fraction of bunched neutron emission in the presence of a Poisson background.

INTRODUCTION

Since the first announcement by Fleischmann and Pons [1] and shortly thereafter by Jones et al [2] of the observation of cold fusion reactions in palladium electrolytically loaded with deuterium, various theories and speculations have been put forward as possible mechanisms for the same. All the schemes proposed so far may be classified into two broad categories Those that lead to fusion reactions taking place one at a time i.e. wherein occurrence of one fusion reaction does not directly influence the probability of occurrence of another. In this case one can assign a certain probability per second per deuteron for the reaction rate. A figure of 10^{-20} has for example been deduced for this by Jones et al.

The second category of mechanisms leads to a cascade or sharp bursts of fusion reactions. One of the earliest speculations [3,4] attributed the cold fusion phenomenon to muon catalysis triggered by cosmic ray produced muons. It was pointed out that each muon could in principle catalyze several hundred fusion reactions within a time span of a couple of microseconds. Recently Rafelski [5] has proposed catalysis by a massive negatively charged particle X^- as being responsible for the observation of bunched neutron emission during cold fusion. Yet another mechanism proposed has been lattice crystal fracture or cracking leading to acceleration of deuterons to energies of 20 to 50 Kev in electric fields generated across fracture crevices. Such internally accelerated deuteron beams are then presumed to cause fusion reactions [6]. Here again the fusion reactions may be expected to occur erratically leading to bunched emission of neutrons. More recently coherent processes [7] have been proposed which could lead to bunched neutron emission.

Since neutrons are one of the end products of cold fusion reactions [8], it may be expected that statistical analysis such as measurement of the multiplicity spectrum of neutron emission can give valuable insight into the possible origin of cold fusion reactions. The emission of neutrons in bunches of two or more can for example be observed by employing two (or more) fast neutron detectors and looking for coincidences amongst detected pulses within a gate interval of say 1 or 10 μs. Since the average background count rate is generally small, the chance coincidence

rate due to background events in such small intervals would be negligible making the task of establishing the occurrence of multiple neutron emission events quite easy.

An alternate technique of detecting fast neutron multiplicity is to employ a thermal neutron detector surrounded by a hydrogenous moderator such as paraffin. This type of detector system has the interesting property that a bunch of fast neutrons simultaneously incident on it would be temporally seperated due to the statistical nature of the neutron slowing down process and get detected as individual neutrons within a time span governed by the neutron die-away time $(1/\lambda)$ in the moderator-detector assembly. It is this type of thermal neutron detector that is considered in the present studies. The pulse train issuing from such a detector can then be analysed by any of the techniques developed for the purpose in the fields of reactor noise [9] and more recently the passive neutron assay of plutonium for safeguards applications [10].

One of the most straightforward methods is to measure the frequency distribution of counts registered in short counting intervals and to relate it to the statistical characteristics of the neutron emitting source. This method was used by us to study the statistics of neutron emission from the Milton Roy commercial electrolytic cell [11] as well as some D_2 gas loaded Ti targets [12] and is described below.

STATISTICAL ANALYSIS USING PC BASED SYSTEM

Theory of Multiplicity Analysis

If the events producing neutrons are random in time and result in one neutron per event, then the number of counts observed in a time interval τ would be distributed according to the Poisson law as follows:

$$P_r = \frac{(N_0\tau)^r}{r!} e^{-N_0\tau} \qquad (1)$$

where P_r is the probability of obtaining r counts in time τ and N_0 is the average count rate. Thus when the average count rate is small i.e. when $N_0\tau \ll 1$, one can set $\exp(-N_0\tau) \sim 1$. In this case the probabilities of detecting one, two and three neutrons in the time interval τ are $(N_0\tau)$, $(N_0\tau)^2/2$ and $(N_0\tau)^3/6$ respectively. In particular note that the ratio of doubles to singles is $(N_0\tau/2)$ while that of triples to doubles is $(N_0\tau/3)$ and so on.

On the other hand if there are S_b events per second which result in emission of neutrons in bunches, say ν neutrons per bunch, then in a time interval τ which encompasses the bunched nuclear event, the probability (P_γ) of obtaining r counts in time τ would be given by a binomial distribution as follows:

$$P_r = \binom{\nu}{r}(1-\varepsilon)^{\nu-r}\varepsilon^r \qquad (2)$$

It is presumed here that the interval τ is large compared to the neutron die-away time in the detection system. It is also assumed that the source event rate S_b is so small that only one such event occurs in the the interval τ. Here ε is the overall counting efficiency. In the limit of $\nu \gg 1$ and $\varepsilon \ll 1$ Eq. (2) simplifies to give

$$P_\gamma = \frac{(\nu\varepsilon)^r}{r!} e^{-\nu\varepsilon} \qquad (3)$$

Note that while the probabilities of various multiplicities due to the random background depend on the product $(N_0\tau)$ that due to the bunched neutronic events depend mainly on ν and ε. Table I gives the expected frequency distributions of multiple neutron counts for typical values of N_0, ε, and ν. The counting time interval (τ) is kept fixed at 20 ms while the bunched neutron producing event rate (S_b) is taken as 10^{-2}/s. The data presented is for a total of 10^5 sampling time intervals. It is clear from the table that while the average count rate for Poisson events is much greater than for bunched events, the frequencies of higher

count multiplicities (>2) is much larger for the bunched events. This means that if some of the cold fusion neutrons are released in bunches, it is much easier to detect these in the presence of a random background if the multiplicity distribution of counts in short time intervals is measured. Secondly, measurement of the multiplicity distribution of counts would also enable us to distinguish between the neutrons emitted in singlets and those emitted in bunches and to derive quantities like the average number of neutrons per bunch and the fraction of neutrons produced in bunches.

Let us consider a situation wherein neutrons are produced in singlets as well as in bunches. Let S_1 denote the source event rate of the former and S_b that of the latter such that $S=S_1+S_b$ represents the total source event rate. The fraction of events (f_e) that result in bunched neutron emission and the fraction of neutrons (f_n) produced in bunches can then be written as follows:

$$f_e = \frac{S_b}{S_1 + S_b} \qquad (4)$$

$$f_n = \frac{\bar{\nu} S_b}{S_1 + \bar{\nu} S_b} = \frac{\nu f_e}{1 - f_e + \nu f_e} \qquad (5)$$

In the situation encountered in cold fusion experiments, the product $N_0 \tau$ is small compared to unity and the product $\nu\varepsilon$ is ~ 5 as we shall see later. Thus the measured frequency distribution of counts clearly seperates into two components viz that governed by Eq. (1) and that governed by Eq.(3), thus making the task of deriving the parameters f_n and ν fairly easy. The component corresponding to single neutron emission lies in the low multiplicity region while that due to bunched neutron emission extends into the region of high multiplicities. Moreover, since the peak of the latter distribution appears at the multiplicity given by the product $\nu\varepsilon$, it is possible to deduce ν since ε can be measured using a calibrated neutron source. On the other hand f can be simply taken as the ratio of the sum of the high frequency events to the total frequency.

TABLE I

Expected Frequency Distribution of Counts for Poisson and Bunched Neutronic Events for Typical Sets of Parameters

Multiplicity of counts	Frequency of Counts in 20ms Intervals for 10^5 Samples					
	Poisson Events		Bunched Events ($S=10^{-2}$ per sec)			
			ν = 100	ν = 100	ν = 500	ν = 500
	N_0=0.3 cps	N_0=3.0 cps	ε = 0.005	ε = 0.015	ε = 0.005	ε = 0.015
			$S\nu\varepsilon$ = 0.005	$S\nu\varepsilon$ = 0.015	$S\nu\varepsilon$ = 0.025	$S\nu\varepsilon$ =0.075
0	99940	99402	99992	99984	99980	99980
1	60	597	6.1	6.6	4.00	0.07
2	$\sim 10^{-2}$	1.7	1.5	5.0	5.1	0.3
3	$\sim 10^{-5}$	$\sim 10^{-2}$	0.2	2.5	4.2	0.8
4	$\sim 10^{-9}$	$\sim 10^{-5}$	0.03	1.0	2.6	1.5
5	$\sim 10^{-13}$	$\sim 10^{-8}$	0.003	0.33	1.3	2.2

Neutron Counts Data Acquisition System

Neutrons from the cold fusion source were counted by a bank of thermal neutron detectors embedded in a paraffin moderator block. One bank comprised of three BF_3 counters while the other was made up of three He^3 counters. The neutron die-away time in each of these was ~25 μs. The BF_3 bank was mounted close to the Milton Roy Pd-Ni electrolytic cell [11] and the He^3 bank near a D_2 gas loading apparatus [12] about 1.5 m^2 away. While one counter was being used as signal counter in one experiment the other bank served as background monitor and vice versa. The efficiency (ε) of detection for the cold fusion source neutrons was typically in the range of 0.5% to 1.5% depending on the exact distance between the cold fusion source and the detector assembly as well as the pulse height discriminator bias setting.

The outputs of both these counter banks were fed to scalers whose readings could be read off by a Personal Computer (PC) at the end of each counting interval which was controlled by the clock in the PC. By taking the difference in the scaler readings corresponding to the end of two consecutive counting intervals the number of counts recorded in a given counting interval is computed and stored by the PC. It took the PC typically about 280 ms to carry out these operations following each sampling time. Hence a set of 1000 samples consumed a real time of~5 minutes. From such data accumulated over several hours, the frequency distribution of counts recorded in 20 ms intervals could be computed.

Multiplicity Spectrum Measurements and Results

To begin with the statistics of background counts was studied to ensure that the equipment was functioning satisfactorily. For this purpose all potential cold fusion sources were removed from the room where the detectors were located. Data acquisition of background counts continued in an uninturrupted manner for 63 hours over a week end (from 1800 hrs on Friday 2nd June to 0900 hrs Monday 5th June, 1989). During this run the average background count rate in the BF_3 bank was ~0.023 cps and in the He^3 bank ~0.43 cps. Table II presents the results of the frequency distribution of counts obtained in this long background run. It is heartening to note that, as expected on the basis of Poisson distribution, not even once out of the ~750,000 odd samples were 3 or more counts registered by either of the detector banks. The ratio of doubles to singles frequency further conforms to Poisson statistics, indicating that the equipment was functioning properly. Sparking in any of the counters for example would have given rise to significant non-Poisson behaviour.

Table III represents the results of our first attempt to measure multiplicity distribution of neutrons from an electrolytic cell. The data was accumulated overnight (1805 hrs on 26th May to 0645 hrs on 27th May) with the BF_3 bank viewing the Milton Roy cell which was quiescent i.e. the cell current was not on. Besides, a plastic scintillator (NE 102A) biased to register only neutrons of energy > 9 MeV monitored cosmic ray and other background events. The first column of the table gives the probability distribution of counts of the BF_3 bank for 20 ms intervals. The average count rate works out to 5.6 cps. It is clear from the frequencies of 2s, 3s and higher

TABLE II

Frequency Distribution of Background counts in Two Detector Banks

Counting interval 20 ms
Total counting time 63 hrs

Multiplicity of counts	Frequency BF_3 Bank	Frequency He^3 Bank
0	750035	743948
1	339	6413
2	1	14
3	0	0
4-20	0	0
N_0	0.023cps	0.43cps
$N_0\tau$	5×10^{-4}	0.0086

TABLE III

Frequency Distribution of Counts in BF_3 Bank and Plastic Scintillator with Quiescent Milton Roy Cell

Counting period	12hrs
Counting interval	20 ms
Total number of sampling intervals	144000

Multiplicity of couts	Gross Frequency	Frequency in those samples in which plastic scintillator records a count
1	11941	114
2	2760	31
3	111	0
4	19	0
5	2	0
6	13	0
7	9	0
8	3	0
9	5	0
10	1	0
11	0	0
12	1	0
13	0	0
14	0	0
15	1	0
16	0	0

multiplicities that there is considerable contribution of non-Poisson events. The second column of the table gives the frequency distribution of the same counts data whenever there was a pulse recorded by the plastic scintillator also during a 20 ms interval. From this we conclude that only about 1% of the multiple neutron events occurring in the BF_3 bank can be attributed to cosmic ray showers.

Table IV presents the frequency distribution results of the Milton Roy cell run of 12th to 14th June, 1989. As may be seen from Fig. 1, six neutron bursts of five minutes duration each were recorded during this period, the first about 50 minutes after cell electrolysis commenced on 12th June, the second and third about an hour thereafter and the remaining three a few hours after the cell current was switched off on the evening of 14th June. During the burst phase, the count rates were in the range of ~0.5 to 1.7 cps which is about 4 to 14 times that of the background value (~0.12 cps). However it is noteworthy that in 4 out of the 6 bursts observed, count multiplicities of 2,3,4,5 and even 10 have been recorded at least once each. This type of behaviour is clearly indicative of high multiplicity neutron emission events. Throughout this run lasting several days the background counter did not record any noticable increase in count rate.

TABLE IV

Frequency Distribution of Counts for 1000 Sampling Intervals Each of 20ms During Six Periods of High Neutron Activity (Milton Roy Cell Run of 12th to 14 th June '89)

Multiplicity of counts	Frequency 12th June A	B	C	14th June D	E	F	Total (A to F) Observed	Expected
1	27	0	2	7	29	22	87	117
2	0	0	0	0	3	0	3	1
3	0	1	0	0	0	0	1	$\sim 10^{-3}$
4	0	0	1	0	0	0	1	$\sim 10^{-5}$
5	0	0	1	1	0	0	2	$\sim 10^{-7}$
6	0	0	0	0	0	0	0	$\sim 10^{-10}$
7	0	0	0	0	0	0	0	$\sim 10^{-12}$
8	0	0	0	0	0	0	0	$\sim 10^{-15}$
9	0	0	0	0	0	0	0	$\sim 10^{-18}$
10	0	1	0	0	0	0	1	$\sim 10^{-20}$

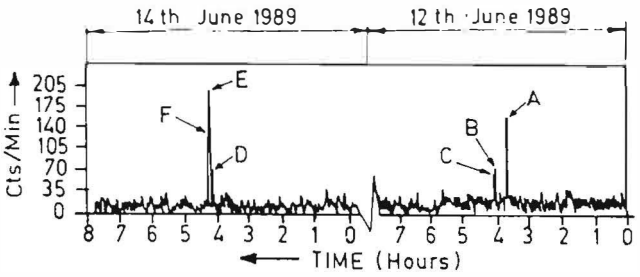

Fig.1. Neutron Bursts of Initial Part of Run Number 2 of Milton Roy Cell.

Table V summarises the frequency distribution measured during the 2.5 hour long neutron burst recorded on 16 th June, 1989 from 1900 hours onwards with the Milton Roy electrolyser. It may be noted that the cell had not been operated for the previous ~52 hours. The count rate during this wide neutron burst attained a value as high as 20 cps at the peak. The background neutron monitor which was only 1.5m away also indicated a small increase in count rate commensurate with its efficiency for neutrons emanating from the Milton Roy cell. Careful scrutiny of these results indicates that the frequency distribution essentially corresponds to a Poisson distribution. However, the fact that multiplicities of 5 or more are recorded several times again points to the sporadic occurrence of multiple neutron emission events. It is noteworthy that around 1950 hrs (close to the peak) there were more than 20 such high multiplicity cascade events within a time span of 5 minutes.

Table V

Frequency distribution of count for 1000 Sampling Intervals of 20ms Each
During Periods of High Neutron Activity
(Milton Roy Cell Run of 16 th June)

Multiplicity of countsf	Frequency													Total(A to L)	
	A	B	C	D	E	F	G	H	I	J	K	L	M	Observed	Expected
1	124	54	335	320	243	315	295	492	447	104	355	345	24	3429	3166
2	21	9	54	82	13	35	24	51	42	13	49	99	7	492	616
3	4	1	7	10	4	3	0	3	2	4	1	16	3	55	80
4	1	0	2	0	0	1	1	2	1	0	1	2	3	11	8
5	0	0	1	0	1	0	0	0	1	0	0	0	2	3	0.6
6	0	0	0	0	0	0	0	0	1	1	1	0	1	3	0.03
7	0	0	0	0	0	0	0	0	0	0	0	0	1	0	$\sim 10^{-3}$
8	0	0	0	0	0	0	0	0	0	0	0	0	1	0	$\sim 10^{-4}$
9	0	0	0	0	0	0	0	0	0	0	0	1	1	1	$\sim 10^{-6}$
10	0	0	0	0	0	0	0	0	0	0	0	0	1	0	$\sim 10^{-7}$
11	0	0	0	0	0	0	0	0	1	0	0	0	2	1	$\sim 10^{-8}$
12	0	0	0	0	0	0	0	0	0	0	0	0	2	0	$\sim 10^{-10}$
13	0	0	0	0	0	0	0	0	1	0	0	0	1	1	$\sim 10^{-11}$
14	0	0	0	0	0	0	0	0	0	0	0	0	0	0	$\sim 10^{-13}$
15	0	0	0	0	0	0	0	0	0	0	0	0	5	0	$\sim 10^{-14}$
16	0	0	0	0	0	0	0	0	0	0	0	0	2	0	$\sim 10^{-16}$
17	1	0	0	0	0	0	0	0	0	0	0	0	1	0	$\sim 10^{-18}$
18	1	0	0	0	0	0	0	0	0	0	0	0	1	0	$\sim 10^{-20}$
19	1	0	0	0	0	0	0	0	0	0	0	0	1	0	$\sim 10^{-21}$
20	0	0	0	0	0	0	0	0	0	0	0	0	0	0	$\sim 10^{-22}$

TABLE VI

Frequency Distribution of Counts from Deuterated Zr Ti Sponge
Counting Interval 20 ms

Multiplicity of counts	Frequency BF_3 background	Frequency He^3 signal
0	67778	67493
1	281	557
2	5	11
3	0	5
4	0	2
5	0	0
6	0	0

Tables VI & VII summarise the results of multiplicity distribution measurements carried out with two D_2 gas loaded Ti targets. During the weekend run of 9th to 11th June, 1989 with 15 grams of Ti-Zr deuteride (see Table VI) the average count rate measured was only 0.42 cps. Since this corresponds to an $(N_0 \tau)$ value of 0.008, we expect a doubles to singles ratio of 0.004 only. While the relatively high doubles events in both the background and the signal counter could possibly be attributed to statistics, or cosmic ray induced events the 3s and 4s in the He^3 detector viewing the target can only be attributed to high multiplicity neutron emissions in the deuterated Ti- Zr target. Absence of such high multiplicity events in the background channel further strengthens this conjecture. Table VII presents a similar result from a D_2 loaded Ti disc target. As may be seen from Fig. 2, the neutron active phase of this target lasted almost 85 minutes during which it

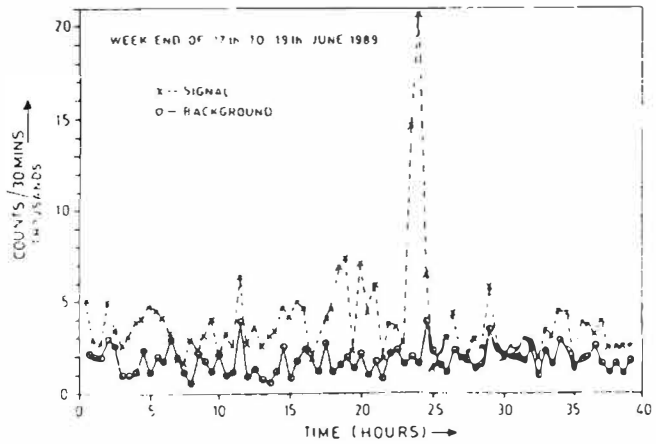

Fig.2. Neutron Output from a Deuterated Ti Disc.

is estimated to have emitted 5×10^5 neutrons in all. On the whole this target also points to the occurrence of a significant number of high multiplicity neutron emission events.

The last columns of Tables IV, V and VII give the total frequency distribution for the entire duration i.e. the sum of all the columns. Also shown are the theoretical frequency distributions expected on the basis of Poisson statistics. It is worth noting that except for the background case (Table II),in all the cold fusion measurements the observed frequencies fall according to the Poisson law for low multiplicity events but there is a distinct tendency for them to show a slight peak between the multiplicities of 4 and 6. If we assume that this peak is due to the superposition of bunched neutronic events on a Poisson background, we deduce the value of ν to be in the range of 400 to 600 since the peak of the

Table VII

Frequency Distribution of Counts from a Deuterated Disc for 1000 Sampling Intervals of 20 ms Each During Periods of High Neutronic Activity

Multiplicity of counts	Frequency A	B	C	D	E	F	G	H	I	J	K	L	M	N	O	P	Q	Total(A to Q) Obs.	Exp.
1	11	9	7	8	4	9	0	20	32	50	36	37	42	26	38	33	23	385	440
2	0	0	0	0	0	0	1	0	1	1	0	0	2	1	2	2	0	10	6
3	0	1	0	0	0	0	2	0	0	0	0	0	0	0	0	0	0	3	0.05
4	0	0	1	1	0	0	1	0	0	0	0	0	1	0	0	0	0	4	10^{-4}
5	0	0	0	0	1	0	1	0	0	0	0	0	0	0	0	0	0	2	10^{-6}
6	0	0	0	0	0	1	1	0	0	0	0	0	0	0	0	0	0	2	10^{-8}

binomial distribution occurs at the multiplicity value of the product $\nu\varepsilon$ and ε values in the experiment are typically ~ 0.01. Further, since the expected frequency of high multiplicities is given by $S_b \tau J$, where J is the total number of sampling intervals, we deduce that the average source event rate S_b for such events during the neutron emitting phase is very roughly about 10^{-2} per second.

In summary the multiplicity distribution of counts in 20 ms intervals has so far been measured six times during cold fusion experiments. While the background displays strictly Poisson behaviour, in the three experiments where distinct excess over background was recorded, between 10 and 25% of the neutrons appear to display high multiplicity characteristics. The observed frequency distributions can be explained as being due to bunched neutronic events superposed over a Poissonian background. Such occasional neutron bursts resulting in several hundred neutrons have also been observed by Menlove [13].

The duration of the counting interval selected viz ~20 ms was a compromise between the total volume of data required to be stored and the time resolution. Ideally the counting interval should have been of the order of the neutron die-away time in the moderator detector assembly to ascertain whether the "neutron bunches" are spread out over the entire 20 ms interval duration or whether they are in fact emitted in micro second time scales. Better time resolution is therefore called for and one of the simplest techniques, for achieving this, viz the artificial dead time method [14-15] is described in the following section.

THE ARTIFICIAL DEAD TIME METHOD

This technique was first introduced by Jacquesson [14] for estimation of the fraction of Pu^{240} in a sample and independently by Srinivasan [15] for measuring α the prompt neutron decay constant of a reactor assembly. It has since been developed as into field unit for nondestructive assay of plutonium [16]. In its simplest form the method consists of feeding the pulse train from a detector monitoring the test source to two scalers in parallel. While the pulses reach the first scaler directly, they are filtered through an artificial dead time unit before being fed to the second scaler. In this process the second scaler records a count rate lower than the first as some of the counts are lost during the dead time. In what follows we derive an expression [17] for the dead time filterd count rate and show how it is possible to distinguish between random Poisson events and bunched events and to deduce therefrom the fraction f_n of neutrons emitted in bunches.

Theory

We assume that during each counting time interval employed, the source event rate S for production of neutrons (be it in singlets or in multiplets) does not vary with time and can be described as a stationary Poisson process. It is then permissible to use the formula derived in [18] for the count rate as a function of dead time. It was shown there that in the presence of a dead time of the extendable type the observed count rate N_d is given by

$$N_d = \left\{ S \sum_{r=0}^{\infty} \frac{(-1)^r \varepsilon^{r+1}}{(r+1)!} M_{r+1} \left(1 - e^{-\lambda d}\right)^r \right\}$$

$$\exp\left[S \sum_{r=1}^{\infty} \frac{(-1)^r \varepsilon^r}{r!} M_r \left\{ \sum_{\ell=1}^{r} (-1)^{\ell} \binom{r}{\ell} \left(\left(\frac{1}{r} - \frac{1}{\ell}\right) e^{-\ell\lambda d} + \frac{1}{\ell} \right) + \lambda d + \left\{ \frac{1}{r} \right\} \right] \right\} \quad (6)$$

where ε is the detection efficiency, M_r the r th factorial moment of the multiplicity distribution of source neutrons, λ the inverse of the neutron die-away time and d the artificial dead time introduced. In the kind of situation encountered in cold fusion experiments, the count rates are rather small compared to λ ($1/\lambda$ is typically 25-60 μs). Hence the argument of the exponential (in square brackets) is very small and the exponential may be set equal to unity. Moreover, if we choose the dead time d such that $\lambda d > 3$, the above expression reduces to

$$N_d = S\varepsilon M_1 - \frac{S\varepsilon^2 M_2}{2!} + \frac{S\varepsilon^3 M_3}{3!} - \cdots \quad (7a)$$

or

$$\frac{N_d}{N_0} = 1 - \frac{\varepsilon M_2}{2!M_1} + \frac{\varepsilon^2 M_3}{3!M_1} - \cdots \quad (7b)$$

where we have written N_0 for $S\varepsilon\nu$, the count rate in the absence of dead time.

The factorial moments M_ν can now be written in terms of the individual source event rates S_1 and S_b and the factorial moments of the multiplicity distribution of bunched neutron emision viz $\bar{\nu}$, $\overline{\nu(\nu-1)}$ etc. as follows:

$$M_1 = \frac{S_1 + \bar{\nu}S_b}{S_1 + S_b} = 1 - f_e + \nu f_e \quad (8a)$$

$$M_2 = \frac{\overline{\nu(\nu-1)}S_b}{S_1 + S_b} = \overline{\nu(\nu-1)}f_e \quad (8b)$$

$$M_3 = \frac{\overline{\nu(\nu-1)(\nu-2)}S_b}{S_1 + S_b} = \overline{\nu(\nu-1)(\nu-2)}f_e \quad (8c)$$

As noted earlier, f_e represents the fraction of events that result in neutron bunches. Eq. (7b) can then be rewritten as follows

$$\frac{N_d}{N_0} = 1 - \frac{\varepsilon\overline{\nu(\nu-1)}f_e}{2!(1-f_e+\bar{\nu}f_e)} + \frac{\varepsilon^2\overline{\nu(\nu-1)(\nu-2)}f_e}{3!(1-f_e+\bar{\nu}f_e)} - \cdots \quad (9)$$

or

$$\left[1 - \frac{N_d}{N_0}\right] = \left(\frac{f_e}{1-f_e+\bar{\nu}f_e}\right)\left[\frac{\varepsilon\overline{\nu(\nu-1)}}{2!} - \frac{\varepsilon^2\overline{\nu(\nu-1)(\nu-2)}}{3!} + \cdots\right] \quad (10)$$

If $\bar{\nu} \gg 1$ it may be permissible to approximate $\overline{\nu(\nu-1)}$, $\overline{\nu(\nu-1)(\nu-2)}$ etc by $\bar{\nu}^2$, $\bar{\nu}^3$ etc. Writing simply ν instead of $\bar{\nu}$ and summing the resulting power series we get

$$\left[1 - \frac{N_d}{N_0}\right] = f_n\left[1 - \frac{1 - e^{-\nu\varepsilon}}{\nu\varepsilon}\right] \quad (11)$$

It is clear from Eq. (11) that the fractional loss of counts $[1-N_d/N_0]$, which represents the deviation from Poisson behaviour, is a product of two factors : the first being f_n, the fraction of neutrons that are emitted in bunches and the second being dependent on the product $\nu\varepsilon$. Interestingly, the dependence on $\nu\varepsilon$ is similar to the dependence of the variance/mean ratio (of reactor noise theory) on the product αt. The fractional loss of counts increases with all the three parameters viz f_n, ν and ε. In Fig. 3 we show the variation of the fractional loss of counts $[1-N_d/N_0]$ with the product $\nu\varepsilon$ for various values of f_n.

In the above derivation it was assumed that the dead time introduced is of the extendable type. However under the conditions prevailing in cold fusion experiments, viz a count rate that is very small compared to λ and $\lambda d > 3$, it turns out that Eq. (11) is valid irrespective of whether the dead time is of the extendable or the non-extendable type.

Discussion

It is clear that by simply using two scalers one without any dead time and the other with an artificial dead time filter of ~50-100 μs it is possible to distinguish between the two kinds of events. Since the fraction of neutrons which are emitted in bunches in cold fusion experiments appears to be in the region of 0.1 to 0.25, the magnitude of the product $\nu\varepsilon$ required to give measureable values of fractional count loss (> 0.05) can be seen from Fig. 3 to be about 3.0. Since ν in these experiments is found to be about 400 - 600 neutrons, we conclude that an efficiency in the region of ~ 1 (which is easy to achieve) should be adequate to give measurable results. The method has the advantages of simplicity but the amount of information

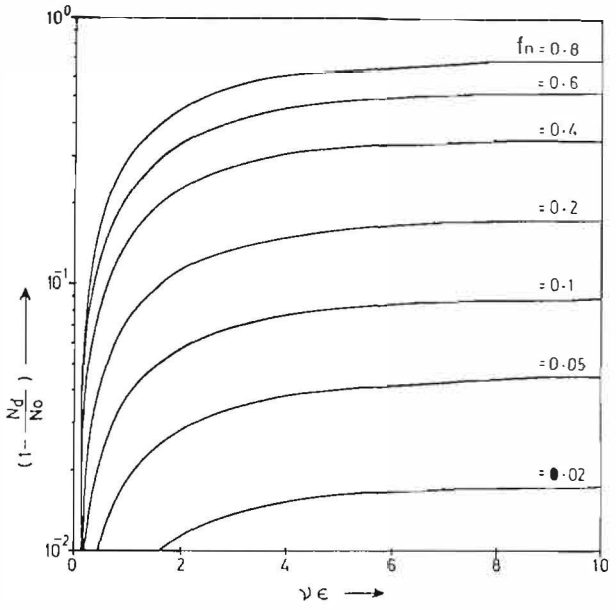

Fig.3. Variation of $(1-N_d/N_o)$ with $\nu\epsilon$

available is less than that from a full multiplicity spectrum measurement, since only two quantities viz N_0 and N_d are measured and therefore it is not possible to uniquely derive either f_n or ν. This is in contrast to the passive neutron assay problem where it is possible to derive the spontaneous fission rate and (α,n) rate even with two measurements because there the multiplicity distribution of spontaneous fission neutron emission is well known. However by conducting the experiment with two different values of the detection efficiency ε, it should be possible to derive both the parameters ν and ε. The choice of the two values of ε should be such that while one results in a fractional count loss comparable to f_n the other gives about half this value.

REFERENCES

1. M. Fleischmann and S. Pons, "Electrochemically Induced Nuclear Fusion of Deuterium", J. Electroanal. Chem. 261, 301 (1989)
2. S.E. Jones et al, "Observation of Cold Nuclear Fusion in Condensed Matter", Nature 338, 737 (1989)
3. M.W. Guinan, G.F. Chapline and R.W. Moir "Catalysis of Deuterium Fusion in Metal Hydrides by Cosmic Ray Muons", UCRL preprint 100881 (1989)
4. Report on the Workshop on Cold Fusion held at Santa Fe, Mexico, USA during May 1989, Science News, June 3, (1989)
5. J. Rafelski et al, "Nuclear Reactions Catalyzed by a Massive Negatively Charged Particle" To appear in Fus. Tech. (1989)
6. T. Takeda and T. Takizuka, "Fractofusion Mechanism", J. Phys. Soc of Japan, 58, 3073 (1989)
7. P.L. Hagelstein, "Status Report on Cold Fusion Theory" Proc. 1 st Annual Conf. on Cold Fusion, Salt Lake City, Utah (1990)
8. P.K.Iyengar and M.Srinivasan, "Overview of BARC Studies in Cold Fusion", Proc. 1 st Annual Conf. on Cold Fusion, Salt Lake City, Utah, (1990)
9. R.E.Uhrig, "Random Noise Techniques in Nuclear Reactor Systems", Ronald Press, New York (1970)
10. N.Ensslin, M.L. Evans, H.O. Menlove, and J.E.Swansen, "Neutron Coincidence Counters for Plutonium Measurement", Nucl. Mat. Mgmnt. Summer Isuue (1978)
11. M.S. Krishnan et al. "Cold Fusion Experiments Using a commercial Pd-Ni Electrolyser", To appear in Fusion Tech. (Aug. 1990)
12. V.S. Srikande and K.C. Mittal,"Deuteration of Titanium Targets for Cold Fusion Experiments" To appear in Fusion Tech. (Aug. 1990)
13. H. Menlove, "High Sensitivity Measurements of Neutron Emission from Ti Metal in Pressurised D_2 gas" Proc. 1 st Annual Conf. on Cold Fusion, Salt Lake City, Utah (1990)
14. J.Jacquesson J. Phys 24 Suppl to No. 1 112-116A (1963)
15. M. Srinivasan, "On the Measurement of α by a Simple Dead Time Method", Nucleonik 10, 224 (1967)
16. G. Birkhoff, L. Bondar and N. Coppo, Report EUR-4801e (1972)
17. S.B. Degweker and M. Srinivasan, "A Simple Dead Time Method for Measuring the Fraction of Bunched Neutronic Emission in Cold Fusion Experiments", Submitted for publication to Ann. Nucl. Energy (1990))
18. S.B.Degweker, "Effect of Deadtime on the Statistics of Time Correlated Pulses: Application to the Passive Neutron Assay Problem",Ann.Nucl. Energ. 16, 409 (1989)

THE EFFECT OF VELOCITY DISTRIBUTION AND ELECTRON SCREENING ON COLD FUSION

Robert A. Rice, Gary S. Chulick, and Yeong E. Kim

Department of Physics
Purdue University
West Lafayette, Indiana 47907

ABSTRACT

It is demonstrated that electron screening, in combination with a particle velocity distribution, greatly enhances the cross sections and reaction rates for deuteron–deuteron (D–D) and proton–deuteron (p–D) fusion for low kinetic energies ($E \leq 20$ eV, center of mass frame). p–D fusion rates are shown to be comparable to D–D fusion rates for $E \sim 10$ eV, so that in electrolysis experiments with equal amounts of H and D, p–D fusion should compete with D–D fusion as a reaction mechanism.

I. INTRODUCTION

Recently, the effect of a velocity distribution [1] in the context of a surface reaction mechanism [2,3] was shown to be very important in reducing the discrepancy between the electrolysis fusion results [4-9] and the conventional estimates [10-11] of cold fusion rates. More recently, it has been suggested [12] that the effect of electron screening may become significant at low energies and further reduce the discrepancy. In this paper, we present results of our detailed calculations of the deuterium–deuterium (D–D) and proton–deuterium (p–D) fusion rates including both a velocity distribution and electron screening. In section II, definitions and expressions for the Coulomb barrier penetration factor, fusion cross sections and fusion rates are described. In section III, the calculated results are presented and discussed. Finally, section IV contains conclusions.

II. THEORETICAL FORMULATION

Three dominant fusion reactions occurring at low energies are

$$D^+ + D \rightarrow {}^3H(1.01\text{MeV}) + p(3.02\text{MeV}) \ , \quad (1a)$$

$$D^+ + D \rightarrow {}^3\text{He}(0.82\text{MeV}) + n(2.45\text{MeV}) \ , \quad (1b)$$

and

$$\begin{aligned} H^+ \ + \ D &\rightarrow {}^3\text{He} + \gamma(5.5\text{MeV}) \\ \left(\text{or } D^+ \ + \ H \right. &\left. \rightarrow {}^3\text{He} + \gamma(5.5\text{MeV})\right) \end{aligned} \quad (1c)$$

Reaction (1a) is not a "real" fusion reaction but a neutron–transfer reaction, while reaction (1b) is a fusion reaction in which two protons are fused to form a ^{3}He nucleus. Because of the complexity of the four–nucleon system, no rigorous theoretical calculations of the D–D fusion rates and branching ratios and of the H–D fusion rates have been carried out at low positive energies. Since there are no direct measurements of the fusion cross sections, $\sigma(E)$, for reactions (1a) and (1b), below $E_D \lesssim 4$ keV (laboratory (LAB) frame), and for reaction (1c) below $E_H \lesssim 24$ keV (LAB), $\sigma(E)$ has to be extrapolated using the measured values of $\sigma(E)$ at higher energies as is conventionally done in astrophysical calculations [13,14] for $kT \gtrsim 1.5$ keV. In our case, an extrapolation down to the order of 10 eV is required. We describe in the discussion below the extrapolation method used in the astrophysical calculations [13,14] which assumes equal branching ratios for reactions (1a) and (1b). In the following, a theoretical formulation will be given in detail only for reactions (1a) and (1b), as it is similar to that for reaction (1c).

II.1. Velocity Distribution

Since the precise form of the D^+ velocity distribution in electrolysis experiments is not known at present, we will assume a Maxwell–Boltzmann distribution with and without a cut–off for high velocity components. The temperature term, k_BT, will be replaced by the "average" kinetic energy, E_{DD}, in the center of mass (CM) D–D frame, which is related to the most probable velocity v (CM) by $E_{DD} = \frac{M}{2}v^2$ (CM) with the reduced mass $M = M_D/2$.

For a Maxwell–Boltzmann velocity distribution,

the D–D fusion rate, Λ ($\sec^{-1}/D$–D pair), for reaction (1a) or (1b) is given by [13,14]

$$\Lambda\,(E_{DD}) = \frac{n_D}{2}\,\langle\sigma v\rangle\ , \tag{2}$$

with

$$\langle\sigma v\rangle = \frac{(8/\pi)^{1/2}}{M^{1/2}(E_{DD})^{3/2}}\int_0^{E_c}\sigma(E)E\,e^{-E/E_{DD}}dE\ , \tag{3}$$

where the cross section, $\sigma(E)$, has been parameterized as [13]

$$\sigma(E) = \frac{S(E)}{E}\,e^{-(E_G/E)^{1/2}} \tag{4}$$

which is the conventional form assuming (1a), (1b), and (1c) are non–resonant charged particle reactions. E_G is the "Gamow energy" given by $E_G = (2\pi\alpha Z_D Z_D)^2\ Mc^2/2$ or $E_G \approx 31.39\ (keV)^{1/2}$ with the reduced mass $M \approx M_D/2$ for reactions (1a) and (1b) and $E_G^{1/2} = 25.64\ (\text{keV})^{1/2}$ for reaction (1c) with the reduced mass $M = m_p M_D/(m_p + M_D) \approx M_D/3$. E is in units of keV in the center of mass (CM) reference frame. The S–factor, $S(E)$, is extracted from the experimentally measured values [15,16] of the cross section, $\sigma(E)$, for $E \gtrsim 4$ keV and is nearly constant [13,16], $S(E) \approx 52.9\ \text{keV} - b$, for both reactions (1a) and (1b) in the energy range of interest here, $E \lesssim 1$ keV. For reaction (1c), $S(E) \approx 2.50 \times 10^{-4}\ \text{keV} - b$ [13]. The deuterium density n_D is assumed to be $\sim 6\times10^{22}\ cm^{-3}$. E_C in eq. (3) is the upper integration limit beyond which the high velocity components are cut off. With a Taylor series expansion of $S(E)$ [13]

$$S(E) \approx S(O) + S'(O)E + \frac{1}{2}\,S''(O)E^2\ , \tag{5}$$

the integral in eq. (3) can be carried out numerically.

For a sharp velocity distribution, which has been used in the argument against the possibility of D–D fusion at room temperature, the D–D fusion rate ($\sec^{-1}/D$–D pair), Λ_δ, is given by

$$\Lambda_\delta(E) = \frac{n_D}{2}\,\sigma(E)v(CM) \tag{6}$$

where $E = E_{DD} = \frac{M}{2}\,v^2(CM) = \frac{M_D}{4}\,v^2(LAB) = \frac{1}{2}\,E_D(\text{LAB})$, and $\sigma(E)$ is from eq. (4).

II.2. Electron Screening Effect

In electrolysis fusion experiments and other fusion processes, D^+ is incident on D, which is shielded by electron clouds and is electrically neutral outside the electron screening range, r_s. The expression for $\sigma(E)$ given by eq. (4) is derived for the case in which one D^+ is incident on another D^+. Therefore, the Coulomb barrier penetration factor ("Gamow factor") in eq. (4)

$$P_G(E) = \exp\left(-(E_G/E)^{1/2}\right) \tag{7}$$

is appropriate only for the $(D^+ + D^+)$ reaction and needs to be modified for the case of $(D^+ + D)$ in reactions (1a) and (1b), and for the case of $(D^+ + H)$ in reaction (1c). The modified Coulomb barrier penetration factor, $P_s(E)$, is the probability of tunneling through the barrier to reach the nuclear surface and can be computed from solutions of the Schroedinger equation for a $(D^+ + D)$ system in which an attractive Coulomb potential $V_s(r)$ due to the presence of shielding electrons is included with the original repulsive Coulomb potential between two D^+'s (two protons).

The modified Coulomb barrier penetration factor, $P_s(E)$, which includes the effect of $V_s(r)$, can be calculated in the Wentzel–Kramers–Brillouin (WKB) approximation as

$$P_s(E) = \exp\left[-2\left(\frac{2M}{\hbar^2}\right)^{1/2}\int_{r_N}^{r_a}(V_c(r) + V_s(r) - E)^{1/2}dr\right] \tag{8}$$

where $V_c(r)$ is the repulsive Coulomb potential between two D^+'s,

$$V_c(r) = \frac{Z_D Z_D e^2}{r}\ , \tag{9}$$

and $V_s(r)$ is the potential due to the shielding electrons. The effective nuclear interaction range, $r_N \approx 8F$ (twice the deuteron radius), can be set to zero in eq. (8) without loss of accuracy. The integral in eq. (8) cannot be carried out analytically in general, but can be written for an attractive potential, $V_s(r) < 0$, as

$$2\left(\frac{2M}{\hbar^2}\right)^{1/2}\int_0^{r_a}(V_c(r) + V_s(r) - E)^{1/2}dr = \frac{(E_G)^{1/2}}{(E + E_s(E))^{1/2}} \tag{10}$$

where $E_s(E)$ is determined by carrying out the integral numerically for each value of $E > 0$. The modified penetration factor, $P_s(E)$, is then given by

$$P_s(E) = \exp\left(-E_G^{1/2}/(E + E_s(E))^{1/2}\right) . \quad (11)$$

When $V_s(r) = 0$, $E_s(E)$ vanishes, and we recover the conventional Gamow factor, $P_s(E) = P_G(E)$, given by eq. (7).

The classical turning point, r_a in eq. (8), is determined by

$$V_c(r_a) + V_s(r_a) = E . \quad (12)$$

From eqs. (10) and (12), it can be easily shown that $E_s(E)$ in eqs. (10) and (11) satisfies $|V_s(r_a)| < E_s(E) < |V_s(0)|$ [12]. Using $P_s(E)$, the new extrapolation formula appropriate for reactions (1a), (1b), (1c), and other fusion reactions can now be written as

$$\sigma_s(E) = \frac{S(E)}{E} \exp\left(-E_G^{1/2}/(E + E_s(E))^{1/2}\right) . \quad (13)$$

The parameterization [13] of $S(E)$ used in eq. (4) can also be used in eq. (13), since $S(E)$ is determined from the measured cross sections at higher energies $E \gg E_s(E)$ where the electron screening effect is negligible.

The screening energy term $E_s(E)$ can be extracted from the measured values [15,16] of $\sigma_{\rm exp}(E)$ for reaction (1a), $D(D,p)^3$H. The values of $E_s(E)$ extracted from $\sigma_{\rm exp}(E < 4$ keV$(CM))$ [15,16] using eq. (13) are $(40 - 60)$ eV [12] and have large uncertainties. Therefore, it is important to carry out precise measurements of $\sigma_{\rm exp}(E)$ with improved accuracies for $E < 4$ keV(CM). The experimental values $\sigma_{\rm exp}(E)$ [15,16] were measured with D_2 gas targets for which the electron screening potential is expected to be approximately that of the $1s$ hydrogen electron with $E_s(E) = e^2/a_0 \approx 27$ eV. However, for solid targets such as TiD and PdD, the electron screening range could be as small as a tenth of the Bohr radius, $a_0/10 \approx 0.05$ Å [17]. Thus the extracted values of $E_s(E)$ from solid metal deuteride targets may be up to ten times ($E_s(E) \approx 300$ eV) larger than values ($E_s(E) \approx 40 - 60$ eV) extracted from D_2 gas targets [15,16].

For the case of the Yukawa screening potential, $V(r) = (Z_D Z_s e^2/r)e^{-r/r_s}$, the electron screening potential is given as

$$V_s(r) = V(r) - V_c(r) = -\frac{Z_D Z_s e^2}{r}\left(1 - e^{-r/r_s}\right) . \quad (14)$$

Since the magnitude of $V_s(r)$ decreases monotonically from a maximum value of $|V_s(0)|$ to $|V_s(r_a)|$ as r increases from 0 to r_a, $E_s(E)$ is bounded by

$$\frac{Z_D Z_s e^2}{r_a}\left(1 - e^{-r_a/r_s}\right) < E_s(E) < \frac{Z_D Z_s e^2}{r_s} . \quad (15)$$

The recent elaborate calculations [17,18] yield $r_s \gtrsim 0.05$ Å. $r_s \approx 0.05$ Å for TiD and PdD can be justified also on physical grounds since the electron number density in the solid phase is expected to be 10^3 times larger than that in the gas phase; hence a radius scale such as r_s is expected to be 10 times smaller.

Since the precise form of the effective electron screening potential, $V_s(r)$, will depend on experimental conditions and is not yet known, we shall use a simple potential of the form

$$V_s(r) = -\frac{Z_D Z_s}{r_s}\Theta(r_a - r) \quad (16)$$

which has one parameter Z_s/r_s, where Z_s is the effective electron charge and r_s is the screening radius. $V_s(r)$ given by eq.(16) can be generated from a spherical shell charge distribution, $\rho_e = (Z_s e/4\pi r_s r_a)\delta(r - r_a)$. When $V_s(r)$ given by eq. (16) is used in eq. (8), the penetration factor becomes

$$\tilde{P}_s(e) = \exp\left(-E_G^{1/2}/(E + \tilde{E}_s)^{1/2}\right) \quad (17)$$

where $\tilde{E}_s = Z_D Z_S e^2/r_s = E_s(E)$. Equation (17) has previously been used for D_2 molecular fusion calculations [11] and for the analysis of D_2O cluster fusion [19]. Finally, for the screening potential of eq. (16), eq. (13) becomes

$$\sigma_s(E) = \frac{S(E)}{E} \exp\left(-E_G^{1/2}/\left(E + \tilde{E}_s\right)^{1/2}\right) . \quad (18)$$

III. RESULTS

We calculate the fusion cross sections and reaction rates, σ_{DD} (E_{DD}) and $\Lambda_{DD}(E_{DD})$, using eqs. (18) and (2), respectively, for reactions (1a) and (1b) for $\tilde{E}_s = 0, 1, 4$, and 10 e^2/a_0. n_D is assumed to be 6×10^{22} cm^{-3} and the parametric values for $S(E)$

given in reference 13 are used in eq. (18). The calculated results for $\sigma_{DD}(E_{DD})$ and $\Lambda_{DD}(E_{DD})$ are plotted as functions of $E_{DD} \leq 20$ eV in Figs. 1 and 2, respectively; $\Lambda_{DD}(E_{DD})$ is for the sum of reactions (1a) and (1b), assuming equal branching ratios. In evaluating $\Lambda_{DD}(E_{DD})$, the cut-off energy E_c in eq. (3) is assumed to be infinite. The case where $\tilde{E}_s = 0$ in Figs. 1 and 2 corresponds to the use of the conventional Gamow factor, eq. (7), as in eq. (4). As can be seen from Figs. 1 and 2, the electron screening effect ($\tilde{E}_s \neq 0$) becomes increasingly significant for $\sigma_{DD}(E_{DD})$ and $\Lambda_{DD}(E_{DD})$ for reactions (1a) and (1b), as E_{DD} decreases below 20 eV.

In order to study the effect of the velocity distribution, we calculate the fusion rates $\Lambda_\delta(E_{DD})$ with a sharp (delta function) velocity distribution using eq. (6) for reactions (1a) and (1b). The calculated results for $\Lambda_\delta(E_{DD})$ with $\tilde{E}_s = 0$, 4, and 10 e^2/a_0 are plotted and compared in Fig. 3 with the corresponding cases of $\Lambda_{DD}(E_{DD})$ with a Maxwell-Boltzmann velocity distribution. As can be seen from comparing Λ_δ and Λ_{DD} in Fig. 3, the effect of the velocity distribution becomes increasingly important as E_{DD} decreases, but is less so as $\tilde{E}_s$ increases for reactions (1a) and (1b).

To study the effect of introducing a high-energy cut-off (E_c in eq. (3)) for the Maxwell-Boltzmann velocity distribution, we calculate the fusion rates $\Lambda_{DD}(E_{DD})$ of eq. (2) for the sum of reactions (1a) and (1b) as a function of E_c for the cases $E_{DD} = 5$ and 10 eV with $\tilde{E}_s = 0$, 4, and 10 e^2/a_0 in eq. (18). The calculated results are plotted in Fig. 4. As can be seen from Fig. 4, the effect of a cut-off in the velocity distribution is substantially less for the case of $\tilde{E}_s = 10\ e^2/a_0$ than for the case of $\tilde{E}_s = 0$ (no electron screening effect).

For reaction (1c), we calculate the fusion cross section and rates, $\sigma_{pD}(E_{pD})$ and $\Lambda_{pD}(E_{pD})$, using eqs. (18) and (2), respectively, with the replacements of $n_D/2$ in eq. (2) and M and E_{DD} in eq. (3) by n_H, $M = m_p M_D/(m_p + M_D) \approx M_D/3$, and $E_{pD}(CM)$, respectively. Parametric values of $\tilde{E}_s = 0$, 1, 4, and 10 e^2/a_0 are used. n_H is assumed to be $n_H = n_D = 6 \times 10^{22}\ cm^{-3}$, and the parametric values for $S(E)$ for reaction (1c) given in reference 13 are used in eq. (18). E_c in eq. (3) is set to infinity. The calculated results for $\sigma_{pD}(E_{pD})$ and $\Lambda_{pD}(E_{pD})$ are plotted in Figs. 5 and 6, respectively. The $\tilde{E}_s = 0$ case in Figs. 5 and 6 corresponds to the use of the conventional Gamow factor,

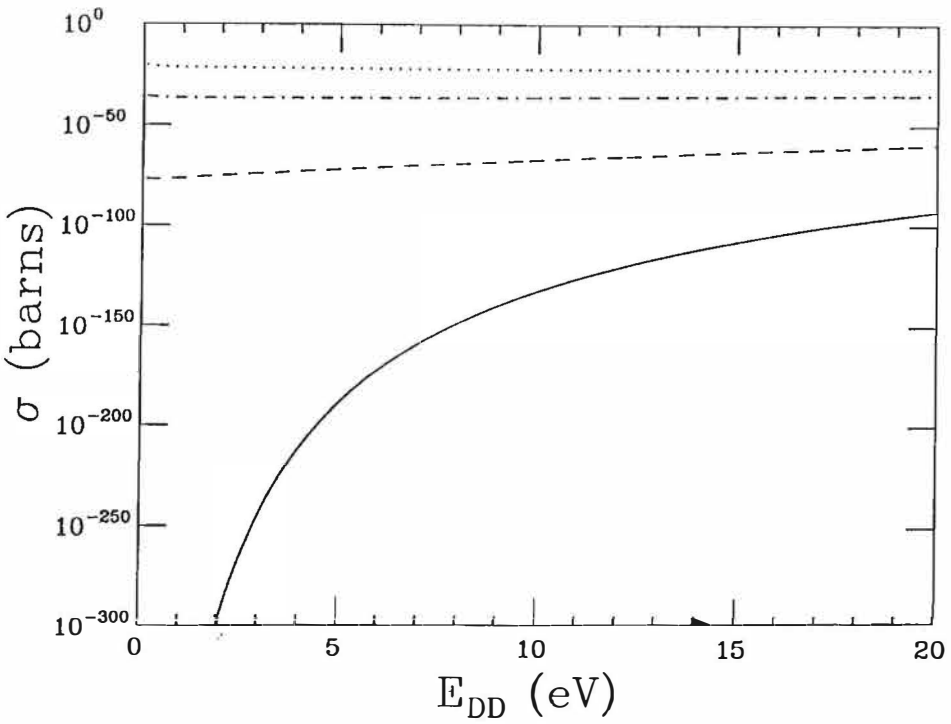

Fig. 1. The calculated cross sections $\sigma_{DD}(E_{DD})$ for reactions (1a) and (1b), $D(D,p)^3H$ and $D(D,n)^3$He, for $E_{DD} \leq 20$ eV with $\tilde{E}_s = 0$, 1, 4, and 10 e^2/a_0. $e^2/a_0 = 27.17$ eV with $a_0 = 0.53$ Å. In this and subsequent figures, the solid, dashed, dash-dotted, and dotted lines refer to the results of calculations using $\tilde{E}_s = 0$, 1, 4, and 10 e^2/a_0, respectively.

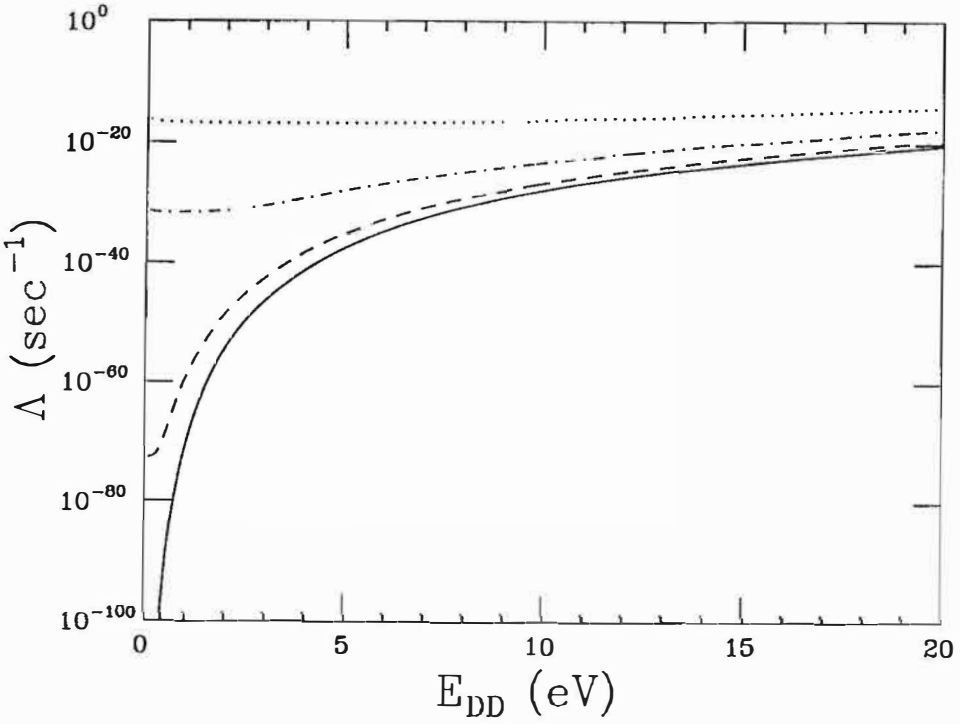

Fig. 2. The calculated fusion rates $\Lambda_{DD}(E_{DD})$ for reactions (1a) and (1b), $D(D,p)^3H$ and $D(D,n)^3$He, for $E_{DD} \leq 20$ eV with $\tilde{E}_s = 0$, 1, 4, and 10 e^2/a_0.

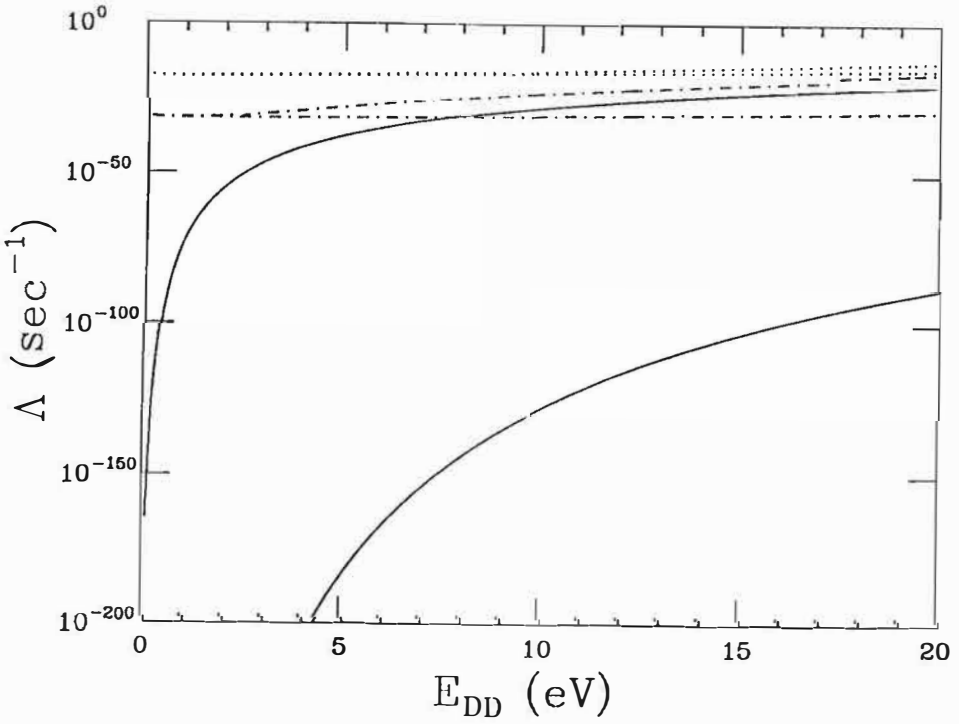

Fig. 3. Comparison of the D–D fusion rates $\Lambda_{DD}(E_{DD})$ with a Maxwell–Boltzmann velocity distribution (upper curve in each pair) and the D–D fusion rates $\Lambda_{\delta}(E_{DD})$ with a sharp velocity distribution (lower curve in each pair) with $\tilde{E}_s = 0$, 4, and 10 e^2/a_0. $E_{DD} < 20$ eV.

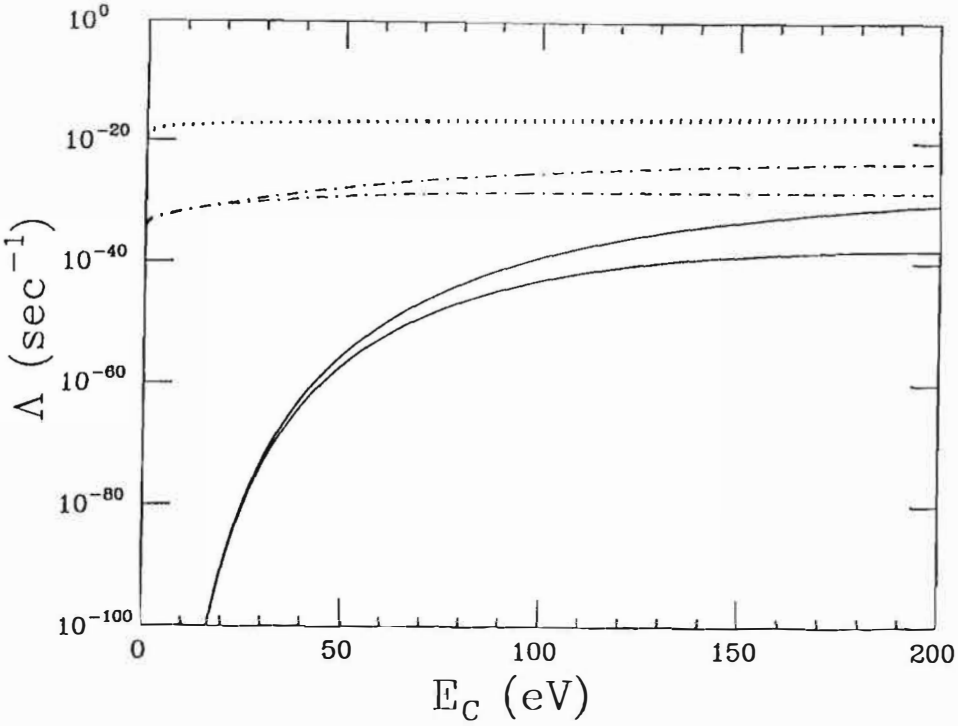

Fig. 4. The calculated D–D fusion rates $\Lambda_{DD}(E_{DD})$ as a function of the cut–off energy E_c with a Maxwell–Boltzmann velocity which is cut off above $E = E_c$. $E_{DD} = 5$ (lower curve in each pair) and 10 eV (upper curve in each pair) with $\tilde{E}_s = 0$, 4, and 10 e^2/a_0 are shown.

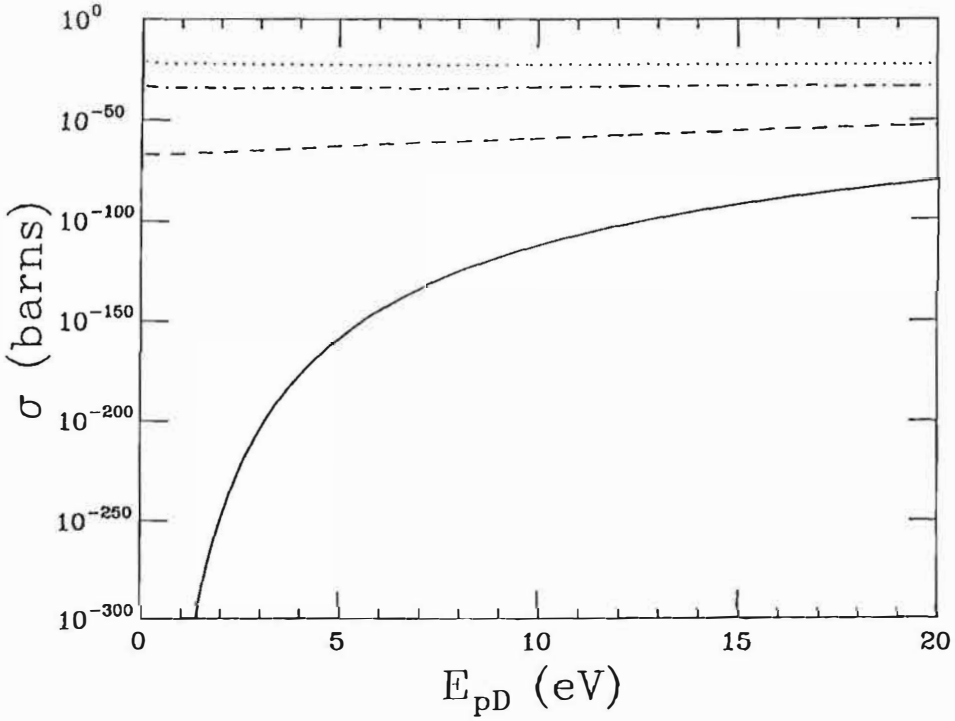

Fig. 5. The calculated cross sections $\sigma_{pD}(E_{pD})$ for reaction (1c), $D(p,\gamma)^3$He, for $E_{pD} \leq 20$ eV with $\tilde{E}_s = 0$, 1, 4, and 10 e^2/a_0.

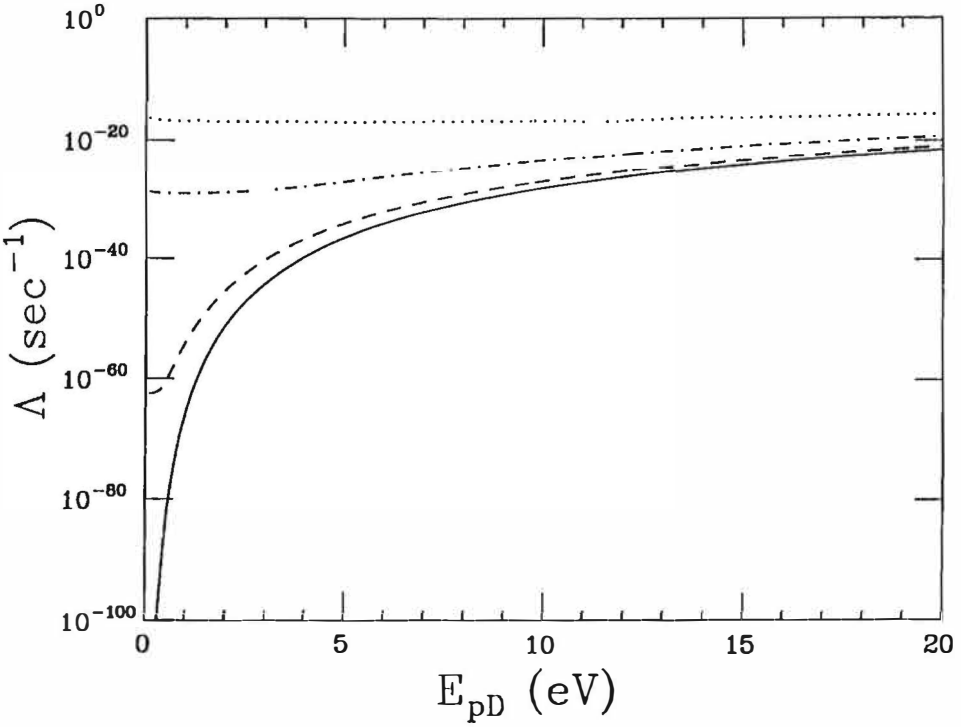

Fig. 6. The calculated fusion rates $\Lambda_{pD}(E_{pD})$ for reaction (1c), $D(p,\gamma)^3$He, for $E_{pD} < 20$ eV with $\tilde{E}_s = 0$, 1, 4, and 10 e^2/a_0.

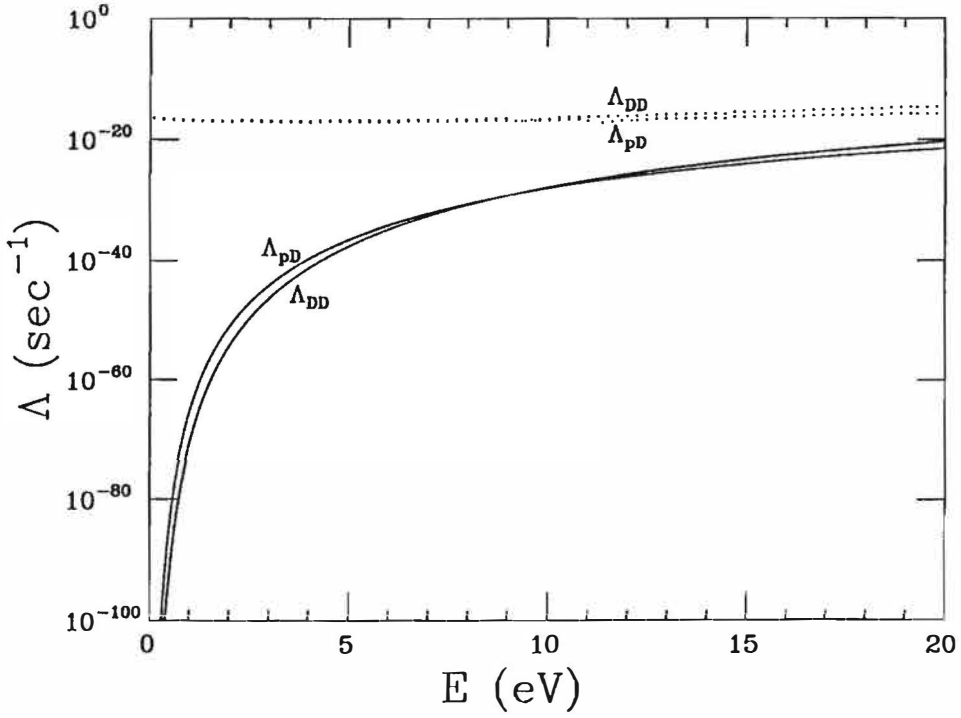

Fig. 7. Comparison of the p–D fusion rates $\Lambda_{pD}(E_{pD})$ and the D–D fusion rates $\Lambda_{DD}(E_{DD})$ for $E(= E_{pD} = E_{DD}) \leq 20$ eV with $\tilde{E}_s = 0$ and 10 e^2/a_0.

eq. (7), as in eq. (4). As in the case of reactions (1a) and (1b) (Figs. 1 and 2), the electron screening effect ($\tilde{E}_s \neq 0$) becomes substantial for $\sigma_{pD}(E_{pD})$ and $\Lambda_{pD}(E_{pD})$ at very low energies.

In order to see whether reaction (1c) will compete with reactions (1a) and (1b) in electrolysis experiments, we compare $\Lambda_{pD}(E_{pD})$ and $\Lambda_{DD}(E_{DD})$ in Fig. 7 for the cases $\tilde{E}_s = 0$ and $10\ e^2/a_0$. As can be seen from Fig. 7, $\Lambda_{pD}(E_{pD})$ is comparable to $\Lambda_{DD}(E_{DD})$ for the case ($\tilde{E}_s \neq 0$) and $n_H = n_D$. Therefore, for a typical value of the H/D ratio, $n_H/n_D \approx 10^{-3}$, in electrolysis experiments, reactions (1a) and (1b) will dominate over reaction (1c). However, reaction (1c) can compete with reactions (1a) and (1b) if $n_H \approx n_D$ is maintained in electrolysis experiments.

IV. CONCLUSIONS

It is shown that the effect of electron screening in conjunction with a particle velocity distribution greatly enhances the cross sections and reaction rates for D–D and p–D fusion at kinetic energies $E \lesssim 20$ eV (CM).

The D–D fusion rate for reaction (1a), $\Lambda^T_{\rm exp}(1a) \approx 10^{-19}\ sec^{-1}$, inferred by Fleischmann et al. [4] from the measurement of tritium production, and also the D–D fusion rate for reaction (1b), $\Lambda^n_{\rm exp}(1a) \approx 10^{-23}\ sec^{-1}$, obtained by Jones et al. [5] are often criticized as being impossible or incorrect when compared to estimates of Λ in bulk matter (an upper limit of $\Lambda \lesssim 10^{-47}\ sec^{-1}$) [10] or to the result of Λ_δ shown in Fig. 3 (lowest curve). Our results for Λ (upper curves) shown in Fig. 3 indicate $\Lambda^n_{\rm exp}(1b) \approx 10^{-23}\ sec^{-1}$ [5] and $\Lambda^T_{\rm exp}(1b) \approx 10^{-19}\ sec^{-1}$ [4] are consistent with calculated values of $\Lambda_{DD}(E_{DD}) \approx 10^{-23}\ sec^{-1}$ and $\Lambda_{DD}(E_{DD}) \approx 10^{-19}\ sec^{-1}$ for $E_{DD} \approx 10$ eV and 17 eV, respectively, with $\tilde{E}_s = 4e^2/a_0$. Therefore, the claimed values of $\Lambda^n_{\rm exp}(1b)$ and $\Lambda^T_{\rm exp}(1a)$ are physically acceptable values for the D–D fusion rate in electrolysis experiments if the applied potentials are 20 V and 34 V, respectively.

To match the D–D fusion rate $\Lambda_{DD}(E_{DD})$ from eq. (1a) to the rate, $\Lambda^{heat}_{\rm exp}(1a) \approx 10^{-10}\ sec^{-1}$ [4] inferred from excess heat measurements [3,5,6], an "average" kinetic energy of $E_{DD} \approx 70$ eV is needed with $\tilde{E}_s = 4\ e^2/a_0$, or $E_{DD} < 70$ eV for $\tilde{E}_s > 4\ e^2/a_0$.

The calculated p–D fusion rates $\Lambda_{pD}(E_{pD})$ for reaction (1c) are comparable to the D–D fusion rates for reactions (1a) and (1c) with $\tilde{E}_s = 10\ e^2/a_0$ and E_{pD}(and E_{DD}) < 20 eV as shown in Fig. 7. Therefore, p–D fusion can compete with D–D fusion if an H/D ratio of $n_H/n_D \approx 1$ can be maintained in both the H_2O–D_2O mixture and the Pd cathode during electrolysis fusion experiments.

REFERENCES

1. R.A. Rice, G.S. Chulick, Y.E. Kim, and J.-H. Yoon, "The Role of Velocity Distribution in Cold Deuterium-Deuterium Fusion," Purdue Nuclear Theory Group Report PNTG-90-5 (January 1990), to be published in Fusion Technology.
2. Y.E. Kim, "Nuclear Theory Hypotheses for Cold Fusion," to be published in the Proceedings of the NSF/EPRI Workshop on Anomalous Effects in Deuterated Metals, Washington, D.C., October 16-18, 1989.
3. Y.E. Kim, "Fission-induced inertial confinement hot fusion and cold fusion with electrolysis," to be published in LASER INTERACTION AND RELATED PLASMA PHENOMENA, Volume 9 (H. Hora and G.H. Miley eds.).
4. M. Fleischmann and S. Pons, "Electrochemically Induced Nuclear Fusion", J. of Electroanal. Chem. **261**, 301 (1989); and errata **263**, 187 (1989).
5. S.E. Jones et al., "Observation of Cold Nuclear Fusion in Condensed Matter," Nature **338**, 737 (27 April 1989).
6. A.J. Appleby, S. Srinivasan, Y.J. Kim, O.J. Murphy, and C.R. Martin, "Evidence for Excess Heat Generation Rates During Electrolysis of D_2O in LiOD using a Palladium Cathode—a Microcalorimetric Study," in the Proceedings of the Workshop on Cold Fusion Phenomena, May 23-25, 1989, Santa Fe, New Mexico, to be published in J. Fusion Energy, March 1990.
7. A. Belzner, U. Bischler, G. Crouch-Baker, T.M. Gur, G. Lucier, M. Schreiber, and R. Huggins "Two Fast Mixed-conductor Systems: Deuterium and Hydrogen in Palladium-Thermal Measurements and Experimental Considerations," in the Proceedings of the Workshop on Cold Fusion Phenomena, May 23-25, 1989, Santa Fe, New Mexico, to be published in J. Fusion Energy, March 1990.
8. K.L. Wolf, N.J.C. Packham, D.R. Lawson, J. Shoemaker, F. Cheng, and J.C. Wass, "Neutron Emission and the Tritium Content Associated with Deuterium Loaded Palladium and

Titanium Metals," in the Proceedings of the Workshop on Cold Fusion Phenomena, May 23-25, 1989, Santa Fe, New Mexico, to be published in J. Fusion Energy, March 1990.

9. P.K. Iyengar, "Cold Fusion Results in BARC Experiment," in the Proceedings of the 5th International Conference on Emerging Nuclear Energy Systems (ICENES V), Karlsruhe, West Germany, July 3-6, 1989.

10. A.J. Leggett and G. Baym, "Exact Upper Bound on Barrier Penetration Probabilities in Many-Body Systems: Application to Cold Fusion," Phys. Rev. Lett. **63**, 191 (1989).

11. K. Langanke, H.J. Assenbaum, and C. Rolfs, "Screening Corrections in Cold Deuterium Fusion Rates," Z. Phys. A. Atomic Nuclei **333**, 317 (1989).

12. Y.E. Kim, "Surface Reaction Mechanism and Lepton Screening for Cold Fusion with Electrolysis," to be published in the Proceedings of the First Annual Conference on Cold Fusion, Salt Lake City, Utah, March 28-31, 1990.

13. W.A. Fowler, G.R. Caughlan, and B.A. Zimmermann, "Thermonuclear Reaction Rates," Ann. Rev. Astr. Astrophys. **5**, 525 (1967); "Thermonuclear Reaction Rates II," **13**, 69 (1975).

14. M.J. Harris, W.A. Fowler, G.R. Caughlan, and B.A. Zimmerman, "Thermonuclear Reaction Rates III," Ann. Rev. Astr. Astrophys. **21**, 165 (1983).

15. A. von Engel and C.C. Goodyear, "Fusion Cross-Section Measurements with Deuterons of Low Energies," Proc. Roy. Soc. A **264**, 445 (1961).

16. A. Krauss, H.W. Becker, H.P. Trautvetter, and C. Rolfs, "Low-Energy Fusion Cross Sections of D+D and D + ^{3}He Reactions," Nucl. Phys. **A465**, 150 (1987).

17. S.N. Vaidya and Y.S. Mayya, "Theory of Screening–Enhanced D–D Fusion in Metals," Jap. J. Appl. Phys. **28**, L2258 (1989).

18. K.B. Whaley, "Boson Enhancement of Finite–Temperature Coherent Dynamics for Deuterium in Metals," Phys. Rev. **B41**, 3473 (1990).

19. M. Rabinowitz and D.H. Worledge, "An Analysis of Cold and Lukewarm Fusion," to be published in Fusion Technology **17**, (1990).

SURFACE REACTION MECHANISM AND LEPTON SCREENING FOR COLD FUSION WITH ELECTROLYSIS

Yeong E. Kim

Department of Physics, Purdue University
West Lafayette, IN 47907

ABSTRACT

A surface reaction mechanism and the effects of electron and muon screening are described for electrolysis fusion experiments. A general expression is given for the modified Coulomb barrier penetration factor which includes the lepton screening effect and which can be used for extrapolating the fusion cross sections to lower energies. It is shown that, when combined with the effect of velocity distribution in the context of the surface reaction mechanism, the electron screening effect may explain the claimed results of recent electrolysis fusion experiments and may also explain why it is difficult to reproduce the same result with different samples in electrolysis experiments. Experimental tests of the effects of electron and muon screening are suggested both for electrolysis experiments and for inelastic scattering experiments.

I. INTRODUCTION

Recently, a surface reaction mechanism [1,2] was proposed for electrolysis fusion experiments [3-8] in which deuterium-deuterium (D-D) fusion takes place in the surface zone of a palladium (Pd) cathode where whiskers and asperities of metal deuterides form during the electrolysis experiments, in order to explain the discrepancy of 24-60 orders of magnitude between the conventional estimates [9-10] and the electrolysis fusion results [3-8]. It has been shown that the calculated fusion reaction rate can increase by as much as 60 orders of magnitude [11] if an appropriate Maxwell-Boltzmann velocity distribution is used in the context of the proposed surface reaction mechanism.[1,2] It has also been argued that the conventional theoretical estimates of the cold D-D fusion rate may not be reliable since the extrapolation method used may not be valid at low energies.[1,2,12]

In this paper, it is shown that the electron screening effect becomes significant at low energies and hence the conventional Coulomb barrier penetration factor (the "Gamow" factor) used to describe the D-D fusion rate is no longer valid at low energies. A modified Coulomb barrier penetration factor and a new extrapolation method for the cross-section and rate are proposed for the cold D-D fusion reaction in electrolysis experiments and for other fusion reactions in physical processes. When combined with an appropriate velocity distribution arising from the surface reaction mechanism, the new extrapolation formula which includes the electron screening effect is expected to be able to explain the results [3-8] of electrolysis fusion experiments.

In section II, the D-D and hydrogen-deuterium (H-D) fusion reactions are described in terms of the surface reaction mechanism. In section III, the effect of a velocity distribution on D-D fusion is discussed in the context of the surface reaction mechanism. In section IV, the electron screening effect is described in detail for fusion reactions and an appropriate modification of the Coulomb barrier penetration factor is presented. A new extrapolation formula for the fusion cross sections is given. The physical consequences of the effects of both velocity distribution and electron screening are discussed for electrolysis fusion experiments. In section V, the muon screening effect is discussed and its implications are described for the results of the recent electrolysis experiments. In section VI, the branching ratio for the D-D fusion reactions is discussed. Finally, a brief summary is given in section VII.

II. FUSION PROCESSES IN THE SURFACE ZONE

In electrolysis experiments where the Pd cathode is immersed in D_2O with $LiOD$ electrolyte, many spherical and hemispherical D_2 gas bubbles of varying sizes (radii ranging from a few μm to a few mm) will be produced continuously in the surface zone outside the Pd cathode where they will stay for a certain time duration before they move out of the electrolysis cell. Many of these D_2 gas bubbles in the surface zone will have surface whiskers (PdD or LiD) protruding into them. This will create very high electric fields around the sharp tips of the whiskers, which are many orders of magnitude larger than the average field due to the applied potential. D^+ ions in a given bubble will gain kinetic energies with a statistical distribution which depends on the bubble size and the values of the widely varying electric field inside the bubble. When the applied potential is $\sim$ 10 V, the average laboratory kinetic energy of the D^+ ions in each bubble is expected to be $\sim$ 10 eV. A small fraction of the D^+ ions are expected to gain additional kinetic energy beyond the average value due to several acceleration processes, such as (i) acceleration of the ion due to a change of the polarity of D^+ to D or D^- near the whisker tips (this process $D^+ \rightarrow D^-$ may increase the the D kinetic energy by a factor of two, or more by the use of a high AC voltage with a correct modulation frequency), (ii) acceleration of D when D^+ is picked up and carried by a group of fast electrons [13], and (iii) other such processes [13].

The accelerated D^+ ions (deuterons) (also smaller amounts of D^- and D) in the bubble will be incident on the electrically neutral D (or H present as an impurity) in the D_2O or in the Pd cathode (whiskers and surface areas). The dominant fusion reactions are:

$$D^+ + D \rightarrow {}^3H(1.01\ MeV) + p(3.02\ MeV), \quad (1a)$$

$$D^+ + D \rightarrow {}^3He(0.82\ MeV) + n(2.45\ MeV), \quad (1b)$$

and

$$H^+ + D \rightarrow {}^3He + \gamma(5.5\ MeV). \quad (1c)$$

Reaction (1c) is included since it has been recently shown that the H-D fusion cross-section and reaction rate are larger than those for reactions (1a) and (1b) for $E \leq 8eV$ in the center of mass (CM) frame [14] and is thus expected to compete with the D-D fusion below $E(CM) \approx 2.5$ eV for an impurity ratio of $H/D \approx 10^{-3}$ in electrolysis experiments. Experiment values of the cross-section, $\sigma(E)$, for (1a), (1b), and (1c) have been parameterized as [15]

$$\sigma(E) = \frac{S(E)}{E} e^{-(E_G/E)^{1/2}} \quad (2)$$

where E_G is the "Gamow energy" given by $E_G = (2\pi\alpha Z_D Z_D)^2\ Mc^2/2$ or $E_G^{1/2} \approx 31.39(keV)^{1/2}$ for the reduced mass $M \approx M_D/2$ for reactions (1a) and (1b) and $E_G^{1/2} = 25.64\ (keV)^{1/2}$ for reaction (1c) with the reduced mass $M = m_p M_D/(m_p + M_D) \approx M_D/3$. E is in units of keV in the center of mass (CM) reference frame. The S-factor, S(E), is extracted from the experimentally measured values [16,17] of the cross-section, $\sigma(E)$, for E $\gtrsim$ 4 keV and is nearly constant [17], $S(E) \approx 52.9$ keV - b, for both reactions (1a) and (1b) in the energy range of interest here, $E \lesssim 1$ keV. For reaction (1c), $S(E) \approx 2.50 \times 10^{-4}\ keV - b$. In the following, the theoretical formulation will be given only for reactions (1a) and (1b), as it is similar for reaction (1c).

Reaction rates, R_{calc}, for both reactions (1a) and (1b) for an incident deuteron kinetic energy E_i in the laboratory (LAB) frame, are given by

$$R_{calc}(1a) = R_{calc}(1b) = \Phi P(E_i), \quad (3)$$

where Φ is the incident D^+ flux

$$\Phi = (0.625 \times 10^{19} D^+\ 's/sec) I \quad (4)$$

with the current I in units of amperes, and $P(E_i)$ is the probability for a deuteron to undergo a fusion reaction (1a), (1b), or (1c) while slowing down in the deuterated Pd electrode, which can be written as

$$\begin{aligned} P(E_i) &= \int dx\ n_D\ \sigma(E_{DD}) \\ &= \int_o^{E_i} dE_D \frac{1}{|dE_D/dx|} \sigma(E_{DD}). \end{aligned} \quad (5)$$

E_D and E_{DD} are the deuteron kinetic energies in the LAB and CM frames, respectively ($E_{DD} = E_D/2$). The stopping power [18] for $E_D \lesssim 12$ keV is given by

$$\frac{dE_D}{dx} = 3.70 \times 10^{-15} n_{Pd} \sqrt{E_D}\ eV - cm^2 \quad (6)$$

for D in Pd and

$$\frac{dE_D}{dx} = 0.89 \times 10^{-15} n_D \sqrt{E_D}\ eV - cm^2 \quad (7)$$

for D in D. Therefore, the stopping power for D in PdD is given by the sum of eqs. (6) and (7),

$$\frac{dE_D}{dx} = 3.1 \times 10^5 \sqrt{E_D}\ keV/cm \quad (8)$$

for $n_{Pd} = 6.767 \times 10^{22} cm^{-3}$ and $n_D = n_{Pd}$. E_D in eq. (8) is in units of keV in the LAB frame.

With the given choice of parameterizations, eqs. (2) and (8), the integration in eq. (5) can be done

analytically to yield the following expression for eq. (3).

$$R_{calc}(1a) = R_{calc}(1b) = 2.3 \times 10^{12} I\ exp(-44.24/\sqrt{E_i}), \quad (9)$$

with I in units of amperes and E_i in units of keV (LAB).

Calculations for R_{calc} (1a), R_{calc} (1b), and R_{calc} (1c) for the case in which D^+ is incident on D (or H) in D_2O (or H_2O) can be carried out in the same way, but the results will not be given here.

The range $R(E_i)$ of D^+ in PdD can be obtained from eq. (8) as

$$R(E_i) = \int dx = \int_o^{E_i} (\frac{dE}{dx})^{-1}\ dE$$

or

$$R(E_i) = 0.645 \times 10^{-6} \sqrt{E_i(in\ keV)}\ cm \quad (10)$$

which yields $R(E_i) = 2.04\mathring{A}$, $6.45\mathring{A}$, and $20.4\ \mathring{A}$ for $E_i = 1\ eV$, 10 eV, and 100 keV, respectively. The range $R(E_i)$ of D^+ in D_2O is slightly larger than that of D^+ in PdD. Since individual D in Pd is separated by $\sim 2\mathring{A}$, D^+ penetrates into 2, 4, and 11 layers from the surface of PdD when the incident D^+ energies (LAB) are 1 eV, 10 eV, and 100 eV, respectively. Therefore, D-D fusion takes place within the first few surface layers of PdD and of D_2O surrounding the bubbles in electrolysis experiments.

III. THE EFFECT OF VELOCITY DISTRIBUTION

In order to compare with the experimental rates which are usually given in units of sec^{-1} per deuterium, the theoretical D-D fusion rate ($sec^{-1}/D-D\ pair$), Λ_δ, is defined as

$$\Lambda_\delta = \frac{n_D}{2}\ \sigma(E)v(CM) \quad (11)$$

for a sharp (delta-function) velocity distribution where $E = E_{DD} = \frac{M}{2}v^2(CM) = \frac{M_D}{4}v^2(LAB) = \frac{1}{2}E_D(LAB)$ and $n_D \approx 6 \times 10^{22} cm^{-3}$. The estimated values of $\Lambda_\delta(E)$ calculated from eqs. (2) and (11) for a sharp velocity distribution have been used to argue against the possibility of D-D fusion in electrolysis experiments. However, a statistical velocity distribution is more appropriate in electrolysis experiments as discussed in section II. It has been argued [1,2] and shown [11] that the D-D fusion rate with a Maxwell-Boltzmann D^+ velocity distribution can become very large at low energies compared to that with a sharp velocity distribution.

Since the precise form of the D^+ velocity distribution in electrolysis experiments is not known at present,we assume a Maxwell-Boltzmann distribution with and without a cut-off for high velocity components. The temperature term, k_BT, will be replaced by the "average" kinetic energy, E_{DD}, in the center of mass (CM) D-D frame, which is related to the most probable velocity v(CM) by $E_{DD} = \frac{M}{2}\ v^2$ (CM) with the reduced mass $M = M_D/2$.

For a Maxwell-Boltzmann velocity distribution, the D-D fusion rate, $\Lambda(sec^{-1}/D-D\ pair)$, for reaction (1a) or (1b) is given by [15]

$$\Lambda(E_{DD}) = \frac{n_D}{2} < \sigma v >, \quad (12)$$

with

$$< \sigma v > = \frac{(8/\pi)^{1/2}}{M^{1/2}(E_{DD})^{3/2}} \int_o^{E_c} \sigma(E) E e^{-E/E_{DD}} dE, \quad (13)$$

where the cross-section, $\sigma(E)$, is parameterized (E is in the C.M. frame) by eq. (2) which is the conventional form assuming non-resonant charged particle reactions for reactions (1a) and (1b).

The D-D fusion rate for reaction (1a), $\Lambda^T_{exp}(1a) \approx 10^{-19} sec^{-1}$, inferred by Fleischmann et al.[3] from the measurement of tritium production, and also the D-D fusion rate for reaction (1b), $\Lambda^n_{exp}(1b) \approx 10^{-23} sec^{-1}$, obtained by Jones et al.[4] are often criticized as being impossible or incorrect when compared to estimates of Λ in bulk matter (an upper limit of $\Lambda \lesssim 10^{-47}\ sec^{-1}$) [9] or to the result of Λ_δ obtained from eq. (11). Our recent results [11] for Λ calculated from eqs. (12) and (13) indicate that Λ^n_{exp} (1b) $\approx (10^{-23}/sec)$ [4] and $\Lambda^T_{exp}(1a) \approx (10^{-19}/sec)$ [3] are consistent with calculated values of $\Lambda(E_{DD}) \approx 10^{-23} sec^{-1}$ and $\Lambda(E_{DD}) \approx 10^{-19} sec^{-1}$ for $E_{DD} \approx 15eV$ and 20 eV, respectively. Therefore, the claimed values of $\Lambda^n_{exp}(1b) \approx (10^{-23}/sec)$ [4] and $\Lambda^T_{exp}(1a) \approx (10^{-19}/sec)$ [3] are physically acceptable values for the D-D fusion rate in electrolysis experiments if the applied potentials are 30V and 40V, respectively. To match the D-D fusion rate $\Lambda(E_{DD})$ of eq. (1a) to the rate, $\Lambda^{heat}_{exp}(1a) \approx (10^{-10}/sec)$ [3], inferred by excess heat measurements [3,4,6], an "average" kinetic energy of $E_{DD} \approx 75eV$ is needed. In the following section, it will be shown that the above remaining discrepancies can be explained by the effect of electron screening.

IV. ELECTRON SCREENING EFFECT

The expression for $\sigma(E)$ given by eq. (2) is valid only for a reaction in which D^+ is incident on another D^+. In electrolysis fusion experiments as well

as in other physical processes [14], D^+ (also D^- or D) is incident on D which is shielded by an electron cloud; i.e., the target D is electrically neutral outside the electron shielding radius ($\lesssim$ 0.53 Å, the Bohr radius). Therefore, the Coulomb barrier penetration factor ("Gamow factor") in eq. (2)

$$P_G(E) = exp(-(E_G/E)^{1/2}) \tag{14}$$

which is appropriate only for the $(D^+ + D^+)$ reaction has to be modified for the case of the $(D^+ + D)$ reactions (1a) and (1b), and the $(D^+ + H)$ reaction (1c). The modified Coulomb barrier penetration factor,$P_s(E)$, is the probability of tunneling through the barrier to reach the nuclear surface. It can be computed from solutions of the Schroedinger equation for the $(D^+ + D)$ system in which an attractive Coulomb potential $V_s(r)$ due to the presence of shielding elections is included with the original repulsive Coulomb potential between two D^+'s (two protons):

$$\{-\frac{\hbar^2}{2M}\nabla^2+V_N(r)+V_c(r)+V_s(r)\}\,\psi_{DD}(\vec{r}) = E\psi_{DD}(\vec{r}) \tag{15}$$

where $V_N(r)$ is an effective attractive nuclear potential of range $\sim$ 8F (twice the deuteron radius of 4F) and $V_c(r)$ is the repulsive Coulomb potential between two D^+'s,

$$V_c(r) = \frac{Z_D Z_D e^2}{r}. \tag{16}$$

The modified Coulomb barrier penetration factor, $P_s(E)$, which includes the effect of the electron screening potential $V_s(r)$ given in eq. (15) can be calculated in the Wentzel- Kramers-Brillouin (WKB) approximation as (retaining only the s-wave contribution)

$$P_s(E) = exp[-2(\frac{2M}{\hbar^2})^{1/2}\int_{r_N}^{r_a}(V_c(r)+V_s(r)-E)^{1/2}dr] \tag{17}$$

The effective nuclear interaction range, $r_N \approx 8F$, can be set to zero in eq. (17) without loss of accuracy. The integral in eq. (17) cannot be carried out analytically, but can be written for an attractive potential, $V_s(r) < 0$, as

$$2(\tfrac{2M}{\hbar^2})^{1/2}\int_o^{r_a}(V_c(r) + V_s(r) - E)^{1/2}\,dr = \frac{(E_G)^{1/2}}{(E+E_s(E))^{1/2}} \tag{18}$$

where $E_s(E)$ is determined numerically as a function of E by carrying out the integral numerically for each value of $E > 0$. The modified penetration factor, $P_s(E)$, is then

$$P_s(E) = exp(-E_G^{1/2}/(E + E_s(E))^{1/2}). \tag{19}$$

When $V_s(r) = 0$ and hence $E_s(E)$ vanishes, we recover the conventional Gamow factor, $P_s(E) = P_G(E)$. The classical turning point, r_a, in eq. (17) is determined by

$$V_c(r_a) + V_s(r_a) = E. \tag{20}$$

From eqs.(18) and (20), it can be easily shown that $E_s(E)$ in eqs.(18) and (19) is bounded by $|V_s(r_a)| < E_s(E) < |V_s(0)|$. In the following, two models for the electron screening potential $V_s(r)$ will be described.

(a) The ls Hydrogen Electron Screening Potential.

The electron screening potential for the target D (or H) in D_2 gas (or H_2 gas) can be approximated, to reasonable accuracy, via the electron probability density $\rho_e(r)$ of the 1s hydrogen electron,

$$\rho_e(r) = -q\ e^{-ur}, \tag{21}$$

where $q = Z_s e/\pi a_o^3$ and $u = 2/a_o$. $Z_S, Z_D = 1$, and a_o are the effective charge of the screening electrons, the deuteron nuclear charge, and the Bohr radius ($a_o \approx 0.53\mathring{A}$), respectively. $\rho_e(r)$ is normalized such that $\int \rho_e(r)d^3r = -Z_s e$. The Coulomb potential generated by $\rho_e(r)$ as seen by an incident deuteron(D^+) is then

$$\begin{aligned} V_s(r) &= Z_D e \int \frac{\rho_e(r')}{|\vec{r}-\vec{r}'|}\,d^3r' \\ &= -\frac{Z_D Z_S e^2}{r}[1 - e^{-ur}(1 + ur/2)], \end{aligned} \tag{22}$$

which approaches to $-Z_D Z_S e^2/r$ as $r \to \infty$, as expected.

We note that $V_s(r)$ is negative for $r \geq 0$ and $|V_s(r)|$ has the maximum value $|V_s(0)| = Z_D Z_S\, e^2/a_o$ = 27.17 $Z_D Z_S eV$ at $r = 0$. Since $|V_s(r)|$ decreases monotonically as r increases, $E_s(E)$ is bounded by $E_s(E) \leq |V_s(0)|$. As an example, at the classical turning point of $r = r_a = a_o$ corresponding to $E = 7.35eV, |V_s(a_o)| = 19.8\ Z_D Z_S eV$, and hence $E_S(E)$ is bounded by 27.17 $Z_D Z_S eV > E_S(E) >$ 19.8 $Z_D Z_S eV$. It is interesting to note that for $Z_S = Z_D$, $V(r) = V_c(r) + V_s(r) = Z_D^2 e^2(e^{-ur}/r)(1 + ur/2)$ which is similar to the Debye screening potential in condensed matter and plasma physics, $Z^2e^2(e^{-kr}/r)$ with $k^{-1} = r_s = (k_B T/4\pi n_e e^2)^{1/2}$.

(b) Spherical Shell Charge Electron Screening Potential

For a simpler potential generated by a spherical shell charge distribution, $\vec{\rho_e}(r) = (Z_s e/4\pi r_s r_a)\ \delta(r - r_a), V_s(r)$ can be written as

$$\tilde{V}_s(r) = -\frac{Z_D Z_S}{r_s}\Theta(r_a - r). \tag{23}$$

When $\tilde{V}_s(r)$ is used in eq. (18) the penetration factor becomes

$$\tilde{P}_s(E) = exp(-E_G^{1/2}/(E+\tilde{E}_s)^{1/2}) \qquad (24)$$

where $\tilde{E}_s = Z_D Z_S e^2/r_s$ is a constant independent of E. Eq. (24) has been previously used for D_2 molecular fusion [10] and for analysis of D_2O cluster fusion.[13]

Using eq. (19), the new extrapolation formula appropriate for reactions (1a), (1b), (1c), and other fusion reactions is

$$\sigma_s(E) = \frac{S(E)}{E} exp(-(E_G/(E+E_s(E))^{1/2}). \qquad (25)$$

The screening energy term $E_s(E)$ can be extracted from the measured values [16,17] of $\sigma_{exp}(E)$ for the D-D fusion reaction (1a) and be compared with the values of $E_s(E)$ given by the two models described above. The values of $E_s(E)$ extracted from $\sigma_{exp}(E < 4keV$ (CM)) [16,17] using eq. (25) are listed in Table I, and have large uncertainties. Therefore, it is important to carry out precision measurements of $\sigma_{exp}(E)$ with improved accuracies for $E < 4keV$ (CM). The experimental values of $\sigma_{exp}(E)$ [16, 17] listed in Table I are measured with D_2 gas targets for which the electron screening potential is expected to be approximately that of the 1s hydrogen electron. However, for solid targets such as $Ti D$ and PdD, the electron screening range could be as small as a tenth of the Bohr radius , $a_o/10$, since the Debye screening length k^{-1} is $k^{-1} = r_s = (k_B T/4\pi n_e e^2)^{1/2} \approx$ 0.05Å with $T = 300°K$ and $n_e \approx 6 \times 10^{22} cm^{-3}$. A more elaborate calculation [19] yields also $k_s \approx$ 0.05Å at $T = 300°K$ for D^+ in Pd. Therefore, the extracted values of $E_s(E)$ from the solid metal deuteride targets may be up to ten times larger than values ($E_s(E) \approx 40 - 60\ eV$) extracted from the D_2 gas target [16, 17]. Improved measurements are presently being carried out at Purdue by D. Elmore, Y.E. Kim, D.S. Koltick, E. Michlovich, and R.G. Reifenberger.

Since the precise form of $V_s(r)$ will depend on experimental and physical conditions and is not known for electrolysis experiments, it is useful to replace $E_S(E)$ of eq. (19) with an energy independent parameter $\tilde{E}_s$ as in eq. (24) within a reasonable range of parametric values for $\tilde{E}_s$.

Since $E_s(E)$ in eq. (25) is expected to be of the order of 270 $Z_s eV$ for the metal deuteride targets, the electron screening effect will play a very important role when $E \lesssim 270\ Z_s eV$ in for electrolysis fusion experiments and for other fusion processes, as shown by a recent calculation [20] and may act in part as a catalyst of cold fusion. The electron screening effect may explain why it is difficult to reproduce the same result with different cathode samples in electrolysis experiments and may also explain why the reported tritium production [7,8] lasts only for a finite period in electrolysis experiments, since the fusion rate and cross section are very sensitive to variation of flux and kinetic energies of D^+ and also to the electron density and screening potential around D in the cathode surface layer, which may be difficult to maintain and could be different for each electrolysis experiment due to the a non-equilibrium situation and other experimental conditions. The extracted values of $E_s(E)$ from $\sigma_{exp}(E)$ using eq. (25) should enable us to determine an effective electron screening potential and also the corresponding electron density surrounding the deuterium nucleus in the metal surface layer.

V. MUON SCREENING EFFECT

The screening effect is expected to be substantially larger for a muonic atomic or molecular target, since the muonic Bohr radius, a_o^μ, is much smaller than a_o, $a_o^\mu \approx a_o/196 \approx 2.7 \times 10^{-3} Å$ for D ($a_o^\mu \approx a_o/186$ for H) and thus $|V_s^\mu(0)| \approx 196|V_s(0)| \approx 5318$ eV (5054 eV for H) for $Z_S = Z_D$. In order to study the muonic screening effect on fusion reactions, the fusion cross-sections should be measured as a function of energy using a muonic atom (or molecule) beam and/or target for reactions, (1a), (1b), and (1c). This expected large increase of the muonic deuterium fusion rate brings up an interesting possibility that a minute amount of the background muonic hydrogen or deuterium atoms, produced by cosmic rays and present in electrolysis experiments might participate in fusion reactions that compete with or dominate over the regular fusion reactions (1a), (1b), and (1c).

For the muon screening effect on reactions (1a) and (1b), order of magnitude estimates for the fusion rates can be made with reasonable accuracy using eq. (11) for the rate $\Lambda_\delta^\mu(E)$ with a sharp velocity distribution. This is because the values of $E_s(E) > |V_s^\mu(r_a)|$ are substantial larger than the corresponding values of $E < 0.1\ keV$. For the 1s hydrogen muon screening potential $V_s^\mu(r)$, the Bohr radius a_o in eq. (22) is replaced by the muonic Bohr radius a_o^μ. Assuming that $E_s(E) = |V_s^\mu(r_a)|$ (which is an underestimate), the fusion rate, $\Lambda_\delta^\mu(E) = n_D^\mu \sigma(E) v(CM)$, for the sum of the two reactions (1a) and (1b) is calculated at several values of E(CM) and summarized in table II.

As can be seen from table II, the observed rates of Λ_{exp}^n $(1b) \approx 10^{-23}\ sec^{-1}/D$ [4] and Λ_{exp}^T $(1a) \approx 10^{-19}\ sec^{-1}/D$ [3] can be explained if very small densities of $n_D^\mu \approx 10^3$ and $10^7\ cm^{-3}$, respectively, are

assumed (in D_2O or PdD), using Λ_δ^μ (E = 2.1 eV) $\approx n_D^\mu(3.9 \times 10^{-26}\ cm^3/sec)$. However, it is difficult to maintain the background density of $n_D^\mu \approx 10^3 \sim 10^7\ cm^{-3}$ from the cosmic ray muons (produced by pions, neutrino, etc.)[21]. Nevertheless, it is useful to study the muon screening effect for reactions (1a), (1b), and (1c) by carrying out two types of experiments: (a) scattering experiments in which a muonic atom (or molecule) beam or target is used, and (b) electrolysis experiments exposed to muon (or pion) beam from an accelerator. This later type of experiment should be examined as a possible prototype for a practical fusion reactor.

VI. BRANCHING RATIO FOR THE D-D FUSION REACTIONS

The suppression of reaction (1b) and the enhancement of reaction (1a) at low energies have been observed in electrolysis experiments [3,7,8] contrary to the conventional assumption of nearly equal rates based on the charge symmetry and the charge independence of the nuclear force.

After the incident deuteron penetrates through the Coulomb barrier within an effective nuclear interaction range of 8F (twice the deuteron radius), nuclear dynamics take over for this system of four nucleons. One possible explanation for the unequal rates is that there may be a broad resonance behavior in $\sigma(E)$ for reaction (1a) but not in $\sigma(E)$ for reaction (1b) at low energies, which is plausible since the final state Coulomb interaction is present for reaction (1a) but not for reaction (1b). If $\sigma(E)$ happens to have resonance behavior near $E \approx 0$, the extrapolation may yield erroneous values for $\sigma(E \approx 0)$, since the non-resonant relation (2) is not applicable to resonance reactions. Therefore, it is very important to investigate the possibility of resonance behavior for $\sigma(E)$ near $E \approx 0$ theoretically, and also to measure $\sigma(E \approx 0)$ directly with precision experiments. Recent observation of neutron bursts at $-30°C$ at a rate of $\Lambda \approx 10^{-23} sec^{-1}$ reported by Menlove et al. [22] may be interpreted as the existence of a sharp resonance in the reaction channel (1b).

At present, there are neither direct experimental measurements nor theoretical calculations of the branching ratios for reactions (1a) and (1b) for $E \lesssim 3\ keV$. One would expect the branching ratio of reaction (1a) to be larger than that of reaction (1b), since reaction (1b) involves a fusion of two protons to form ^3He while reaction (1a) does not fuse two protons but merely transfers a neutron from one deuteron to another to form ^3H. Theoretical calculations of the reaction cross- sections and branching ratios of reactions (1a) and (1b) should be carried out based on non-relativistic four-nucleon scattering theory [23] using nucleon-nucleon forces and the Coulomb interaction.

VII. SUMMARY

It has been shown that the effect of electron screening may be essential in describing the electrolysis fusion experiments and other related physical processes. When combined with the effect of velocity distribution in the context of the surface reaction mechanism, the screening effect may be able to explain the claimed values of $\Lambda_{exp}^T(1a) \approx 10^{-19}/D$ [3] and $\Lambda_{exp}^n(1b) \approx 10^{-23}\ sec^{-1}/D$ [4]. The effects of velocity distribution and electron screening may also be able to explain the claimed value of $\Lambda_{exp}^{heat} \approx 10^{-10}\ sec^{-1}/D$ [3].

It is important to improve the accuracy of the measurements of the cross section for reaction (1a) below 4 keV (LAB) in order to determine the magnitude of the electron screening effect on the Coulomb barrier penetration factor and fusion rates. It is suggested that the screening effect should be investigated with metal deuteride targets and also with a muonic atom (or molecule) beam and/or target for reactions (1a), (1b), and (1c), since the screening effect is then expected to be substantially larger. The electron screening effect may provide a plausible explanation for the results of the electrolysis experiments and also for other physical processes [24] such as the earth's internal heating [4] and the excess heat radiation from other outer planets [24].

The observed suppression [3,7,8] of the branching ratio for reaction (1b) is expected to be due to nuclear resonance and dynamic effects which involve the attractive short-range nuclear forces among four nucleons (two neutrons and two protons) and the Coulomb repulsive barrier between the fusing protons within the range of 1.6 F (twice proton radius) to 8F (twice the deuteron radius). These effects will modify the S(E) factor in eq. (25).

ACKNOWLEDGEMENT

The author wishes to thank Gary S. Chulick and Robert A. Rice for helpful discussion and suggestions.

REFERENCES

1. Y.E. Kim, "Nuclear Theory Hypotheses for Cold Fusion", to be published in the Proceedings of the NSF/EPRI Workshop on Anomalous Effects in Deuterated Metals, Washington, D.C., October 16-18, 1989.

2. Y.E. Kim, "Fission-induced inertial confinement hot fusion and cold fusion with electrolysis", to be published in LASER INTERACTION AND RELATED PLASMA PHENOMENA, Volume 9 (H. Hora and G.H. Miley eds.).

3. M. Fleischmann and S. Pons, "Electrochemically Induced Nuclear Fusion" J. of Electroanal. Chem., **261**, 301 (1989); and errata, **263**, 187 (1989).

4. S.E. Jones et al., "Observation of Cold Nuclear Fusion in Condensed Matter", Nature **338**, 737 (27 April 1989).

5. A.J. Appleby, S. Srinivasan, Y.J. Kim, O.J. Murphy, and C.R. Martin, "Evidence for Excess Heat Generation Rates During Electrolysis of D_20 in LiOD using a Palladium Cathode - a Microcalorimetric Study", in the Proceedings of the Workshop on Cold Fusion Phenomena, May 23-25, 1989, Santa Fe, New Mexico, to be published in J. Fusion Energy, March 1990.

6. A. Belzner, U. Bischler, G. Crouch-Baker, T.M. Gur, G. Lucier, M. Schreiber, and R. Huggins "Two Fast Mixed-conductor Systems: Deuterium and Hydrogen in Palladium-Thermal Measurements and Experimental Considerations", in the Proceedings of the Workshop on Cold Fusion Phenomena, May 23-25, 1989, Santa Fe, New Mexico, to be published in J. Fusion Energy, March 1990.

7. K.L. Wolf, N.J.C. Packham, D.R. Lawson, J. Shoemaker, F. Cheng, and J.C. Wass, "Neutron Emission and the Tritium Content Associated with Deuterium Loaded Palladium and Titanium Metals", in the Proceedings of the Workshop on Cold Fusion Phenomena, May 23-25, 1989, Santa Fe, New Mexico, to be published in J. Fusion Energy, March 1990.

8. P.K. Iyengar, "Cold Fusion Results in BARC Experiment", in the Proceedings of the 5th International Conference on Emerging Nuclear Energy Systems (ICENES V), Karlsruhe, West Germany, July 3-6, 1989.

9. A.J. Leggett and G. Baym, "Exact Upper Bound on Barrier Penetration Probabilities in Many-Body Systems: Application to Cold Fusion", Phys. Rev. Lett. **63**, 191 (1989).

10. K. Langanke, H.J. Assenbaum, and C. Rolfs, "Screening Corrections in Cold Deuterium Fusion Rates", Z. Phys. A. Atomic Nuclei **333**, 317 (1989).

11. R.A. Rice, G.S. Chulick, Y.E. Kim, and J.-H. Yoon, "The Role of Velocity Distribution in Cold Deuterium-Deuterium Fusion", Purdue Nuclear Theory Group Report PNTG-90-5 (January 1990), submitted to Fusion Technology.

12. Y.E. Kim, "Cross-Section for Cold Deuterium-Deuterium Fusion", to be published in Fusion Technology, May, 1990.

13. M. Rabinowitz and D.H. Worledge, "An Analysis of Cold and Lukewarm Fusion", to be published in Fusion Technology **17**, (1990).

14. Y.E. Kim, R.A. Rice, and G.S. Chulick, "The Role of the Proton-Deuterium Fusion Cross Section in Physical Processes", PNTG-90-7 (February 1990), submitted to Fusion Technology.

15. W.A. Fowler, G.R. Caughlan, and B.A. Zimmermann, "Thermonuclear Reaction Rates", Ann. Rev. Astr. Astrophys. **5**, 525 (1967); "Thermonuclear Reaction Rates II", **13**, 69 (1975).

16. A. von Engel and C.C. Goodyear, "Fusion Cross-Section Measurements with Deuterons of Low Energies", Proc. Roy. Soc. A **264**, 445 (1961).

17. A. Krauss, H.W. Becker, H.P. Trautvetter, and C. Rolfs, "Low-Energy Fusion Cross Sections of D+D and D + ^3He Reactions", **A465**, 150 (1987).

18. H.H. Anderson and J.F. Ziegler, "Hydrogen Stopping Powers and Ranges in All Elements", Pergamon Press, New York (1977).

19. S. N. Vaidya and Y. S. Mayya, "Theory of Screening-Enhanced D-D Fusion in Metals", Jap. J. of Appl. Phys. **28**, L2258 (1989).

20. R.A. Rice, G. S. Chulick, and Y. E. Kim, "The Effect of Velocity Distribution and Electron Screening on Cold Fusion", to be published in the Proceedings of the First Annual Conference on Cold Fusion, Salt Lake City, Utah, March 28-31, 1990.

21. S. Hayakawa, *Cosmic Ray Physics*, Wiley, New York (1969).

22. H. O. Menlove et al., "The Measurements of Neutron Emissions from Ti Plus D_2 Gas", in the Proceedings of Workshop on Cold Fusion Phenomena, May 23-25, 1989, Santa Fe, New Mexico, to be published in J. Fusion Energy.

23. O. A. Yakubovsky, Yad. Fiz. **5** 1312 (1967) [Sov. J. Nucl. Phys. **5**, 937 (1967)]; P. Grassberger and W. Sandhas, Nucl. Phys. **B2**, 181 (1967); E. O. Alt, P. Grassberger and W. Sandhas, J.I.N.R. Report No. E4-6688 (1971).

24. Y. E. Kim, R. A. Rice, and G. S. Chulick, "The Electron Screening Effect on Fusion Cross-Sections and Rates in Physical Processes", Purdue Nuclear Theory Group Report PNTG-90-9 (March, 1990).

Table I

Extracted values of the electron screening parameter, $E_s(E)$, for eq. (25) from the experimental values of the D-D fusion cross section, $\sigma_{exp}(E)$, for reaction (1a), $D(D^+,p)^3H$, at low energies, $E < 4keV$ (CM). $\sigma_{calc}(E)$ is calculated with the conventional extrapolation formula, eq.(2), with $S(E) = 52.9keV - b$ and $E_G^{1/2} = 31.39(keV)^{1/2}$. The superscripts a and b in the first column refer to references 16 and 17, respectively.

E (keV in CM)	$\sigma_{exp}(E)$ (barn)	$\sigma_{calc}(E)$ (barn)	$E_s(E)$ (eV)
2.0^a	$(8.4 \pm 4.6) \times 10^{-9}$	6.06×10^{-9}	$59 \pm {}^{79}_{143}$
2.98^b	$(2.54 \pm 0.37) \times 10^{-7}$	2.25×10^{-7}	$40 \pm {}^{46}_{52}$
3.98^b	$(2.19 \pm 0.13) \times 10^{-6}$	1.95×10^{-6}	$58 \pm {}^{30}_{32}$

Table II

The fusion rate, $\sigma(E)\ v$(CM), for reactions (1a) and (1b), $D(D^+,p)^3H$ and $D(D^+,n)^3He$, calculated from eq. (25) with the muon screening energy term $E_s(E) = |V_s^\mu(r_a)|$. The classical turning point r_a is in units of the muonic Bohr radius $a_o^\mu \approx a_o/186 \approx 2.85 \times 10^{-3}$ Å.

E (eV)	r_a (a_o^μ)	$\lvert V_s^\mu(r_a)\rvert$ (keV)	$\sigma(E)$ (b)	$\sigma(E)\ v(CM)$ (cm^3/sec)
0.036	6	0.844	2.1×10^{-9}	5.6×10^{-28}
0.276	5	1.01	5.4×10^{-9}	3.9×10^{-27}
2.12	4	1.26	1.9×10^{-8}	3.9×10^{-26}
16.7	3	1.67	1.0×10^{-7}	5.8×10^{-25}

ON ASPECTS OF NUCLEAR PRODUCTS

by

G. H. Miley, M. H. Ragheb, and H. Hora[+]
Fusion Studies Laboratory
University of Illinois
Urbana, IL 61801

[+]Department of Theoretical Physics, University of New South Wales,
Kensington, New South Wales, Australia

ABSTRACT

Reaction product measurements are not yet conclusive and often appear contradictory. Still the measurement of tritium in several different laboratories appears most convincing. However, there is growing evidence that the tritium production rate can only account for a few percent of the heating rate while the neutron rate is only 10^{-5} to 10^{-8} times the tritium rate.

Various mechanisms proposed to explain these observations are reviewed. The often favored candidate for tritium production, $D + D \rightarrow (^4He)^* \rightarrow T + p + 3.7$ MeV, with the excess energy carried by phonons or electrons, would not explain heat production rate that would require $(^4He)^*$ decay by collective dissipation of 23.8 MeV. Thus it appears likely that several different reactions are involved. The need for improved diagnostics to provide a time correlation for the appearance of products and to measure X rays, gamma rays and energetic charged particles is stressed. The significance of the search for transmutation of Pd and Li isotopes on electrode surfaces is also discussed.

INTRODUCTION

The key objective for measurements of nuclear products is to identify the reaction mechanism (or mechanisms) that are occurring in the current cold fusion experiments. In addition to this identification, an understanding of the nuclear products is essential for the determination of future applications of cold fusion. For example, are we developing small radiation free cells for heat and electrical production or does this device better lend itself to tritium production?

The degree of correspondence between experimental measurements and theory is generally viewed as a gauge of the maturity of any new scientific endeavor. In that sense it appears that, as of today, cold fusion is not very mature; certainly when compared to hot fusion. However, cold fusion has an important advantage in that experiments can be done relatively cheaply in small cells in a variety of laboratories. Consequently, a wide data base can develop rapidly. Thus, it seems reasonable to expect that the field will quickly reach the point where measurements and theory converge to provide a clear understanding of the phenomena involved.

COMMENTS ABOUT REACTION PRODUCT MEASUREMENTS

As shown in Fig. 1, measurements in any experiment should cover a wide variety of possible reaction products[1]. These range from neutrons, gamma rays, X rays and neutrinos on to energetic charged products and isotopic abundances of electrode and electrolytic materials. Also, the importance of continuing the search for helium-4 and helium-3 in both the off gas and electrodes is widely recognized. In addition to measurement of specific products, it is essential that time correlations between various particle and radiation products and also heat production be established. As seen from the present meeting, several attempts to do this have been made[2]. However, due to complications associated with the "burst nature" of the phenomena, time correlations have been difficult to obtain. Not only are time correlations an essential element in the effort to identify the mechanism involved, but they should help resolve the issue of whether different mechanisms occur at different times in a given experiment or in uniquely

Neutrons

Gammas, x-rays, neutrinos

Charged Products

protons, ^4He, ^3He, tritium, betas (β^+ and β^-)

Transmuted Pd isotopes, Li isotopes, O isotopes

Figure 1. Possible Reaction Products from Experiments. Note: Different mechanisms may occur in various experiments, resulting in a different grouping of products.

Tritium/neutron rates ~ ratio of 10^5 to 10^8

Tritium Rx heat rate/heating rate < 5%

Burst character

neutron bursts { sec to 10s min duration; up to 100 n./50 μs bursts

heat bursts: long term "bursts," delayed initiation

Surface enrichment of ^{106}Pd ? ^{7}Li

appearance of Rh, Ag, Cu ?

3-MeV protons (bursts) ?

Autoradiograph: active surface "spots," K X rays

Neutron "avalanche," > 10^8 n/s, in "on-off" exps.

Gamma-rays ?

14-MeV neutrons doubtful

Figure 2. Characteristics observed in various experiments.

different experiments. Specifically, a key current issue is whether or not tritium production is correlated with heat and neutron production.

GENERAL OBSERVATIONS

At present it is difficult to provide firm conclusions about reaction products based on experimental data due to the non-reproducible nature and the intermittent bursts of heat and neutrons encountered in most cells. However, a rough impression is summarized in Fig. 2.

Most important, a pattern appears to be emerging where the tritium to neutron production rates occur in a ratio of 10^5 to 10^8[3,4]. Further, the heating rate that would accompany tritium production appears to be less than 5% of the overall heating rate. Indeed, not all experiments have demonstrated both tritium production and heating, so there may not even be a connection between the two. (For example, experiments at Oak Ridge National Laboratory reported at this meeting[5] were cited for excess heat but no measurable tritium. The Los Alamos National Laboratory experiments cited for tritium production[6,7] have not been instrumented for simultaneous heat measurements.) Still, the ratios cited here may be viewed as a "time average" over various experiments.

In addition to tritium production, a variety of other miscellaneous characteristics listed in Fig. 2 have been noted in various experiments. These include, both neutron and heat bursts[4,8]. Also the possible redistribution in surface layers of palladium and lithium isotopes as well as trace impurities in the electrodes has been observed in some instances[9,10]. MeV proton bursts have been reported in several instances. Further, the spotty nature of X-ray and/or gamma-ray production has been demonstrated in autioradiographic measurements[3]. Other phenomena include the observation of massive neutron avalanches in "on-off" experiments and occasional reports of gamma emission in other cells[5,11]. It is important to note that, to date, no experiment hasreported 14-MeV neutron production. Neither has there been a measurement reported which would verify ^4He or ^3He production -- the measurements attempted being inconclusive[12].

Since many of these observations occur on different cells and are not always reproducible, an interpretation is difficult. For example, the segregation of trace impurities and enrichment of some isotopes on electrode surfaces observed in several experiments appears to be associated with electrically driven transport processes rather than a nuclear

reaction. However, some of these phenomena may enable the reaction, or alternatively quench it. More work needs to be done to clarify these issues. Thus for present purposes, we will mainly concentrate on tritium and heat reactions since data for these phenomena has been most widely reported.

When searching for reaction mechanisms, it is important to keep in mind that there are two key issues that require resolution. The first is a quantitative explanation of the reaction rates, i.e., the tritium production rate and also the heating rate in the cell. The second issue though, is the relative production of the reaction products, i.e., to the branching ratio between reaction "channels."

TRITIUM PRODUCTION MECHANISMS

As seen from the list of possible two-body reactions, given in Table 1 (taken from Ref. 13), very few reactions can lead to tritium production. The D-D reaction itself is the most obvious candidate. If this is not the source of tritium, then we must jump to other reactions such as:

$$^{2}_{1}D + {}^{7}_{3}Li \rightarrow {}^{3}_{1}T + {}^{6}_{3}Li, \text{ or:}$$

$$^{2}_{1}D + {}^{17}_{8}O \rightarrow {}^{3}_{1}T + {}^{16}_{8}O$$

which, due to smaller abundances of the Li-7 and O-17 isotopes and smaller classical reaction cross sections, seem less likely. While the possibility of tritium production by a multibody mechanism cannot be ruled out, there does not appear to be a reasonable candidate. Thus we conclude here that the D-D reaction is the most probable source of tritium. This conclusion must be viewed in light of additional observations summarized in Fig. 3 that are connected with tritium production. The many orders of magnitude higher tritium production rate vs. neutron rate suggests that the D-D reaction must proceed through the t + p channel rather than the He^3 + n branch. Also, if the absence of 14-MeV neutrons is confirmed, it appears that the tritium must be born at abnormally low energies. In the "conventional" D-D reaction, corresponding to Fig. 3, tritium would be released at 3 MeV. Then, as it slows down in the dense deuterium medium, D-T reactions would occur providing a measurable 14 MeV neutron signal (see, for example, Ref. 14). The failure to observe 14-MeV neutrons is not completely conclusive, however. Such measurements are difficult in view of the erratic behavior of cells. Also the relatively low yields make detection difficult. Thus continued stress should be placed on a search for possible 14-MeV neutrons. Another issue which should be considered is that anomalous slowing of the fast tritium due to collective effects could result in a very low yield of 14-MeV neutrons. At the moment, however we will simply assume that no neutrons are observed and that a classical Fokker-Planck behavior of tritium slowing-down occurs. In that case, cf. Fig. 3, there are limited possible explanations for tritium production. One popular explanation for the strong tritium channel (originally advocated by the authors), is an Oppenheimer-Phillips type D-D reaction. However, this reaction would still proceed with the production of 3-MeV tritium so the 14-MeV neutron argument seems to rule it out. This leaves the possibility of "deuteron tunneling" as proposed earlier by G. Collins[15] and discussed in detail by J. Schwinger[16] at this conference. As indicated in Fig. 3, this reaction produces tritium at 0.08 MeV with the transfer of 3.97 MeV of energy to the surroundings (see the energy level diagram of Fig. 4). G. Collins originally proposed that this excess energy was carried off by electrons while J. Schwinger's recent theory is based on transfer to phonons. In either case, the reaction products are identical. Thus an identification of the exact carrier of the excess energy is not crucial to the present discussion. Further, it should be stressed that in either theory the energy released per triton formed is also identical. Thus the heating rate associated with tritium production is unambiguous, and this is important in any comparison of the tritium production rate to the cell heating rate.

While tritium might be produced via various reactions with lithium, experiments appear to make this possibility unlikely. For example, lithium isotope substitution experiments have not confirmed the need for a specific isotope in order to produce tritium[17]. Substitution of the sodium equivalent for

TABLE I

Possible Two-Body Reactions, Their Products, and Q Values

Reactants	Product 1	Product 2	Product 3	Q Value (MeV)
$p + d$	^{3}He	γ		5.4
$d + d$	t ($\beta t_{1/2} = 12.3$ yr)	p		4.03
	^{3}He	n		3.27
$p + {}^{6}$Li	^{7}Be ($\epsilon t_{1/2} = 53.3$ days)	γ		5.61
	^{3}He	α		4.02
$p + {}^{7}$Li	^{8}Be ($2\alpha t_{1/2} = 0.07$ fs)	γ		17.25
	α	α		17.35
$d + {}^{6}$Li	^{8}Be ($2\alpha t_{1/2} = 0.07$ fs)	γ		22.28
	α	α		22.37
	^{5}He (α, $n\Gamma = 0.6$)	^{3}He		0.84
	^{3}He	α	n	1.80
	^{7}Li	p		5.03
	^{7}Be ($\epsilon t_{1/2} = 53.3$ days)	n		3.38
	^{5}Li (α, $p\Gamma = 1.5$)	t ($\beta t_{1/2} = 12.3$ yr)		0.60
$d + {}^{7}$Li	^{9}Be	γ		5.61
	^{8}Be ($2\alpha t_{1/2} = 0.07$ fs)	n		15.03
	^{5}He (α, $n\Gamma = 0.6$)	α		15.16
	α	α	n	15.12
$p + {}^{12}$C	^{13}N ($\epsilon t_{1/2} = 9.96$ min)	γ		1.94
$d + {}^{12}$C	^{14}N	γ		10.27
$p + {}^{16}$O	^{17}F ($\epsilon t_{1/2} = 64.5$ s)	γ		0.6
$d + {}^{16}$O	^{18}F ($\epsilon t_{1/2} = 110$ min)	γ		7.53
$p + {}^{102}$Pd	^{103}Ag ($\epsilon t_{1/2} = 1.10$ h)	γ		4.24
	m (IT$t_{1/2} = 5.7$ s)			4.11
$p + {}^{104}$Pd	^{105}Ag ($\epsilon t_{1/2} = 41.3$)	γ		5.01
	m (ϵ, IT$t_{1/2} = 7.2$ min)			4.97
	^{101}Rh ($\epsilon t_{1/2} = 3.3$ yr)	α		2.85
	m (ϵ, IT$t_{1/2} = 4.34$ days)			2.69
(Similar reactions in ^{106}Pd, ^{108}Pd, ^{110}Pd: see Ref. 1)				
$d + {}^{102}$Pd	^{103}Ag ($\epsilon t_{1/2} = 1.1$ h)	n		2.01
	m (IT$t_{1/2} = 5.7$ s)			1.88
	^{103}Pd ($\epsilon t_{1/2} = 17.0$ days)	p		5.38
(Similar reactions in ^{104}Pd, ^{105}Pd, ^{106}Pd, ^{108}Pd and ^{110}Pd: see Ref. 1)				

Nomenclature

d = deuteron

IT = isomeric transition (gamma-ray and conversion-electron decay)

m = isomeric state

n = neutron

p = proton

t = triton

$t_{1/2}$ = half-life

α = alpha decay

β = negative beta decay

ϵ = positive beta decay including electron conversion

Γ = level width for particle-unstable nuclides (MeV)

Tritium

T/n rates ~ 10^{5-8}

no 14-MeV neutrons ?

$$D + D \rightarrow \begin{cases} T + D \rightarrow \alpha + n + 17.6\ MeV \\ \uparrow \\ T + p + 4.02\ MeV \\ {}^3He + n + 3.27\ MeV \end{cases}$$

Low energy T ? Possible Explanations

- D + D Oppenheimer-Phillips Reaction - predicts high energy T however.
- D or n tunneling (Δ carried by electrons or phonons)

$$D + D \rightarrow {}^4He\ (20\ MeV) + \Delta(3.7\ MeV)$$
$$\downarrow$$
$$T(.08\ MeV) + p(0.23\ MeV)$$

- D + Li reaction ? (Inconsistent with tritium reported in non Li containing cells)

$^6Li(n,\alpha)T$ $\quad$ $^6Li(d,\alpha,p)T$

$^7Li(n\alpha,n)T$ $\quad$ $d(^6Li,\alpha,p)T$

- D + O reaction ? ${}^2_1D + {}^{17}_8O \rightarrow {}^3_1T + {}^{16}_8O$

Other mechanism issues:

Surface vs Volume

Local fields via surface projections vs. Surface Potential

} crucial to scaling relations

How to account for the heating observed? Second reaction independent of tritium producing reaction needed?

Figure 3. Observations connected with tritium production.

the lithium electrolyte did, however, reduce excess heat production[17]. Thus the role of the electrolyte is not clear. Further, there are some reports of tritium in cells that do not contain lithium at all. (An example is T. Claytor's experiment at Los Alamos National Laboratory[18].) In summary then, the D-D reaction associated with n/D tunneling shown in Figures 3 and 4 must be viewed as a possible explanation.

A number of associated issues also need resolution. The most obvious is the location of the reaction, i.e, whether it occurs only on the surface versus in the volume of the electrode. The surface is favored in several theories, e.g., deuteron acceleration by local fields created by dendrites or by a double potential layer at the surface[2,19]. Indeed, thus far, some experimental data appears to favor a surface reaction, but there are contradictions and the data is ambiguous.

Perhaps the most important issue is whether the tritium reaction can also account for the observations of excess heat; i.e., is there a second independent heat producing reaction? Indeed, the latter seems likely since the energy release in the tritium reactions of Figs. 3 and 4 does not account for more than 5% of the heating reported in strong

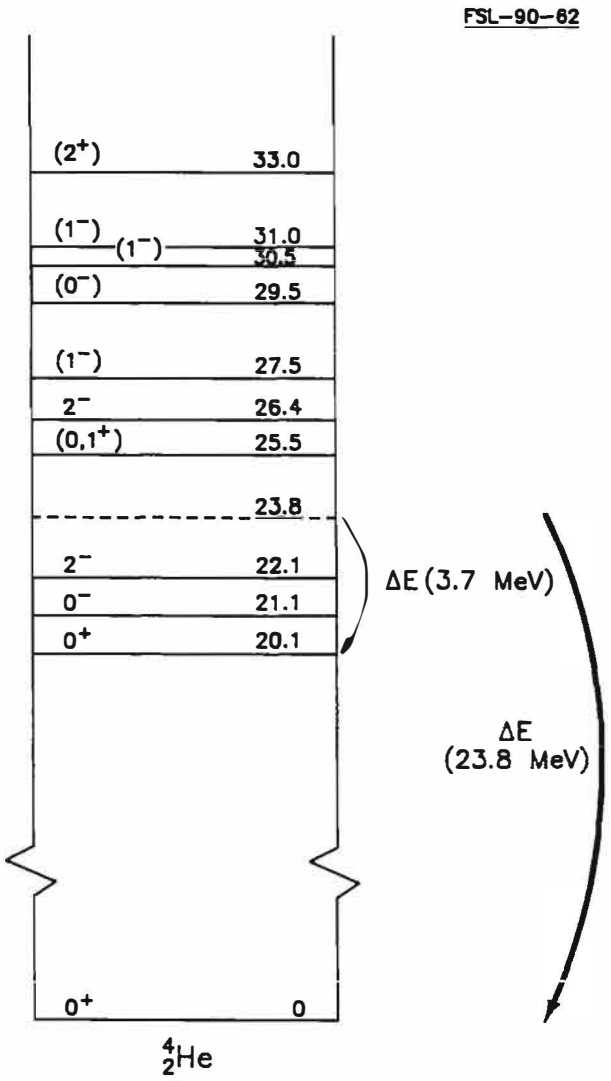

Figure 4. Energy Level Diagram for the ^{4}He Compound Nucleus.

"heating" experiments[2,3]. Although the lack of correlated measurements admittedly clouds this issue, we will choose to treat heat production as a separate issue in the present discussion.

HEAT PRODUCTION REACTIONS

The most crucial, but to date, the least understood mechanism associated with cold fusion experiments is the observation of excess heat. The observation of tens of megajoules energy release in various experiments seems to rule out all possible sources except nuclear reactions[2,20].

Characteristics observed in calorimetric experiments of heat production are summarized in Fig. 5. As stressed earlier, the ratio of heat production to the heating rate associated with tritium production appears to be a factor of 20 to 100. In addition, the heat production must be quite aneutronic since the tritium reaction itself is so much stronger than the neutron rate.

Various reaction mechanisms which have been discussed in connection with heating are also outlined in Fig. 5. The "deuteron tunneling" reaction in deuterium is quite similar to one discussed earlier in connection with tritium production. However, now, as shown earlier from the energy level diagram in Fig. 4, 23.8 MeV must be dissipated (as opposed to 3.7 MeV[1]). Initial theoretical studies of cold fusion proposed several mechanisms for dissipation of this large amount of energy[21,22], but the present consensus is that this is unlikely. The point is that the lifetime of the ^{4}He compound nucleus is extremely short[13] so that a collective dissipation of the 23.8 MeV's would have to occur to distribute order of an eV/photon (or multi-eV/electron) quickly enough to prevent decay to other products, i.e., to avoid the "classical" D-D reaction.

Another reaction that has been considered is D-^{6}Li with the release of two alpha particles carrying a total of 22.4 MeV[30]. In addition to the appearance of high energy alphas, this reaction should produce copious X rays. A search for such emission is just starting. A dependence on ^{6}Li should also be apparent in the cells, but this has not been confirmed yet, and, indeed there is some evidence to the contrary.

Another mechanism which has been considered in several different forms involves a chain reaction carried by neutrons[23,24]. The "closing" of the chain typically assumes a gamma interaction with deuterium which reproduces the chain carrying neutron. However, calculations of the relative reaction rates do not appear to justify this closure, i.e., it appears that the chain would be very short. Thus, this mechanism does not seem likely.

A third possibility which has been discussed by the present authors is an Oppenheimer-Phillips reaction between the deuterium and the palladium itself[1,25]. (In this case, an Oppenheimer-Phillips reaction involving D-D would occur

Heating Observations

- $\dot{H}$ / $\dot{T}$ ~ 20 - 100 x ?
- aneutronic

Reaction Possibilities

- D + D → + ^{4}He + 23.8 MeV ?
- D + ^{6}Li → 2^{4}He + 22.4 MeV ?
- neutron chain chain rate ?
- Q-P

  D + ^{A}Pd → $^{A+1}$Pd + p ~ 4.8 MeV

  Pd isotope shift ??
- n-D tunneling

  ^{6}Li + ^{6}Li → ^{7}Li + p + α + 3.6 MeV
  ^{6}Li + ^{6}Li → 2α + t + p + 1.1 MeV
- Coherent
  Cluster (Nattoh Model)
  Bose Block Condensate (BBC)

  Various products
  MeV particles/alphas X rays
  } ?
- X^- catalysis

  Xd + α → X^- + ^{6}Li + 1.48 MeV
  (tritium production: ??) → simulated tritium: Xp
  } ?

Figure 5. Characteristics observed in calorimetric experiments.

simultaneously, producing tritium and suppressing the neutron branch. However, as discussed earlier and also in Ref. 1, this view would require rationalization of the relative D-Pd and D-D reaction rates as well as an explanation of the lack of observed 14-MeV neutrons from the energetic tritium.) Again there is considerable difficulty in justifying the reaction rate that would be needed to match the observed heating. However, this reaction would be a prime candidate if palladium isotope transmutations are found[1,25]. Indeed, as indicated by D. Rolison et al.[9] at this meeting, palladium isotopic shifts may have been observed in one instance, but this result has not been reproduced. Further, no indication of such a shift has been found in several cases where surface measurements of electrodes have been carried out in other laboratories[10]. Unless experimental confirmation of an isotope shift is found, this mechanism must be ruled out.*

A fourth possible mechanism is the counterpart of the deuteron tunneling mechanism proposed by Collins[15] as applied to lithium. For example, lithium-6 reactions would yield lithium-7 plus a proton and alpha particle. Something of this nature might be inferred from some data. For example, lithium isotopic shift

*Note, however, that as discussed in Ref. 1, transmutations by the Oppenheimer-Phillips reaction will occur in different ratios than those due to "free" neutrons. The relative shifts in the former will be less, so a very careful examination of relative isotopic abundances is essential to evaluate this possibility.

on electrode surfaces noted by several workers at the present meeting[10] seems suggestive of such a reaction. However, again there is no explanation for the reaction rate that would be required to provide the heating rate reported in various experiments. Also this explanation would not be consistent with experiments where lithium-6 was not present when heating was obtained[2,17]. Thus this mechanism also seems unlikely.

Another category of mechanisms includes a variety of multibody reactions with energy being carried off by coherent effects. These include the general theory of coherent reactions[16,26,27], the multibody cluster ("Nattoh") mechanism[28], Bose-Block Condensate[29], the transmission resonance concept[30], etc. These various mechanisms have not been explored in depth yet and require more study to fully evaluate, however. Reaction products have not been clearly identified in all of the proposed mechanisms either, although helium production is a common product which could be detected. Also, these phenomena generally result in MeV charged particles with accompanying gamma-ray and/or X-ray emission. Thus experimental studies of these radiations are crucial to the evaluation of possible mechanisms.

Another hypothesis revolves around the issue that a strange particle, namely the X^- particle, could catalyze cold fusion[31]. The X^- particle is postulated as a remnant from the early formation of the universe. If it exists, the bombardment of the earth by a flux of Xp could result in a finite concentration of Xd in heavy water. Thus, in the cold fusion cell, energy could be released by the interaction of Xd with alpha particles contained in other nuclei, freeing the X^- and yielding Li^6 and heat. The X^- particle would continue to interact in a chain-like reaction. This theory might even provide an explanation for tritium observations since an Xp particle would have an electronic structure capable of simulating tritium emission. While such a phenomena cannot be ruled out, much more effort would be necessary to provide convincing evidence, especially since the X^- has not previously been observed.

An alternate theory involves the formation of a new neutral particle, designated as Neutrium (Nu) which consists of two bound neutrons [32]. The Nu can be absorbed by deuterium, Pd or other heavy nuclei, producing a source of heat. Nu, alternately called the dineutron, was originally studied with respect to the T-T reaction

$$ {}_1^3T + {}_1^3T \rightarrow 2\,{}_0^1n + {}_2^4He \quad . $$

In conclusion then, the search for the heat producing reaction in cold fusion remains as the greatest mystery of cold fusion. Of the various possibilities discussed here, perhaps the D-D reaction with 23.8 MeV coherent dissipation remains as the most plausible but has no complete theoretical justification. To solidify this position, we must find a theory for rapid dissipation of this huge amount of energy and intensify the search for He^4 production. On the other hand, if the report of an isotopic shift of either palladium or lithium is confirmed, obviously a strong focus would develop on the reactions involving these species.

The measurement of charged particles and of gammas should provide a strong insight into the various multibody reaction possibilities. The observation of high-energy charged particles, in particular, would provide a strong clue. Indeed, several new experiments aimed at charged particle detection are being developed (see, for example, Ref. 33). These include plans to incorporate solid-state detectors into special design cells. Another approach which has started to receive some emphasis is the possible use of CR-39 plastic foil for charged particle tracking[34,35]. The advantage of such foils is their low cost and the relative ease of inserting them into the experiment.

As stressed by several investigators, any mechanism which is proposed must be consistent with the frequently observed burst behavior and long wait prior to initiation which is observed in many experiments. The explanation for these characteristics must be an inherent feature of the mechanism. An example is the high sensitivity of the tritium production rate to key parameters in the exponential functions in Schwinger's theory[16]. On the other hand, this "delay" could be due to other physical

conditions that must be brought together in order to enable the mechanism to proceed. For example, a special surface composition might be required. Along that line, some comment is worthwhile about the difference between microscopic hot fusion and cold fusion. In some theories, such as crack propagation, the electric field accelerates deuterium causing reactions by a high energy particle interacting with the cold background (known in the hot fusion community as beam-target interactions). This might help explain the reaction rate but does not explain how the branching occurs. A complete theory must resolve both issues. Indeed, attempts are now being made to incorporate aspects of both reaction rate and branching phenomena in a unified theory (e.g., see Rice, et al.[36]).

SUMMARY

In summary, there is not a consistent picture as to the mechanism and the associated reaction products. However, with the rapid rate of advance and accumulation of experimental data there is every hope that the situation should be cleared up in the near future. One difficulty revolves around the danger that mistakes will be made due to the possible existence of multiple mechanisms which might occur simultaneously during a given experiment or at different times in different experiments.

The level of sophistication of diagnostics of cold fusion has increased dramatically in the past year. There is strong hope that this will help in the resolution of the reaction mechanism. Of course, to fully understand the cell operation, one needs a full array of diagnostics capable of covering a variety of particle and radiation as indicated earlier in Fig. 1. This must be combined with the capability for extensive surface and volume metallurgy. Finally, all these diagnostic techniques must be combined with good control of the experimental conditions in the cell.

REFERENCES

[1] G. H. Miley, M. Ragheb and H. Hora, "Comments About Diagnostics for Nuclear Reaction Products From Cold Fusion," NSF/EPRI Workshop, Washington, D.C., Oct. 16-18, 1989 (in press).

[2] For example, see J. O'M. Bockris, G. H. Lin and N. J. C. Packham, "Nuclear Electrochemistry Among the Hydrogen Isotopes," The First Annual Conference on Cold Fusion, Salt Lake City, UT, March 28-31, 1990.

[3] Government of India, Atomic Energy Commission Report BARC-1500, P. K. Iyengar and M. Srinivasan (Eds.), September (1989).

[4] K. L. Wolf, D. E. Lawson, J. C. Wass and N. J. C. Packham, Proceedings of the EPRI/NSF Conference on Cold Fusion Phenomena, Washington, D.C., October (1989).

[5] C. D. Scott et al., "Measurement of Excess Heat and Apparent Coincident Increases in the Neutron and Gamma Ray Count Rates During the Electrolysis of Heavy Water," The First Annual Conference on Cold Fusion, Salt Lake City, UT, March 28-31, 1990.

[6] E. Storms and C. Talcott, "Electrolytic Tritium Production," *Fusion Technology*, in press (1990).

[7] E. Storms and C. Talcott, "A Systematic Study of Electrolytic Tritium Production," The First Annual Conference on Cold Fusion, Salt Lake City, UT, March 28-31, 1990.

[8] H. O. Menlove, "High Sensitivity Measurements of Neutron Emission From T_i Metal in Pressurized D_2 Gas," The First Annual Conference on Cold Fusion, Salt Lake City, UT, March 28-31, 1990.

[9] D. Rolison et al., "Anomalies in the Surface Analysis of Deuterated Palladium Metals," The First Annual Conference on Cold Fusion, Salt Lake City, UT, March 28-31, 1990.

[10] D. R. Coupland et al., "Some Observations Related to the Structure of Hydrogen and Deuterium in Palladium," The First Annual Conference on Cold Fusion, Salt Lake City, UT, March 28-31, 1990.

[11] Y. Arata and Y-C. Zhang, "Achievement of Intense 'Cold' Fusion Reaction," *Fusion Technology* (July 1990, in press).

[12] N. Hoffman, Rockwell International, "Panel Discussion - Nuclear Phenomena," The First Annual Conference on Cold Fusion, Salt Lake City, UT, March 28-31, 1990.

[13] D. Mueller and L. R. Grisham, "Nuclear Reaction Products That Would Appear if Substantial Cold Fusion Occurred," *Fusion Technology*, *16*, 379, 1989.

[14] R. W. Bussard, "Virtual-State Internal Nuclear Fusion in Metal Lattices," *Fusion Technology*, *16*, 231, 1989.

[15] G. S. Collins, "Deuteron Tunneling at Electron-Volt Energies," Abstracts, Workshop on Cold Fusion Phenomena, Santa Fe, NM, May 23-25, 1989.

[16] J. Schwinger, "Nuclear Energy in an Atomic Lattice," The First Annual Conference on Cold Fusion, Salt Lake City, UT, March 28-31, 1990.

[17] S. Srinivasan and A. J. Appleby, Proceedings of the EPRI/NSF Conference on Cold Fusion Phenomena, Washington, D.C., October (1989).

[18] Described by H. Menlove in Panel Discussion at NSF/EPRI Workshop, Oct. 16-18, 1989 (to be published).

[19] H. Hora, G. H. Miley, and M. Ragheb, "Plasma and Surface Tension Model for Explaining the Surface Effect of Tritium Generation in Cold Fusion," *Nuovo Cimento*, *12* , 393 (1990).

[20] S. Pons, "Calorimetry of the Palladium-Deuterium System," The First Annual Conference on Cold Fusion, Salt Lake City, UT, March 28-31, 1990.

[21] P. L. Hagelstein, "A (Slightly Revised) Simple Model for Coherent DD Fusion in the Presence of a Lattice," Abstracts, Workshop on Cold Fusion Phenomena, Santa Fe, NM, May 23-25, 1989.

[22] J. R. McNally, "On the Possibility of a Nuclear Mass-Energy Resonance in D + D Reactions at Low Energy," *Fusion Technology*, *16*, 237, 1989.

[23] J. C. Jackson, "Cold Fusion Results Still Unexplained," Scientific Correspondence, *Nature, 339*, 345, 1989.

[24] Y. E. Kim, "New Cold Nuclear Fusion Theory and Experimental Tests," Abstracts, Workshop on Cold Fusion Phenomena, Santa Fe, NM, May 23-25, 1989.

[25] M. Ragheb and G. H. Miley, "On the Possibility of Deuteron Disintegration in Electrochemistry-chemically Compressed D+ in a Palladium Cathode," *Fusion Technology*, *16*, 243, 1989. Also see: Abstracts, Workshop on Cold Fusion Phenomena, May 23-25, 1989, Santa Fe, NM (to be published, *Journal of Fusion Energy*).

[26] P. L. Hagelstein, "Status Report on Coherent Fusion Theory," The First Annual Conference on Cold Fusion, Salt Lake City, UT, March 28-31, 1990.

[27] G. Preparata, "Some Theoretical Ideas on Cold Fusion," The First Annual Conference on Cold Fusion, Salt Lake City, UT, March 28-31, 1990.

[28] T. Matsumoto, "'NATTOH' Model for Cold Fusion," *Fusion Technology*, *16*, 532, 1989.

[29] S. R. Chubb and T. A. Chubb, "Quantum Mechanics of 'Cold' and 'Not So Cold' Fusion," The First Annual Conference on Cold Fusion, Salt Lake City, UT, March 28-31, 1990.

[30] R. T. Bush, "Isotopic Mass Shifts in Cathodically-Driven Palladium via Neutron Transfer Suggested by a Transmission Resonance Model to Explicate Enhanced Fusion Phenomena (Hot and Cold) Within a Deuterated Matrix," The First Annual Conference on Cold Fusion, Salt Lake City, UT, March 28-31, 1990.

[31] J. Rafelski, et al., "How Cold Fusion can be Catalyzed," Report AZPH.Th/90-08, Univ. of Arizona, Tucson, AZ, Feb. 15, 1990 (in press, *Fusion Technology*).

[32] G. Andermann, "A Theoretical Model (Nu-Q) for Rationalizing Electrochemically Induced Nuclear Events Observed in Deuterium Loaded Pd Cathodes," The First Annual Conference on Cold Fusion, Salt Lake City, UT, March 28-31, 1990.

[33] S. Jones, "Cold Nuclear Fusion in Condensed Matter: Recent Results and Open Questions," The First Annual Conference on Cold Fusion, Salt Lake City, UT, March 28-31, 1990.

[34] X. L. Jiang and L. J. Han, "Micropinch in Cold Nuclear Fusion," Report DMPL/89-03, Lanzhow University, China, Sept. (1989).

[35] R. Ilic, et al., "Investigations of the D-D Fusion Reaction in Cast, Annealed and Cold Rolled Palladium, Internal Report, J. Stefan Institute, Yugoslavia, March 1990 (in press, *Fusion Technology*).

[36] R. A. Rice, et al., "The Effect of Velocity Distribution on Cold Deuterium Fusion," The First Annual Conference on Cold Fusion, Salt Lake City, UT, March 28-31, 1990.

ISOTOPIC MASS SHIFTS IN CATHODICALLY-DRIVEN PALLADIUM VIA NEUTRON TRANSFER SUGGESTED BY A TRANSMISSION RESONANCE MODEL TO EXPLICATE ENHANCED FUSION PHENOMENA (HOT AND COLD) WITHIN A DEUTERATED MATRIX

Robert T. Bush

Physics Department
California State Polytechnic University
3801 West Temple Avenue, Pomona, CA 91768

Abstract: The transmission resonance model previously presented by the author [3] to explicate cold fusion phenomena is now extended to treat the full range of enhanced fusion phenomena, from "hot" to "cold", within a deuterated matrix. Such seemingly disparate effects as low-level neutron emission, tritium production, the Pons-Fleischmann effect (i.e.,excess heat production in electrolytic cold fusion) [1],[2], and "cluster-impact" fusion (i.e., hot fusion within a lattice), may share a commonality as enhanced fusion phenomena resulting from the resonant transmission of de Broglie waves within a deuterated matrix. A new phenomenon is suggested as a possible source of excess heat; "transmission resonance-induced neutron transfer" (t.r.i.n.t.), which, in its effect, is essentially equivalent to Teller's hypothesized "catalytic neutron transfer" [4], and gives added support to a research suggestion of Teller [4]. An expression is given for relative excess power in the electrolytic case in terms of temperature and current density, and is suggestive when applied to new data on excess power. A postscript in this section indicates an apparent breakthrough for the model. The relative excess power expression is incorporated into a relation to give absolute excess power. When combined with the data it is found that the cross-section for the nuclear process that is the ultimate source of the excess power is on the order of 10^{-24} cm^2; viz., one barn.

INTRODUCTION

The transmission resonance model as applied strictly to cold fusion will first be updated and summarized in order to provide a framework for its generalization to predict enhanced fusion phenomena, hot and cold, in a deuterated matrix; e.g., palladium deuteride or titanium deuteride. The generalized model suggests that neutron emission (such as that observed in experiments employing pressurized deuterium gas and titanium shavings), electrolytic cold fusion, tritium production, and "cluster-impact" fusion (hot fusion) may all be examples of such enhanced fusion phenomena within a deuterated matrix. The model suggests a new phenomenon, "transmission resonance-induced neutron transfer" (t.r.i.n.t.), as a possible source of excess heat which, in its effect, is essentially equivalent to Teller's hypothesized "catalytic neutron transfer"[4]. A research proposal of Teller's [4] thus receives additional support from the transmission resonance model. A relative excess power expression is introduced for electrolytic cold fusion and compared to new data. A postscript in this section indicates that the model has achieved a breakthrough. An absolute excess power relation for electrolytic cold fusion is introduced and employed to derive a nuclear cross-section for the nuclear reaction that is the ultimate source of the excess heat.

THE TRANSMISSION RESONANCE MODEL (TRM) FOR COLD FUSION

Model Basis

The central assumption of the model is a transmission resonance condition for the de Broglie waves associated with diffusons, e.g. diffusing deuterons (hereafter: D's), within a deuterated matrix (usually a metal deuteride lattice) that is a simplification of a recent conjecture by L. Turner of L.A.N.L. [5],[6]. Combined with this central assumption are an energy distribution for the diffusons (taken as a Maxwell-Boltzmann distribution at the surface of the sample), and the

effects of "phonon exchange" between the interstitial D's in the matrix and the matrix; e.g., a palladium lattice. Finally, the boson nature of the D's is invoked at several stages.

Transmission Resonance Condition

Turner [5],[6] has recently suggested that cold fusion may involve transmission resonances for D's diffusing through a periodic array of wells formed by the "ascending walls of neighboring Coulomb barriers" of interstitial D's within the Pd lattice. He points out that "conventional quantum mechanics yields a transmission coefficient of unity whenever the resonance condition of

$$\int_0^L k(x)dx = (n + 1)\pi \qquad (1)$$

is satisfied by the wavenumber of the particle crossing the potential well between the two barriers." [k(x) in (1) is the wavenumber of the diffusing particle, and L is the well width. [An excellent treatment leading to (1), and indicating when the term on the righthand side should be replaced by (n + 1) is provided in Chap. 12 of Bohm's Quantum Theory 7].] If λ is now taken to be the average de Broglie wavelength within the potential well, it is easily seen that (1) is simplified to

$$(2n + 1)\lambda/4 = L, \quad n = 0, 1, 2, \qquad (2)$$

(If the well were reasonably flat, λ would be essentially constant within it.)

Physical Meaning

Based upon the condition expressed by (2), we will assume that transmission occurs through a barrier-well-barrier combination whenever an odd quarter number of de Broglie wavelengths of the diffuson fit into the well width L. If we consider a de Broglie wave incident from left to right upon the barrier-well-barrier combination, then the physical meaning of the high transmissivity through the combination is as follows: That part of the wave reflected from the second barrier is interfering almost totally destructively with that part of the wave reflected from the first barrier to yield essentially zero reflected wave for the combination. (See Fig. 1, below.) With regard to this situation Bohm 7] notes: "It is especially interesting that although a single high and thick barrier has a very small transmissivity, two such barriers in a row can be completely transparent for certain wavelengths. This behavior can be understood only in terms of the wavelike aspects of matter. The high transmissivity arises because, for certain wavelengths the reflected waves from inside interfere destructively with those from the outside so that only a transmitted wave remains." The resonance condition also leads to a relatively high amplitude of the wave inside the well, and Bohm [7] demonstrates that the energy levels associated with (2) correspond to metastable states.

It is of course this resonant transmission that is assumed to result in a diffuson (e.g., a D) getting close enough to a relatively fixed particle within the lattice to give the two particles a large probability of undergoing a nuclear reaction compared to the case when the condition (2) is not satisfied. Thus, in this model it is this resonant transmission phenomenon that is invoked to explain the central mystery of cold fusion; viz., how is it possible to have two charged particles, such as two deuterons, have a large enough probability to undergo a nuclear reaction in a metal lattice at room temperature to provide credibility for the purported effects, e.g. the amount of "excess heat" claimed.

As an example of a well-known wave-mechanical phenomenon involving a high transmissivity associated with a quantum resonance condition we need only to recall the Ramsauer effect: Electrons incident upon a noble gas, such as argon, are found not to be scattered if their de Broglie wavelengths satisfy condition (1) with the factor (n + 1/2) on the righthand side replaced by (n + 1). [See Bohm's Quantum

Theory [7], Chap. 12, to understand why the wave relation expressing resonance here is altered from that of (1).]

Metastable States: Lifetimes and the Effect of Coherence

The physical picture that emerges is one in which the lack of a reflected de Broglie wave causes the amplitude of the wave to become relatively large inside the well as it bounces back and forth between he barriers as shown qualitatively in Fig 1. It is the "leakage" of this large amplitude wave through the barrier on the far side that leads to a wave of amplitude low compared to that in the well, but of comparable amplitude to the wave incident upon the first barrier. Thus, transmissivity is essentially 100%.

Since the transmission resonance condition is also the condition for a "metastable state"; i.e., a relatively long-lived state, the question arises as to whether there are states with short enough lifetimes to allow them to be associated with the the excess power phenomenon. Elsewhere [8] we show that, without bringing in considerations involving the coherence of the bosons, the lifetimes of the first four metastable states corresponding to orders n = 0, 1, 2, and 3 are, respectively, 0.76×10^{-10} s, 1.36×10^{-8} s, 4.4×10^{-6} s and 1.7×10^{-3} s. Thus, all four states have short enough lifetimes to be operable in an excess heat scenario based upon the transmission resonance model (hereafter: TRM). The next three states, i.e. n = 4, 5, and 6 have lifetimes that make them interesting candidates for the "heat bursts" reported by some observers: Respectively, they are 0.7 s, 3.1×10^{2} s (approximately 5 min.), and 1.4×10^{5} s (approximately 39 hours). (The n=7 state, however, already has a lifetime of about 2 years.)

If considerations of coherence are employed for the bosons (the D's), however, it is possible to show [8] that, depending upon the effective "coherence volume", a number of higher order states can be brought into play: The basic idea, here, is that for the coherent case, when one particle makes the transition through the second barrier they essentially all do. So, it becomes a question of figuring out how long one would have to wait to see one particle emerge for the case in which the wavefunction is considered to be appropriately enhanced and the number of parallel, but interdependent-via-coherence, " transmission experiments" is vastly increased. In essence, then, coherence produces a totally new situation that we might liken to a large number of "phase-locked" de Broglie wave lasers operating over the coherence volume. For a coherence volume equal to 1% of the active region the new lifetimes corresponding, respectively, to metastable states of order n =15, 16, 17, 18, and 19, would be 2ms, 0.1 s, 51 s, 2.5×10^{3} s (0.7 hrs), and 1.4×10^{7}s (162 days). So states of order n = 0 through n = 15 would here be available for what is observed to be the "steady" production of excess heat. And, again, the longer-lived of these might conceivably account for "heat bursts". Of course it is clear that even the "steady-state" production of excess heat has a "burst" nature if one looks on a small enough time scale. In this context we note that Huggins [9] has remarked that the production of

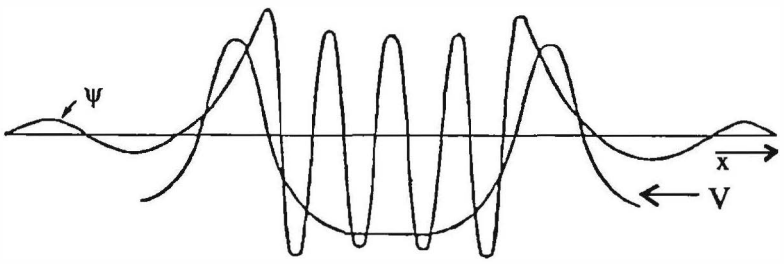

Fig. 1. Barrier-Well-Barrier Combination with de Broglie Wave Incident from Left.

excess heat is essentially a "non-equilibrium phenomenon", as opposed to a steady-state phenomenon.

The symmetry of the boson wavefunctions with the additional strict requirements of periodicity imposed by the periodicity of the crystalline lattice (Floquet's theorem) appear capable of producing the sort of coherence for the bosons (D's), which make them behave in a given coherence region almost as a single particle. It is this collective behavior that would presumably be responsible, for example, for "neutron bursts" and for "heat bursts". (In this regard we note that Bush and Eagleton [10] have previously emphasized the importance of the boson nature of the D's combined with the periodicity of the crystalline lattice. More recently this has also been stressed by S.R. Chubb and T.A. Chubb [11] of N.R.L. .)

The harshest critics of cold fusion have claimed that " it is done with mirrors." It is a wry observation that, if the picture presented here involving metastable states with the reflections of de Broglie waves is correct, it is indeed done with mirrors. Lots of them! This would, in fact, be how nature accomplishes the feat of "cold fusion".

An Optical Analogue For Transmission Resonance

It is possible to give a rather nice optical analogue for the transmission resonance phenomenon which we have taken as explaining the central mystery of cold fusion. With reference to Fig.2, two forty-five degree prisms have between them an optically flat piece of glass 9e.g., a microscope slide) of uniform thickness separated from the prisms by two air gaps on the order of a wavelength in thickness, but not necessarily of the same width. In this analogue, the piece of glass plays the role of the potential well , while the two air gaps play the part of the potential barriers, and the photons in the laser beam are analogues of the diffusons. Recall that, if the angle of incidence θ is equal to the critical angle θ_c or greater, all of the incident light, (I), is reflected, (R). On the other hand, if, in addition, the wavelength λ satisfies the transmission resonance condition (2), that an odd integral number of wavelengths fit into the plate width, transmission occurs as indicated by (T), with the reflected intensity becoming small. A variation of this is suggested by Bohm[7]: Let white light in a beam distributed across the face of the first prism replace the laser light. Only those colors satisfying the condition (2) for resonant transmission will be transmitted and (T) will be colored. If in addition, a flaw is introduced into the interior of the glass plate, the flaw will glow strongly in the colored light demonstrating in addition the strong buildup of light intensity within the glass plate characteristic of a metastable state.

Transmission Level Energies

The energies, E_n, associated with the resonant transmission levels specified by (2) are readily found by combining relation (2) with the kinetic energy relation, $E_n = p_n^2/2m$ and the definition of the de Broglie wavelength, $\lambda_n = h/p_n$;

$$E_n = (2n + 1)^2h^2/32mL^2, \qquad (3)$$

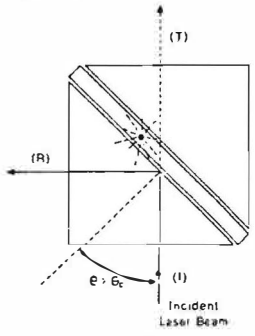

Fig.2. Optical Analogue for Transmission Resonance.

with h as Planck's constant and m as the mass of the diffuson. It will turn out to be convenient, and also, as will be shown, physically meaningful, to label these energy levels by the temperatures T_n, where we define the T_n by

$$E_n = kT_n, \qquad (4)$$

so that (3) and (4) yield

$$T_n = (2n + 1)^2h^2/32mL^2. \qquad (5)$$

Warning!: In what follows it is important to realize that the ambient temperature will be indicated by T, and not T_n. We will soon show from the model, however, an important physical significance for the condition $T = T_n$.

Many-Body Tunneling as Counterintuitive to the Two-Body Case

Two-body tunneling reaction theory has generally been extremely discouraging to the hypothetical prospects for cold fusion. The transmissivity for the two-body, or Gamow, case may be expressed by

$$T = \exp[-\gamma Z_1 Z_2 (m/E)^{1/2}], \qquad (6)$$

where γ is a constant, the Z's refer to the number of protonic charges on the two interacting particles, m is the mass of the lighter particle considered the tunneling particle, and E is the energy of its approach in a frame where the heavier particle is considered at rest. Thus, consider two separate hypothetical cases in which all factors are the same except the mass of the tunneling particles. Clearly, from (6), a slight increase in mass is enough to give a tremendous advantage to the less massive particle in terms of transmissivity, and thus the nuclear reaction rate.

Counterintuitive to this, on the other hand, is the many-body case of tunneling associated with transmission resonances within a deuterated metal lattice. Recall that the de Broglie wavelength can also be expressed in terms of the mass and energy of the particle as,

$$\lambda = h/(2mE)^{1/2}. \qquad (7)$$

Thus, for equal energies E, the diffuson with the greatest mass will have the lowest λ. However, this means that for an equal distribution of energy for two different species of diffusons of masses m and M (M>m), the latter will be associated with the largest density of transmission resonance levels per unit energy. This is apparent from (2), since, at least hypothetically we can find orders N and n (n<N) for the transmission resonance levels for the two species of masses M and m, respectively such that

$$(2N + 1)\lambda_M = (2n + 1)\lambda_m = 4L, \qquad (8)$$

This means that there are more transmission "windows" for the diffusons of larger mass, giving them an advantage, at least in this respect, in terms of the number of candidates available for nuclear reactions. This is clearly exhibited in Fig. 3, where the density of transmission levels is observed to increase for the three cases involving palladium deuteride as a matrix as we go from left to right for the successive cases of deuterons, and lithons (Li^6 and Li^7, respectively). It must again be emphasized that this increased opportunity for tunneling in this many-body case is strictly counterintuitive to the two-body case for which slight mass increases, assuming other factors to be the same, radically diminish the chances for a nuclear reaction.

Fit of the Model to Data: Level Schemes

In the neutron emission experiments of Menlove, Jones, et al. [12] involving pressurized D_2 gas and titanium shavings the temperature of -30C (243K) was observed to be a recurring temperature associated with neutron emission in bursts. It was, thus, hypothesized within the context of this model by the author [3] that this temperature corresponds to one of the transmission levels in a sequence of levels

specified by equation (5) for the case of deuterons diffusing within a titanium deuteride lattice. (The physical rationale for this hypothesis is presented in a later section:) Substitution of T_n = 243K into (5) for an as yet unknown integer order n leads to the following generating formula for the possible compatible well widths, L_n:

$$L_n = (2n + 1)(0.349A) \qquad (9)$$

Corresponding to the respective integers 0,1, 2, 3, 4, etc. this relation generates the well widths 0.349A,
0.047A, 1.75A, 2.44A, 3.14A, etc. Based upon the independent crystalline data of Sidhu et al.[13] for the γ phase of titanium deuteride, a separation of interstitial deuterons is known to be 1.047A in excellent agreement with the generated value of L above corresponding to the order n = 1. The value L = 1.047A is then reinserted into equation (5), with the mass m as that of the deuteron as diffuson, to yield the following level scheme for the case of a titanium deuteride lattice with deuterons as the diffusons:

$$T_n = (2n + 1)^2(27K). \qquad (10)$$

This is portrayed in Fig. 3 showing only the first two transmission levels at T_o = 27K and T_1 = 243K (i.e., -30C). Higher energy transmission levels are specified by T_2 = 675K (402C), T_3 = 1323K (1050C), etc. It has previously been noted that this level scheme is also compatible with the experimental results of Mazzoni and Vittori [14] involving neutron emission in the case of titanium blades pressurized with D_2 gas at high temperatures. Since there was no neutron emission data for the case of PdD, the model fitting procedure was then repeated for the case of electrolytic cold fusion taking room temperature, i.e. 293.2K, to be one level in a level scheme for the case of palladium deuteride as the lattice and the following respective diffusons: Deuterons (D), Li^6 lithons , and Li^7 lithons. The optimism for employing this result was based on the success of Pons and Fleischmann [1] at room temperature. (In this respect, it should be noted that Turner [5],[6] also employed room temperature as a significant one for the electrolytic case.) These other three level schemes are also portrayed in Fig.3. The dashed lines on either side of the solid levels in Fig.3 indicate representative thermal widths for the levels. [The relation for thermal width, ΔT_n , is given in equation (12).] All four cases, along with a comparison of the selected generated well width with the well width obtained from independent crystalline data, are summarized in the Table on the next page. Note from that Table that the poorest agreement of the four comparisons is still to within three percent. Finally, it should be indicated, however, that ,

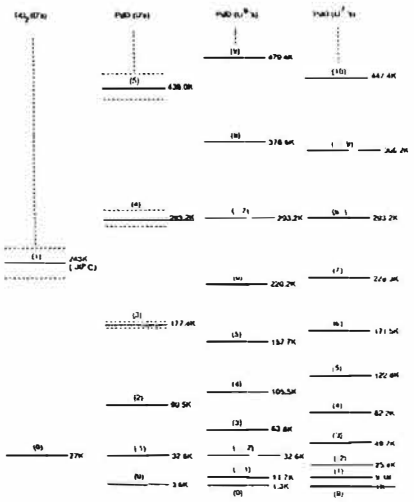

Fig.3. Transmission Resonance Energy Level Schemes.

Lattice	Diffuson	Well Width from Crystalline Data		Well Width from Model
TiD_2	d	1.047A	vs.	1.047A
PdD	d	2.85A	vs.	2.86A
PdD	Li^6	2.85A	vs.	2.76A
PdD	Li^7	2.85A	vs.	2.89A

TABLE of Well Widths

unlike those pressurized gas neutron emission cases in which there is no applied voltage, the electrolytic experiments usually involve an "overpotential"; i.e. the potential drop across the double layer in the electrolyte next to the cathode surface, that is just as important as the ambient temperature in determining the energy distribution of the diffusons. The new developments in the model involving overpotential will be treated in a later section.

MAXWELL VELOCITY DISTRIBUTION AND THE EFFECTS OF PHONON EXCHANGE

A Maxwell velocity distribution is assumed for the diffusing D's. However, it is important to realize that for sharp values of the resonant velocities v_n corresponding to the de Broglie wavelengths for the various transmission orders n there are no candidate diffusons, corresponding to the fact that the area under a point on the distribution curve is zero. Candidates for transmission exist because of the the spread in well widths produced by phonon exchange between the interstitial deuterons and the metal lattice. Thus, Fig. 4 portrays three different velocity distributions overlying transmission resonance "windows": For the nth order resonance the window is centered upon v_n and lies between $v_n - \Delta v_n/2$ and $v_n + \Delta v_n/2$. The areas underneath the distribution curve lying within the windows provide relative measures of the number of candidate diffusons for transmission associated with the respective transmission orders at the temperature T. (The portrayal is not to scale. In addition, it should be noted that the widths of the transmission windows increase with the temperature T.) For PdD it is relatively easy to show that

$$\Delta v_n = 0.2(T_n T)^{1/2} \text{ m/s.} \qquad (11)$$

Thus, for n=0, for which the velocity $v_o = 173$m/s, $\Delta v_o = 7$m/s. We have previously shown that ΔT_n for TiD_2 is given by,

$$\Delta T_n = (4.1 \times 10^{-3})\, T_n T^{1/2}. \qquad (12)$$

Since this formula has been shown elsewhere [3] to scale inversely as the well width, the width of the energy window for a Maxwell-Boltzmann energy distribution not shown) for the nth order transmission resonance energy is given by approximately

$$\Delta E_n = k\Delta T_n = (1.3 \times 10^{-7})(T_n T^{1/2}) \text{ eV.} \qquad (13)$$

Thus, for the n=4 transmission resonance level the energy window is centered on $E_4 = 25$meV, while ΔE_4, the width of the energy transmission window is approximately 0.7meV around room temperature.

A second effect of phonon exchange, in addition to providing transmission candidates among the diffusons, is a negative one: It limits the maximum order of the transmission resonance that can contribute transmission candidates. Thus, as the order n increases, the de Broglie wavelength decreases as seen from (2). When the variation in the well width due to phonon exchange is no longer small compared to the de Broglie wavelength of the diffuson (and the period of well vibration is comparable to, or less than, the time of passage of a particle through the well) the resonance condition (2) can no longer be said to be obeyed: Transmis-

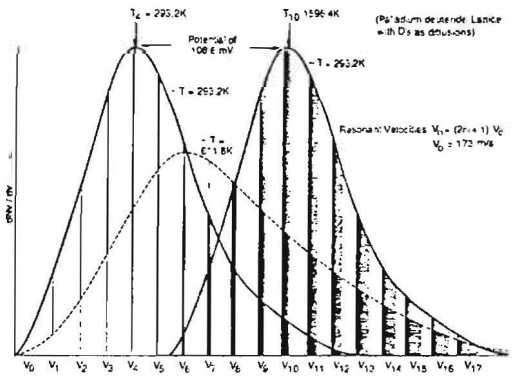

Fig.4. Maxwell Velocity Distributions for Diffusons showing Transmission Resonance Windows.

sion resonance no longer occurs for states above n_{max}. For the wells formed by neighboring Pd atoms we show elsewhere [8] that $n_{max} = 16$ at room temperature. However, for wells formed by neighboring D's in interstitial sites the situation is far more severe: Here, the corresponding $n_{max} = 0$, due to the fact that the variation in well width associated with thermal vibration scales inversely as the square root of the mass of the particles forming the wells as we have previously shown [3]. (Note that the Pd-channel well widths are essentially the same as for the D-channel.) (I am grateful to David Worledge of E.P.R.I. for asking me how thermal vibration might affect my model [15].) The fact that the Pd-channel for resonant transmission is thus far more robust than the D-channel within PdD will be shown to have profound ramifications.

Finally, we note that we have previously shown [3] that the peak of the Maxwell velocity distribution is centered at vn when the temperature T is equal to Tn. Thus, neutron bursts associated with the Tn level might be seen to occur upon warming of the sample when the temperature has reached that value of T such that the peak is associated with vn. However, we note that the envelope of the distribution also includes other values of vn. so it isn't clear what would prevent them from contributing. Perhaps, however, since small numbers of neutrons are observed, it is predominantly those associated with the peak that are numerous enough to be observable. In that regard it should be noted that neutron production will be associated in a later section with the D-channel, which will restrict the neutron numbers even more severely, as just discussed.

THE TRM APPLIED TO ELECTROLYTIC COLD FUSION

A Formula for Relative Excess Power

We will employ a Maxwell-Boltzmann energy distribution for the diffusons. While this might seem most appropriate for a reaction near the surface of the cathode it should be noted that most researchers, e.g., the Appleby group of Texas A&M [16], have found evidence for an excess heat reaction occurring within about 5 microns or so of the cathode surface. Thus, the relative heights of the transmission resonance windows are governed by the Maxwell-Boltzmann "envelope" for the temperature T and energy E expressed by

$$\Delta N(E) \propto T^{-3/2}E^{1/2}\exp(-E/kT)\Delta E. \qquad (14)$$

A particular transmission resonance window of order n will thus make a relative contribution to the candidate pool for nuclear reactions expressed by (14) with E replaced by E_n. The candidate number is also proportional to the current density i in the case of a given sample. Then, since it has been shown elsewhere [3] that

$$\Delta E_n \propto T^{1/2}T_n, \qquad (15)$$

it might seem that an appropriate expression for relative power for the purpose of comparing the theoretical excess power from the same sample at different current densities and temperatures would be given by

$$P_r = iT^{-1}\Sigma_n E_n^{1/2}\exp(-E_n/T)\,(T_n). \qquad (16)$$

However, this would ignore the fact that, at the surface, there is an additional energy gained by the diffusons associated with the overpotential, η, of $q\eta$, where q is the charge on the diffuson. Since the net effect is to add this energy to the diffusons, the Maxwell velocity distribution or the Maxwell-Boltzmann energy distribution is shifted to the right without a change in shape. This rightward shift without a change in shape is expressed mathematically by subtracting $q\eta$ from E in the two places where it occurs in (14), so that (16) is transformed as follows:

$$P_r = iT^{-1}\Sigma_n (E_n - q\eta)^{1/2}\exp[-(E_n - q\eta)/kT](Tn) \qquad (17)$$

We present the details of the incorporation of the the formalism of the Butler-Volmer equation

from electrochemistry elsewhere [8]. Finally, employing $E_n = kT_n$, and throwing away a factor of $k^{1/2}$, (17) is transformed into the following relation, which we take as defining the relative excess power, P_r:

$$P_r = i^3 i_o^{-2} T^{-1} \Sigma_n \{ [T_n - 2T\ln(i/i_o)]^{1/2} T_n \exp(-T_n/T) \}, \qquad (18)$$

where i_o is the "equilibrium current density" when no net current flows to the cathode and serves as the adjustable parameter in this model. The sum is only over those values of n from 0 to about 15 for which the quantity $T_n - 2T\ln(i/i_o)$ is positive. (Recall that the upper limit upon n enters because of the fact that thermal changes in the well width have become comparable to the de Broglie wavelength of the particle for periods of vibration comparable to, or shorter than, the time of passage of the particle across the well.) We now investigate to see whether the expression in (18) is meaningful, by comparing it to new calorimetric data obtained by Eagleton and Bush [17] of Cal Poly, Pomona.

Comparison with Data

Fig. 5 is a plot of excess of power versus current density for T = 300K. The data is from Eagleton and Bush [17], where the experiment is described in thorough detail. However, a few details may be of interest here: The calorimeter is of a steady-flow design and the flow rate is periodically checked. The entrance and exit ports of the bath in which the electrolytic cell resides have thermocouples to monitor their temperatures. Two thermocouples inside the cell are employed to obtain temperature readings near the cathode. Separate calibration curves for each of these in-cell thermocouples are rectilinear, as one would expect. A value of excess power is guaged from a thermocouple reading and the corresponding calibration curve. The two values are then averaged to provide the experimental excess power that appears in Fig. 5 . The system is fast-mixed since a magnetic stirrer is employed. In addition the cell is closed and a recombiner is used. The cathode was gently loaded for about two and one half weeks at a charging current density of about 70mA/cm². The total integrated input power from the beginning of charging until the end of the experiment; i.e., until the end of the excess power output, was approximately 2.0MJ, while the total integrated excess power output for the approximately 36 hours of excess power production was about 0.35MJ. However, during that final 36 hours of the experiment, i.e. that period in which excess power could be observed, the excess power was rather spectacular, being, on average, about 30% of the input power associated with the applied current. Nevertheless, we refer to "excess power" rather than "excess heat" since the 0.35MJ obtained was less than the applied energy of 2.0MJ. (In this connection, however, it should be noted that other researchers, e.g. Pons and Fleischmann [1] and Huggins [18], have observed excess heat. Moreover, the excess heat is on the order of megajoules per mole of material, rather than kilojoules per mole of material, with the thousandfold difference clearly indicative of a nuclear source for the excess energy as opposed

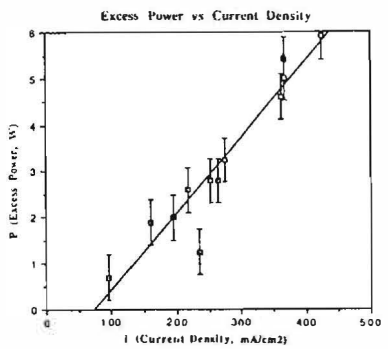

Fig.5. Experimental Excess Power versus Current Density.

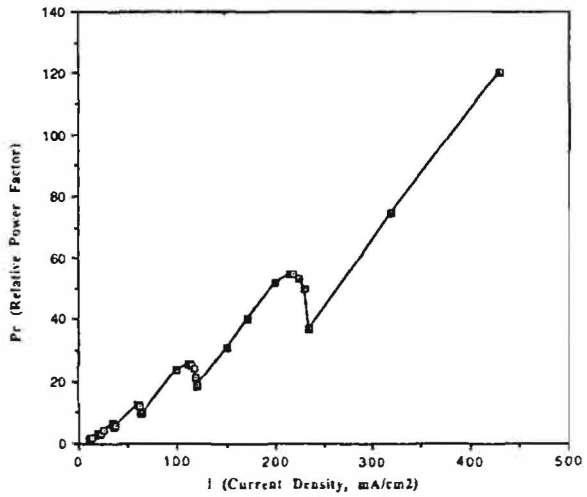

Fig.6. Relative Power versus Current Density on tne Transmission Resonance Model

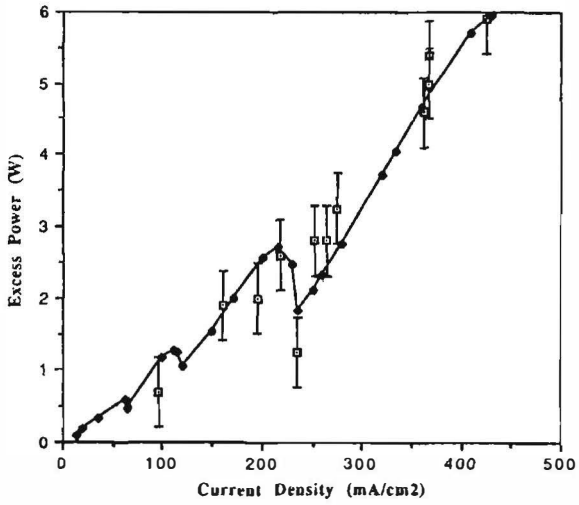

Fig.7. Comparison of Transmission Resonance Model to Data of Fig.5.

to a chemical source.)

The data of Fig. 5 appears to be quite typical. In particular, with the exception of the low-lying data point at 235mA/cm^2 it seems to indicate a linear relation between excess power and the applied current density over the range of values shown.. Another typical feature is that the effect apparently is no longer observable when the applied current
density is lowered to a value (found by extrapolation here) of about 60mA/cm^2 . Fig 6 shows a plot based upon the TRM: The relation for relative excess power in (18) was employed to plot theoretical excess power versus applied current density for T = 300K. The values of T_n for the transmission resonance levels of PdD are taken from (10) with the 27K for TiD2 replaced by the 3.62K appropriate for PdD with D's as diffusons. . A value for the adjustable parameter of i_o = 1.47mA/cm^2 was shown to give the best fit to the data. This is displayed in Fig.7 with the curve based upon the model shown as a solid line with dark squares showing the theoretical points entered in the Cricket graph. Note that a relative minimum of the theoretical curve, a sort of "cusp", corresponds to the low-lying data point at 235mA/cm^2. In my presentation at the Cold Fusion Symposium I indicated that, while this was rather "flimsy" evidence for the model , nevertheless, I would stick my neck out by indicating that I felt it would turn out to be prophetic. [**Postscript:** Since the First Annual Cold Fusion Symposium at the end of March we (Bush and Eagleton) have obtained additional important evidence of the sort of fine structure seen in the model curve of Fig.6 and Fig.7. This will be made available in references [8] and [17]. Thus, the model with its ability to relate relative excess power to applied current density and temperature near the surface of the electrode according to the formula in (18) appears to be quite meaningful. In addition, the fact that in these post-Symposium studies there is finally a reasonable physical model providing a good fit to data on excess heat appears to provide an enormous boost to the credibility of the Pons-Fleischmann effect, itself. In a word it seems that the transmission resonance model has achieved a genuine breakthrough in the study of "cold fusion". Implicit in this model, which now combines physics and electrochemistry, is an extremely important role for the overpotential. To be sure, acceptance of the TRM will depend upon independent confirmation of our results by other researchers.]

TRANSMISSION RESONANCE-INDUCED NEUTRON TRANSFER (t.r.i.n.t.)

Excess Heat Source in "Cold Fusion"

It has already been observed that the phonon exchange effect associated with vibration of the potential wells limits the Pd-channel for transmission resonance to an order n of about 15, but limits the D-channel to only about n=o, due to the greater amplitude of well vibration for the far less massive deuteron wells. Two effects arise from this: First of all, the vast majority of D-on-D reactions would occur in the n=o state, which means that the relative velocity of approach of the two D's would be only about 173m/s corresponding to an energy of only about 3×10^{-4}eV! Under this circumstance we would anticipate a large polarization effect due to the two protons residing on the D's. This should lead to a stripping process, or Oppenheimer-Phillips type process, in which this massive polarization effect favors the exchange of a neutron to yield a T (triton) plus p (proton) as opposed to the exchange of a p to yield an He^3 nucleus plus a neutron. Thus, the TRM may be able to account for the "anomalous" branching ratio on the order of 10^8 favoring the production of tritium over neutrons that several observers have noted.

The second effect is that the nuclear reaction of a D with a Pd nucleus will be a far more common occurrence than will be a D+D reaction in the D-channel. (From the standpoint of the Gamow reaction this would not be reasonable, due to the much larger charge on a Pd nucleus than on a D. Again, however, the many-body tunneling reaction implicit in the transmission resonance phenomenon is counterintuitive to the Gamow case: All that counts is whether the transmission resonance condition holds for the wells formed by the potential curves of neighboring Pd nuclei.) (Remember that the spacings of neighboring Pd's will be essentially the same as that of neighboring D's.) Employing the above reaction as a prototype we again suppose that polarization effects due to the positive charges in the two particles (D and Pd) vastly favor the transfer of a neutron to the Pd nucleus from the D leaving a heavier isotope of Pd and a proton. We will refer to this reaction as a "transmission resonance-induced neutron transfer" ("t.r.i.n.t."), or by the acronym trint (reaction). (D+D to give T + p is a special case of a trint reaction.) (The greater velocities of approach for the higher order states would be compensated for in terms of this polarization process by the larger positive charge on the Pd nucleus.) Because of the fact that the D is a loosely bound nuclear structure, the greater binding energy per nucleon in the heavier Pd nucleus would be the ultimate source of the energy finally showing up as excess heat.

Based upon spin considerations the only acceptable trint reactions for the Pd isotopes are,

$$D + Pd^{105} \rightarrow p\,(7.35MeV) + Pd^{106},$$

and,

$$D + Pd^{106} \rightarrow p(4.31MeV) + Pd^{107},$$

where Pd^{107} β-decays with a half-life of 7×10^6 years (35keV β) to Ag^{107}, which,in turn, decays with a halflife of 42s by emitting a 93keV gamma ray. It will not be easy to demonstrate the existence of these isotope shifts based upon either mass spectroscopy or the β-decay of Pd^{107}. The best bet would, perhaps, be to run the same cathode over and over again to enhance the isotopic shift in the Pd metal. It has been estimated that a 5 gram Pd cathode would have to produce about 100MJ of excess heat, assuming the validity of trint, before the β-decay of the Pd^{107} would be detectable. (When rerun, the surface of the cathode should be made clean again. If cracking due to the D's gets too severe it may also be necessary to recast the Pd cathode being careful to avoid other Pd contamination.)

Similarity to Teller's Hypothesized "Catalytic Neutron Transfer"

Teller [4] has hypothesized a reaction, "cata-

lytic neutron transfer", in which a hitherto unknown neutral particle would catalyze the transfer of a neutron between, for example, two D's. In essence the trint reaction hypothesized above has the same end result as Teller's hypothesized reaction, but requires no unknown particle as a catalyst.

An Experiment to Convince Physicists

Teller has suggested (4) in connection with his hypothesized "catalytic neutron transfer" reaction that U^{235} be employed cathodically in an electrolytic cold fusion experiment because "uranium's response to absorbing a neutron is well-known." The TRM with the hypothesized trint reaction also suggests trying this experiment: Thus, one uranium cathode enriched with U^{235} and loaded with D's from a heavy water electrolyte should emit many more neutrons than should an essentially identical uranium cathode loaded with protons via an electrolyte made from ordinary water. The contrast in neutron emission should be impressive enough to convince those physicists who need to see particle emission in order to believe that a nuclear reaction is occurring at room temperature inside a metal lattice.

APPLICATION TO 'HOT' NUCLEAR PHENOMENA WITHIN A DEUTERATED MATRIX (T.R.E.N.D.)

Introduction

Phonon exchange implies that transmission resonance states above about order n=15 will not make a contribution for a lattice temperature around 300K for the Pd-channel. However, at high enough velocities for which the transit time through a barrier-well-barrier system becomes short compared to the period of vibration of the well width due to thermal effects it may again be possible to see the effects of transmission resonance. Thus, we might anticipate reaction yields for such cases that would be larger than Gamow theory based on a two-body reaction at those energies predicts. This condition is met near the lower end of the range at which the elegant "cluster-impact" fusion experiments of Beuhler,Friedlander, and Friedman [19] have been carried out; viz. at around 1keV per deuteron of the heavy water clusters used as projectiles upon a TiD_2 target.

"Cluster-Impact" Fusion

Beuhler has, in fact, indicated [20] that the calculated theoretical yields for "cluster-impact" fusion are "highly unflattering" for their experiment. It seems highly likely that their actual experimental yields of protons, tritons, and He^3 nuclei are in fact higher than conventional nuclear physics would predict because a sizeable fraction of the reactions that result in particle transfer between a "diffusing" D and either a D or a Ti nucleus in the TiD_2 lattice are examples of "transmission resonance-enhanced nuclear phenomena", or "TREND.": In this case, particles would, via transmission resonance within the lattice, get much closer together in this environment than in the asymptotically-free environment of a hot plasma. Note that the D-channels would now be competitive with the Ti-channels since the well widths are virtually "frozen " during the transit time of a D. Neutrons as reaction by-products are apparently not yet being studied by them. However, based upon the ratios of T's and p's to He^3's the branching ratio appears to be 1:1. This is what we would anticipate based upon the much larger relative velocity of approach of the particles at these higher energies: The polarization effect associated with the positive charges on the two particles which has time to be important for the Oppenheimer-Phillips type process in the case of low relative velocity of approach now has no time to produce a noticeable effect. One mystery, however, is this: If the Ti-channels are competitive with the D-channels with regard to this effect, it appears that Beuhler et al. should be seeing a branching ratio of in favor of proton-triton production over that of

He^3. In addition, the protons from the Ti-channel reactions would have energies ranging from about 6MeV to about 9.3MeV, making them rather difficult to confuse with the 3 MeV protons from the D-on-D reaction. The answer to this may be that the wider range of well widths (larger amplitude of vibration) for the D-wells give this channel a large advantage over the Ti-channel. That is, there is a larger number of possibilities in the D-channel case all of which are essentially equally likely in the transition resonance "lottery" at these energies. The result would be relatively few Oppenheimer-Phillips type reactions involving the Ti-channel with negligible chance of seeing Ti-isotope ratio shifts except in the case of a target that is employed over and over with relatively large currents.

An experiment that might show whether transmission resonance is effective here involves employing a single TiD_2 crystal as a target: If transmission resonance is involved, changing the orientation of the crystal axis relative to the beam direction should produce variations in the yields. Such an effect would be evidence in support of TREND. Of course, due to the "splattering" nature of the water "droplets", perhaps the more random the target the better. In this regard it should be indicated that, in addition to obtaining good results with polycrystalline TiD_2 targets, Beuhler et al. [20] have also had excellent results with more "random" targets such as polydeuteroethylene in which ordinary hydrogen atoms have been replaced by deuterium atoms. Here again there is a large range of well widths available for TREND. An indication of this "randomness effect" might also be obtained by employing a sintered TiD_2 target to attempt to see an enhancement of yield over that for their usual polycrystalline targets.

THE TRM AND THE TRITIUM PUZZLE

Introduction

Some researchers, the most prominent being Bockris [21] of Texas A&M, have suggested that tritium is produced on the surface of the cathode in association with the growth of "dendrites". According to this argument the dendrites would produce enormous fields, e.g. 10^5V/cm, near their tips which would accelerate D's onto their surfaces to plough into other D's. It is further argued that the polarizations produced by these fields would shift the branching ratio strongly away from the neutron branch towards the tritium branch of the D+D reaction. Potential drops on the order of 20kV have been hypothesized, so that such a reaction would, in actuality, be a "hot" nuclear reaction. Thus, the reaction would have a lot in common with the "fracto-fusion" reaction hypothesized in connection with observations of low-level neutron production by Jones, Menlove, and others. Bockris [22] has recently been very clever in apparently correlating dendrite growth times with the appearance of tritium in the electrolyte. However, this dendrite hypothesis appears to face two difficulties: Most researchers grant the existence of the high fields, but cannot see these as being extensive enough to give anywhere near the potential drops required for the scheme to operate. (Bockris claims that these high potential drops are attained intermittently.) A more telling difficulty, however, is the fact that tritium production is sometimes observed in the absence of dendrites. It is this observation which, notwithstanding the ingenuity of the dendrite hypothesis, renders it difficult to accept.

The Role of Lithium

Whether or not lithium, either Li^6 or Li^7, plays a major role in tritium production is not clear. What suggests that it does not is that tritium has been observed for both relatively pure Li^6-component electrolytes and relatively pure Li^7-component electrolytes. In addition Iyengar et al. [23] have reported tritium production in the case of electrolytic cold fusion where sodium was used in place of lithium. Also, excess heat production has been observed [16] for both

relatively pure Li^6 and Li^7 cases.

Thus, the role of lithium is not clear. Appleby's group at Texas A&M [16] has, however, established that both Li^6 and Li^7 are found to about a depth of 5 microns in those cathodes evidencing excess heat when they employ the naturally-occurring ratio in their electrolyte. So,there may then be an important role for the lithium since the heat reaction appears to involve this sort of active depth. One possibility, suggested previously by the author [3] is that of a heat producing reaction

$$D + Li^6 \rightarrow He^4 + He^4$$

However, we would have to suppose that there is still enough Li^6 contaminant in the relatively-pure Li^7 electrolyte to still produce observable excess heat. Also, if this is a transmission resonance reaction it would seem likely that the D's are the diffusons rather than the Li^6's. The depth of Li^6 penetration would then reflect the extent of the Li^6 participation in the lattice and/or as interstitials for enough reactions with diffusons (D's) to occur for observable excess heat production.

Another role for lithium has been suggested by Storms [24] of L.A.N.L. and, independently, by Marshall [25]. Hydrogen dissolves well in both palladium and lithium. Perhaps the combination is even more effective. Maybe a lithide compound of Pd is formed, for example, which promotes the absorption of hydrogen. In this scenario the lithium simply helps to achieve a high enough loading of the D's to make the reaction go in this region. It may also aid the process of filling interstitial sites by occupying those interstitial sites that the D's do not occupy. Presumably, sodium might play the same sort of role.

Explaining the Bockris Curve

Bockris [26] has presented a curve for excess heat production which is mirrored by a lower-level curve for the production of tritium, although with an initial lag behind excess heat production of about five days. In this connection it is interesting that the TRM, if limited to the first four metastable states (n=0,1,2,3) for heat production (Pd-channel) (except for bursts of heat as described earlier) and the first state (n=0) (D-channel) for tritium appears able to account for the situation described by the two-component Bockris curve: Thus, in this TRM scenario, initially the overpotential shifts the energy distribution so far to the right that none of three shorter-lived metastable states are operative. However, as the electrode is "platinized" via cathodic deposition, the overpotential decreases, and the energy shift of the D's that we have associated with it decreases so that first the n=3 state is brought into play as the curve shifts leftward followed by the n=2 state etc. Thus, excess heat is now being observed, but tritium will not be produced in observable amounts until the leftward shift of the envelope via the decreasing overpotential allows it to overlap the n=0 state. In this connection, the P_r value (See ( ).) for the n=0 state (i.e. P_r evaluated for just n=0) is about 0.1% of that for the sum of the P_r values for the states n=0,1,2,3 (i.e. P_r evaluated with the sum over the first four states), which is in agreement with Bockris' estimate of the percentage correlation between the production of "excess heat" and tritium production.

CALCULATION OF A NUCLEAR CROSS-SECTION

We show elsewhere [8], that the relative excess power factor can be incorporated into the following expression for absolute excess power:

$$P = \{8k/qL(\pi m\omega^2)^{1/2}]A(\rho/M)N_o f N_C E_1 \tau\sigma i^3 i_o^{-2} T^{-1}\} \cdot \\ \cdot \Sigma_n\{[(2n+1)^2 T_o - 2T\ln(i/i_o)]^{1/2} \cdot \\ \cdot (2n+1)^2 T_o \exp(-T_u/T)\}, \qquad (19)$$

where q is the charge on a D, L is the well width (meters), m is the mass of a D, ω is the angular frequency of vibration (average) for the interstitial D's, A is the surface area of the cathode, ρ is the density of the palladium , M is the gram-

molecular weight of Pd, N_o is Avogadro's number, f is the "sticking factor" (i.e. the number of D's that enter the surface for each electron passing in the current), N_c is the number of singly-charged positive particles in a Coulomb of charge, E_1 is the energy released in a single nuclear reaction (taken here to be about 5MeV), τ is the depth of the active region (taken to be about 5 microns), and σ is the nuclear cross-section. To estimate σ we employ the data of Fig.7 taking P to be 2W for an applied current density of $i=250mA/cm^2$ and $i_o = 1.47mA/cm^2$. The relative power factor from the computer program was 4,280. The result is,

$$\sigma = (2.8/f) \times 10^{-26}\ cm^2. \qquad (20)$$

Thus, if the sticking factor is on the order of 3/100, the cross-section for the nuclear reaction would be on the order $10^{-24}\ cm^2$, viz., a barn, which seems not unreasonable.

CONCLUSION

The transmission resonance model appears to account for the Pons-Fleischmann effect of excess heat production: The model gives an excellent fit to data, strengthening the likelihood that it is correct, and boosting the credibility of the effect, itself. Nevertheless, the results indicated must be confirmed by other researchers. That the TRM stands a good chance,also, of explicating both the phenomena of low-level neutron production and the higher-level production of tritium is very apparent, though there is much work remaining to be done in order to sort this out.

Finally, if the the model is correct it appears that there is little new physics involved. Rather, the Pons-Fleischmann effect is, quite simply stated, the most startling of the consequences of the wave nature of matter discovered thus far.

ACKNOWLEDGEMENTS

Robert D. Eagleton, my colleague in the cold fusion project (Physics, Cal Poly, Pomona) is appreciated for discussions on all aspects of the work and for his continued encouragement. **Earl Pye** and **Fred Bet-Pera** (Chemistry, Cal Poly) are thanked for discussions. I would also like to acknowledge helpful discussions with the following: **Robert Beuhler** (Brookhaven National Laboratory), **John Bockris** (Chemistry. Texas A&M), **Don Hutchinson** (O.R.N.L.), **Steve Jones** (Physics, Brigham Young), **John Marshall** (Marshall Laboratories, Denver), **Howard Menlove** (L.A.N.L.), **Nigel Packham** (Chemistry, Texas A&M), **Chuck Scott** (O.R.N.L.), **Ed Storms** (L.A.N.L.); **Edward Teller**, Associate Director Emeritus of the Lawrence Radiation Laboratory (Livermore) and Fellow of the Hoover Institute (Palo Alto); **Kevin Wolfe** (Cyclotron Institute, Texas A&M), and **David Worledge** (E.P.R.I., Palo Alto). **David Thompson** and **Johnson-Matthey** are thanked for a metals loan, and **Phillip Armstrong**, **Ron Ellis**, and **The Los Alamos National Laboratory** are appreciated for metals fabrication. **Dr. Ray Shiflett**, Dean of the College of Science and **Dr. Raymond Fleck**, Director of Research (Cal Poly) are both thanked for their enthusiastic support. Finally, it is a pleasure to express gratitude to **Southern California Edison** (Coordinator: **Kert Kertamus**) and **Wind River Resources, Inc.** of Denver, (President: **Joe Ignat**) for the continued financial support that has made the Cal Poly cold fusion project possible.

REFERENCES

[1] M. Fleischmann, S. Pons, "Electrochemically Induced Nuclear Fusion of Deuterium", J. Electroanal. Chem, Vol.261, p.301,1989.

[2] S. Pons, "Calorimetry of the Palladium-Deuterium Systems", presentation at The First Annual Conference on Cold Fusion (Hereafter: The Utah Conference), March 28-31, 1990, University Park Hotel, Salt Lake City, Utah.

[3]R. Bush, "A Transmission Resonance Model for Cold Fusion", presented at the Winter Meeting of The American Society of Mechanical Engineers, San Francisco Hilton, Dec. 12, 1989, A.S.M.E. Archive Number: 89-WA/TS-3.

[4]E. Teller, Research News, Science, p.449, Oct 27, 1989, Based upon remarks at the NSF/EPRI Workshop on Anomalous Effects in Deuterated Materials (Hereafter: NSF/EPRI Conference), Washington D.C., Oct. 16-18, 1989.

[5]L. Turner, "Preregrinations on Cold Fusion" , poster presented at the Workshop on Cold Fusion Phenomena (Hereafter:The Santa Fe Conference), May 23-25, Santa Fe, N.M., accepted for publication by J. Fus.Energy.

[6]L. Turner, "Thoughts Unbottled by Cold Fusion", Letter to the Editor, Physics Today, pp. 140-142,Sept., 1989.

[7]D. Bohm, Quantum Theory, Prentice-Hall, Inc., Englewood Cliffs, N.J.,1951.

[8]R. Bush, " 'Cold Fusion': The Transmission Resonance Model Predicts Optimal "Trigger" Points to Achieve Excess Heat and Suggests a Hitherto Unknown Nuclear Reaction as the Ultimate Source of that Energy", submitted for publication to J.Fus.Tech.

[9] R. Huggins, Remarks at the Utah Conference.

[10]R. Bush , R.D. Eagleton,' 'Cold Nuclear Fusion': A Hypothetical Model to Probe an Elusive Phenomenon", poster presented at the Santa Fe Conference, May 23-25, 1989, accepted for publication in J Fus.Energy.

[11]S.R. Chubb, T.A. Chubb, "Quantum Mechanics of 'Cold' and'Not-So-Cold' Fusion", presentation at Utah Conference.

[12]H. Menlove, S. Jones, et al., "The Measurement of Neutron Emissions from Ti plus D_2 Gas", presented at the Santa Fe Conference.

[13]S. Sidhu,et al., Acta Cryst., Vol.9, pp 607-614, 1956.

[14]Mazzoni and Vittori, results reported at the Santa Fe Conference by F. Scaramuzzi et al., "Neutron Emission from a Titanium-Deuterium System".

[15]D.Worledge, private communication.

[16]O. Murphy, J. Appleby, and S.Srinivasan, "Palladium/Hydrogen Isotope Systems: Microcalorimetric Measurements and Surface Analyses", presented at the Utah Conference.

[17]R.Eagleton, R. Bush, "Calorimetric Evidence Supporting the Transmission Resonance Model" , submitted for publication to J. Fus.Tech..

[18]R. Huggins et al.,"Recent Measurements of Excess Energy Production in Electrochemical Cells", presented at the Utah Conference.

[19]R. Beuhler, G. Friedlander, and L. Friedman, "Cluster-Impact Fusion", Phys. Rev. Lett., Vol. 63, No. 12, pp. 1292-1295, 1989.

[20]R. Beuhler, private communication.

[21]J. Bockris, K. Wolf, et al.,"Production of Tritium from D_2O Electrolysis at a Palladium Cathode", accepted for publication in J. Fus.Tech.

[22]J. Bockris et al., panel discusion remarks at the Utah Conference.

[23] P.Lyengar, "Overview of BARC Studies in Cold Fusion", presented at the Utah Conference.

[24]E. Storms, private communication.

[25]J. Marshall, private communication.

[26] J. Bockris, presentation at NSF/EPRI Conference.

A ZERO GRADIENT CALORIMETER FOR THE MEASUREMENT OF ANOMALOUS HEAT FROM THE ELECTROLYSIS OF DEUTERATED METALS

Lee John Droege and Thomas F. Droege

1715 Karlann Drive, Black Hawk, CO 80422
2 S. 942 Thornecrest La., Batavia, IL 60510

ABSTRACT

A null balance calorimeter has been designed for the measurement of anomalous heat in electrolytic cells containing deuterium and palladium. Early measurements indicate an accuracy of less than 1% of the total energy processed through the calorimeter. Anomalous heat has been observed at the 4% level for palladium cathodes, or 4w per cc. Measurements have been made of cathode material resistance change and cathode gas absorption during electrolysis. Cell voltage variations over time have been correlated with cell gas evolution. Attempts have been made to correlate radiation with cell activity.

INTRODUCTION

The announcement of Fleischmann and Pons [1] brought great excitement. Here was an experiment that amateurs could perform in their basement. No single discipline appeared to have an advantage. After many excited telephone calls between brothers in Colorado and Illinois, it was decided that our goal was to be the first to hold the land speed record for a "cold fusion" powered car. Since we are engineers, we planned to attack the problem of optimizing palladium cells for high power output. The approach was to design a sensitive calorimeter. Sensitivity was desired so that small improvements could be detected as we searched for optimum palladium conformations including intentionally rifted structures along various crystal planes [2]. Some time was spent searching for an old float zone refiner (Pfann) to make single crystal Palladium. But the machines we had used in the past all seem to have made it to the junk yard for their stainless steel weight as little as two weeks ahead of us. Eventually this effort was abandoned and it was decided to use readily available numismatic palladium. By the time construction work started it was obvious that neutron measurements would be difficult, so even though one of us had some skill in nuclear instrumentation this further confirmed our selection of heat as the primary measurement.

Video tapes of the Santa Fe conference [3] were obtained and provided great help in designing the experiment. The debates over re-combination of hydrogen and oxygen, and how to take into account the refrigeration effects seemed to be more suitable to monks, angels and pins. A completely sealed cell with a catalyst was designed to avoid these arguments.

We believe that it is often very helpful to hear of other's mistakes and disasters. We report a few of ours here. We believe that the dry impartial style of technical papers prevents young people from discovering the joy of research. We consciously allow our excitement to show while attempting to report objectively.

DESIGN

Calorimeter Design

Early criticism of the technique of Fleischmann and Pons made it desirable to avoid heat flow measurements which depended on Newton's law of cooling, stirring, and thermometers. A Peltier thermoelectric cooler (TEC) had been recently purchased from a surplus house because it looked like a fun toy for experimentation. A quick experiment determined that it would be possible to use this device to build a calorimeter which would avoid the defects which had been so heavily criticized. The

design uses two concentric copper shells (Figure 1) both of which are held at the same constant temperature by analog computer driven power amplifiers. The outside of each shell is insulated with 1 1/2" of foam. The inner shell contains a single window in the foam insulation where a thermoelectric cooler (TEC1) connects it to the outside shell through blocks of aluminum. The design effort was to control

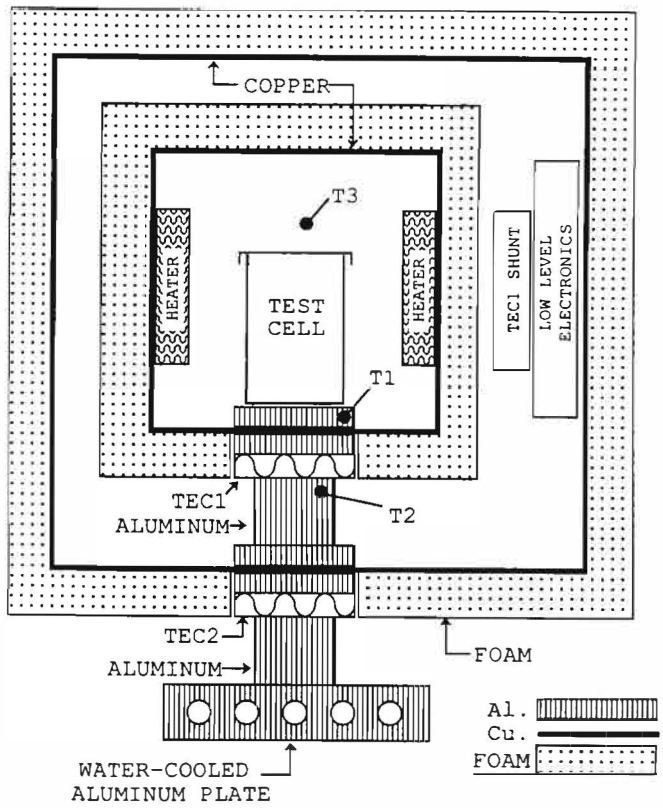

Figure 1. Calorimeter Layout. The calorimeter consists of an inner and outer copper shell heavily insulated with foam. Thermal electric coolers move heat between the shells and from the outer shell to a heat sink. Solid state thermometers control electronics to maintain both shells at the same temperature. The electronics reduces drive to the balance heater in the inner shell to compensate for heat added by the test cell.

the heat path so that all heat would be forced to flow through TEC1.

The outer shell is held at a computer-controlled temperature by connection through a second set of TECs to a water cooled plate. The TEC connecting the inner shell to the outer shell is driven by a precision constant current. The inner shell temperature is controlled to match the outer shell temperature by driving a distributed precision balancing heater glued to the inner wall of the inner shell. Our tests have shown that a constant current through a TEC with both faces at the same temperature produces a constant heat flow through the device.

Since the two shells are controlled to the same operating temperature to 10 millidegrees RMS, heat leaks between the inner and outer shell are reduced. The heat path through TEC1 is significant since TECs are not only heat pumps, but also thermal conductors. We have measured the thermal resistance to be 2.85 degrees Celsius per watt. Heat conduction through the TEC is compensated by placing a sensitive solid state thermometer (T1 and T2 of Figure 1) on each side of the TEC and making appropriate corrections to the heat balance computation.

The sensitive electronics is located in the constant temperature environment between the inner and outer shell. Circuits in this space are selected for constant heat dissipation. The current shunt for the between shells TEC1 is also located in this space. Temperatures are measured with the AD590 integrated circuit temperature sensor [4]. Analog circuits use the OP270 [5] for high stability and the OPA404 [6] for moderate stability and low leakage where circuits require long time constants. Very high stability of the sensitive circuits is assured through operating the OP270 amplifiers, which feature less than 0.6 microvolt per degree Celsius offset drift, in an environment which is maintained within 50 milidegrees of its set point. Our tests have confirmed that the balancing heater maintains its precision over the operating power range. This heater is composed of 40 metal film resistors selected in value for a best temperature coefficient. The assembly temperature coefficient has been measured at 17 ppm per degree Celsius. Resistance change at the operating point has been tested by operating at full power, then quickly removing the drive and measuring the resistance change. Checks over time have confirmed stability.

The configuration is not optimum. There are temperature gradients in both the inner and outer shell. There is typically 30 degrees Celsius rise between T1 and T3 of Figure 1 when operating at a 6 watt cell power. The test cell must discharge heat through convection. This produces a very long time constant of 1 1/2 hours which is

a nuisance when performing calibrations. This also prevents measurement of the fine time structure of the anomalous heat when running 100 hour cell tests. By the time the tops of the shells are cut off and formed into plugs for access, there are many opportunities for errors in heat flow.

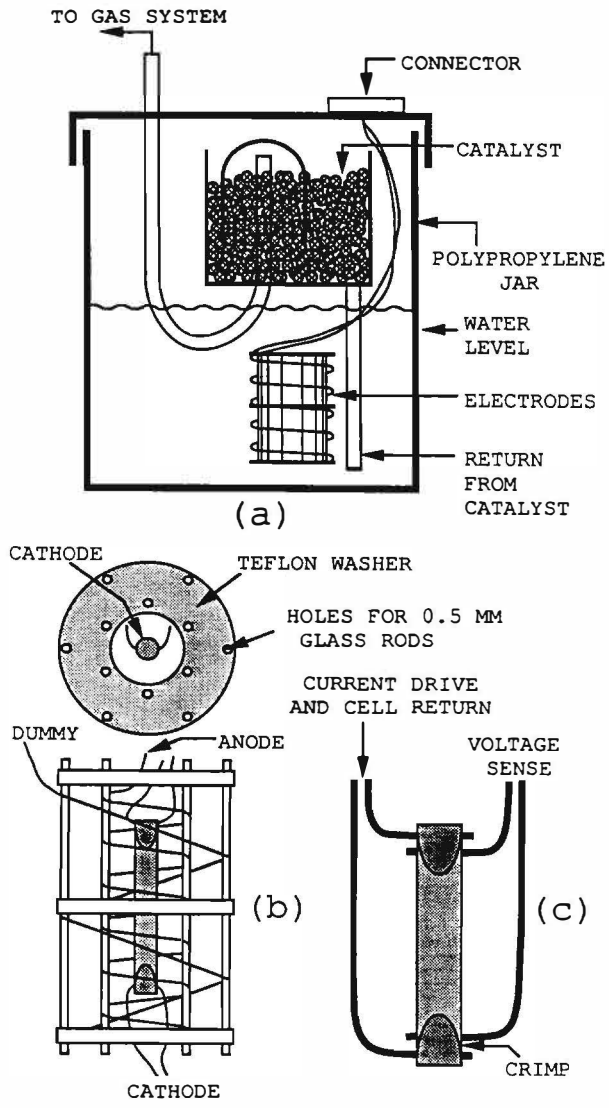

Figure 2. Cell Construction. a)Overall Cell Layout. b)Electrode Detail. c)Cathode Lead Connections.

Many unexpected things contribute small amounts of heat in the inner shell. Lead and connector losses must be considered at a level unusual in electronic design. While many of these problems have been found and cured, many others have been identified but are not correctable in this design. These details are far more limiting to the accuracy than the stability of the scheme. We are thus quite optimistic that future designs will achieve much greater accuracy.

Cell Design

Cells are built into 4 oz. polypropylene jars, Figure 2(a). The top contains 30 grams of Engelhard Catalyst D in the form of small cylinders. The catalyst is arranged so that the evolved gas has an extended path to the output pipe and recombined water is returned to the bottom of the cell.

The anode is wound on glass rods which are compression fit into teflon washers, Figure 2(b). Two layers are wound. The inner layer is the anode, the outer layer is used as a "dummy" as described below. The cathode is prepared as in Figure 2(c). The Palladium anodes are fabricated from slices of a one ounce Engelhard 99.9% Palladium bar purchased from a numismatic dealer. The slices are then turned on a small lathe until approximately round. Primitive equipment, limited skill, and the nasty machining properties of the coin palladium assure that no two cathodes are alike. Two holes are drilled in each end of the cathode by breaking numerous #80 drills. Platinum wires are inserted, and the cathode ends are squeezed in a vice. This cold welds the wires which are then operated in the Kelvin connection for the measurement of cathode resistance. Support structures are fabricated from polypropylene mesh, spot welded with a temperature controlled soldering iron.

Electrolyte is prepared by adding Lithium metal degreased with perchlorethylene to either Deuterium oxide, 99.9% atom% D, Aldrich Chemical Co. or ACS ultra pure water. The amount added is determined by weight after observing the solvent evaporation on a scale. The operation is carried out in very dry mountain air, at 9300 ft, but no special precautions are taken to prevent contamination.

A wide variety of cell configurations have been used as different fabrication techniques were tried. A typical cell contains 70 grams of electrolyte, 30 grams of catalyst, a 2mm by 25mm Palladium cathode, and sufficient .25mm Platinum anode wire to achieve a 5 to 1 anode to cathode area ratio.

Gas System

The cell is vented outside the calorimeter through sections of 1/16" dia. stainless

steel tubing interconnected with PVC tubing. Figure 3 shows the gas measurement system. Gas from the cell is connected to

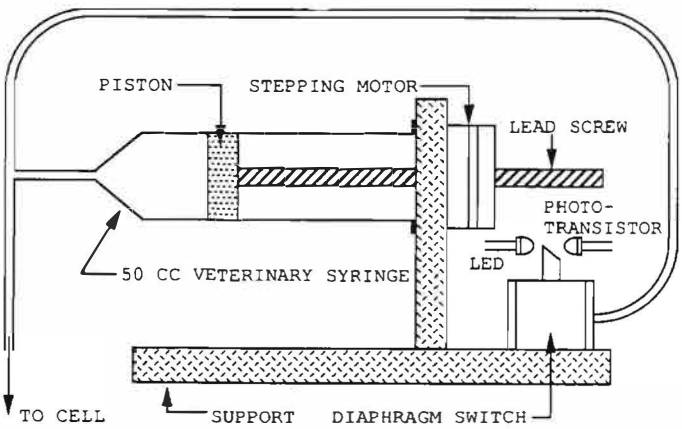

Figure 3. Gas Measurement Servo Pressure from the gas released by the test cell moves a latex rubber diaphragm with an attached flag. The flag moves between the light emitting diode and the photo transistor of a common solid state limit switch. The photo transistor output is read by an analog to digital converter and used to control a stepping motor connected to the piston of a large syringe. The piston is driven to restore the diaphragm position. A computer program measures the gas released by counting the steps required to maintain the balance.

a diaphragm switch and to a 50 cc disposable syringe obtained from a veterinarian. A metal vane is glued to the 0.006" latex rubber diaphragm. The vane is arranged to pass between a solid state limit switch of the type used to locate the home position for computer printers. This device contains a light source and a photodiode. It is normally connected to digital logic to give a beam interrupted signal. The device used gives full on to full off signals for about 0.002" travel. For this application the photodiode is read with the 12 bit precision data system. This allows resolution of a micro-inch of diaphragm travel. The vane position is sensed periodically by a computer program. The program controls a stepping motor with an internally threaded armature which drives a lead screw connected to the syringe piston. Each step displaces 0.014 cc of gas. By noting the direction of travel, varying the step rate in proportion to the error, and backing up to always close the error from the same direction, gas volume is measured to within one step. Hysteresis loop tests have confirmed this precision. A water manometer has been used to determine that pressure changes from ambient are less than our measurement accuracy, which is 1/20" of water. Absolute accuracy is dependent on temperature and barometric pressure for which no corrections are made. The experiment is operated below grade in a residential basement where the temperature has been constant to within 2 degrees Celsius during most runs.

We operate the gas system in two modes. The normal mode measures the gas evolved from the electrolytic cell. This is measured to a precision of 0.014 cc. The normal volume measurement limit is the 50 cc syringe capacity. This can be extended by withdrawing gas into additional syringes with some loss of accuracy. For small gas changes, the system can be operated open loop and the evolved gas measured by the photodiode signal. This mode has a precision of 0.062 micro liters, a peak to peak noise level of 0.5 micro liters, and a range of +/- 62 micro liters. To observe small changes, the system is first operated in the closed loop mode to set the sense switch to the middle of its range. The loop is then opened and measurements are attempted before the system drifts off scale.

Radiation Measurement System

The primary radiation detector is a 1" National Radac NaI(Tl) crystal and RCA6199 photomultiplier tube. Both were purchased in 1954 and surprisingly survived prospecting for Uranium in the Mojave desert and 36 years in the junk box during an uncountable number of moves. A radium test source was secured from a second hand store for $2 by searching a pile of broken watches for one that glowed in the dark. An earlier attempt for a source used ore from the mine in Colorado which supplied Mme. Curie. Unfortunately, this proved not to be radioactive. High voltage is provided by a high stability circuit similar to those used in high energy physics experiments [7]. The photomultiplier signal is amplified by a low noise J-FET amplifier similar to those used in high energy physics calorimeters [8]. The amplifier output is differentiated, discriminated, and pulse shaped before counting. The photomultiplier voltage is set as high as possible in an attempt to detect single photons associated with soft x-rays. This results in a majority of the counts being

due to photomultiplier tube noise.

The NaI(Tl) counter is placed above and outside the calorimeter. Its position is such that it is 7" away from the working electrodes. There is 0.040" of copper, 3" of plastic foam, 3/4" of catalyst, and approximately 1" of electrolyte between the cell electrodes and the detector.

Data collection system

An inexpensive ($295) data system card was purchased and installed in an 80286 based personal computer for control of the experiment. The analog measurement section consists of an 8/1 CMOS multiplexer circuit, a sample and hold amplifier, and a 12 bit analog to digital converter. The measurement is bi-polar providing 11 bit precision. The card also contains three 16 bit counters and a digital I/O channel.

A second electronics card was designed for this experiment and is located in the space between the two calorimeter shells. The electronics in this location is selected for constant power dissipation. The constant temperature environment assures minimal problems from precision resistor and amplifier drift. The experiment is controlled by four 14 bit digital to analog converters (DAC) located on this card. These are loaded by computer program. Once set, the DACs control the calorimeter through analog computer techniques allowing the digital computer to be turned on and off without affecting operation. An uninterruptable power supply is essential as neighborhood chipmunks like to chew on the distribution transformers.

To guard against false settings of the DACs over the long running times they are reloaded every ten minutes. The result of commands are also recorded independently. For example, the cell current is commanded to a particular value. This command value is read by one channel. The cell current as measured by a shunt is read through another channel. This allows continuous monitoring of the experiment to verify that it is actually running where commanded. More than once this has prevented calling a press conference.

A CMOS multiplexer assures that all channels have the same gain. A zero volt reference and a -5 volt reference are measured as a system accuracy check. Most signals are measured differentially to reduce common mode and noise problems. 100 samples of each of 18 variables are taken during 20 seconds of each one minute time interval. Because of the limited storage capacity of the data collection system (floppy disks) means of this data are recorded each minute. Since the cell voltage and current are critical and can vary widely, their RMS values are computed and recorded.

OPERATION

Cell Preparation

Before placing in the calorimeter, a cell is subjected to a series of operating cycles designed to remove hydrogen which may have been diffused into the cathode, to prepare the cathode for charging, and to remove impurities from the system. The removal of hydrogen is encouraged by cycling gas in and out of the cathode [10].

A voltage versus current curve is first taken in both the forward and reverse connection. The cell is then operated reversed at several currents in the expected operating range. Hoare [13] suggests that this may prepare the cathode for charging by removing a blocking layer which can develop while exposed to hydrogen in the gas phase. This then continues for 10 to 20 hours as a continued attempt to remove absorbed hydrogen. The cell is then placed through 10 or more cycles alternating forward and reversed at different currents in the operating range. This is followed by operation with anode and cathode tied together as the anode with the "dummy" as the cathode. This operation starts at the highest operating current and is reduced to zero over about an hour. This technique is used by electroplaters to improve plating operations when their solutions no longer produce a bright finish. The process tends to cause impurities to be deposited on the dummy where they are held by a very small current. Appropriate control runs have not been made to verify this procedure; however, the long charging times reported by others for cathodes of similar size have not been observed. All cathodes have been cut from the same Engelhard 1 ounce numismatic bar. All cells have shown excess heat within a day of high current operation. This is inconclusive, however,

since no fresh cells have been prepared since the discovery that CO2 diffusion into the cell was producing initial heat.

Another technique used in an attempt to remove hydrogen from a cathode is to operate it in the calorimeter under the control of a computer program which alternates between a high and low cell current. A typical program alternates between 0 and 500 ma per square cm on an eight minute cycle. This results in gas amounting to .2 D/Pd atomic ratio "breathing" in and out of the cathode during each cycle.

Calibration

Calibration is started by selecting an operating power point and temperature. Most of the work reported below was done at a calorimeter power level of 8.052 watts and cell base temperature (T1 and T2 of Figure 1) of 320 degrees Kelvin. The power point is determined by varying the current in the TEC and noting the power in the balance resistor. A cell which physically matches the test cells but which contains resistors in an oil bath is now inserted into the inner shell and operated at various currents. The calorimeter should come to a balance at each test current so that the E*I power added into the inner shell by the test cell is matched by a reduction in E*E/R power in the balance resistor. Through careful selection of the balance resistor, accurate calibration of shunts, and differential measurement of all voltages to reduce common mode errors, calibration of the power balance should be within 0.1%, or better. Since the time constant of the system is 1.5 hours, each calibration point requires 10 hours to settle to 0.1%.

Due to the pressure of actually making measurements on the phenomena, ultimate calibration was not pursued. Because the calorimenter was designed and built in two weeks, we did not have time to properly consider requirements, so the design did not couple the test cell tightly to the inner calorimeter shell. Better coupling would significantly reduce the time constant and make calibration faster. Since the phenomena was supposed to take weeks to appear, this was not considered to be important to the design.

It was a mistake not to build calibration resistors into the cells. A second set of heater resistors should be added for future designs. The next design will allow using the Pt anode wire as a heater to allow calibration by inserting heat at the location where it is generated during operation. The moderate effort made to reduce common mode rejection and other measurement errors, proved not to be good enough. Summation of the elements contributing to the heat balance cannot be made to the desired 0.1% precision.

As experienced analog circuit designers, we are aware that the design requirements are quite difficult and require great care in planning and execution. Instrumentation amplifiers are essential. Each wire in the calorimeter has to be carefully designed for heat dissipation. The method and location of lead attachment for voltage measurement is critical. It is not safe to use connectors since they are apt to introduce uncontrolled heat.

Resistance Measurement

Every ten minutes, a current pulse is passed through the outer connections of the Palladium cathode (Figure 3c) to measure its resistance. This proved to be more difficult than expected. The four terminal Kelvin connection used normally solves problems measuring low value resistance. These cells have several added problems which have only approximate solutions. The cell operating current passes through the cathode. Depending on the grounding choice, this produces an end-to-end voltage which is measured as if it were the result of the test current. While the computer can be programmed to command the cell current to zero during the measurement, this does not appear to be wise from the view point of understanding cell operation. Further, there appear to be long term cathode end-to-end voltages which change during the measurement if the cell current is turned off. Measurements were taken by reading the cathode end-to-end voltage before and during the application of the test current. This would be acceptable if done fast enough. Unfortunately, the current driver was not designed for fast response time. Thus the one second pulse periods chosen for this design and the rather rapid cell voltage variations assure large errors. Measurements are taken at two current values to investigate cathode ionization.

Cell Power Checks

At the Santa Fe meeting Richard Garwin [9] proposed that there might be a problem in accurately computing the power into an electrolytic cell. To check this, we compute the cell power two ways and record the ratio as a "Garwin" number. During the 20 second interval of each minute when the parameters are measured 100 samples of each are taken. Cell voltage and current are arranged to occupy adjacent channels of the 18 multiplexed readings so that they are measured as closely together as possible. The sequence is to scan through all channels then to repeat the scan 100 times in this same 20 second interval. Power is computed by taking the mean of the voltage readings and multiplying it by the mean of the current readings. Power is also computed by taking the product of the instantaneous readings and then taking the mean of these products. With either ideal constant voltage or constant current operation of the cell these computations are mathematically equivalent. However, with real current sources differences are possible. The ratio of these computations is recorded as the Garwin number and is used as an indication of the quality of the power measurement.

EXPERIMENTAL RESULTS

We have operated this calorimeter about 5000 hours in a variety of experiments designed to survey cell operation in an attempt to find where interesting work might be performed. All data should be considered preliminary. We report results to indicate where we plan continued work.

CO2 Problems

About 3400 hours of experimental data was discarded as worthless after it was discovered that CO2 had diffused into the cells through a water trap which served as a pressure relief. This would convert most of the cell lithium hydroxide to a lithium carbonate in about two weeks operation for what was thought to be a .1N cell (see below). The result was a gradual increase in cell voltage which eventually went beyond either the calorimeter power capacity or the voltage drive capacity of the servo. Fortunately the electrolyte from all the runs had been saved. Measurement indicated that most old cells had a pH in the range of 7 to 9. All had started at a pH of 12.5 or higher as determined from reference samples. The last run made before this discovery was an H2O Pt-Pt cell filled with 1N LiOH. It appeared to show an "anomalous heat" level of 100 mw. This run was repeated after replacing the H2O in the safety trap with NaOH ("Easy Off" oven cleaner) which absorbs CO2. The "anomalous heat" disappeared and was then within the calorimeter error. The system has since been completely sealed, the water trap having been replaced with a "blow out" piston formed from a second syringe.

After the surprise finding of the CO2 effect, we bought a pH meter and began to check cell pH. We found it lower than expected, and eventually found that the chain of our balance had come off its pivot at some unknown time. While the pH comparisons above are valid since we kept reference samples, we were working with lower pH electrolyte than planned since the scale problem produced low weights of Lithium. Because pan weights were needed for the 1N sample, it was near the expected value.

It is thought that CO2 may be a more serious problem for the closed cell operation used here. With open cells the very large gas flow out of the cell may purge CO2 from the cell to an acceptable level. The partial pressure dynamics of such a situation are unknown to us.

Resistance Measurements

The history of cathode #9 is typical. This cathode is 2mm in diameter and 19mm long with 16 mm spacing between the inner measurement connections. The initial measurement of #9 was 300 micro-ohms. This increased to 600 micro-ohms after operating for 2 hours at 60 ma per square cm. See Figure 4. After 20 hours of operation the resistance had reached the 750 micro ohm range. There was then little change over a variety of operating currents during 1400 hours of runs with six changes of electrolyte. During long off periods, or electrolyte changes, the resistance would reduce to the vicinity of 600 micro-ohms. It never approached the initial value. Since gas content varied widely over the many runs after the initial charging, resistance measurement does not appear to be as valuable as we had hoped as an

indication of the cathode status.

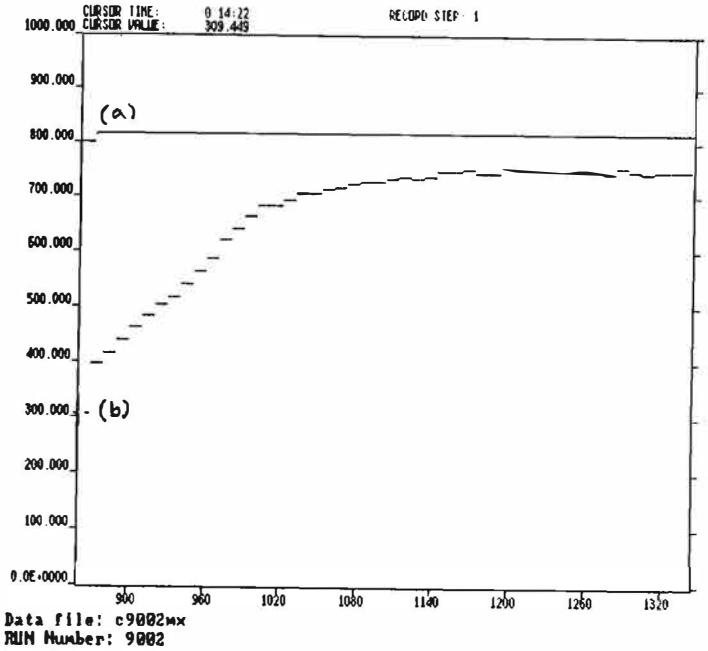

Figure 4. Cathode Resistance During Charging. The upper trace is cell current showing charging at 60ma per sq. cm. The lower trace is cathode resistance. The Vertical Scale is in micro-ohms with major divisions at 100 micro-ohm intervals. The Horizontal scale is in minutes with major divisions at one hour.

Resistance measurements are performed at .1 and 1 ampere. There is some indication that for very long electrolysis, the resistance is nonlinear. The lower current has been found to produce a higher resistance reading. This is consistent with an ionization process as reported by Moore [11].

Radiation measurement

Counts accumulated during each one minute time interval by the NaI(Tl) counter are recorded. Attempts have been made to correlate the radiation count with other experimental parameters.

A series of runs were made where the cell current was alternated between a high and low value with an eight minute period. Count rates were compared between the high and low current levels with no result. Other combinations were tried. Scaramuzzi[12] reported observation of neutrons on dynamically loading Titanium with deuterium. In an attempt to measure this, comparison was made between high, high going low, low, and low going high bin periods on the assumption that there would be a different radiation pattern depending on the direction and rate of gas flow to the cathode. During these tests there was a cyclical gas change amounting to .1 D/Pd atomic ratio. There was nothing of statistical significance observed. Tests with a four hour period show a hint of a relation. The great length of time required to remove counter drifts has prevented a definitive experiment from being performed to date.

By watching the cell voltage variation with time and adding the radiation counter pulse to the cell voltage with the A+B feature of an oscilloscope, it is possible to imagine that there is often a radiation pulse at the cell voltage peak as might be the result of a fusion event causing a cell voltage change. Binning of radiation counts by cell voltage revealed nothing significant.

Tests were made with film wrapped around the cell during runs which displayed "anomalous heat." Development revealed darkened film with images of the absorber we had inserted between the cell and film. Control runs at the same temperature and with similar metal objects next to the film demonstrated that this was a temperature effect.

Electrolyte from a closed cell which had displayed "anomalous heat" was analyzed for tritium content. There was no difference between it and a reference sample.

We have binned all data accumulated so far on cells which indicate excess heat against the direction and quantity of gas flow during the one minute data interval. This reveals a small but persistent effect which indicates the possibility that there are slightly fewer counts in the detector during the one minute intervals in which a small amount of gas has left the cathode. The theory is that first something happens to produce heat. The heat causes some gas to leave the cathode. While gas is out of the cathode, fewer radiation events occur. This is not yet statistically significant.

Long term gas measurements

All the gas measurements are indirect. What is measured is gas which appears in the system. This is presumed to be the left over oxygen from the disassociated hydrogen or deuterium absorbed by the

Palladium. Due to limited resources we have not confirmed this by chemical analysis of gas samples. Figure 5 is a typical gas run. The dotted line indicates

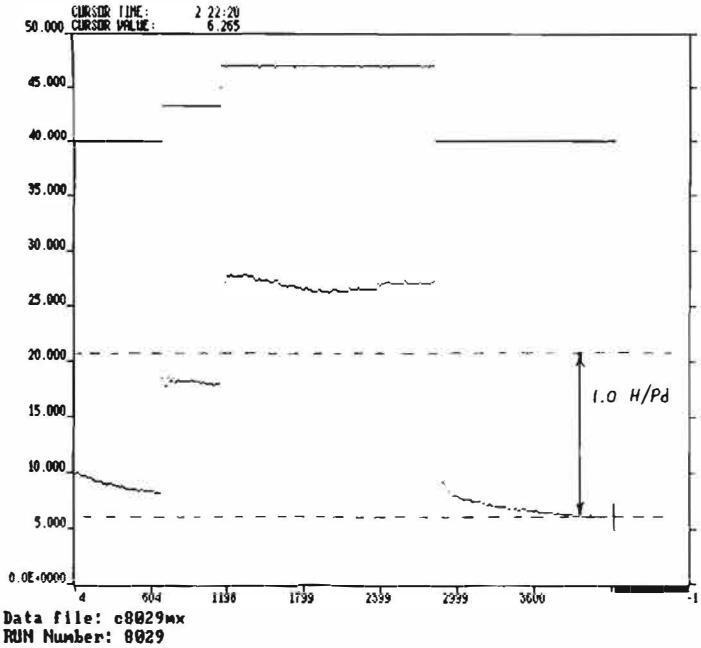

Figure 5. Gas Absorption by the Cathode for an H2O cell. The upper trace shows cell current starting at 500 ma per square cm, stepping to 1 amp per sq cm, then returning to zero. Lower trace is the gas absorbed by the cathode. The vertical scale is in cc with 5 cc major divisions. Dotted lines indicate gas for 1/1 H-Pd ratio. Horizontal axis is in minutes with major divisions at 10 hours.

gas change for 1.0 H/Pd atomic ratio. This cathode has been through many charging cycles so the initial content of gas is unknown. Because of the failure of the resistance to return to its initial value, it is believed to be non zero. Hoare [13] suggests it might be close to .6 H/Pd. This is cell #8 which has a cathode area of 0.686 square cm, and a volume of .0229 cc. The run starts with 11 hours of operation at zero current. During this time, the cell is outgassing due to previous operation on the bench. Note that the operation of the catalyst produces a reduction of gas volume for gas leaving the cathode. After applying .5 amp per square cm. the cathode quickly gains gas amounting to .7 H/Pd. Later application of 1 amp per square cm. pushes the increase of H/Pd to the area of 1.3. After removal of current the gas slowly returns to near the initial value though it is still outgassing after more than 20 hours. For cells showing anomalous heat there is a general trend, for example, Figure 11. The gas enters the cathode quickly, particularly for cathodes which have undergone many current changes cycles. After the first few hours, the gas slowly decreases. After more time, there is a gradual increase in gas content, during which time there is displayed an apparent increase in anomalous power level.

Short Term Gas Measurements

Figure 6 shows the changes of gas seen in Figure 5 to higher time resolution. The dots are at one minute intervals. Figure 6(a) shows first gas entry. Since this is

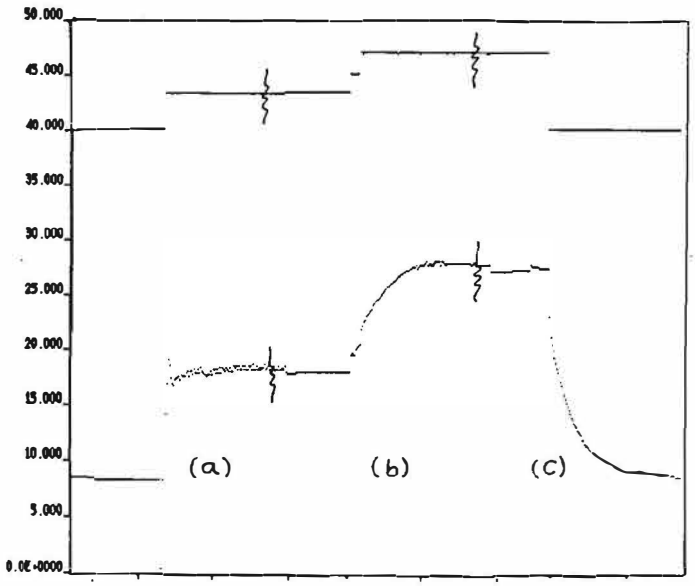

Figure 6. Detail of Cathode Gas Absorption Shown in Figure 5. Left section shows detail of turn on. Center section shows switching from .5 to 1 amp per square cm. Last section shows evolution of gas on current turn off. Vertical scale is in cc with major divisions at 5 cc. The curves are plotted with dots at one minute intervals.

a cathode that has a history of 28 previous runs totaling 598 hours, gas enters quickly. The overshoot at the beginning is presumably caused by the catalyst failing to recombine the gas at the evolution rate when it is cold. After a few minutes the recombination heat allows it to catch up. Later, when going to high current density, gas absorption is slower, Figure 6(b). Finally in Figure 6(c) the gas release on turn off is shown. About 20% of the gas is evolved during the first minute after current turn off. Estimating gas content by removing the cathode and weighing is difficult as it is not clear how to extrapolate back to time zero. The gas servo can be observed to be stepping within a second of the application or removal of

current.

Voltage and Gas Observations

During calibration runs with resistors in oil, and H2O cell operation, the Garwin number is constant to a few parts in 10E6. This is well beyond the precision of the system and can only be explained by the averaging technique used. Thus for these runs it is easy to measure the power correctly.

Because Garwin prompted us to use our oscilloscope, we have observed that the cell voltage follows a saw tooth wave form. The data collection program has been arranged so that it can be interrupted briefly allowing a minute of "high speed" data taking. During this time cell voltage, current, radiation and gas are measured at .1 or .02 second intervals. Data is stored directly in memory to avoid errors caused by disk waits. For gas measurement, the servo is turned off and gas volume is measured by the relative position of the flag interrupting the photo diode.

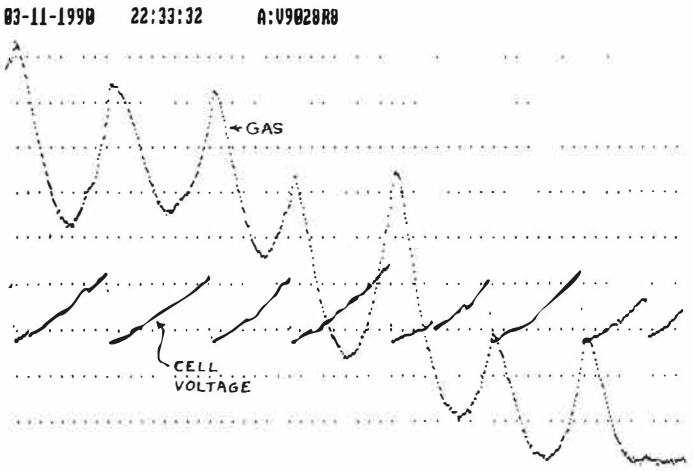

Figure 7. Cell Voltage and Gas Relationship The upper trace is the cell gas volume. The lower trace is the cell voltage. The vertical scale for the gas is 12.5 micro liters per major division. The vertical scale for the voltage is one volt per major division. The horizontal scale is one second per dot.

Figure 7(b) is the voltage waveform from a cell operated at 285 ma per square cm. We have observed that the frequency and amplitude of the cell voltage change with current density and cathode gas content. These measurements were taken with the cell driven from a constant current source. Cells operated with a constant voltage source display a current saw tooth.

For D2O runs which show "anomalous heat", the saw tooth wave form and the limited band width of the current source cause the Garwin number to show variations as large as 2 parts in 1000. The variation as observed is always in the same direction, the mean of the instantaneous products being smaller than the product of the means. As a conservative approach, the product of the means is used in the energy balance which tends to decrease the "anomalous heat" seen.

At first it was thought that the saw tooth wave form was caused by bubble formation and release at the anode producing a negative resistance. Visual observations do not confirm this.

We speculate that the cathode pulses as a surface film forms, becomes unstable like the heated earth's surface, and breaks off like a thermal bubble in the earth's atmosphere. During the process it seems likely that some compressed gas will also escape resulting in a cell gas volume increase. Whatever the source, the cell appears to alternate long periods, of order 1 to 60 seconds, of positive resistance with short periods, of order 50 milliseconds, of negative resistance. It is not surprising that a relaxation oscillation occurs under these conditions.

Figure 7 shows simultaneous measurements of the cell voltage 7(b) and gas volume 7(a). Each time the cell voltage drops, the gas volume starts to decrease. Because of the complexity introduced by the catalyst, it is not entirely obvious whether this is a gas release or absorption by the cathode. Since there is a hint of a gas release pulse just before the gas decreases, gas release is favored. This will be clarified by further study.

The saw tooth waveform is seen with D2O Pt-Pd cells and is not seen with H2O Pt-Pt cells. The status of H2O Pt-Pd cells has not been resolved.

Calorimeter Calibration

We wish to stress that we are running a completely closed system. Much of the early criticism of Fleischmann and Pons' work was concerned with estimates of energy that left the cell with the disassociated gas. Those problems are avoided here. All runs end with the cell at the same

condition as it was when the run began. Differences, if any, relate to the amount of gas that remains absorbed in the palladium cathode.

All of the curves except the heat balance are printed directly from the raw data. For the heat balance, a single set of calibration constants has been computed from a calibration run and is used throughout. In addition, a factor for the thermoelectric cooler is computed for each run from the period when the cell is operated at zero current. When observing the energy balance curves, the reader should keep in mind that they are the differences between numbers which are many times the size of the displayed scale range.

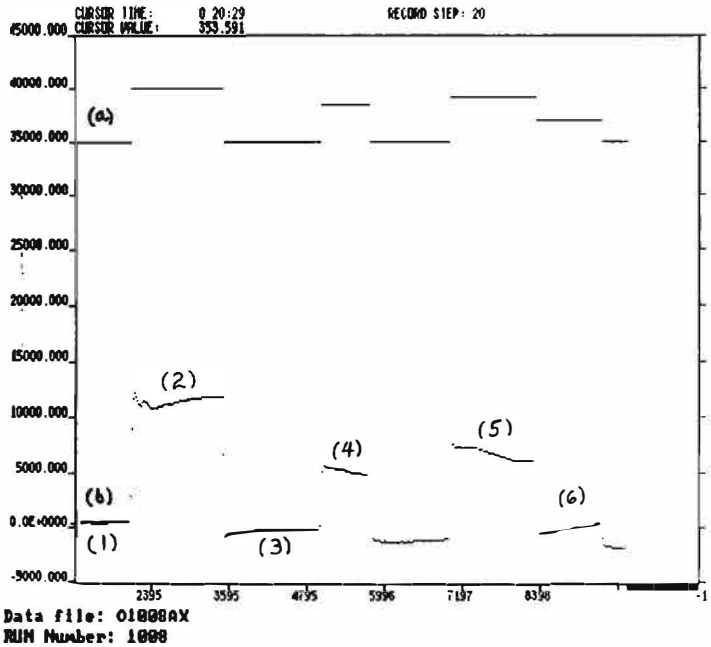

Figure 8. Calibration Run Using a Resistor Cell Filled with Oil The upper trace is the cell current. Currents start at zero. Successive current values are .5, .35, .43, and .2 amperes. The lower trace is the energy balance in joules. The vertical axis is in joules with major divisions of 5000 joules. The horizontal axis is in minutes with major divisions of 20 hours.

Figure 8 is a typical 141 hour calibration run. Here a cell of the same shape as the test cells is filled with oil and power resistors.

The cell was allowed to come to the calorimeter temperature for 8 hours before data taking started. Data starts with a 17 hour period (1) where the cell is operated at zero current. The bottom curve is the net power into the cell in joules. Positive on the curve indicates that more energy has been put into the calorimeter shell than has been taken from it.

During the 23 hour period (2) the cell was operated at 500 ma. During the transition, the calorimeter accumulates heat. A perfect design would not do this, but this design contains a better conduction path through lower specific heat copper for the heaters. Thus when the primary source of heat transfers from the heaters to the test cell, the copper shell gets only slightly cooler. The cell on the other hand, transfers heat mostly by convection so that it gets much hotter and so causes a net accumulation of heat in the calorimeter shell.

The whole process reverses at (3) when the cell current is commanded back to zero. In order to return exactly to zero, the I*I*R computation of the heater power must track exactly the E*I computation of the cell power. This can be guaranteed at one operating power point if things are stable by picking calibration constants. To assure that the computation is correct when the test cell operates at a different power point than the calibration cell, calibration is done at several points, (4), (5).... A curve is then fit for the best calibration.

This curve is then used for a set of H2O and D2O test cells. For this calibration, a balance was maintained over 141 hours to 2 kilo-joules out of a total of 4 mega-joules which passed through the calorimeter. This represents a drift of 4 mw. A more practical measure is the worst drift rate during the run caused by imperfect compensation at the various operating points. This is somewhat less than 20 mw for the above run. We do not have enough runs to compute any meaningful statistics for the calorimeter drift rate. We have measured the worst drift observed for a calibration run which otherwise appeared to function correctly. This is 50 mw.

H2O Runs

Figure 9 shows the operation of an H2O cell. The run consisted of 11 hrs at zero current, 35 hrs. at 500 ma. per square cm, and 22 hrs at zero current. Figure 9(a) is

the current. Figure 9(b) shows the voltage which slowly increases from 5.2 to 5.8 volts during the run. Because the voltage is slowly increasing, the temperature above the cell, Figure 9(c), slowly increases by 1 degree Celsius during the run. This

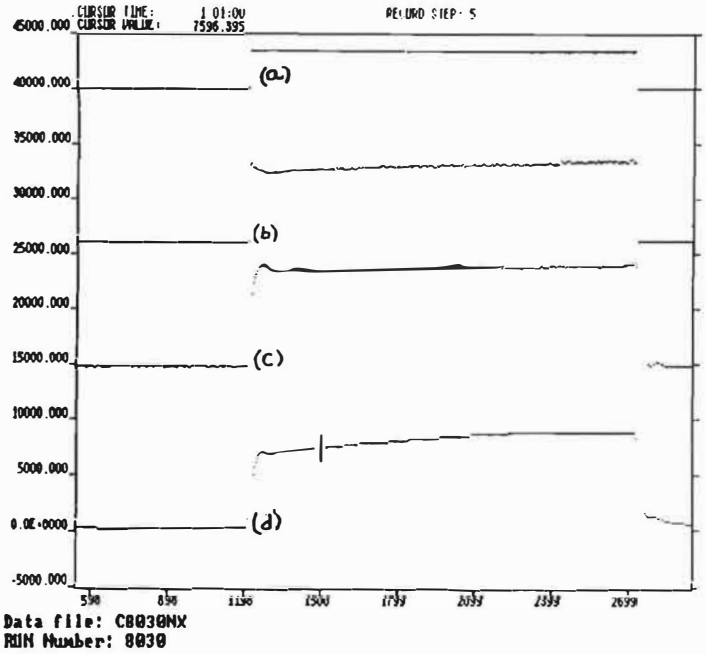

Figure 9. H2O Cell Operation Trace a) is the cell current of 500 ma per square cm. Trace b) is the cell voltage. Trace c) is the temperature above the cell. Trace d) is the energy balance. The vertical scale is energy in joules. Major divisions are 5000 joules. The horizontal axis is in minutes with major divisions at 5 hours.

results in the net energy curve, Figure 9(d) slowly increasing as the cell contents get hotter. When the current is removed, the net energy curve returns to zero as the contents of the cell return to the initial temperature. For this run, energy drift has been removed to illustrate the energy balance.

D2O Runs

Figure 10 is the energy balance for a D2O cell which shows "anomalous heat". We show drift range on this curve representing the worst drift observed during oil and H2O cell runs. Since the aforementioned CO2 problems ruined many calibration runs the six or so remaining do not provide meaningful statistics. This was the 19th run for this cell but the first since a change of electrolyte where the cell was open and exposed to the air for about 1 hour. After current is applied there is a

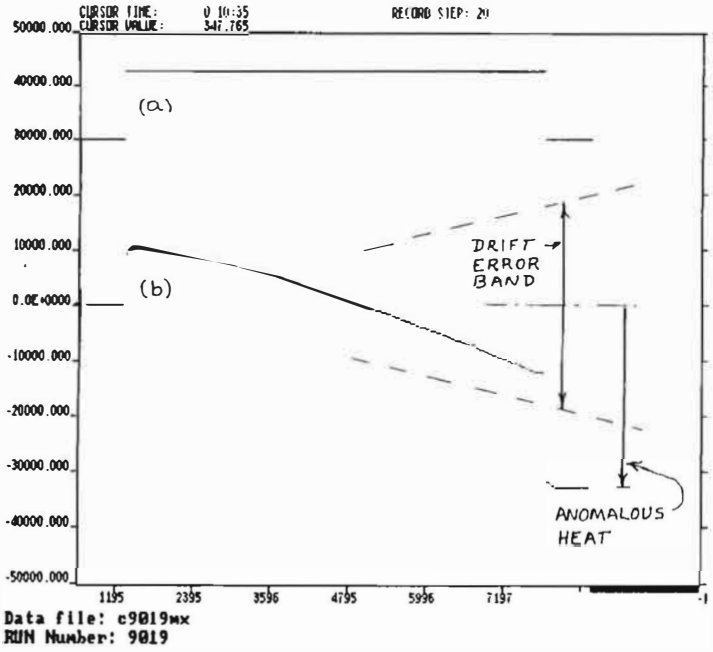

Figure 10. D2O Cell Operation The upper trace (a) is the charging current of .46 amps per sq. cm. The lower trace shows the net energy during the run. The vertical scale is energy in joules with major divisions at 10,000 joules. The horizontal scale is in minutes with major divisions at 20 hours. Dotted lines indicate the largest drift observed.

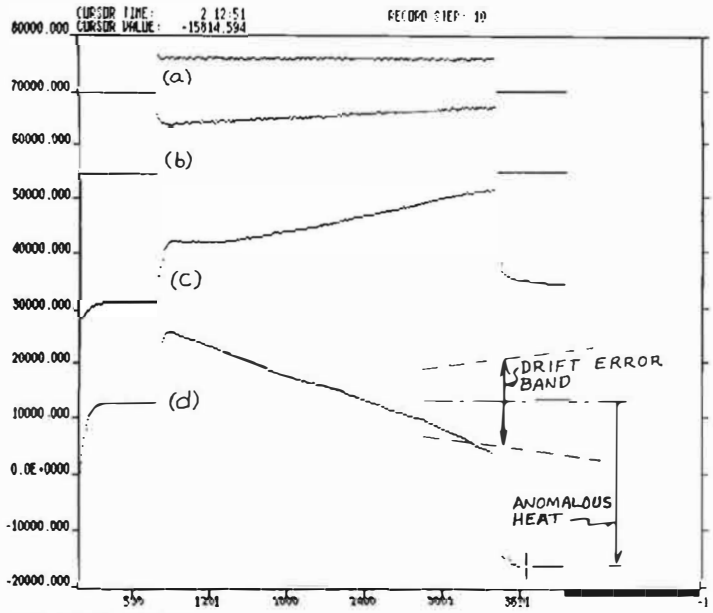

Figure 11. D2O Cell Operation The upper trace (a) is the charging current of .46 amps per sq. cm. Trace (b) i the cell voltage. Trace (c) is the gas volume. Trace (d) is the net energy during the run. The vertical scale is energy in joules with major divisions at 10,000 joules. The horizontal scale is in minutes with major divisions at 20 hours. Dotted lines indicate the largest drift observed.

period of about 15 hours during which the cell maintains an approximate heat balance.

The balance then changes in the direction of "anomalous heat" with a gradual acceleration during the run. Towards the end of the run, "anomalous heat" is being produced at nearly twice the maximum probable drift rate. We do not see this change of slope on the H2O or oil runs.

Examination of the detail of D2O cell operation, Figure 12(e), shows that there are alternating periods of heat release and balanced operation. There is some suggestion that the gas system is more active when heat is being produced. Comparison of a D2O run showing "anomalous heat" Figure 12, with an H2O run Figure 13,

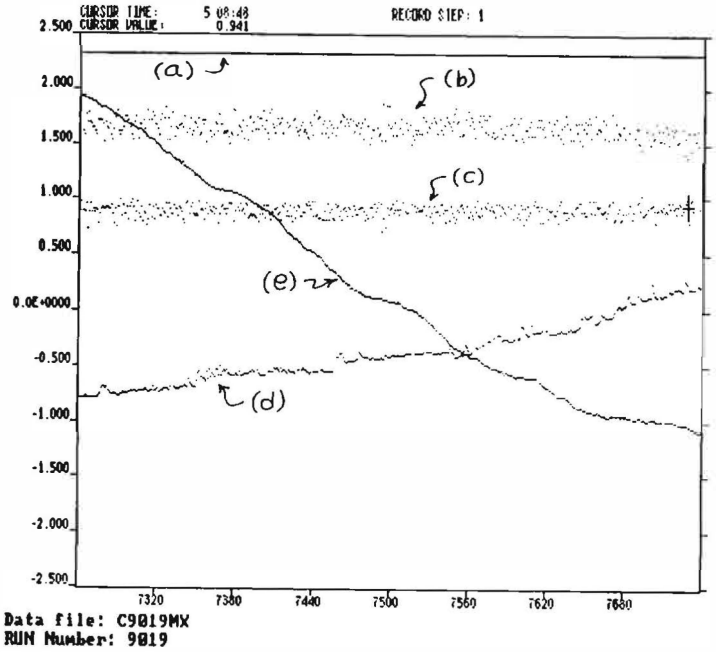

Figure 12. D2O Cell Operation Detail The upper trace (a) is the charging current. Trace (b) is the Garwin number variation. Trace (c) is the RMS cell voltage. Trace (d) is the gas volume. Trace (e) is the energy balance. The vertical scale is the RMS cell voltage. The horizontal scale is in minutes with major divisions at one hour. All scales are the same as for Figure 13.

indicates that the gas system is more active, the RMS cell voltage is higher, and the Garwin number is farther from one. Figure 12 and 13 use the same scales for the various variables. Unfortunately, because the cell of figure 13 used a 1mm dia. cathode vs 2mm for the cell of Figure 12, a direct comparison cannot be made. We show this comparison because other data indicate that there may be valid differences. The great length of time required for runs and the availability of only a single calorimeter preclude the completion of the obvious experiments.

Between D2O run C9019 (Figure 10) and D2O run c9020 (Figure 11) an H2O calibration run, C8030 (Figure 9) was performed. This run indicated a calorimeter drift of 33 mw which was removed from the elthalpy curve for the purpose indicated. This drift happened to be in the direction of "anomalous heat", however other H2O runs have drifted in random directions. There followed run C9020 which accumulated 29,064 joules during a 2,612 minute run for an average "anomalous heat" of 185 mw. Run C9020 shows an increasing heat release which averages about three times the estimate of maximum drift from the various calibration runs. This data is representative of the last 2000 hours of calorimeter operation where we have alternated D2O runs with oil or H2O calibration runs. These runs are ongoing and continue to show similar results.

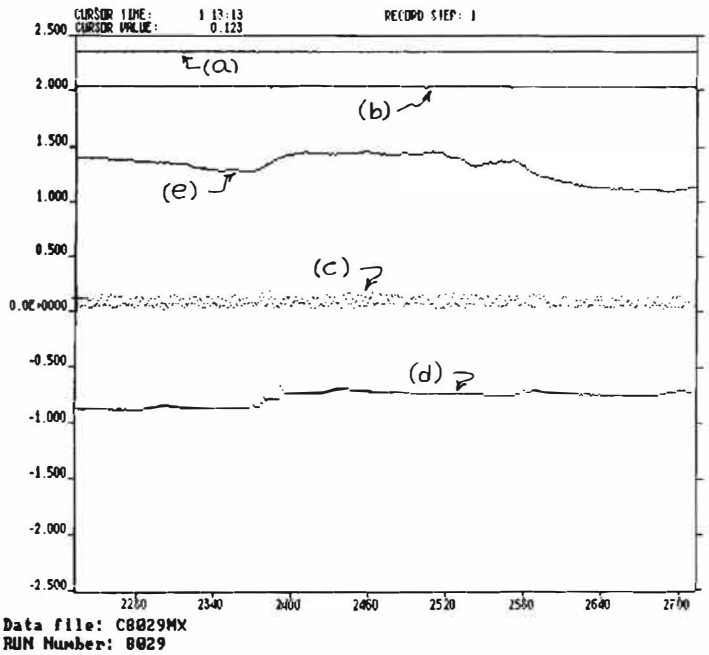

Figure 13. H2O Cell Operation Detail The upper trace (a) is the charging current. Trace (b) is the Garwin number variation. Trace (c) is the RMS cell voltage. Trace (d) is the gas volume. Trace (e) is the energy balance. The vertical scale is the RMS cell voltage. The horizontal scale is in minutes with major divisions at one hour. All scales are the same as for Figure 12.

DISCUSSION

We find the evidence for "anomalous heat" to be persuasive but not absolutely convincing. We have presented data that we

believe to be representative. Still, there are enough calibration runs which show too much heat and D2O runs which show little or no heat that the whole process could be noise. We present our willingness to continue work without financial support as a measure of our conviction. We continue to see differences between D2O and H2O cells which indicate that something is happening beyond normal chemistry.

Once we are at an operating point, we have not observed calibration data which indicates a change in drift rate of more than a few mw. We therefor consider runs such as C9019, Figure 11, to be highly significant. We can only conclude that something is changing in the cell to cause it to increase in heat output.

While the calorimeter concept is very promising, the current implementation produces a different calorimeter every time we open it up to change cells. The 50 mw drift rate claimed is believed to be conservative, even for our string and glue construction. There is every indication that this can be reduced to the area of 1 mw when it is rebuilt to allow reassembly to a constant configuration.

Garwin was correct in advising caution in the measurement of cell power. The saw tooth wave form is subject to measurement error if proper technique is not used.

The resistance measurements indicate that the change to the beta phase occurs rather quickly. As the material is exercised it stays at high resistance, indicating that considerable gas remains in the material. The cathode accepts gas long after the beta transition appears to be complete, indicating that gas may be going into the "rifts in the slip planes" [11] as described by Moore.

The use of cell preparation seems to speed up the appearance of "anomalous heat." We have not yet done a proper control experiment. Ultra clean procedures do not appear to be required to observe "anomalous heat." However, our observations are about a factor of five below other reports. The materials used, except D2O, were of commercial quality. We did not discover the CO2 problem until working together over Christmas, so all the cells operated to date contain lithium carbonate encrustations which have accumulated over several electrolyte changes.

We have just begun to learn how to make these measurements. We understand how to do almost everything an order of magnitude better. It is a pleasure to work where there appear to be endless interesting possibilities to be explored. While we have not yet climbed into the drivers seat of our fusion car, we could not be having more fun.

ACKNOWLEDGEMENT

We thank Charles A. Nelson, Jr., Ming-Jen Yang, and Dick Gustafson for physics advice and review. We particularly thank Charlie Nelson for always finding an ordinary explanation for our 30 sigma effects. (We could kill him.) We thank Ming-Jen Yang for computer analysis software. Dick Gustafson and Moyses Kuchnir provided useful stuff. Merle Watson is thanked for building the electronics and for being an enthusiastic spectator. Gary Drake is thanked for the amplifier design and simulation of the calorimeter. Thanks to Rick Mouche' for appearing with pH paper at a crucial time and for teaching one of us a little chemistry. Douglas R. O. Morrison is thanked for integrating the field with his "Cold Fusion Notes". Last, we thank the USA tax system for supplying a significant portion of our expenses.

REFERENCES

[1] M. Fleischmann, S. Pons, and M. Hawkins, *J. Electroanal. Chem.* 261,301-308 (1989).
[2] G.A. Moore, Dissertation. Princeton, (1939).
[3] Workshop on Cold Fusion Phenomena, *Los Alamos Video Tape*, Santa Fe, (1989)
[4] AD590 Data Sheet, Analog Devices, Inc.
[5] OP-270 Data Sheet, Precision Monolithics, Inc.
[6] OPA404 Data Sheet, Burr-Brown Corp.
[7] United States Patent #4,888,763
[8] G. Drake et. al., *IEEE Nuclear Science Symp.*, San Francisco (1985).
[9] ibid., Workshop, Day 2 Discussion.
[10] T. B. Flanagan and F. A. Lewis, *J. Electrochem. Soc.*,108,473 (1961)
[11] ibid., Moore, 91
[12] ibid.,Workshop
[13] J. P. Hoare, *J. Electrochem. Soc.*, 107,635 (1960)

ELECTRIC FIELD DISTRIBUTION OF THE PALLADIUM CRYSTAL LATTICE

K. J. Bunch and R. W. Grow

Cold Fusion Institute
University of Utah
Salt Lake City, Utah 84112

ABSTRACT

Palladium has always been a metal of interest for its hydrogen absorption qualities [1] and, more recently, for its use in cold fusion experiments [2]. An atomic model of the metallic crystal would give a better overall understanding of the palladium-hydrogen system. Unfortunately, a computer simulation of the wave mechanical properties of palladium based on solving the three-dimensional Schrödinger equation is a major undertaking [3, 4] that is probably unnecessary for calculating many useful characteristics of palladium. A simpler approach, based on a Thomas-Fermi model [5] for palladium, is proposed by the authors. This semiclassical model averages the effects of all the electrons within an atom to approximate the electric field distribution everywhere. Overlapping these distributions approximates the electric fields within the palladium crystal. This model predicts a crystal that is a bit too stiff, but overall it gives reasonable results; it is also simple to use. It is expected that this model will broaden the understanding of the interaction of hydrogen with palladium.

INTRODUCTION

This paper presents preliminary investigations into the electric field distribution within palladium metal based on the Thomas-Fermi statistical model [5-7]. This model has a long and fruitful history [8-12], but it has largely been displaced by self-consistent field techniques [3, 13-20] for calculating molecular properties. Recently, however, Lieb and Simon [10] have revived interest in the Thomas-Fermi model by showing that the model becomes exact as the atomic number approaches infinity. Further, various corrections have been proposed to make this model more exact for finite atomic number [21-24].

THE THOMAS-FERMI MODEL

The basic Thomas-Fermi model [7] assumes the electrons in a central field satisfy Fermi-Dirac statistics and that the potential varies little within an electron wavelength. The number of electron states contained within a cube of length L is given by

$$N = 2\left(\frac{L}{2\pi}\right)^3 dk_x\, dk_y\, dk_z \qquad (1)$$

The factor of 2 comes from the 2 possible electron spin states. The number of states for which the momentum $p = \hbar k$ is less than P_o is

$$2\left(\frac{L}{2\pi}\right)^3 \int_0^{P_o/\hbar} \int_0^{\pi} \int_0^{2\pi} k^2\, dk \sin\theta\, d\theta\, d\phi = \frac{P_o^3 L^3}{3\pi^2 \hbar^3} \qquad (2)$$

Assuming a central field, the maximum kinetic energy an electron can have is $-V(r)$; otherwise, electrons would escape the field. A relation between the density of electrons and the potential energy is then

$$n(r) = \frac{[-2m\, V(r)]^{3/2}}{3\pi^2 \hbar^3} \qquad (3)$$

From Poisson's equation,

$$\nabla^2 V(r) = \frac{-n(r)}{\varepsilon} \qquad (4)$$

A differential equation for the potential is obtained by eliminating the electron density:

$$\frac{1}{r^2}\frac{d}{dr}\left[r^2\frac{d(-V)}{dr}\right] = \frac{[-2m\ V(r)]^{3/2}}{3\pi^2\ \epsilon\hbar^3} \qquad (5)$$

Making the following substitutions:

$$V(r) = \frac{-Ze^2}{4\pi\epsilon r}\phi = \frac{-14.3998}{r}\phi$$

(r in A, V in e.v.) (6)

$$r = bx \qquad (7)$$

$$b = \frac{0.885341\ a_o}{Z^{1/3}} = \frac{0.468502}{Z^{1/3}} \qquad (8)$$

where Z is the nuclear charge and a_o is the Bohr radius (0.5292 A). Equation 5 becomes

$$\frac{d^2\phi}{dx^2} = \frac{\phi^{3/2}}{\sqrt{x}} \qquad (9)$$

which is the Thomas-Fermi equation. A numerical solution was found by Bush and Caldwell [25] sufficiently accurately for the purposes of this paper. For palladium, Z = 46 and

$$V(r) = \frac{-662.39}{r}\phi \qquad (10)$$

$$r = 0.13076x \qquad (11)$$

For the ionization energy of a palladium atom stripped of 1 electron, ϕ has to drop from its value at x = 0 (ϕ = 1) to 1/Z = 0.0217. From the tabulated values of ϕ given by Bush and Caldwell [25],

$$x \approx 10.16$$

$$r = 1.33\ A$$

$$V(r) = 10.8\ e.v.$$

The actual ionization energy is 8.3 e.v. [26], reasonably close to that predicted by the Thomas-Fermi model. As a further example, for a palladium atom stripped of 4 electrons, the measured radius is 0.64 A [26]. ϕ = 4/46 = 0.087 and

$$x \approx 4.7$$

$$r = 0.615\ A$$

$$V = 93.7\ e.v.$$

The results are reasonable.

THE PALLADIUM LATTICE MODEL

The palladium lattice is assumed to be a simple superposition of Thomas-Fermi atoms. The electric potential at any point in space is assumed to be the superposition of the potentials from all the neighboring atoms. The atoms themselves are assumed to be noninteracting, and so this model cannot predict the binding energy of the palladium metal. Even if the interaction is taken into account, however, the Thomas-Fermi model is unable to produce a binding interaction [27, 28]; corrections to this model can produce binding, however [12].

Palladium is a face-centered cubic structure, and if a single atom is placed at the center of an x, y, z coordinate system, any other atomic center can be located through the primitive vectors [4]

$$\vec{t}_1 = \frac{r}{\sqrt{2}}(\hat{y} + \hat{z}) \qquad (12)$$

$$\vec{t}_2 = \frac{r}{\sqrt{2}}(\hat{x} + \hat{z}) \qquad (13)$$

$$\vec{t}_3 = \frac{r}{\sqrt{2}}(\hat{x} + \hat{y}) \qquad (14)$$

$$\vec{R} = \ell\vec{t}_1 + m\vec{t}_2 + n\vec{t}_3 \qquad (15)$$

r is the nearest neighbor distance (2.49 A [29]) and ℓ, m, n are the integer indices 0, ±1, ±2, ... At any location x, y, z in the lattice, the distance to any atomic center is given by

$$P = \frac{r}{\sqrt{2}}[(m + n - x)^2 + (\ell + n - y)^2 + (\ell + m - z)^2]^{1/2} \qquad (16)$$

The calculation of the potential anywhere within the lattice involves solving the Thomas-Fermi differential equation (Eq. 9), and summing up the contributions to the potential at each of the distances given by Eq. 16. The indices are increased until the contributions to the potential from higher indices is negligible.

PREDICTED BULK MODULUS AND VELOCITY OF SOUND

The bulk modulus is a measure of the compressibility of a material and the stiffness of the crystal lattice. It is defined by [26]

$$B = \frac{-\Delta P}{\Delta V/V} = -V \frac{dP}{dV} \qquad (17)$$

where P is the pressure on all sides of the material, and V is the volume given by [26]

$$V = \gamma r^3 \qquad (18)$$

where r is the nearest neighbor distance and $\gamma = 2^{-1/2}$ for the face-centered cubic structure. The pressure in Eq. 17 is the change of energy of the crystal with respect to a change in volume

$$P = -\frac{dU}{dV} \qquad (19)$$

so that the bulk modulus becomes

$$B = \frac{1}{9\gamma r}\left[\frac{-2}{r}\frac{dU}{dr} + \frac{d^2U}{dr^2}\right] \qquad (20)$$

Consider removing the atom at the origin of the coordinate system and replacing it with a test charge. The bulk modulus can be determined by calculating the potential changes at the origin as the nearest neighbor distance (r) is varied. The removal of the atom at the origin does not affect this calculation, since this atom is stationary with respect to lattice variations, and all the atoms are non-interacting. Figure 1 shows the bulk modulus calculated over changes in nearest

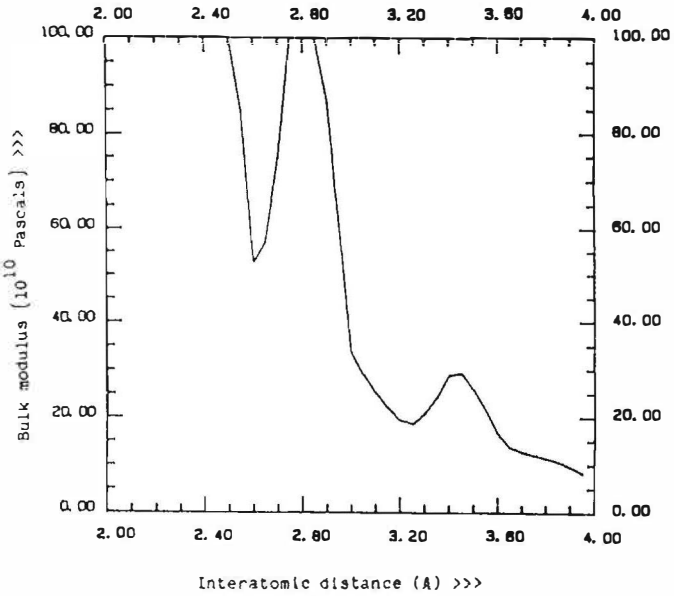

Fig. 1. The predicted bulk modulus over lattice spacing.

neighbor distance. The experimental value for palladium is 1.87×10^{11} pascals [30], whereas the calculated value at r = 2.49 A is 5×10^{11} pascals, about 2.7 times too high. In other words, this model predicts too stiff a lattice.

The velocity of sound can be similarly calculated. Brillouin [31] gives the following formula for the speed of a wave traveling down a one-dimensional string of particles:

$$V = r\sqrt{\frac{1}{m}\frac{d^2U}{dr^2}} = 953.65\, r\sqrt{\frac{d^2U}{dr^2}} \qquad (r \text{ in A, } U \text{ in e.v.}) \qquad (21)$$

From Eq. 10,

$$\frac{d^2V}{dr^2} = -662.39\left\{\frac{d^2\phi}{dr^2} - \frac{2}{r}\frac{d\phi}{dr} + \frac{2\phi}{r^2}\right\} \qquad (22)$$

Using the solution to the Thomas-Fermi equation (Eq. 9) [25], the predicted velocity of sound is 5,000 m/s, whereas the experimental value is 3,000 m/s [32]. The pressure of the surrounding atoms in the lattice will increase this value so that this model again predicts a lattice that is too stiff.

ELECTROSTATIC CALCULATIONS OF PALLADIUM

Figure 2 shows the Bravais cube of the palladium lattice along with the path of the electrostatic field plots. The profile of the potential is calculated across the main (4.76 Å) and sub (2.75 Å) diagonals along the face of the primitive cell. Figures 3 and 4 show the potential profiles at the face of the primitive cell; Figs. 5 and 6 show the profiles at the center of the cell. The interesting fact to notice is that the lattice has definite preferred "channels" through which hydrogen can diffuse. Of course, any lattice imperfections will disrupt this flow.

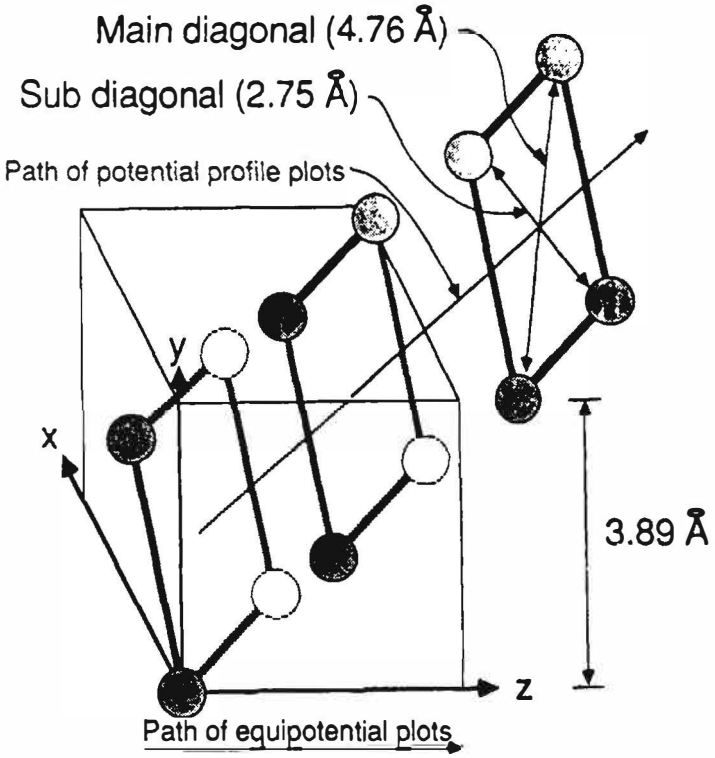

Fig. 2. The Bravais cube showing the primitive cell and the path for subsequent potential plots.

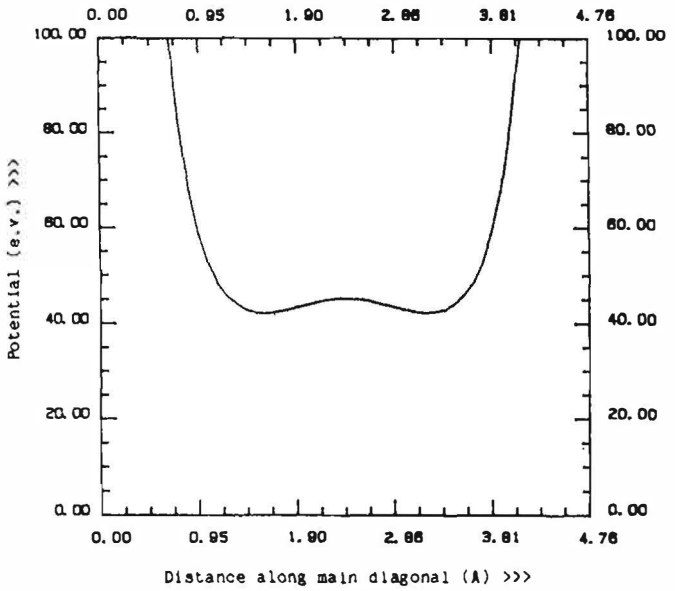

Fig. 3. The potential profile along the main diagonal of the primitive cell.

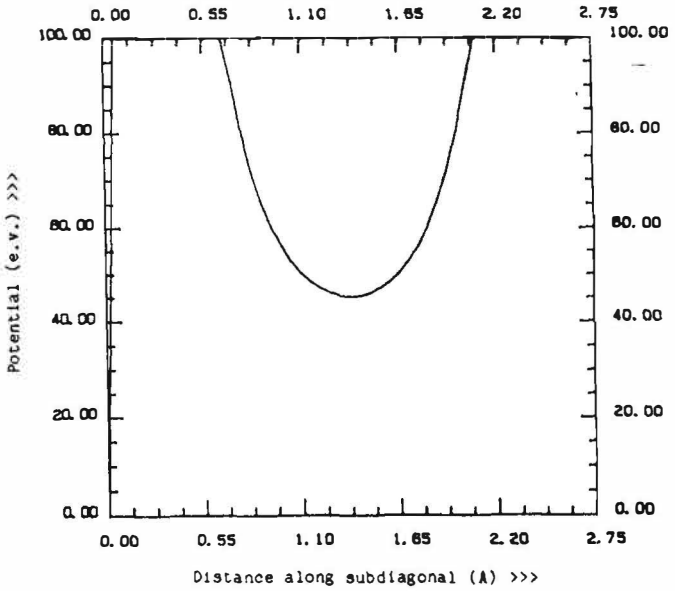

Fig. 4. The potential profile along the subdiagonal of the primitive cell.

The next series of figures shows the equipotential lines along the Bravais lattice shown in Fig. 2. Figure 7 shows the equipotential lines in the x-y plane at z = 0. The potential value of the lines is 50 e.v., a convenient value to measure the channel sizes. Figures 8-10 show the same potential lines for z = 1, 2, and 3 Å.

Figures 3-10 show, not surprisingly, that this model predicts palladium to be relatively hard spheres of an approximate diameter of 2.14 Å. This simplification arises from the noninteracting nature of this model; the electron gas is not allowed to redistribute itself to lower the lattice energy. Of course, this model has the advantage of being able to represent actual lattices with their consequent

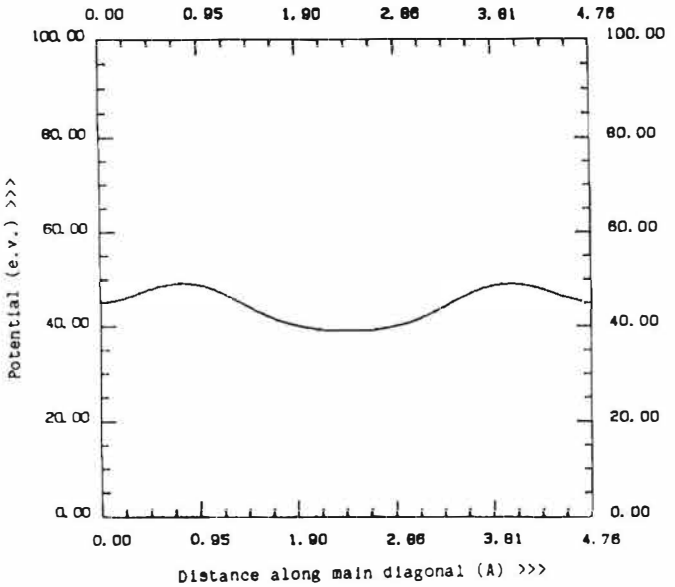

Fig. 5. The potential profile along the main diagonal at the center of the primitive cell.

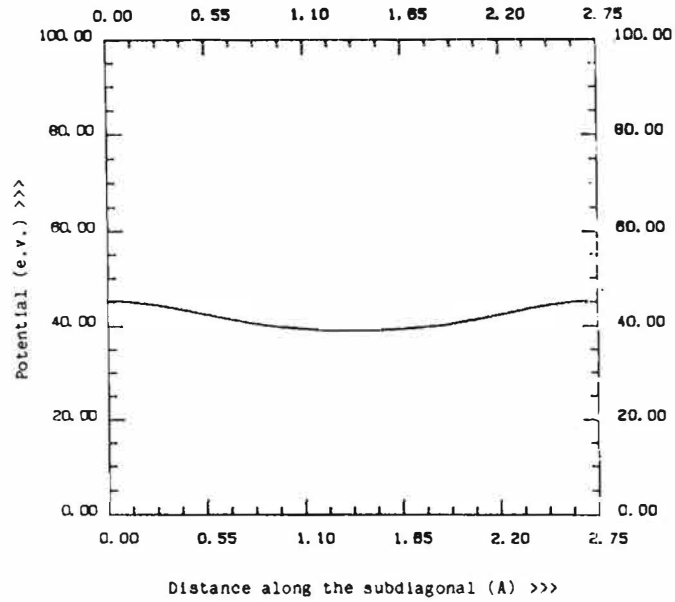

Fig. 6. The potential profile along the subdiagonal at the center of the primitive cell.

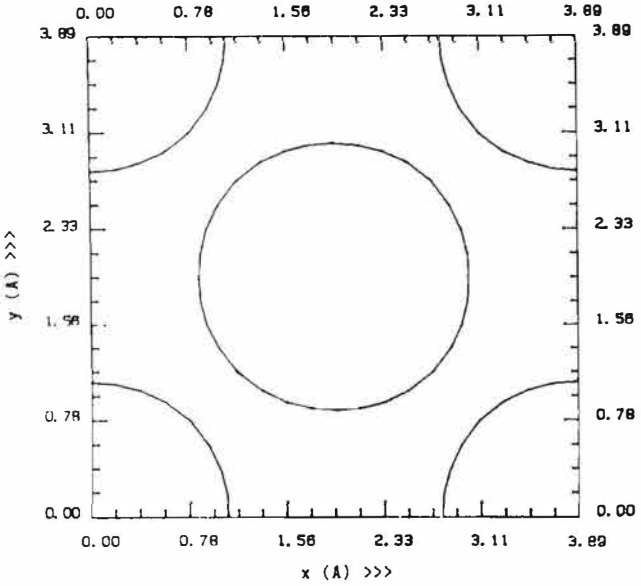

Fig. 7. The equipotential (50 e.v.) lines in the x-6 plane of the Bravais cell for z = 0 Å.

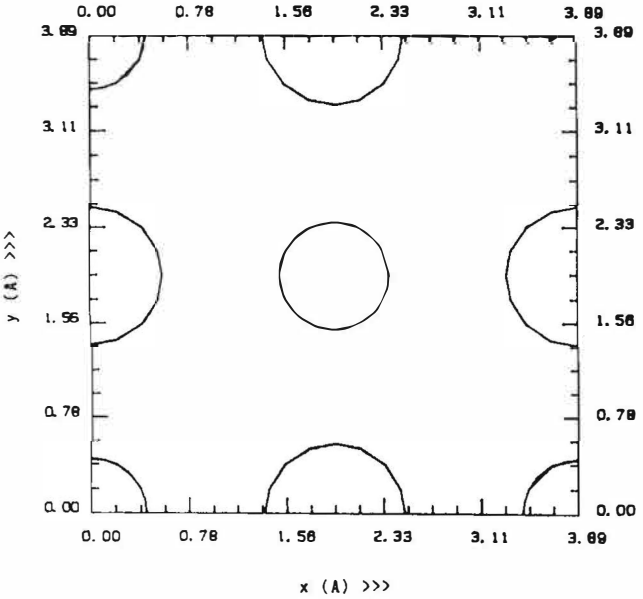

Fig. 8. The same as Fig. 7 for z = 1 Å.

defects and impurities. These effects are difficult to model with other methods, such as with SCF calculations [3]. Further, it may be possible to retain the essential simplicity of this model while including the lattice binding through enforcing boundary conditions at the interfaces of the atomic spheres [9].

CONCLUSIONS

This paper has presented a preliminary investigation into the electrostatic field distribution within the palladium lattice. The palladium atoms are assumed to follow Thomas-Fermi statistics. This approach has the advantage of simplicity as well as the ability to model latice defects and impurities. The model predicts a lattice that is too stiff for palladium, and it fails to take into account any binding within the material. This model can be used to predict the interaction of hydrogen with palladium showing the locations at which hydrogen can collect and the channels through which hydrogen can flow.

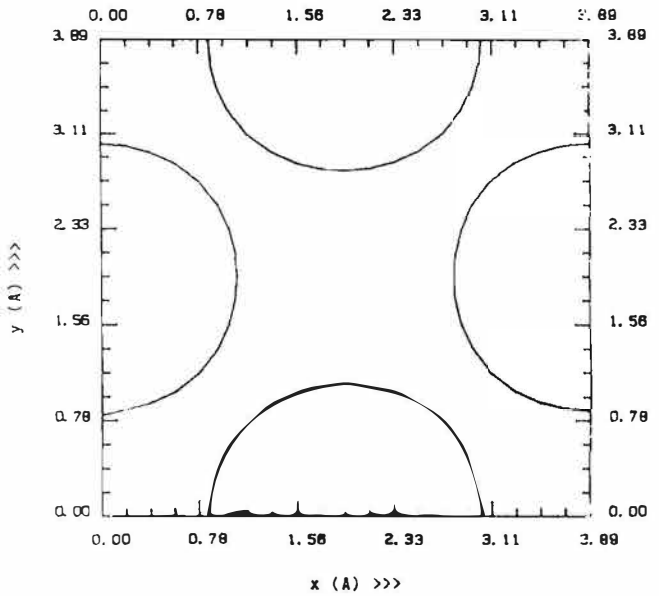

Fig. 9. The same as Fig. 7 for z = 2 Å.

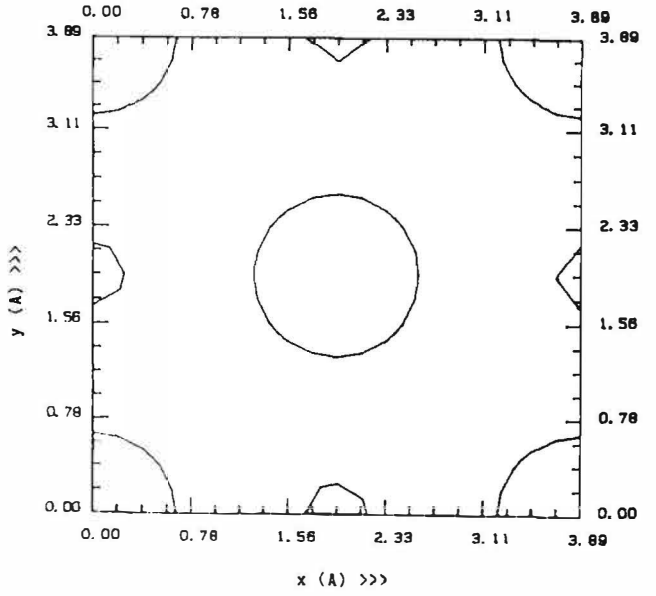

Fig. 10. The same as Fig. 7 for z = 3 Å.

REFERENCES

[1] F. A. Lewis, The Palladium Hydrogen System, Academic Press, New York, 1967.

[2] F. D. Peat, Cold Fusion, Contemporary Books, Chicago, Illinois, 1989.

[3] R. McWeeny, Coulson's Valence, 3rd Edition, Oxford University Press, Fair Lawn, New Jersey, 1979.

[4] J. C. Slater, Quantum Theory of Molecules and Solids, Vol. 2, McGraw-Hill Book Company, New York, 1965.

[5] L. H. Thomas, "The Calculation of Atomic Fields," Proceedings of the Cambridge Philosophical Society, Vol. 23, 1927, pp. 542-548.

[6] E. Fermi, "Eine Statistische Methode zur Bestimmung Einiger Eigenschaften des Atoms und Ihre Anwendung auf die Theorie des Periodischen Systems der Elemente," Zeitschrift fur Physik, Vol. 48, 1928, pp. 73-79.

[7] L. I. Schiff, Quantum Mechanics, 2nd Edition, McGraw-Hill Book Company, Inc., New York, 1955.

[8] P. A. M. Dirac, "Note on Exchange Phenomena in the Thomas Atom," Proceedings of the Philosophical Society, Vol. 26, 1930, pp. 376-385.

[9] N. H. March, "The Thomas-Fermi Approximation in Quantum Mechanics," Advances in Physics, Vol. 6, No. 21, January 1957, pp. 1-101.

[10] I. H. Lieb and B. Simon, "Thomas-Fermi Theory Revisited," Physical Review Letters, Vol. 31, No. 11, September 1973, pp. 681-683.

[11] R. Benguria and E. H. Lieb, "Many-Body Atomic Potentials in Thomas-Fermi Theory," Annals of Physics, Vol. 110, 1978, pp. 34-45.

[12] E. H. Lieb, "Thomas-Fermi and Related Theories of Atoms and Molecules," Reviews of Modern Physics, Vol. 53, No. 4, October 1981, pp. 603-641.

[13] C. C. J. Roothaan, "New Developments in Molecular Orbital Theory," Reviews of Modern Physics, Vol. 23, No. 2, April 1951, pp. 69-89.

[14] C. A. Coulson, "Present State of Molecular Structure Calculations," Reviews of Modern Physics, Vol. 32, No. 2, April 1960, pp. 170-177.

[15] C. C. J. Roothaan, "Self-Consistent Field Theory for Open Shells of Electronic Systems," Reviews of Modern Physics, Vol. 32, No. 2, April 1960, pp. 179-185.

[16] R. S. Mulliken, "Self-Consistent Field Atomic and Molecular Orbitals and Their Approximations as Linear Combinations of Slater-Type Orbitals," Reviews of Modern Physics, Vol. 32, No. 2, April 1960, pp. 232-238.

[17] R. K. Nesbet, "Computer Programs for Electronic Wave-Function Calculations," Reviews of Modern Physics, Vol. 35, No. 3, July 1963, pp. 552-557.

[18] S. M. Blinder, "Basic Concepts of Self-Consistent-Field Theory," American Journal of Physics, Vol. 33, No. 6, June 1965, pp. 431-443.

[19] J. C. Slater, The Calculation of Molecular Orbitals, John Wiley & Sons, New York, 1979.

[20] A. Hinchliffe, Computational Quantum Chemistry, John Wiley & Sons, New York, 1988.

[21] J. Schwinger, "Thomas-Fermi Model: The Leading Correction," Physical Review A, Vol. 22, No. 5, November 1980, pp. 1827-1832.

[22] J. Schwinger, "Thomas-Fermi Model: The Second Correction," Physical Review A, Vol. 24, No. 5, November 1981, pp. 2353-2361.

[23] P. Benguria, H. Brezis, and E. H. Lieb, "The Thomas-Fermi-Von Weizsäcker Theory of Atoms and Molecules," Communications in Mathematical Physics, Vol. 79, 1981, pp. 167-180.

[24] V. C. Aguilera-Navarro, M. de Llano, O. RoJo, and S. L. L. Verardi, "The Thomas-Fermi-Scott-Schwinger Expansion and the Schrödinger Ground State Energy of Complex Neutral Atoms," Journal of Chemical Physics, December 1982, pp. 6131-6133.

[25] V. Bush and S. H. Caldwell, "Thomas-Fermi Equation Solution by the Differential Analyzer," Physical Review, Vol. 38, November 1931, pp. 1898-1902.

[26] G. S. Zhdanov, Crystal Physics, Academic Press, New York, 1965.

[27] E. Teller, "On the Stability of Molecules in the Thomas-Fermi Theory," Reviews of Modern Physics, Vol. 34, No. 4, October 1962, pp. 627-631.

[28] E. H. Lieb, "The Stability of Matter," Reviews of Modern Physics, Vol. 48, No. 4, October 1976, pp. 553-569.

[29] W. B. Pearson, A Handbook of Lattice Spacings and Structures of Metals and Alloys, Pergamon Press, New York, 1958.

[30] C. J. Smithells, Metals Reference Book, 4th Edition, Vol.s I-III, Plenum Press, New York, 1967.

[31] L. Brillouin, Wave Propagation in Periodic Structures, 2nd Edition, Dover Publications, Inc., New York, 1946.

[32] C. J. Smithells, Metals Reference Book, 1st Edition, Butterworths Scientific Publications, London, 1949.

HIGH-SENSITIVITY MEASUREMENTS OF NEUTRON EMISSION FROM Ti METAL IN PRESSURIZED D_2 GAS

H. O. Menlove
Group N-1, MS E540
Los Alamos National Laboratory
Los Alamos, NM 87545

ABSTRACT

Recent measurements of neutron emission from Ti metal in pressurized D_2 gas have established the multiplicity distribution of neutron bursts emitted from the samples. A new ^{3}He detector system with high sensitivity has been used to lower the detection limit so that small bursts emitting from 2-10 n can be distinguished from the cosmic-ray background. The frequency distribution of the neutrons indicates that the lower multiplicities occur much more frequently than the higher multiplicities as shown in Fig. 1. The improved sensitivity in our new detector system was obtained by using low radioactive background stainless-steel tubes, a small detector volume with high efficiency, and additional cosmic-ray shielding. The detector consists of two independent segments making up inner and outer rings of ^{3}He tubes. The inner detector has nine ^{3}He tubes (2.5 x 30 cm), and the outer detector has forty-two ^{3}He tubes (2.5 x 50 cm). The combined total efficiency is 44%. The low-background inner detector has a singles count background of 97 counts/h and a coincidence count background of only 0.67 counts/h. The corresponding singles efficiency (2.3-MeV neutrons) is 19% and the coincidence efficiency is 3.6%.

This system has been used to detect low multiplicity neutron emissions from samples where the yield is 5-10 times larger than the background level for intervals of many hours. This improved sensitivity makes it possible to monitor the neutron yield characteristics of samples at a much lower level than was previously possible. We have shown that the most frequent events emit neutrons with 1-10 n and the larger burst events 20-200 n occur much less frequently. Figure 2 shows an example of the multiplicity distribution we measured for a sample containing Ti metal chips in D_2 gas pressurized to 800 psi. The active period lasted for several days following three weeks and six liquid-nitrogen temperature cycles that were inactive. On the right side of Fig. 2 is the multiplicity distribution for a control sample of Ti metal chips in H_2 gas that was measured for the same amount of time both before and after the active sample runs.

These multiple small burst events (2-10 source neutrons) give us the ability to study the details of the

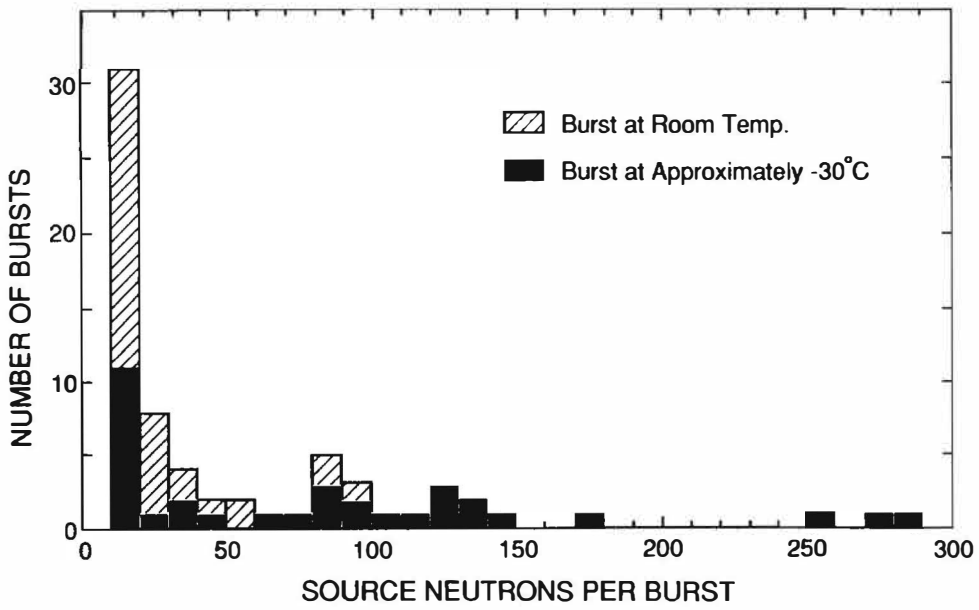

Fig. 1. Neutron burst multiplicity frequency distribution for 13 active samples of Ti metal in pressurized D_2 gas.

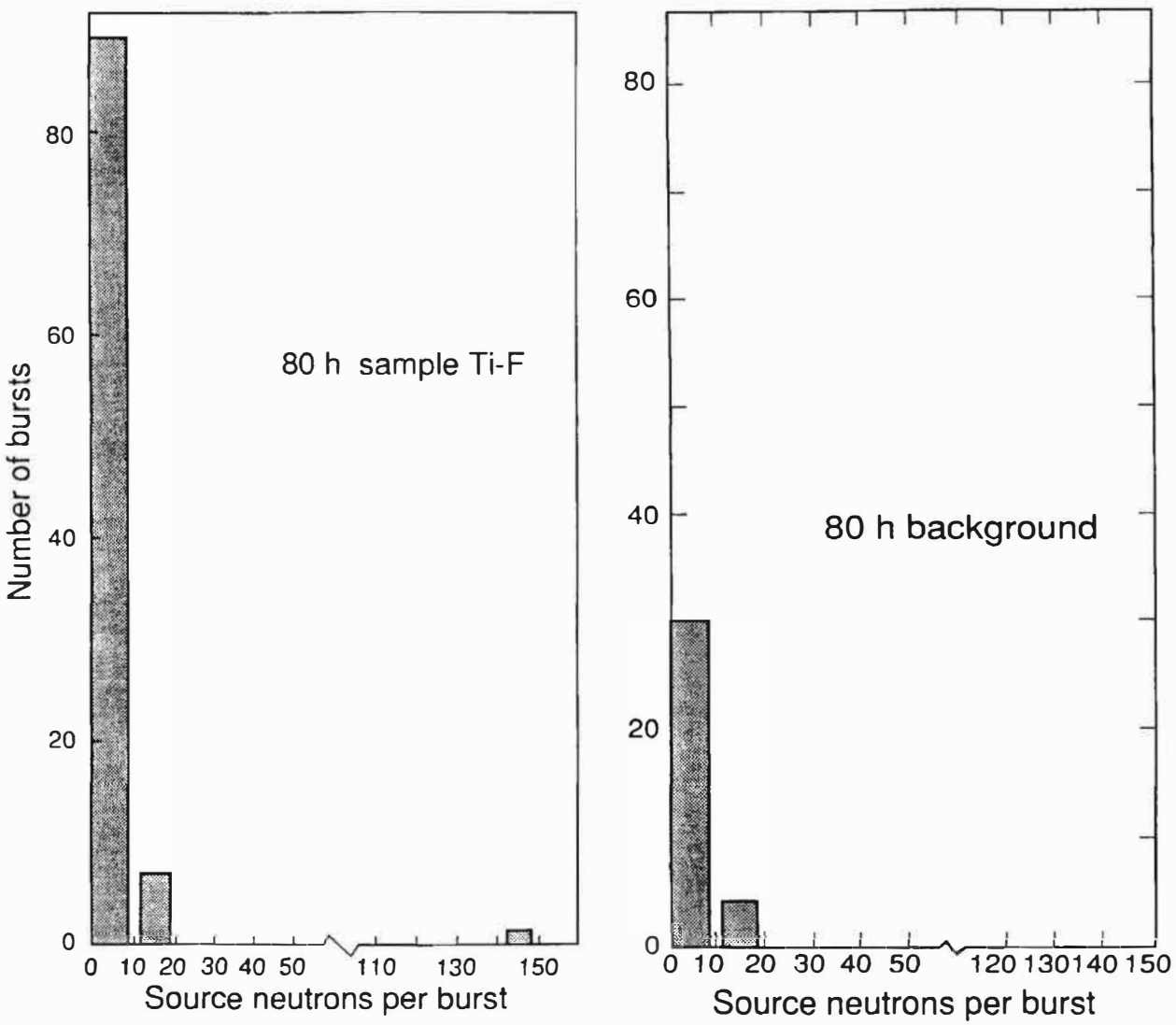

Fig. 2. Neutron source multiplicity frequency distribution for a single Ti sample showing the high frequency for the low number of source neutrons per burst.

phenomena that were not observable before. The results are now reproducible in that we can remove an active sample from one detector system and still measure the excess yield for the same sample in the adjacent detector system. The neutron emission rate is very low (0.001 n/s), and we can detect it only by means of our time-correlation counting and underground laboratory.

Only an abstract is given for this paper because the full paper has been submitted for journal publication.

TECHNICAL STATUS OF COLD FUSION RESULTS

David H. Worledge

Electric Power Research Institute
P.O. Box 10412, Palo Alto, California 94303

ABSTRACT

Experimental results in cold fusion research up to the end of the 1989 are reviewed to gain a perspective on the credibility of the phenomena. The review does not attempt to be comprehensive but concentrates on the highest quality experiments claiming to give positive results. The results are used to formulate a strategy for continuing to support cold fusion research in 1990.

INTRODUCTION

During the past 12 months, many improvements have been made in experiments done to attempt to verify the Fleischmann-Pons phenomena. These changes have, in part, been a response to valid criticisms of the early work, and in part due to a natural process of refinement that has come with having more time and resources. Considerable attention has been paid to 1) reducing the probability of contamination in experiments finding tritium, 2) reducing backgrounds and increasing efficiency in neutron counting, 3) improving calibration methods and reducing sensitivity to spatial variations of temperature in calorimetry, and 4) using closed cells. Many different laboratories including some national laboratories and organizations in foreign countries have reported positive findings.

Despite these advances we have not yet succeeded in producing a recipe that can be handed to independent research groups that will lead to reproducible results.

Furthermore, we see the positive results against a background of statistically over-whelming negative evidence from other research groups too numerous to mention. In many cases, these groups are just as credible and experienced as those producing positive results. Because of this, most of us are still undecided as to the truth of the cold fusion claims, and there is no question that scientific demonstration of the phenomena has simply not been achieved.

How should we view this situation? It is not hard to find reasons why many experiments may have failed. One issue is the way in which adequate loading of the metal lattice with deuterium can be hindered, particularly since concentrations of electrolyte contaminants of order ppb or less can obscure the cathode surface after a period of electrolysis. Further reasons can be found, perhaps, in too long integrating times for neutron counting(~hr) when the adventitious neutron signal may endure for no longer than a few minutes. Whatever the reasons, they amount at best to plausible rationalizations. On the other hand, just as plausible rationalizations may be stated, a priori, for the neutrons to be background-related artifacts, or for the tritium to be the result of occasional spot contamination of the materials, perhaps more deeply trapped than expected. To get beyond such trite rationalizations requires a close look at a large fraction of the data. We should be willing to let the evidence accumulate and let the data speak for itself, without allowing beliefs or prejudices about the outcome to influence our judgement. Long before the final outcome is known, however, we have to make decisions about research funding and which experimental directions to emphasize.

This paper reports a technical review of the results available at the end of 1989 and focuses on the factors that lend support to their credibility and those which point to remaining problems. The review is not comprehensive. It leans heavily on results that have been published or that have been presented at specialist meetings. Most of them either preceded or are part of results discussed or reported in the proceedings of this meeting. I have scarcely referred to the original published data of Fleischmann and Pons [1] nor of Jones *et. al.* [2] because, as the progenitors of all that followed, they hardly need further comment. Including them would not change my conclusions.

TRITIUM

At Texas A&M University Bockris and Wolf have reported [3] that 11 electrolytic cells using a single source of palladium for cathodes and nickel anodes produced tritium in amounts from 7×10^3 to 5×10^7 dpm/ml (10^6 times background). In a controlled batch of 6 cells having external recombiners and 6 accompanying H_2O cells, one D_2O cell has given ~10^6 dpm/ml. The first Bockris cell reported to give a significant amount of excess heat has been the first cell to produce tritium twice while in a calorimeter [4]. Detailed assay

procedures and results are described in references 1 and 2. More than 25 other cells have not produced any tritium, including those operated by Appleby.

At Los Alamos National Laboratory, Storms and Talcott [5] have reported that seven of nine new closed cells have produced tritium in amounts up to six times the background concentration in the electrolyte. At least two earlier open cells (of 16) produced tritium, one of which had 80 times the background. A further batch of 16 closed cells gave no tritium. No H_2O control cells have been run.

Several groups at the Bhabha Atomic Energy Research Center (BARC) have reported [6] that at least nine electrolytic experiments were conducted yielding more than sixty samples where tritium was not produced. However, in experiments described in papers A1, A2, A3, A6, and A8 of reference 4, quantities of tritium were produced exceeding 10^{12} atoms. Some of the experiments used reflux condensers and cold traps to remove D_2O carryover, a recombination catalyst to remove stoichiometric D_2 and O_2, a copper oxide catalyst to remove desorbed D_2, further cold traps and a bubbler. These experiments desorbed all D_2 at the end of the experiments by heating the cathodes in a similar apparatus. All fractions were counted and added to give a tritium assay to better than 10%. Table 1 summarizes the results.

Two pressure loading experiments (papers B3 and B4 of ref. 4) have given tritium after D_2 gas was absorbed into Ti and Pd-Ag alloy discs, wafers and cones and Pd-black powder. Tritium presence in amounts $>10^{10}$ to 10^{11} atoms was confirmed by a combination of surface activity measurement using 1) direct contact with scintillation cocktail, 2) autoradiography, 3) X-ray spectrum analysis, and 4) desorption in H_2O followed by scintillation counting. The count rates correspond roughly to an enhancement of the t:d ratio by factors of 10^2 to 10^4. The overall hit rate in gas absorption experiments was low. No blanks had been run using H_2 gas. Several blanks had been run without gas absorption or after annealing the samples. No tritium activity was observed in these controls.

Several other laboratories have reported tritium generation in the electrolyte at only three to six times the initial concentration, often but not exclusively in open cells. Electrolytic isotopic concentration in open cell electrolyte using palladium can account for about a factor of two at room temperature although this factor depends on the metal at the surface of the cathode and on the temperature. Impurities on the cathode surface may, therefore, affect the isotopic concentration. Such results may be significant but assay technique details, surface conditions, and systematic and random errors are not generally available. It is, therefore, even more difficult to assess the significance of these particular results.

Also at Los Alamos, Claytor [7] claims almost reproducible tritium production from a non-electrolytic device involving the passage of a pulsed electric current through a stack of thin discs made alternately of Si and Pd. The stack had previously absorbed D_2 gas to equilibrium at 110 psi to a D/Pd ratio of 0.7. In a 90-hour run, 10^{12} to 10^{15} tritium atoms were produced. Annealing the sample before the experiments at

TABLE 1. BARC TRITIUM RESULTS

No.	Cathode	Anode	Tritium Concentration/ Background	Atoms of Tritium	Duration of Tritium Generation (Days)	Controls
A1	Pd/Ag Alloy	Ni	20,000	8.10^{15}	3	No
			4,000	5.10^{14}	2	No
A2	Pd/Ag Alloy	Ni	3,455	4.10^{15}	<1	No
A3	Ti	Stainless Steel	1,000	$1.4.10^{14}$	<1	One
A6	Pd	Pt	12,500	2.10^{15}	2	No
			>5	$\geq 10^{12}$	7	No
A7	Pd	Pt	3	2.10^{11}	17	Several
A8	Pd	Pt	1.5	7.10^{11}	49	Three

high temperature should have eliminated the most obvious potential source of tritium contamination.

The tritium facility at Los Alamos National Laboratory contains some of the country's foremost experts on tritium handling and assay. The Isotope Production Group, Health Physics Division and Heavy Water Division personnel at BARC have been dealing with tritium for over 20 years. Their approach displays considerable expertise in tritium handling and assay. They have performed the most comprehensive total tritium assays in the field so far, without appearing to be on a learning curve.

The laboratories at Texas A&M University, BARC and LANL each adopt several independent instruments and give extensive attention to calibration, background, chemiluminescence, quenching and spectrum analysis. Independent assays (by five different laboratories in the case of Texas A&M) confirm that tritium is present in the samples.

The extraordinary spectre of intentional contamination should be essentially ruled out by the facts that 1) the results occur in different organizations, 2) security measures are in effect at all three laboratories, 3) at least one of the Texas cells was inaccessible beneath shielding and detectors, 4) in at least one instance, tritium was increasing in samples taken over 3 days, and 5) Storm's data show evidence of many small tritium bursts in some cells.

The chance of accidental contamination should be reviewed in light of the following facts: 1) most of the experiments were sealed; 2) pre-annealing was done on many metal samples; 3) post-test analysis of blank (unelectrolyzed or unused) cathode samples yielded no tritium; 4) Texas A&M assay of glassware, plastic tubes, rubber bungs and syringes yielded no tritium; 5) LANL assay of Bockris' Ni anodes yielded no tritium; 6) careful pre- and post-assay of D_2O and D_2 gas used at all stages verified background levels of tritium; 7) strongly differing partition of tritium between electrolyte, off-gas and cathode can be explained for several different experimental set-ups; 8) BARC, at least, regularly monitors tritium activity in the laboratory atmosphere in the Heavy Water Division; 9) amounts of tritium in the neighborhood of 10^{14}-10^{16}atoms exceeds conceivable contamina-tion sources (e.g., even a standard laboratory solution of 1 m Ci/ml contains only 2×10^{13} tritiums/ml, whereas most of the Texas cells had only 15 ml volume); 10) the laboratory at Texas A&M Cyclotron Institute had never been used for tritium production or assay; 11) the overwhelming majority of cells only gave tritium once, inconsistent with random in-process contamination; 12) adjacently placed cells were not contaminated by those producing tritium; 13) H_2O control cells gave no tritium; 14) no tritium was produced often during many weeks of charging during which it would have been flushed out of either electrode, if present initially; and 15) previously contaminated Pd would lose tritium by diffusion to air at room temperature in <100 hours for the dimensions used.

CONCLUSION ON TRITIUM

Although better controls are needed and reproducibility is clearly lacking, the evidence is becoming stronger that tritium is generated in the experiments. This evidence is from three credible and experienced organizations with multiple independent checks in many different kinds of experiment. We shall see that the evidence on tritium generation is the strongest of the three types of evidence for cold nuclear reactions, i.e. tritium, neutrons, and heat. It seems no longer reasonable to assume these results are necessarily wrong solely because of theoretical improbability based on current understanding. My view is that the results deserve to be taken seriously even though they are a long way from providing proof of the phenomena.

NEUTRONS

The earliest confirmation of neutrons from electrolytic cells was reported by Bertin *et al.* [8] in a low background tunnel under the Gran Sasso Massif. Two NE213 scintillation counters recorded similar count rates when exposed alternately to a group of three cells. In each case, the alternate counter measured the background simultaneously eitht meters away. The energy specrtum and a Monte Carlo simulation indicated the neutrons had 2.5 MeV energy. The source rate was 14.5 neutrons per minute (~58 n/min/cm^3). This background corrected rate was almost 5 σ.

In 200 early experiments on 25 electrolytic cells at Texas A&M University, statistically significant neutron emission from three separate experiments using the same piece of palladium was obtained by Wolf *at. al*[9]. In more recent experiments, five different electrodes (6 mm ϕ x 2 cm) have given neutrons for ~10 hours. Count rates were three to five times background corresponding to source strengths of 50 n/min (~500 n/min per cm^3).

A fast plastic scintillation counter in an electronically shielded low background configuration gave 0.8 c/min overall background, and 0.5 background c/min in the energy range 1 to 2.5 MeV. The counting system obtained the neutron energy spectrum with energy discrimination against cosmic background. Two different pulse shape discrimination systems were used against gamma background. Large geometric efficiency, common-mode electronic noise rejection, broad range frequency noise scans, thermal isolation of the detector, and detector temperature monitoring give additional confidence against artifacts. The detector neutron efficiency was determined with three techniques including ^{252}Cf time-of-flight measurement specific for 2 MeV neutrons, and the cyclotron was always off during measurements. Two independent theoretical calculations of response of the detector to 2.45 MeV neutrons are consistent with the measured spectrum shape. Additionally, one $1/r^2$ test confirmed neutrons from a source at the cell.

In addition, the neutron spectrum is quite different from that observed from a fission source, from (α,n) reactions of light elements and neutrons from cosmic ray shower-induced reactions in surrounding materials. The same spectrum and signal was measured with a second detector of the same type. The 200 experiments contained several H_2O blanks and

TABLE 2. SUMMARY OF BARC NEUTRON RESULTS

EXPERIMENT NO.	A1	A2	A3	A7	A8
CATHODE	PdAg	PdAg	Ti	Pd	Pd
NEUTRON DETECTORS	BF_3, ^3He, Plastic	BF_3,Plastic	^3He, Plastic	^3He	BF_3
SEPARATE B/G DETECTOR	^3He, Second run	No	Plastic	No	BF_3
BACKBROUND COUNT RATE (per second)	0.2(BF_3), 2 (plastic)	1.3 (BF_3), 1.7 (plastic)	24 (^3HE)	1.6	20
NEUTRON COUNT) (TIMES B/G)	2-200(BF_3), 2-40 (plastic)	150 (BF_3), 120 (plastic)	2	1,000	56
DURATION OF NEUTRONS (minutes)	5 to 150	4	150	2,400	8
DELAY BEFORE NEUTRONS	2 days; 1 hour	4 hours	3 hours	14 days	a fewhours
NEUTRON YIELD (source)	4×10^7	4×10^6	3×10^7	2×10^8	1.4×10^6
TRITIUM YIELD (atoms)	8×10^{15}	4×10^{15}	10^{14}	$>2 \times 10^{11}$	7×10^{11}
NEUTRON/TRITIUM RATIO	10^{-8}	$>10^{-9}$	2×10^{-7}	$<10^{-3}$	1.7×10^{-6}
NEUTRONN SOURCE 10^4 n/min/cm^3	6	20	0.3	10	1.4
10^6 n/cm^3	6	0.8	0.5	300	1.4
10^5 n/cm^2	1.3	0.1	3	100	2

dummy cells. None produced neutrons.

Iyengar [6] reports at least five different kinds of experiments done by different combinations of Neutron Physics Division, Heavy Water Division, Water Chemistry Division, Desalination Division, Isotope Production Division, Analytical Chemistry Division and Reactor Operations and Maintenance Division at the Bhabha Research Center (i.e. groups of varied expertise were brought together). Table 2 gives a summary of the neutron results.

In general, the experiments were not significantly shielded and little electronic processing was done on the detector signals. A combination of ^3He, BF_3 and plastic scintillation detectors was used. BARC neutron counting details equivalent to the Texas information are not at hand to enable confidence to be stated in count rates only 2 to 5 times the background; for example, the extent of efforts to eliminate and monitor noise sources or variation of count rate with mass close to the detector. Conclusions included here are, therefore, only from higher signal-to-noise ratios. However, the Neutron Physics group apparently conducted extensive searches for noise sources and demonstrated counter stability and background rates over a period of about five weeks prior to some of the experiments [10].

In three of the experiments a separate, sometimes diverse, counter monitored background about 2 meters from the cell. At least four experiments (A1, A2, A7, A8) gave count rates from 30 to 1,000 times the background, although the background rate was relatively high at 2 to 20 per second. In experiments A1 (BF_3, NE102A), A2 (BF_3, NE102A) and A3 (BF_3, NE102A) neutrons were recorded simultaneously in the two detector types, at high rates in A1 and A3. Control experiments with H_2O or stainless steel cathodes did not give neutrons. Neutron emission is also reported from TiDx gas absorption experiments.

Menlove and Jones report [11] several hundred neutrons occurring in bursts less than 120 μsec in duration from palladium electrolytic cells, as well as from TiDx in gas absorption experiments. These neutrons have no time correlation with accompanying acoustic emissions. But the bursts are repeatable in a statistical sense.

The reported random (multiplicity one) neutron emission of Jones [2] corresponds to a source strength of 24 n/min (~240 n/min/cm^3), about the same as Wolf (500 n/min/cm^3), and two to three orders of magnitude less than those found at BARC. Jones' H_2O control experiments did not give neutrons.

CONCLUSIONS ON NEUTRONS

Although the quality of experiments claiming to measure neutrons is high at least at BYU, Texas A&M, LANL, and BARC, the low counting rates at Texas A&M and BYU do not support high confidence in these results. The burst nature of neutrons at LANL at rates well above background are a clearer signal but conceivably could be due to micro-hot fusion. The results at LANL and at Texas A&M have so far been observed only using a single detector at a time. On both these bases the BARC results appear, perhaps, to be the most definitive. We will benefit greatly from having more specific input on the quality of these results at this meeting. Until then, the neutron evidence must be seen as less compelling than that from tritium.

NEUTRONS, TRITIUM AND HEAT COMPARED

Neutrons are not always, or even usually, observed concurrent with tritium. In electrolytic experiments where neutrons and tritium were observed simultaneously or close in time correlation, Table 3 shows total neutrons, tritium and their ratios. This measured ratio is very different from the expected value of approximately unity for d-d fusion proceeding through ^{4}He compound nucleus levels.

TABLE 3. NEUTRON TO TRITIUM YIELD RATIO

	Neutrons	Tritiujm Atoms	Ratio (n:t)
Wolf, Texas A&M BARC, Bombay	7×10^4	$>10^{13}$	$<5 \times 10^{-8}$
A1	4×10^7	8×10^{15}	5×10^{-9}
A2	4×10^6	4×10^{15}	10^{-9}
Claytor, LANL	10^3	10^{12}	10^{-9}
Claytor, LANL	10^6	10^{15}	10^{-9}

Although excess heat levels are not discussed until later, I will assume an excess power of 1 watt for comparison. 2×10^{12}/sec d-d fusions leading to the n, ^{3}He branch are needed to supply 1 watt. The Jones and Wolf neutron rates are ~ 10^{-12} of this. Table 3 shows total numbers of tritium atoms supposed to have been produced, concurrent with neutrons, over periods of roughly 10^5 second (1 day). They correspond to 10^9 -10^{11} tritium atoms per second. The maximum amount reported from the Bockris laboratory is 10^{16} tritiums. It is not known if excess heat accompanied this tritium production.

One watt from the p,t branch of the d-d reaction requires 1.6×10^{12} events/second. The tritium observed accounts for less than 1% of this. In a recent experiment [4] Bockris claims excess heat roughly concurrent with tritium (the first cell to give two episodes of each concurrently). The amount of tritium accounts for only about 0.1% of the excess heat.

If tritium is the nuclear product associated with excess heat we must explain why heat has many times been observed without tritium. Even in the Bockris cell giving heat and tritium there was an extended period of excess heat before any tritium appeared.

OTHER NUCLEAR MEASUREMENTS

Protons must accompany tritium from d-d fusion whatever the mechanism or the n:t branching ratio is. Taniguchi [12] claims to have observed protons in 6 out of 23 experiments using a 10 μm palladium foil cathode as one side of an electrolytic cell. The count rate was of the same order of magnitude as the Jones and Wolf neutron rates (~10 to 100/hour but from a much smaller volume). The surface area was about the same.

The protons had energies extending down from 2 MeV. The 3 Mev protons from d-d fusion would lose about 1 MeV in traversing the palladium foil. Very few protons had 2 MeV energy. The spectrum implies that the protons were produced close to the inside surface or, if distributed through the bulk, have lower energy than energy conservation demands. Even if all protons were initiated on the surface at 3 MeV, the authors state the spectrum shape is inconsistent with integration over the angular acceptance of the detector. The (ambiguously stated) implication is that no matter where the protons were produced, energy is only conserved if d-d fusion is not responsible or if it leads to three or more bodies in the final state. This is to be compared to Wolf's observation that lack of 14.1 MeV secondary neutrons implies the tritium has lower energy than expected from d-d fusion.

Taniguchi did not have positive particle identification, so it is possible he is not seeing protons at all.

Rasmussen (UC Berkeley) [13] observed no protons in a similar experiment, but he used cathode foils 76 μm thick, beyond the range of 3 MeV protons in palladium. Rasmussen also maintained low current densities throughout the experiments, but so did Taniguchi *et al* . (only about 5 mA/cm^2). Ziegler [14] did not observe any protons in a similar experiment. However, Cecil has pointed out that Ziegler's foils (25 μm Pd) were thick. Only if the protons had >3 MeV energy or some were produced close to the outside surface would they have been observed.

The story on protons is extremely important because of the low sensitivity of small volume silicon surface barrier detectors to neutrons and gammas. Extremely low count rates in the MeV region can be measured with good energy resolution and close to 100% efficiency. Positive findings in such experiments could greatly improve confidence in the nuclear products.

Wolf, Lewis [15] and others have searched unsuccessfully for palladium coulomb excitation gammas. High resolution detectors were used. The inference from the work to date seems to be that there are no energetic gammas accompanying neutron or tritium emission, strongly implying that the protons have lower energy than expected or do not exist at all. Gammas from possible (n,γ) reactions are also not observed. This is important with respect to data from the Naval Research Laboratory concerning palladium isotope ratios (below). No 23.84 MeV gammas are seen (from the d-d threshold to ^{4}He ground state) nor gammas from other transitions in ^{4}He.

21 KeV Pd K-Xrays would probably not have been observable with confidence in any electrolytic experiments done to date. However, it should be possible to observe them with an appropriate cell design if they are present. Given the adventitious occurrence of neutrons, tritium and excess heat, it is essential that cells active in all of these three ways be moni-

TABLE 4. SUMMARY OF ROUND ROBIN ^{4}HE ANALYSIS

Laboratory	As Received (x 10^{13} atoms)	Electrolyzed (x 10^{13} Atoms)	Factor Increase
#1	2.0	6.3	3.15
#2	1.25	7.0	5.60
#3	0.31	2.4	7.74
#4	0.37	1.6	4.32
	0.35		4.57
#5	0.84	4.6	5.48
		8.3	9.88

tored over long periods for X-ray emission.

O'Grady and Rollison [16] reported substantial changes in palladium isotopic abundance after electrolysis in D_2O/Li_2SO_4 and D_2O/LiOD. The changes were confined to the outer surface layer of the cathode. They did not appear when using an H_2O based electrolyte or when using non-electrolyzed palladium. The isotope ratios reverted to the natural abundances at depth. The inference is that a total of several percent of the palladium atoms in the outer 1 μm were transmuted in some nuclear reaction. For the active agent to be completely absorbed in this small thickness would need an interaction cross-section of order 10^5 barns. The result is so far unconfirmed.

ETEC/Rockwell has analyzed cathode samples from Texas A&M University that had apparently produced some excess power and has found no helium 3 or helium 4 above a detection threshold which is $5x10^9$ atoms. If produced at the surface, helium would all escape with evolved gases. EPRI, through ETEC/Rockwell, participated in a double-blind Round Robin assay by five laboratories of samples as received and as electrolyzed by Pons. The Round Robin results are shown in Table 4. There is a wide scatter on results from different laboratories (and within each laboratory depending on the spot selected for analysis) but all found an increase by a factor of 3 to 10 between the as received and the electrolyzed samples. The most accurate result has probably been obtained subsequently by ETEC as an average of 13 measurements. Although small in absolute terms, the number of helium atoms "produced" (~2.7 x 10^{13} - ETEC) in the test sample is about right to account for the heat claimed (only 3-4 mW for 10^5 sec). The background ^{4}He in the as-received material from Johnson Mathey was curiously high (by a factor of ~10^4) indicating some exposure to ^{4}He in the manufacturing process. This anomalous ^{4}He in the as-received material makes it impossible to interpret the results of the Round Robin experiment.

In a one gram sample of metal, it is not possible to detect less than about 10^{11} helium atoms. For comparison, atmospheric helium at a concentration of 5 ppm in air represents 10^{16} atoms in a minimum sample of ~125 cm^3 of air at STP. This means that samples of gas must be free of air (to <10 ppm) to take advantage of the detection limit. When vastly diluted with deuterium helium detection becomes even more difficult. Even if all the helium that might be produced at the electrode surface were collected in ~100 ml of gas, to exceed that due to atmospheric contamination would require 40 KJ of excess heat. A good signal to noise ratio and the added difficulty of detection against the deuterium background would probably require one to two orders of magnitude more than this --0.4 MJ to 4 MJ. This is at the limit of what has been oberved but such assays for helium in the off-gas have not yet been done.

Rao (BARC) reports an assay for He which failed to find any above their detection limit of 10 ppm.

IMPLICATIONS OF NUCLEAR RESULTS

The mysteries are: 1) charged particle nuclear reactions seem to occur at high rates at thermal energy, 2) d-d fusion branching ratio is wrong by 10^8, 3) energy conservation in d-d reaction is violated unless the final t+p state has a third body, 4) tritium or ^{4}He do not appear to account for the heat by many orders of magnitude, 5) nuclear products do not correlate with each other, 6) excess heat is seen unaccompanied by neutrons or tritium 7) no radiative deexcitations are seen, 8) effects are stochastic and not reproducible.

No known reactions can explain these results. The reaction is certainly not normal d-d fusion and whether nuclear or

chemical in origin might involve many different reactions.

EXCESS HEAT

Appleby and Srinivasan at Texas A&M University [17] have used a sensitive heat flow commercial calorimeter not dependent on temperature distribution. The particular instrument appears to be working properly; for example, it gives the same calibration with the same resistive heat input whether an electrolytic cell is in position or not. They claim excess power up to 50 mW in 0.5 mm ϕ palladium cathodes ~ 0.01 cm^3 in volume in at least 10 cells with 90% reproducibility (up to ~15 W/cm^3 when extrapolated). The cells are open but the results could therefore be conservative, i.e. heat losses through the top are ignored.

Excess power could be result of ~20% O_2/D_2 recombination in the cell. So far, a clear demonstration of the absence of recombination is lacking, although in many experiments in this laboratory and in others it has been shown there is less than a few percent (<5%) recombination for cases not producing excess heat. Calibrations have been done using a resistance heater. The cells are not run isothermally. A smaller number of H_2O and Pt/D_2O control cells have not produced excess power.

Bockris [4] at Texas A&M University has obtained recent results using a calorimeter cell, closed to tritium but having a recombiner external to the calorimeter. Sensitivity to temperature distribution is greatly diminished by vigorous stirring inside the cell.

One cell of five produced two episodes of tritium generation while generating ~15% excess power (ΔT~5°C). Tritium generation episodes corresponded roughly in time, although not quantitatively with increases in excess power (9 W/cm^3 when extrapolated). Total integrated energy exceeded 1.5 MJ. In this case an upper limit on recombination of O_2/D_2 in the cell was placed by one measurement of the recombinant liquid volume in comparison with the coulombic expectation. The limit set was less than 2% recombination. This is not enough to account for the excess heat. Bockris is calibrating using both a resistance heater and electrolytic power scans but is not running isothermally. Data on statistical errors are not at hand.

Oriani at the University of Minnesota [18] has used an open cell in a heat flow calorimeter not sensitive to temperature distributions. An H_2O control gave no excess power. Two D_2O cells gave up to 2 watts excess in ~ 1/50 cm^3 cathode, i.e. up to ~100 W/cm^3 extrapolated. Total integrated energy was 0.075 MJ.

Hutchinson at Oak Ridge National Laboratory originally reported excess power in one open cell of two after 100 days of charging. Hutchinson now reports [19] four cells (of four) have generated up to 9 watts excess power (equivalent to 3 $watts/cm^3$). Total integrated energy is greater than 3MJ. The four cells are closed in a flow type calorimeter with external recombiners. The recombinant volume accurately equals coulomb expectation during excess power generation. So gas recombination is apparently ruled out. The excess power is up to 18% of the input but scales linearly with current giving maximum temperature excesses of 25° C.

More recent results from Scott at Oak Ridge are reported at this meeting.

Huggins at Stanford University [20] has developed a new style calorimeter, insensitive to the temperature distribution, with a cell having internal and external recombiners. The calorimeter's main feature is rapid lateral heat dissipation along aluminum walls combined with a very large thermal impedance in the radial direction. Shakedown tests and 3-D heat transfer modeling confirm the insensitivity to internal temperature distribution. Recombination has been ruled out by measurement.

Huggins has measured 1.4 W (7 $Watts/cm^3$) excess power for 12 days. Total integrated energy was 1.4 MJ. Three of these cells (of five) have given excess power, using Englehardt palladium, after a long period of inactivity. Huggins also reports total excess energy net of the electrical charging energy. More recent results are reported at this meeting.

McKubre at SRI [21] has run a new closed cell in a sensitive flow calorimeter at 850 psi to avoid gas evolution. The cell is extensively instrumented. The calorimeter is run isothermally, backing off a resistance heater to compensate for anomalous heat generation. It is also calibrated using electrolytic power scans. Preliminary indications are that excess power of order 2W (20% of input) was observed for 14 days with subsequent increases to 50% of input. Total integrated energy is about 2.4 MJ. Further results are reported at this meeting.

Wadsworth at the University of Utah [22] has reported that up to 56 W excess power (~60W/cm^3) were generated in 5 open cells on several occasions in a calorimeter somewhat susceptible to non-uniformities of temperature distribution. Only one temperature measuring device was in each cell which was not stirred except by evolved gases. Laser doppler measurements show considerable fluid motion but it is known from subsequent similar cells, with three thermocouples present, that 2° C temperature differences exist in the cells.

Heater calibrations performed on the later cells show all three thermocouples exhibiting the (heater calibration) transients together. However, because of the temperature uncertainties the original large heat bursts can probably not be shown to be real with high confidence.

CONCLUSIONS ON EXCESS HEAT

The excess energies reported are frequently in excess of 1MJ for cathodes of a fraction of a cubic centimeter volume. At the generous investment of 5eV per chemical bond only 0.05 MJ/cm^3 of excess heat can be produced by chemical binding or by solid state phase changes even if every atom of palladium or deuterium in the cathodes were involved.

The best calorimetry method is using a device not sensitive to temperature distributions [flow type (McKubre, Hutchinson) or thermo junction type (Appleby, Oriani), or lateral heat dissipation type (Huggins).]

The cells should be entirely closed within the calorimeter (McKubre) or should at least have external recombiners with checks of recombinent volume against coulomb calculation

(Bockris, Huggins, and Hutchinson) during the period of excess heat. Calibrations should be both electrolytic with ascending and descending power (Bockris, Huggins, McKubre, Hutchinson, Oriani) as well as isothermal checks by backing off a resistance heater (McKubre). The results of McKubre indicate.that the more recent closed cell experiments do appear to have produced excess power, even when mass transfer and electrolyte changes are eliminated.

Few of the above experiments used all these optimal techniques although all the techniques have now been used. The calorimetry work is now of high quality with attention paid to uncertainties. Although the results are still not reproducible, they appear to be quite repeatable. It seems no longer reasonable to assume that these results must necessarily be wrong solely because of lack of a nuclear explanation and lack of reproducibility.

However, problems of electrolyte concentration changes, variations in stirring, effects of bubbles, sporadic partial unloading of deuterium gas, O_2/D_2 recombination, and stability issues surrounding constant current or constant voltage operation, continue to cloud the interpretation of many experiments. Such issues will continue to cause the excess heat results to be called into question.

It is not likely that this picture will change significantly until reproducibility is achieved, ie until the many researchers totally unsuccessful in producing excess heat can be given a good hit-rate recipe, or at least until the large power bursts reported by Wadsworth appear in experiments incorporating the above desirable features. It also seems to be the case that these large power excursions reported by several groups last summer have not been repeated, despite continued reports of the lower levels of excess power.

RESEARCH STRATEGY

Reproducibility is the most important current objective. Reasons for its importance are: 1) lacking it wastes resources on fruitless experiments; 2) the time elapsed while "waiting and hoping" for positive results slows down the program; and 3) variability in magnitude of effects, when eventually obtained, prevents discrimination between experiments unless statistically significant numbers of experiments are run for each set of conditions. This increases the size of an experimental program .

Reproducibility may be difficult to achieve because of the large number of variables to be investigated and the possibility that entirely new domains of physics may have to be explored (new particles, states of matter). Without reproducibility, the global scientific community will not turn significant resources to cold fusion. Advances towards reproducibility will thus be severely slowed down.

Even if the effects turn out to be real EPRI cannot expect to solve the reproducibility problems with its own limited resources, unless a way can be found to strongly focus the effort. A "fishing" approach of running very large numbers of cells and continuing to monitor heat, tritium, helium and neutrons is likely to fail unless one of these nuclear products is found to be directly correlated with excess heat, which seems unlikely on present knowledge. Such a fishing approach is likely to fail on three counts: 1) it would not provide further assurance of verification of the Fleischmann/Pons effects beyond the level we currently have, i.e. simply more repeated findings, lacking reproducibility, will not provide 'proof' acceptable to science, 2) it would not uncover the nuclear reactions involved; without this knowledge, there is no rational basis for acceptance of sporadic heat effects, and 3) as described above, it is likely to provide too slow and costly a path to reproducibility.

Since nuclear diagnostics can be sensitive, non-invasive, and more specific than measuring heat (1 W ~ 10^{12} nuclear reactions per second), there should be an emphasis on finding a nuclear product that could be responsible for excess heat. The sensitive detectability of this product could offer an efficient route to reproducibility. Finding the product and success in identifying the reactions involved would automatically account for the levels of heat. Continued failure to find such a product must be viewed as strong evidence against cold fusion. Success in identifying the nuclear products and nuclear reactions will also provide the starting point for theoretical developments. Particularly important is work to discover the energy of the participating species and the energy spectrum of the products for what they can tell of the location of the reactions as well as their origin.

Notwithstanding the main focus on nuclear products other areas must be pursued in parallel. Chief among these is to properly benchmark cathode materials and cell preparations that already show promise of approaching reproducibility of excess power. Ways of triggering the cells into periods of activity should be studied, not only because of achieving faster results but because of what may be learned of the mechanisms involved. In general, it will be wise to look beyond electrochemical cells because several alternate experimental configurations, e.g. pressure loading of titanium, appear to offer faster routes to positive results with fewer problems of surface contamination. Although not covered in the foregoing review, many electrochemical cells have proved to be contaminated with foreign substances that have coated and concealed the entire surface of the cathode with chromium, zirconium, iron, ruthenium, rhodium, carbon, etc. It is essential that cathode surface activation and maintenance of active surfaces be readily achieved and understood before we get drawn into very large experimental matrices using electrochemical cells that may be run for long periods. In the meantime, pressure loading and ion implantation experiments can help alleviate these problems .

To summarize, at EPRI, we believe that we have a well focused, cost-effective program for 1990 that employs the following strategy:

1. Monitor for nuclear products from active cells, e.g. X-rays, protons, tritium, neutrons etc.

2. Benchmark excess power, making promising materials available to other groups.

3. Study triggering methods.

4. Favor short experiments in alternate configurations, e.g. pressure loading, ion implantation.

5. Study maintenance of active surfaces in electrolytic cells.

6. Using promising cathode materials and cell preparation procedures study alternate electrolytes.

7. At an appropriate point, investigate the parameter space of electrolytic cells.

Following this route should lead to progress toward a scientifically sound basis for either rejecting the Fleischmann-Pons phenomena or for establishing a rational explanation for them.

REFERENCES

1. M. Fleischmann and S. Pons, J. Electroanalytical Chemistry 261, 301-308, 1989.

2. S. E. Jones et al, "Observation of Cold Nuclear Fusion in Condensed Matter", Nature 338, 737-740, 1989.

3. N.J.C. Packham, K. L. Wolf, J. C. Wass, R. C. Kainthla, and J.O.M. Bockris, "Production of tritium from D_2O electrolysis at a palladium cathode", J. Electroanalytical Chemistry 270 451-458.: 1989.

4. G. H. Lin, R. C. Kainthla, N. J. C. Packham, O. Velev, J. O'M. Bockris, submitted to Journal of the Electrochemical Society, November, 1989.

5. E. Storms and C. Talcott, "Electrolytic tritium production," presented at the EPRI/NSF Workshop on Anomalous Effects in Deuterated Materials, October, 1989.

6. P.K. Iyengar and H. Srinivasan, "BARC Studies in Cold Fusion," Bhabha Atomic Research Center, Report BARC-1500, November 1989, Bombay.

7. T. N. Claytor at al, "Tritium and neutron measurements of a solid state cell", Los Alamos National Laboratory preprint LA-UR-89-39-46, presented at the EPRI/NSF Workshop on Anomalous Effects in Deuterated Materials, October, 1989.

8. A. Bertin *et al.* "Experimental Evidence of Cold Nuclear Fusion in a Measurement under the Gran Sasso Massif", Nuovo Cimento 101A, No. 6, 997-1004, June 1989.

9. K. L. Wolf et al "Neutron emission and the tritium content associated with deuterium loaded palladium and titanium metals", presented at Workshop on Cold Fusion Phenomena, May 1989, Santa Fe.

10. M. Srinivasan, private communication.

11. H. O. Menlove, S. Jones et al., submitted to Nature and presented at Workshop on Cold Fusion Phenomena, May 1989, Santa Fe.

12. R. Taniguchi, T. Yamamoto, and S. Irie, Japanese Journal of Applied Physics 28 No. 11, 659-661, November 1989.

13. J. Rasmussen, private communication

14. J. F. Ziegler et. al. Phys. Rev. Letters, 62, 2929, 1989.

15. N.S. Lewis et al, "Searches for low-temperature nuclear fusion of deuterium in palladium," California Institute of Technology, Nature 340 525-530, (August 1984).

16. D. R. Rollison and W. E. O'Grady, "Elemental and Mass/charge Anomalies in Pd after Electrochemical Loading with Deuterium," Proceedings of the NSF/EPRI Workshop on Anomalous Effects in Deuterated Materials, Washington DC, October 1989.

17. A.J. Appleby, Srinivasan, Y.J. Kim, O.J. Murphy, C.R. Martin, "Evidence for excess heat generation rate during electrolysis of D_2O in LiOD using a palladium cathode - a microcalorimetric study", presented at Workshop on Cold Fusion Phenomena, Santa Fee, N.M., May, 1989

18. R. Oriani, J. C. Nelson, S. K. Lee, J. H. Broadhurst, "Calorimetric measurements of excess power output during the cathodic charging of deuterium into palladium", Proceedings of the NSF/EPRI Workshop on Anomalous Effects in Deuterated Materials, Washington DC, October 1989.

19. D. Hutchinson et al. Proceedings of the NSF/EPRI Workshop on Anomalous Effects in Deuterated Materials, Washington DC, October 1989.

20. R. Huggins, private communication.

21. M. McKubre, private communication

22. J. G. Byrne, S. Guruswamy, J. Lee, M. E. Wadsworth. Proceedings of the NSF/EPRI Workshop on Anomalous Effects in Deuterated Materials, Washington DC, October 1989.

TRITIUM MEASUREMENTS AND DEUTERIUM LOADING IN D_2O ELECTROLYSIS WITH A PALLADIUM CATHODE

R. R. Adzic*, D. Gervasio, I. Bae, B. Cahan and E. Yeager
Case Center for Electrochemical Sciences and Chemistry Dept.
Case Western Reserve University
Cleveland, Ohio 44106

ABSTRACT

Measurements have been performed to check on the Fleischmann-Pons (F-P) phenomena. They involved 1) measurements of tritium in the cell solution and the gas above it; and 2) determination of the D/Pd ratio by coulometry. Enhancement of tritium in the D_2O solution was found in these two open glass cells, as well as in another four cells with Ni-anodes. The largest enhancement factor found was ~50. The neutron measurements were inconclusive.

INTRODUCTION

Fleischmann, Pons and Hawkins (1) and Jones et. al. (2) have reported evidence for nuclear fusion of deuterium electrochemically injected into palladium. Excess heat generation, neutron and γ-rays emission and tritium enhancement (1) were found by the first group and neutron emission (2) by the second group. These results have been met with much skepticism, especially after several reports of negative results by other workers (3-5). Subsequently there have been a number of reports of excess heat generation (6-8) and tritium enhancement (9,10) or both (11).

The present research was motivated by the necessity for experiments under well defined conditions. In order to verify excess heat generation calorimetric measurements were done with a modified (Fleischmann-Pons) type open cell and calorimetric measurements with a closed cell with internal D_2/O_2 recombination. Some excess heat generation was observed. The results, however, require further evalution and will be reported at a future date. Careful determination of tritium was done in electrolytic solution and also in the water obtained from the recombined gases outside the cell. Surface analysis of Pd cathode was performed and the D/Pd ratio determined. Neutron radiation measurements were attempted, but difficulties in making background corrections interfered with the interpretation.

EXPERIMENTAL

Electrodes

Pd from several sources was used for cathodes. The rods 0.2 x 10 cm were obtained from Engelhard Corporation. Wire of 0.5 mm diameter and 99.9% purity, was obtained from Johnson Matthey - Aesar. 1 mm wire (grade A) and 4 mm rod of 99.9% purity were obtained from Johnson-Matthey, England. The Engelhard Pd was also used by Westinghouse to prepare 2 mm rods by recasting, drawing or swaging. The pretreatments used with various samples are indicated in the tables.

Anodes were made of Engelhard's Pt ribbon or wire cages of 99.9% purity Pt or Ni foil (99.9%), obtained from Fischer Scientific Co.

Electrolytes

0.1 M LiOD was used as the electrolyte in all glass cells, while 0.1 M and 1 M LiOD were used in Ni encased cells. LiOD attacks glass, which leads to a deposition of Si and other constituents of glass onto the Pd. The SIMS measurements showed that even in 0.1 M LiOD after several weeks Si could be easily detected on the Pd surface. The electrolytes were prepared from once distilled Norell (99.5%) or Isotech (99.9%) D_2O. 1 M LiOD was prepared from Li_2O (99.9%) Cerac, Inc. in a glove bag. Upon diluting this stock solution, 0.1 M LiOD was obtained. Time constants did not permit yet to run blank experiments with LiOH electrolyte solution.

*Permanent Address: Institute of Electrochemistry, ICTM, University of Belgrade, Belgrade, Yugoslavia.

Tritium Measurements

The analyses of the solution for tritium were performed by Westinghouse Electric Company using liquid scintillation counting on a Packard 4030 counter. The liquid scintillation cocktails were prepared with OPTI-FLOUR scintillator. Typically, four consecutive 60 min. counts were recorded and averaged. Another precaution against any possible complications caused by components in the electrolyte solution was a vacuum distillation of the solution before tritium measurements. While this procedure minimized the possibility of interference effects with some constituents of the electrolyte it causes some loss of dissolved T_2 and DT. For this reason some experiments were done without distillation after neutralization of the alkaline electrolyte. The electrolytic solution from the cells with Ni anodes was neutralized, filtered and centrifuged to remove suspended nickle oxide particles. Distillation was also used with a centrifuged sample which showed high counts in order to ensure that solid particles within the electrolytic solution were not responsible for the high count rate.

Neutron Radiation Measurements

The neutron detection was attempted by using two BF_3 counters coupled with a multichannel analyzer. The authors are not satisfied that the background was adequately taken into account with this experimental arrangement and hence the results are considered inconclusive. Solid state track recorders may prove attractive for the measurements in the future.

RESULTS AND DISCUSSION

Tritium

Fleischmann and Pons (1) reported enhancement of tritium concentration in the electrolyte as one evidence for a cold fusion of deuterium. The enhancement factor (see Eq. 4) is, however, close to the deuterium/tritium separation $S_{D,T} \simeq 2$, as recently determined by Corrigan and Schneider (12). Bockris et al. (13) and Wolf et al. (14) reported recently enhancements of 4 to 7 orders of magnitude over the background. In this work we have measured tritium concentrations in open F-P cells, closed cells with the Ni casing and in four open cells designed for studying the tritium enhancement.

In open cells a change in tritium concentration will occur due to the addition of D_2O containing T and due to removal by electrolysis. The isotopic separation factor of T to D is defined as

$$S = (n_D/n_T)_g/(n_D/n_T)_s \quad (1)$$

where n_D and n_T are numbers of deuterium and tritium atoms in the gas (g) and the solution (s) phases.

It can be shown (14) that the enhancement of tritium in a cell at time (t) obeys the following expression

$$n_T(t)/n_T(o) = S-(S-1)\exp(-t/T) \quad (2)$$

where T is the tritium build-up time constant.

Thus, at very long times the tritium concentration in the solution due to isotopic separation is S times the tritium concentration in the original solution.

If the recombination of D_2 and O_2 is carried out in the cell or outside the cell and the D_2O returned to the cell, the change in tritium concentration in the electrolyte could be brought about either by having substantial tritium in the palladium or other cell components or by a nuclear reaction. The palladium was stripped of hydrogen and its isotopes by electrochemical oxidation for 24 h in LiOD solution. This treatment has removed any tritium that might possibily be present in the Pd samples.

In all our experiments, in which an enhancement of T was observed, a long time electrolysis of the order of several weeks was necessary before observation of the increase in tritium concentration. In two open cells with Pt anodes excess tritium was found. These cells also were the only ones out of five which generated excess heat.

Table 1 gives the cell parameters for which enhancement of tritium concentration was observed. In four open cells, which

were designed to study tritium accumulation and generation, were essentially test tubes 3 cm in diameter with a Teflon cell top. Cathodes were 5 cm long, spot welded to a nickel ribbon as an electrical contact; 0.25 cm thick Ni foil was used as anode. During a long term electrolysis a black residue, most probably nickel oxide, accumulated in the electrolyte in only two cells. The electrolyte was filtered and centrifuged to remove these particles and then neutralized by HCl before determination of T. When large tritium counts the solution was distilled and counted again. In some instances (cells 1, 2) the solution was vacuum distilled and only the distillate was added to the scintillating liquid to avoid possible complications with various species in the solution.

The results are given in Table 2. All measurements were done in four runs during several to 24 h. The average of 4 counts is given with the standard deviation indicated. The decrease in the count rates for the distilled vs. neutralized samples was negligible. The samples were taken in intervals of 15-20 days. According to Bockris et al. (13) after reaching the maximum level, the tritium content considerably decreases after a few days, eventually down to the separation factor. If this is applicable to our measurements, it may mean that we have not observed the maximum amount of tritium probably due to a low frequency of sampling. The calculation of the tritium concentration was done in the following way:

$$\frac{\text{Net count rate}}{\text{c ml}^{-1}} = \frac{\text{average count rate}}{\text{cml}^{-1}} - \frac{\text{blank count rate}}{\text{c ml}^{-1}} \quad (3)$$

$$\text{Enhancement ratio} = \frac{\text{sample net count rate}}{D_2O \text{ net count rate}} \quad (4)$$

The number of disintegrations per minute per ml was calculated by dividing the net count rate with the efficiency factor, which is 0.224 c/d for this instrument.

$$\text{dpm ml}^{-1} = \frac{\text{net count rate/cpmml}^{-1}}{0.224 \text{ c/d}} \quad (5)$$

For cells number 1 and 2 for which some excess heat generation was observed, the tritium level amounted to 766.43 and 1730 dpm ml^{-1} respectively.*

Let us compare the excess heat generated in these open cells with the amount of T found. If all of the energy were coming from the tritium generating reaction,

$$D + D \rightarrow T + H + 4.03 \text{ MeV} \quad (6)$$

this would produce 4.03 MeV = $4.03 \cdot 10^6$eV $\cdot$ 1.6022 $\cdot$ 10^{-19}J/eV = 6.46 $\cdot$ 10^{-13} J/reaction. If 1 mW of power is produced in a cold fusion reaction, per 1 cm^3 of Pd the corresponding number of T atoms would be 10^{-3} W/(6.46 x 10^{-13} W s/reaction) = 1.55 x 10^9 reactions/s; i.e. 1.55 x 10^9 T atoms would need to be produced. Tritium decays by the reaction

$$T \rightarrow {}^3He + \beta^- + \nu^- \quad (7)$$

where β^- is a beta particle and ν^- is a antineutrino. Tritium decay is, as with all radioactive nuclei, first order. For N atoms of T, the decay rate is (16)

$$\frac{dN}{dt} = -\lambda N \quad (8)$$

The decay constant, related to the half life, is (17)

$$\lambda = 1.782 \times 10^{-19} \text{ s}^{-1} \quad (9)$$

For 1 mW one should observe

$$-\frac{dN}{dt} = (1.782 \times 10^{-9} \text{ s}^{-1})(1.55 \times 10^9) = 2.76 \text{ dps} = 166 \text{ dpm of T} \quad (10)$$

Therefore, the observed 766 and 1730 dpm ml^{-1} can account only for $\simeq$ 4-10 mW. Much

*The tritium concentrations in the samples of electrolyte from these cells have been confirmed to be similar to those found by Westinghouse, S. Landau of Case Western Reserve University and Z. Minevski of Texas A&M University, whose help in this matter is acknowledged.

The endpoint of the charging process was difficult to assign since PdD_x formation and D_2 evolution can occur simultaneously as discussed above. The discharging process at +0.83 V was easily spotted because the current goes to zero when discharge is complete. Although the charging of D into Pd (bottom curves in Figs. 1 and 2) took over 10 h, discharging of D from Pd at +0.83 V (see top curves in Figs. 1 and 2) was completed after ~70 minutes. Using the linear diffusion law, this endpoint suggests a effecctive diffusion coefficient for discharging D from Pd, $D_{discharging}$, of ~2 x 10^{-8} cm^2s^{-1}. One analogous feature in the discharge chronoamperometry curve, not noticeable in Fig. 1, is a sinusoidal ripple in the curve between 1 1/2 and 8 minutes. This ripple is possibly due to a sudden phase transition in the cathode from the α to β phase as it loses ~40% of the total 106.5 C of charge in this time interval.

Several other charging potentials were tried, but the optimal charging potential was ~-0.3 V vs. RDE. The rate of charging Pd with D was impractically slow at lower overpotentials (i.e., potentials more positive than -0.25 V). On the other hand, the rate of charging Pd with D was not noticeably increased at greater overpotentials (i.e., more negative than -0.3 V), although the rate of D_2 evolution did appear to increase with increasing overpotential. Figure 6 shows the chronocoulometry curve for loading D into Pd at -0.35 V (see bottom curve). Comparing this and the analogous curve in Fig. 7 for loading at -0.3 V, one can see that at any given time there was more total negative charge for the loading of -0.35 V versus at -0.3 V. Furthermore, even though the total charge collected at -0.35 V (-255 C) was greater than the total charge collected at -0.3 V (-142 C), both experiments gave roughly the same total value for discharge at +0.83 V, namely +107 C. Similarly, the total charge collected at -0.4 V was -289 C (and was accompanied by even stronger D_2 bubble evolution), but still discharging the Pd cathode loaded this way gave just +122 C.

The mass of the Pd in the electrode was 0.12 g which corresponds to 1.1 x 10^{-3} moles of Pd. Assuming that the positive charge collected at +0.83 V is due only to the discharge of D from Pd, the moles of D in Pd can be calculated from Faraday's law, moles(D) = Q(discharge)/nF, in which n is 1 for the discharge of 1 D from Pd and F is Faraday's constant (9.65 x 10^4 C/equivalent). The results are summarized in Table 3. All three cases indicate that there was one D absorbed per Pd atom in the electrode over this range of loading potentials with 0.1 M LiOD and D_2O as the electrolyte solution.

The loading and discharging processes were essentially reversible when the loading potentials were more positive than -0.4 V. When larger overpotentials, e.g., -0.6 V vs. RDE, were used the value of the subsequent discharge fell to ~+90 C, i.e., the corresponding ratio of D to Pd in the charged electrode was ~0.8. This suggests that charging Pd cathodes at high overpotentials (or alternatively at high constant currents) may result in irreversible damage to the electrode, which may prevent attaining higher ratios of D to Pd.

GENERAL DISCUSSION AND CONCLUSIONS

The results reported here support, to a certain extent, the claims of tritium generated in the electrolysis of D_2O on Pd of deuterium reported by Fleischmann, Pons and Hawkins (1). The following conclusions have been reached:

1. Enhancement of tritium was found in two out of five open cells with Pt-anodes and four out of four cells with Ni-anodes. The largest enhancement factor with respect to D_2O is ~50. The heat level is by three orders of magnitude larger than the heat corresponding to the observed tritium levels.

2. The ratio of deuterium to palladium atoms was found to be 1 for 0.25 mm wire, charged at E = -0.3 - 0.65 V.

3. The neutron radiation measurements were inconclusive due to the uncertainty in determining the background correction.

In general, on the experimental side there are, however, many questions to be answered in order to increase the understanding of this phenomenon, These

smaller, but still significant, enhancement of tritium was found in the gas phase for cells 1 and 4 after recombination of O_2 with D_2 and TD. Based on the separation factor one would expect a lower concentration of tritium in the gas phase, if tritium originates from the solution phase. Smaller concentrations of T in the gas phase than in the liquid phase were found by Bockris et al. (13) for long electrolysis times. In certain short intervals, e.g., one day, however, a higher concentration in gas phase was observed. The frequency of our measurements was not sufficient to detect such short-lived changes.

In an experiment of this importance one should address the question of the contamination by T of materials used in the experiments. The question can be ruled out on the grounds that the same materials have been used for the cells that gave zero tritium enhancement and the necessity for the long charging of Pd before observation of T. Electrochemical oxidation of H, D, or T, annealing and catalytic combustion, during the pretreatment make unlikely the possibility that tritium came from the palladium samples contaminated by tritium before the experiments.

Coulometric Determination of D absorbed in Pd Cathodes

Metallic Pd can absorb D to form a solid PdD_x solution. For cathodes equilibrated with air at ambient temperature and pressure, a value of x of about 0.7 to 0.8 is widely accepted. The reactivity of D in Pd may vary considerably with x, particularly if x exceeds 0.8, and therefore a coulometric determination of x was made. The working electrode was a coil of Pd wire (diameter = 0.025 cm, area = 1.86 cm^2, mass = 0.12 g; 99.997%, Puratronic grade, Johnson Matthey) crimped together with the end of a gold wire (d = 0.05 cm; 99.9985%, Puratronic, Johnson Matthey) which served as the lead to the potentiostat. A three compartment electrochemical cell was used. The electrolyte, 0.1 M LiOD was continuously and vigorously degassed with N_2 (99.995%, Ultrapure, Matheson). The counter electrode , a Pd coil (A = 2 cm^2), was in a chamber chamber connected to the working chamber by a glass tube filled with a glass wool plug. The reference electrode was a reversible deuterium electrode (RDE).

The working electrode was rinsed with 0.1 M LiOD and D_2O electrolyte solution and cycled between 0.25 and 1.35 V until the steady state voltammogram shown in Fig. 1 (dashed line) was obtained. The cell was then rinsed and refilled with fresh electrolyte solution and sparged with N_2 gas. When the cell was left at open circuit for several days, it came to rest at +0.83 V, and it always returned to +0.83 V at open circuit whether it was offset to positive or negative potentials. When the working electrode was potentiostated at 0.83 V, no current flowed.

Figure 2 shows the chronoamperometry curves for the charging of Pd with D at -0.3 V and discharging of D from Pd at +0.83 V. During the charging at -0.3 V, there was no noticeable D_2 gas evolution at the working electrode. This suggests that when D is formed on the Pd surface at -0.3 V, initially most of the D is absorbed into the bulk Pd. During charging at -0.3 V, the magnitude of the current was ~10 mA in the first minute, gradually dropped to ~1.5 mA after 10 hours, and finally stabilized at ~0.7 mA after 1 day.

There is an inflection in the chronocoulometry charging curve at ~0.3 V (Fig. 1, bottom curve) after 10 h. It was also noticed that after 10 or more hours that if the N_2 bubbler was lifted over the electrolyte solution, D_2 bubbles were visible and slowly nucleating at the Pd surface. These observations suggest that after 10 h the charging of the Pd with D is nearly completed. The linear diffusion law is stated as, $\langle x \rangle^2 = 2\,D\,t$, with $\langle x \rangle$ being the mean distance travelled in time, t, with diffusion coefficient, D. An effective diffusion coefficient of D through Pd for the charging process, $D_{charging}$, can be calculated by using t = 10 hours and $\langle x \rangle$ = 0.0125 cm (the radius of the electrode), and the value for $D_{charging}$ is ~2 x 10^{-9} $cm^2 s^{-1}$. The transport of D into Pd wire is more complicated than that represented by simple linear diffusion because during D loading the electrode would be modelled better as a cylinder which is slowly expanding.

include the irreproducibility and sporadicity of the phenomenon, necessity for a prolonged electrolysis before the excess heat or tritium production occur, the role of the microstructure and of the trace impurities in palladium, the difference between the amount of excess heat in open and closed cell, the role of surface impurities and the role of lithium, if any.

On the theoretical side the questions appear even more difficult. Table 4 lists possible fusion reaction of deuterium. According to the accepted theories the evidence for fusion of deuterium requires, besides the heat generation, a corresponding amount of neutrons, tritium and ^3He. The branching ratio of reaction A and B (Table 3) is approximately one. The cross section for reaction C is on the order of 10^7 lower than for A and B (1). γ-rays should be observed if the reaction K occurs in the electrochemical cell.

No data on electrochemically induced fusion satisfies undisputably any of these requirements. In order to overcome these difficulties several new mechanisms of fusion have been proposed. These include the mechanisms in which the energy from the reaction C dissipates into the lattice as heat rather than γ-photon (17, 18), or in which two deuterons as bosons are squeezed together in a sphere of an octahedral site (19). Dendrites on Pd surface have been suggested as a explanation for tritium generation, due to increased electric fields around the dendrite tips (13). Fracto-fusion was also mentioned as a possible explanation in anology with the explanation of neutron generation upon fracturing LiD single crystals (19). There is, obviously, a need for more work in order to estimate the merits of these explanations, as well as reach a complete understanding of the Fleischmann and Pons phenomenon.

ACKNOWLEDGEMENTS

The authors are indebted to Westinghouse Electric Corporation and C. Blackburn for tritium measurement and palladium metallurgy, Ford Motor Company and Eltech Systems Corporation for the loan of palladium samples, Eveready Battery Company for the use of their facility and NASA and the ONR for partial support. Discussions with J. Blue, H. Wroblowa, F. Ruddy, J. Jackovitz, U. Landau and D. Corrigan are very much appreciated.

REFERENCES

1. M. Fleischmann, S. Pons and M. Hawkins, J. Electroanol. Chem 261 (1989) and Errota 263 (1989) 187.
2. S. E. Jones, E. P. Palmer, J. B. Czirr, D. L. Decfer, G. L. Jensen, J. Thorne and S. F. Taylor, Nature, 338, 737 (1989).
3. M. Goi, S. L. Rugori, R. H. France, B. J. Lund, Z. Zhao, A. J. Davenport, H. S. Isaacs and K. G. Lyun, Nature, 340, 29 (1989).
4. N. S. Lewis, et. al. Nature, 340, 525 (1989).
5. D. E. Williams, D. J. S. Findley, D. H. Creston, M. R. Sene', M. Bailey, S. Croft, B. W. Hooton, C. P. Jones, A. R. J. Kucernak, J. A. Mason and R. I. Taylor, Nature, 342, 375 (1989).
6. A. J. Appleby, S. Srinivasan, A. J. Appleby, O. J. Murphy and C. R. Martin, Workshop on Cold Fusion Phenomena, Sante Fe, May 22-25, 1989.
7. R. A. Huggins, Workshop on Cold Fusion Phenomena, Sante Fe, May 22-25, 1989.
8. R. A. Oriani, J. C. Nelson, S. K. Lee and J. H. Broadhurst, The Electrochemical Society Meeting, October, 16-20, 1989, Hollywood, Florida.
9. N. J. C. Packham, K. L. Wolf, J. C. Wass, R. C. Kainthle and J. O'M. Bockris, J. Electroanal. Chem., 270, 451 (1989).
10. P. K. Iyengar, Fifth International Conference on Emerging Nuclear Energy Systems (ICENESV) Karlsruhe, West Germany, July 1989.
11. U. Landau, The Electrochemical Society Meetings, October 16-20 Hollywood, Florida.
12. D. A. Corrigan and E. W. Schneider, submitted to J. Electroanol. Chem.
13. G. H. Lin, R. C. Kainthle, N. J. C. Packham, O. Velev and J. O'M. Bockris, p. 3. Manuscript submitted to J. Electrochem. Soc.

14. K. L. Wolf, N. J. C. Packham, D. L. Lawson, J. Shoemaker, F. Cheng and J. C. Wass, Manuscript submitted to J. Fusion Energy.
15. D. Albolgi, R. Ballinger, V. Commoroto, X. Chen, R. Crooks, C. Fiore, M. Gaudreau, I. Hwang, C. K. Li, P. Linsay, S. Luekhardt, R. R. Parker, R. Petrasso, M. Schoh, K. Wenzel and M. Wrighton Manuscript submitted to the Journal of Fusion Energy.
16. P. Clark Souers, Hydrogen Properties for Fusion, Energy, University of California, Berkely 1986.
17. P. L. Hagelstein, Proc. of the Cold Fusion Workshop, J. Fusion Energy, in press.
18. J. Rafelski, M. Gaide, D. Harley and S. E. Jones, Unpublished results.
19. B. V. Deryagin, V. A. Klyuev, A. G. Lipson and Yu. T. Toporov, Kolloiidnyi Zhurnal, 48, 12 (1986).

Table 1: Cell parameters for Tritium measurements

Cell	Electrode size d x l (cm x cm)	Supplier	Pretreatment	Anode	Current (mA/cm^2)
1	0.4 x 6	JM[a]	oxid. of H_{abs}	Pt	5-400
2	0.2 x 10	E[b]	"	Pt	60-120
3	0.1 x 5	JM	"	Ni	10-120
4	0.2 x 5	E	"	Ni	10-120
5	0.1 x 5	JM	Annealing	Ni	10-120
6	0.2 x 5	E	"	Ni	10-120
7	0.2 x 10	E	"	Pt	10-120

[a] - JM refers to Johnson Matthey.
[b] - E refers to Engelhard.

Table 2 : Tritium Measurements

Cell	Days	ACR[a] (cpm)	NCR[b] (cpm)	$\frac{NCR^{sample}}{NCR^{D_2O}}$	DPM/ml[c]
1	42	21.13	5.13	1.6	44
	48	20.72	16.72	1.5	148
	58	35.08	19.08	6.5	170
	68	107.63±1.20	85.99±0.99	24.6±8.3	766
gas phase	68	42.66±2.32	24.06±0.93	8.3±2.3	114
	75	34.05	18.05	6	160
gas phase	75	20.93	4.93	1.6	44
2	25	209.27±0.80	193.80	6.2	1730
	45	120.06±0.49	103.06	4.1	920
3	26	159.14±1.83	143.24±1.88	49.4±13.8	1278
gas phase	26	26.53±0.86	9.63±0.96	3.3±0.9	85
	36	39.14±1.95	22.73±1.97	14.2	202
4	26	91.58±1.58	75.68±1.64	26.1±7.3	675
	36	36.94±0.54	20.53±0.60	12.8	183
5	26	58.11±0.27	42.21±0.51	14.6±4.1	376
	36	40.24±0.34	23.83±0.43	14.8	212
	76[d]	37.03±0.40	19.63	9.67	87
gas phase	76[d]	29.00±0.40	11.60±0.71	5.71±1.94	51
6	26	80.54±0.48	64.64±0.64	22.3±6.2	577
gas phase	26	39.40±0.86	23.50±0.96	8.1±2.3	209
	36	25.35±0.37	8.94±0.46	5.5	79
gas phase	56[d]	33.88±0.55	16.48±0.81	8.12±2.75	73
	76[d]	35.94±0.55	16.48±0.81	9.13±3.09	82
gas phase	76[d]	26.62±0.38	9.22±0.70	4.54±1.56	41
7	16	22.21±0.49	6.31±0.65	2.18±0.65	56
	36	20.93±0.86	4.52±0.63	2.8	40
	76[d]	21.76±0.86	4.36±1.04	2.15±0.88	19

[a] ACR - average (4 replicates) count rate per 0.5 ml.
[b] NCR - net count rate per 0.5 ml.
[c] DPM - disintegrations per minute.
[d] Sample size = 1 ml.
Typical background count rate = 16 cpm.
ACR(Norell D_2O) = ~46 cpm; ACR(Isotech D_2O) = ~19cpm.

TABLE 3

Summary of the Calculated Amount of the D Loaded in Pd[a] at Different Overpotentials

η(volts)	$Q_{discharge}$(C)	moles D
-0.30	106.5	1.1×10^{-3}
-0.35	170.0	1.1×10^{-3}
-0.40	111.7	1.2×10^{-3}

[a] Mass of Pd electrode was 0.12 g before and after the experiment. This corresponds to 1.1×10^{3} moles Pd.

TABLE 4

Nuclear Fusion Reactions

Reaction	Equation
A	$D + D \rightarrow n$ [2.45 MeV] + ^{3}He [0.82 MeV]
B	$D + D \rightarrow H$ [3.02 MeV + T [1.01 MeV]
C	$D + D \rightarrow \gamma$ [23.0 MeV] + ^{4}He [0.08 MeV]
D	$D + {}^{6}Li \rightarrow n$ [2.96 MeV] + ^{7}Be [0.43 MeV]
E	$D + {}^{6}Li \rightarrow {}^{4}He$ [11.2 MeV] + ^{4}He [11.2 MeV]
F	$D + {}^{6}Li \rightarrow H$ [4.39 MeV] + ^{7}Li [0.63 MeV]
G	$D + {}^{7}Li \rightarrow n$ [13.36 MeV] + ^{8}Be [1.67 MeV] $\rightarrow$ n [13.36 MeV] + ^{4}He [0.85 MeV] + ^{4}He [0.85 MeV]
H	$D + {}^{7}Li \rightarrow \gamma$ [16.7 MeV] + ^{9}Be [0.02 MeV]
I	$D + {}^{7}Li \rightarrow p + {}^{8}Li$ (endoergic, -1.01 MeV) $\rightarrow \rightarrow p + {}^{4}He$ [8.05 MeV] + ^{4}He (8.05 MeV]
J	$D + {}^{7}Li \rightarrow T + {}^{6}Li$ (endoergic, -1.81 MeV)

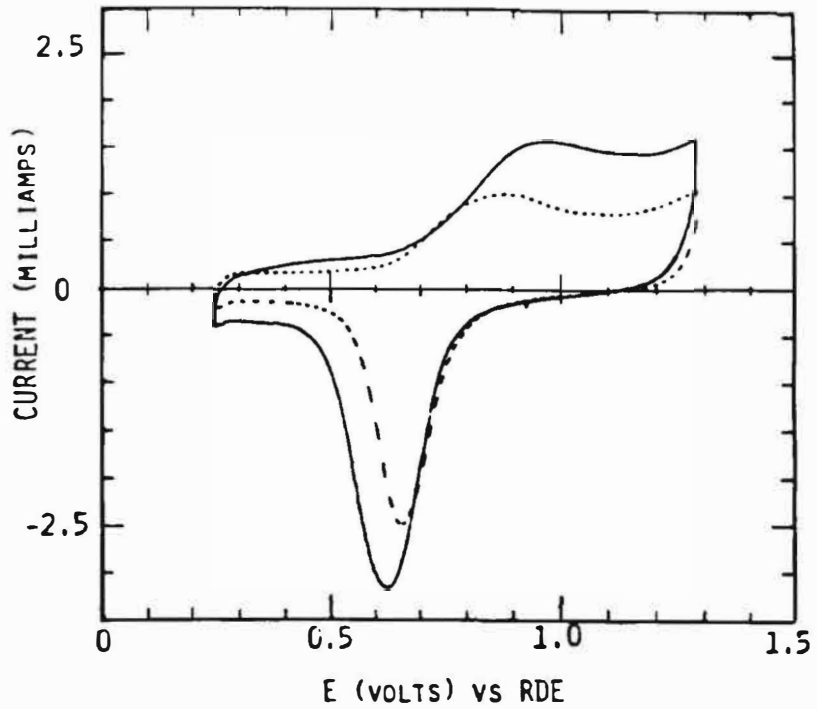

Fig. 1. Cyclic voltammograms of Palladium wire (d = 0.03 cm) in D_2O with 0.1 M LiOD under a N_2 atmosphere. Dashed line is the steady state voltammogram. Solid line is the voltammogram recorded after charging the Pd with D at -0.4V for 24 hours, followed by discharging the D at +0.83 V for 60 minutes. Scan Rate = 100 mV/s. Electrode area = 1.86 cm^2. Counter electrode: Pd.

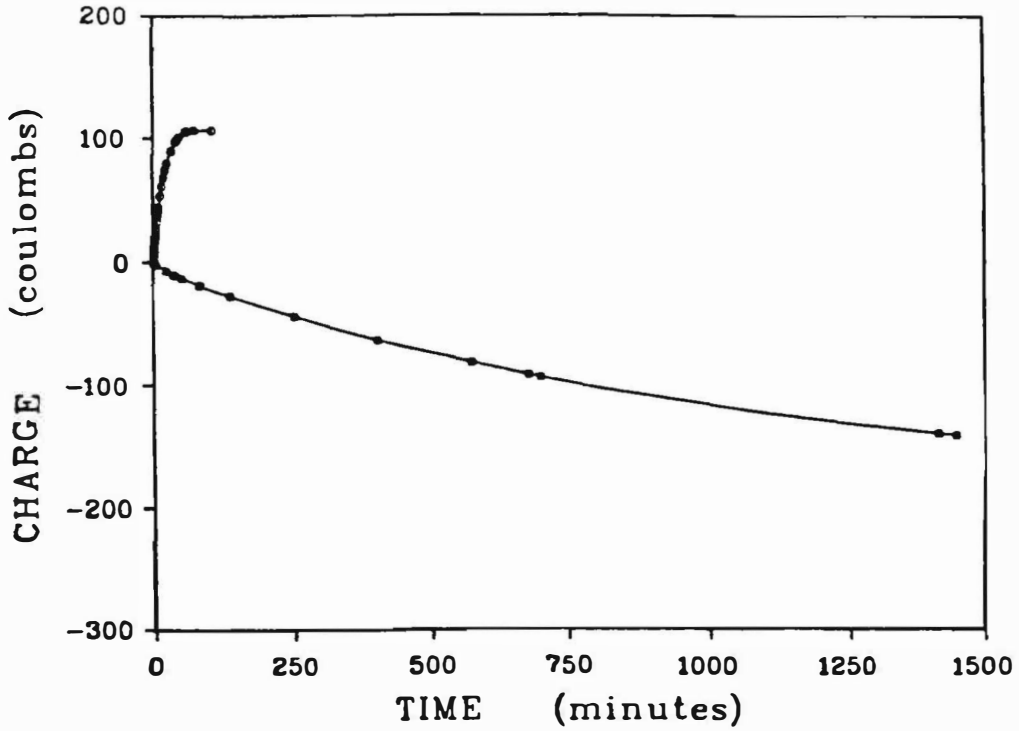

Fig. 2. Chronocoulometry curve for the charging (negative charge) and discharging (positive charge) of D into palladium wire (d=0.03 cm). Electrode area = 1.86 cm^2. Electrode mass = 0.12 grams. Electrolyte: 0.1 M LiOD in D_2O. Charging potential = -0.3 V vs RDE. Discharging potential = +0.83 V vs RDE.

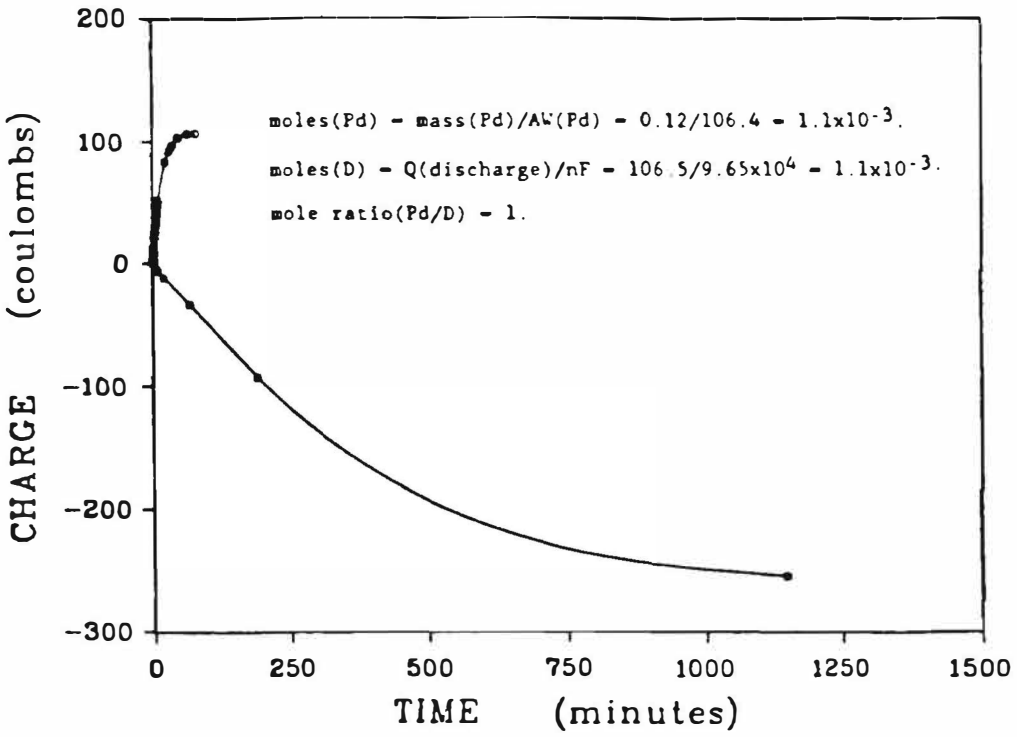

Fig. 3. Chronocoulometry curve for the charging (negative charge) and discharging (positive charge) of D into palladium wire (d=0.03 cm). Electrode area = 1.86 cm^2. Electrode mass = 0.12 grams. Electrolyte: 0.1 M LiOD in D_2O. Charging potential = -0.35 V vs RDE. Discharging potential = +0.83 V vs RDE.

ANOMALIES IN THE SURFACE ANALYSIS OF DEUTERATED PALLADIUM

Debra R. Rolison, William E. O'Grady, Robert J. Doyle, Jr.[1],
and Patricia P. Trzaskoma[2]

Surface Chemistry Branch, Code 6170; [1]Code 6110; [2]Code 6320
Naval Research Laboratory
Washington, DC 20375-5000

ABSTRACT

The surface and near-surface analytical characterization of thin palladium foils after the electrolysis of H_2O or D_2O was performed with X-ray photoelectron spectroscopy (XPS), high resolution mass spectrometry, time-of-flight secondary ion mass spectrometry (TOF-SIMS), and scanning electron microscopy (SEM). These surface characterizations revealed a number of anomalous results, as summarized below.

INTRODUCTION

Our studies of the Pd-D_2O system, precipitated by the announcement of the Fleischmann-Pons effect [1], have centered on the exploration of the surface character of thin palladium foils before and after electrolysis of pH-neutral solutions of D_2O and H_2O [2-4]. The importance of understanding and controlling the nature of the electrode surface, so as to understand and control electron-transfer reactions occurring at the electrode surface, underlies the field of electrochemistry and has previously been emphasized as critical for the successful hydrogen loading of Pd [5]. In light of the variability of observations made by the myriad researchers exploring the Pd-D_2O system, the imperative need to determine the physical, chemical, and metallurgical nature of the palladium surface has recently been stressed [6,7].

EXPERIMENTAL

Electrochemistry and Chemicals

All electrolyses were performed, with one exception, in 0.1*F* Li_2SO_4/D_2O or H_2O, as appropriate. The one exception was a solution of 0.1*F* LiOD in D_2O prepared by dissolving lithium metal in D_2O. H_2O was triply distilled from quartz, 99.9% D_2O [MSD Isotopes for the preliminary experiments, Cambridge Isotope Laboratories for the majority of the experiments] was used as received. Li ribbon [Alfa] and Li_2SO_4 [Alfa, anhydrous] were used as received.

All electrolyses were performed with 99.9% Pd foil, 0.127-mm thick [historical supply of precious metals, Naval Research Laboratory]. X-ray diffraction analysis of this foil showed that it was preferentially oriented, primarily in the <200> direction [2]. The foils were acid etched in 1:1 HCl:HNO_3 to remove surface oxide, rinsed well, and then sonicated in the appropriate solvent prior to use. The anode, with one exception described below, was 99.999% Pt wire [Alfa], wound around a glass-rod cage so as to concentrically surround the Pd cathode.

The Pd foils were cathodically charged at 10 mA/cm^2 using the galvanostatic mode of a EG&G PAR Model 173 potentiostat/galvanostat; higher current densities were then usually applied. The cells and experimental procedure have been described in greater detail elsewhere [2-4].

Mass Spectrometric Measurements

The mass/charge profile encompassing the Pd isotope range (m/z range 100-115) was measured using the static SIMS mode of a TOF-SIMS built in-house at the Naval Research Laboratory [8,9]. Positive-ion spectra were obtained by using primary ions of 14.0-keV cesium ions from a pulsed alkali-ion gun containing a thermionic emitter. Each reported spectrum is the average of two-to-three million spectra. Samples were argon-plasma cleaned, *in situ*, prior to analysis.

High resolution ($m/\Delta m$ > 50,000) analysis of m/z 3, 4, 5, and 6 of the gases emitted by electrochemically loaded PdD_x was made using a ZAB-2F double-focusing mass spectrometer. Slivers were cut from the Pd foil immediately after electrolysis and placed in glass capillaries; the capillaries were introduced into an electron ionization source via a standard solids probe. This experiment was performed for one sample only. Background pressure was 10^{-8} torr.

The mass/charge region encompassing the Pd isotope window (m/z 102-110) was obtained by wrapping the foils (before and after electrolysis) around a solids probe and fast-atom bombarding with 8 keV Xe; resolution was $m/\Delta m$ = 3300. 6-10 spectra were signal averaged to produce the obtained spectrum. To gauge the presence of interfering polyatomic species at m/z 106, the ions comprising m/z 106 were mass selected and collided with helium neutrals to induce dissociation of polyatomics.

To obtain the ratio of m/z 7 to m/z 6, lithium salts were dissolved to $\approx 0.1F$ with H_2O and aliquots of the solution were evaporated on the solids probe.

Bulk and Surface Elemental Analysis

Atomic emission spectrographic analysis of the stock Pd foil showed significant concentrations of the following metals [3]:

Element	*Concentration/ppm*
Ni	200-300
Pt	200
Ag	100
Rh	50
Cu	50
Si	20-40

Elemental analysis of the Pd surface before and after electrolysis was performed with a Surface Sciences Instruments Model SSX-100-03 X-ray photoelectron spectrometer with a small-spot capability and equipped with an Al anode. Foils analyzed immediately after electrolysis outgassed so severely (> 10^{-7} torr background pressure) that $\approx$12 h were required to reduce the pressure to the typical analysis pressure of < 5 x 10^{-9} torr [3]. Binding energies are referenced to the adventitious C1s line at 284.6 eV. Overlapping lines were deconvoluted with a graphics package using a χ^2-minimization calculation.

Scanning Electron Microscopy

Scanning electron microscopy was performed with a Hitachi Model S-800 Field Emission Microscope. Photomicrographs were taken in the normal mode (using the secondary electrons emitted from the sample) and, to accentuate surface topography, in the differential mode.

RESULTS and DISCUSSION

X-ray Photoelectron Spectroscopic Analyses

Survey scans of the etched Pd, an example of which is shown in Figure 1*a*, consist of the characteristic Pd lines with a trace amount of spectrometer-derived carbon. The small peak at $\approx$50 eV is due to $Pd5p_{3/2}$; the other platinum-group metals also have weak, higher valence lines in this area making any post-electrolysis assignment of Li1s, by XPS, ambiguous.

After electrolysis of D_2O for an accumulation of 1.9 x 10^5 Coulombs of charge, other elemental lines are now evident in the survey scan (Figure 1*b*), *e.g.*, O1s (the small contribution seen for $Pd3p_{1/2}$ at 560 eV shows that the line at 530 eV is predominantly O1s and not $Pd3p_{3/2}$), Na1s (and a Na Auger line), Pt4f, a Mg Auger line, Zn2p, Si2p, S2p, and Cu2p. While elemental components derived from the glass cell (Si, Mg, Na) are present, as is Pt (electrodeposited at the surface as Pt metal from Pt ions generated by the oxidative dissolution of the anode), the surface retains a Pd signature.

Although Rh and Ag are present in our Pd stock at a concentration below the limit of detection by XPS, after electrolysis of either D_2O or H_2O, Rh and Ag can be detected at the surface of the Pd by signal averaging tens of high resolution scans. The concentrations of Rh and Ag maximize at 3 and 1 atom%, respectively, relative to the Pd signal [3].

Rh and Ag do not electrodeposit, but rather they concentrate towards the interface as a function of the long duration and high accumulated charge of the electrolysis. This was determined in two ways: *(i)* by the absence of Ag signals for the one sample electrolyzed in LiOD - this sample had no Pd signal and strong Pt signals due to electrodeposited Pt; and *(ii)* by using the small-spot capability of the spectrometer, the analysis was centered on a slight scratch made in the surface before placing the sample in the spectrometer - this procedure emphasizes bulk material brought to the surface; the $Pt4d_{5/2}$ line was found to strongly decrease while the area due to the $Rh3d_{3/2}$ line remained unchanged. Both of these results are consistent with a Pt signal dominated by Pt derived from electrodeposition and Ag and Rh signals derived from surface enrichment of Rh and Ag residing in the bulk Pd.

The concentration of the Rh increased as a function of total accumulated charge, but plateaued at $\approx$3 atom% [3]. The magnitude of the surface enrichment can be gauged by

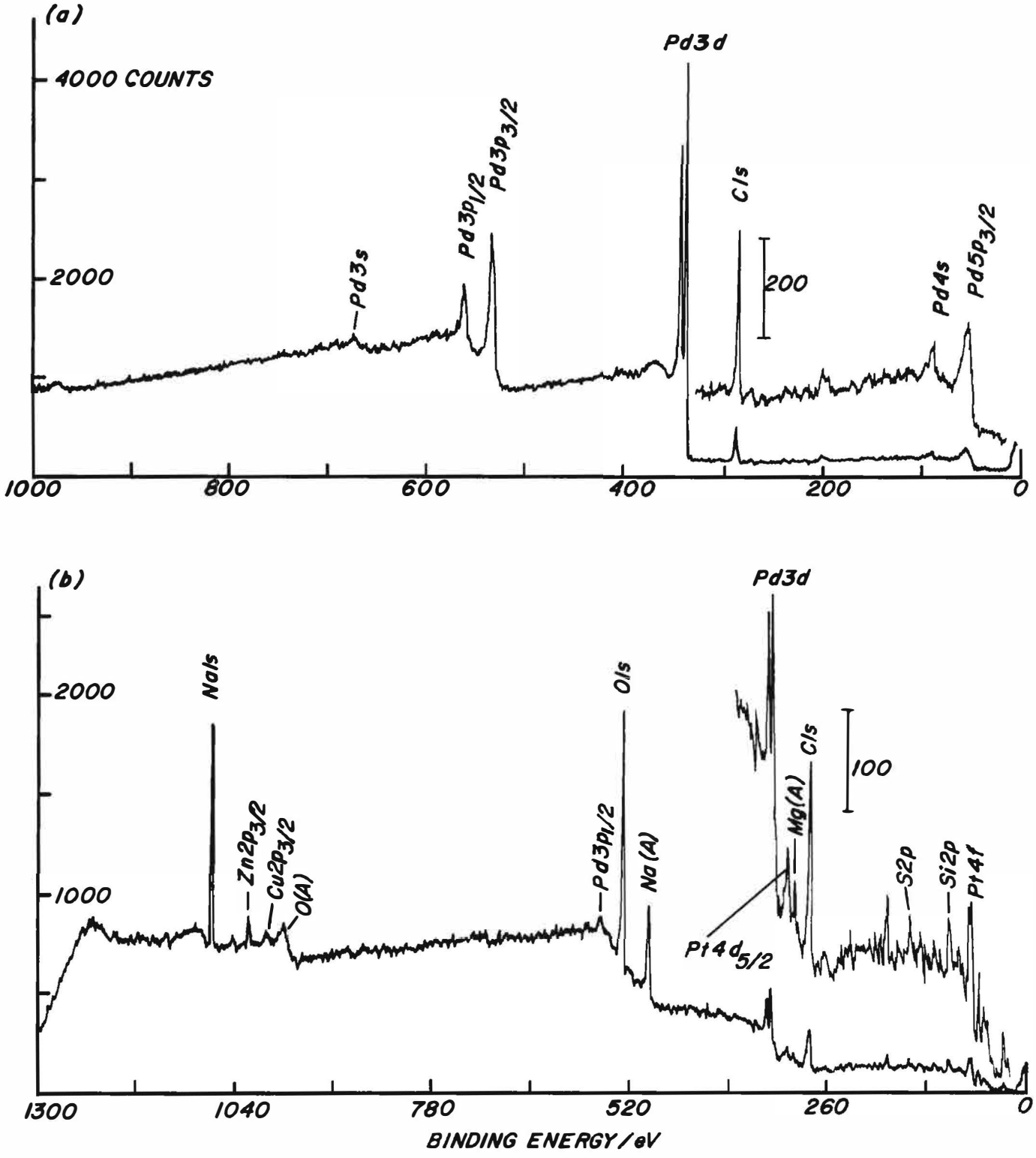

Figure 1. X-ray photoelectron survey scans of Pd foil: *(a)* after etching in 1:1 HCl:HNO_3; and *(b)* after electrolysis in 0.1*F* Li_2SO_4/D_2O for a total accumulated cathodic charge of 1.9 x 10^5 C.

estimating the depth of the enriched layer assuming a uniform 3 atom% concentration. This layer would be ≈0.1-μm thick - which is a serious degree of migration/segregation in a foil on the order of 10^2-μm thick. As both Ag and Rh appear at the surface of Pd charged in either D_2O or H_2O, a mechanism based on surface segregation and forced diffusion as the Pd lattice is filled with H· or D· atoms seems more probable than one relying on known neutron activation reactions of Pd isotopes, some of which yield stable Ag and Rh isotopes [10]. Intriguing though this latter prospect may be, experiments with 99.999% Pd would be required before a physical transport mechanism could start to be discounted.

Mass Spectrometric Analyses

Pd

TOF-SIMS measurements of the Pd blank (the Pd starting material prior to electrolysis) and Pd electrolyzed in H_2O yielded mass-to-charge **vs.** amu intensities which mirrored the expected sequence for the stable Pd isotopes (neglecting the 1.02% abundant ^{102}Pd). The ideal abundances are [11]:

Isotope	*Natural Abundance/%*
^{104}Pd	11.14
^{105}Pd	22.33
^{106}Pd	27.33
^{108}Pd	26.46
^{110}Pd	11.72

Two samples electrolyzed in D_2O exhibited greater than 20% enrichments in m/z 106 intensity and diminutions in m/z 105 intensity [2]. This result is provocative because of the implication that ^{105}Pd obtained a neutron to generate ^{106}Pd. The more startling ^{106}Pd enrichment (≈100% over ideal) was observed for the only sample electrolyzed in LiOD; an enrichment of ≈45% was observed for one of the samples electrolyzed in Li_2SO_4. It was shown using the Pd blanks and the sample used to electrolyze H_2O that the conditions of the TOF-SIMS measurements, including *in-situ* plasma cleaning of the samples, were not responsible for the enrichment/diminution phenomena [2].

Subsequent fast-atom bombardment, high-resolution mass spectrometric measurements on the LiOD sample replicated the TOF-SIMS results, however, mass selecting the ions at m/z 106 and using collisional-induced dissociation showed a loss of oxygen atoms indicating that the intensity at m/z 106 was compromised by the presence of polyatomic ions. It was shown that the species was $^{90}Zr^{16}O$, a species with a nearly coincident mass to ^{106}Pd, 105.8992 and 105.9032, respectively. The zirconium isotopic distribution allows ZrO species to unfortunately overlap most of the Pd isotopic distribution (see Figure 2*b*), making high resolution measurements of this region (or the Pd dimer mass/charge region) necessary [12]. After 30 min of bombardment, the isotopic distribution reflected the expected abundances for Pd. The zirconium was present at the surface as ZrO_2 (confirmed by XPS), at trace levels, and it derived from the electrochemical (or post-electrolytic) conditions and not from a plasma-generated contaminant.

The Li_2SO_4-derived, ^{106}Pd-enriched sample was Zr-free according to TOF-SIMS data, see Figure 2*a*; unfortunately, it no longer existed in a form compatible with surface-sensitive high resolution mass spectrometry (having earlier been dissolved in 1:1 HCl:HNO_3 to pursue other analytical chimera). Other Pd foils used to electrolyze D_2O have shown, by high resolution mass spectrometry, a mass/charge distribution in this region which matches the expected Pd isotopic distribution, including a sample only mildly etched, so that the cold-worked overlayer remained.

The source of the anomaly in the Pd isotopic distribution for the one Li_2SO_4-derived sample remains unexplained. We have recently recognized that this sample was coincidentally contaminated with Cd due to an impurity in the Pt-gauze used as an anode while awaiting receipt of the 99.999% Pt wire. (^{106}Cd is a stable isotope but has an abundance of 1.25% [11]; signals for the significantly more abundant ^{112}Cd (24.13%) and ^{114}Cd (28.72%) are absent in the TOF-SIMS spectrum.) Cd has a high overvoltage for the evolution of hydrogen [13], *i.e.*, the back reaction of D· atoms recombining to form D_2 gas is inhibited. Cd may have provided a serendipitous, low-level surface poison and it is conceivable that higher D:Pd levels were achieved in this one experiment than in subsequent experiments. Experiments to test this possibility are in progress.

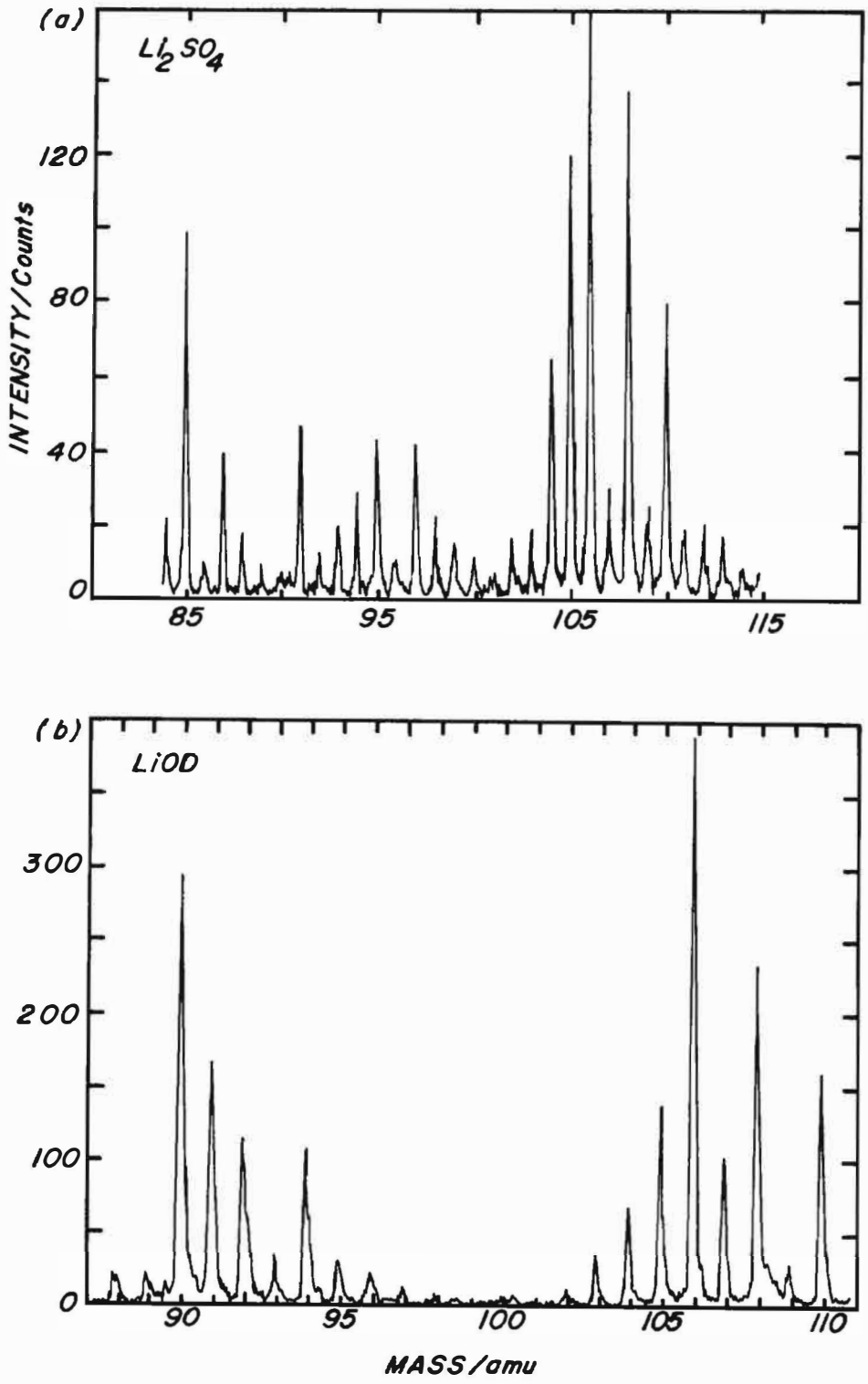

Figure 2. TOF-SIMS spectra obtained for Pd foil after electrolysis in *(a)* 0.1*F* Li_2SO_4/D_2O for a total accumulated cathodic charge of > 8 x 10^3 C; and *(b)* 0.1*F* $LiOD/D_2O$ for a total accumulated cathodic charge of 1.4 x 10^6 C. The m/z range is chosen to encompass the Zr and Pd isotopic distributions.

Li

As has been pointed out by others, the natural abundance of Li isotopes (^{7}Li, 92.5% abundant and ^{6}Li, 7.5% abundant) is not necessarily found in commercial lithium salts due to the extraction of the neutron-scavenging ^{6}Li isotope. Consequently, any determination of the ^{7}Li-to-^{6}Li ratio for Pd after electrolysis of Li^+/D_2O electrolytes needs to be balanced against the ratio of the starting lithium electrolyte salt. Sampling, via fast-atom bombardment mass spectrometric analysis, of some lithium salts stocked at our laboratory shows how variable the ^{7}Li-to-^{6}Li ratio can be, as summarized below:

Li salt	*^{7}Li-to-^{6}Li ratio*	*Source*
Natural Abundance	12.3	Big Bang
LiOD	31 ± 1	Li metal, Alfa
$Li_2B_4O_7$	18.2	Johnson Matthey
LiI	11.6	Alfa
LiI	19.4	Aldrich
$LiBO_2$	16.1	Johnson Matthey

H/D/T

The copious explosion of gas that bursts from the surface of the Pd cathode when the electrochemical circuit is broken is followed by long-term outgassing, as can be observed by the gas bubbles that form when the Pd cathode is stored under water after electrolysis. Likewise, even slivers of material cut from the Pd after electrolysis provide ample gas to analyze by mass spectrometry. High resolution analysis of the gases emitted from one Pd foil after charging in Li_2SO_4/D_2O showed that the m/z 3, 4, 5, and 6 peaks were composed of the dimers and readily formed trimers of hydrogen and deuterium with no detectable quantities of tritium-based species.

Scanning Electron Microscopic Analyses

SEM has been used to explore Pd foil before and after use as cathodes to electrolyze H_2O and D_2O [4]. After sufficient etching to leave visible crystal grains, the majority of the grains are roughened, but ≈20-30% of the grains remain smooth and unfeatured even at high magnification (> 15,000 x). The surface morphology changes after electrolysis, with the roughened grains restructuring to yield greater intragranular homogeneity and features of higher surface area, however, smooth and unfeatured grains persist after electrolysis of both D_2O and H_2O electrolytes.

Three characteristic grains have been observed for PdD_x from highly etched stock, the smooth, unstructured grains, and two structured morphologies. On the micrometer scale, as seen in Figure 3, one structure consists of rugged, parallel, thin-edged ridges (Figure 3*a*), and the other is an intertwined structure (Figure 3*b*, lower half), which at higher magnification, might be the beginning of crystal faceting [4].

The degree of the initial etch governs the development of the surface structures that form with electrolysis. SEM survey scans of Pd cathodes after electrolysis must be placed in the context of the initial microscopic morphology of a portion of the *same* piece of Pd. We attempted to control this by etching a large piece of Pd foil and then using portions of it for electrolytic preparation of PdH_x and PdD_x using comparable electrolytic histories.

Three PdD_x samples have been prepared, yielding comparable characteristic morphologies, and one PdH_x sample has been prepared, electrolytically analogous to one of the three PdD_x samples. The PdH_x sample also produced restructured grains with greater intragranular homogeneity and higher surface area than the initial etch morphology, however the resulting restructured morphologies differed between H- and D-exposed Pd. The surface of the structured grains for PdH_x appeared more polished and had features that were less deep and developed than those on the comparably treated PdD_x. An additional series will be run to confirm this difference in morphology between electrolytically prepared PdH_x and PdD_x.

Cracks and fissures do not appear to be part of the morphology after electrolysis for either system; this may be due to the well-defined grain boundaries, resulting from the etch, which provide non-catastrophic paths for gas release when the electrical circuit is broken.

Photomicrographs taken in the differential mode indicated that intergranular elevational differences resulted between the smooth, unstructured grains and the roughened and structured grains, as seen in Figure 4*a*. Stereopairs made in 2-3 locations for PdH_x, all three PdD_x samples, and reserved samples of the initially etched Pd confirmed the intergranular elevational differences and showed that the structured grains are uplifted relative to

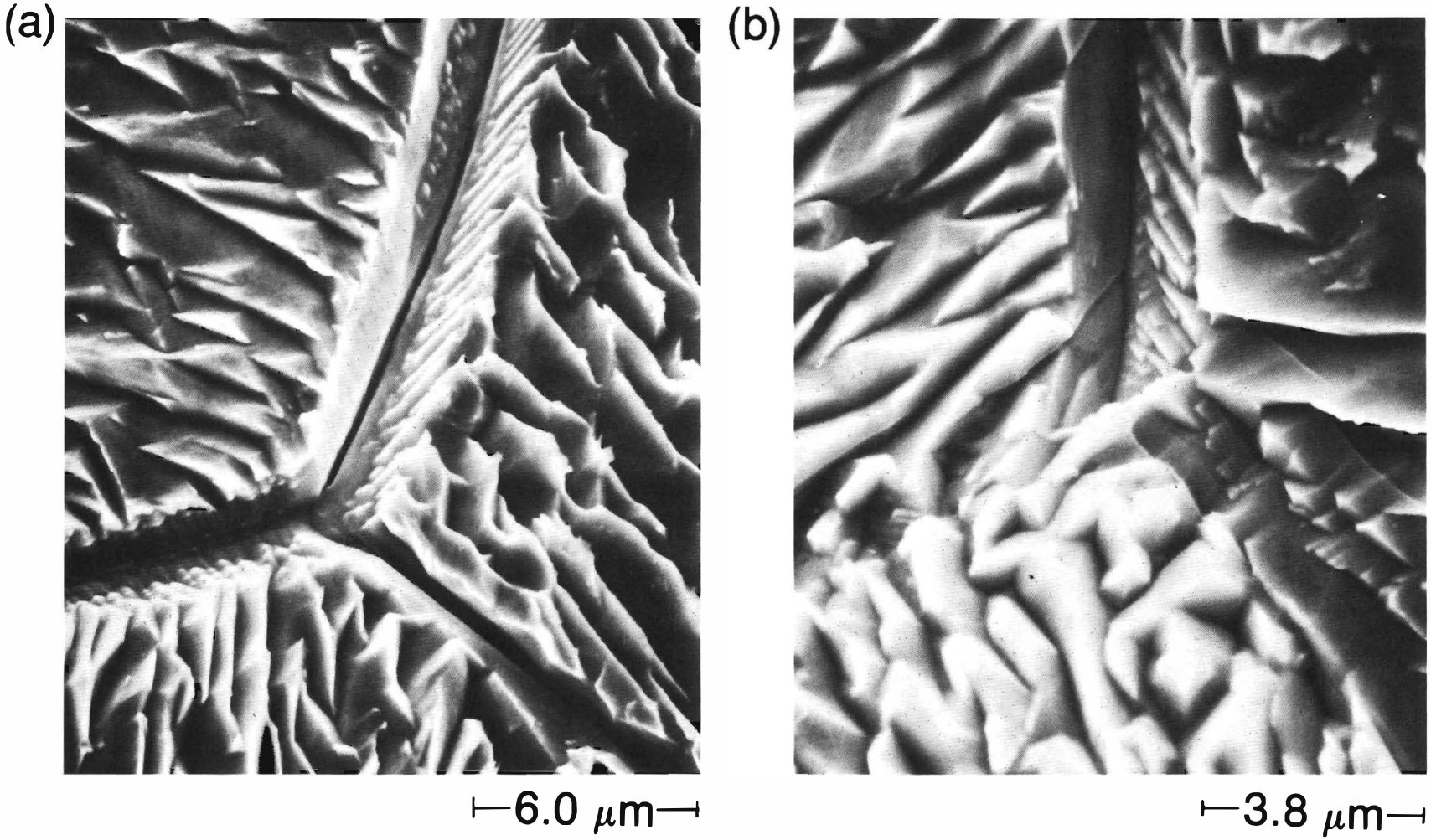

Figure 3. Photomicrographs (normal mode) of the two characteristic restructured grains observed on highly etched Pd foil after electrolysis of 0.1*F* Li_2SO_4/D_2O (total accumulated cathodic charge = 1.9×10^5 C): *(a)* morphology described as rugged, parallel thin-edged ridges (tilt = 30°, 5000x); and *(b)* morphology described as an intertwined structure, lower half (tilt = 22°, 8000x).

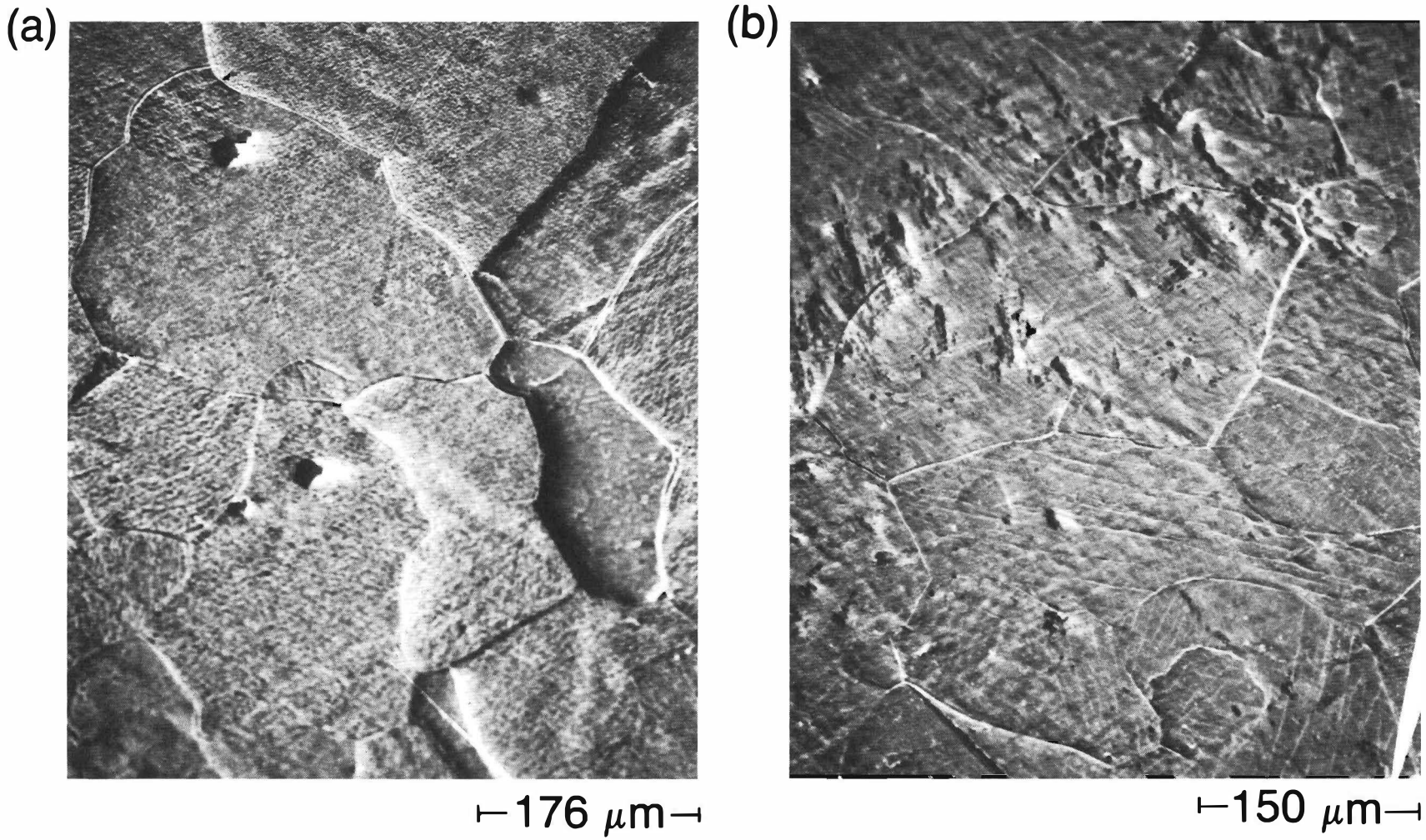

Figure 4. Photomicrographs (differential mode) showing *(a)* the presence of intergranular elevational differences for the sample of Figure 3 (tilt = 30°, 170x); and *(b)* the absence of intergranular elevational differences after fast-atom bombardment of the surface (tilt = 30°, 200 x).

the smooth, unstructured grains, but only for the PdD_x samples.

This topography is somewhat restricted to the near-surface region in that all intergranular differences in elevation disappeared after a piece of the sample shown in Figure 3 was subjected to ≈10 min of fast-atom bombardment, as seen in Figure 4*b*. In addition, the high surface area features are now absent. Quantifying the depth of the profile is not routinely done in this experiment, so the restructured layer can only be estimated as greater than nanometer, but less than micrometer in depth.

We assign the process for uplifting to the premier, rapid episode of outgassing because *(i)* deformation due solely to lattice expansion upon formation of the hydride or deuteride would have produced greater deformation for the PdH_x sample since palladium hydride expands more than does palladium deuteride [5]; *(ii)* one of the three PdD_x samples was subjected to multiple charge/outgassing cycles and showed a qualitatively similar degree of uplifting as singly outgassed samples; *(iii)* the smooth grains appear structurally indifferent to hydrogen or deuterium loading; and *(iv)* the outrush of gas is visibly more explosive for the PdD_x system than it is for the PdH_x system.

CONCLUSIONS

Our surface analytical characterizations of Pd-H_2O and Pd-D_2O systems have produced a number of unusual results involving:

(i) a relative enrichment at m/z 106 that cannot be attributed to heretofore-identified plausible chemical interferents;

(ii) segregation of metallic impurities (present in the bulk Pd at 10^2-ppm levels) to the surface of the more resistive, but still conductive PdD_x or PdH_x at atom-% levels;

(iii) differently structured morphologies for PdD_x and PdH_x;

(iv) grains which remain smooth and unstructured even after electrolysis of D_2O or H_2O solutions to 10^5 C of accumulated charge; and

(v) intergranular uplift for the structured grains relative to the unstructured grains, but only for PdD_x samples.

Obviously the surface and near-surface characterization of electrolytically prepared PdD_x systems requires great care and attention, but with the reward of unusual results.

ACKNOWLEDGMENTS

We are grateful to Dr. Steven M. Hues (NRL) for the TOF-SIMS measurements, to Mr. John Norris (National Institute of Standards and Technology) for the atomic emission analyses, and to Dr. Robert Jones (NRL) for the X-ray diffraction measurements. Funding for this research was provided through the Office of Naval Research.

REFERENCES

[1] M. Fleischmann, S. Pons, and M. Hawkins, *J. Electroanal. Chem.*, **261** (1989) 301; errata, **263** (1989) 187.

[2] D. R. Rolison and W. E. O'Grady, *Proc. NSF-EPRI Workshop on Anomalous Effects in Deuterated Metals*, 16-18 October 1989, Washington, DC, (1990).

[3] D. R. Rolison and W. E. O'Grady, *Anal. Chem.*, submitted.

[4] D. R. Rolison and P. P. Trzaskoma, *J. Electroanal. Chem.*, submitted.

[5] F. A. Lewis, **The Palladium Hydrogen System**, Academic Press: London, 1967.

[6] Panel Discussions, 1*st* Annu. Conf. on Cold Fusion, 28-31 March 1990, Salt Lake City, UT.

[7] L. E. Murr, *Scripta Metallurg. Mater.*, **24** (1990) 783.

[8] S. M. Hues, R. J. Colton, R. L. Mowery, K. J. McGrath, and J. R. Wyatt, *Appl. Surf. Sci.*, **35** (1988-89) 507.

[9] S. M. Hues, R. J. Colton, J. R. Wyatt, and J. A. Schultz, *Rev. Sci. Instrum.*, **60** (1989) 1239.

[10] D. Taylor, **Neutron Irradiation and Activation Analysis**, Van Nostrand: Princeton, NJ, 1964.

[11] J. Emsley, **The Elements**, Clarendon Press: Oxford, 1989.

[12] We would like to emphasize, yet again, that we have always referred to this observation as a mass/charge anomaly and not as an isotopic anomaly. The result, while valid for this one sample, and certainly intriguing, can only legitimately be described as a mass/charge anomaly when using this experimental approach and the resolution of this experiment.

[13] R. J. Latham and N. A. Hampson, **Encyclopedia of Electrochemistry of the Elements**, *Vol.* 1, A. J. Bard, Ed., Marcel Dekker: New York, 1973, 155.

A more readable copy of this paper is here: http://lenr-canr.org/acrobat/BassRWonempirica.pdf

ON EMPIRICAL SYSTEM ID, POSSIBLE EXTERNAL ELECTROMAGNETIC/ELECTRONUCLEAR STIMULATION/ACTUATION, AND AUTOMATIC FEEDBACK CONTROL OF COLD FUSION

by

Dr. Robert W. Bass

Registered Patent Agent, P.O. Box 6337, Thousand Oaks, CA 91359

ABSTRACT

This paper reviews some basic results from modern systems theory, which may prove useful to experimenters researching the cold fusion phenomenon from the point of view of attempting to learn how to stimulate, initiate, regulate, control by command at will, and terminate excess enthalpy, rate of tritium production, neutron count, etc.

Empirical System ID Technology regards an unknown system, to which information-theoretic signals or inputs may be injected, and from which responding outputs may be recorded, as an "arbitrary black box". There are many procedures for performing systematic input-output testing from which the internal dynamics of the unknown processes in the box may be inferred. There are available System ID software packages for processing the data produced by input-output experiments, and then using other software packages in the CACE (Computer Aided Control Engineering) category to design automatic feedback control systems which can be implemented by means of a Controller or Control Computer that converts the system into a closed-loop system by means of processing the output signals to generate appropriate input signals which will regulate the state of the process at a given set-point, or drive it toward a varying state in response to dynamic commands

This procedure can be applied to a Fleischmann-Pons electrochemical cell as follows. Introduce in proximity to the cathode one or more *actuators* selected from the category of all possible external physical stimuli whose effects are to be studied. Such a stimulus might be *electrical* (e.g. additional resistive heating of the electrolyte and/ or electrodes, or an external electrostatic field, or external radiant heating), or *magnetic* (e.g. an external static magnetic field), or *electromagnetic* (e.g. ion or electron cyclotron-resonant heating), or *electro-nuclear* (e.g. high-voltage, fast-switch triggered neutron flashers), etc. The system *inputs* will be the signals controlling such an *actuator suite.*

Now install a *sensor suite* comprising one or more measuring instruments selected to monitor the cell's physical properties of interest. Such monitors might include a continuous measurement of excess enthalpy, temperature of either electrodes or electrolyte, rate of tritium production, neutron count, etc. The signals from these sensors constitute the system's *output.*

Suppose that the system is near a steady state ("autonomy"), and that small inputs give small outputs ("linearizability near equilibrium"), and that bounded inputs give bounded outputs ("stability of equilibrium"). Suppose there are l outputs, m inputs, and that in addition to the preceding hypotheses the unknown process dynamic is either "finite dimensional" or adequately so approximable. Then according to the Ho-Kalman Lemma there must exist a finite integer n, and constant matrices F, G, H of dimensions respectively $n \times n$, $n \times m$, $l \times n$ such that the unknown process can be characterized for control purposes by the $l \times m$ matrix of scalar transfer functions T_{ij} or *transfer matrix*

$$T(s) = H(sI_n - F)^{-1}G.$$

This paper by a systems engineer will outline to experimenters available automatic data-reduction procedures (e.g. the *MATLAB State Space Identification Toolkit*) for determining the matrices (F, G, H) from records of systematic input-output experiments, and available automatic synthesis procedures (e.g. the *MATLAB Robust Control Toolkit*) for designing an optimal *controller* $C(s)$ to close the loop via feedback control.

Figure 1 illustrates *open-loop* control, and Figure 2 depicts *closed-loop* or *feedback* control.

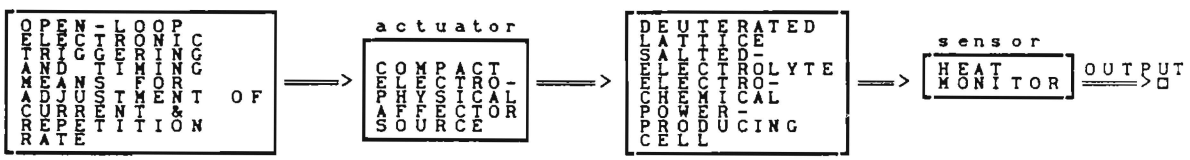

OPEN-LOOP CONTROL SYSTEM FOR STIMULATION, INITIATION & MAINTENANCE

Figure 1

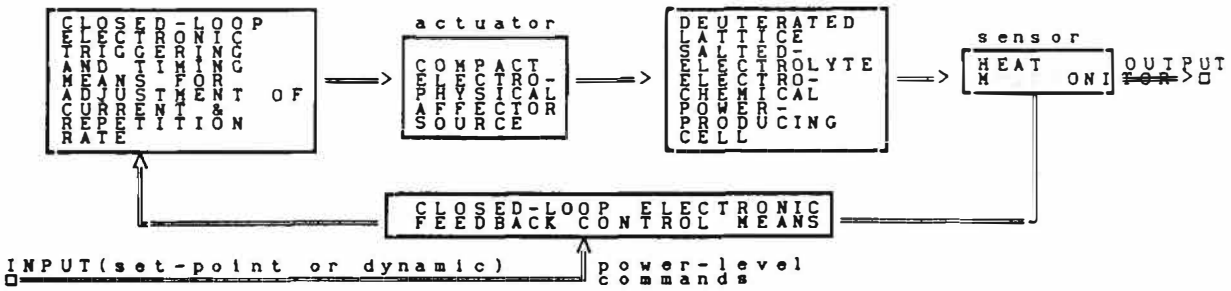

CLOSED-LOOP CONTROL SYSTEM FOR STIMULATION, REGULATION & CONTROL

Figure 2

TEXT

The rather negative report on Cold Fusion by the DOE Advisory Panel contains the statement that *"The claims of cold fusion, however, are unusual in that even the strongest proponents of cold fusion assert that the experiments, FOR UNKNOWN REASONS, are not consistent and reproducible at the present time. ...".* [Emphases added.]

The University of Utah's National Cold Fusion Institute [NCFI] has stated that *"the protocol of the [NCFI] focuses on* THREE *CENTRAL* ISSUES:

- *REPEATABILITY of this ... phenomenon;*
- *Understanding of the* trigger *mechanism which INITIATES [it];*
- *IDENTIFICATION of nuclear by-products ....".* [Emphases added.] As mentioned by Dr. Peter Hagelstein, the third *desideratum* may be subordinated to the first two, for if the phenomenon could be started and stopped at will and maintained reliably for indefinite periods of time, then operation for sufficiently many hours would cause the nuclear "fuel" to disappear and nuclear "ash" to appear in macroscopically measurable quantities, which would then settle definitively the nature of the principal nuclear processes at work.

In other words, it is the presently erratic behavior of the process which needs most to be cured. A Systems Engineer with my background might say that the process appears to lack *controllability* and *observability.*

My own field of specialization is Control Theory. For examples of the use of automatic feedback control in Cold Fusion experiments, see Figure 3.

Control Theory is a a branch of Information Science which analyzes and seeks to synthesize physical systems in terms of the *quantitative characterizations* of *Observability* and *Controllability* introduced in 1960 by R.E. Kalman, who recently received the $350,000 Kyoto Prize for his pioneering work in Mathematical Systems Theory.

To show that these concepts are susceptible to a precise Information-Theoretic definition, I will digress for a moment.

Suppose that the Fleischmann-Pons Effect can be affected *somehow* by any conceivable *external* physical agency. If the secret of mastery of the phenomenon lies in Material Science or Metallurgy, then I myself have not a clue; but if the secret lies in *any known physical affect whatsoever* [e.g. externally imposed electrostatic or magnetostatic fields, or electromagnetic fields, or heat or cold, or particle flux, etc.] then the *completely general* and systematic procedure which I have outlined in the preceding Abstract is certain to discover it, sooner or later. All that one has to do is to arrange for physical *actuators* to affect the process, and physical *sensors* to monitor the results of said actuation, and there is a well-known and frequently employed technique in engineering for doing what is called *"identification of the process dynamics of an unknown arbitrary black box"*, about which nothing is known except that input-output 'experiments' can be performed and recorded. (Such *TESTS* should not be called "experiments" because of the Patent Law forbidding patenting of a result which calls for *"UNDUE experimentation"* on the part of the prospective user, but since they are systematic and rational and do not get bogged down in the *"curse of dimensionality"* [too many unknown parameters to be able to do enough 'experiments' to identify them all], I would refer to them as "standardized systematic measurements".)

For examples of possible *input* variables u_i $(i = 1,2,\cdots,m)$ and *output* variables y_j $(j = 1,2,\cdots,l)$, see Figure 4. The input-output testing is illustrated in Figure 5.

After the input-output measurements have been completed, one processes this multi-channel data by any one of upwards of a hundred different "data reduction packages" available. I use MATLAB (available for less than $5,000 for use on either a 386-based AT-type PC or

a Workstation); however, if I were going First Class I would also get MATRIX-X for about $50,000 and run it on a mainframe, from which it can synthesize Control Laws that can be "downloaded" into a proprietary Digital Controller (the S-100) available from Integrated Systems Inc. for about $150,000.

Also there is available NASA's wonderful program "Modified Maximum Likelihood Estimation, release 3" [MMLE3], at no cost (in the public domain) for mainframe computers, and available as a *State Space Identification Toolkit* add-on to MATLAB from The Mathworks Inc.

The results of such a *test-data-reduction* are completely summarized in one easily understood n-vector and five easily understood matrices, generally written in the notation introduced at the Moscow IFAC by Rudolf Kalman in 1960 as (F,G,H,Q,R,b). The matrices are respectively of dimensions $n\times n$, $n\times m$, $l\times n$, $n\times n$, $l\times l$, where the point to keep in mind is that the dimensions m *and* l *are known* (because the engineer is using m actuators and l sensors), but the all-important dimension n is *NOT KNOWN IN ADVANCE* (because the insides of the black box or arbitrary process are unknown).

However the engineer can find out n very easily by a one-parameter search (which the patent office cannot call "undue" experimentation), performed not by him but by a computer. The computer simply tries out systematically $n = 1$, $n = 2$, $n = 3$, $\cdots$, until it finds that the residual error in the "fit" to the data has stopped decreasing and started increasing, which is then, *EMPIRICALLY*, the best choice of n. I could go into many technical reasons why I am sure that even as large values as $n = 100$ or $n = 150$ (which is the case for modern aircraft flight control systems and inertial navigation systems for submarines and ICBMs) can be handled effectively by existing software. Having found out n, then the engineer says that the system has been "identified", in the sense that the input-output process dynamics, near equilibrium (and so linearizable), can be represented by a *transfer matrix* [$l\times m$ matrix of (lm) scalar transfer functions, or ratios of Laplace transforms of outputs to Laplace transforms of inputs, in terms of the complex Laplace variable s]

$$\Phi = \Phi(s) = H(sI_n - F)^{-1}G, \quad [s = \textit{complex frequency}]$$

where now the physical interpretation of the matrices is:

- F = *dynamical* coefficient matrix
- G = *input* distribution matrix
- H = *output* distribution matrix

The important point is that according to the Ho-Kalman Lemma, the *pair* (H,F) must [is guaranteed *a priori* to] satisfy Kalman's condition of *Observability*, and the *pair* (F,G) must satisfy his condition of *Controllability*. See Figure 6.

These conditions are applications of the *Fisher Information Matrix*. (Here by $^{\bullet}$ one denotes the operation of matrix *transposition*.) They are:

$$\textit{Observability: } rank(H^{\bullet},F^{\bullet}H^{\bullet},(F^{\bullet})^2H^{\bullet},\cdots,(F^{\bullet})^{n-1}H^{\bullet}) = n$$

$$\textit{Controllability: } rank(G,FG,F^2G,\cdots,(F)^{n-1}G) = n$$

If the system is Single-Input, Single-Output (SISO), i.e. if $l = m = 1$, then it has been proved by Kalman that Controllability and Observability are always present, which explains why these concepts were not discovered during the period of Classical Control Theory. The Modern Control Theory era began when Kalman considered Multiple-Input, Multiple-Output (MIMO) systems, in which case one cannot perform Computer Aided Control Engineering (CACE) effectively without first checking the system's observability and controllability. See Figure 8.

To explain the practical importance of Controllability and Observability one must look at one more abstraction. The transfer function formulation conceals the *time*-domain *state-vector* differential equation formulation

$$dx/dt = Fx + Gu + v(t), \qquad (x \in \mathbb{R}^n),$$

$$y = b + Hx + w(t),$$

where now x is the *state vector* of the unknown system's open-loop process dynamics (an element of real Euclidean n-space $\mathbb{R}^n$). Here the zero-mean Gaussian "white noise" processes $v(t)$ and $w(t)$ are, respectively, the system's *process disturbance* and *measurement noise* vectors, respectively; the reason one needs to know Q and R as well as (F, G, H) is that Q is the *covariance matrix* of v and R is the *covariance matrix* of w. Also the l-vector b is the vector of *sensor biases*. In the Sampled Data case, Figures 9 and 10, the preceding differential equations are replaced by the system of difference equations

$$x^{k+1} = \Phi\cdot x^k + \Gamma\cdot u^k,$$

$$y^k = H\cdot x^k,$$

where for simplicity we have neglected sensor noise and process disturbance, and where the *state transition matrix* is given by a matrix exponential

$$\Phi = exp(F\cdot\Delta t),$$

and where Δt is the *sampling interval* and where Γ is given in terms of F and G as in Figure 10.

To recapitulate, you get a tape of MMLE3 or equivalent, you run your input-output "tests" (*not* "experiments") for a time $0 \le t \le T$, and you end up with m-channel recordings of the m inputs $\{u(t)\,|\,[t,T]\}$ plus l-channel recordings of the l outputs $\{y(t)\,|\,[t,T]\}$, which data are to be processed by MMLE3.

Then MMLE3 spits out *THE ANSWERS*:

$$(n,\ F,\ G,\ H,\ Q,\ R,\ b),$$

and you have succeeded in *identifying* the unknown arbitrary black box!

The physical significance of Controllability and Observability is that, as Kalman proved at the 1960 Moscow IFAC, if the system is Controllable then there *must exist* at least one control command input policy (or "control law") which will drive the system's state vector to *any* prespecified terminal state, *provided* that either $l = n$ and the n sensors are sufficient to measure all n state variables (components of x) or else (the usual case in engineering, where $l = 1$ or 2 or 3, but $n = 30$) the system is also Observable, in which case there exists at least one filtering policy (filter law) which can provide *in real time and on-line* actual *MINIMAL VARIANCE* ("optimal") estimates of all unmeasured state variables, and using these with the theoretically ideal state-feedback control law ("certainty-equivalence principle") is guaranteed *a priori* to succeed (up to minimum irreducible steady-state errors related to the size of Q and R). (His discovery is this "Control/Filter *Separation* Principle.")

An author in the IEEE *Spectrum* has said that Kalman Filtering is the biggest advance in electrical engineering since World War II. Kalman himself once said to me that "the reason that Kalman-Bucy Filtering turned out to be more important than Wiener Filtering is that Newton is more important than Gauss!" (That is, it is more important to know F somewhat accurately than to know Q and R accurately.)

Around 1961 I gave a one-week course at NASA Langley on "Modern Control Theory"; one participant, Dr. E. Armstrong has since devoted more than a decade to numerical analysis and programming of the basic necessities of Optimal Regulation and Control of Linear Systems (ORACLS) and his control synthesis toolkit is

now in the public domain as a NASA-supplied minimal-cost alternative to MATRIX-X or MATLAB. (It is also available in a hardback book called ORACLS from Marcel Dekker.) I agree that Q and R are less important than endowing the *closed-loop* successor to F with certain properties called *fidelity* and *robustness*. In my Langley lectures I presented closed-form algorithms for choosing the state-variable feedback gains so as to place the complex frequencies of the resultant controlled system at *any prespecified location* in the complex-frequency plane. Kalman in a chapter of a book on *Mathematical Systems Theory* has called my result "The Fundamental Theorem of Control Theory." Professor Kailath of Stanford on page 298 of his standard text on *Linear Systems* refers to the "Bass-Gura formula" as the most direct route to "pole placement", also called "eigenstructure assignment".

In other words, once the engineer completes the above-summarized process of *EMPIRICAL SYSTEM IDENTIFICATION*, the game is essentially over, for given the *reduced* data (n, F, G, H, Q, R, b), one can input this data to such a program as ORACLS and *instantly* find out the "control/filter law" to embody in an algorithm in a *control computer* which closes the loop by operating upon the system's sensor outputs and feeding the results back into the command signals to the system's actuator inputs. You can then make the closed-loop process "jump through arbitrary hoops" upon command.

If you want to go First Class, you don't have to understand any of the preceding theoretical results. You just go to Integrated Systems Inc. of Palo Alto and purchase MATRIX-X for $50,000 plus their proprietary Control Computer S-100 for $150,000. You then take this equipment to your unknown system (say a full-scale airplane in a wind-tunnel that can be tested but has never flown). You "exercise" all the input-output channels in a systematic way (operating every actuator signal to wiggle every control surface and stimulate output from every gyro, accelerometer, alpha-meter, or other sensor), recording the results on tape. Then have MATRIX-X process the data and *DOWNLOAD* its "optimal" closed-loop control/filter algorithms into their proprietary black-box S-100. You then stick S-100 into the airplane's electronics, take it out of the wind tunnel, and fly off into severe turbulence and return during a thunderstorm and zero-visibility to make a completely automatic landing. In other words, with these *Automatic Synthesis Procedures* (which are the descendent's of the ASP program of Kalman, Englar, and Bucy), you can accomplish in one day what would have previously taken hundreds of man-years by old-fashioned methods.

If what I am sketching above were not more or less true, then we could not have launched the thin-walled, flexible Saturn V booster on automatic pilot through shearing wind gusts, nor landed a man on the moon, nor achieved ICBM CEP's [Circular Error Probable] rumored by Astronomer Jastrow in the popular press to be about 100 feet, nor pressured the Soviets into preferring to end the Cold War rather than compete in an SDI space-arms race.

The above vast theory (of which I have only hinted at the tip of the iceberg) is every bit as rich and powerful as, say , Quantum Mechanics, but today's physicists, complacent over doing their own engineering during the Manhattan project, don't want to acknowledge its existence, nor contemplate the use of engineers other than as subordinates. That is why I am certain that it is easer to apply the above-sketched procedure to control of a Hot Fusion magnetic bottle (say the high-beta toroidal pinch Scyllac, which was canceled for uncontrollable instabilities) than it is to control a soft-landing Lunar Excursion Module (LEM), but the physicists in charge would never listen to a systems engineer and now their entire empire is starting to fall apart.

This is why I am hoping to gain the ears of the people pioneering the new field of Cold Fusion, in case it turns out that the process cannot be operated successfully in a scaled-up version without automatic regulation, because the above is the *SCIENTIFIC* way to go about it. (The above is called Empirical Systems Control; it is better to perform it in parallel with A Priori Modeling Control, as we did on the Saturn V, in which fundamental physics and engineering is used to derive theoretical formulae for (F, G, H) [see Greensite's two-volume book published in the USA in 1970 by Spartan Books and distributed in the UK by Macmillan & Co. Ltd.], because if the empirical tests yield a value of F which is in close agreement with your expectations -- as it was on the Saturn V -- then you can have even greater confidence in the "scientific" validity of your approach; in the case of Saturn V, the input-output tests involved placing the assembled vehicle in a vertical cradle for "shake testing", in which the engines were swiveled and the vibrations 300 feet above at the nose were recorded; on its *first flight*, all 29 state-variables were recorded by special instruments and telemetered back to the ground, and none deviated more than 10% from "nominal".

My UCLA collaborator Dr. Don Wiberg has applied Kalman-type multivariable methods to study the control of Fission Reactors. He submitted a proposal during the early stages of the Three Mile Island project which, he says, if it had been acted upon would have resulted in a more controllable system and prevented their disastrous partial melt-down!

POSTSCRIPT.

Hearing Dr. Stan Pons's impressive empirical identification of half-a dozen coefficients in a nonlinear "black box" input-output model reminded me that I should have said that not only does one want to find (F,G,H,Q,R,b) but *very importantly* one also needs to know the *variances* (ΔF,ΔG,ΔH,ΔQ,ΔR,Δb) which correspond to the data. His reference to the Levenberg-Marquardt Algorithm for Nonlinear Regression in the book *Numerical Recipes* [Press *et al*, Cambridge U. Press] is a valuable alternative to my references above. (Cf. also J.C. Nash's improved version in his *Compact Numerical Methods* [Wiley] and *Nonlinear Parameter Estimation* [Marcel Dekker].)

EXAMPLES OF
AUTOMATIC FEEDBACK CONTROL

1. **Peripheral systems:**
   - **Constant-temperature bath [regulator]**

2. **Electrochemical cells**
   - **D. Gozzi et al (Rome)**
     Nuovo Cimento, vol. 103A (1990), No 1, pp. 143-154

"Time, electrode temperature, palladium electrode potential vs. reference and the potential difference between Pt and Pd electrodes, were simultaneously transferred into a computer. The data acquisition system was programmed, for safety reasons, to switch off the applied current when the electrode temperature was over 80 C"

Figure 3

l = # of OUTPUT signals (SENSOR states)

m = # of INPUT signals (ACTUATOR states)

n = # of STATE variables

EXAMPLES of possible OUTPUT variables

y_1 = excess power (watts)
y_2 = cathode temperature (degrees K)
y_3 = anode temperature (degrees K)
y_4 = electrolyte temperature (degrees K)
.
.
.
y_l = ?

EXAMPLES of possible INPUT variables

u_1 = current (amperes)
u_2 = potential (volts)
u_3 = pressure (pascals)
u_4 = heating/cooling (watts)
.
.
.
u_m = ?

SISO = Single-Input Single-Output ($l = m = 1$)
MIMO = Multiple-Input Multiple-Output ($l > 1$ or $m > 1$)

Figure 4

HO-KALMAN LEMMA

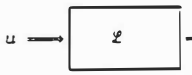

$(u \in \mathbb{R}^m,\ y \in \mathbb{R}^l)$

there exists a finite integer n and matrices

(F, G, H)

of dimensions $n \times n$, $n \times m$, $l \times n$, respectively

such that

for some initial state vector $x^0 \in \mathbb{R}^n$, & $t \geq 0$

$$\dot{x} = Fx + Gu, \quad x(0) = x^0, \quad (\dot{} = d/dt),$$
$$y = Hx,$$

where the system (F, G, H) is

CONTROLLABLE & OBSERVABLE

Figure 6

ARBITRARY UNKNOWN PROCESS

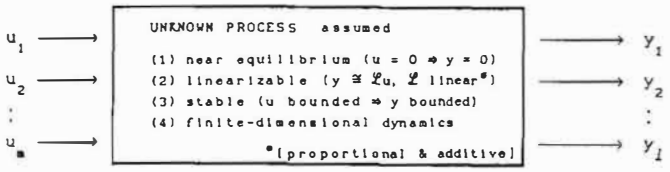

$$\begin{pmatrix} u_1 \\ u_2 \\ \vdots \\ u_m \end{pmatrix} = u \in \mathbb{R}^m, \qquad y = \mathcal{L}u, \qquad \begin{pmatrix} y_1 \\ y_2 \\ \vdots \\ y_l \end{pmatrix} = y \in \mathbb{R}^l$$

can RECORD $u(t)$, $y(t)$ for future time: $0 \leq t < +\infty$

$$y(\cdot) = \mathcal{L}\{u(\cdot)\}$$

Figure 5

CACE =
Computer Aided Control Engineering

SISO systems are always both controllable & observable.

MIMO systems must be checked:

(1) If not controllable, add more or different kinds of actuators;
(2) If controllable, optimize controllability by adjusting actuator parameters (e.g. location, size etc.)
(3) If not observable, add more or different kinds of sensors;
(4) If observable, optimize observability by adjusting sensor parameters (e.g. location, scaling, etc.)

Figure 8

CONTROLLABILITY & OBSERVABILITY

the pair (F,G) is *controllable* if $rank(G) = n$ and

$$det(\mathfrak{C}) > 0,$$

$$\mathfrak{C} = \mathfrak{G}\cdot(G^{*}G)^{-1}\cdot\mathfrak{G}^{*}, \quad \mathfrak{G} = (G, FG, F^{2}G, \cdots, F^{n-1}G).$$

a quantitative measure of the amount of controllability is

$$\gamma = \|\mathfrak{C}^{-1}\|.$$

the pair (F,H) is *observable* if $rank(H) = l$ and (F^{*},H^{*}) is controllable

- CONTROLLABILITY $\Rightarrow$ $\exists$ input $u(\cdot)$ which drives state X to any assigned state
- OBSERVABILITY $\Rightarrow$ $\exists$ a linear filter which will give an unbiased minimal-variance estimate of the state $x(t)$ from $\{y(\tau) \mid 0 \le \tau < t\}$

Figure 7

SAMPLED-DATA VERSION

$$t_{k} = k\cdot\Delta t, \quad (k = 1,2,3,\cdots)$$

$$v^{k} = v(t_{k}), \quad v \in \mathbb{R}^{p}$$

$$x^{k+1} = \Phi x^{k} + \Gamma u^{k},$$

$$y^{k} = Hx^{k},$$

$\Phi = e^{F\Delta t}$ = state transition matrix,

$$\Gamma = F^{-1}(\Phi - I_{n})G.$$

Figure 10

y = output vector

u = input vector

x = state vector

F = dynamical coefficient matrix

G = input distribution matrix

H = output distribution matrix

$\Delta\tau$ = sampling interval

$\Phi = e^{F\Delta\tau}$ = state transition matrix

$\Gamma = F^{-1}(\Phi - I_{n})\,G$ = discrete-time input distribution matrix

If $\Delta t \ll 1$, then

$\Phi = I_{n} + F\Delta t + \ldots$

$\Gamma = \Delta t G + \ldots$

Figure 9

IDENTIFIABILITY CANONICAL FORM

$$x^{k+1} = \Phi x^{k} + \Gamma u^{k},$$

$$y^{k} = Hx^{k},$$

$$\Gamma = \begin{pmatrix} 0 \\ I_{m} \end{pmatrix}, \quad H = (I_{l}, 0).$$

only Φ is unknown

Figure 11

STATE OF THE ART

EMPIRICAL ID & MULTI-INPUT, MULTI-OUTPUT (MIMO) CONTROL

1. Identify process state-transition matrix using e.g. *MATLAB State-Space Identification Toolbox* with input-output experiments
2. Design process Controller (algorithms for control computer) using e.g. *Matrix-x* software or NASA's (public domain) *ORACLS* software or *MATLAB Robust Control Toolbox*.

Figure 12

CURRENT R&D

INTELLIGENT SYSTEMS TECHNOLOGY

1. Use input-output records of actual process to train a *neural network* to mimic the process. Then the *synaptic weight matrix* of the trained net is just the state transition matrix (in identifiability canonical form).
2. Use *fuzzy-logic* techniques and *AI* techniques (rule-based expert systems) to implement a self-tuning or adaptive controller.

Figure 13

REFORMULATION OF THE COLD FUSION PROBLEM: HETEROGENEOUS NUCLEATION - A LIKELY CAUSE OF THE IRREPRODUCIBILITY AND INTERMITTENCY OF COLD FUSION OBSERVATIONS

Peter H. Handel, Physics Department, University of Missouri, St. Louis, MO 63121

ABSTRACT

The Irreproducibility and intermittency of the observed cold nuclear fusion effects is linked to the known difficulties affecting the observation of homogeneous nucleation of D_2 bubbles on the surface of the cathode in the electrolysis of D_2O. In general some nucleation centers are present, allowing for heterogeneous nucleation of D_2 bubbles at the Pd, Ti or Zr cathode, long before the chemical potential of D in the cathode reaches the levels necessary for cold fusion. By carefully eliminating the impurities and surface defects which can act as nucleation centers, one can create homogeneous nucleation conditions which correspond to higher values of the cathodic D chemical potential, provided the cathode is completely covered by the electrolyte, or extremely large currents are applied to the cell. A decrease of the surface tension due to tensio-active impurities in the electrolyte must also be avoided. A well-known collective lattice effect is the increased effective mass of the electrons which can lead to increased D-D nuclear fusion rates and to enhanced multiphonon generation amplitudes, i.e., to non-radiative dissipation of the reaction energy. At the very low center-of-mass energies of the order of 1eV encountered in this form of the fusion reaction we expect a breakdown of the charge-invariance of inter-nucleonic forces which can lead to a strong preference of the tritium channel over the He^3 fusion channel.

INTRODUCTION

The observation of excess heat production in the electrolysis of D_2O by Pons and Fleischman [1] as well as other indications of electrolytic cold fusion [2,3] have met with many negative reactions, because few people were able to reproduce the initial results. Even the few "lucky" experiments which produced excess heat and/or neutrons and/or tritium proved in general to be very unreliable, with an intermittent character. Indeed, most experiments yielded negative results, causing most workers to doubt the correctness of the initial claims, while the few positive results could not be reproduced at will. In fact, electrolytic cells, inactive for several weeks, suddenly could turn active, putting out excess energies in the MJ range which cannot be explained in the absence of nuclear reactions. After an arbitrary time period which could last from minutes to weeks, an active cell would suddenly become inactive to the outmost frustration of the "lucky" experimentalists. It appears that the reaction is switched on and off by factors beyond control. This situation reminds us of the most frustrating experiments known from the studies of homogeneous nucleation of new phases in condensed matter physics and in the related fields of cloud physics, metallurgy of alloys, and surface phenomena.

It is well-known that in the absence of any impurities which could act as nucleation centers, a liquid can be cooled far below the melting point, or a vapor can be pushed to supersaturations of the order of 40% or higher, right to the homogeneous nucleation limit. This limit appears when the rate of spontaneous germ creation approaches unity. A germ is defined as a spontaneous aggregate of molecules which is large enough to continue growing on its own, in spite of the large surface energy required to separate the new phase. Under normal atmospheric conditions condensation occurs already at supersaturations of 1-3%, due to the ubiquity of condensation centers which waives the large supersaturation requirement needed to produce a condensation germ homogeneously. In the case of supercooled liquids, or of supersaturated solutions, it is again the omnipresence of solid mesoscopic impurities acting with various degrees of efficiency as nucleation centers, which causes heterogeneously nucleated phase transitions at various supersaturation levels, all considerably lower than the homogeneous supersaturation limit. Even the most meticulous purification attempts were not able to insure the reproducible homogeneous nucleation conditions except for a few "lucky" cases, in which no qualifying impurities must have been present. Finally, in spite of the frustrating and uncontrollable randomness of the experimental results, a consensus about the homogeneous nucleation limit emerged in reasonable agreement with the elementary theory [4], and in better agreement with more advanced molecular models [5].

The present paper considers the nucleation of D_2 bubbles at the surface of a deuterium absorbing cathode in the electrolysis of D_2O and evaluates the corresponding homogeneous nucleation barrier. If impurities and defects can be controlled to inhibit heterogeneous nucleation, a considerable

increase in the achievable D chemical potential, roughly equal to the homogeneous nucleation barrier, can be realized, as we show in the following section. This increased chemical potential could switch on the fusion reaction and could therefore explain the difference between the active and inactive states of an electrolytic fusion cell. Based on this reformulation and new understanding of the intermittent and irreproducible character of cold fusion, we make some recommendations concerning the cathode geometry and configuration.

In the subsequent section a brief discussion of the increased electronic effective masses in deuterium absorbing metals is presented. An estimate of the average electronic mass observed in specific heat measurements performed on these metals yields about 3 times the free electron mass, while hydrogen rejecting metals do not show a sizable increase of the thermal effective mass. The thermal effective mass measured at low temperatures in the so called heavy fermion compounds is much larger than the free electron mass, up to 1000 times. The enhanced electronic mass is a collective lattice effect related to Bragg reflection on a large number of crystalline planes which can strongly bind together a pair of deuterons, can bring them close enough for nuclear fusion and can cause large multiphonon emission amplitudes which help carry away the reaction energy.

Finally we discuss the breakdown of the charge invariance in the low-energy interaction between nucleons as a possible cause of the preference of the tritium channel in the D-D reaction.

NUCLEATION LIMIT TO CATHODIC D LOADING

If all trivial routes of deuterium loss have been eliminated in the electrolysis of D_2O, the increase $\Delta\mu$ in the electro-chemical potential μ of D in the cathode will be limited by the surface tension barrier for homogeneous nucleation of D_2 bubbles at the interface between the cathode and the electrolyte.

In principle, a small gas bubble, i.e., a germ of the gas phase which appears at the interface, would be bound on one side by the cathode with surface tension σ_{cd} and on the other side by the electrolyte with surface tension σ_{wd}. The effective surface tension would then be $(2\sigma_{cw}-\sigma_{wd}-\sigma_{cd})/2$. Here σ_{cw} is the surface tension at the cathode to electrolyte interface. However, since $\sigma_{cw}>\sigma_{wd}$ and $\sigma_{cw}>\sigma_{cd}$, a thin film of electrolyte will creep in between the gas and the electrode at a certain point in the nucleation process, creating a barrier, which hinders the further growth of the germ, strongly depressing the nucleation rate and enhancing the effective nucleation energy barrier ΔF_g, while replacing the effective surface tension with σ_{wd}. The homogeneous nucleation energy barrier [6] for a D_2 germ of area Ω_g is $\Delta F_g = \sigma_{wd}/3$.

The nucleation rate J of germs is given by

$$J = c_{D_2} w_D \Omega_g Z \exp[-\Delta F_g/kT], \qquad (1)$$

where

$$Z=[\Delta F_g/3\pi kTg^2]^{1/2}$$

$$= (2v/\Omega_g)\,(\sigma/kT)^{1/2} \qquad (2)$$

is a Zeldovich correction factor. In Eq.(2) g is the number of D_2 molecules in a germ corresponding to the maximum of ΔF_g, w_D is the flux density of incoming D_2 molecules at the interface, and c_{D_2} is the concentration of D_2 molecules in the electrolyte. The value of ΔF_g for which the nucleation rate is J=1 bubble/cm^3s will be taken as the effective achievable potential.

The rate w_D at which D_2 molecules reach the germ is the rate by which they scale the energy barrier from the adsorbed state on the cathode surface to the germ, plus the rate by which they reach the germ from the electrolyte. The latter will be neglected, because the concentration of D_2 in the electrolyte will not exceed the saturation concentration at 1 atm very much. The rate is therefore given by the absolute reaction rate theory [7,8].

$$w_D = (N_c kT/h)\exp(-\Delta F_a/kT), \quad (3)$$

where h is Planck's constant and N_c is the number of deuterium molecules present in the absorbed state on the cathode in contact with the unit area of the germ. the rate thus becomes

$$J =$$

$$c_{D_2}(N_c kT/h)\exp(\Delta F_a/kT)\Omega_g Z\exp(\Delta F_g/kT)=$$

$$c_{D_2}(N_c kT/h)\exp[(\Delta F_a+\Delta F_g)/kT]2v(\sigma/kT)^{1/2} \qquad (4)$$

Nucleation takes place when the free energy difference ΔF_g is sufficiently large, so that the nucleation rate J becomes of the order of the unity. Setting J=1 we can find the free energy threshold

$$(\Delta F_a+\Delta F_g)/kT$$

$$= \ln[c_{D_2}(N_c kT/h)\ 2v\ (\sigma/kT)^{1/2}] \quad (5)$$

$$= \ln\{10^{17}cm^{-3}(10^{15}\ cm^{-2}4\ 10^{-14}erg$$

$$/6\ 10^{-27}erg\ s)7\ 10^{20}cm^3$$

$$[(150erg/cm^2)/4\ 10^{14}erg]^{1/2}\}$$

$$= \ln\ [6\ 10^{32}] = 75.6;$$

$$\Delta_o\mu = \Delta F_a+\Delta F_g = 1.9\ eV. \quad (6)$$

Thus, to move from the adsorbed state on the electrode surface to the gas phase by creating a small D_2 bubble, deuterium molecules must overcome a potential barrier $\Delta_o\mu$ of about 1.9 eV. The activation energy ΔF_a can be found in the literature [9] and is 0.7 eV for a pair of D atoms. Therefore, we obtain for the homogeneous nucleation barrier ΔF_g=1.9 eV - 0.7 eV = 1.2 eV. Provided no nucleation centers which would induce heterogeneous nucleation are present on the cathode-electrolyte interface, this means that through electrolysis the effective electrochemical potential of D_2 at the cathode surface and in the bulk of the cathode can be raised 1.2 eV above the level applicable in the absence of the homogeneous nucleation barrier, i.e., above the level achievable at low electrolytic currents, when the cathode is not completely immersed in the electrolyte, so that the deuterium can slowly diffuse through the electrode and escape into the atmosphere. Even in the presence of nucleation centers at the surface of the cathode, there will be a small effective (heterogeneous) nucleation barrier present, which we consider negligible.

It is interesting to calculate the D_2 gas pressure increase over a standard D_2 pressure of p_o=1 atm at the dry cathode surface, which would correspond to the same ΔF_g=1.2 eV increase in the electrochemical potential. Setting $\Delta F_g = kT\ln(p/p_o)$, which implies ideal gas behavior, we get $p=p_o e^{48} = 10^{20}$ *atm,* because p_o =0.1 atm. for D_2. This is an extremely high D_2 gas pressure. It also provides a general idea of the pressure which would have to be present above the dry part of the electrode protruding out of the electrolyte during electrolysis, in order to stop the slow loss of D_2.

The first trivial route of D escape is thus the heterogeneous nucleation of D_2 bubbles at the cathode surface. Unfortunately, this route has not been blocked in general so far. Only a few lucky experiments may have avoided heterogeneous nucleation. Even in these lucky experiments, once homogeneous nucleation sets in, the nucleation process will be induced by the now-existing bubbles which act as nuclei, and tends to become gradually heterogeneous, which corresponds to lower $\Delta\mu$ values. This impairs the reproducibility of the achieved $\Delta\mu$ and of $\Delta\mu$-dependent results of any nature, leading to an intermittent operation at best, or to an activity in the form of bursts, and would let us understand claims of sporadic heat generation by cold fusion, limited to time periods in which no nucleation centers happened to be present, periods marked also by an increased voltage drop at the cathode surface.

The second trivial route of D escape is the above-mentioned emergence of electrodes from the electrolyte, which leads to current-dependent, somewhat lower, achievable $\Delta\mu$ values, limited by the diffusion rate of D through the cathode. The third difficulty, also connected to the second escape route, is caused by the electric connection wires. To avoid the emergence of parts of the cathode from the electrolyte, the electric connection must be done under the electrolyte surface.

The electrode geometry suggested here is thus characterized by the presence of a cylindrical protrusion of the electrode material, electrolytically covered with a sufficiently thick *layer of metal* which most strongly *rejects* the hydrogen isotopes, e.g, Cr, Ni, Cu, Ag, Au, Mo, W, Co, Pt, Mg, Cd, Zn, Al. This layer carries the electric connection soldered at the far end of the cylindrical protrusion. On top of this layer of metal, and on the connecting wires, there should be an electrically insulating layer of chemically inert plastic or paint which keeps the electrolyte from making contact with any conductor other than the electrode material.

After this description of the electrode geometry, it is useful to clarify the terms used in the description. *Strong D-rejection* by a metal means a large negative difference $2d_\alpha$-d_g between the energy $2d_\alpha$ released when two isolated deuterium atoms are brought from infinity into the bulk of the metal in the α-phase on one hand, and the dissociation energy d_g of an isolated D_2 molecule on the other hand. The solubility decreases on cooling in this case. The α-phase describes deuterium in metals at low atomic fractions (<0.1 in Pd at room temperature). In *D-absorbing metals* ($2d_\alpha$-d_g>0, such as in Sc, Y, Er, Tu, Lu, La, Ti, Zr, Hf, V, Nb, Ta, Pd, and some additional rare earths and actinides) the solubility of D increases on cooling, and at higher atomic D-fractions, various phase transitions from the α-phase to other phases are observed.

Finally, a physical example may help in nailing down the main concept of deuterium

cramming with the help of the homogeneous nucleation barrier for bubbles at the surface of the electrode, which is the primary notion developed in this section in the context of cold electrolytic nuclear fusion. Consider a carbonated soft drink or beer poured into a glass. After the foam at the surface has dissipated, it becomes very easy to notice that bubble formation continues at a low rate for a long time from a few points on the bottom of the glass and on the walls, which are the active nucleation centers. This is heterogeneous nucleation, and is observed as strands of rising bubbles, coming from each of the nucleation centers. Through special surface treatment which eliminates impurities and defects from the surface of the glass, we can reduce the number of these centers. By removing a large regular Quartz crystal at the top from an even larger crystal in vacuum, we can imagine getting closer to the ideal case of a container with perfectly clean and homogeneous crystalline surfaces presenting no nucleation centers at all. In this ideal Gedanken-experiment case, a relatively large supersaturation is needed before CO_2 bubbles are formed on the walls, this time by what we call homogeneous nucleation, because no point on the bottom or on the walls of this ideal container or "glass" is different from any other point, or offers a lower nucleation barrier (except, perhaps, for the corners). Our homogeneous nucleation is still heterogeneous with respect to the whole volume of the liquid, because the points on the surface present a lower nucleation barrier than points in the volume of the impurity-free liquid, but we do not take this into account here either.

A real quartz beaker will have a few nucleation points even if it is monocrystalline, e.g. where dislocation lines reach the otherwise perfect surfaces. Due to random migration of thermally activated impurities to and from the surface along the dislocation lines, a process which is well known in many crystals, we can witness the intermittent activation and deactivation of nucleation centers. If only a few potential nucleation center points are present, sometimes the surface may remain with no active centers for certain time periods. A similar process is likely to be present at the surface of experimental electrolytic cold fusion devices, and we suggest here that it causes large fluctuations of the chemical potential in the cathode material, which result in the observed erratic intermittent activation and deactivation of the cold nuclear fusion reaction in the fusion cells. This would qualitatively explain the observed intermittency of tritium- and excess heat- production in the cells, as a restriction to periods with no deuterium bubble nucleation centers left, centers that would offer a low or negligible nucleation barrier. The randomness would be caused by the migration of impurities and defects to and from the cathode surface.

QUALITATIVE INTERPRETATION OF COLD FUSION IN TERMS OF HEAVY FERMIONS, PREFERENTIAL NEUTRON TUNNELING AND MULTIPLE GENERATION OF PHONONS

Due to their interaction with the periodic potential of the rigid crystal lattice, as well as due to interactions with phonons, and with other electrons, the electrons in the cathode acquire new dynamical properties which can be described by a larger effective mass. This larger effective mass of the electrons in certain states, in turn, could allow them to bind together deuterons in pairs much tighter than the normal-mass electrons. The electrons in states characterized by very large effective masses are quasi-particles called heavy fermions. We suggest here that heavy-fermion effects could also lead to increased fusion rates compared to the extremely low rates expected, e.g., in D_2. This heavy-fermion-fusion effect would bear some similarity to cold fusion catalysed by muons, although in this case the applicable effective mass may not be quite so large as the mass of the muon ($m_\mu = 207 m_e$), and although the fusion rate may be only slightly enhanced everywhere in the crystal where pairs of deuterons appear. The presence of heavy fermions in metals has been established experimentally through electronic low-temperature specific heat measurements and through the De Haas van Alphen effect. We shall first provide below a general discussion, and then a qualitative illustration of the plausibility of our suggestion, followed by an examination of the corresponding low-energy nuclear reaction.

The heat capacity of metals contains contributions from phonons ($\sim T^3$) and from electrons ($=\gamma T$). At low temperatures, the electronic contribution becomes dominant. By looking at the known experimental data (see Table I), we find that the values of the *electronic specific heat coefficient* γ are of the order of 1 mJ/(mol K^2) for most D-rejecting metals, an order of magnitude higher (10 mJ/molK^2) for most D-absorbing metals (9.42 mJ/mol K^2 for Pd), and two or three orders of magnitude higher at low temperatures in some inter-metallic compounds discovered after 1974, known as heavy fermion compounds, and containing ions with f-electrons, such as $CeAl_3$, $CeCu_2Si_2$, $CeCu_6$, UBe_{13}, UPt_3, UCd_{11}, U_2Zn_{17}, $NpBe_{13}$, $CePb_3$, $CeSn_3$ with up to $m_{th} \approx 1000$ m.

Table I

Electronic specific heat coefficients in mJ/K^2mol

1. D-Rejecting metals: $2d\text{-}d_g < 0$

Mg	Cr	Mo	W	Fe	Co	Ni	Pt	Cu	Ag	Au	Zn	Cd	Al
1.3	1.4	2	1.3	4.98	4.73	7.01	6.8	0.7	0.65	0.73	0.64	0.69	1.35

Average: 2.45 mJ/K^2mol, corresponding to $\mathbf{m_{th} \approx m}$

2. D-Absorbing: $2d\text{-}d_g > 0$

Pd	Se	Ti	V	Y	Zr	Nb	La	Hf	Ta
9.42	10.7	3.35	9.26	10.2	2.8	7.79	10	2.16	5.9

Average: 7.16 mJ/K^2mol, corresponding to $\mathbf{m_{th} \approx 2.92\ m}$

It is well known that the electronic heat capacity of metals is given only by the active electrons within an energy interval kT of the Fermi surface; their concentration is of the order of nT/T_F, where $T_F = \varepsilon_F/k = \hbar^2k^2_F/2m_{th}k$ is the Fermi temperature, ε_F the Fermi energy, $k_F = (2\pi^2n)^{1/3}$ the Fermi wave vector, m_{th} the thermal effective mass of the electrons, and n the electronic concentration, all in the approximation of a spherical Fermi surface. In the free electron model, the molar heat capacity contribution of the electrons is thus of the order of $3RT/T_F$ (more precisely $\pi^2RT/2T_F = \gamma T$), where R=Nk is the ideal gas constant, and γ is identified as $\gamma = \pi^2R/2T_F = \pi^2Rm_{th}k/\hbar^2k_F{}^2$. The large values of γ thus correspond to large values of the effective mass m_{th} of the electrons in these metals, or in a more appropriate formulation, to the large dynamical mass of the single-particle elementary excitations. The ratio of the thermal effective mass to the free electron mass is thus $m_{th}/m = \gamma_{exp}/\gamma_{free\ electron}$. For Pd this ratio is difficult to evaluate, since in metallic Pd the 4d band is not completely filled, about 0.36 holes being present; the Fermi surface includes therefore also sections (containing 0.36 electrons) located in the 5s band, and is very different from the simple spherical (free electron) example considered above. Nevertheless, the measured electronic specific heat coefficient of Pd would indicate a thermal effective mass of about m_{th} = 4 m in the Fermi sphere model, based on $k_F=(3\pi^2n)^{1/3}$ and $n=0.36(6.8\ 10^{22}cm^{-3})$ for metallic Pd.

The stoichiometric hydride PdD has a NaCl structure and is more relevant for our problem, since electrolytically loaded Pd electrodes will be close to this Pd/D ratio, and will try to exceed stoichiometry by as much as possible. However, for PdD we also expect at least m_{th} = 3m, from a comparison of the measured and calculated electronic specific heats by Switendick [10].

The increased effective mass will cause both a (roughly m/m_{th} times) lower distance between deuterons wherever pairing occurs, and a (roughly m/m_{th} times) larger pair binding energy, making the statistical occurrence of pairs energetically affordable and much more likely. Indeed, by introducing the notations $(m_{th}/m_D)^{1/2} = \rho$ and $m_{th}m_De^4/\hbar^2(m_{th}+m_D) = U$, we obtain [11] the deuteron pair binding energy

$$W = [-0.0697 - 0.06681(\pi/4 - \arctan\rho)^2 - 0.16736(\pi/4 - \arctan\rho)^4]U. \quad (7)$$

The corresponding separation of the deuterons of a pair is about 0.25 Å, for m_{th}=3. For this reduced internuclear distance one can calculate [3] a fusion rate of about $10^{-20}\ s^{-1}$ per deuteron pair.

Palladium is known [12,9] for its very high diffusion coefficient for all hydrogen isotopes; it increases with the isotopic mass and it increases exponentially with temperature. Although most of the diffusion is thermally activated, there is also a relatively large tunneling matrix element which had been underestimated earlier by Kehr [13] with a Bloch/Mathieu functions approach. More realistic calculations performed by Sugimoto and Fukai [14] yield 0.1 meV for D in Pd. An additional correction factor was introduced by Kondo [15], taking into account also the interactions with conduction electrons. As a result, in Pd super-diffusion can occur in certain circumstances with very high effective diffusion coefficients, leading to almost instantaneous deuteron motion under certain circumstances. With almost 100% occupation of the octahedric lattice positions, deuteron diffusion can only proceed through occasional double occupancy of these sites. These occasional D_2 pairs are the ones we refer to everywhwhere in this paper. Deuteron diffusion involves to a certain extent delocalization of the deuterons in Wannier states, which implies more than single-occupancy in PdD. We conclude that for the observation of cold fusion in the metallic lattice two conditions must be satisfied. First D loading must have reached a state close to stoiciometry (PdD or TiD_2, e.g.), at least in certain regions. Second, considerable D motion must be present, leading to a large macroscopic probability of double occupancy, with a fraction of mutiply-occupied sites not smaller than about 0.01. In this situation the deuteron pairs will be bound by electrons described in terms of nonlocalized but weakly overlapping electronic states, including also f-states with very high effective mass values. The large effective mass leads to the close approach between deuterons, of about 0.25 Å, mentioned above as being conducive to a nuclear fusion rate of the order of 10^{-20}/s.

Finally, the (m/m_{th} times) reduced size of the electronic states which cause the deuteron-deuteron binding, will allow the states to fit even better into the octahedric positions of the fcc palladium lattice. It is also likely that heavy fermion effects from the lowered, initially empty, 4f states participating in the deuteron pair binding, play a certain role in the stronger deuteron pair binding in the Pd lattice, as well as in rare earth intermetallic compounds such as $CeAl_3$, $CeCu_2Si_2$, $CeCu_6$, UBe_{13}, UPt_3, UCd_{11}, U_2Zn_{17}, $NpBe_{13}$, $CePb_3$, $CeSn_3$, which are therefore suggested here as most promising replacements of Pd for cold fusion purposes.

Preferential tunneling of neutrons. The single-nucleon tunneling attempt frequency between the deuterons of a deuteron pair separated by 0.25 Å in the Pd cathode is very large, but the nuclear potential barrier transparence is extremely low, both for neutrons and for protons at room temperature, in spite of the aerated structure of the deuterons, of their d-state component, and of their low 2.2 MeV binding energy. At the very low energies in the center of mass (CM) system of the deuterons of such a pair, small differences caused between the slow tunneling rates of protons and neutrons by the electromagnetic interaction get to be amplified in the presence of resonance effects by the small barrier transmission factor. Therefore, the reaction rates in the $_2He^3 +_0 n^1$ channel can be depressed many orders of magnitude with respect to the $_1H^3 +_1 H^1$ channel which is based on neutron tunneling. This "piezonuclear" fusion process is quite different from the usual reaction mechanisms involving nucleon stripping processes, or formation of a compound nucleus. These usual reaction mechanisms require more than 1 KeV in the CM system for an observable fusion rate, and are applicable when DD collisions are produced through the acceleration of deuterons, or by raising the temperature to thermonuclear levels.

To describe these considerations in more detail, we note that the D-D reaction rate can be written in a first approximation as the product of a barrier penetration factor T_b and an intrinsic nuclear reaction rate Γ_n

$$\Gamma = T_b \Gamma_n \qquad (8)$$

In this approximation the deuterons are considered as point particles tunneling through the Coulomb barrier. The point particle model is reasonable as long as the distance between the two tunneling deuterons exceeds a value of the order of 100 fm = 10^{-11}cm. For shorter distances, the polarization of the deuterons can no longer be neglegted, due to the strong electric field present, and the point particle description breaks down. It is therefore convenient to write the barrier penetration factor as a product of two penetration factors, and to replace the second factor by an expression which also allows for individual tunneling of the nucleons which make up the deuteron. The reaction rate can then be written in the form

$$\Gamma = T_{b1}(\alpha T_{b2}\Gamma_n + \beta T_{bN}\Gamma_N + \beta T_{bP}\Gamma_P), \qquad (9)$$

where T_{b2} is the Coulomb barrier tranparence to deuterons on the last 100 fm, and similarly T_{bN} and T_{bP} are the combined nuclear and Coulomb transparence factors on the last 100 fm for neutrons and protons, respectively. Due to the absence of the Coulomb repulsion for neutrons, $T_{bN} >> T_{bP}$. The coefficients α and β indicate the

probabilities for survival and for desintegration of the deuteron. At very low energies of the relative motion of the two deuterons in the CM system we expect β to be much larger than α, so that finally $\beta T_{bN}\Gamma_N >> \alpha T_{b2}\Gamma_n$, in spite of $T_{bN} << T_{b2}$. Indeed, in the limit of very low CM energies the probability β of disintegration of the deuteron on the last 100 fm interval becomes very large, and may lead to the dominance of the tritium channel of reaction. This may explain the extremely low branching rates observed for the He^3 channel in cold fusion experiments. Our simplistic approach highlights the distance of 100 fm arbitrarily in order to provide a clear picture. However, a more realistic calculation will replace Eq.(9) through a more complicated relation which superposes many expressions similar to Eq.(8), with different partitions of the barrier, i.e., with all possible distances replacing our choice of 100 fm.

Finally, the large effective masses of electrons, obtained, e.g, with the help of d&f-electron tight-binding and LDA calculations are instrumental in bringing the D nuclei close together in delocalized states, and since the large electronic masses arise from delocalized coherent Bragg reflection on the whole lattice, they should also allow for the delocalized multiphonon processes which carry away most of the large nuclear reaction energy.

The author is indebted to D. Reago for his participation in many helpful discussions on nucleonic tunneling.

REFERENCES

[1] M. Fleischman, S. Pons and M.J. Hawkins: J. Electroanalyt. Chem **261**, 301 (1989); **263**, 187 (1989) erratum.

[2] S.E. Jones, E.P. Palmer, J.B. Czerr, D.L. Decker, G.L. Jensen, J.M. Thorne, S.F. Taylor, J. Rafelski: Nature **338**, 737 (1989).

[3] J. Rafelski, M. Gajda, D. Harley and S.E. Jones, unpublished manuscript, April 1989.

[4] R. Becker and W. Döring, Ann. d. Physik **24**, 719 (1935).

[5] P.L. Plummer and B.N. Hale, J. Chem. Phys. **56**, 4329 (1972).

[6] H.R. Pruppacher and J.D. Klett: "Microphysics of Clouds and Precipitation", D. Reidel Publishing Co., Dordrecht, Holland (1978).

[7] S. Glasstone, K.J. Laidler and H Eyring: "The Theory of Rate Processes", McGraw-Hill, New York (1941).

[8] H. Eyring and M.S. Jhon: "Significant Liquid Structures", J. Wiley, New York (1969).

[9] See, e.g., E. Wicke and H. Brodowski in "Hydrogen in Metals", Vol. II, G. Alefeld and J. Völkl Eds., Springer, New York (1978), p. 85.

[10] A.C. Switendick, "Hydrogen in Metals", Vol. I, G. Alefeld and J. Völkl, Eds., Springer, New York (1978).

[11] P.H. Handel: "Approximate Expression for the Binding Energy of Isotropic Biexcitons", Phys. Rev. B **7**, 5183-5186 (1973).

[12] Y. Fukai and H. Sugimoto: "Diffusion of hydrogen in metals", Adv. in Phys., **34**, 263-326 (1985).

[13] K.W. Kehr, in "Hydrogen in Metals", Vol. I, G. Alefeld and J. Völkl, Eds., Springer 1978, p. 197.

[14] H. Sugimoto and Y. Fukai, J. Phys. Soc. Japan, **53**, 2592 (1985).

[15] J. Kondo, Physica B **124**, 25; **125**, 279; **126**, 377 (1984).

A NEW THEORETICAL MODEL ($Nu\text{-}Q^*$) FOR RATIONALIZING VARIOUS EVENTS OF 'COLD FUSION' IN DEUTERIUM LOADED PALLADIUM CATHODES

George Andermann, Department of Chemistry and Hawaii Natural Energy Institute, University of Hawaii at Manoa, Honolulu, HI 96822

ABSTRACT

A model is proposed based on di-neutrons, Nu, to rationalize most of the high energy and some of the low energy events observed in electrochemically induced 'cold fusion'. Using pressure induced electron capture (EC) by deuterons as the triggering mechanism for the creation of Nu, this model calls for the absorption of Nu by deuterons, creating a highly unstable isotope Quatrium, Q^*, which decays instantly to yield tritium and neutrons. Because of electron spin considerations the dominant EC mechanism is shown to yield two kinds of Nu, namely, a low lying Nu_L and a less stable higher lying Nu_H. Thus, the $Nu\text{-}Q^*$ mechanism is shown to yield a doublet in the gamma ray spectrum. Another form of di-neutron, Nu^*, is also expected to be created from the coalescence of neutrons. The theoretically calculated gamma ray lines are in excellent agreement with the experimentally observed lines. Another possible coalescence is that of neutrons with deuterons which may result in significant heat production. Heat production is also rationalized as being due to neutron and di-neutron absorption of heavier elements in the cathode, as well as from UV photon emission which is the by-product of EC mechanisms.

THEORY

The model proposed here gets around some of the difficulties inherent in the usual deuterium-deuterium (D•D) collision-fusion model. The weaknesses of the D•D fusion model have been reviewed recently[1]. Accordingly, the fusion model's inherent weakness is the forbidding Coulomb barrier. The proposed model does not have this problem because of the use of di-neutrons. It is suggested that under the conditions of electrolysis of heavy water, a di-neutron, hereafter designated as Neutrium (Nu) is formed according to the following electron capture (EC) mechanism[2], a process which is enhanced by pressure[3],

$$ {}^{0}_{-1}e + {}^{1}_{1}H \xrightarrow{(EC)} {}^{2}_{0}Nu + \upsilon + \gamma \qquad (1), $$

where υ represents a neutrino. Since this process is not favored for low Z, it is essential to enhance it by very high pressures. Moreover, since the EC process is the initiating mechanism, the problem of irreprodicibility, well known to be associated with the 'cold fusion' phenomena, may be assigned to not having sufficiently high and/or reproducible pressures. The biggest problem with this model, however, is that a di-neutron has never been observed before. However, it should be noted that Teller suggested some time ago[4] that some sort of a hitherto unobserved neutral particle is involved in 'cold fusion'. If Nu can be created, then its reaction with D is no longer fusion but rather conventional absorption of cold neutral particles, and, therefore, the 'cold fusion' terminology should be disbanded in favor of cold absorption of Nu by D which is pressure induced. More specifically,

$$ {}^{2}_{0}Nu + {}^{2}_{1}H \rightarrow {}^{4}_{1}Q^* \qquad (2), $$

where the completely unstable isotope Quatrium, Q^*, can yield the following reactions:

$$ {}^{4}_{1}Q^* \rightarrow {}^{4}_{2}He + {}^{0}_{-1}\beta + \bar{\upsilon} \qquad (3), $$

and

$$ {}^{4}_{1}Q^{*} \rightarrow {}^{3}_{1}H + {}^{1}_{0}n + \gamma \qquad (4) $$

It is pertinent at this point to recall that the D•D fusion model has 3 branches, one branch producing ^{4}He and γ, another producting Tr, and ^{1}H, and the third yielding ^{3}He plus neutrons and γ. Thus, there are significant qualitative differences between the Nu-D absorption (coalescence) model and the D•D fusion model, the most important of which is that Tr and n are produced in the same branch with the Nu-D model but ^{3}He is not produced, a substance that has not been observed to date. In terms of quantitative evaluation between the two models, the most significant differentiation is that the γ-ray signatures observed do not agree at all with the γ-ray signatures called for by the fusion model. In contrast, as shown below, the coalescence model accurately assigns three such lines.

Since di-neutrons have not been observed before, it is essential to evaluate whether or not Nu would be stable with respect to its formation out of neutrons.

$$ {}^{1}_{0}n + {}^{1}_{0}n \rightarrow {}^{2}_{0}Nu^{*} + \gamma^{*} \qquad (5) $$

Whether or not Nu^{*} is exothermic depends on the rest mass of Nu^{*}. As a first approximation it can be assumed that the coalescence via equation (5) is thermodynamically equivalent to the EC mechanism of (1), i.e.,

$$ M(Nu^{*}) = M(D) + M(e) \qquad (6) $$

or more simply,

$$ Nu^{*} = D + e \qquad (7) $$

Under this stipulation γ^{*} in (5) has a value of 2.496 MeV, which is exactly the experimental value reported by the Univ. of Utah (UU) group[5]. Thus, if this assignment is correct, then Nu^{*} is highly stable with resepect to dissociation to isolated neutrons formed out of coalescence.

However, in the EC mechanism of equation (1) it is not necessarily true that the enthalpy, Q = 0. Moreover, previous discussion of the EC process did not take into account the nature of the proton (p) and neutron (n) spins in their ground state configuration, and this may be important for deuteron but not for higher Z. The stable ground state configuration[2] of D is $^{3}S_{0}$, which means that p and n have parallel spins, that is, $(p\uparrow)(n\uparrow)$. Consequently, since due to Pauli forces, Nu must have a ground state configuration of $(n\downarrow)(n\uparrow)$, the EC mechanism can create two kinds of di-neutrons depending upon the spin of the incoming electron. If the electron spin is down, then there are no problems since the transitional configuration just prior to neutralization is $(e\downarrow)(p\uparrow)(n\downarrow)$, which readily relaxes to the desired singlet configuration $^{1}S_{o}$ of $(n\downarrow)(n\uparrow)$, yielding a stabilized low lying singlet for Nu, labelled Nu_{L}. On the other hand, if the spin of the incoming electron is up, then the transitional configuration would yield $(e\uparrow)(p\uparrow)(n\uparrow)$, which would yield an anti-Pauli configuration of $(n\uparrow)(n\uparrow)$. To circumvent this, the electron spin of the incoming electron needs to be flipped just as it enters the nucleus, yielding $(e\downarrow)(p\uparrow)(n\uparrow)$, which would yield a desired singlet Nu_{H}, but at a higher level. The maximum energy of this spin flip mechanism cannot exceed .51 Mev, i.e., the rest mass of the electron.

Using this more sophisticated version of the EC process for equation (1) a doublet is expected in the gamma ray spectrum, namely γ_{H} and a γ_{L} with a maximum energy separation of 0.51 MeV and to be in the region of 2.74 and 3.76 MeV, which corresponds to the rest mass range of $D \pm e$. The published experimental observations of the UU group[5] mentions a

doublet at 3.01 and 3.52 MeV yielding values of (D + .55e) for Nu_H and (D - .45e) for Nu_L.

Still another possible mechanism for Nu creation is the coalescence of a neutron with D, i.e.,

$$ {}_0^1n + {}_1^2H \rightarrow {}_0^2NU^{**} + {}_1^1H + \gamma^{**} \qquad (8) $$

Again, conventional scattering (collisional) experiments between n and D have not produced a di-neutron, but again it is suggested that under the conditions of very high pressure in these electrolytic experiments it may be possible to do so. If the rest mass resulting from this kind of coalescence is designated by Nu^{**}, and if Nu^{*} is set equal to Nu^{**}, then γ^{**} would have a value of 0.27 MeV, and this could definitely yield appreciable heat in the electrolytic cell. Moreover, mechanism (8) together with (4) constitute a chain reaction.

With respect to the absorption of thermal di-neutrons by the various Pd isotopes, it can be shown readily that the γ-ray spectra would be very complex but should be observable somewhere between 7 and 8 MeV. Fundamentally, there are three possible mechanisms for each of the isotopes. The three different kinds of mechanisms are, thermal absorption of n and of di-neutrons with and without dissociation of the di-neutrons. Moreover, for each of the di-neutron absorptions there are three different kinds of Nu involvements yielding over 30 possible γ ray lines.

The (102) Pd isotope enrichment presents a very special case since

$$ (102) + Nu \rightarrow (103) + n + \gamma \qquad (9) $$

However, (103) decays according to an exothermic EC process, namely,

$$ {}_{46}^{103}Pd + {}_{-1}^{0}e \rightarrow {}_{45}^{103}Rh + \gamma + \upsilon \qquad (10), $$

where the decay energy is .57 MeV, thus leading to some heat production as well. Moreover, according to the rules of EC mechanism there should be a detectable Rh-K emission spectrum, and this could be used to monitor the overall process. Of the other possible enrichment, Oxygen is another interesting one since that could be used to monitor any oxygen involvement in the cathode. Finally the involvement of Li in the overall process could also be used to reveal why Li appears to be so critical in most of the present experiments. Considering the importance of gamma ray signatures for monitoring the various thermal absorption processes, it appears crucial to monitor these signatures with relatively high resolution and accurate calibration.

So far it has been shown that low energy gamma rays are involved in some heat production. Another very important source of heat production is due to the filling of the vacancy left behind upon electron capture. This kind of vacancy has not been treated before. While the details of the filling of this kind of vacancy is a very interesting topic by itself, briefly, the electronic transitions that may be involved yield photons primarily in the UV region. The filling of this vacancy is exactly equivalent to the phenomena with higher Z elements, more specifically with Z>3, where the filling of the vacancy yields characteristic X-rays involving the isobaric nucleus. In this case the isobaric Nu is free to go as it pleases, so the filling of this vacancy may have nothing to do with the properties of Nu and more with the partial density of states of p character of the atoms surrounding the vacancy. This, of course, assumes that the vacancy will remember its original character.

DISCUSSION

While the proposed coalescence model appears to be more suitable than the conventional D•D fusion model, the most important weakness of the proposed model is that di-neutrons have never been observed before. As already argued, just because di-neutrons have not been observed before under low pressure-high energy

scattering experimental conditions does not mean that di-neutrons could not be created under low energy (cold) high pressure conditions. If the energy calibration of the gamma ray spectrum is correct, then the gamma ray signatures assigned here represent a good validation of the proposed model. Moreover, even if the MIT group's argument[6] about 2.5 MeV really being 2.8 MeV is correct, everything presented here would still be valid, since the 3.01 and 3.52 MeV lines would be merely shifted by the same amount. The argument by the MIT group that the lines reported by the UU group must be instrumental artifacts is fallacious because this group assumed that these lines were due to conventional neutrons arising from D•D. collision. All the MIT group can claim is that the 'cold fusion' model is invalid, and, of course, this discussion offers further proof. Here, the argument is presented that the UU group's gamma lines are real and represent a partial verification of the di-neutron coalescence model.

While the subject matter of low energy events, heat buildup, and their irreproducibility has not been dealt with in detail, all of these phenomena may be shown to be connected to di-neutron formation where the EC step represents the crucial initiating and dominant mechanism. Since the EC process is extremely sensitive to the pressure buildup, which may vary from grain to grain and from surface to bulk of each grain, it is suggested that if the model presented is valid, then the understanding and monitoring of the pressure on a microscopic and macroscopic basis and as a function of grain depth may be one of the important ways for understanding most of the frustrating aspects of the so-called 'cold fusion' phenomenon.

REFERENCES

(1) D. Lindlay, Commentary Nature, 344, 375 (1990).

(2) R.D. Evans, "The Atomic Nucleus", McCraw Hill Book Co., (1952).

(3) W.K. Hensley et al., Science 181, 1164 (1978).

(4) E. Teller, Research News, Oct. 1990.

(5) M. Fleishmann, S. Pons, R.I. Hoffman, Nature, 339, 667 (1989).

(6) R.D. Petrasso et al., Nature 339, 183 (1989) and Ibid, 667 (1989).

SOME OBSERVATIONS RELATED TO THE PRESENCE OF HYDROGEN AND DEUTERIUM IN PALLADIUM

D R Coupland, M L Doyle, J W Jenkins, J H F Notton, R J Potter and D T Thompson.

Johnson Matthey Technology Centre, Blounts Court, Sonning Common, Reading, RG4 9NH, England.

SUMMARY

Surface and bulk analytical work carried out on Pd rod samples returned to JM by Fleischmann and Pons indicate that a number of elements, including Pt and Li were deposited on the surface during electrolysis in D_2O.

One electrolysed rod exhibited recovery of part of the wrought microstructure which would ordinarily require a temperature of > ca. 200°C, and another rod showed recrystallisation of a portion of its length and this would normally require a temperature of > ca. 300°C. These effects cannot be readily explained by known processing history and could not be reproduced by filing or sawing.

Temperature programmed hydrogen absorption/ desorption profile measurements on a range of Pd samples indicates wide differences in properties; for example a rod electrolysed in LiOH absorbed hydrogen more readily than a similar rod electrolysed in NaOH. This technique would therefore seem to be of value in characterising the Pd electrode.

Electrochemical measurements conducted in H_2O show that there are significant differences between the behaviour of Pd in LiOH and in NaOH and KOH solutions.

1. ANALYSIS OF PALLADIUM RODS RETURNED TO JMTC BY FLEISCHMANN AND PONS

SLIDE 2

Three rods were returned. The dimensions are given on this slide.

1.1 Surface Analysis

SLIDE 3

There were two principal objectives here. Firstly, an assessment of the surface texture of the rods; and secondly, analysis of the surface to detect the presence of gross contaminants or a layer of electro- deposited material formed during use.

SLIDES 4 - 7

SEM EDX analysis profile plots for Cu, Fe, Zn and Pt percentages for various positions along the rod are given on these four slides. Penetration depth is ca 1μ.

SLIDE 8

XPS analysis using the Kratos XSAM 800 surface analyser showed that the immediate surface of all the rods showed a very high signal for carbon - probably from the plastic bags used for transport.

The surface was etched back, over an area greater than the analysis area, using a beam of argon ions at 4keV and the analysis repeated. It was proposed to repeat this procedure with each specimen until signals indicated that bulk metal had been reached.

Elements found were as follows:

Rod 1 - oxygen, nitrogen, sodium, chlorine and palladium.

Apart from Pd, these elements presumably represent handling contamination, although the levels of chlorine are too low compared to the sodium found for normal handling residues.

Rod 2 - oxygen, sodium, silicon and platinum.

Rod 3 - oxygen, silicon, iron, sodium, platinum, zinc and copper.

The composition profiles for the surface layer showed that sodium and silicon were removed fairly rapidly during the etching process; for Rod 2 after 100Å, and for Rod 3 after 600Å.

After removal of the Na and Si the other metallic contaminants, Pt, Cu, Fe and Zn became detectable and achieved maximum values which declined again as the bulk metal was approached. Pt, Cu, Fe and Zn were present as metals.

Spectral line overlaps interfered with the detection and measurement of Li in the presence of Fe and the measurement of O in the presence of bulk Pd.

Instead of a sharp demarcation at the palladium surface the impurities showed a gradual fall off. This is interpreted as an effect of the roughness of the surface with a surface film of variable thickness within the analysis area.

SLIDE 9

Time of flight SIMS analysis has been carried out on two palladium rod samples recovered from the experiments carried out by Professors Fleischmann and Pons. The samples examined were the as received 4mm Rod 1 and the 2mm Rod 2, which was electrolysed at 64mA/cm^{-2}. The equipment used was a Cambridge Mass Spectrometry TOF/SIMS. It was operated so that not more than 1 monolayer of metal was ablated in a twenty minute period during spectrum collection so that isotope ratio measurements were not confused by depth profiling effects. The surface of the sample was ablated by a gallium ion beam. This has the advantage that oxide species are not present to complicate the mass spectrum as is normally the case when an oxygen ion beam is used. The values measured for the two rods are closely similar. The values differ somewhat from values quoted in the literature; no explanation is currently offered for this in terms of instrumental parameters.

SLIDE 10

No lithium was detected at the centre of either rod.

Lithium was detected at a very low level on Rod 1 after the removal of 4 monolayers and only as the isotope of mass 7. This was considered to be a trace contaminant.

After removal of 4 monolayers on Rod 2 a larger amount of lithium was detected with both isotopes being found.

The measured values for isotope 6 seem to be consistently different from the expected values. So far as can be ascertained from an inspection of the mass spectra there is no possibility of a significant interference with isotope 7 so that the effect is considered to be real. There was no opportunity to measure the ratio on the lithuim used in the electrolysis cell.

This work is regarded as preliminary in that better information might be expected to be gained from a rod electrolysed at a higher current density. A continuation of the profiling which was not attempted in this case would show how deeply the lithium has penetrated into the rod.

Before the analysis the rods were washed in water, hot arklone and ultra-pure hexane to remove any lithium not chemically bound to the surface.

SLIDE 11

Conclusions from surface analyses.

1.2 Bulk Analysis

SLIDE 12

Spectrographic analysis for trace impurities is normally made on pure metals produced by JM. The batch analysis for the materials supplied to Fleischmann and Pons is given here.

SLIDE 13

Samples for ICP were dissolved in aqua regia in closed containers (to minimise loss of Ru). Rods 1 and 2 were analysed in quadruplicate and Rod 3 in duplicate.

Li, and Pt show increases from Rod 1 to Rod 3.

B, Al, Cu, Au values are substantially constant, low levels of Rh and Ru were found in all these analyses.

1.3 Metallography

SLIDES 14-16

The end of Rod 2 furthest from the spot weld exhibited microstructural variation from the norm, i.e. recovered grain structure, consistent for instance with temperatures of greater than 200°C having been generated for a short period. Rod 3 showed complete recrystallisation over a distance of approximately 4mm from the non-spot welded end, consistent with a temperature of >300°C having been generated. However, we do not know the total history of the rods after they passed out of our hands so we cannot independantly draw definite conclusions.

Vigorous filing and sawing of virgin and hydrogenated rods did not produce this recrystallisation phenomenon.

2. TEMPERATURE PROGRAMMED HYDROGEN ABSORPTION/ DESORPTION ON VARIOUS PD SAMPLES

2.1 Temperature Programmed Absorption/Desorption Technique

SLIDE 17

Hydrogen absorption and desorption is measured by monitoring changes in the exit hydrogen concentration of a 10% H_2 in N_2 stream passing over the sample at a slow rate (25ml/minute). The sample itself can be heated or cooled at a linear rate. The method allows for the measurement of very small amounts of hydrogen and the temperature at which it is absorbed (or reacted) and desorbed. Typically the temperature is cycled between ambient and 400°C at 5°C per minute, one complete cycle therefore lasting some three hours.

For samples which have been electrolytically charged the total hydrogen content, usually expressed as a H/Pd atomic ratio, and the temperature at which the hydrogen is desorbed can both be measured. The latter reflects the combined effects of changes in hydride structure, changes in the cleanliness and catalytic effectiveness of the surface, and the effects of changes in surface to volume ratio reflecting changes in physical dimensions. Changes in the results between successive cycles can reflect changes in the surface, i.e. reactivation, which can occur during the high temperature part of the desorption cycle.

Our rationale for making such measurements lies in our belief that the differences which seem to occur among different palladium samples should be related to their ability to trap hydrogen or deuterium under non-equilibrium conditions, particularly under conditions of incipient temperature increases.

2.2 Measurement of Palladium Hydride/Deuteride Decomposition/Formation

SLIDE 18

What then would one normally expect from such temperature programmed desorption and absorption measurements? SLIDE 18 shows typical literature data for the decomposition and formation of palladium deuteride and hydride at one atmosphere pressure as the temperature is changed. At the risk of belabouring the point, as the temperature of a loaded sample is increased, one might expect a rather sharp evolution of hydrogen or deuterium at a relatively low temperature, say below 100°C, as the β- hydride decomposes followed by a small loss as the temperature increases and the α-hydride decomposes. Cooling the sample should incur a hysteresis effect, absorption taking place at a lower temperature than the corresponding desorption. These temperatures should be lower for a deuterided sample than for one which has been hydrided. SLIDE 19 gives the Pd-H phase diagram.

SLIDE 20

Since the samples available were very different in geometry and surface condition, the magnitude of the peaks cannot be compared, but this technique does give an indication of the adsorption/desorption characteristics of the samples.

In fact the hydride decomposition of these massive electrode samples can be very difficult and in some cases the temperature rises close to the critical temperature (ca. 300°C) before decomposition occurs. SLIDE 20 shows the qualitative results for decomposition of six different samples of various surface to volume ratios. From this figure it is seen that for the palladium sponge and the palladium wire the results are very much what we might have expected from information on hydride formation shown in the previous figure, that is a sharp decomposition around 100°C. As we pass to the 2mm rod there is this marked shift in decomposition temperature with no evidence of any significant gas evolution at 100°C. One might expect that the difficulty that the gas would have in permeating to the surface might explain this observation at least in part. The results for the 4mm, 6.3mm and 8mm rods do not however seem to fit this simple explanation so some other factor(s) would seem to be involved.

You can imagine how very much we would like to find out what these are when I point out that the 2 and 4mm rods are from the original experiments in which excess heat was observed and that the 8mm rod sample was tested at the same time and apparently failed to generate excess heat. In other words there would seem to be a possible connection between the hydride stability as determined in this way and the heat generation under electrolytic conditions, in line with our original rationale.

SLIDE 21

One can get some indication of the effect of surface poisoning by repeating the absorption/desorption cycles as shown in SLIDE 21 for the same 4mm rod which we have just seen. Of course when re-hydriding in the absorption apparatus with the 10% H_2 for a relatively short time the hydrogen uptakes are much less, as shown. What is most striking is that a significant desorption spike is now seen at 100°C and that this increases substantially for the third cycle. The total amount desorbed also increases along with this increase in low temperature desorption but in both cases a second desorption peak at around 200°C is seen which seems to agree with the peak observed after electrolytic charging. This second peak seems to remain about the same size. It would seem to be significant that a sample of the same rod when processed in the hydrogen absorption apparatus and never exposed to an electrolyte or polarising current showed only a trace of a low temperature desorption spike, most of the desorption occurring in a broad peak centred on 225°C.

2.3 Comparison Between Re-hydriding Characteristics of Pd Electrolysed in 0.1M LiOH and 0.1M NaOH

SLIDE 22

One other interesting observation, another part of the mystery and possibly part of the solution is shown in SLIDE 22. This concerns part re-hydriding in the hydrogen absorption apparatus of two similar 6.3mm bar

samples hydrided electrolytically in 0.1M LiOH and 0.1M NaOH electrolytes respectively. The initial desorption results, one of which is shown in the previous slide, were identical as a broad peak with a maximum at 200°C. Upon cooling the samples in hydrogen the results shown in SLIDE 22 were obtained. These show similar hydrogen re-absorptions at elevated temperatures but a marked difference at the lower temperature at which the sample treated in LiOH absorbed hydrogen readily but that treated in NaOH did not; in fact, the pattern of the NaOH case was similar to that of an untreated rod. The low temperature absorption was matched by a corresponding low temperature desorption peak on the next desorption cycle.

Clearly the temperature programmed absorption measurements are showing large sample differences. Interpreting how these differences arise and in what way they can be manipulated to advantage is still very much an open question.

SLIDE 23

Conclusions for temperature programmed absorption/desorption.

3. ELECTROCHEMICAL MEASUREMENTS IN H_2O

3.1 Galvanostatic Charging of Pd electrodes

SLIDE 24

In order to establish whether there are major differences between 'Pd hydride' formed by electrolysis in LiOH and other alkali metal hydroxides, a series of galvanostatic charge/discharge experiments have been carried out on Pd foil and rod electrodes in LiOH, NaOH and KOH solutions. The charging process is highly sensitive to surface conditions in all of the electrolytes examined. In one experiment (LiOH, 60°C), which as yet we have been unable to reproduce, the overpotential during charging reached a maximum and then steadily declined and the electrode subsequently acted as an efficient hydrogen evolver.

The result obtained with LiOH electrolyte at 60°C could possibly be explained by the surface of the Pd electrode becoming progressively covered with Pt from the anode. The galvanostatic charging experiments carried out to date give (with one exception) similar results in the three electrolytes tested. However there is some tentative evidence to suggest that galvanostatic discharge is somewhat inhibited in the case of LiOH.

SLIDE 25

The "steady-state" voltammetry shows that Pd electrochemistry is sensitive to the nature of the alkali-metal cation present. The comparatively diminished reoxidation wave in the LiOH system is consistent with the galvanostatic discharge behaviour, i.e. some form of inhibition for the hydride dissolution reaction is present. However the possibility that a surface Pd-Li alloy is involved cannot be ruled out.

SLIDE 26

Pd electrochemistry is sensitive to the nature of the alkali-metal cation, Li shows comparatively anomalous behaviour.

SLIDE 27

Conclusions.

ACKNOWLEDGEMENTS

The authors thank members of the Analytical Department (JMTC) for the SEM EDAX, XPS, TOF SIMS and bulk analysis measurements. These include Drs P Whitehead, D R Hepburn, J A Busby and Mr M J Lovell.

SOME OBSERVATIONS RELATED TO THE PRESENCE OF HYDROGEN AND DEUTERIUM IN PALLADIUM

1. ANALYSIS OF FLEISCHMANN AND PONS RODS RETURNED FROM D_2O EXPERIMENTS.

2. TEMPERATURE PROGRAMMED HYDROGEN ABSORPTION/DESORPTION ON VARIOUS PALLADIUM SAMPLES.

3. ELECTROCHEMICAL EXPERIMENTS IN H_2O.

SLIDE 1

FLEISCHMANN AND PONS RODS ANALYSED AT JMTC

ROD 1

4 MM DIAMETER, 10CM LONG

AS RECEIVED CONDITION.

ROD 2

2 MM DIAMETER, 9CM LONG

USED AS CATHODE AT 64 MA/CM².

ROD 3

2 MM DIAMETER, 1.2CM LONG

USED AS CATHODE AT 512 MA/CM².

SLIDE 2

SURFACE ANALYSIS – SEM

INSTRUMENT USED - Cambridge Stereoscan 250 Mark II fitted with Princeton Gamma Tech (PGT) System 4 energy dispersive X-ray analyser. Instrument is capable of producing clear images up to a magnification of about x20,000 and can detect X-rays from sodium and elements with greater atomic number.

1. SURFACE FEATURES INCLUDE CRACKS AND SCRATCHES
   - INTENSITY OF FEATURES INCREASES FROM ROD 1 TO ROD 3.

2. NO SIGNIFICANT SURFACE CONTAMINATION IN ROD 1.

3. Fe, Cu, Pt, Zn DETECTED ON USED RODS.

SLIDE 3

SEM EDX ANALYSIS OF PALLADIUM RODS
Analysis for Copper

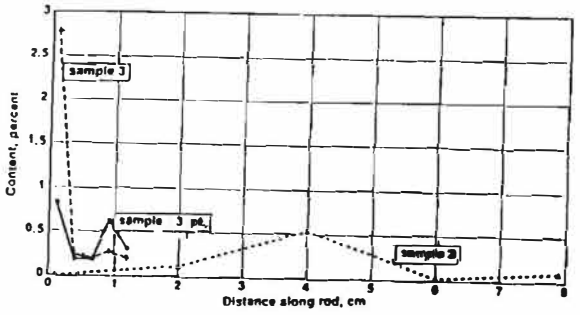

SLIDE 4

SEM EDX ANALYSIS OF PALLADIUM RODS
Analysis for Iron

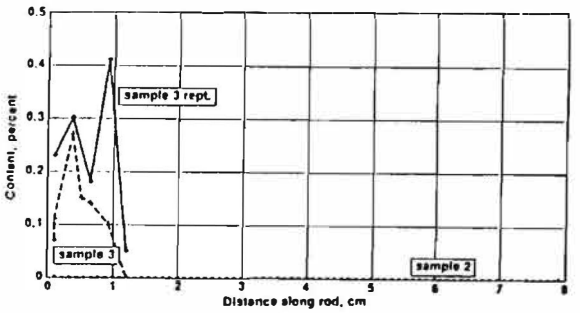

SLIDE 5

SEM EDX ANALYSIS OF PALLADIUM RODS
Analysis for Zinc

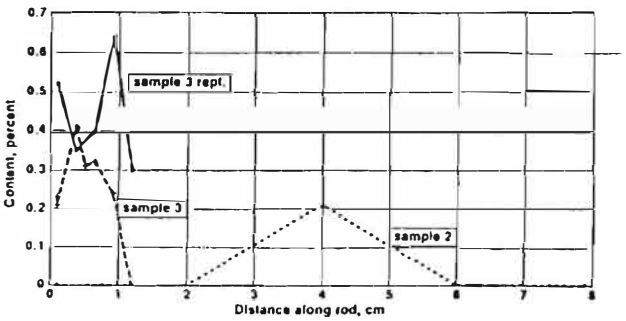

SLIDE 6

SEM EDX ANALYSIS OF PALLADIUM RODS
Analysis for Platinum

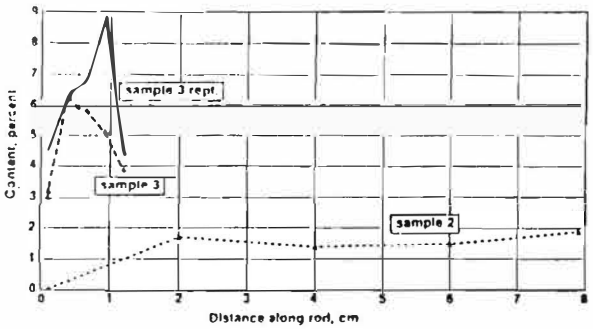

SLIDE 7

SURFACE ANALYSIS - TOF SIMS

INSTRUMENT USED - CAMBRIDGE MASS SPECTROMETRY TOF/SIMS

LITHIUM ISOTOPE RATIOS (%)

ISOTOPE	REPLICATE MEASUREMENTS			LITERATURE VALUES
6	4 0	4 8	4 7	7 5
7	96 0	95 3	95 3	92 5

SLIDE 10

SURFACE ANALYSIS - XPES

INSTRUMENT USED - Kratos XSAM 800 surface analyser using Mg K alpha radiation at 15kV and 10mA. The area analysed was 1.5mm square.

ROD 1 - Oxygen, nitrogen, chlorine, palladium
(Etching --> 100Å depth).

ROD 2 - Oxygen, sodium, silicon, platinum
(Etching --> 300Å depth).

ROD 3 - Oxygen, silicon, iron, sodium, platinum, zinc, copper
(Etching --> 1800Å depth).

SLIDE 8

SURFACE ANALYSIS - CONCLUSIONS

1. Pt DETECTED ON ELECTROLYSED RODS BY ALL TECHNIQUES USED.

2 O, Si, Fe, Na, Zn, Cu, Li, Cl ALSO DETECTED.

3. Pt, Cu, Fe AND Zn PRESENT AS METALS.

SLIDE 11

SURFACE ANALYSIS - TOF SIMS

INSTRUMENT USED.- CAMBRIDGE MASS SPECTROMETRY TOF/SIMS

PALLADIUM ISOTOPE RATIOS (%)

ISOTOPE	VIRGIN ROD No 1	USED ROD No 2	LITERATURE VALUES
102	1.28	1.31	0 92
104	11 58	11 50	10 43
105	22 96	23 77	22.33
106	28 00	28 39	27 23
108	25 25	23 90	26 70
110	10 91	11.10	12 36

SLIDE 9

BULK ANALYSIS - SPECTROGRAPHIC

Element	Ingot 1 ppm	Ingot 2 ppm
Al	5	10
B	20	20
Ca	30	30
Cr	2	3
Cu	10	10
Fe	10	10
Ni	1	1
Ag	1	1
Pt	10	10
Au	30	30

Mg and Si were detected at levels below 1 ppm.

SLIDE 12

BULK ANALYSIS – ICP MASS SPECTROMETRY

INSTRUMENT USED - VG Plasma Quad PQ2.

Element	ROD 1 ppm	ROD 2 ppm	ROD 3 ppm
Li	6	9	12
B	25	25	31
Al	7	8	9
Cu	13	14	15
Zn	< 1	< 1	6
Rh	1	1	2
Ru	0.4	0.4	0.3
Au	13	13	13
Pt	6	16	27
Pb	0.2	0.3	0.6

Elements not detected:
< 0.1 ppm Bi, Th, U, Te, Re, Hf, In.
< 0.2 ppm Hg, Tl, Os, Ir, Cs, Ba, Sb, Nb, Mo, Y, Sr, Rb, Mn, Co and all lanthanides.
< 1 ppm W, Te, Zr, Ga.
< 2 ppm Ni, Mg, Ti.
< 5 ppm Ge.
< 10 ppm Cr.
Not determined:- Cd, Ag, V, Na, Ca, Si, P, K, As, Fe, Se and halogens.

SLIDE 13

METALLOGRAPHY

RECOVERY AND RECRYSTALLATION OF THE ENDS ONLY OF RODS 2 AND 3 INDICATE LOCAL TEMPERATURES OF > 200°C AND > 350°C RESPECTIVELY.

NOTES

1 THIS PHENOMENON OBSERVED AT ENDS AWAY FROM SPOT WELD.

2 FILING OR SAWING DID NOT PRODUCE THIS KIND OF RECRYSTALLISATION IN HYDROGENATED OR UNHYRODGENATED RODS.

SLIDE 16

LONGITUDINAL SECTION FROM ROD 3 SHOWING AN ABRUPT CHANGE IN MICROSTRUCTURE INDICATIVE OF RECRYSTALLATION

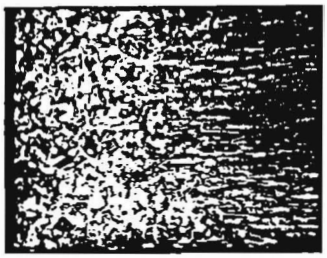

SLIDE 14

TEMPERATURE PROGRAMMED HYDROGEN ABSORPTION/DESORPTION APPARATUS

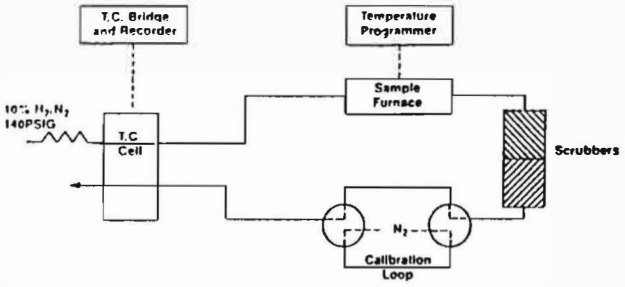

SLIDE 17

LONGITUDINAL SECTION OF END (BOTTOM) OF ROD 2 SHOWING A RECRYSTALLISED MICROSTRUCTURE

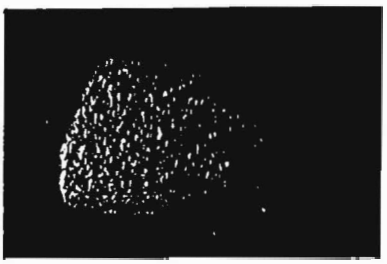

SLIDE 15

ABSORPTION/DESORPTION OF HYDROGEN OR DEUTERIUM AT ONE ATMOSPHERIC PRESSURE vs TEMPERATURE (SIEVERTS)

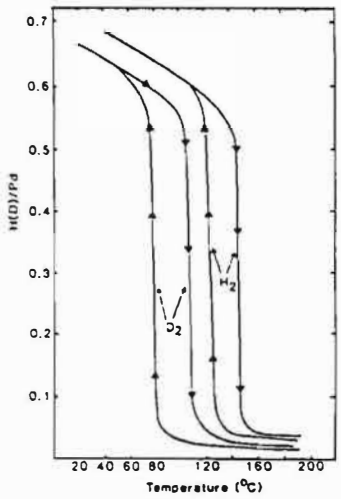

SLIDE 18

Pd - H PHASE DIAGRAM

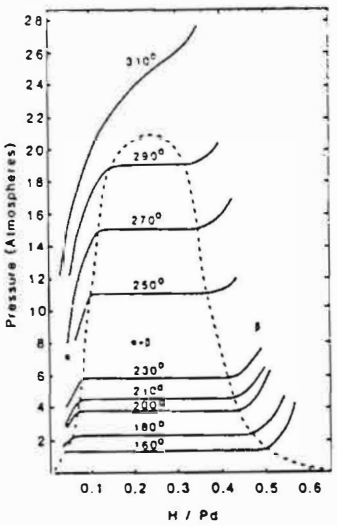

SLIDE 19

TEMPERATURE PROGRAMMED DESORPTION CURVES FOR VARIOUS Pd HYDRIDE/DEUTERIDE SAMPLES

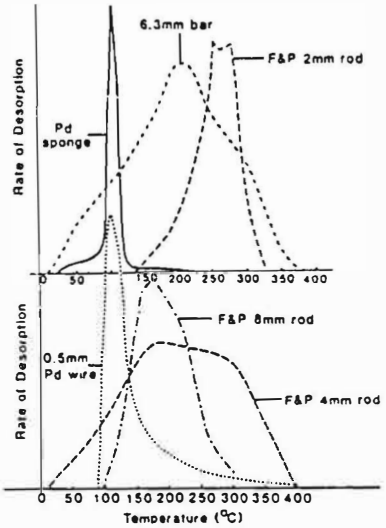

SLIDE 20

SEQUENTIAL TEMPERATURE PROGRAMMED DESORPTION ON HYDRIDED ROD 1

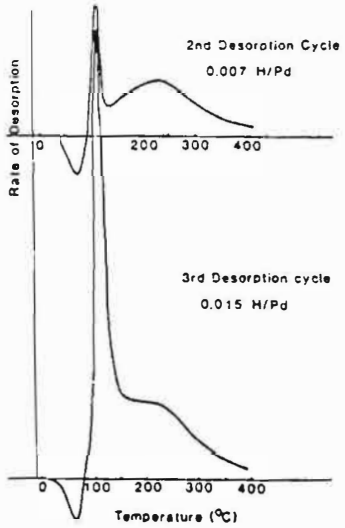

SLIDE 21

REHYDRIDING OF 6.3mm Pd BAR ELECTROLYSED IN 0.1M LiOH and 0.1M NaOH

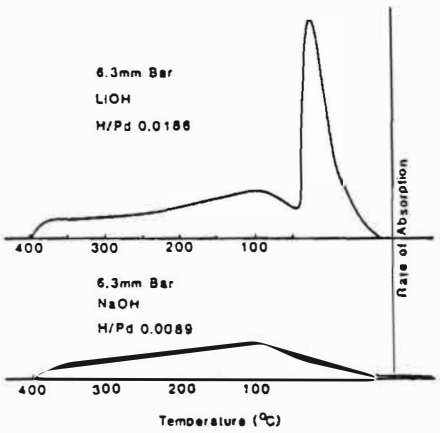

SLIDE 22

TEMPERATURE PROGRAMMED/ABSORPION/DESORPTION – CONCLUSIONS

1 Pd SPONGE AND Pd WIRE BEHAVE AS EXPECTED

2 Pd RODS GIVE RANGE OF RESULTS PROBABLY DEPENDANT TO SOME EXTENT ON SURFACE CONDITION OF Pd

3 ROD ELECTROLYSED IN LiOH ABSORBED HYDROGEN MORE READILY THAN SIMILAR ROD ELECTROLYSED IN NaOH.

SLIDE 23

GALVANOSTATIC CHARGING CURVES FOR 0.05cm THICK Pd FOIL in 0.1M LiOH AT 20° & 61°C.

J = 25mA/cm², SURFACE AREA ~ 0.9cm²

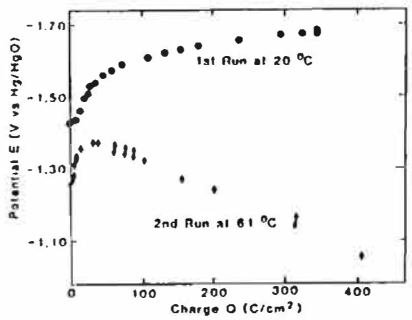

SLIDE 24

STEADY-STATE VOLTAMMOGRAMS FOR A Pd DISC ELECTRODE

(SURFACE AREA ~ 3.1x10⁻²cm²) IN a)0.1M LiOH, b)0.1M NaOH, c)0.1M KOH. 20°C, SWEEPRATE 30mV/s

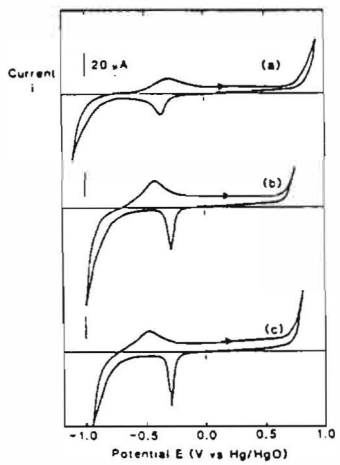

SLIDE 25

MEASUREMENTS IN H_2O – CONCLUSIONS

1 HYDROGEN EVOLUTION/DISSOLUTION IS SUBJECT TO SURFACE CONDITIONS ON Pd

2 SIMPLE EXPERIMENTS IN LIGHT WATER INDICATE THAT THERE ARE SIGNIFICANT DIFFERENCES IN THE ELECTROCHEMISTRY OF PALLADIUM IN LITHIUM HYDROXIDE COMPARED TO SODIUM AND POTASSIUM HYDROXIDE SOLUTIONS.

SLIDE 26

GENERAL CONCLUSIONS

1. A NUMBER OF ELEMENTS INCLUDING Pt AND Li ARE DEPOSITED ON Pd-CATHODE SURFACE DURING ELECTROLYSIS IN D_2O.
2. Li^6/Li^7 ISOTOPE RATIO SEEMS TO BE UNUSUALLY LOW BUT NO ORIGINAL REFERENCE IS CURRENTLY AVAILABLE.
3. RECOVERY AND RECRYSTALLISATION HAS BEEN OBSERVED IN RETURNED Pd RODS.
4. TEMPERATURE PROGRAMMED HYDROGEN ABSORPTION/ DESORPTION SEEMS TO BE A USEFUL TECHNIQUE FOR CHARACTERISING THE Pd ELECTRODES.
5. ELECTROCHEMICAL BEHAVIOUR OF A Pd ELECTRODE IN LiOH DIFFERS SIGNIFICANTLY FROM ITS PERFORMANCE IN NaOH AND KOH.

SLIDE 27

THREE DIMENSIONAL COMPUTER SIMULATION OF AN ISOPERIBOLIC CALORIMETER FOR COLD FUSION EXPERIMENTS

J. Chao, EPRI, W. Layman, EPRI, C.M. Kang, AET
T. Gur, M. Schreiber, R. Huggins, G. Lucier, J. Ferrante
Stanford University

ABSTRACT

The three dimensional heat conduction computer code HEATING5 was used to simulate the isoperibolic calorimeter being used for cold fusion experiments at Stanford University. The simulation results confirm the measured temperature distribution in the calorimeter. Computer analysis also demonstrates that temperature measurements for this particular calorimeter are independent of the heat source position in the calorimeter. A numerical procedure was developed to derive the transient behavior of the heat generation in the cold fusion cell from the transient temperature measurements. This procedure was exercised using a measured temperature pulse. The transient behavior of the power pulse was in the form of square-wave and its magnitude was slightly higher than the on-line calculation based on a steady-state approach.

INTRODUCTION

This paper describes the numerical simulation of heat generation and heat conduction in an isoperibolic calorimeter used for cold fusion experiments at Stanford University. An analytical procedure is developed for predicting the excess heat source from the temperature measurements. The objective of this work is to confirm the steady state and transient measurements by detailed computer simulation and thus to elucidate the observed phenomena.

ISOPERIBOLIC CALORIMETER

The isoperibolic calorimeter used in the experiment consists of two concentric aluminum cylinders, and an electrolysis cell which is housed in the inner cylinder. The gap between the two cylinder walls is filled with the aluminum oxide (Al_2O_3). Figure 1 illustrates the arrangement of materials and dimensions in the calorimeter.
The design principles of the isoperibolic calorimeter are:

- The temperature distribution is nearly uniform within the aluminum blocks,

- The aluminum oxide is a good insulator and a thick aluminum oxide insulation in the axial direction causes the heat to flow radially,

- The measurement of excess heat generation is based on the temperature difference between the two aluminum blocks,

- The measurement is independent of the location of the heat source.

Further details of the isoperibolic calorimeter are discussed in a separate paper presented in this conference.[1,2]

NUMERICAL SIMULATION

The simulation of heat transfer was performed by using the HEATING5 computer code. HEATING5 is a steady-state and/or transient heat conduction code in three dimensions including the Cartesian, cylindrical, and spherical coordinates. The thermal conductivity, density, and specific heat may be both spatially and temperature dependent. Heat generation rates may be dependent on time, temperature, and position. The boundary conditions may be specified for surface-to-boundary or surface-to-surface, and can be temperatures or any combination of prescribed heat flux, forced convection, natural convection, and radiation. The boundary condition parameters may be time and/or temperature dependent.

HEATING5 uses the finite difference scheme to discretize the heat balance equation in space time domains. The steady state problem may be solved by a direct matrix inversion method for one or two dimensional problems, or the point successive over-relaxation iterative method with a modified Aitken extrapolation process. The transient problem may be solved using the Crank-Nicholson method, the backwards Euler method, or an explicit method which is stable for a time step of any size (Levy's modified explicit method).

In order to estimate the heat source from the measurement, a separate numerical technique has been developed. We approximate the heat source in terms of discrete unit step functions in time,

$u_i(t)$, $i=1,\ldots,N$:

$$S(t) = \sum_{i}^{N} a_i u_i(t)$$

where

a_i = amplitude

$$u_i(t) = \begin{cases} 1 & t_i \le t < t_{i+1} \\ 0 & \text{otherwise} \end{cases}$$

Let $r_i(t)$ denote a response function representing the temperature difference between two aluminum blocks due to the unit heat source $u_i(t)$. For example, $r_i(t)$ can be determined by running HEATING5 for the given heat source $u_i(t)$.

If $T(t)$ is the measured temperature difference due to the heat source $S(t)$, then the heat source can be approximated by requiring that the integral of squared errors between the measurement and approximation is minimal with respect to variations of a_i, that is

$$\frac{\partial}{\partial a_j} \int \left[T(t) - \sum_{i}^{N} a_i r_i(t) \right]^2 dt = 0$$

These equations lead to a system of linear equations for a_i's, which can be solved to determine the unknown heat source.

RESULTS AND DISCUSSION

The isoperibolic calorimeter was modeled in two or three dimensions using HEATING5 for the purpose of the model calibration and heat source analyses of the measurements.

The temperature distribution within the two aluminum blocks at a steady state was computed by using HEATING5 and is shown in Figure 2. This result indicates that the temperature is quite uniform within the aluminum blocks.

Figure 3 compares temperature differences in aluminum blocks computed by using a

fixed temperature condition and a forced convection boundary condition on the surface of the colorimeter. In this analysis the transient was initiated by a stepwise increase of heat generation rate from 5 watts to 6 watts at time zero. It is shown in this figure that the temperature difference between two aluminum blocks is relatively insensitive to the type of boundary condition used.

Figure 4 compares the measured temperature difference against the simulation of the measurement using HEATING5. Measured heat sources were used in modeling this calibration experiment. The agreement between the measurement and simulation is shown to be quite good confirming the adequacy of the HEATING5 and modeling input parameters.

Next the transient data obtained from the isoperibolic calorimeter was analyzed to determine the heat source using the source discretization method discussed above. Figure 5 shows the heat generation obtained by an on-line calculation neglecting the time delay effect of heat conduction from the source to the instruments. The total heat generation (areas under the curves) are conserved in both curves. However, the time of heat generation and the magnitude of peak are different in the two cases due to the time lag and heat dissipation during the heat conduction through materials.

Finally, Figure 6 compares the temperature difference between measurement and HEATING5. In HEATING5 calculation, the predicted heat generation rate shown in Figure 5 was used as the heat source. A good agreement between the measurement and simulation is observed, which confirms the accuracy of the procedure for estimating heat source from the measurement.

CONCLUSION

The three dimensional heat conduction computer code HEATING5 was used to simulate the isoperibolic calorimeter being used for cold fusion experiments at Stanford University. The simulation results confirm the accuracy of the temperature measurements in the calorimeter. The Computer analysis also demonstrates that temperature measurements for this particular calorimeter are independent of heat source position in the calorimeter. The working principles of this type of calorimeter are verified by the computer simulation.

REFERENCES

1. Martha Schreiber, Turgut M. Gür, George Lucier, Joseph Ferrante, Jason Chao, and Robert Huggins, "Recent Measurements of Excess Energy Production in Electrochemical Cells Containing Heavy Water and Palladium," this volume.

2. Turgut M. Gür, Martha Schreiber, George Lucier, Joseph Ferrante, Jason Chao, and Robert Huggins, "Experimental Considerations in Electrochemical Isoperibolic Calorimety," this volume.

FIGURE 1

A Conduction Calorimeter

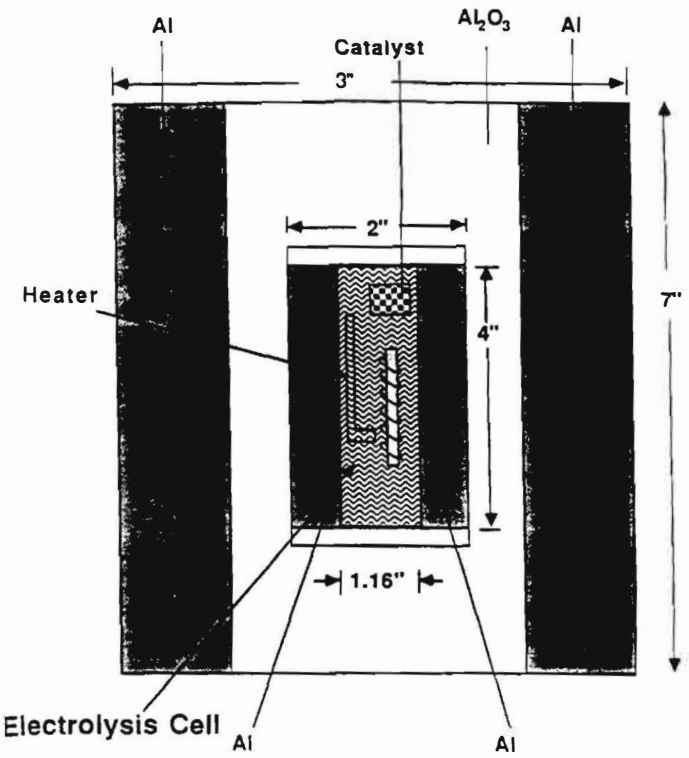

FIGURE 2

TEMPERATURE DISTRUTION

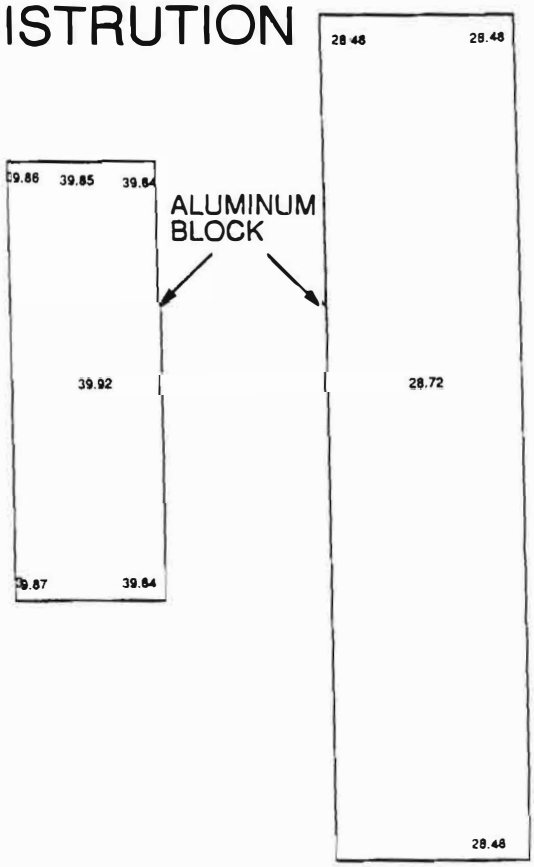

FIGURE 3

TEMPERATURE VS TIME

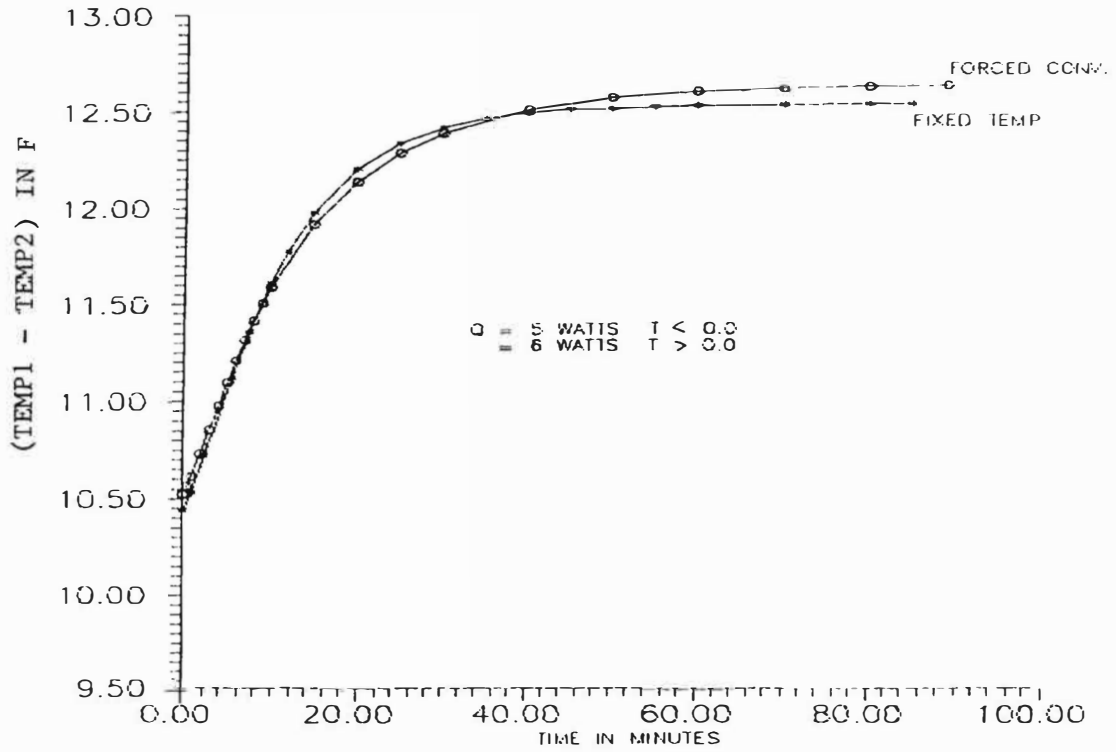

FIGURE 4

TEMPERATURE DIFFERENCE

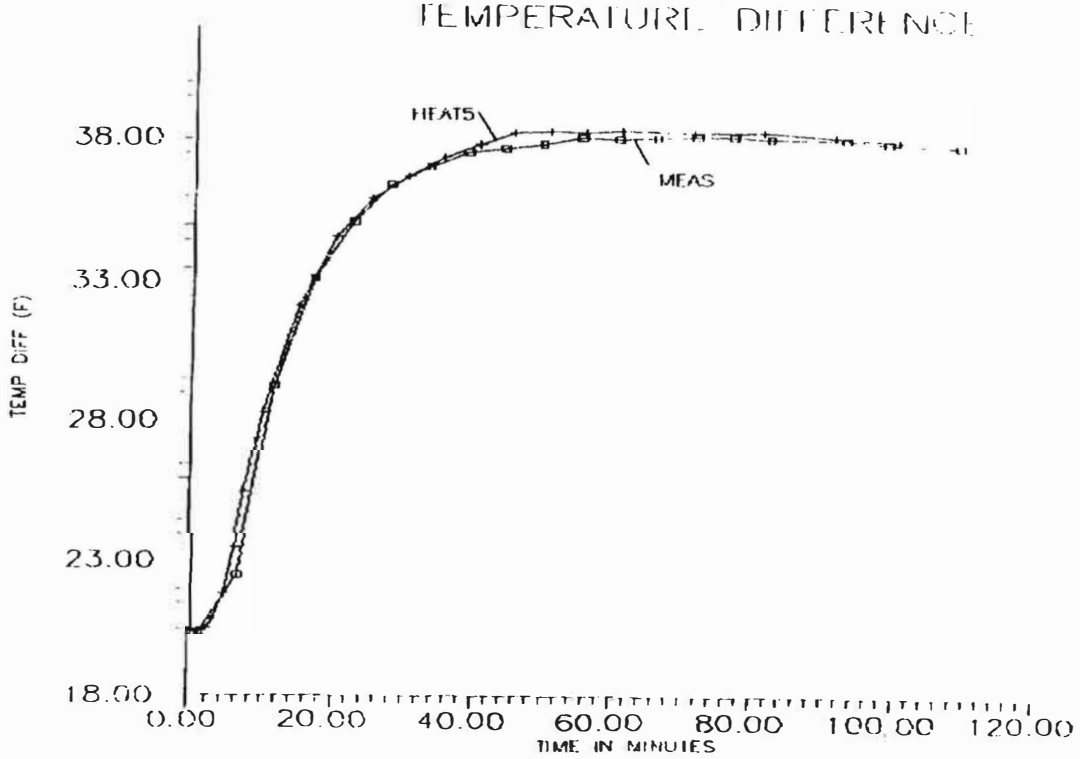

FIGURE 5

TRANSIENT DATA FROM AN ISOPERIBOLIC CALORIMETER

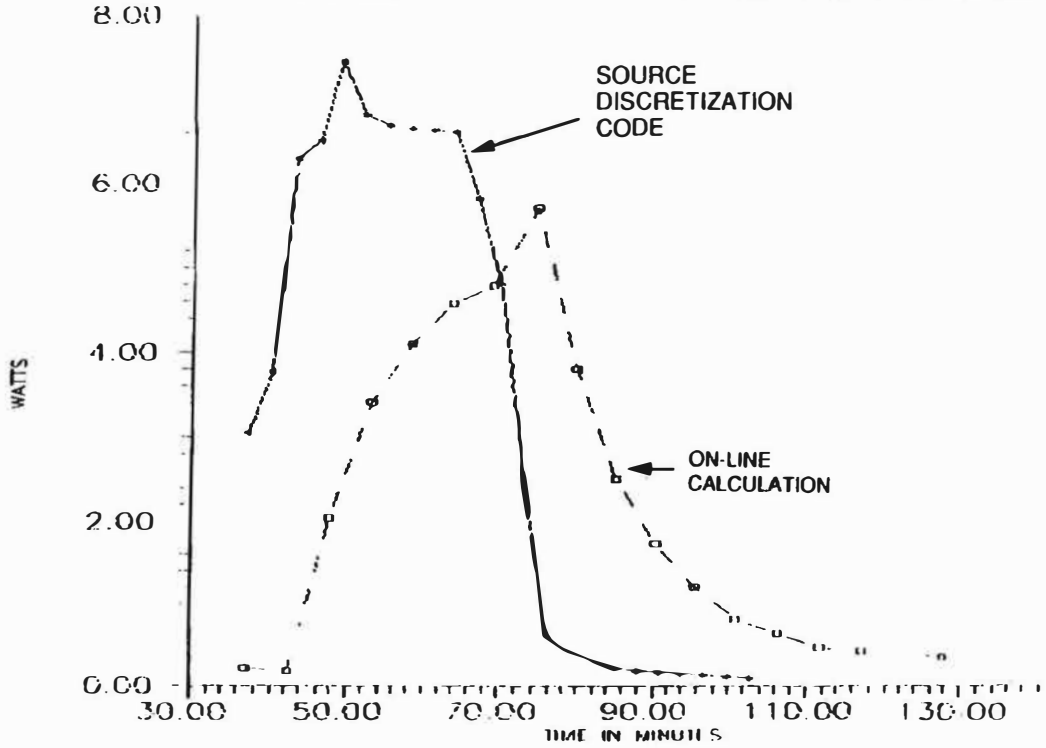

FIGURE 6

TRANSIENT DATA FROM AN ISOPERIBOLIC CALORIMETER

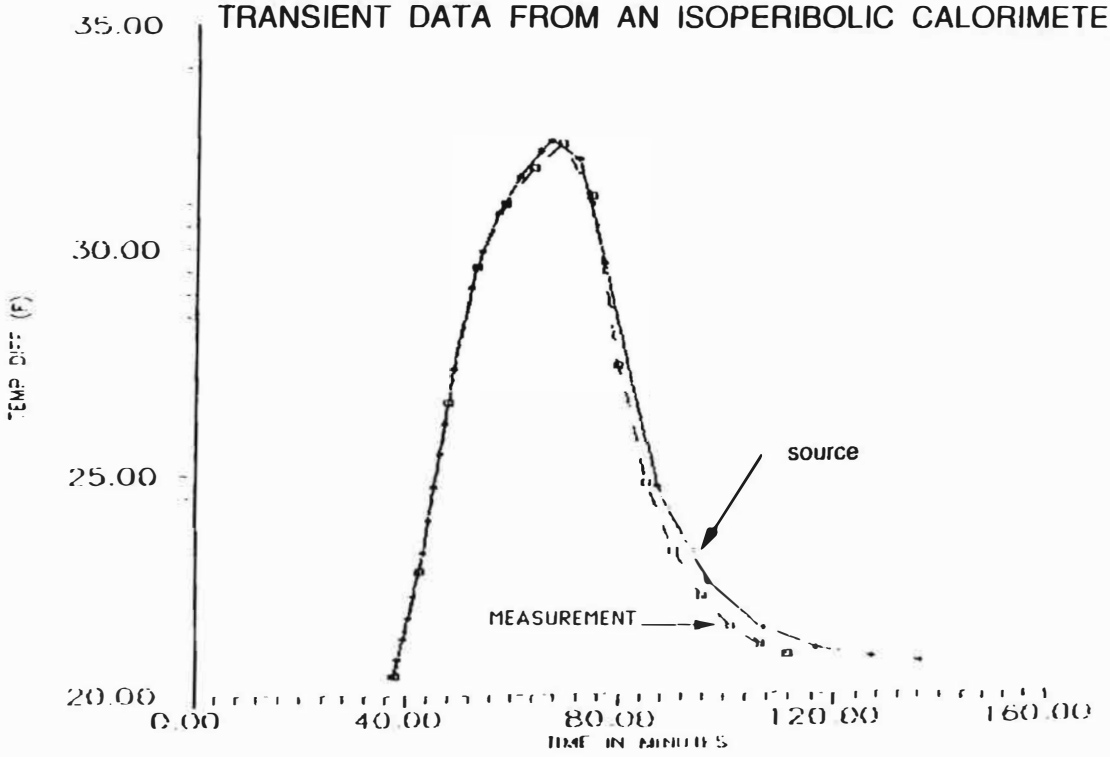

A more readable copy of this paper is here: http://lenr-canr.org/acrobat/GuruswamySmetallurgi.pdf

METALLURGICAL ASPECTS IN COLD FUSION EXPERIMENTS

SIVARAMAN GURUSWAMY and MILTON E. WADSWORTH

National Cold Fusion Institute, University of Utah

ABSTRACT

Deuterium loading of palladium cathodes in Pons-Fleischmann type electrolytic cells has been observed to result in generation of excess heat on several occasions. Metallurgical examination of some of the electrodes showed extensive damage associated with deuterium loading. Surfaces have been found to be covered with large number of impurities. Initiation and sustaining these heat bursts, monitoring of nuclear products and materials aspects of these electrolytic cells have been the focus of our current efforts. As D/Pd loading appear to be critical, the measurement of deuterium loading using dilatometry as a function of current density, surface and heat treatment of the cathode and poisoning are currently being investigated.

INTRODUCTION

High hydrogen gas fugacities or gas pressures at the cathode surfaces during aquous electrolysis is not new to electrochemists or metallurgists, but the idea of Pons and Fleischmann [1] that such electrochemically imposed pressures can be utilised to create conditions for fusion in the metal lattice was revolutionary. This appealing concept and the apparent simplicity of the experiment, resulted in the feverish international activity to replicate and as well as to provide explanations for their observations. Despite many negative claims, a significant number of laboratories report excess heat either at low continuous level or large short duration heat bursts [1-11], tritium at levels as high as 10^6 times the background [2,6,7,12,13], neutron bursts at levels of 10^{-8} times tritium level [6,7,12] and 3 MeV proton emissions [14] in electrolytic cells. These provide signals that nuclear processes may be occuring in these deuterated metals as suggested by Pons and Fleischmann. However there has been no consistent pattern in observations and the reproducibilty of experiments have been very poor. These may be attributed to the large number of metallurgical and electrochemical variables involved in these experiment as listed in Table 1.

Excited by the prospects of cold fusion and the key role metallurgists may play in this technolgy, an experimental program was initiated to determine metallurgical changes, structural integrity of the electrodes and possible alternate metals and alloys. After several weeks of charging 4 mm diameter Pd cathodes with deuterium by electrolysis in 0.1 M LiOD solution at high overvoltages, modest to large heat releases were observed. The deuterated electrodes have been examined for changes in metallurgical structure and surface chemistry. The extent of loading under typical electrolysis conditions has been determined using dilatometry and gravimetric techniques. Metallurgical factors influencing D/Pd loading, problems involved in measuring D/Pd ratio by various techniques are discussed. Current efforts are aimed at monitoring in-situ changes in the Pd electrode characteristics,

electrochemical conditions, preparation of Pd electrodes with controlled impurities and additives to enable a better understanding of processes occuring in these cells.

CELL CONFIGURATION AND OPERATION

Different designs of large cells used in our study are shown in figures 1 a,b & c. Large 4mm diameter x 10 cm long Pd rod cathodes and Pt windings or mesh or sheet supported by a glass rod cage anodes are used in these cells. Continuous heavy water addition to the cell is done using syringe pumps. The first cell design (Figure 1a) had one thermocouple to measure the cell temperature. To have redundancy in temperature measurement, three temperature sensors, one at the top, one at the middle and one at the bottom section of the cells, were used in the latter designs. Internal / external recombination of deuterium and oxygen from the electrolysis was done in most of our cells. The cells were operated mostly in a constant current mode. The cell operation is automated both in D_2O addition and data recording. Temperature, voltage, current and other signals are sampled every 10 seconds and recorded every 1 minute. When sudden changes in cell operating conditions were sensed, recording then occurs every 10 seconds. The temperatures inside the cell and the temperature of the bath in conjunction with calibration curves are used to measure the power output level. Bath temperature is maintained within 0.01°C. Thermal calibration is done by performing electrolysis at different power levels as well as by using an internal heater. Laser Doppler measurement of bubble velocities in the cell (Figure 1d) showed excellent stirring by the evolved gas bubbles resulting in very uniform temperature distribution, within 1 °C over most regions of the cell. Flow patterns in the cell were studied by measuring velocities of the gas bubbles using a Laser. Lithium concentration, electrolyte conductivity and pH are monitored periodically. Li concentration is measured using DCP analysis. The cathode metals tested were palladium, titanium and zirconium. However most of the attention was focussed on palladium. Platinum and nickel wire, gauze and sheets have been used as anodes. The experimental variables tested included the form of the platinum anode, anode to cathode surface area, anode to cathode distance, separation of deuterium and oxygen using a Nafion membrane that allows deuterium ion to pass through but not the anion, preloading of deuterium under high pressure deuterium gas, and variation in the heat and surface treatment of the palladium cathode.

TEMPERATURE EXCURSIONS SHOWING EXCESS POWER GENERATION

During the first week of May, 1989, frequent explosive popping of the cells (Figure 2a) were observed, some with minimal damage and some with the destruction of the assembly. The temperature excursions were associated with some of these events which were initially dismissed as being due to deuterium and oxygen recombination. Again in the third week of May, a large temperature excursion of about 12°C was observed, the cell temperature rise lasting about 90 minutes (Figure 2a). The temperature-time profiles showed a similar pattern to an earlier temperature excursion (Figure 2b). This particular cell was operating at constant current mode at current setting of 0.95 amperes during the heat excursion shown in Figure 2a. The voltage was recorded continuously while the current was manually recorded. The temperature excursion was interrupted by the make up D_2O addition. During the burst shown in Figure 2b, the cell was being operated in a constant voltage mode and the voltage and current readings

were manually recorded. Explosive popping of the cell interrupted the large heat burst and dislodged the electrodes. The cell was put back together immediately and the cell temperature remained at a level well above the normal values corresponding to the gross power input to the cell (about 9.6 Watts). Thermal calibration curves showed that excess heat generated during these two events were about 240,000 Joules during the 91 minute burst and around 1 MJ during the 40 minute burst followed by a 30 hour excess heat generation at a lower level. During the bursts the power outputs were as high as 6-7 times the input power which was less than 10 Watts. This level of energy output could not be explained by burning of all the deuterium stored in the Pd cathode, the heat of solution of deuterium in palladium, or the heat of formation of PdD_x. We also checked the possibility of storing energy in the solution in the form of peroxide. Analysis of electrolyte samples from all the operating cells showed peroxide concentration was less than 10^{-4} moles/cm^3 as expected from the instability of peroxide under high cathodic overvoltage conditions. The tritium level in the electrolyte after degassing of the electrode that showed the 90 minute heat burst and the starting solutions were checked by 3 different laboratories. The level of tritium was found to have increased by a factor of 3-4 which is more than can be accounted for by separation during electrolysis. The electrode (JM 2) involved in the above two large heat bursts was the same and had been obtained from Johnson Mathey and had a purity of 99.95%. The heat treatment involved annealing at at 600 °C in ultra high purity argon atmosphere. Figures 2c and 2d show two consecutive bursts in a same cell using a high purity Pd rod, (Electrode #5), from Metalor, USA. In all the above heat excursions cell design shown in figure 1a had been used. Single thermocouple was used to monitor the cell temperatures.

Figure 2e shows operating cell data for Cell 9 (Figure 1b). Each point corresponds to an average temeprature and power input data for a period during which the cell was operated at a given current level. During a period when the cell was operated at a current level of 2.0 Amperes, the temperature of the cell was about 1.8°C (about 7.6 excess Watts) above the expected value suggesting excess power production during this period. No excess tritium was seen in this cell. On 11 different occasions, we have seen events which seem to have genearted excess heat.

Our earlier cells were designed to use large cathodes to provide enough material for subsequent metallurgical characterisation and therefore limited to detect only large excess heats. But these cells had rapid thermal response times of about 90 seconds. Our recent cell design with an external acrylic jacket (Figure 1c) has a cell constant of about 0.5 W/°C and a nearly linear response. Excess power of the order of 200 -300 mW can be detected in these new cells. The relaxation time is less than 10 minutes and the size of the electrode / maximum power input to the cells is lower.

METALLURGICAL EXAMINATION OF ELECTRODES THAT SHOWED HEAT BURSTS

BULK ANALYSIS

A single palladium electrode has shown heat bursts illustrated in Figures 2a and 2b. This electrode was degassed and the electrolyte was sent for tritium analysis. The electrode was cleaned with distilled water and dried. Resistance measurement by four probe technique showed a two fold increase in resistivity. The electrode was then examined by positron annihilation technique.

The Doppler line broadening of the electron-positron annihilation

peak at 512 KeV showed a 6% change in the Peak/Width ratio which is rather large indicative of a large increase in defect density. The surface hardness along the length was first measured using a Vickers indentor at 1 kg load. Soft and hard spots at adjacent locations were observed. This is likely to be due to subsurface cracks and to hardness measurements on a curved surface. Smaller lengths of the electrode were cut from the lower half of the electrode and hardness measurements were made on the cut section. The hardness values obtained were very uniform showing values of 102 +5 VHN. The hardness value for this material before the cell exposure was 69 VHN.

While the above electrode JM2 did not show visual cracking, another electrode from the same batch showed after more than 11 months of operation showed a high density of visual cracks on the surface. A 99.995 purity Pd rod from a different source deuterated for nearly 11 months showed extensive visual damage as shown in Figure 3. The surface contains a high density of fine cracks. Hardness measurements on the cross section show wide variation from 110 VHN to 180 VHN due to extensive microcracking in the sample. The optical microscopy image of the cross section shows extensive cracking and surface relief associated with sursurface cracks. Extensive cracking was also observed in electrode 17 which is a 0.5 mm wire subjected to current densities from 1000 - 3000 mA/ cm^2 over a period of about 3 months.

TRANSMISSION ELECTRON MICROSCOPY

Thin slices cut from electrode JM2 were mechanically polished and then electro-chemically thinned for observation of the internal structure. The diffraction pattern confirmed the presence of β hydride phase which is a metastable phase. The electrode after the cell operation, showed extensive deformation and much larger dislocation density compared to the annealed starting material as can be seen from Figures 4 a & b. The damage observed may be due to large strain associated with β hydride phase formation and/or the deformation resulting from high pressure hydrogen bubbles. In the future it will be very important to make a comparison of the internal damage for identical rods, one of which has experienced excess heat generation.

Figure 4c shows a TEM micrograph of electrode 5 after about 11 months of electrolysis. Specimen preparation of this sample was particularly difficult and image is less clear due to extensive strain, high dislocation density and microcracks.

X-RAY DIFFRACTION

An X-ray diffraction pattern showed that the major phase was β hydride. Only minor amounts of α phase were observed. The D/Pd ratio in the sample was estimated to be around 0.7.

SURFACE ANALYSIS

Surface chemical analysis was done using diffrent techniques. A quick examination of the near surface region was performed using the state of the art CAMECA 50 SX electron microprobe. This showed only palladium with trace amounts of Rh and Br. Possible rhodium contamination from the platinum anode is possible. Sampling volume in this technique is 1 μm^3 and light elements below carbon and trace elements may not be detected by this technique. XPS, Auger electron spectroscopy and SIMS analysis were performed at the Battelle Nothwest laboratories. Perkin-Elmer Physical Electronics 550 multiprobe surface analysis system was used. AES analysis was done using 5 kV electron beam. XPS data was generated using Mg K_α X-rays. The SIMS analysis was performed using a

5 KV Ar ion beam to detect trace impurities. The quantitative estimates of different elements present in the first few nanometers of the surface region using XPS and Auger analysis are shown in Tables 2 and 3. Both XPS and AES data shows that the surface is highly contaminated with O and C contaminants that come from handling. Other minor contaminants are expected, except probably Co, from the electrolyte, anode, quartz glass vessel or from handling. SIMS profile over a depth of about 600 nm is shown in Figure 5 (sputtering rate of about 6 nm/mt) and Li signal amplitudes at different depths ratioed to Pd signal are summarised in Table 4. High surface enrichment of Li and a surprisingly very small amount of Pd. Surface is covered with elements such as Al^{27}, Na^{23}, Li^{7}, Ca^{40}, Fe^{56}, Li^{6}, C^{12}, Pd^{106} and Cd^{113}. Of these Cd is an impurity that was unexpected.

EPMA on the electrode 5 surface and cross section showed no extensive contamination and predominantly Pd. The near surface composition examination by SIMS and Auger is currently underway. EPMA on electrode 17, a 0.5 mm wire, run at extremely high current densities of greater than 3000 mA/cm^2 shows extensive Pt transfer from anode to cathode. Pt concentration on the surface observed range from 30-40% with the remainder being predominantly Pd.

BULK ISOTOPIC ANALYSIS

SIMS analysis of the palladium cathode JM2 and a reference pure palladium sample were analysed using a primary beam of 10.5 keV O_2^+ and positive spectrometry. Small deviations of isotopic abundance compared to pure Pd reference is noted but considered not significant.

ROOM TEMPERATURE MASS SPECTROMETRY

H, H_2, HD and D_2 were found but no evidence of He^4 was found.

SCANNING ELECTRON MICROSCOPY

Scanning electron microscopy on the electrode JM2 showed half the surface covered with pits. Whether it was present prior to testing is not known. Pits were covered with a thin oxide layer. Evidence of S and Ca on the surface were found. Grain boundaries were deeply etched but no apparent composition difference across the boundary was observed. Electrode 5 as mentioned earlier, showed extensive micro and macro cracks.

DIFFERENTIAL SCANNING CALORIMETRY OF DEUTERATED CATHODES

DSC was done on small pieces of electrode 5 and electrode 17 in an argon atmosphere at a scannning rate of 10 °/minute. Figures 6 show the DSC data for electrode 5. The initial endothermic peak corresponds to D desorption. The amount of D desorbed is small indicating that in this extensively cracked electrode the bulk of the deuterium had already desorbed prior to the DSC run. The exothermic peaks around 350°C from points 2-4 correspond to recovery and recrystallization processes.

DETERMINATION OF D/Pd RATIO

Monitoring the D/Pd ratio may be done by measuring the resistivity change, dilation, shift in rest potential,or gravimetry. All methods have certain drawbacks, making estimation of D/Pd ratio difficult. Most of these measurements are most likely to overestimate the measured D/Pd ratio when there is cracking or deformation and any data presented must be used with caution. While gravimetry is direct, insitu measurement is difficult due to bubble evolution, and density change due to internal cracks. Defects introduced during charging can influence resistivity values. Cracks or fissures and plastic deformation can influence D/Pd estimation. In-situ dilatometry was adopted in this work for

the D/Pd ratio estimation because of the relative ease of the technique. Use of intermittent diameter measurements and gravimetry to correlate dilation to D/Pd ratio allows reasonable prediction of D/Pd ratio. Errors due to internal and external cracks and bending of the rods can introduce errors. However, this technique allows one to evaluate effects of different variables such as poisons, current density, surface treatments and microstructure on the D uptake of the electrode with realtive ease. Figure 7 shows the length change as a function of charging time of 99.995 Pd cathode with no surface treatments at a current density of 100 mA/cm^2 in a 0.1 molar LiOD. In about 4-5 days, a plateau in the loading versus time curve was reached. Weight and diametral measurements of the electrode were done immediately after the electrolysis was stopped and were used in conjunction with the axial dilation value to determine the D/Pd laoding. Loading beyond a D/Pd ratio of 0.93 has been observed using 100 mA/cm^2 current density in LiOD. Higher loadings may be possible with increase in current density, lower temperatures, change electrolyte pH or with the addition of poisons. Figure 7 shows change in dilation in an annealed Pd rod initially at a current density of 100 mA/cm^2, then increased to 200 mA/cm^2, then with the addition of arsenic poison in the form of arsenate to the electrolyte, the power switch off and finally anodic discharge. The original length is not regained after the entire cycle. Change due to increase in current density is small and includes the small length change due to change in cell temperature. Addition of the poison did not have much effect. Turning the power off results in a rapid length change in the first two hours. In another experiment, even after several weeks, we find no change in length until the anodic discharge is done, indicating the metastable nature of the deuteride. These studies are continuing at the present time.

The hydrogen pressures vary exponentially with overvoltage (deviation from the equilibrium voltage at which the forward and reverse rates for this reaction are equal) and astronomical pressures can exist at the cathode/electrolyte interface. Such high surface pressures and favorable surface conditions can increase the uptake of D or H in the metal. D atoms absorbed into the metal occupy octahedral sites, first forming the random solid solution and at higher pressures forming an ordered β phase. The β phase can reach stoichiometry at high pressures such as that obtained during electrolysis at high overvoltages. In this PdD_x interstitial metallic alloy, deuterium has a metallic behavior. This hydride phase has metallic character and D in PdD is considered an deuteron. No clear picture of the behavior of the stoichiometry phase exists at this time. The hydrogen /deuterium loading level in Pons-Fleischmann type cells is much larger than that normally encountered in electroplating, hydrogen storage or conventional metals processing situations. Even in those conventional levels of H or D in metals, understanding of the behavior of H or D is still far from complete.

NUCLEAR RADIATON MONITORING

The nuclear monitoring capabilities of the Physics group at NCFI include (a) A 4" x 8" diameter sodium iodide crystal with associated electronics giving the capability of sensitive measurements of all gamma rays with energies in the range 0.5 MeV to 25 MeV, (b) A HP Ge detector with associated power supplies, amplifiers and multi-channel analyzer, giving the capability of giving high resolution measurement of gamma rays in the range from 5 keV to 10 MeV. This system complements the sodium iodide detector, having a lower efficiency

and a higher resolution, (c) A Si(Li) detector with the capability of measuring x-rays with energies between 1 keV and 60 keV and (d) A neutron spectrometer with large-area cosmic-ray veto counters to make low-level neutron study possible. Beckman scintillation unit capable of automatic measurement of several hundred samples per day is used for routine tritium monitoring of the cells.

REPRODUCIBITY AND FUTURE OF COLD FUSION RESEARCH

Table 1 lists the different variables that we currently feel are involved in these experiments. Questions about the electrode material, probable involvement of a third element in the nuclear process, contaminants from the electrolyte or cell wall that may be influence the surface reaction are currently being asked and are being examined.

Palladium rods during routine casting and drawing are likely to pick up carbon from the molds of the extrusion die. Also trace amounts of O,N, and H are likely to be picked up during fabrication and handling. The levels of these interstitial impurities is likely to be different in electrodes used by different investigators. All these interstitials will compete for the octahedral sites and will reduce the maximum Pd/D ratio. Also these elements may likely block potential defect sites that may be involved as they normally segregate to these defect sites. Unique atomic configurations are possible at special grain boundaries which may likely assist the D-D fusion in the palladium lattice.

Other critical variables include critical loading ratios of deuterium/Pd, surface chemistry of the palladium electrode, the electrolyte composition, temperature, role of lithium, role of deuterium recombination poisons, and rapid variations in operating conditions such as current density required to initiate the heat bursts.

This large number of variables require statistically large numbers of experiments to isolate the conditions under which fusion at room temperature may occur. The fact that a significant but a small number of well established research groups have been able to reproduce some aspects of this effect, requires that research in cold fusion continue on a larger accelerated scale. Currently work is in progress to systematically examine some of the key metallurgical and electrochemical variables.

ACKNOWLEDGEMENTS

Many graduate students and faculty have contibuted to this work in particular Prof. J.G. Byrne, Prof. Rajamani, Dr. John Peterson, Jun Li, Ilesh Shah, H. Hwang, Narendran Karattup, Jose Hevia and Jim Noland and their contribution is gratefully acknowledged. We are thankful to Dr. John Morrey of Battelle Northwest Laboratories, for the help with surface analytical work. We are also thankful to the Physics group at NCFI for their help with nuclear radiation monitoring.

REFERENCES

[1] M. Fleischmann, S. Pons, and M. Hawkins, J. Electroanal. Chem., 261 (1989) 301.

[2] R.C. Kainthla, O. Velev, N.J.C. Packham, L. Kaba, and J.'O.M. Bockris, Proc. of NSF/EPRI conf. on Cold Fusion, Washington, D.C., October, 1989.

[3] S. Srinivasan and A.J. Appleby, Proc. of NSF/EPRI conference on Cold Fusion, Washington, D.C., October, 1989.

[4] M. Mckubre, Proc. of NSF/EPRI

Conf. on Cold Fusion, Washington, D.C., October, 1989.

[5] A. Azdic, D. Gervasio, I. Bae, B. Cahan and E. Yeager, Personal Communication, Feb., 1990.

[6] P.K. Iyengar, Fifth Intl. Conf. on Emerging nuclear Systems, Karlsruhe, FRG, July, 1989.

[7] Government of India, Atomic Energy Commision Report BARC-1500, P.K. Iyengar and M. Srinivasan, Eds., Dec, 1989.

[8] A. Belzner, U. Bischler, S. Crouch-Baker, T. Gur, G. Lucier, M. Schreiber and R. Huggins, Proc. of Workshop on Cold Fusion Phenomenon, Santa Fe, New Mexico, May 1989.

[9] C.D. Scott, J.E. Mrochek, E.Newman, T.C. Scott, G.E. Michaels and M. Petek, DOE Report ORNL/TM-11322, November, 1989.

[10] D. Hutchinson, Personal Communication, Feb., 1990.

[11] R.A. Oriani, J.C. Nelson, S.K. Lee and J.H. Broadhurst, Submitted to Nature (1989).

[12] K. Wolf, D.E. Lawson, J.C. Wass and N.J.C. Packham, Proc. of the NSF/EPRI Conf. on Cold Fusion, Washington, D.C., October, 1989.

[13] E. Storms and C. Talcott, J. Fusion Tech., in Press (1990).

[14] R. Taniguchi, T. Yamamoto, and S. Irie, Jap. J. Appl. Phy., 28 (1989) 2021.

Table 1. Some of the known variables involved in electrolytic cold fusion experiments.

1. EXPERIMENTAL CONDITIONS
   - CURRENT DENSITY
   - TEMPERATURE
   - ELECTROLYTE COMPOSITION
   - POISONS IN ELECTROLYTE
   - NEED FOR INITIATION (ELECTRICAL, MAGNETIC, THERMAL or ULTRASONIC SHOCK)
   - H, CO_2 PICK UP
   - CELL DESIGN

2. ELECTRODE PURITY
   - SUBSTITUTIONAL IMPURITIES
     - PRIMARY Pd (Cu, Ni, Fe, Zr, Te, As, Sb, Cd, Mg, Ca, Li...)
     - RECYCLED Pd (LARGE NO. OF ALLOYING ELEMENTS)
   - INTERSTITIAL IMPURITIES
     - PICKED UP DURING PROCESSING & HANDLING (C, O, N, H)

3. IMPURITIES IN ELECTROLYTE
   - IMPURITIES FROM PROCESSING & HANDLING (C, S, Cu, Zr ...)

4. ELECTRODE MICROSTRUCTURE
   - GRAIN SIZE, DISLOCATION DENSITY & DISTRIBUTION

5. POSSIBLE ROLE OF A THIRD ELEMENT IN THE NUCLEAR REACTION

6. CELL DESIGN: ELECTRODE GEOMETRY, ELECTRODE SPACING, ETC.

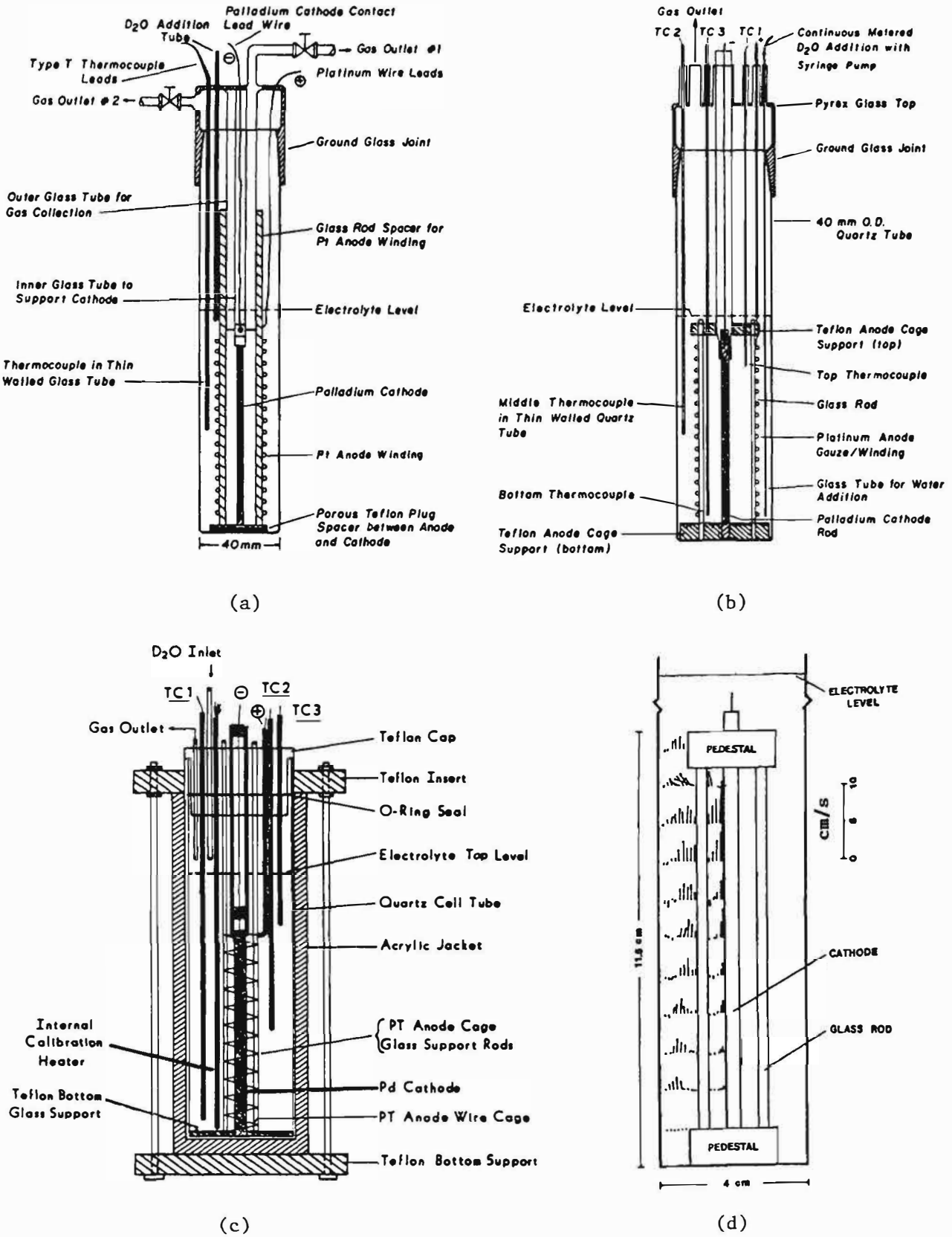

Figure 1. (a,b & c) Different electrolytic cell configurations used and (d) Laser Doppler measurement of gas bubble velocities in the electrolyte under typical operating conditions of cell 1a.

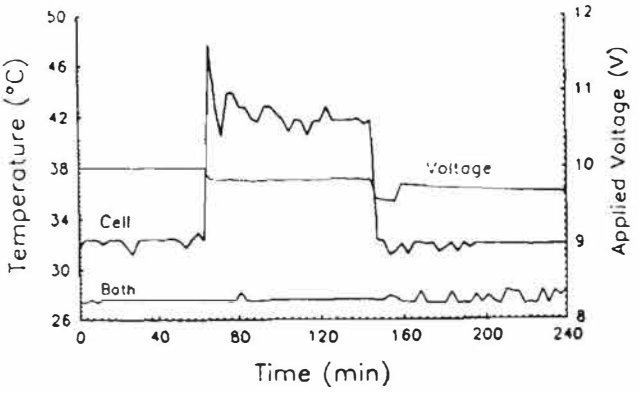

(a)

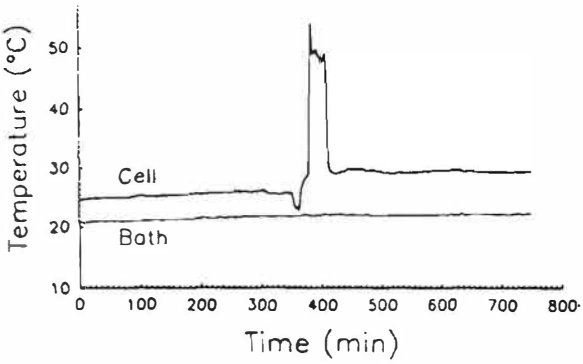

(b)

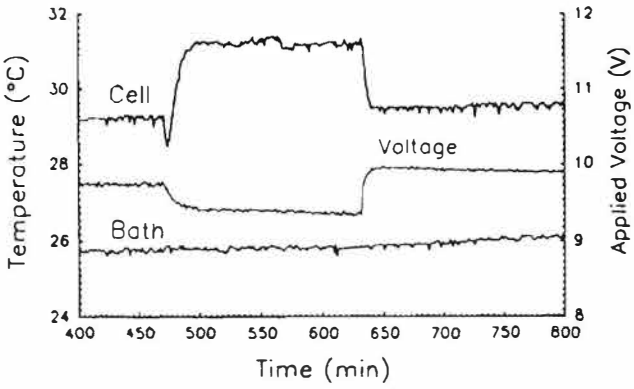

(c)

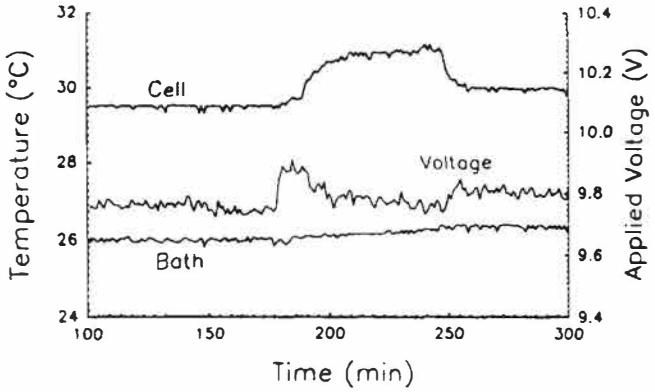

(d)

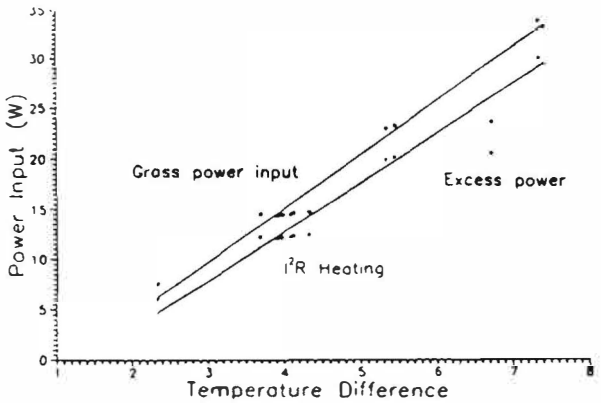

(e)

Figure 2. Temperature excursions observed during electrolytic D loading of Pd cathode. (a and b) Cell 3, cathode JM2; (c&d) Cell 5, cathode PD5; and (e) Cell 9, cathode JM1.

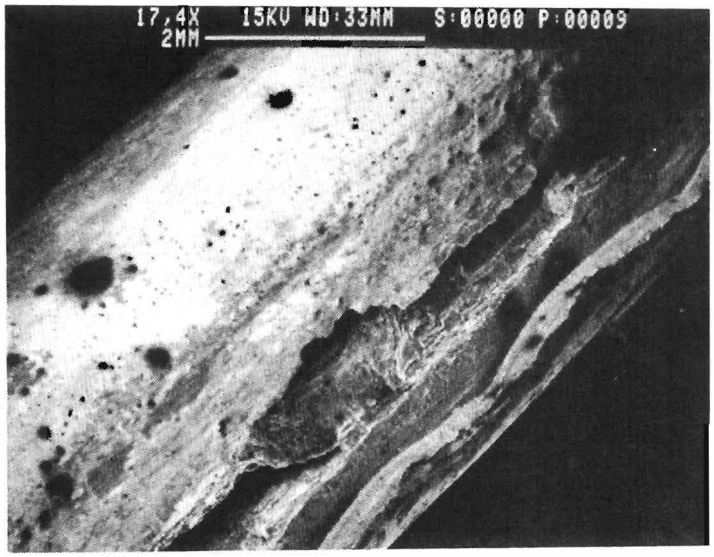

(a)

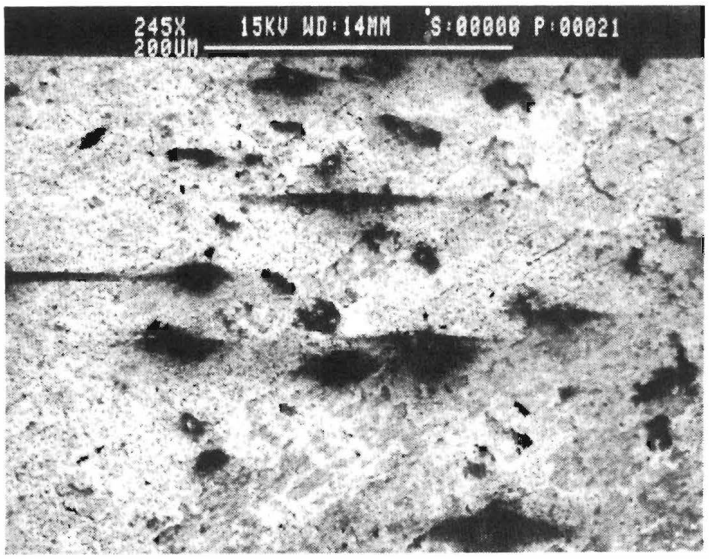

(b)

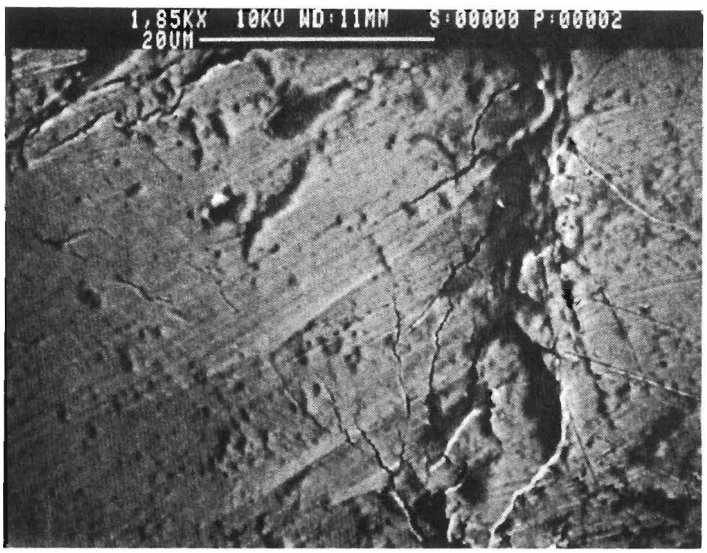

(c)

Figure 3. Scanning electron micrographs showing extensive cracking in palladium cathode 5 after 11 months of D charging. (a&b) Surface region; and (c) interior region of the cathode.

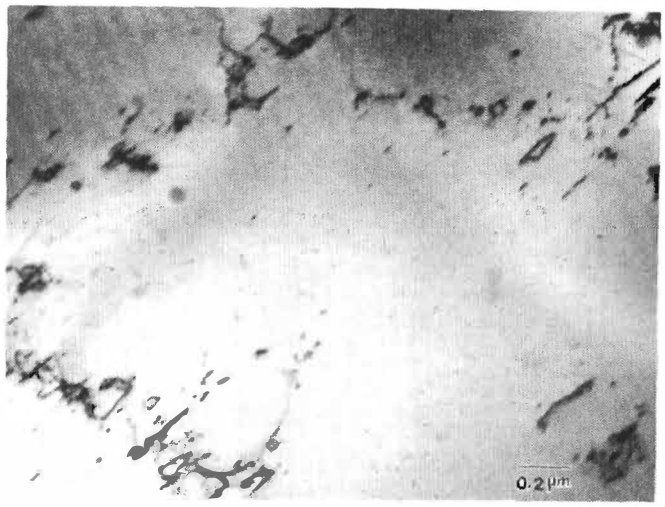

(a)

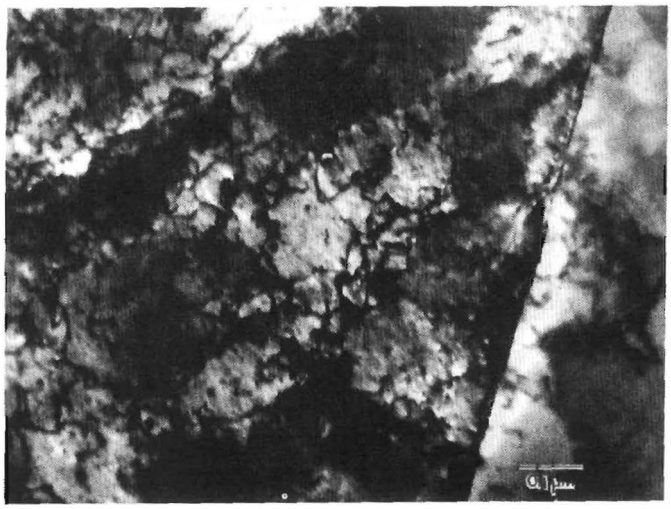

(b)

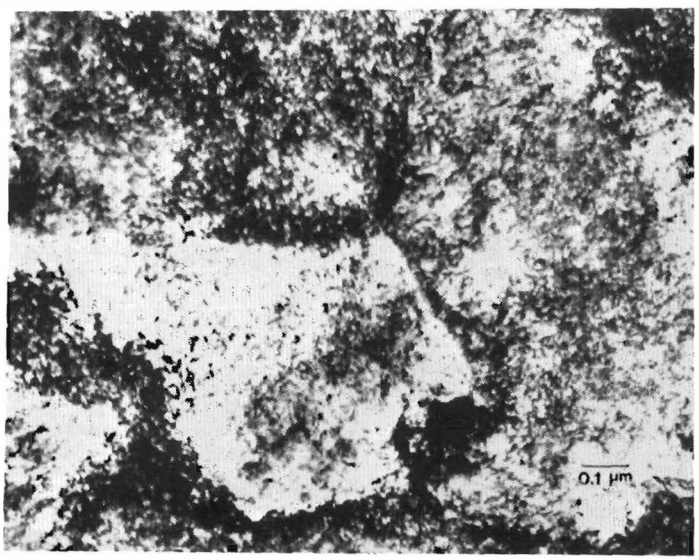

(c)

Figure 4. TEM micrographs of palladium cathodes. (a) After annealing at 600°C for 1 hour (Electrode JM2); (b) after deuterium loading for 3 weeks (Electrode JM2); and (c) after 11 months of deuterium loading (Electrode 5).

Table 2. AES analysis of the near surface region of Pd cathode JM2 after the heat burst shown in figure 2a.

ELEMENT	SIGNAL	SENS. FACTOR	AT%
Si	0.45	0.25	6.71
S	0.40	0.75	1.83
Cl	0.59	1.00	2.02
C	2.14	0.14	52.37
Pd	1.00	0.85	4.01
O	2.48	0.40	21.24
Cu	0.34	0.23	< 5.07
Na	0.38	0.25	5.14
Co	0.18	0.23	< 2.61

Table 3. XPS analysis of the near surface region of Pd cathode JM2 after heat burst in figure 2a.

ELEMENT	SIGNAL	SENS. FACTOR	AT%
Si	0.03	0.27	2.31
C	0.78	0.25	64.52
Pd	0.28	2.70	2.16
O	0.89	0.60	30.62
Cu	0.06	4.20	0.30
Sn	0.01	4.30	0.05
Co	< 0.01	0.23	< 0.04

Table 4. Ratio of Li and Pd signals as a function of sputtering time of the surface of Pd cathode JM2 after heat burst shown in figure 2a.

TIME mts	Pd^{106} Cts.	Li^{7} Cts.	Li/Pd
0.00	1876	96159	51.26
10.00	966	28534	29.54
20.00	730	15002	20.55
30.00	674	10331	15.33
40.00	596	8171	13.71
50.00	567	6675	11.77
60.00	486	5855	12.05
70.00	450	5328	11.84
80.00	446	4885	10.95
90.00	442	4407	9.97

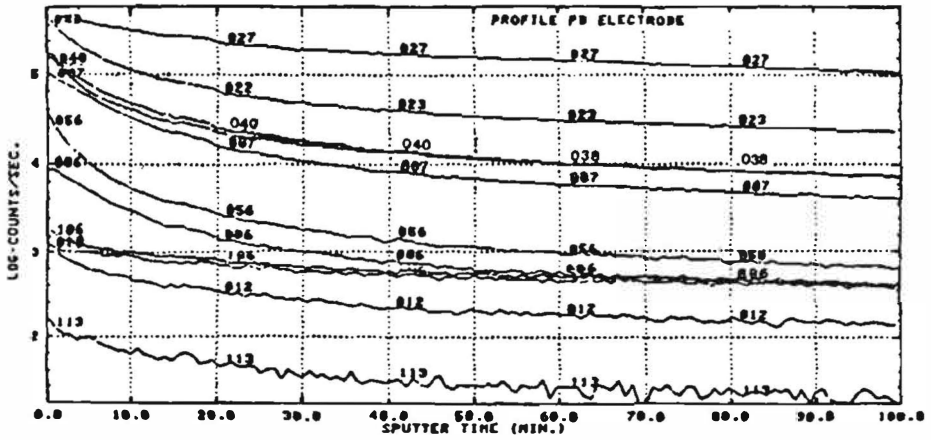

Figure 5. SIMS profile of palladium cathode JM2 after heat burst shown in figure 2a.

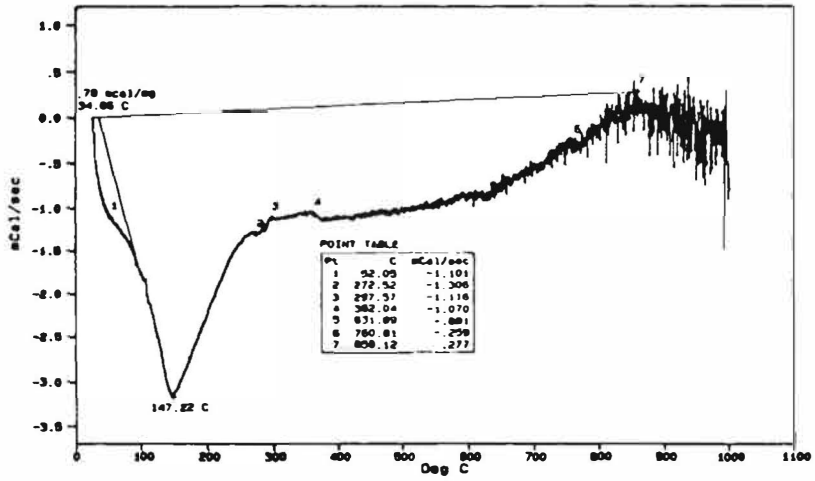

Figure 6. DSC scan of Pd cathode 5 after 11 months of elctrolytic charging and three temperature excusion events.

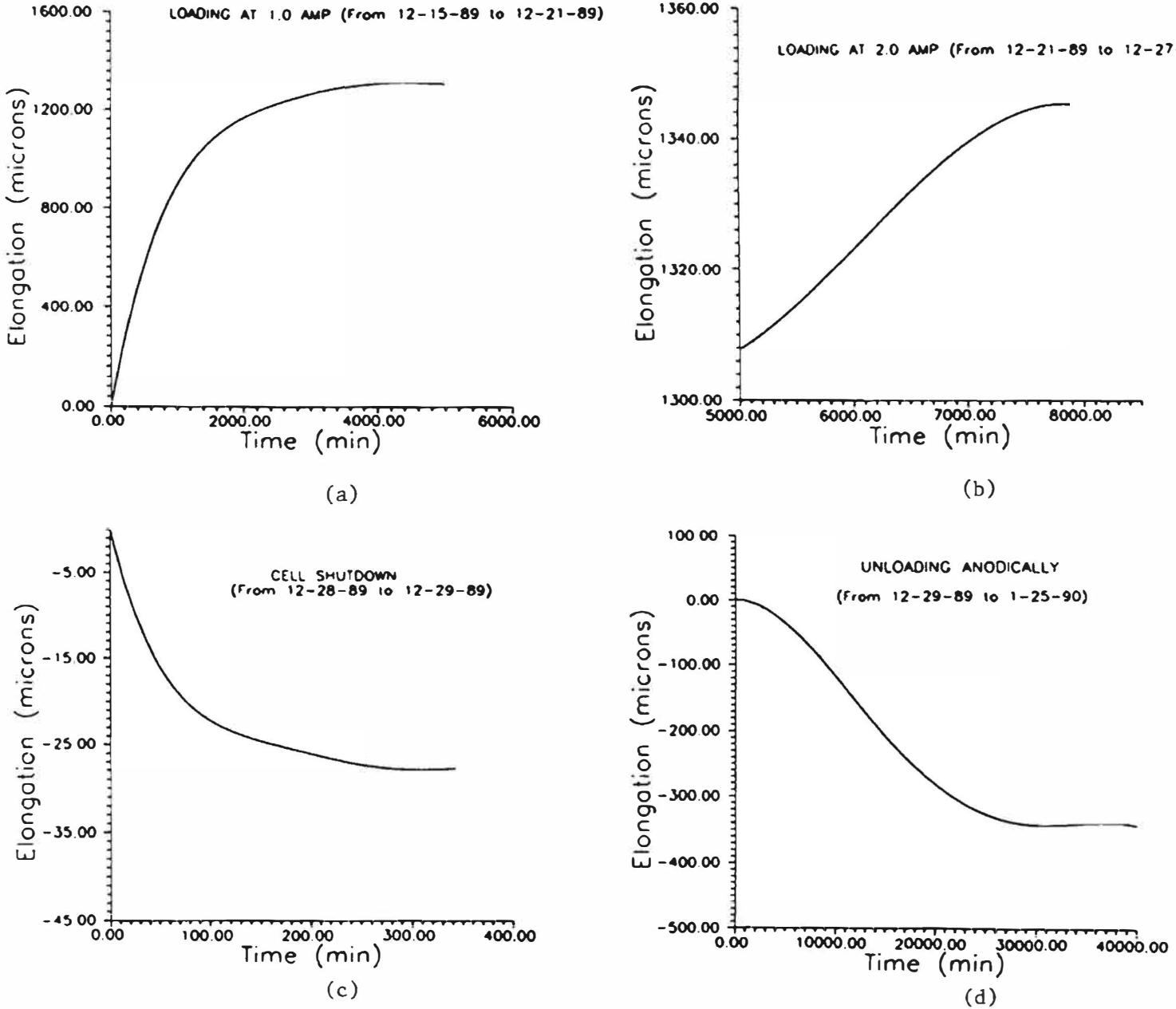

Figure 7. Electrode elongation measured in-situ during (a) loading at 100 mA/cm^2, (b) after current density change to 200 mA/cm^2, (c) after power was turned off and (d) during anodic D discharge.

ELECTROCHEMICAL CALORIMETRIC STUDIES OF THE COLD FUSION EFFECT

M. H. Miles, K. H. Park, and D. E. Stilwell

Chemistry Division, Research Department
Naval Weapons Center, China Lake, CA 93555

ABSTRACT

Several types of calorimetric cell designs were used in attempts to measure excess enthalpy during the electrolysis of LiOD/D_2O using palladium cathodes. Control experiments were run by using light water in place of D_2O or by using platinum cathodes in place of palladium. Initial experiments using thin palladium cathodes of an unknown purity gave no significant differences between the Pd/D_2O cells and the controls. For example, the ratio of heat out to Joule heat in was 1.00 ±0.04 for one study and 1.065 ±0.04 for another study in LiOD/D_2O compared to 1.075 ±0.07 in LiOH/H_2O. The use of a much thicker palladium rod (99.96%, d = 0.635 cm) from Johnson Matthey, however, resulted in calorimetric evidence for excess enthalpy in five out of six cells. The excess rate of heating averaged 0.39 W/cm^3 over a 9-day period in one experiment. The total excess enthalpy observed was 110,000 J. This excess enthalpy is difficult to explain by chemical reactions. Similar experiments conducted in H_2O did not produce significant amounts of excess enthalpy. Possible experimental errors in these calorimetric studies are being investigated.

INTRODUCTION

The electrochemically induced nuclear fusion of deuterium using a palladium electrode reported by Pons, Fleischmann, and Hawkins [1] has sparked a flurry of experimental measurements and considerable controversy [2-6]. The conditions under which this fusion may or may not occur will eventually be determined by many experiments at various laboratories. Enthalpy excesses that can exceed 10 W/cm^3 of the palladium electrode have been claimed [1]. Similar experiments by Jones and coworkers [7] also report evidence for cold nuclear fusion; however, the fusion rates reported are far too small to be detected by calorimetry. The experiments, described below, are an attempt to detect any excess heat output by calorimetric studies during the electrolysis of deuterium oxide containing LiOD at palladium cathodes. Control measurements were run using light water with palladium cathodes or heavy water with platinum cathodes. Radiation levels were also monitored by various methods.

EXPERIMENTAL

The calorimetric cell design used in most experiments is shown in Figure 1. The electrolysis cell in this configuration can be visualized as a resistive heater with the temperature being measured in the secondary compartment (gap) surrounding the

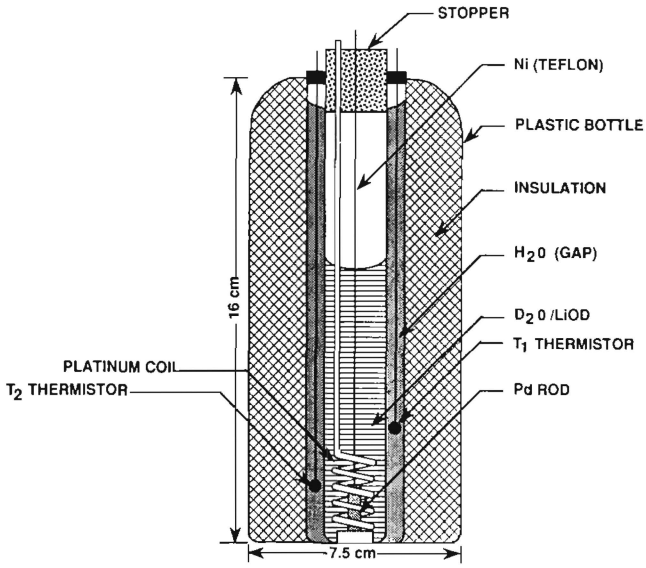

Figure 1. Calorimetric Cell Design.

electrolysis cell. The electrolysis cell initially contained 18-20 g of 0.1 m LiOD/D_2O (99.9%, Cambridge Isotope Laboratories) while the gap contained 68-70 g of distilled water. The alkaline solutions were prepared from lithium metal (ROC/RIC, 99.95%). This cell design minimized the decrease in the calorimetric cell constant with the decrease in the electrolyte solution volume which occurs during electrolysis. Both the electrolysis cell and plastic bottle (polyethylene) were stoppered and wrapped with parafilm to reduce evaporation and contamination. The evaporative losses from both the inner and outer glass vessels were 1% by weight per day. Make up water and heavy water were periodically added to the two compartments. After correcting for evaporation, the measured loss of D_2O due to electrolysis was always within ±1% of the calculated value. The palladium rod cathode (Johnson Matthey, 99.96%, d = 0.635 cm, A = 2.64 cm^2) was spot-welded to a nickel lead. Both the anode and cathode leads were covered with heat shrinkable Teflon tubing to prevent exposure of the bare metal to the gases in the headspace. Two

thermister thermometers (Cole-Parmer, Model 8502-16) calibrated within ±0.01°C were inserted into small glass tubes placed in the gap H_2O and positioned 4.6 cm (T_1, T_4) and 1.9 cm (T_2, T_5) from the bottom of the cell. Two identical calorimetric cells containing two thermistors each as shown in Figure 1 were always run simultaneously in a constant temperature bath (T_{bath} = 27.50°C). Identical coils of Pt - 20% Rh (5.35 g, d = 0.1 cm) served as the counter electrodes.

Earlier experiments used a palladium wire cathode (d = 0.14 cm, A = 2.64 cm^2, Wesgo) of an unknown purity spot-welded to a Pt - 20% Rh lead that was covered with heat-shrinkable Teflon tubing. Platinum wire cathodes (d = 0.12 cm, A = 2.64 cm^2) were used in several control experiments. Precision thermometers graduated in units of 0.1°C were used in these earlier studies. Several other calorimetric cell designs were also used that involved measuring the temperature directly in the electrolysis cell and using a correction factor to compensate for the decrease in the calorimetric cell constant with solution volume.

The constant current source for electrolysis was a Princeton Applied Research (PAR) potentiostat/galvanostat (Model 373) set at 264 mA (100 mA/cm^2). Calorimetric cell constants were usually determined during the first day of electrolysis when no excess enthalpy is expected. Experiments using palladium cathodes in H_2O or platinum cathodes in D_2O gave nearly the same cell constants. In earlier experiments, calorimetric cell constants were determined by Joule heat calibrations with a 29 ohm resistor.

RESULTS

Calorimetric studies using the thin palladium and platinum wire cathodes in 0.1 m LiOD/D_2O are presented in Figure 2. The equation

$$X = \frac{\text{Heat out}}{\text{Joule heat in}} = \frac{K \cdot \Delta T}{(E - E_H^o) \cdot I} \qquad (1)$$

was used for these experiments where K is the calorimetric cell constant, E is the cell voltage, E_H^o is the thermal neutral potential for the cell reaction, and ΔT is the temperature difference measured within the gap and the outer surface of the polyethylene bottle (Fig. 1). The daily mean values from a series of measurements are shown in Figure 2. The overall mean value of $\bar{X}$ = 0.97 ±0.06 for the platinum cathode indicated that the calorimetric design was satisfactory. Further-more, the overall mean value of $\bar{X}$ = 1.00 ±0.04 for palladium showed that there was no measurable excess enthalpy generation due to the cold fusion effect in this experiment.

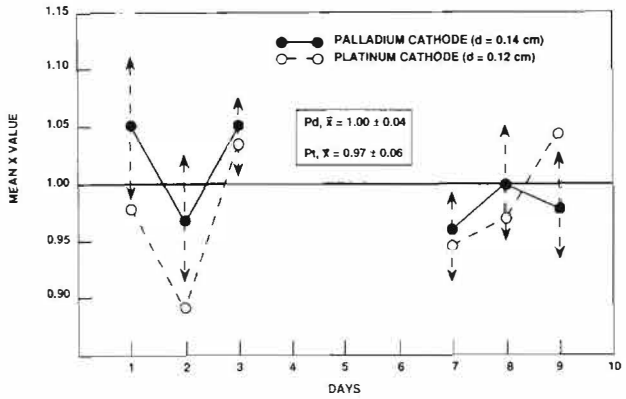

Figure 2. Comparison of Palladium and Platinum Wire Cathodes in LiOD/D_2O. The standard deviation for each day is indicated for the palladium cathode. Both cells were charged at 20 mA/cm^2 between days 3 and 7. Current density was 100 mA/cm^2 for all other days except day 3 (200 mA/cm^2).

Earlier experiments in a thermos-type cell with a precision thermometer placed directly in the electrolyte solution yielded mean values of $\bar{X}$ = 1.065 ±0.04 for the palladium wire cathode in LiOD/D_2O compared to 1.075 ±0.07 in LiOH/H_2O. In these studies, the equation used to correct the K values due to the volume change was

$$K_t = (0.964\ V_t/V_o + 0.036)\ K_o \qquad (2)$$

where K_o and V_o represent the initial cell constant and volume, respectively. The initial cell constants determined by Joule heat calibrations were 0.0435 ±0.0015 W/°C for the D_2O cell and 0.0458 ±0.0016 W/°C for the H_2O cell. These experiments support the conclusion that no excess enthalpy was generated using the palladium wire cathode. However, most of these experiments were of relatively short duration (1-3 days). Details of these earlier studies that failed to show any excess enthalpy are reported elsewhere [8].

The use of the much thicker palladium rod from Johnson Matthey resulted in calorimetric evidence for excess enthalpy as shown in Figure 3. For the two cells run simultaneously, one cell gave a heat ratio of $\bar{X}$ = 1.31 ±0.05 for the 11th day while the other cell gave a ratio of only $\bar{X}$ = 1.05 ±0.04 for measurements that day. The major difference between these two cells was the tighter wrapping of the counter electrode coils about the palladium in the cell that gave the greater X values. The

discontinuation of the electrolysis overnight after the 18th day showed that the X values returned to near unity. Results from the thermistors positioned higher in the gap were similar (Figure 4), hence any thermal inversion is unlikely. The daily average for the room temperature ranged from 21.8 to 23.8°C in this study with a mean of 23.0 ±0.6°C.

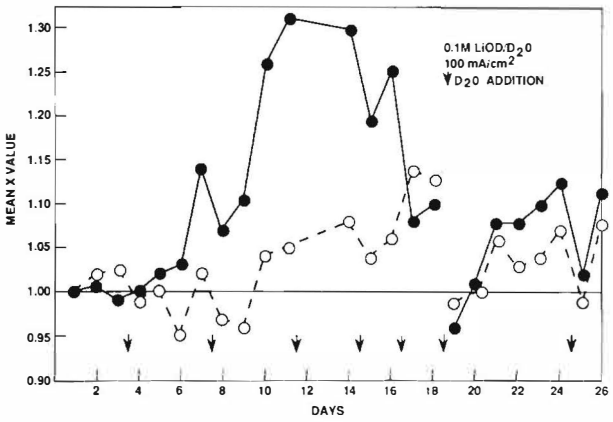

Figure 3. First Cold Fusion Study Using Palladium Rod (Johnson Matthey, d = 0.635 cm). Cell A (broken line, T_2) and cell B (solid line, T_5).

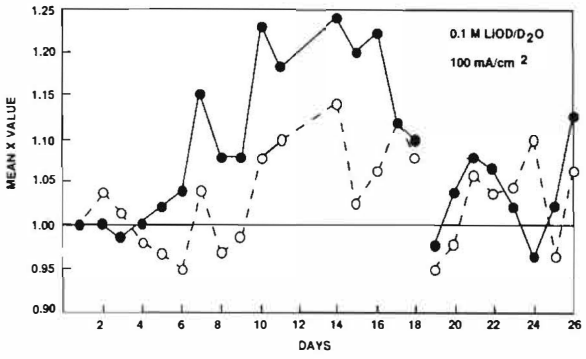

Figure 4. First Cold Fusion Study Using Palladium Rod (Johnson Matthey, d = 0.635 cm). Cell A (broken line, T_1) and cell B (solid line, T_4).

A continuation of this cold fusion study following a 10-day shutdown is shown in Figure 5. The excess enthalpy peaks are not as large and appear to be much more periodic with the D_2O additions than before. The additions of small amounts of ZnO to one cell and sulfur to the other cell had no measurable effects. The room temperature control was not as good in this study since the time frame (October, November) involved the onset of cooler weather. The daily average for the room temperature ranged from 19.7 to 23.4°C with a mean of 22.0 ±1.0°C.

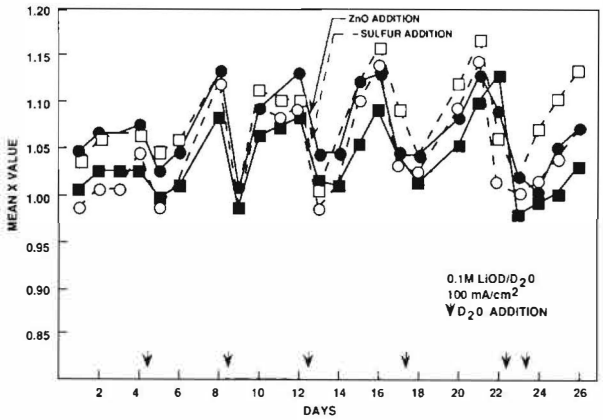

Figure 5. Second Cold Fusion Study Using Palladium Rod (Johnson Matthey, d = 0.635 cm). Cell A (broken lines), cell B (solid lines), T_1 (open circle), T_2 (open square), T_4 (solid circle), and T_5 (solid square).

Similar studies using the same palladium rod electrodes in cells containing H_2O rather than D_2O are shown in Figure 6. The striking difference from the

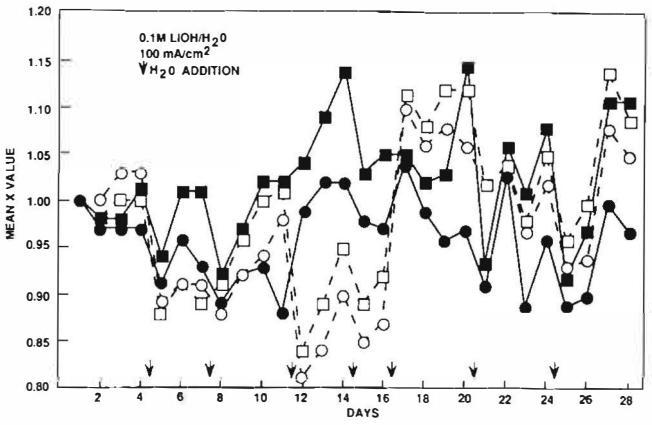

Figure 6. Studies in Water Using Palladium Rod (Johnson Matthey, d = 0.635 cm). Symbols for cell A, cell B, T_1, T_2, T_4, and T_5 same as in Figure 5.

previous experiments in D_2O are the excursions of the daily mean X values into regions of less than unity. Some rather large differences between the two thermistors in cell B (solid lines) suggest that thermal inversions were occasionally occurring. At times, a temperature instability was noted that was likely due to a mixing of the air in the glass thermistor tube. A portion of the thermistor tube extended above the calorimetric cell and was subjected to cooling by the room air. In later experiments, the thermistor tubes were made flush with the cell top resulting in more uniform temperatures and X values within the same cell. All H_2O measurements were made within an average daily room temperature range of 19.9-22.8°C with a mean of 21.5 ±0.7°C. Only a weak

relationship between the daily X values and the room temperature could be established in this study with a slope less than 0.02 per degree Centigrade and a correlation coefficient less than 0.3.

A third cold fusion study using the same palladium rod cathodes in fresh LiOD/D_2O solutions is shown in Figure 7. Excellent agreement between the two thermistors in each cell was realized in this study where the thermistor tubes were flush with the cell top. This experiment shows a nearly consistent excess enthalpy production with only a few days yielding near unity for the heat ratio. However the daily mean X values are noticeably less than those for the first study with a freshly prepared palladium cathode (Figures 3 and 4). The daily average room temperature ranged from 22.4 to 24.5°C in this study with a mean of 23.4 ±0.5°C.

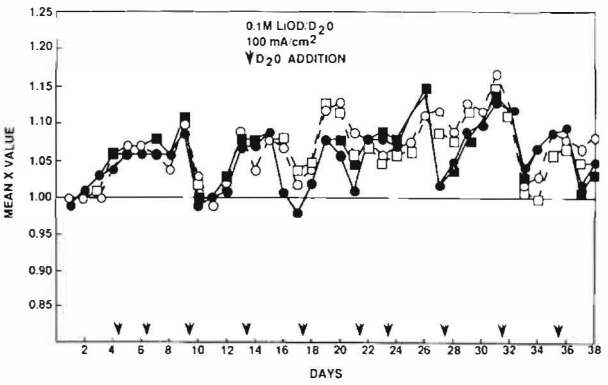

Figure 7. Third Cold Fusion Study Using Palladium Rod (Johnson Matthey, d = 0.635 cm). Symbols for cell A, cell B, T_1, T_2, T_4, and T_5 same as in Figure 5.

Tritium measurements on the LiOD/D_2O solutions following the first two experiment using the palladium rods were negative. The two LiOD/D_2O solutions gave 22.99 ±2.63 cpm and 22.18 ±1.06 cpm versus 19.34 ±0.57 cpm for a LiOD/D_2O sample that was never subjected to electrolysis. Results from a second laboratory gave similar conclusions. Theoretical calculations based on the total observed excess enthalpy (563 kJ) yield 4.4 x 10^7 T atoms mL^{-1} when the 10^{-9} disparity factor between excess heat and tritium production is used [1]. Assuming no loss of tritium to the gas phase and a 100% counting efficiency, this amount of tritium would only yield 4.7 cpm, hence, the tritium produced would have been difficult to detect from the background.

DISCUSSION

Interpolations of the results reported by Pons, Fleischmann, and Hawkins [1] yield an expected heat ratio of X = 1.95 for our palladium rod at 100 mA/cm^2. Such a high X value would unquestionably be well outside the range of any calorimetric errors. Statistical tests must be applied to our smaller X values to determine any significant difference from unity. Nevertheless, the comment [5] that it is most unlikely that the excess thermal energy due to a fusion process would be of the same order of magnitude as the electrical energy input is perplexing. An order of magnitude larger fusion effect involving D_2O electrolysis with a palladium cathode, however, likely would have been discovered years ago.

The overall mean heat ratios obtained from the various experiments using the palladium rod cathodes as well as the 99% confidence intervals are presented in Table I. The first five days of data were omitted to allow the palladium to become charged with deuterium (n is the number of days of data considered). The excess enthalpy for cell B ($\bar{X}_4$, $\bar{X}_5$) was significant at the 99% confidence level in all three D_2O experiments. For cell A ($\bar{X}_1$, $\bar{X}_2$), the excess enthalpy was significant at the 99% level in all except the first D_2O experiment that had the widely spaced counter electrode coils. The experiment in H_2O yields mean heat ratios close to unity for both cells A and B. The overall mean heat ratios and confidence intervals using all data yields similar conclusions. The main difference is that the mean X values are generally somewhat smaller for the Pd/D_2O experiments when the first five days are included.

Table I. Mean Heat Ratios and Confidence Intervals for Data After 5 Days of Charging. $\mu - \bar{X} = \pm 2.58\ \sigma/\sqrt{n}$ (99%).

Experiment	$\bar{X}_1$	$\bar{X}_2$	$\bar{X}_4$	$\bar{X}_5$	
Pd ROD/D_2O (I)	1.04 ±0.05	1.04 ±0.05	1.145[a] ±0.06	1.17a ±0.08	(n=11)
Pd ROD/D_2O (II)	1.06[a] ±0.03	1.10[a] ±0.03	1.08[a] ±0.03	1.05[a] ±0.03	(n-19)
Pd ROD/H_2O	0.96 ±0.05	0.995 ±0.05	0.96 ±0.03	1.03 ±0.03	(n=23)
Pd ROD/D_2O (III)	1.08[a] ±0.02	1.07[a] ±0.02	1.06[a] ±0.02	1.07[a] ±0.02	(n=33)

[a]Excess enthalpy (99% confidence level).

The t-test can also be used to determine if there is a significant difference from unity for the various mean heat ratios in Table I. Results for the t-test at the 99.5% confidence level are given in Table II. The same Pd/D_2O cells as before show a significant positive difference from unity at the 99.5% confidence level. Both cell A and cell B in the

Pd/H_2O experiment fails to show any significant positive differences from unity. The value for t_4 (-4.21), however, is a significant negative difference at the 99.5% confidence level. Although the third cold fusion experiment (Figure 7) did not yield the highest heat ratios, the length of this study (n = 33 days) along with its small mean standard deviation (s = ±0.02) yielded exceptionally large t values.

Table II. The t Test for Excess Enthalpy for Data After 5 Days of Charging. $t = (X - \mu)\sqrt{n}/s$.

Experiment	t_1	t_2	t_4	t_5	t (99.5%)
Pd ROD/D_2O (I) (n=11)	2.30	2.10	6.64[a]	5.56[a]	3.58
Pd ROD/D_2O (II) (n=19)	5.27[a]	8.27[a]	7.84[a]	4.93[a]	3.25
Pd ROD/H_2O (n=23)	-2.23	-0.28	-4.21	2.25	3.15
Pd ROD/D_2O (III) (n=33)	10.94[a]	10.25[a]	8.55[a]	9.01[a]	3.08

[a]Excess enthalpy (99.5% confidence level).

Table III shows that the differences in the calorimetric cell constants measured in various experiments were not a significant factor. The cell constants for cell A (K_1, K_2) tended to be slightly larger than for cell B (K_4, K_5). The cell constants determined in H_2O were very close to those determined in D_2O.

Table III. Calorimetric Cell Constants Determined in Various Experiments Using $K_{cell} = (E\text{-}E^o_H)\ I/\Delta T$ Where E^o_H = 1.53 V for D_2O and E^o_H = 1.48 V for H_2O.

Experiment	K_1 (W/°C)	K_2 (W/°C)	K_4 (W/°C)	K_5 (W/°C)
Pd ROD/D_2O (I)	0.141	0.145	0.133	0.132
Pd ROD/H_2O	0.135	0.138	0.137	0.134
Pd ROD/D2O (III)	0.139	0.143	0.133	0.134
Mean	0.138 ±0.003	0.142 ±0.004	0.134 ±0.002	0.133 ±0.001

Possible calorimetric error sources for our cell design (Figure 1) include room temperature fluctuations, the exposure of the glass thermistor tubes to the room air, the level of H_2O in the gap, the level of the electrolyte in the electrolysis cell, thermal inversions in the gap or thermistor tubes, hydrogen/oxygen recombination within the cell, and deviations from Newton's Law of cooling. Many of these error sources are small and they all tend to cancel since cell constant determinations were made under nearly the same conditions. Furthermore, these error sources should affect the Pd/H_2O experiments in the same manner, yet mean heat ratios close to unity were obtained in the H_2O studies. However, the level of the gap H_2O must be carefully controlled in our cell design. Experiments where measured amounts of the gap H_2O up to 10 mL were withdrawn showed nearly a 2% increase in X per mL of H_2O withdrawn. Although the loss due to evaporation was small (and could be entirely eliminated), the effect of the gradual loss of gap H_2O often became experimentally measurable after several days and likely contributed to the periodic trends of Figure 5. The effect of the electrolyte level was much less important for our cell design, hence no correction for this was needed. There was never any evidence for deuterium/oxygen recombination within the cell.

It is interesting to consider the excess enthalpy produced by the various Pd rod/D_2O cells. For example, using the data from either Figure 3 or 4, an average of at least 18% excess enthalpy is observed for a 9-day period (days 9-18). This corresponds to an average excess power of 0.14 W (0.39 W/cm^3) and a total excess enthalpy of 110 kJ. It can be shown that the complete combustion of the palladium electrode in the form of Pd_2H to yield PdO and H_2O would give an excess enthalpy of only 6.2 kJ. The recombination of D_2 and O_2 to yield 110 kJ of enthalpy would require the formation of 0.37 moles (7.4 g) of D_2O within the cell, yet only normal amounts of make-up D_2O were required during this 9-day period. Hence, it is difficult to explain the 110 kJ of excess enthalpy by chemical reactions. Similar calculations based on data in Table I yields total excess enthalpies of 213 kJ for cell B in Exp. I, 217 kJ for cell A in Exp. II, and 301 kJ for cell A in Exp. III. No excess enthalpies were measured in the H_2O experiment.

Deviations from Newton's Law of cooling have been recently discussed as a possible calorimetric error source [9]. Although this concern applies mainly to Dewar calorimeters where most heat transfer occurs by radiation, it is interesting to see how such errors would affect experimental X values in any type of calorimeter. If heat transfer from the calorimetric cell occurs only by radiation (Q_R) and conduction (Q_C), then

$$Q_R + Q_C = K_R\,(T_i^4 - T_o^4) + K_C(T_i - T_o) \quad (3)$$

The substitution $T_i = T_o + \Delta T$ yields

$$Q_R + Q_C = [K_R^0\,(1 + \Delta) + K_C]\,\Delta T \quad (4)$$

where $K_R^o = 4K_R T_o^3$ and $\Delta = 3\,\Delta T/2\,T_o + (\Delta T)^2/T_o^2 + (\Delta T)^3/4\,T_o^3$. Thus the ratio of heat in to heat out becomes

$$X = \frac{[K_R^o(1+\Delta) + K_C]\,\Delta T}{(E - E_H^o) \bullet I} \qquad (5)$$

rather than Eq. 1. If there is Joule heating only, then $X = 1.00$, $\Delta T = \Delta T_J$, and $\Delta = \Delta_J$. If there is a fusion contribution to the heat, then $X > 1.00$, $\Delta T = \Delta T_J + \Delta T_F$, and $\Delta = \Delta_F$. Thus

$$X = \left(1 + \frac{\Delta T_F}{\Delta T_J}\right) \bullet \left[\frac{(1+\Delta_F) + K_C/K_R^o}{(1+\Delta_J) + K_C/K_R^o}\right] \qquad (6)$$

If the heat transfer occurs mainly by conduction as in our calorimeter, then $K_C >> K_R^o$, hence

$$X = 1 + \frac{\Delta T_F}{\Delta T_J} = X_N \qquad (7)$$

which corresponds to Newton's Law of cooling. If the heat transfer occurs mainly by radiation, then $K_C << K_R^o$, hence

$$X = \left(1 + \frac{\Delta T_F}{\Delta T_J}\right)\left(\frac{1+\Delta_F}{1+\Delta_J}\right) \qquad (8)$$

Since $\Delta_F > \Delta_J$, larger X values would be obtained using Eq. 8 rather than Newton's cooling law (Eq. 7). For example, assuming $\Delta T_J = 10$ K, $\Delta T_F = 2$ K, and $T_o = 300$ K yields $X_N = 1.20$ from Newton's law and $X = 1.21$ from Eq. 8. Hence calibrating a Dewar type cell under conditions of Joule heating only and measuring a fusion heat contribution would yield somewhat higher X values if the more exact expression (Eq. 8) is used rather than Newton's cooling law.

The exposure to neutrons and other harmful radiation can be a matter of concern in cold fusion experiments. Theoretical calculations of dose rates were performed for our cell design (Figure 1) using the Group 16 model for neutron energies. Assuming a source of 10^4 neutrons from the palladium, calculated dose rates were 0.28 mrad/hr at the outer surface of the bottle and 0.012 mrad/hr at the top of the bottle (1 rad = 0.01 J/kg). These calculations suggest safe dose rates for people near the cold fusion experiment. Radiation exceeding weekly safe limits could only be reached by holding the cold fusion bottle against the body for an entire 40-hour-work week. These theoretical calculations also showed that the flux of thermal neutrons would not be sufficient to activate gold or copper metal placed at the surface of the bottle. Gold and copper metal samples were always kept near the cold fusion experiments, but radiation measurements gave essentially only background levels. Neutron monitoring for safety concerns carried out with a Ludlum Model 15 counter never gave any response significantly above the background levels.

The upper limit for isotopic changes in metals due to an electrochemical fusion process that produces neutrons can be illustrated by a simple calculation. Assuming an excess power of 1 W/cm^3 resulting from the fusion reaction

$$^2D + {}^2D \rightarrow {}^3He + n + 3.27\ MeV \qquad (9)$$

yields 1.91×10^{12} neutrons/cm^3 s. If all of these neutrons were absorbed by the palladium electrode, then the time requried to convert 1% of the palladium to other isotopes is given by

$$t = \frac{(6.79\times10^{22}\ \text{Pd atoms/cm}^3)\,(0.01)}{1.91\times10^{12}\ \text{neutrons/cm}^3\ \text{s}} =$$

$$3.55\times10^8\ \text{s} \qquad (10)$$

which translates into 11 years. Considering the relatively short duration of most electrochemical fusion experiments and the low thermal neutron capture cross-section for the various palladium isotopes, any change in the isotopic composition of the palladium electrode would be difficult to detect. The rate of ^{3}He production would be equally small and difficult to detect, especially considering its possible escape through cracks and fissures.

CONCLUSIONS

Heat ratios greater than unity can be measured in calorimetric experiments for Pd rod/D_2O cells that are significant at the 99.5% confidence level. However, these heat ratios are frustratingly small in many experiments. Nevertheless, the total excess enthalpies are difficult to explain by chemical reactions.

ACKNOWLEDGMENT

We would like to thank Bruce Tufts of the California Instute of Technology and Philip Aisen of the Albert Einstein College of Medicine for the tritium measurements, and Robert Miles of Rocky Flat/EG and G for neutron flux and dose rate calculations. We are also grateful to John France for assistance in

obtaining supplies and equipment. K.H.P. and D.E.S. express appreciation for ONT/ASEE postdoctoral fellowships.

REFERENCES

1. M. Fleischmann, S. Pons, and M. Hawkins, "Electrochemically Induced Nuclear Fusion of Deuterium," J. Electroanal. Chem., Vol. 261, pp. 301-308 (1989).

2. M. Gai, S. L. Rugari, R. H. France, B. J. Lund, Z. Zhao, A. J. Davenport, H. S. Isaacs, and K. G. Lynn, "Upper Limits on Neutron and γ-Ray Emission from Cold Fusion," Nature, Vol. 340, pp. 29-34 (1989).

3. D. E. Williams, D. J. S. Findlay, D. H. Craston, M. R. Sené, M. Bailey, S. Croft, B. W. Hooton, C. P. Jones, A. R. J. Kucernak, J. A. Mason, and R. I. Taylor, "Upper Bounds on Cold Fusion in Electrolytic Cells," Nature, Vol. 342, pp. 375-384 (1989).

4. D. Morrison, "The Rise and Decline of Cold Fusion," Physics World, Vol. 3, pp. 35-38 (1990).

5. R. D. Armstrong, E. A. Charles, J. Fells, L. Molyneux, and M. Todd, "Some Aspects of Thermal Energy Generation During the Electrolysis of D_2O Using a Palladium Cathode," Electrochim. Acta, Vol. 34, pp. 1319-1322 (1989).

6. N. J. C. Packham, K. L. Wolf, J. C. Wass, R. C. Kainthla, and J. O'M. Bockris, "Production of Tritium from D_2O Electrolysis at a Palladium Cathode," J. Electroanal. Chem., Vol. 270, pp. 451-458 (1989).

7. S. E. Jones, E. P. Palmer, J. B. Czirr, D. L. Decker, G. L. Jensen, J. M. Thorne, S. F. Taylor, and J. Rafelski, "Observation of Cold Nuclear Fusion in Condensed Matter," Nature, Vol. 338, pp. 737-740 (1989).

8. D. E. Stilwell, K. H. Park, and M. H. Miles, "Electrochemical Calorimetric Studies on the Electrolysis of Water and Heavy Water (D_2O), " J. Fusion Energy (in press).

9. V. J. Cunnane, R. A. Scannell, and D. J. Schiffrin, "$H_2 + O_2$ Recombination in Non-Isothermal, Non-Adiabatic Electrochemical Calorimetry of Water Electrolysis in an Undivided Cell," J. Electroanal. Chem., Vol. 269, pp. 163-174 (1989).

Thoughts on Warm Fusion versus Cold Fusion

Yi-Chen Cheng, W-Y. P. Hwang, and Shin Nan Yang

Department of Physics
National Taiwan University
Taipei, Taiwan 10764, R.O.C.

ABSTRACT

We propose a mechanism that may allow for understanding of the cluster-impact fusion experiment of Beuhler, Friedlander, and Friedman. When the cluster of D_2O molecules collides with the metallic surface, the cluster dissociates into a collection of D and O atoms. In the process, a significant portion of the translational kinetic energy of the cluster is converted to thermal energy, so that the system thermalizes to become a "warm atomic plasma". The neutral D atoms in the warm atomic plasma then fuse with the D atoms in the lattice via direct scattering, without going through the doorway step of forming D_2 molecules. As a rough estimate for the fusion reaction rate, the velocity distribution of the thermalized D atoms is taken to be Maxwell-Boltzmann, leading to results in qualitative agreement with the experimental observations for a cluster of about $100 - 300$ molecules.

I. Introduction

Recently, Beuhler, Friedlander, and Friedman (BFF) [1] claimed that the nuclear fusion reaction $d+d \rightarrow^3 H+p$, detected via the $3-MeV$ protons produced, has been observed to take place as singly charged clusters of 25 to 1300 D_2O molecules, accelerated to 200 to 325 keV, impinge on TiD targets. The BFF experiment has often been cited as another evidence to support the result reported earlier by S.E. Jones *et al.* [2] who have observed deuteron-deuteron fusion at room temperature during low-voltage electrolytic infusion of deuterons into metallic titanium or palladium electrodes. Nevertheless, the situation concerning "cold fusion" (CF) remains rather confusing and is certainly far from being settled. Some claimed [3] that they have seen CF, while others [4] declared the opposite.

In this work, we attempt to explore if the BFF experiment can be understood on plausible grounds. To this end, we noted that in the BFF experiment each D atom in the D_2 molecular cluster, which will dissociate upon impinging on the target, has energy around 20 to $300eV$. (Here and henceforth we shall use D and d to denote a deuterium atom and a deuteron nucleus, respectively.) It seems rather unlikely that these energetic D atoms will give up all their kinetic energies and form D_2 molecules with D atoms on the lattice such that fusion reactions take

place after the formation of D_2 molecules. Instead, it is likely that fusion reactions take place via direct scattering between the energetic incoming D atoms and the D atoms inside the target. Recent calculations [5] of the interaction potentials between two D atoms inside Pd and Ti suggest that the shortest stable equilibrium distance between two D atoms inside the metals is not shorter than that in a free D_2 molecule. This in turn suggests that, if the fusion reactions took place by going through a doorway step of forming D_2 molecules, then the fusion reaction rate inside the metals would be less than that in the free space, contradicting some people's belief that the metals enhance the reaction rate. It is also likely that in the BFF experiment, when the singly charged D_2O clusters impinge upon the target, the dissociated D atoms will be mostly neutral. Accordingly, the interaction potential in the scattering process is more like $D+D$, i.e., atom-atom interaction rather than the usually assumed $d+d$, i.e., bare Coulomb interaction. The assumption is supported by the neutral $He+He$ and $H+He$ collision experiments [6] in the laboratory energy range of 200 to $500eV$, where one sees that complete ionization does not occur very often. When the free space $D+D$ interaction potential is used, the fusion cross section is 6 orders of magnitude larger than that of the pure Coulomb $d+d$ interaction potential for the center-of-momentum energy of about $150eV$. Although this is a significant improvement, the predicted fusion reaction rate is still lower than the observed one by more than 19 orders of magnitude. As suggested by the title of the BFF experiment, however, "cluster" and "impact" are the two ingredients which appear in the BFF experiment but not in atom-atom scattering in free space. A possible effect of "cluster-impact" is that the translational motion of the cluster will be stopped by the target and a dissociation of the cluster into D and O atoms occurs. The lost kinetic energy of the translational motion of the cluster may be redistributed to the dissociated atoms. If the cluster is large enough, a quasi-thermal equilibrium state may be reached, forcing the system to form a "warm atomic plasma" of some sort. For a crude approximation the velocity distribution of the dissociated atoms may be taken as Maxwell-Boltzmann. With the above proposed scattering process and the velocity distribution our calculated results for the fusion rate are in qualitative agreement with the observations in the BFF experiment. We call this type of nuclear fusion as "warm fusion" (WF) which is to be distinguished from the so-called cold fusion (CF) and the much studied hot fusion. Cold fusion is usually referred to fusion which could take place at room temperature or below. Hot fusion refers to deuterons with thermal energy as high as 10^9 degrees and above. Our proposed warm fusion, which occurs via formation of a warm atomic plasma, provides another type of fusion. When the D_2O cluster impinges upon the target with energy around 300 keV, the dissociated D atoms are thermalized up to a temperature of around 10^6 to 10^7 degrees and therefore a "warm" fusion.

Thermalization of the D atoms in the cluster enhances the fusion rate by more than 15 orders of magnitude, in comparison with the delta-function velocity distribution, in the energy range we considered. Therefore the establishment of quasi-thermal equilibrium state is essential for this type of nuclear fusion to be observed. It is possible that some kind of redistribution of velocity of the D atoms (or d ions), which will enhance the fusion rate, also occur in the low-voltage electrolysis experiments performed by Jones *et al.* [2] and Fleischmann *et al.* [3] and others. However in this work we will concentrate only on the cluster-impact experiment of BFF and will not elaborate on the electrolysis experiments. In the following we

present the theory and the calculated results of the above proposed mechanism for warm fusion.

II. Nuclear Fusion via Direct Atomic Scattering

In the cluster-impact experiment of Beuhler, Friedlander [1], and Friedman, the observed reaction rate is related to the fusion cross section $\sigma(E)$ as follows:

$$R = n\sigma(E)\Phi t A \tag{1a}$$

$$= 2N_i n\sigma(E) t I_d, \tag{1b}$$

where n is the density of the deuterium atoms in the target material, t and A are respectively the thickness (or the penetration depth) and the cross section area of the target, Φ is the incoming flux of the deuterium atoms, I_d is the incoming dc current and N_i is the number of heavy-water molecules contained in the singly charged cluster. The fusion cross section $\sigma(E)$ is given by the standard formula

$$\sigma(E) = \frac{S(E)}{E} e^{-G}, \tag{2a}$$

$$G = 2\int_a^{r_0} k(r)dr, \tag{2b}$$

$$k(r) = \{2\mu(V(r) - E)\}^{1/2}, \tag{2c}$$

where E and μ are respectively the kinetic energy in the center-of-momentum (CM) frame and the reduced mass of the deuteron pair, and $S(E)$ is the astrophysical S factor for the specific process. ($S(E \approx 0) \approx 55\, keV - barn$ for $d+d \rightarrow^3 H+p$ and $d+d \rightarrow^3 He+n$.) $V(r)$ is the repulsive interaction potential between the reacting particles, $d+d$, $d+D$, or $D+D$. When the reacting particles are $d+d$, the e^{-G} term is the standard Gamow Coulomb barrier penetration factor in the WKB approximation. When the reacting particles are $d+D$ or $D+D$, the e^{-G} term still represents the penetration factor but its value is many orders of magnitude larger than the standard Gamow factor for E in the energy range we considered. Note that r_0 in Eq. (2b) is the classical turning point as the two deuterons approach each other, while the inner distance a ($< r_0$) is such that $V(a) = V(r_0)$. In practice, we may set $a \approx 0$.

We begin our investigations by comparing the results corresponding to three different choices of the potential $V(r)$, viz.: (1) the pure $d+d$ Coulomb repulsive potential shown as the long dashed curve in Fig. 1, (2) the screened $D+D$ potential $V(r)$, as obtained in the calculation on D_2 molecule by Kolos and Wolniewicz (KW)[7], shown as the solid curve in Fig. 1, and (3) the partially screened $d+D$ potential in D_2^- shown as the short dashed curve in Fig. 1. A glance at Fig. 1 already suggests that the difference between the $D+D$ and $d+D$ cases is much less dramatic than that between the $D+D$ and $d+d$ cases.

In Fig. 2, the calculated fusion cross section is shown as a function of the atom-atom CM kinetic energy E_d. In the long dashed curve is the prediction for the $d+d$ Coulomb repulsive potential, in the solid curve for the $D+D$ potential in D_2 [7], and in the short dashed curve for the partially screened $d+D$ potential in D_2^-. It is clear that the predicted cross section is the largest in the case of the fully screened $D+D$ potential.

As two deuterium atoms scatter from each other, there is of course some chance that both atoms become ionized. In the case that both deuterium atoms are ionized, $d+d$ fusion is dictated by the need to penetrate the pure Coulomb potential. The penetration factor e^{-G} is found to be 10^{-35} at $E = 150eV$ (the energy relevant for the BFF experiment). On the other hand, if both deuterium atoms remain electrically neutral, the penetration factor becomes 10^{-29} which is an enhancement of about 6 orders of magnitude. It is thus an experimental question to decide the level of complete ionization as two deu-

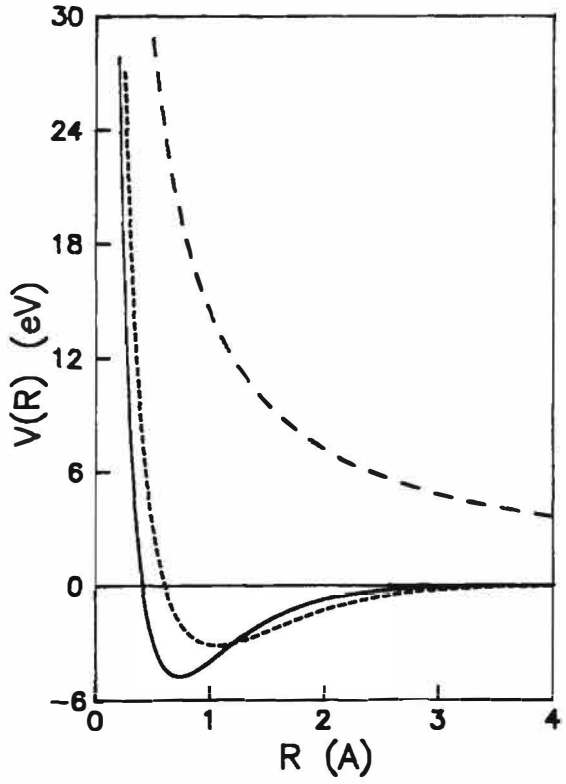

Fig. 1. The potentials which we choose to consider in this work. The long dashed curve refers to the pure $d + d$ Coulomb repulsive potential, the solid curve is the $D + D$ potential $V(r)$ in D_2 molecule as obtainede by Kolos and Wolniewicz[7], and the short dashed curve is the partially screened $d + D$ potential in D_2^-.

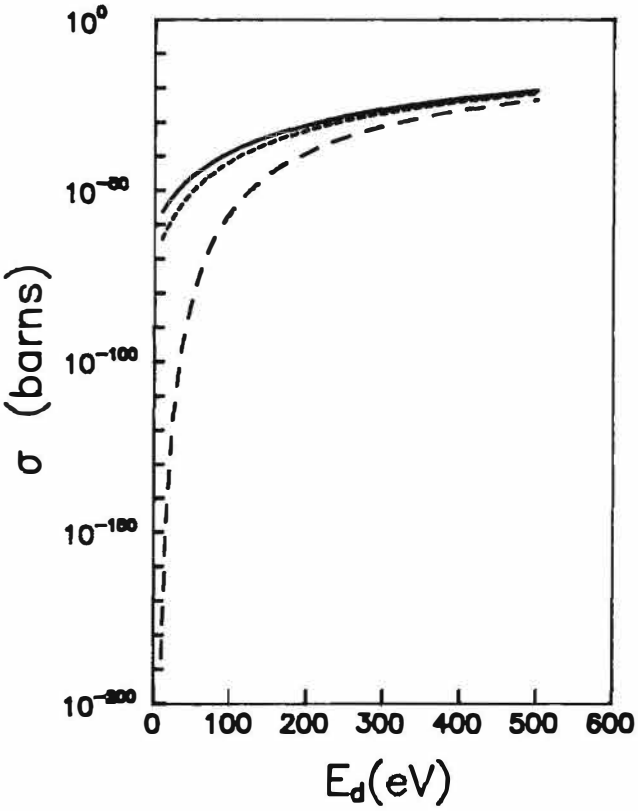

Fig. 2. The deuteron-deuteron calculated fusion cross section as a function of the CM kinetic energy E_d. In the long dashed curve is the prediction for the $d + d$ Coulomb repulsive potential, in the solid curve for the $(D+D)$ potential in D_2 molecule [7], and in the short dashed curve for the partially screened $d + D$ potential in D_2^-.

terium atoms collide. A similar question for $He + He$ and $H + He$ collisions has been studied [6], indicating that elastic atomic scattering dominates in the laboratory energy range of 200 to 500 eV. So long as there is a significant fraction of time that complete ionization is irrelevant, the approximation to consider only the atom-atom collisions through the KW potential should yield a reasonable estimate for the fusion cross section, at least in terms of the order of magnitude.

Koonin and Nauenberg [8] have considered the scenario in which a D_2 molecule is formed prior to nuclear fusion by tunneling through the KW potential. They obtain the rate for $d + d$ fusion which is some 10 orders of magnitude faster than previous estimates, but still far below the value that might be needed to account for those experiments which claim to have seen CF. In such scenario, the Coulomb barrier remains very high although trapping of the two deuterium atoms in the potential well improve the the chance for penetration for nuclear fusion

(as there is more time to do so). It turns out that the gain really cannot outweigh the loss in the penetration factor.

While the consideration of the nuclear fusion via unionized atom-atom scattering can improve the calculated results many orders of magnitude, this picture alone is not enough for understanding the BFF experiment since our calculated rate is still lower than the observed one by about 19 orders of magnitude. Nevertheless, the cluster-impact experiment such as BFF has an additional feature that, upon impact, the cluster may dissociate into D and O atoms and a large portion of the translational kinetic energy of the cluster may convert to thermal energy. The thermalization process causes redistribution of the velocities among the D atoms. This will enhance the reaction rate by more than 15 orders of magnitude. We call this thermalization induced fusion "warm fusion" and will discuss it in the following Section.

III. Nuclear Fusion via Formation of a Warm Atomic Plasma

The experimental situation of the BFF experiment has an important feature that the cluster is large. It seems likely that, within a limited numbers of layers in the lattice, the impinging flow of D_2 cluster already suffer from a large number of collisions (electromagnetic in origin) between particles in the beam and those in the target such that the cluster dissociates into D and O atoms and redistribution of the kinetic energy occurs. Accordingly, the system thermalizes to become a "warm atomic plasma" of some sort. It is clear that such evolution of cluster flow can in fact be described by the well-known Boltzmann transport equation with the interactions between particles in the flow and those in the target giving rise to the "force term" [9].

$$(\frac{\partial}{\partial t} + \mathbf{v}_1 \cdot \nabla_{\mathbf{r}} + \frac{\mathbf{F}}{m} \cdot \nabla_{\mathbf{v}_1}) f_1 = \int d\Omega \int d^3 v_2 \mid \mathbf{v}_1 - \mathbf{v}_2 \mid \frac{d\sigma}{d\Omega} (f_2' f_1' - f_2 f_1), \tag{3}$$

with $f_1 \equiv f(\mathbf{r}, \mathbf{v}_1, t)$, $f_2 \equiv f(\mathbf{r}, \mathbf{v}_2, t)$, $f_1' \equiv f(\mathbf{r}, \mathbf{v}_1', t)$, and $f_2' \equiv f(\mathbf{r}, \mathbf{v}_2', t)$. $d\sigma/d\Omega$ is the differential cross section for the collision $\{\mathbf{v}_1, \mathbf{v}_2\} \rightarrow \{\mathbf{v}_1', \mathbf{v}_2'\}$.

As the zeroth-order approximation [9], the distribution function is locally Maxwell-Boltzmann,
i.e. $f(\mathbf{r}, \mathbf{v}, t) = (\frac{M}{2\pi\theta})^{3/2} exp\{-\frac{M}{2\theta}(\mathbf{v} - \mathbf{u})^2\}$ with θ and $\mathbf{u}$ slowly varying functions of the position $\mathbf{r}$ and the time t. At a time t_0 when the flow is almost stopped ($\mathbf{u} \approx 0$) and a quasi-equilibrium state, i.e., a warm plasma of neutral atoms ("warm atomic plasma"), has been reached.

It is likely that the neutral D atoms in the warm atomic plasma then fuse with the D atoms in the lattice via direct scattering, without going through the doorway step of forming D_2 molecules. Qualitatively speaking, the total thermal energy of the flow may be only about a half of that of the original flow but the flow now contains a fraction of high-energy deuterium atoms, enhancing the warm fusion cross section in a significant way. For example, the Gamow Coulomb barrier penetration factor, the e^{-G} term, is 10^{-29}, 10^{-21}, or 10^{-18} for $E = 150\,eV$, $300\,eV$, or $450\,eV$, respectively. As long as the redistribution according to the Boltzmann transport phenomenon yields a non-negligible fraction of deuterium atoms of energies several times of the initial value, say a couple of per cent, the enhancement of the fusion cross section can easily be in the range of more than 10 orders of magnitude.

In the process of forming the warm atomic plasma, the thermal energy, as converted from a portion of the translational kinetic energy $E_{cluster}$ of the cluster, is specified by $\alpha E_{cluster}$.

$$E_{thermal} = \alpha E_{cluster}. \quad (4)$$

Assuming that, by equipartition theorem, the thermal energy is shared equally among $3N_i$ dissociated D and O atoms, the temperature of the plasma is given as

$$\frac{E_{thermal}}{3N_i} = \frac{3}{2}k_B T. \quad (5)$$

α will be treated as a parameter characterizing the fraction of the kinetic energy retained by the projectile flow of deuterium atoms after the flow has been stopped. Most of collision processes yield $\alpha < 1$. In our opinion, $\alpha \sim \frac{1}{2}$ would be a reasonable estimate and $\alpha = 1$ helps to set the optimal upper bound.

We may use

$$f(\mathbf{v}) = (\frac{M}{2\pi k_B T})^{3/2} exp\{-\frac{M}{2k_B T}\mathbf{v}^2\}, \quad (6)$$

with M the deuteron mass and $\mathbf{v}$ the deuterium velocity seen in the rest frame of the target material (the laboratory frame). Assuming that fusion takes place between the deuterium atom in the cluster projectile and that in the target material, we obtain the CM kinetic energy:

$$E = \frac{1}{2}E_d^L \equiv \frac{1}{2}\mu v^2. \quad (7)$$

On the first sight, the cross section to be used in connection with Eq. (1) would be given by

$$< \sigma >= \int_0^{N_0 k_B T} \sigma(E) f(\mathbf{v}) d^3 v, \quad (8)$$

where $\sigma(E)$ is obtained from Eqs. (4). However, a close look at Eq. (1) indicates that $\sigma(E)\, v$ is the quantity to be replaced by

$$< \sigma\, v >= \int_0^{N_0 k_B T} \sigma(E) \mid \mathbf{v} \mid f(\mathbf{v}) d^3 v, \quad (9)$$

since the flux Φ, contains the relative velocity between the two fusion particles. A temperature-dependent cut-off $N_0 k_B T$, with $N_0 = 6 - 10$, has been introduced in Eqs. (8) and (9) to avoid the "high energy" region where the WKB approximation is no longer justified while the contribution to warm fusion cross section is likely to be of less importance.

In Figs. 3(a) and 3(b), we show our predictions, for the case $N_i = 150$, together with the results from the BFF experiment, for the quantity $< \sigma\, v >$ as a function of the energy respectively for $\alpha = 1$ and $\alpha = 0.5$. The long dashed and solid curves are results obtained with $N_0 = 10$ and 6, respectively. The experimental results are extracted with the use of Eq. 1 and the following estimates,

$$n \approx 6 \times 10^{22}/cm^3, \qquad \Phi \approx 1.25 \times 10^{12} cm^{-2} sec^{-1}$$
$$t \approx 10^{-5} cm, \qquad A \approx 1\, cm^2. \quad (10)$$

It is seen that the shape of the energy dependence seen in the BFF experiment is reproduced very well. In addition, our predictions are surprisingly close to the points extracted qualitatively from the BFF experiment. Considering the fact that our estimates can easily be off by a couple of orders of magnitude and that there are many effects which can give rise to modification in the range of a couple of orders of magnitude, we have come a long way to resolve the mystery of 10's orders of magnitude in understanding the BFF experiment.

Fig. 4, shows our predictions, together with the results from the BFF experiment, on the quantity $< \sigma\, v >$ as a function of the number of D_2O molecules in the cluster projectile for fixed cluster incident energy $E_{cluster} = 300keV$ and $\alpha = 1$. Here it is seen that additional cluster effects set in as the size of the cluster increases. This can be taken as another evidence for our conjecture that the projectile flow can in fact be described as a Boltzmann transport phenomenon of some sort. As the cluster size

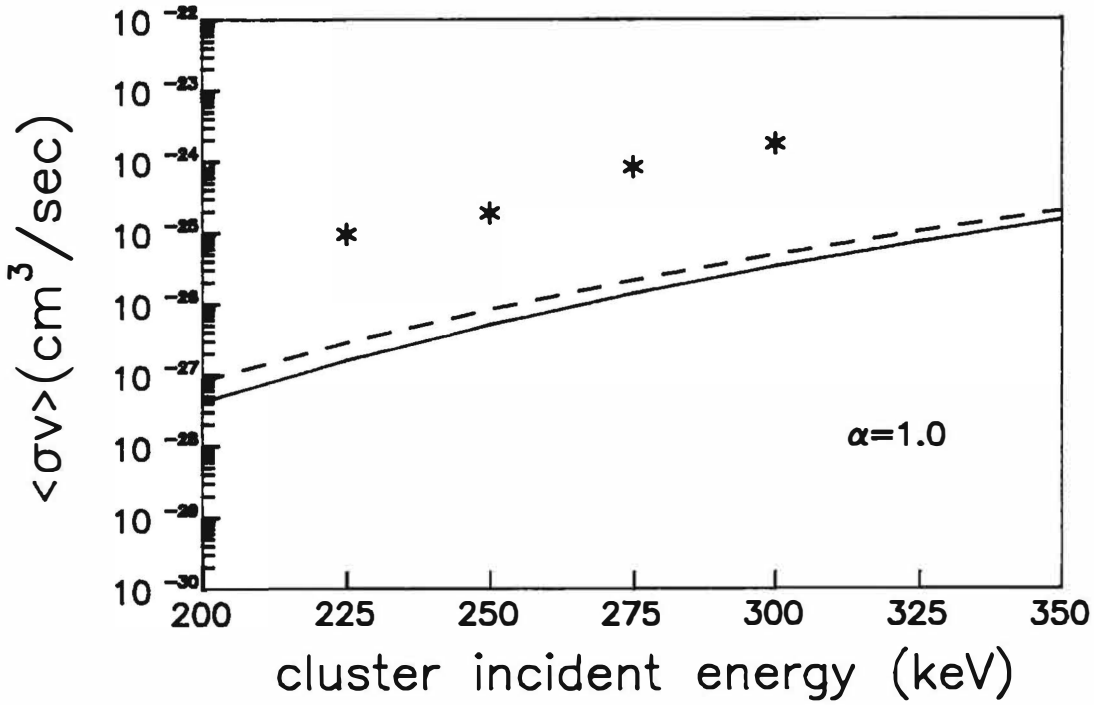

Fig. 3a. Our predictions, together with the results from the BFF experiment, on the quantity $< \sigma v >$ shown as a function of cluster incident energy with $\alpha = 1$, for the case that cluster projectile contains 150 D_2O molecules. The long dashed and the solid curves are results obtained with different choices of cut-off energy, i.e., $N_0 = 10$ and 6, respectively.

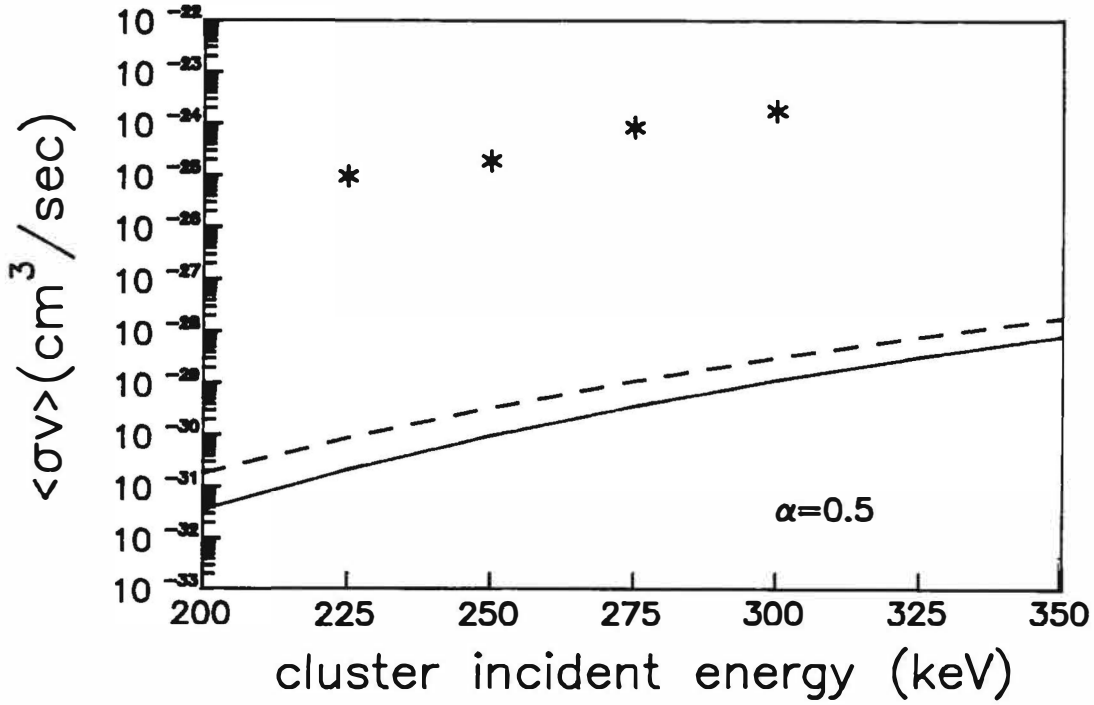

Fig. 3b. Same as in Fig. 3a, but with $\alpha = 0.5$.

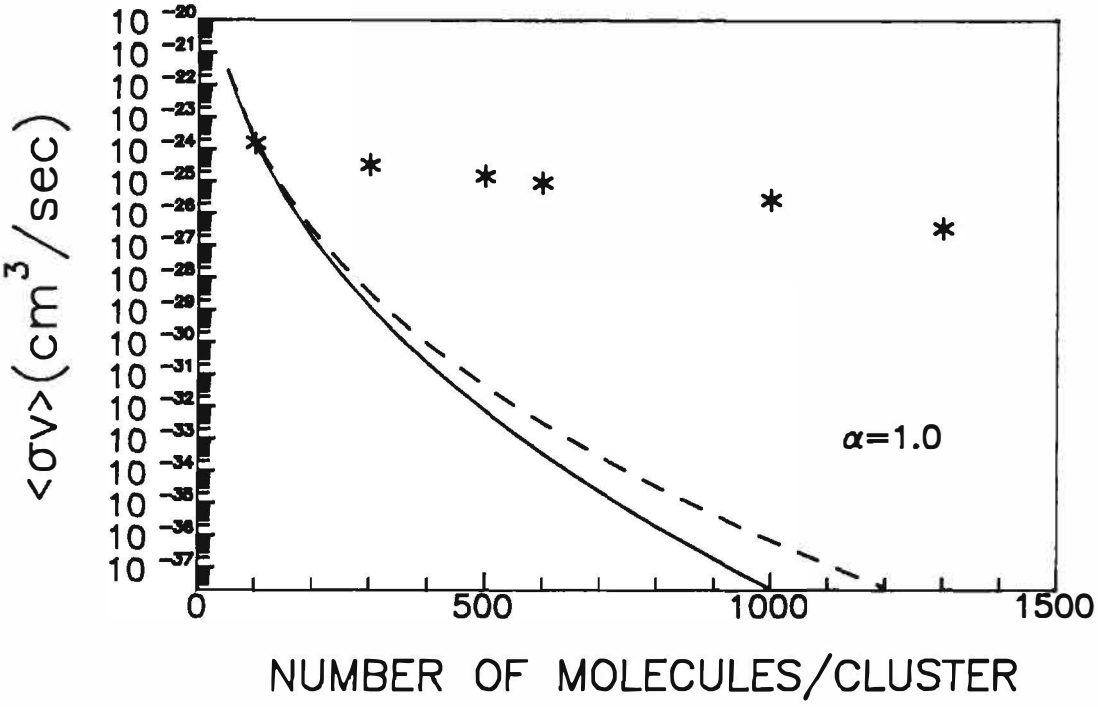

Fig. 4. Our predictions, together with the results from the BFF experiment, on the quantity $< \sigma v >$ shown as a function of the number of D_2O in the cluster at fixed cluster incident energy of $300keV$ with $\alpha = 1$. The long dashed and the solid curves are results obtained with different choices of cut-off energy, i.e., $N_0 = 10$ and 6, respectively.

increases, the approach in which only the deuterium atoms in the cluster projectile are assumed to be "thermalized" becomes too limited since compression forced on the target material by the large cluster should become of great importance.

IV. Concluding Remarks

In this work, we have proposed a mechanism that may allow for understanding of the cluster-impact fusion experiment of Beuhler, Friedlander, and Friedman [1]. As caused by a large number of collisions due to the interaction between the cluster and the lattice, the cluster dissociates into a collection of D and O atoms when the cluster of D_2O molecules collides with the metallic surface. In the process, a significant portion of the translational kinetic energy of the cluster is converted to thermal energy, so that the system thermalizes to become a "warm atomic plasma". The neutral D atoms in the warm atomic plasma then fuse with the D atoms in the lattice via direct scattering, without going through the doorway step of forming D_2 molecules. As a rough estimate for the fusion reaction rate, the velocity distribution of the thermalized D atoms is taken to be Maxwell-Boltzmann. When the cluster is of the size that it contains about $100 - 300$ molecules, our results are in qualitative agreement with the experimental observations. As the cluster size increases, our results could be as far as 10 orders of magnitude smaller than

the experiemental observations. This indicates that the approach in which only the deuterium atoms in the cluster projectile are assumed to be "thermalized" becomes too limited since compression forced on both the target material and the cluster should become very important.

Acknowledgement

We wish to acknowledge Mr. S.-T. Lee and Mr. C.Y. Wu for helps in numerical calculations. This work is supported in part by the Atomic Energy Council of the Republic of China.

REFERENCES

[1] R.J. Beuhler, G. Friedlander, and L. Friedman, Phys. Rev. Lett. **63**, 1292 (1989).

[2] S.E. Jones, E.P. Palmer, J.B. Czirr, D.L. Decker, G.L. Jensen, J. M. Thorne, S.F. Tayler, and J. Rafelski, Nature **338**, 737 (1989).

[3] M. Fleischmann and S. Pons, J. Electroanal. Chem. **261**, 301 (1989); N.Wada and K.Nishizawa, Japanese J. Applied Phys. **28**, L2017 (1989); R. Taniguchi, T. Yamamoto, and S. Irie, *ibid.*, **28**, L2021 (1989).

[4] R. B. Campbell and L. J. Perkins, Fusion Technology, **16**, 383 (1989); M. A. Butler, D.S. Ginley, J. E. Schirber, and R.I. Ewing, *ibid.*, **16**, 388 (1989); J. E. Schirber, M.A. Butler, D.S. Ginley, and R. I. Ewing, *ibid.*, **16**, 397 (1989); H. Werle, G. Fieg, J. Lebkücher, and M. Mõschke, *ibid.*, **16**, 391 (1989); V.C. Rogers, G.M. Sandquist, and K.K. Nielson, *ibid.*, **16**, 523 (1989); D. J. Gillespie, G. N. Kamm, A. C. Ehrlich, and P. L. Mart, *ibid.*, **16**. 526 (1989); A.G. Gu, R.K.F. Teng, M.S. Miller, and W. J. Sprouse, *ibid.*, 248 (1989).

[5] X. W. Wang, S. G. Louie, and M. L. Cohen, Phys. Rev. **B40**, 5822 (1989); K. Sohlberg and K. Szalewicz, Phys. Lett. **A144**, 365 (1990).

[6] R. Morgenstern, M. Barat, and D. C. Lorents, J. Phys. B: Atom. Molec. Phys. **6**, L330 (1973); C. Benoit and J. P. Gauyacq, *ibid.* **9** L391 (1976).

[7] W. Kolos and L. Wolniewicz, J. Chem. Phys. **41**, 3663 (1964); **49**, 404 (1968); W. Byers-Brown and J.D. Power, Proc. Roy. Soc. Lond. **A 317**, 545 (1970).

[8] For a discussion on cold fusion in isotopic hydrogen molecules, see, e.g., S. E. Koonin and M. Nauenberg, Nature **339**, 690 (1989).

[9] Kerson Huang, *Statistical Mechanics* (John Wiley & Sons, Inc., New York - London - Sydney, 1963), p.67.

AN OVERVIEW OF COLD FUSION PHENOMENA

Martin Fleischmann

Department of Chemistry
University of Southampton
Southampton, Hants., SO9 5NH
ENGLAND

and

Department of Chemistry
University of Utah
Salt Lake City, UT 84112
USA

Abstract

The present position of research in the field of Cold Fusion has already been outlined in two papers presented at this meeting.[1,2] This report will therefore emphasize the early work and general considerations which led us to investigate the possibility of inducing nuclear reactions of D^+ in palladium electrodes[3] (for some corrections see[4]); this is followed by a brief assessment of the position reached at the end of the first year of research in this field as summarized by the papers presented at this conference.

Historical Background

The discovery of the two major nuclear reaction paths of D^+

$$^2D + {}^2D = {}^3T(1.01MeV) + {}^1H(3.02MeV) \quad (i)$$

$$^2D + {}^2D = {}^3He(0.81MeV) + n(2.45MeV) \quad (ii)$$

was reported by Oliphant, Harteck and Lord Rutherford in 1934 in a brief letter to Nature[5]; the precise values of the energy terms in reactions (i) and (ii) were established by subsequent research. This early work relied on the bombardment of perdeutero inorganic compounds such as $(ND_4)_2SO_4$ by deuterons of intermediate energies (~ 20 keV). The origins of this discovery have been largely forgotten presumably because deuterium and the deuteron were called diplogen and the diplon at that time. This neglect of the early literature is doubly unfortunate because the precise characterization of reaction (i) using cloud chamber methods already showed at that time that a significant number of the tracks of the ^3T and ^1H species emerged at ~ 180°[6,7]! To quote Philip Dee[7]: "this no doubt being the result of transmutations effected by slower diplons which have lost energy by collision in the target."

We believe that these reports are the first indication that there are low energy[1] fusion channels in solid lattices. The bombardment of heavy ice by deuterons of intermediate energy was used subsequently as a relatively intense source of neutrons[9] but the neutron generating processes do not appear to have been further characterized. There have, however, sometimes been other indications that low energy deuterons undergo fusion reactions e.g., the production of neutrons from high density low ion temperature plasmas induced by electron cyclotron resonance heating in magnetic mirror devices.[10]

General Consideration of the Behavior of D^+ in Palladium Cathodes

We have already drawn attention[3,11] to the strange behavior of D^+ electrochemically compressed into palladium cathodes.[12,13] Fig. 1 illustrates a number of the important

---

[1] Recent work on "warm fusion" induced in perdeuterated inorganic and organic materials by relatively low energy heavy water clusters[8] may well be related to these early observations.

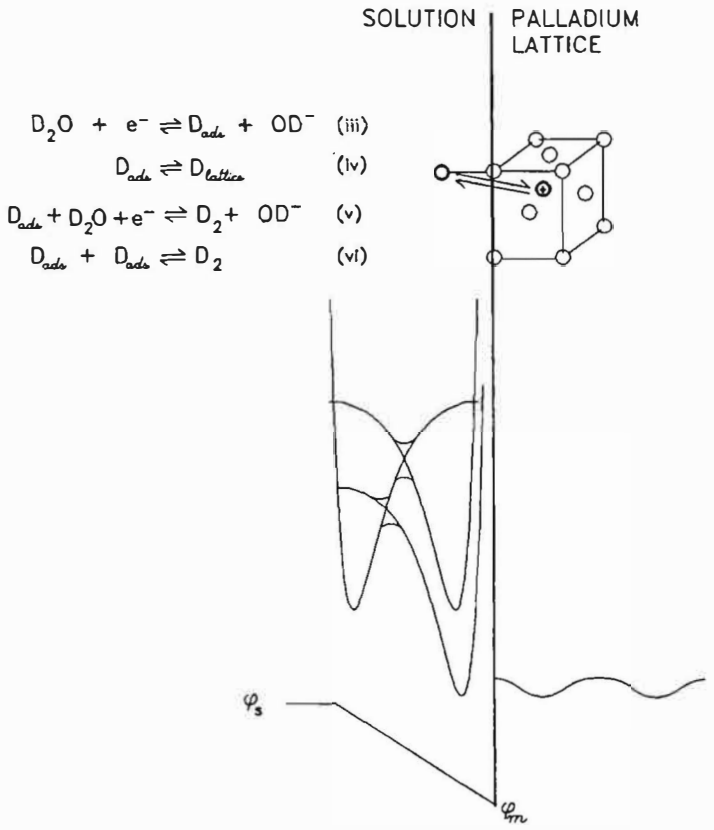

Figure 1. Schematic of the energetics in the solution, at the interface, and in the bulk of a palladium electrode during the electrolysis of heavy water containing LiOD, and a list of the pertinent reactions.

features of the discharge of D_2O and of D_2 evolution for electrolyses in alkaline media as well as of the dissolution of adsorbed D in the palladium lattice. At the reversible potential the initial state of reaction (iii) (a D_2O molecule interacting with its surroundings together with an electron in the Pd lattice) is in equilibrium with the final state (an adsorbed atom and a deuteroxide ion again interacting with their surroundings). For experiments close to atmospheric pressure the lattice is already in the β Pd-D phase. Increases in the difference of the galvani potential between the metal and the solution $|\Delta(\phi_m - \phi_s)|$ (shown here in a highly simplified form as a linear drop in potential across the Helmholtz double layer) from the value at the reversible potential stabilize the final state with respect to the initial state to an extent $\Delta(\phi_m - \phi_s)F$ joules mole^{-1}. The adsorbed atoms are therefore "driven" onto the surface and, in turn, the adsorbed species are "driven" into the FCC lattice, step (iv) where they exist as D^+ ions, almost certainly in the octahedral positions. The adsorbed species are desorbed in the further step (v). At very negative potentials, the D^+ species behave as classical oscillators.[13]

The concentration of D^+ in the lattice under equilibrium conditions is already very high (D/Pd $\approx$ 0.6 - 0.7). The composition of the lattice at high negative potentials is still a subject of debate but it would be surprising if the D/Pd ratio did not approach or even exceed unity under these conditions (see results presented at this meeting).[14] The dominant effect of the increase in cathodic potential must, however, be an increase in the activity of the dissolved deuterium. The activity will be determined under steady state conditions by the rates of steps (iii), (v) and (vi) but we will restrict attention here to a quasi-thermodynamic argument based on an hypothetical equilibrium of reactions (iii) and (iv). For such an equilibrium

we can equate the electrochemical potentials of the initial and final states

$$\bar{\mu}_{D^+,m} + \bar{\mu}_{OD^-,s} = \mu_{D_2O,s} \quad (1)$$

or

$$\mu_{D^+,m} + \phi_m F + \mu_{OD^-,s} - \phi_s F = \mu_{D_2O,s} \quad (2)$$

i.e.

$$\mu_{D^+,m} = \mu_{D_2O,s} + \mu_{OD^-,s} - (\phi_m - \phi_s)F \quad (3)$$

In this expression $\mu_{D_2O,s}$ and $\mu_{OD^-,s}$ will be close to the standard state values. It should be noted that $\mu_{D^+,m}$, $\mu_{OD^-,s}$ and $(\phi_m - \phi_s)$ are quantities which are not accessible to thermodynamic measurement but the change in the chemical potential of the dissolved D^+, $\Delta\mu_{D^+,m}$, due to a change in the galvani potential difference $\Delta(\phi_m - \phi_s)$, from the value existing at the reversible potential is thermodynamically defined (as is $\Delta(\phi_m - \phi_s)$).

Values of $\Delta(\phi_m - \phi_s)$ as high as 0.8V can be achieved using conventional electrochemical systems and values even higher (in excess of 2V) could be achieved under special conditions.[15] While the energy values $\Delta(\phi_m - \phi_s)F$ may appear to be modest, they are, in fact, of astronomical magnitude. Thus, if one were to attempt to achieve the same activity of dissolved D^+ by the compression of D_2 using steps (iv) and (vi) under equilibrium conditions (as is customary in heterogeneous catalysis) we would need to satisfy the condition

$$2\mu_{D^+,m} + 2\mu_{e,m} = \mu^{\circ}_{D_2,g} + RT \ln P_{D_2} \quad (4)$$

where P_{D_2} is the fugacity of the gaseous D_2. We obtain

$$\mu_{D^+,m} = \mu^{\circ}_{D_2,g}/2 - \mu_{e,m} + RT/2 \ln P_D \quad (5)$$

and, it can be seen that a 0.8 eV shift of the potential of the electrode corresponds to a $\cong 10^{27}$ fugacity of D_2:

$$0.8F = RT/2 \ln P_{D_2} \quad (6)$$

Such high hydrostatic pressures are naturally not achievable on earth and, even if they were, other phenomena would intervene such as the formation of metallic D and collapse of the host lattice. The argument set out above is instructive, however, from several points of view: in the first place it points to the importance of the "poisoning" of the desorption steps (v) and (vi) so as to drive (iii) as close to equilibrium as is possible; secondly, it points to the special role of cathodic polarization in causing the "compression" of D^+ into the lattice; thirdly, it suggests that clusters of D^+ must form in the lattice under such extreme conditions by analogy to the nucleation of metals. Our interest in nucleation phenomena and our knowledge of the prediction of the formation of metallic hydrogen (and deuterium) at extreme compressions in United States and Soviet work during the mid 70's (e.g., see[16]) was, in fact, a key element in the initiation of this research project. The clustering of D^+ would be initiated at special sites or, possibly, at octahedral sites which would distort so that these sites would then be more correctly described as being parts of dislocation loops.

There were (and are) a number of further factors which point to the possibility of inducing nuclear reactions of electrochemically compressed deuterium. The dissolved D^+ is, in fact, a very high density, low ion temperature plasma existing in an high electron concentration. We can therefore pose the following conundrum: it would be expected that the s-electron density around the nuclei would be high but this would lead to the formation of D_2. As this is not observed, the s-electron density must in fact be low. While we do not subscribe to the notion of the formation of heavy electrons, we recognize that the electron density in the clusters must be highly asymmetric and that it is necessary to develop a priori calculations about the many-body problem (taking into account the presence of the lattice) before it is possible to make any predictions of the Coulomb repulsion and nuclear motion in the clusters in the host

lattice[2] as well as the stability of the D^+ species. Such calculations must also provide answers to other conundra such as why the diffusion coefficient of D in Pd/D exceeds those of both H in Pd/H and T in Pd/T.[17] We recognize that some[18] (many?) regard the principle of asymptotic freedom as sacrosanct and, therefore, that nuclear reactions of D^+ could not be affected by many-body phenomena (coherent processes) in the lattice environment. This point of view is adhered to notwithstanding the fact that it is an approximation which may, or may not, hold in the limit of short space-times, the principle being increasingly called into question for other reasons, e.g.[19-21]. We, for our part, would not have started this investigation[3] if we had accepted the view that nuclear reactions in host lattices could not be affected by coherent processes.

The background to this research has been presented from the point of view of the behavior of D^+ in palladium cathodes since this has been our exclusive concern. A somewhat different account would be relevant to the behavior of deuterium in titanium, the other system which has been the subject of intensive research following the description of the generation of low levels of neutrons during cathodic polarization.[22]

Assessment of the Present Position

Part of our early work leading up to our first publication[3] was based on the search for evidence for reactions (i) and (ii) of D^+ compressed electrochemically into palladium electrodes. To our great surprise we found that excess enthalpy was generated in the cathodes, the magnitude of this excess enthalpy increasing markedly with increase of the current density; levels of 10-20 watts cm^{-3} of the cathode material were reached at 512mA cm^{-2}. The most surprising aspect of the results was that although low levels of tritium and possibly neutron generation could be detected, these levels were far too low to account for the generation of excess enthalpy. There appeared to be a rough equivalence of the rates of tritium and neutron generation at electrodes generating excess enthalpy above 1 watt cm^{-3}. Neutron generation appeared to take place in "bursts."[23] Subsequent work has shown that there are also "bursts" in the excess enthalpy production superposed on the essentially steady state excess enthalpy production reached at long times.[24] Tritium production also appears to take place in "bursts."[25]

The work reported at this meeting (as well as in a number of publications and numerous announcements during the past year) supports most of the first findings.[3,24] Steady state excess enthalpy production and "bursts" in enthalpy have been detected using a variety of calorimeters and calorimetric techniques (e.g., see the papers presented at this meeting). Rates of excess enthalpy generation above 100 watt cm^{-3} have been reached at 1A cm^{-3} [26,27] and these are sustained for times such that the total excess enthalpy is in the range 100-1000MJ cm^{-3} [26]; "bursts" in enthalpy as high as ~16 MJ cm^{-3} have been observed.[26,28] Such excess enthalpy generation clearly cannot be attributed to any chemical process(es).[30] Much higher levels of tritium generation (e.g., see[25,31-33]) than those observed in the original work[3] have now been reported and, as has been noted above, tritium generation also appears to take place in "bursts." The much more detailed and careful measurements of neutron production[34] than those in the original report[3] indicate that this process takes place at a very low steady state level and in "bursts." This appears to be equally true for the Ti-D system where further measurements have been largely confined to gas loading experiments.[35] For the Pd-D system it is becoming apparent that the branching ratio for reactions (i) and (ii) differs markedly from the expected value of ~ 1[31,32]. While this report has concentrated on the work presented at this meeting, we also draw attention to the interesting work on neutron generation induced by gas phase discharges in palladium rods saturated with deuterium[36].

New results reported at this meeting include the detection of soft

---

[2] This was the background to our statement[3] that it is necessary to reexamine the quantum mechanics of D^+ and electrons in such host lattices.

X-rays[31,37] (presumably by some type of coulomb excitation), of γ-rays[38] and the generation of charged particles following ion-implantation into Ti targets.[31,39] As electrochemists we have found the measurements of the low frequency impedance of Pd cathodes at high overpotentials[38] of special interest. The inductive A.C. loop could well be due to the nucleation and growth of a new metallic phase (see above-metallic D?). The theoretical investigations[40-44] have reached some degree of concensus in attributing Cold Fusion to the operation of coherent phenomena be they phonon or photon coupled or related to bound or unbound states. Experimentally testable predictions can be based on some of these theories (e.g., of tritium versus heat generation[41]).

While some of the more recent investigations indicate some degree of parallelism of the various phenomena (e.g. of tritium and neutron production and "bursts" in enthalpy[32,45] it is not yet by any means clear whether we are dealing with bulk or surface processes or both of these and whether and how all the disparate phenomena listed in Table 1 may be linked. The investigation of this aspect must clearly have high priority. It is now also essential to broaden the base of the research to include both the quantitative evaluation of the effects of the many variables leading to the control and optimization of particular outputs (compare[46]) and the extension of the range of systems showing the various effects. For the Pd-D system the central conundrum, the disparity of the excess enthalpy generation and of the expected nuclear products according to reactions (i) and (ii) however remains unsolved. It is clear that there must be other nuclear reaction paths of high cross-section and that these will only be discovered by a careful search for products on the surface and in the bulk of the electrodes (as well as in the solution and gas spaces). Experiments of this type will require electrode preparation under very clean conditions and analyses using XPS, Auger and high mass resolution SIMS measurements[47] as well as other high resolution mass spectroscopy. We arrive at the final conundrum: such experiments are essential to complete the description of the processes and are rightly requested.[48] However, while these experiments are certainly feasible they cannot be initiated, let alone completed, with present day funding levels and funding policies.

Conclusion

It is hardly possible that the

Excess enthalpy Bursts in enthalpy Tritium Bursts in tritium Neutrons Bursts in Neutrons X-rays Bursts in x-rays γ-rays Bursts in γ-rays Reaction products	Bulk, Surface, Special sites

Theory: coherent phenomena

Table I. The various phenomena which have been reported so far in the course of this research.

repeated observation of such a wide range of disparate phenomena can be explained away by the operation of a whole set of different systematic errors nor that we have been attending a seance of true believers.

References

[1] G. H. Miley: this meeting.
[2] D. Worledge: this meeting.
[3] M. Fleischmann, S. Pons, and M. Hawkins, J. Electroanal Chem. 261 (1989).
[4] M. Fleischmann, S. Pons, and M. Hawkins, J. Electroanal Chem. 263(1989) 187.
[5] M. L. Oliphant, P. Harteck, and Lord Rutherford, Nature 133 (1934) 413.
[6] P. I. Dee, Nature 133 (1934) 564.
[7] P. I. Dee, Proc. Roy. Soc. A 148 (1935) 623.
[8] R.J. Beuhler, G. Friedlander and L. Friedman, Phys. Rev. Lett., 63 (1989) 1292.
[9] E.C. Pollard and W.L. Davidson, "Applied Nuclear Physics," John Wileyand Sons, New York, 1942.
[10] W.B. Ard, M.L. Becker, R.A. Dandl, H.O. Eason, A.C. England and R.J. Kerr, Phys. Rev. Lett., 10 (1963) 87.
[11] M. Fleischmann and S. Pons, Proceedings of the Joint N.S.F. - E.P.R.I. Meeting, Washington, D.C., November, 1989.
[12] F. A. Lewis, "The Palladium Hydrogen System, Academic press, London, 1967.
[13] B. Dandapani and M. Fleischmann, J. Electroanal. Chem. 39 (1972) 323.
[14] R. Adzic, D. Gervasie, I. Bae, B. Cahan and E.B. Yeager: this meeting.
[15] M. Fleischmann and S. Pons, to be published.
[16] See the Rand Corporation Reports.
[17] J. Vöelkl and G. Alefeld, Eds., "Hydrogen and Metals", vol. 2, in "Topics in Applied Physics", vol. 29, Springer Verlag, Berlin,(1978), chapter 12.
[18] D. Lindley, Nature, 344 (1990) 375. Dr. Lindley does not phrase his comments in this way but this is what he implies.
[19] G. Preparata, Phys. Rev., A38 (1988) 233.
[20] E. Del Giudice, G. Preparata and G. Vitiello, Phys. Rev. Lett., 61 (1988)1085.
[21] G. Preparata, "Quantum Field Theory of Superradiance" in "Problems of Fundamental Modern Physics," R. Cherubini, P. Dal Piaz and B. Minetti, Eds., World Scientific Press (1990).
[22] S. Jones, E. Palmer, J. Czior, D. Decker, G. Jensen, J. Thorne, S. Taylor and J. Rafelski, Nature 338 (1989) 737.
[23] This has been repeatedly reported in lectures given by us subsequent to our first announcement.
[24] First reported by S. Pons at the 175th Meeting of the Electrochemical Society, Los Angeles, CA, May (1989).
[25] N. J. C. Packham, K. L. Wolf, J. C. Wass, R. C. Kainthla, and J. O'M. Bockris, J. Electroanal. Chem. 270(1989) 451.
[26] S. Pons: this meeting.
[27] R. A. Oriani, J. C. Nelson, S. K. Lee, and J. H. Broadhurst, 176th Meeting of the Electrochemical Society, Hollywood, FL USA October (1989), and submitted to Nature.
[28] M. Fleischmann, S. Pons, M. Anderson, L. J. Li, and M. Hawkins, J. Electroanal. Chem., in the press.
[29] S. Pons and M. Fleischmann, J. Fusion Technology, in the press.
[30] R. C. Kainthla, M. Sklarczyk, L. Kaba, G. H. Lin, O. Velev, N. J. C. Packham, J. C. Wass and J. O'M. Bockris, Inst. J. Hydrogen Energy 14 (1989) 771.
[31] P.K. Iyengar and M. Srinivasan: this meeting.
[32] J. O'M.. Bockris, G.H. Liu and N.J.C. Packham: this meeting.
[33] E. Storms and C. Talcott: this meeting.
[34] M. Srinivasan, A. Shyam, S.B. Degwekar and L.V. Kulkavui: this meeting.
[35] H.O. Menlove: this meeting.
[36] N. Wada and K. Nishizawa, Japanese J. of Appl. Phys., 28(1989)665.
[37] H. Bergerson: this meeting.
[38] M.C.H. McKubre, R.C. Rocha-Filho, S. Smedley, F. Tanzella, B. Chexal, T. Passell and J. Santucci: this meeting.
[39] G.C. Chambers, G. Hubler and K. Grabowski: this meeting.
[40] J. Schwinger: this meeting.
[41] G. Preparata: this meeting.
[42] P.L. Hagelstein: this meeting.

[43] S.R. Chubb and T.A. Chubb: this meeting.
[44] R.T. Bush: this meeting.
[45] C.D. Scott, J.E. Mrochek, M. Petek, T.C. Scott, G.E. Michaels and E. Newman: this meeting.
[46] R.W. Bass: this meeting.
[47] D.R. Rolison, W.E. O'Grady, R.J. Doyle, and P. P. Trzasko: this meeting.
[48] Cold Fusion Research, A Report of the Energy Research Advisory Board to the United States Department of Energy, DOE/S-0073, November, 1989.